

CMBBE 2023 SYMPOSIUM

18th International Symposium on Computer Methods
in Biomechanics and Biomedical Engineering

3 - 5 May 2023, Paris, France

CHALLENGES IN COMPUTATIONAL BIOMECHANICS
FOR TOMORROW'S HEALTHCARE SYSTEMS

ABSTRACT BOOK
ORAL PRESENTATIONS

www.cmbbe-symposium.com



Physics-based modeling and machine learning synergies in human heart modeling

Mathias Peirlinck (1)

1. *Delft University of Technology, Netherlands*

Through computational modeling, we can objectively integrate multi-physics data across the molecular, cell, tissue, and organ scale. For biological tissues, which are intrinsically more complex than most classical engineering materials, this approach has become imperative to understand and simulate the mechanistic emergence of function. For human heart modeling, the field has successfully simulated acute and chronic mechanisms at the tissue and organ scale by integrating various biological, chemical, and mechanical processes at smaller molecular and cellular scales. The resulting insights provide ample opportunities for an improved understanding of cardiac patho-(physiology), the design of new and safe medical devices, and the inception and ethical testing of novel treatment strategies [1]. Despite its predictive power, this higher level of mechanistic detail also introduces many unknowns, both in the form of unknown physics and unknown parameters [2]. Moreover, these frameworks often suffer from high computational costs. These aspects make the inference of these unknowns from sparse and indirect experimental biological and clinical data a challenging endeavor.

In this talk, we will highlight how machine learning approaches, coupled with multiscale modeling, hold important opportunities to overcome these issues and further improve our understanding of cardiac tissue behavior. By means of two studies focusing on the quantification of the predictive power of multiscale cardiac growth frameworks [3] and the differing risk for developing drug-induced arrhythmias between men and women [4], we will highlight various interesting machine learning approaches including Bayesian inference, Markov Chain Monte Carlo, hierarchical modeling, logistic and Gaussian process regression, multi-fidelity modeling and active learning. We will demonstrate how these

approaches enabled us to quantify the quality of sparse experimental data, identify missing information and inform our decisions for collecting additional experimental data or running expensive high-fidelity multiscale simulations. Moreover, we will showcase how multiscale modeling and machine learning mutually benefit from one another to create surrogate models, infer system dynamics and parameters, analyze underlying modeling sensitivities, and quantify uncertainty across the scales to better understand cardiac function.

References

1. Peirlinck, M., et al., Precision medicine in human heart modeling : Perspectives, challenges, and opportunities. *Biomechanics and Modeling in Mechanobiology*, 2021. 20(3): p. 803-831.
2. Alber, M., et al., Integrating machine learning and multiscale modeling—perspectives, challenges, and opportunities in the biological, biomedical, and behavioral sciences. *npj Digital Medicine*, 2019. 2(1): p. 115.
3. Peirlinck, M., et al., Using machine learning to characterize heart failure across the scales. *Biomech Model Mechanobiol*, 2019. 18(6): p. 1987-2001.
4. Peirlinck, M., F. Sahli Costabal, and E. Kuhl, Sex Differences in Drug-Induced Arrhythmogenesis. *Frontiers in Physiology*, 2021. 12(1245).

Acknowledgements

The work that will be presented entails the results of various collaborations with partners at Stanford University, Pontificia Universidad Catolica de Chile, Dassault Systemes Simulia Corp, University of California, San Francisco, Edwards Lifesciences, Thornton Tomasetti, Capvidia, Duke University, and the FDA.



PREDICTING AND UNDERSTANDING THE MECHANICAL BEHAVIOR OF SOFT TISSUE ACROSS THE SCALES BY DEEP LEARNING

Christian J. Cyron (1), Kevin Linka (1), Selda Sherifova (2), Cristina Cavinato (3),
Jay D. Humphrey (3), Gerhard A. Holzapfel (2)

1. Hamburg University of Technology, Germany; 2. Graz University of Technology, Austria;
3. Yale University, USA

1. Introduction

The microstructure and macroscopic mechanical properties of soft tissues like arteries are closely related. While substantial efforts have been made to quantify this relation, it has yet remained impossible for a long time to predict the macroscopic mechanical properties of soft tissues from microstructural information with satisfactory accuracy

2. Materials and Methods

To overcome this problem, we introduce a novel machine learning framework that combines advanced theoretical concepts with deep learning [1,2,3]. This framework receives microstructural information about soft tissue samples (e.g., from multi-photon microscopy and histology) as input. Its output are the mechanical properties of the same samples (i.e., their in general nonlinear and anisotropic strain energy function). Our machine learning architecture is designed such that it incorporates substantial prior knowledge from continuum mechanics and materials theory. This reduces the number of training samples it needs for successful machine learning to $10^1 - 10^2$. We applied our framework both to human [2] and murine [3] aortic data.

3. Results

Our trained machine learning architecture can predict the macroscopic mechanical properties of arterial tissue from microstructural information with high accuracy ($R^2 > 0.9$). Moreover, it cannot only predict mechanical properties in a black-box manner but also identify by layer-wise relevance propagation (LRP) those microstructural features that are most important for the mechanical properties of the tissue.

4. Discussion and Conclusions

To the authors' best knowledge, this is the first time that macroscopic mechanical properties of soft tissues are predicted with such high accuracy from the tissue microstructure. Moreover, our framework can also help to understand the role of different microstructural features for the macroscopic mechanical properties using concepts of explainable artificial intelligence. The automated identification of microstructural features most relevant for macroscopic mechanical properties can guide experiments, that is, help to focus them on measuring exactly those features. Moreover, it can provide advice what features should be paid to particular attention during tissue engineering. Altogether, this way the machine learning framework we present bears promise to be transformative for our understanding of soft tissue mechanics and to provide new insights into the changes of soft tissues during aging and various diseases.

5. References

1. Linka K et al., J Comput Phys. 2021;429:110010 (2021).
2. Holzapfel GA et al., J R Soc Interface. 2021;18(182):20210411 (2021).
3. Linka K et al., Acta Biomat. 2022;147:63-72 (2022).

Acknowledgements:

Funded by the Deutsche Forschungsgemeinschaft (DFG, German Research Foundation) – 257981274, Hamburg University of Technology's I3-Lab program, Graz University of Technology's Lead Project 'Mechanics, Modeling and Simulation of Aortic Dissection' and grants from the US NIH (R01 HL105297, U01 HL142518).

A DATA-DRIVEN COMPUTATIONAL MODEL OF ENGINEERED HEART TISSUES

Javiera Jilberto (1), Samuel DePalma (1), Jason Lo (1), Brendon Baker (1),
David Nordsletten (1,2)

1. Department of Biomedical Engineering, University of Michigan, Ann Arbor, USA; 2. Department of Biomedical Engineering, King's College London, London, United Kingdom.

1. Introduction

Cardiac tissue engineering enables the *in-vitro* study of diseases and drug therapy in patient-specific tissues. However, developing engineered heart tissues (EHTs) that resemble adult heart tissue remains a challenge due, in part, to our incomplete understanding of the mechanobiology of these constructs [1]. This challenge is further exacerbated by the fact that changing extracellular matrix structure and composition, as well as varying cardiomyocyte formation within EHTs, is left to be deciphered through single measures of twitch force. To decode the mechanobiology of EHTs, we develop a computational modelling pipeline to study how the mechanics drive tissue maturity.

2. Materials and Methods

Experimental data was obtained from a mechanically tunable fibroTUG setup, where cells are seeded on top of a fibrous substrate suspended between two flexible posts. Using image processing techniques, the local structural characteristics of the fibrous matrix and the sarcomere network were obtained from images of the fibrous matrix and the titin protein (Fig. 1A-D). We use these quantities to define a constitutive relationship for the EHT. The matrix-specific stiffness and the magnitude of active stress generated by the cells are computed using a system of equations where the post displacement and force are constrained to match experimental data. Using our pipeline, we generated models for different experimental conditions (soft/stiff posts with aligned/random matrices of soft/stiff fibers).

3. Results

In concordance with experimental results, the active stress parameter showed that aligned, soft fibers suspended between soft posts produce more contractile cardiomyocytes. The resulting fiber stress (Fig. 1E) and sarcomere

stretch (Fig. 1F) shows high heterogeneity. We also showed that the magnitude of active stress was more sensitive to fiber alignment than sarcomere alignment (Fig. 1G).

4. Discussion and Conclusions

In this work, we use a data-driven computational approach to study the mechanics of EHTs. The active stress that we compute considers the fiber and sarcomere structure providing a more representative measure of the contractile capacity of the cells compared to traditional approaches. Further, we can generate non-experimental conditions to determine the primary drivers of this value. This work shows the importance of combining *in-silico* with *in-vitro* approaches to understand how mechanics relate to EHT manufacturing.

5. References

1. Depalma, S. J., et al. *Biomaterials Science*, 9(1), 93–107 (2021).

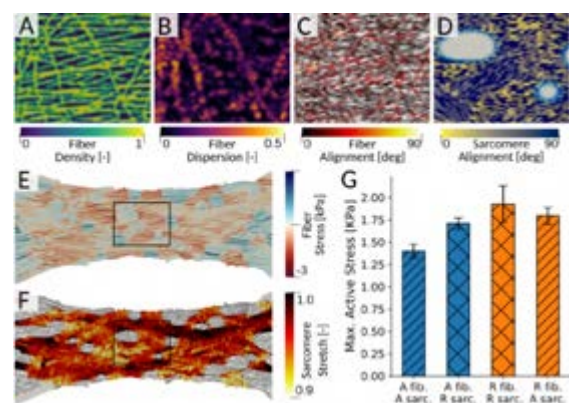


Figure 1: (A) Fiber density, (B) alignment, (C) and dispersion fields obtained from images of the fibrous matrix. (D) Sarcomere density and alignment fields generated from a probabilistic characterization of the sarcomeres. (E) Fiber stress and (F) sarcomere stretch fields. (G) Active stress values for aligned and random matrices of stiff fibers using aligned or random sarcomere fields.



MODELLING ARTERIAL RESPONSE TO MECHANO-BIOLOGICAL CUES: GETTING THROUGH OR BREAKING BAD?

Michele Marino

University of Rome Tor Vergata, Italy

1. Introduction

The physiological behaviour of the cardiovascular system is highly affected by the mechanical response of arterial segments, that is in turn dependent from tissue histological architecture and composition, as well as from its vascular tone. Non-physiological events, such as trauma, increased blood flow, or tissue inflammation, determine a change of mechanobiological conditions in which cells live. A cascade of events is then initiated by cells to react to such altered conditions. This might lead to a change of tissue composition and/or vascular tone that in turn affect arterial mechanical response.

In most cases, changes in arterial response allow to restore a homeostatic state with respect to the non-physiological trigger. Unfortunately, they might be insufficient or lead to the evolution of pathologies, like hyperplastic formations.

2. Materials and Methods

This work presents recent examples from our group on the chemo-mechano-biology of arterial tissues. Models are formulated in a continuum framework. The Ariadne's thread is the coupling between inelastic mechanisms in tissue deformation and reaction-diffusion equations describing systemic events affecting cell biology and molecular pathways [1,2].

Inelastic deformations comprise the active behaviour of smooth muscle cells, plastic mechanisms in collagen fibers, and/or kinematic description of the effects of growth and remodelling [2,3].

The chemo-biological component of the model describes the production/consumption of matrix metalloproteinases (MMPs), growth factors (TGF-beta), nitric oxide (NO) and reactive oxygen species (ROS). Moreover, cell motility (both random and chemotactic), proliferation and phenotype change are explicitly described.

3. Results

Results from two applicative case studies are presented. Firstly, the relationship between arterial remodeling and hypertension is investigated, considering the coupling of bio-chemically-induced vaso-activity, global and local hemodynamics, tissue-level stresses, and histological arrangement of constituents [4]. Secondly, the cascade of inflammatory mechanisms leading to tissue healing as a consequence of collagen damage is addressed [5]. The features of the models are demonstrated presenting several numerical examples using the finite element method where the multi-field problem is solved monolithically.

4. Discussion and Conclusions

Results show that normal as well as pathological outcomes can be reproduced by the presented models, highlighting the added value gained by the proposed chemo-mechano-biological descriptions. In fact, the proposed methods allow us to provide mechanistic explanations of the different behaviours by comparing the evolution of the dynamics of molecular concentrations, of cell behaviour, and of the turnover of tissue constituents over wide time and length scales.

5. References

1. Marino et al., J Royal Society Interface 14:20170615(17) (2017).
2. Gierig et al., Biomech Model Mechanobiol; 20(4):1297–1315 (2021).
3. Marino et al., J Mech Behav Biomed Mat 97:254–271 (2019).
4. Sauty, et al., Proceedings AFRICOMP 2022.
5. Gierig et al., Comp. Med Biol; under review.

Acknowledgements:

Funding from Regione Lazio (POR FESR LAZIO 2014; Progetti di Gruppi di Ricerca 2020; project: BIOPMEAT, n. A0375- 2020-36756) are acknowledged.

Cellular responses to substrate topography: opportunities for computational modeling

Claire Leclech, Bettina Roellinger, Abdul I. Barakat

LadHyX, CNRS, Ecole Polytechnique, Institut Polytechnique de Paris, Palaiseau, France

Adherent cells *in vivo* often reside on extracellular matrices (ECMs) that possess an anisotropic topographical organization at different scales. Various types of engineered microstructured substrates have been developed to study the impact of topographical cues on cell behavior *in vitro*. One such system that we have been using to elucidate the effect of surface topography on cellular structure and function is a substrate that consists of arrays of micro-scale grooves that are intended to mimic the anisotropic organization of the ECM.

We are particularly interested in vascular endothelial cells that line the inner surfaces of all blood vessels. In medium and large arteries, chronic endothelial inflammation is a trigger of atherosclerosis, the disease that leads to heart attacks and strokes. Interestingly, atherosclerotic lesions develop preferentially in arterial regions where endothelial cells are cuboidal and randomly oriented whereas arterial zones that are characterized by highly elongated and aligned endothelial cells remain largely spared from the disease. Therefore, understanding the relationships between endothelial cell shape/alignment and function is of fundamental interest.

In this presentation, I will focus on three specific endothelial cell responses to microgroove substrates where opportunities for mathematical and computational modeling arise. First, I will show how microgroove substrates can be used to noninvasively control endothelial cell shape and alignment and will describe our understanding of the mechanisms that underlie cell shape regulation by microgrooves. Second, I will describe dynamic live-cell recordings that demonstrate that microgrooves can orient the direction of migration of endothelial cells within monolayers and can lead to a unique pattern of collective cell migration that takes the form of antiparallel streams. Modeling the endothelial monolayer as an active fluid with the effect of the microgrooves considered as an energetic constraint on cell orientation predicts the occurrence of the antiparallel streams as well as their dimensions. Finally, I will show how microgrooves lead to extensive deformation of endothelial cells and their nuclei and will evoke the interesting notion of using these deformations to diagnose certain diseases that involve abnormalities in cellular and nuclear mechanical properties. Notions of how multiscale modeling approaches can be used to describe these cellular and nuclear deformations will be evoked.



LAMELLAR UNDULATION, RESIDUAL STRESSES, AND HOMEOSTASIS: A MULTISCALE MATHEMATICAL APPROACH.

Claire Morin (1), Elda Daidone (1), Stéphane Avril (1)

1. Mines Saint-Etienne, Univ Jean Monnet, Etablissement Français du Sang, INSERM, U 1059
Sainbiose, F - 42023 Saint-Etienne, France

1. Introduction

Arterial tissues are made of various fiber networks and cell populations. While the decrimping of adventitial collagen fibers has been widely measured and modelled, less importance has been devoted to the gradual crimp of the elastic lamellae in the media, which progressively uncrimp when subjected to a mechanical load [1]. We propose a multiscale model to study the link between the observed crimp, the presence of residual stresses and the cellular homeostasis.

2. Materials and Methods

As a first step, the medial layer is made of a pile of lamellae and interlamellar space. In the framework of continuum micromechanics [2], a representative volume element (RVE) of the interlamellar space is made of an arrangement of smooth muscle cells modelled as the matrix in which collagen and elastic fibers are embedded. The lamellae are considered as a hierarchical structure, made of two RVEs. At the lower scale, the elastic tissue RVE is made of an elastic fiber network, while the upper scale RVE is an arrangement of oblate spheroids representing the undulation of the elastic tissue, embedded in a surrounding matrix. As a second step, this multiscale model is incorporated in an axisymmetric, finite-element model of the arterial wall. An inner pressure is applied and the resulting macroscopic stress field in the wall is downscaled in the different RVES, inducing microscopic strain rate and vorticity fields, and in turn the straightening of the lamellae, leading to the macroscopic inflation of the tissue. As a third step, a residual stress field is added to the model, which is computed as follows: starting from straight lamellae, a compression is applied until the experimentally observed undulation is reached.

3. Results

The model was validated against pressure-inflations tests performed on different mice arteries [3], see Figure 1.

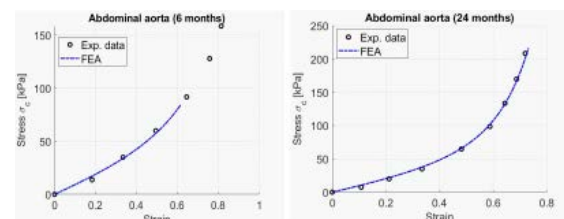


Figure 1: Comparison between experimental data (dots) and model predictions (lines) for the stress-strain curve from inflation tests on young (left) and aged (right) mice abdominal aorta.

4. Discussion and Conclusions

Our approach enables reproducing the main features of inflation tests, adjusting only few parameters for the different curves. It also shows that the gradient in lamellar crimping generates a residual stress field which provides a smooth stress field in the wall, a key ingredient for cellular homeostasis [4].

5. References

1. Yu, X. et al. *J. Mech. Behav. Biomed. Mater.*, 77 :745–753 (2018).
2. Morin C., et al., *Front. Bioeng.* 9:1-18, 2021.
3. Pezet M., PhD thesis, Univ. J. Fourier, Grenoble, France; (2016).
4. Humphrey, J. et al. *Nature Rev. Mol. Cell Biol.*, 15(12), 802–812 (2014).

ECM Mechanics for Early Detection of Diseases

Yanhang Zhang

Department of Mechanical Engineering
Department of Biomedical Engineering
Division of Materials Science & Engineering
Boston University
110 Cummington Mall, Boston, MA 02215, USA
yanhang@bu.edu

The extracellular matrix (ECM) in the arterial wall, composed of elastic fibers, collagen fibers, and ground substances, largely determines the passive mechanical properties of large elastic arteries. Our recent findings on the ECM structural inhomogeneities demonstrated the important roles that they play in contributing to tissue mechanics and homeostasis. Considering ECM structural inhomogeneity is thus important when studying the physiological function and failure of the arterial wall. Aging and diseases could have profound impact on the composition and structure of the arterial wall. This talk will focus on the effect of aging and diseases on ECM structure, and the mechanical function and integrity of the arterial wall. The complex structural and mechanical interplay needs to be considered to advance the current understanding of multi-scale ECM mechanics and calls for new approaches that integrate imaging, mechanical characterization, and computational modeling.



A BOTTOM-UP APPROACH TO MODEL FAILURE IN SOFT COLLAGENOUS TISSUES

Christopher Miller¹, T.Christian Gasser^{1,2}

1. KTH Royal Institute of Technology, Sweden; 2. University of Southern Denmark, Denmark

1. Introduction

Abdominal Aortic Aneurysms (AAA) remain a leading cause of disability and death worldwide [1], and their treatment represents a major healthcare challenge with an enormous socioeconomic impact. No medication is known to prevent AAA from rupture, and success in slowing-down AAA growth is moderate [2]. Moreover, it remains difficult to predict when AAA patients will require treatment. Beyond purely biomechanical approaches [3,4], a Machine Learning-based combination of risk factors provided promising results in predicting the threshold for surgery and rupture [5,6]. However, such approaches are currently limited by our restricted understanding of vascular tissue failure. A versatile constitutive model for load-carrying soft biological tissue should incorporate salient microstructural deformation mechanisms and be able to reliably predict complex load-case scenarios [7].

2. Materials and Methods

We present an extension of our previous microstructural continuum model [8] that includes proteoglycan-mediated collagen fibril sliding towards capturing the non-linear time-dependent properties of collagenous tissue. It incorporates an interfibrillar failure (fibril pull-out) mechanism and gives rise to physiologically reasonable damage-induced mechanical behaviour across several length scales. A bottom-up approach is followed, whereby the microstructural model is employed in a single-element representation of the modes of fracture. A qualitative description of soft tissue rupture is accordingly attained, to which an appropriate cohesive zone model for the equivalent fracture surface is then calibrated. In doing so, a surface-based discontinuous characterization of failure is derived directly from the upscaling of irreversible and dissipative damage mechanisms from the microscale.

3. Results, Discussion and Conclusions

The model has been implemented in FEAP (Univ. of California at Berkley, US) using an in-house PUFEM description [9]. A number of test cases, including the symmetry-constrained Compact Tension (symconCT) test, verified the implementation, see Fig.1. We used an implicit Finite Element implementation that employs an integral interpolation strategy towards collagen fiber stress determination and results in a memory-efficient representation of the model.

Figure 1: Simulation of the symconCT vascular tissue fracture experiment.

5. References

1. J Golledge, Nat. Reviews Cardiology 16, 2019.
2. TP Singh, et al. Eur. J. Vasc. Endovasc. Surg. 64, 2022.
3. L Kubicek, et al. Eur. J. Vasc. Endovasc. Surg. 58, e306-e307.
4. TP Singh, et al. J. Am. Heart Assoc. 10, e019772.
5. M Lindquist Liljeqvist, et al. Sci. Rep. 11,10.
6. M Alloisio, et al. Eur. J. Vasc. Endovasc. Surg. 63, e34-e35.
7. C Miller, TC Gasser, J. Mech. Phys. Solids 154, 104500.
8. C Miller, TC Gasser, J. Mech. Phys. Solids 169, 105086.
9. TC Gasser, GA Holzapfel. Comp. Meth. Appl. Mech. Engrg. 194, 2859-2896, 2005.

Acknowledgements:

Financial support through the project grant No 2020-04447 from the Swedish Research Council.



MECHANOSENSITIVE PROTEASE NETWORK MODELING FOR PATIENT-SPECIFIC HEART FAILURE PREDICTIONS

Amir Yeganegi (1), Saubana Dada (2), Will Richardson (2)

1. *Clemson University, United States of America*; 2. *University of Arkansas, United States of America*

1. Introduction

Cardiac fibrosis is a major contributor to diastolic and systolic dysfunction for millions of heart failure (HF) patients. Unfortunately, current prediction and control over cardiac fibrosis are lacking due in part to complexity within collagen regulation networks and in part to patient-to-patient variabilities in the biochemical and mechanical signals regulating matrix turnover. We hypothesized that computationally integrating biochemical and mechanical information (rather than a single biomarker) will enable personalized fibrosis diagnosis and therapy selection. In this work, we combined HF patient data, a novel model of extracellular matrix turnover, and machine learning (ML) approaches to produce patient-specific fibrotic predictions.

2. Materials and Methods

Collagen turnover depends on a complex balance between the production and processing of collagens, matrix metalloproteinases (MMPs), and tissue inhibitors of metalloproteinase (TIMPs), with a wide range of isoform-specific and mechano-sensitive kinetic rates [1]. We constructed an ODE mass-action kinetics model capturing the interactions of collagen I, collagen III, MMPs 1, 2, 3, 7, 8, 9, 12, 13, 14, TIMPs 1-4, and plasmin, assuming isoform-specific kinetic rates that also depended upon mechanical deformation. To test model predictions, we simulated patient-specific data that was previously collected from 480 healthy, hypertensive, and HF patients including multiplex plasma MMP and TIMP levels, and LV mechanics assessed by echocardiography [2]. Kinetic rate parameters were calibrated from a random subset of patients using a genetic fitting algorithm that maximized the binary classification accuracy between HF vs. non-HF (control and hypertensive) patients. After parameter-fitting,

the ODE-predicted fibrosis score for each patient was integrated with protein biomarker and demographic information in a boosted ML algorithm in order to classify each patient into HF or non-HF groups.

3. Results

Our integrated ODE+ML modelling approach was able to reach 93% accuracy and 95% area-under-the-receiver-operating-characteristic curves for distinguishing between HF and non-HF patients. Post-hoc model interpretability analysis revealed that circulating MMP2, MMP8, TIMP1 levels along with left ventricular volumes were the most significant predictive biomarkers.

4. Discussion and Conclusions

Our results demonstrated that integrating systems biology-based ODE models with machine learning approaches can offer benefit beyond either approach used independently. Importantly, personalized predictions could be made using only information that can be readily obtained in a basic, primary care setting (blood panels and pressure measurements), supporting the value of this approach as a HF-screening tool. Our on-going work is utilizing this modelling framework not just for diagnosis, but also for computational drug screens to enable personalized therapy selection across patient-specific conditions.

5. References

1. Rogers JD, Yeganegi A, Richardson WJ. *Mechanobiology Handbook*. p. 511-530 (2018).
2. Zile MR et al., *Circ Heart Failure*; 4:246-256 (2011).

Acknowledgements:

The authors would like to thank the United States National Institutes of Health (Grant no: HL144927) for providing financial support to this project.

Effect of atheroma plaque on drug transport in a coronary stent

Estefanía Peña^{1,2}, Javier Escuer¹, Estela Pina¹, Miguel A. Martínez^{1,2}

¹*Aragón Institute of Engineering Research (I3A), University of Zaragoza, Zaragoza, Spain*

²*Biomedical Research Networking Center in Bioengineering, Biomaterials and Nanomedicine (CIBER-BBN), Madrid, Spain*

E-mail: jescuer@unizar.es, estelapinaclos@gmail.com, miguelam@unizar.es, fany@unizar.es

Keywords: Drug-eluting Stent; Drug transport; Atheroma plaque

Coronary angioplasty with stenting is currently the most widely used treatment for advanced atherosclerotic lesions. However, in-stent restenosis (ISR) is the main limitation of this technique today. The introduction of drug-eluting stents (DES), which deliver antiproliferative substances to the arterial wall, has contributed to the improvement of IRS. Despite the improvement achieved with DES compared to bare metal stents, ISR remains a major clinical and technological challenge in the design of these intravascular devices. The development of computational models has led to great advances in the understanding of drug transport on DES, but they usually represent simplified healthy straight geometries or highly simplified plaques that do not reproduce the characteristic geometry and composition of them. However, there is growing evidence that plaque composition may well have an impact on drug distribution within diseased tissue.

In an attempt to address some of the limitations of the previously computational models, we perform a series of computational drug transport models to analyse and understand the effect of atheroma plaque composition and structure on spatio-temporal drug uptake within the tissue. To this end, a finite element model of an idealised coronary artery under conditions of atherosclerotic disease between DES and healthy tissue is performed, and the effect of plaque composition and structure on global drug distribution is investigated. Of all the geometric factors to be analysed, we focus on the thickness of the fibrous cap, the total length of the plaque and the length and thickness of the necrotic core and percentage stenosis.

The results clearly demonstrate that the spatio-temporal distribution of drug is highly dependent on the geometrical variables analysed. The composition of the core strongly influences the drug concentrations, due to the different density of binding sites in this region. The results suggest that lipid plaques give rise to higher drug concentrations than fibrotic plaques, while calcified plaques are drug-impenetrable, according to the assumptions assigned to the model. The impenetrability of calcified plaque has potentially important implications and, if large enough, may act as a significant barrier to drug from reaching arterial tissue where smooth muscle cells (SMCs) capable of proliferating and migrating to device-injured areas during implantation reside. The results also suggest that the presence of plaque, regardless of core composition, may slightly delay receptor saturation in the medial layer.

References

- [1] Tzafriri A. R., Groothuis A., Price G S., Edelman E. R. *Stent elution rate determines drug deposition and receptor-mediated effects. Journal of controlled release.*2012;161(3):918–92.
- [2] Escuer J., Aznar I., McCormick C., Peña E., McGinty S., Martínez M. A. *Influence of Vessel Curvature and Plaque Composition on Drug Transport in the Arterial Wall following Drug-eluting Stent Implantation. Biomech Model Mechanob.*2021;20:767–78

AUTOMATIC SEGMENTATION OF VERTEBRAE AND INTERVERTEBRAL DISCS FROM SYNTHETIC CT IMAGES DERIVED FROM MR IMAGES

Joeri Kok* (1), Bert van Rietbergen (1), Yulia Shcherbakova (2), Tom Schlösser (2), Peter Seevinck (2), René Castelein (2), Keita Ito (1,2)

1. Eindhoven University of Technology, Netherlands; 2. University Medical Center Utrecht, Netherlands

*Corresponding author: j.kok@tue.nl

1. Introduction

Finite element (FE) models of the spine are widely used for research. They are most often based on computed tomography (CT) scans, exposing subjects to harmful radiation. Magnetic resonance (MR) imaging does not expose the subject to radiation but is generally better suited for the visualization of soft tissues. With emerging deep-learning methods it is now also possible to visualize bone using MR images [1]. The aim of this study was to develop a method for the automatic segmentation of vertebrae and intervertebral discs (IVD) based on MR images.

2. Materials and Methods

Sagittal in-phase, out-of-phase, fat, and water MR scans were taken from 8 adult volunteers of which one has scoliosis (~30° Cobb angle) (fig. 1A; voxel size: 0.625 x 0.625 x 1 mm³; field of view: 420 x 420 x 100 mm³). Synthetic CT scans were generated from these images using a pretrained deep-learning algorithm (fig 1B; BoneMRI V1.5, MRGuidance). A neural network (nnU-Net) was trained for automatic segmentation of the IVD on a training set of 6 subjects without scoliosis [2]. For segmentation of the vertebrae another pretrained model was selected [3,4]. Using the pretrained models, validation was performed on the remaining 2 subjects, one with scoliosis.

3. Results

For the test set, a Dice score of 0.95 was obtained for the automatic segmentations of the IVD. For validation on the remaining healthy and scoliotic subject, Dice scores reached 0.94 and 0.93, respectively (fig. 1c). For the

vertebrae the Dice scores were 0.94 and 0.96 for the healthy and scoliotic subject, respectively.

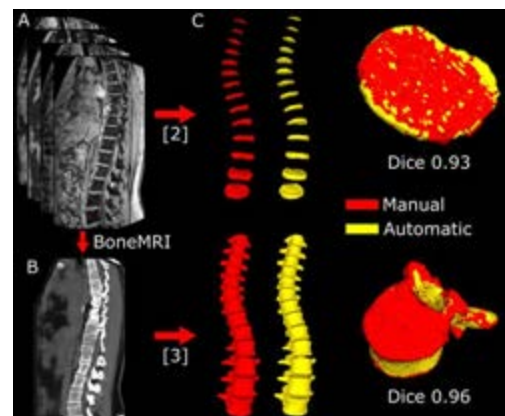


Figure 1: A) MR images for IVD segmentation [2] and creation of B) synthetic CT for vertebra segmentation [3]. C) Comparison between manually and automatically segmented IVDs and vertebrae.

4. Discussion and Conclusions

Synthetic CT imaging enables a unique segmentation of discs and vertebrae without the need for registering CT and MR images. Although the present study involves only low numbers for training, promising results are obtained, even in case of spinal deformities.

5. References

1. Morbée L et al., Eur J Radiol; 144:109999 (2021)
2. Isensee F et al., Nat Methods 18:203-14 (2021).
3. Payer et al., VISAPP conference; 2020. 124-133
4. Sekuboyina A et al., Med. Image Anal.; 73:102166 (2021).

Acknowledgements:

The authors would like to thank the European Research Council (Grant no: 101020004) for providing financial support for this project.



DEEP-LEARNING-BASED 3D RECONSTRUCTION OF THE SPINE FROM LOW-DOSE BIPLANAR RADIOGRAPHS

Matteo Bovio, Wafa Skalli, Laurent Gajny

Arts et Metiers Institute of Technology, Institut de Biomecanique Humaine Georges Charpak, Paris, France;

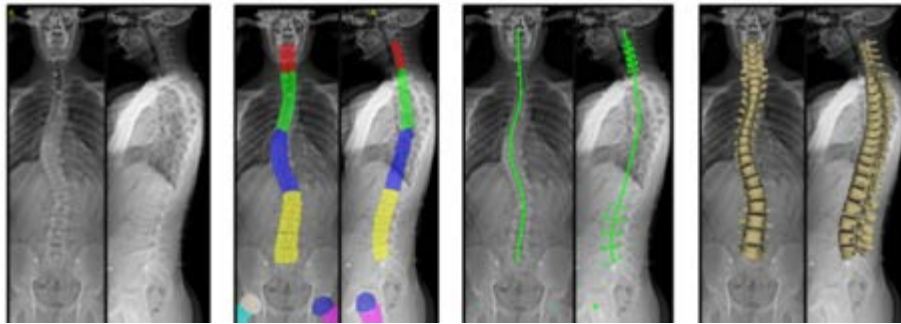


Figure 1. 3D reconstruction of the spine. From left to right, biplanar radiographs; automatic segmentation using deep learning; landmarks extraction using mathematical morphology; 3D model using longitudinal and transversal inferences.

1. Introduction

Personalized 3D reconstruction of the spine based on low-dose biplanar X-rays are available in clinical routine [1]. This method enables 3D visualization and quantification of 3D deformities like scoliosis. Although its validity and reliability have been already evaluated [1], [2], manual input and adjustments still have to be reduced for a large-scale use in clinical routine. To that end, bone detection, classification and segmentation can be of tremendous value for replacing manual inputs. Therefore, we propose a 3D reconstruction method replacing most of the manual inputs with a deep learning framework for classification and segmentation.

2. Materials and Methods

The workflow of the proposed method is illustrated in Fig. 1. A database of 130 biplanar radiographs, with validated spine reconstructions [1, 2], including 20% of scoliotic patients was collected retrospectively. It was first used to train and evaluate a deep learning algorithm (nnU-Net [3]) using a 5-fold cross validation. Classification and segmentation were split into three steps in a coarse-to-fine manner to accurately define spine regions [4]. Segmentations and classifications were manually checked and classifications were corrected if needed. From the obtained segmentation, keypoints bound to replace all but two manual annotations (odontoid tip and

sacral plate) were extracted using mathematical morphology. A previous statistical model based on transversal and longitudinal inferences (statistical model for each vertebra and distribution of vertebrae along the spinal curve) was adapted from [2] to automatically fit to the keypoints. Reconstruction accuracy was evaluated comparing the location of each vertebral body centre to that resulting from the validated reconstructions [1, 2].

3. Results and discussion

Manual intervention was around 30 seconds against 3 minutes in [2]. Out of the 130 patients, only four (3.1%) needed manual checking. Average absolute errors per spine region were minimal along the z-axis, ranging from 0.6 to 1.2 mm (SD = 0.3 to 1.5). Average 3D errors per spine region were ranging from 1.6 to 2.5 mm (SD = 1.0 to 1.8). Accuracy can still be increased in the medio-lateral axis through the use of additional automatically detected keypoints like pedicles.

5. References

1. Humbert L. et al, Medical Engineering and Physics (2009), 31, pp.681–687
2. Gajny L. et al, European Spine Journal (2018), 28(4), pp. 658–664.
3. Isensee F. et al. (2021) Nat Methods 18, 203–211.
4. Bovio M. et al, ICCB 2022 conference

Acknowledgements:

The authors thank the Paristech BiomecAM chair program for its financial support.



DEVELOPMENT OF A SUBJECT-SPECIFIC MUSCULOSKELETAL MODELING FRAMEWORK FOR SPINAL DEFORMITY PATIENTS

Birgitt Peeters (1), Erica-Beaucage-Gauvreau (2), Lieven Moke (3), Ilse Jonkers (2,4), Friedl De Groote (4), Lennart Scheys (1,2,3)

1. Institute for Orthopaedic Research and Training (IORT), Department of Development and Regeneration, Faculty of Medicine, KU Leuven, Belgium; 2. Institute of Physics-based Modeling for in silico Health (iSi Health), Belgium; 3. Division of Orthopaedics, University Hospitals Leuven, Belgium; 4. Department of Movement Sciences, KU Leuven, Belgium

1. Introduction

Adult spinal deformity (ASD) is a spectrum of three-dimensional (3D) spinal malalignments, often resulting in pain and disability [1]. Although these primarily skeletal deformities are associated with severe alterations in muscle structure and function, these are currently neglected in surgical ASD care. Simulations with personalized musculoskeletal models (MSKM) to evaluate the impact of ASD on musculoskeletal dynamics by quantifying functional impairment, show great potential to improve poor surgical outcome [2]. The aim of this project is to develop an efficient image-based framework to create subject-specific ASD MSKMs, which currently do not exist yet.

2. Materials and Methods

The developed workflow creates a subject-specific OpenSim MSKM [3], using Mimics and 3-matic with python interface (v22 and v15, respectively, Materialise, Belgium) in three main steps (Fig. 1): 1) Creation of a full-body model composed of a scaled generic model and a previously validated spinopelvic model based on body segments from computed tomography (CT) and joint definitions from biplanar radiography (BiXR) [2]; 2) Model registration from upright BiXR to supine magnetic resonance imaging (MRI); 3) Semi-automatic muscle definition from MRI: muscle segmentation, definition of lines of action, wrapping surfaces, attachment points, cross sectional area (CSA), and mediolateral and anteroposterior moment arms (MA).

3. Results

A representative subject-specific MSKM of an ASD patient based on the developed workflow is shown in Fig 1. Step 2, i.e. the registration,

had a median distance error below 0.12 mm for each body segment. Muscle segmentation in step 3, was associated with median dice similarity scores for psoas, erector spinae, and multifidus muscles of 0.82-1.00, compared to ground truth [4]. Lines of action, wrapping surfaces, attachment points, CSA, and MA were defined from the muscle segmentations.



Figure 1: Subject-specific modelling workflow.

4. Discussion and Conclusions

The novel developed workflow is the first to allow to semi-automatically generate an image-based personalized MSKM of an ASD patient. The workflow has the potential to provide accurate functional analyses of ASD patients through dynamic MSKM simulations, and will be validated for a larger set of ASD patients.

5. References

1. Ailon et al, Neurosurgery, 2015.
2. Overbergh et al, J. Biomech., 2020.
3. Delp et al, IEEE Trans. Biomed. Eng., 2007.
4. Dice, Ecology, 26:297–302, 1945.

Acknowledgements:

The authors thank Flanders' Fund for Scientific Research (1SE6223N) for financial support.



GENERATION OF SUBJECT-SPECIFIC NUMERICAL MODELS TO INVESTIGATE THE SURGICAL TREATMENT OF AIS

Benedikt Schlager (1), David Volkheimer (1), Hans-Joachim Wilke (1)

Institute of Orthopedic Research and Biomechanics, Ulm University Medical Centre, Germany

1. Introduction

The surgical treatment of adolescent idiopathic scoliotic (AIS) spines is considered as one of the supreme disciplines in orthopaedics. Developing adequate numerical models of the spinal deformities is even harder. In the last decade several finite element models of scoliotic spine were published. Within a clinical setting, these models can be generated based on computer-tomography (CT) images and radiographs in the upright posture and in lateral bending. The CT images are used to construct the geometry, while the lateral bending radiographs can be used to estimate the flexibility of the spine (Gardner-Morse et al., 1990; Petit et al., 2004).

Aim of this study was to analyse the fidelity of generating subject-specific finite element (FE)-models using only the clinical available data of the spine under standardized conditions.

2. Materials and Methods

In-vitro experiments of six intact human lumbar spines ranging from L1-S1 were performed using a spine tester. The range of motion (ROM) was quantified using pure moments of 7.5 Nm around all rotation axes.

Then, FE-models of the subject-specific lumbar spines, which were tested in-vitro, were generated using a parametric approach (Niemeyer et al., 2012; Schlager et al., 2018). Goal of the FE models was to represent the subject-specific ROM of the in-vitro experiments, while incorporating only the subject-specific morphology and lateral bending information of the specimen into the FE-model (same as in a clinical setting).

Assuming a symmetrical spine, the ROM values around the three anatomical rotation-axes need to be defined, which sums up to fifteen unknown ROM values for the five spinal levels on each specimen. Adding the lateral bending information, these unknown ROM-values reduce to eleven.

To estimate the remaining unknowns, we tried to predict the ROM-values using published and in-house in-vitro database, and achieve a level-of-confidence. The material properties of the FE-models were subsequently modified to match the estimated ROM-values within the range of the standard-deviation (SD).

3. Results

According to the in-vitro database, the ROM could vary within the SD of up to 10.8° in flexion-extension, 7.8° in lateral bending and 4.5° in axial rotation on each lumbar spinal level. It was possible to cover the subject-specific ROM in 70% of all spinal levels by varying the ROM within the SD obtained from the in-vitro database.

The maximal deviation between the predicted ROM of the subject specific FE-models and the in-vitro measured ROM values were in flexion-extension 3.3°, in lateral bending 2.1° and in axial rotation 3.4°. Adding the lateral bending information resulted in a maximal deviation to 3.6° in flexion-extension, 1.3° in lateral bending and 0.5° in axial rotation.

4. Discussion and Conclusions

The representation of the morphology and lateral bending information could increase the accuracy of the generated subject-specific scoliosis models. However, the biomechanical model still incorporates a great uncertainty, since the subject-specific load-displacement behaviour of each spinal segment is unknown. Varying the stiffness of the spinal segments within a physiological SD could help cover the real condition, reduce the error, as well as estimate the sensitivity of the gained results.

Acknowledgements:

The authors would like to thank the German Research Foundation (Grant no: Project WI 1352/20-1) for providing financial support to this project.



CAN WE PREDICT THE RISK OF SURGERY REVISION FOR ADOLESCENT IDIOPATHIC SCOLIOSIS USING AN ENERGY-BASED APPROACH

Baptiste Brun-Cottan (1), Pauline Assemat (1), Maxime Pigou (1), Roxane Compagnon (2,3), Tristan Langlais (1,2), Jérôme Sales de Gauzy (1,2), Pascal Swider (1)

1. Institut de Mécanique des Fluides de Toulouse, France; 2. CHU Purpan, Children Hospital, Toulouse, France; 3. Clinique Médipôle Garonne, Toulouse, France

1. Introduction

Idiopathic adolescent progressive scoliosis, in spite of a well-conducted brace treatment, may induce a significant curvature and imbalance requiring a posterior vertebral fusion correction. Choice of instrumented levels [1] and sagittal shape are still empirical. An innovative energetic model was implemented to explore AIS in a patient-specific image-based approach [2]. In the presented study, post-operative responses of vertebral segments remaining free were examined and an energy-based revision criterion was proposed.

2. Materials and Methods

The 3D wireframe model of spine is based on the equilibrium by mechanical energy minimization. The numerical inverse algorithm determines equivalent vertebral segments properties from preoperative biplanar X-ray exam (EOS®).

Design parameters of surgical planning are instrumented length, sagittal shape and surgery reduction. Energy distribution along the corrected spine is obtained using the direct problem resolution [2] and energies of free vertebral segments adjacent to arthrodesis are used to propose the revision criterion. The upper and lower instrumented vertebrae are involved, i.e. UIV and LIV. To explore this innovative approach, a monocentric retrospective study of 18 patients was performed. The cohort includes four patients requiring revision because of either “adding-on” or proximal junctional kyphosis (PJK).

3. Results

Computation time for inverse problem was around 1h, and the surgery simulation took around 1 minute. Summed UIV and LIV energies in frontal vs sagittal plane is shown figure 1 and difference is significant between

patients with or without revision ($p < 0.01$). Revision cases showed energy peaks in both planes at the junction between instrumentation and free segments.

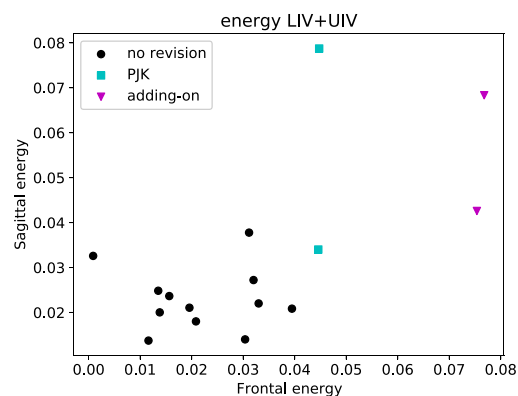


Figure 1: Frontal versus sagittal strain energies of LIV and UIV segments (block: no revision, color: revision).

4. Discussion and Conclusions

An innovative spine model based upon energy balance was faced to an AIS cohort to predict post-operative surgery outcomes. It appeared that strain energies at arthrodesis extremities was a good predictor of post-operative mechanical complications and revision risk. The robustness of our preliminary results could be enhanced by a larger multicenter cohort that would support preoperative planning for clinical teams.

5. References

- Compagnon R et al., OTSR. Vol 108, Iss 6, 2022.
- Brun-Cottan B et al., Biomechanic and modeling in mecanobiology. 20,359-370 (2021).

Acknowledgments:

We thank the Cotrel Foundation and Toulouse Tech Transfer for their financial support.



3D INFERENCE OF THE SCOLIOTIC SPINE FROM DEPTH MAPS OF THE BACK

Nicolas Comte (1, 2), Sergi Pujades (1), Olivier Daniel (3), François Faure (2), Jean-Sebastien Franco (1), Aurélien Courvoisier(3), Edmond Boyer (1)

1. UGA, INRIA, CNRS, INP, LJK, France; 2. Anatoscope, France; 3. Grenoble Alps Scoliosis and Spine Center-Grenoble Alps University Hospital, SPM-TIMC-IMAG, France

1. Introduction

Adolescent idiopathic scoliosis (AIS) is a 3D deformity of the spine progressive during the whole growth. Early detection is mandatory to initiate treatments at an early stage of the deformity. To ease early diagnosis, we propose to use depth information from the surface of the back, acquired with non-ionising sensors, such as depth cameras.

Deep-learning algorithms (DLA) show good performances in the characterization of scoliosis from the back shape analysis [1]. However, existing methods provide yet a limited 2D characterization of the spine. Our goal is to retrieve 3D information, which has been shown to improve spine diagnosis [2].

2. Methods and Materials

Given a population, we first learn a PCA model of the shape of the spine. Then, from depth images of the back, we apply ResNet [5] to learn how to predict the PCA coefficients. These coefficients are further used to reconstruct the vertebrae 3D positions. To this aim, we use paired examples of the surface of the skin and vertebrae locations. Our patient dataset with 3D vertebrae positions from EOS and a surface scan from Grenoble Hospital (GH) is scarce (33 annotated AIS patients). We propose to leverage the public dataset NMDID [3] that contains raw CTs of ex-vivo subjects, mainly asymptomatic in supine position. We segment the spine and the skin of 97 subjects (7% with and 93% without scoliosis) using [4] and obtain therefore additional paired cases of surface skin and 3D vertebrae locations.

3. Results

We performed two experiments, one training solely on the GH (scoliotic data) and one training with GH and NMDID (scoliotic + asymptomatic) data. We used cross-validation with 90/5/5 train/validation/test splits. Tab.1

summarises the results. Values for [6,7] have been computed on different datasets. The sagittal and 3D columns should be interpreted carefully; our method predicts a relative vertebra position in the antero-posterior axis, whereas [6,7] make an absolute prediction.

	Train	Test	Coro	Sagit	3D
Our	scol	scol	6.20 (3.83)	6.87 (4.76)	9.03 (5.04)
Our	scol+ asym	scol	5.97 (3.79)	6.56 (5.17)	8.80 (5.34)
[6]	scol	scol	7.90 (3.66)	8.01 (4.28)	12.62 (5.26)
[7]	asym	asym	NA	NA	10.20 (5.6)

Table 1: Metric comparisons with state of the art. Average distance errors (std) in mm.

4. Discussion and Conclusions

We presented a DLA to predict the 3D spine shape from the subjects' depth map. Our results show good performances compared to the literature [6, 7]. We observe that the inclusion at training time of cadavers in supine position improved the inference on scoliotic cases of the hospital.

5. References

1. Kokabu T et al. The Spine Journal; (2021)
2. Stokes IA. Spine; (1994)
3. Edgar HJH et al. NMDID. (nmdid.unm.edu)
4. Meng et al. MLMIW - MICCAI (2022)
5. He K et al., IEEE CVPR (2016)
6. Caturano et al., MELECON (2022)
7. Nérot A et al. Journal of Biomechanics (2018)

Acknowledgements:

The authors would like to thank the ANRT for providing financial support to this project.



STORAGE DURATION EFFECTS ON THE PROPERTIES OF CORTICAL BONE – MODELLING IMPLICATIONS

Nicholas Daras, Trevor J. Cloete*, Gerald N. Nurick

Blast Impact and Survivability Research Unit (BISRU), Department of Mechanical Engineering, University of Cape Town, Rondebosch, South Africa

*Correspondence Email: trevor.cloete@uct.ac.za

1. Introduction

Computational simulations of human beings subjected to impact events greatly improve design safety, and accurate material models are essential to support this aim. Bone, as a structural material, has been studied for over half a century [1], resulting in a data rich field. Despite this, a large amount of scatter is evident in the reported mechanical properties of bone (e.g. elastic modulus) [1]. A potential reason for this scatter is a lack of consistency across studies regarding specimen preparation procedures, including both storage protocols (e.g. freezing or storage mediums) and storage duration prior to testing. Studies of these effects have been limited, with divergent results [2,3,4]. This paper presents preliminary results from a series of experiments aimed at assessing the effects of long duration freezing on porcine cortical bone specimen properties.

2. Materials and Methods

Cylindrical specimens (5mm diameter and height) were machined from four porcine humeri, obtained from two donor animals. Quasi-static compression tests were conducted after varying durations in storage, over a year. Specimens were divided into three storage protocols; machined-refrigerated (MR), machined-frozen (MF) and frozen-machined-frozen (FMF). The MR and MF specimens were machined within 24 hours of slaughter, from fresh (i.e. never frozen) whole bones and stored in a fridge or freezer, respectively. FMF specimens were machined from whole bones, stored frozen for a specific time period, and then refrozen.

3. Results

MR specimens showed erratic results as the first week of testing progressed, while MF specimens proved more stable. Beyond one

week, MF specimens began to degrade, with a significant decrease in elastic modulus observed after six months in storage. FMF specimens, machined from a whole bone that was stored for two months (2M), exhibited a high initial elastic modulus, but rapid subsequent degradation to similar levels as MF specimens. FMF specimens, machined from a whole bone that was stored for 11 months (11M), exhibited a low initial moduli, signifying severe degradation while stored as whole bone.

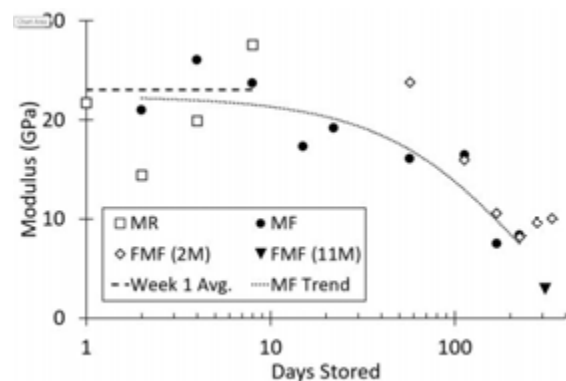


Figure 1: Elastic Modulus Plotted Against Storage Duration.

4. Discussion and Conclusions

This study shows that the fresh cortical bone tests should be conducted within 24 hours of harvesting for the results to be representative of in-situ properties. Similarly, frozen specimens should be tested within one week, while the limit for whole frozen bone storage appears to be two months, although more data is required. These results demonstrate the importance of using fresh bone data to calibrate material models for biofidelic computational simulations.

5. References

1. Johnson TP et al., Acta Biomater. 6 (10) (2010).
2. Lucksanasombool P et al., Biomaterials 22 (23) (2001).
3. Goh J et al., Acta Orthop. Scand. 60 (4) (2009).
4. Stefan U et al., Bone 47 (6) (2010).



AN INTEGRATED FINITE ELEMENT APPROACH TO SIMULATE BONE STRAIN RESPONSE TO PHYSIOLOGICALLY REALISTIC LOADING CONDITIONS

Timo van Leeuwen^{1,2}, Marco Schneider³, Harry van Lenthe⁴, Thor Besier³, Evie Vereecke²

Research Foundation Flanders (FWO), Brussels, Belgium; 2. KU Leuven, campus Kulak, Kortrijk, Belgium; 3. Auckland Bioengineering Institute, Auckland, New Zealand; 4. KU Leuven, Leuven, Belgium

1. Introduction

Bone is an adaptive tissue that is capable of responding to its mechanical environment by remodelling its own morphology in response to mechanostimuli. Understanding the direct relation between bone remodelling and mechanostimuli is immensely valuable to both the biomedical and the biomechanical field as it would facilitate prediction and prevention of bone strain issues and potential bone failure injuries. In order to understand this relation between stimulus and response, accurate assessment of the internal and external loading conditions of bone are paramount. Here we present an integrated finite element (FE) – micro FE (μ FE) approach to assess internal bone strain based on physiologically relevant boundary conditions.

2. Materials and Methods

CT imaging of bones in standardized joint positions is used to generate parametric FE models that simulate external bone loading patterns based on realistic joint interactions. These loading patterns are subsequently aligned and integrated in high resolution, μ CT based, whole bone μ FE models that assess bone strain values at the level of the of the trabecular bone architecture. This method was developed in the primate thumb joint, specifically the trapeziometacarpal joint, but is intended for broader implementations in other joints and taxa. In bonobos, gibbons, and macaques, various grasping types with different thumb positions were CT scanned as input joint positions. The FE approach yields articular loading patterns in which differences per position of the thumb can be identified. These loading patterns are then applied as boundary

conditions to the trapezium bone and solved to assess internal bone strain using μ FE.

3. Results

The results of the μ FE approach show that the strain distributions between the different simulated grasps are highly similar, with dissipation towards the proximo-ulnar cluster of trabeculae regardless of trapezium bone microarchitecture. Strain levels deviating from this pattern are shown to be more likely related to dissimilar, possibly pathological, external joint morphology features rather than internal differences. Evaluation of the corresponding μ FE models shows that the simulated strain values fall within realistic boundaries of mechanical response of bone.

4. Discussion and Conclusions

This approach offers a method to integrate realistic boundary parameters into the assessment of internal bone strain values. Our research collaboration is working on expanding, validating, and further developing the approach open source with the aim of addressing the relation between the stimulus and the response in bone functional adaptation.

Acknowledgements:

The authors thank the Research Foundation Flanders (FWO) and the KU Leuven for providing financial support. This project was developed under the support of the KU Leuven and the FWO. Current and further developments are made possible by the FWO under the postdoctoral fellowship fundamental research grant awarded to Timo van Leeuwen (grant no. 12B3523N).



ANALYSIS OF THE INFLUENCE OF THE GEOMETRIC ANISOTROPY ON THE MECHANICAL BEHAVIOR OF TRABECULAR BONE USING A PARAMETRIC MODEL.

N. Rogalski (1), S. Laporte (1), C. Cluzel (2), J. Girardot (3) & I. Iordanoff (3)

1. Arts et Métiers, Université Sorbonne Paris Nord, IBHGC, Paris, France

2. Université Paris-Saclay, Centrale Supélec, ENS Paris-Saclay, CNRS, LMPS, Gif-Sur-Yvette, France

3. Arts et Métiers, University of Bordeaux, CNRS, Bordeaux INP, INRAE, I2M Bordeaux, France

Corresponding author: nicolas.rogalski@ensam.eu

1. Introduction

Trabecular bone is a network of plates and rods preferentially oriented on local loading axes, resulting in a geometric and mechanical anisotropy [1]. In this study, a parametric model respecting the geometry and the macroscopic mechanical behavior of a target specimen was used to analyze the influence of the geometric anisotropy on the mechanical response of the tissue.

2. Materials and Methods

Trabecular bone samples

170 cylinders of bovine femoral trabecular bone were previously scanned and submitted to compression tests [2]. From the binarized images, morphological parameters were extracted, and preferred orientations of plates and rods were computed [3].

Parametric model

A skeleton of plates and beams was randomly generated for each sample using the geometric data. The skeleton was used as a computational domain in a Discrete Element Method (DEM) simulation [4] and the experimental data were used to calibrate the constitutive properties.

Influence of geometric anisotropy

The preferred orientations of plates and rods were modified within the skeleton, and compression tests were performed with the DEM method. The influence of the geometric anisotropy on the macroscopic Young's modulus and yield strain of the samples was analyzed and the results were compared to the experimental data.

3. Results

An average increase of 140% in the macroscopic Young's modulus was measured

between the main anisotropy direction and the transverse direction (directions 1 & 3) (**Figure 1**). The yield strain was less impacted (average variation of 15%).

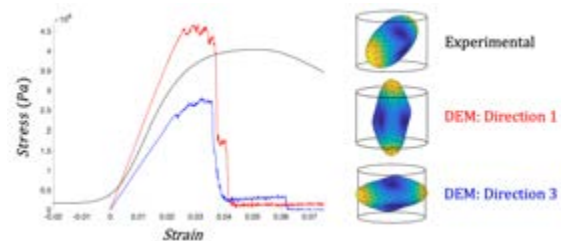


Figure 1: Stress-strain curves obtained by experimental and numerical compression tests (the compression axis corresponds to the cylinder axis). The polar plots represent the geometric anisotropy.

4. Discussion and Conclusions

The proposed framework appears as a promising tool for better understanding the failure mechanism of trabecular bone. While the present study focuses on two directions of anisotropy, a set of directions discretizing the 3D space could be used to calculate all the anisotropic constants of a volume of interest, using an existing formalism [5]. The numerical tests were performed in quasi-static regime as the model does not consider the viscous effects of bone marrow yet. Dynamic simulations could allow the analysis of non-physiological loads occurring in osteoporotic patients, such as fall, in a near future.

5. References

- [1] Cowin, *J. Biomech Eng.*, 1986.
- [2] Prot, These de doctorat, 2015.
- [3] Rogalski et al, *Structmat*, 2020.
- [4] André et al, *CMAME*, 2012.
- [5] Ladevez, 1993

IMPORTANCE OF FIBRIL DISTRIBUTION IN MODELING OF BENNINGHOFF ARCHES IN ARTICULAR CARTILAGE

Courtney A. Petersen, Clark T. Hung, Gerard A. Ateshian

Columbia University, United States of America

1. Introduction

Collagen fibrils in articular cartilage have classically been described to follow an arch-like structure, as proposed by Benninghoff [1], with the fibrils at the superficial zone (SZ) lying tangent to the surface, while deep zone (DZ) fibrils are preferentially oriented perpendicular to the subchondral bone [1]. Techniques such as polarized light microscopy have confirmed this orientation of collagen fibrils. One study used X-ray diffraction to quantify fibril dispersion at three points through the depth of one articular cartilage sample [2]. Aside from this particular study, the fibril distribution about each preferential axis is largely unknown. This study is the first of a series which seeks to elucidate the exact collagen fibril distribution in articular cartilage by using finite element (FE) analysis to replicate experimental strain fields. The aim of the present study is to investigate the importance of fibril dispersion when modeling Benninghoff arches in articular cartilage.

2. Materials and Methods

Axisymmetric FE models of the articular surface of an immature bovine humeral head were created to replicate the experimental setup reported in [3]. Cartilage was modeled as a biphasic material with a neo-Hookean ground matrix whose stiffness varied through the depth [4] and with permeability measured previously [5]. Local material axes were assigned to each of the eight-node hexahedral elements such that the z-axis was normal to and the x-axis was tangent to the articular surface. Collagen fibrils with stiffness measured previously [5] were modeled as either, (1) two discrete fibril bundles oriented along the z-axis in the DZ, arching through the MZ to align with the \pm x-axis in the SZ, or (2) an ellipsoidal fibril distribution with semi-principal axes (a, b, c) set to (3,1,1) in the SZ and (1,1,5) in the DZ to match the distributions reported in [2] and with an

isotropic distribution in the MZ. All simulations used FEBio (febio.org) [6].

3. Results

Magnitudes of normal and shear Lagrange strains in the ellipsoidal distribution model ($E_{xx} = 0.37, E_{yy} = -0.34, E_{xy} = -0.20$) were lower than those in the discrete fibril bundle model ($E_{xx} = 0.64, E_{yy} = -0.43, E_{xy} = -0.32$). The most notable differences in strain distribution was observed in E_{xy} where the maximum occurred near the subchondral surface for the ellipsoidal model and in the MZ for the discrete model (Fig. 1).

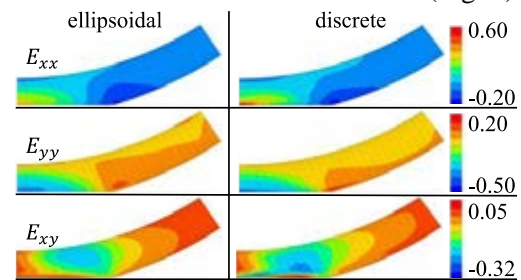


Fig. 1: Strain distributions for distributed and discrete fiber families.

4. Discussion and Conclusions

This study demonstrates that the dispersion of collagen fibrils in articular cartilage, as reported experimentally [2], significantly influences strain distributions in the tissue, even when both modeling approaches account for the arch-like structure of articular cartilage [1]. In future studies we will explore the ramifications of this finding in relation to cartilage damage and wear.

5. References

- [1] Benninghoff, A. *Forschung*, 1925. [2] Aspden, RM & Hukins, DW. *Proc R Soc Lond B Biol Sci*, 1981. [3] Canal, CE.+ *J Biomech*, 2008. [4] Wang, CCB.+ *J Biomech Eng*, 2002. [5] Oungulian, SR.+ *J Biomech*, 2014. [6] Maas SA+. *J Biomech Eng*, 2012

Acknowledgements:

NIH R01 GM083925.



A METHOD TO CHARACTERIZE POSTURE AND THE SCAPULOTHORACIC JOINT USING BIPLANAR RADIOGRAPHY

Sandrine Bousigues (1), Laurent Gajny (1), Wafa Skalli (1), Sawsane Aloui (2), Xavier Ohl (3), Patrice Tétéreault (4), Nicola Hagemeister (2)

1. Arts et Metiers Institute of Technology, Institut de Biomécanique Humaine Georges Charpak, France, 2. Ecole de Technologie Supérieure, Canada, 3. CHU de Reims, France 4. Centre Hospitalier de l'Université de Montréal, Canada

1. Introduction

Shoulder surgical planning aims to predict the size, position and orientation of the implant, in order to restore function after surgery [1]. Recent studies have shown the interest of taking into account both the posture and the scapulothoracic joint during this planning [2, 3]. However, images are generally taken from CT-scan acquisitions in a lying position. In that context, biplanar radiography in standing position could be appropriate to investigate both the scapula-thoracic joint and the spinal alignment.

Scapula, spine and ribcage 3D reconstruction methods exist using biplanar radiography, but the images are not taken with the same patient orientation and no fusion method exists to this day. Hence the objective was to use a fusion method to get a reconstruction containing the different bony segments and evaluate its repeatability.

2. Materials and Methods

5 asymptomatic volunteers were considered (ethical committee: CPP 06036). For each subject, 2 pairs of low dose biplanar X-rays were taken using EOS (EOS imaging, France). One (0° pair) was in conventional free standing position allowing for the spine [4] and rib cage [5] 3D reconstruction. The second (40° pair) was taken in the plane of the scapula (~ 40° rotation of the patient) and used for 3D reconstruction of the scapula [6]. For data fusion, few landmarks were annotated both on the 0° and 40° images, then a rotation angle was computed for scapula gross registration in the 0° pair environment. Finally a manual fine registration was made so that scapula projection best fits the 0° pair X-Rays contours. Following clinical parameters were computed: Protraction, internal rotation, tilt, and upward rotation of the

scapula [2]. To assess intra-observer repeatability, the scapula was registered 3 times for each subject by 1 operator. The results were analysed according to the ISO 5725-2 standard.

3. Results

The clinical parameters repeatability (2 standard deviation) was under 5° for the protraction, the tilt and the upward rotation, and under 6° for the internal rotation of the scapula.

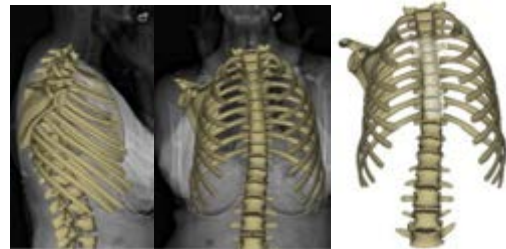


Figure 1 : 3D reconstruction of the spine, ribcage with the scapula

4. Discussion and Conclusions

The proposed method is promising to quantify the position and orientation of the scapula and the posture in a functional position. This method is still preliminary, a collision algorithm is in progress to control bony interpenetration with the rib cage.

5. References

1. J. A. Rodríguez et al., Ann. Joint, 2019
2. P. Moroder et al., JSES, 2020.
3. P. Moroder et al., Clin Orth Relat Res, 2022
4. L. Gajny et al., Eur Spine J, 2019
5. B. Aubert et al., CMBBE, 2014
6. S. Bousigues et al., CMBBE, 2021 conference

Acknowledgements:

The authors thank the NSERC (RGPIN-2017-04080) and the ParisTech BiomecAM chair (COVEA and Société Générale) for providing financial support to this project.

MELT ELECTROWRITTEN GRADIENT SCAFFOLD DEVELOPMENT FOR ROTATOR CUFF ENTHESIS REPAIR

Samuel E. Winston (1), Kirk C. McGilvray (1)

1. Department of Mechanical Engineering, Colorado State University, United States

1. Introduction

Surgical repair strategies of the rotator cuff have re-tear rates upwards of 90%, and these unacceptably high rates can, in part, be attributed to the inability of current treatments to recapitulate the mechanics of a healthy enthesis [1]. Histological evaluations suggest that most currently implemented repair strategies result in a fibrocartilaginous scar across the enthesis with reduced mechanical strength. To overcome these issues, our group has developed a tissue engineering approach that replicates the native gradient in the biomechanical stiffness observed at the enthesis (i.e., a stiff region of bone transitioning to a compliant region of the tendon) to encourage proper cell growth and extracellular matrix deposition. The hypothesis is that by using melt electrowriting (MEW), it will be possible to produce a biomimetic repair scaffold that recapitulates the stiffness gradient at the enthesis resulting in the appropriate formation of bony and tendinous tissues at the repair site.

2. Materials and Methods

Polycaprolactone ($M_n \sim 45$ kDa) (Polysciences, Inc.) angle-ply scaffolds were created with a custom-built MEW system. To generate a mechanical gradient across the scaffold's length, the fiber angle was varied along the length of the scaffold (Fig.1a). This novel approach is advantageous as it allows a single material with a constant fiber diameter to be utilized to create a gradient in the scaffold's mechanical response. Samples were subjected to a uniaxial tensile load of 4% strain at a strain rate of 0.1% strain/s. Localized strain across the scaffold length was measured using standard digital image correlation (MatLab, Jones). Stress was approximated as the measured force divided by the bulk cross-sectional area.

3. Results

The results indicated that variable fiber angle-ply scaffolds could be generated via MEW to control localized mechanics. The localized

elastic modulus of the constructs was shown to vary from 22.1 MPa to 0.6 MPa (Fig 1b).

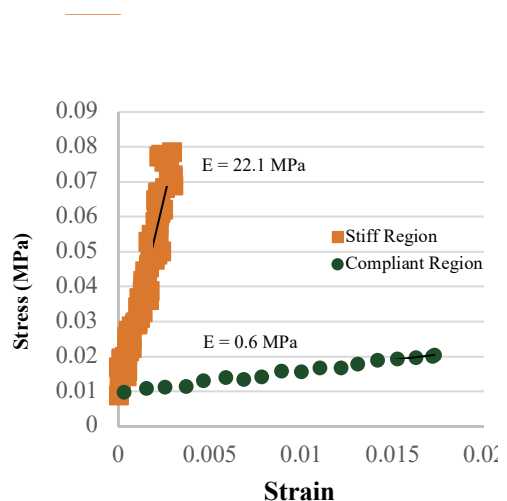
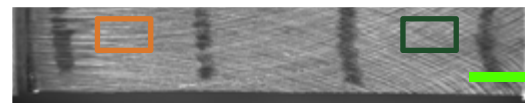


Figure 1: (a) Scaffold before and during mechanical testing with stiff (solid, orange) and compliant (solid green) ROIs highlighted. (b) Representative stress-strain data for two distinct regions of the scaffold

4. Discussion and Conclusions

MEW scaffolds have been successfully fabricated, demonstrating a gradient in the local elastic modulus across the length of the scaffold by a factor of 35x across a very small length. Future work is focused on refining the scaffold's fiber-angle scaffolds to better match the elastic modulus expected in healthy bone and tendons. And since MEW allows for the fabrication of fibers on the order of $5\mu\text{m}$ is postulated that this gradient can be fabricated at a length scale equivalent to a natural enthesis.

6. References

1. Zumstein MA, et al. OTSR. 2017; 103(1):S1-S10 (2017)

ON THE EVALUATION OF POSTOPERATIVE BIOMECHANICAL CONDITIONS IN RECONSTRUCTED HUMAN MANDIBLES: CAN WE PREDICT THE HEALING OUTCOME?

Giorgio Biesso (1), Vincenzo Orassi (1), Clarence Janka (3), Carsten Rendenbach (2), Sara Checa (1)
 1. Berlin Institute of Health at Charité – Universitätsmedizin Berlin, Julius Wolff Institute, Germany;
 2. Charité – Universitätsmedizin Berlin, Freie Universität Berlin, Humboldt-Universität zu Berlin and Berlin Institute of Health, Department of Oral and Maxillofacial Surgery, Berlin, Germany;
 3. Karl Leibinger Medizintechnik GmbH & Co.KG

1. Introduction

Mandibular reconstruction with fibula free flap is associated with a high rate of osseous non-unions (30%). Plate related complications are the most common cause of bone regeneration impairment. Mechanical signals are known to influence the healing outcome in long bones [2], however for mandibular reconstruction the favourable mechanical environment remains largely unknown. Therefore, this study aims to investigate with an *in silico* approach whether the healing outcome in reconstructed patients is related to postoperative biomechanical conditions.

2. Materials and Methods

Subject-specific finite element models (FEMs) were built for two patients reconstructed with a fibula free flap, which reported different bone healing outcomes (successful, non-union). The bone geometry was derived from 6 months postoperative CT scans. Homogeneous and linear elastic material properties were assigned to elements representing bone tissue and callus. The fixation system defined during the virtual surgical plan was reproduced in the model with the same design and position (Fig 1). To ensure a proper occlusion, condylar processes were assumed locked in the mandibular fossa. 14 muscles, modelled as actuators, were added to the FEM through coupling constraints.

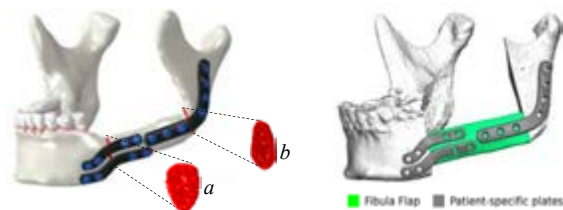


Figure 1: (Left) FEM of mandibular reconstruction with a detailed view of the mesial (a) and distal (b) callus regions. (Right) Virtual surgical plan.

Insertion points, muscle attachments, and force magnitudes were imported as boundary conditions through a musculoskeletal modelling technique.

3. Results

For a unilateral biting task of 50N, mechanical strains between 0.5% - 1.5% (0.003 SD) were determined in the successful healing case. Instead, strain levels less than 0.2% (0.001 SD) were determined in the non-union case.

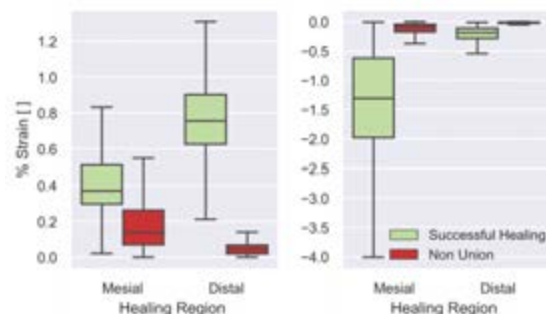


Figure 1: (Left) 1st Principal strain (tensile). (Right) 3rd principal strain (compression).

4. Discussion and Conclusions

Biomechanical conditions of the reconstructed mandibles were different for different healing outcomes. Low strains predicted in the non-union have been previously related to impaired healing [3]. Future studies aim to investigate a larger number of patients.

5. References

- Ritschl et al., Clinical Oral Investigation, 2021.
- Epari et al., Clinical Biomechanics, 2006.
- Elliott D. S. et al., The Bone & Joint Journal, 2016.

Acknowledgements:

This study was funded by the German Research Foundation (Deutsche Forschungsgemeinschaft CH 1123/10-1).



PATIENT-SPECIFIC APPROACH FOR ORTHOGNATHIC SURGERY: IN-SILICO DESIGN AND OPTIMIZATION OF 3D-PRINTED PLATES

Ilaria Rota (1), Andrea Giglio (1), Francesco Grecchi (2), Matteo Bonacina (3), Dario Gastaldi (1)

1. Politecnico di Milano, Department of Chemistry, Materials and Chemical Engineering, Italy;
2. ISI Istituto Stomatologico Italiano, Italy; 3. Ars&Technology Srl, Italy

1. Introduction

Le Fort I osteotomy is an orthognathic surgical treatment used to correct maxillofacial deformities. The maxilla is fixed to ensure the proper occlusion for the patient using titanium plates and screws [1]. Patient-specific plates can be produced with non-uniform thickness by Additive Manufacturing (AM) techniques like Laser Powder Bed Fusion (LPBF) [2].

This study proposes a workflow starting from patient's CT images to optimize the design of orthognathic surgery plates taking advantage of the possibility to produce AM shape-controlled titanium plates. The design is based on providing a trade-off between biomechanical compatibility (namely minimization of dimensions) and mechanical reliability.

2. Materials and Methods

An orthognathic case involving a patient who underwent a Le Fort I osteotomy was investigated. The 3D model of maxillofacial bones of the patient were reconstructed using the CT images. A finite element model was created including two zygomatic implants and two LPBF-titanium plates with fixation screws. Patient-specific bone properties were set using the software Bonemat [3] that assigns appropriate elastic modulus values according to the grey levels of the patient's CTs (Fig. 1).

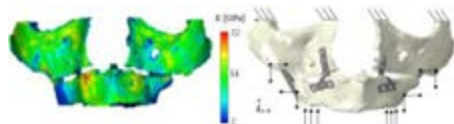


Figure 1: Patient-specific distribution of bone properties and FEM boundary conditions.

Loading and boundary conditions were applied to replicate the physiological conditions of the occlusion. An occlusive load, muscular forces of masseters, lateral and medial pterygoids were imposed, while the upper bone were fully constrained (Fig. 1).

Homogeneous, isotropic and elasto-plastic material properties ($E=107$ GPa, $\nu=0.34$, $\sigma_y=1025$ MPa) were assigned to LPBF-titanium plates following uniaxial and indentation tests. By means of numerical mechanical analysis both in static and cyclic loading conditions, critical and low-stress regions were identified, in order to implement a shape-optimization strategy in terms of optimal thickness design.

3. Results

In Fig.2 the pre-optimization fatigue study reveals a section of the plate that has achieved the number of cycles to failure. After the thickening of the plate the requirement for the cyclic mechanical reliability is satisfied.

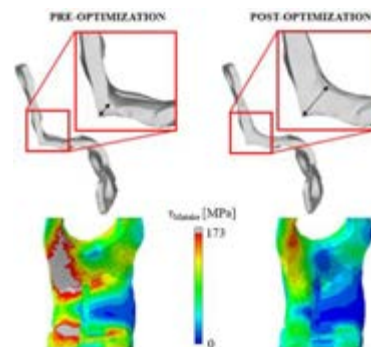


Figure 2: Design optimization and distribution of Mataké's fatigue equivalent stress parameter.

4. Discussion and Conclusions

The optimized plate design guarantees a trade-off between biomechanical compatibility and static and cyclic mechanical reliability. These results suggest that the described patient-specific strategy can be applied for the design optimization of 3D-printed plates.

5. References

1. Grecchi F et al., J. Cranio-Maxillofacial Surg; 2021. p. 114-23
2. Cerea M et al., BioMed Research International; 2018.
3. Taddei F et al., Med Eng Phys; 2007. p. 973-14



IN SILICO EVALUATION OF AN ARTIFICIAL TEMPOROMANDIBULAR JOINT DISC REPLACEMENT

Jason Kuiper* (1), Kevin Labus (1), Christian Puttlitz (1,2,3)

1. Department of Mechanical Engineering, Colorado State University, United States;
2. Department of Clinical Sciences, Colorado State University, United States;
3. School of Biomedical Engineering, Colorado State University, United States;

*Corresponding Author: Jason.kuiper@colostate.edu

1. Introduction

The temporomandibular joint (TMJ) is the articulation between the cranium and mandible. In progressive cases of TMJ degradation, disc excision is a common treatment. However, this increases friction and mechanical stress in the joint and fails to reduce pain in up to 25% of patients [1]. There exists a critical need to develop a robust artificial TMJ disc replacement to arrest joint degradation and improve clinical outcomes. As a first step, we have developed a TMJ finite element (FE) model, simulated jaw clenching to predict TMJ tissue stress distributions, and evaluated an artificial TMJ disc design composed of 25% polyvinyl alcohol (PVA).

2. Materials and Methods

Micro-computed tomography was used to create a unilateral model of the ovine TMJ soft tissues. Abaqus was used for all FE analysis. The TMJ capsule was modeled using non-linear spring elements, and bones were modeled as rigid bodies. Contact and material properties were defined from *ex vivo* experiments on ovine TMJ discs and PVA hydrogels [2,3]. A ramped 25 N load was applied to simulate clenching. To validate the FE model prediction, *ex vivo* experiments were performed on seven ovine TMJs (n=4 left, n=3 right). A ramped 25 N compressive force was applied through the joint, and contact area and pressure were measured using a flexible pressure-mapping sensor. The slope of the peak stress-applied force curve was compared between experimental data, and the native TMJ disc or artificial PVA disc using a one sample t-test. Contact area was defined as the area experiencing pressure greater than 0.1 MPa.

3. Results

The model slope predictions for both the native TMJ disc (97.73 kPa/N, $p = 0.50$) and artificial PVA disc (97.71 kPa/N, $p = 0.51$) were not significantly different from the experimental mean. The predicted contact area fell within the 95% confidence interval of the experimental data for an applied force of 7.5 N, but underpredicted the experimental contact area at higher loads (Figure 1).

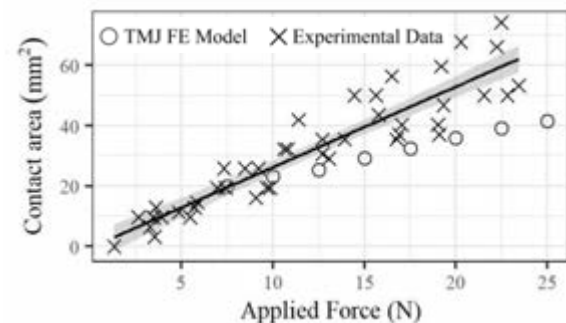


Figure 1: Experimental and predicted contact area, with linear experimental data fit and 95% confidence interval (shaded region).

4. Discussion and Conclusions

The FE model predicts the relationship between applied load and peak pressure. We also demonstrate agreement between peak pressure in the native and artificial PVA discs. Underprediction of the contact area by the FE model will be addressed with localized mesh convergence. Next steps will be to introduce dynamic motion to simulate chewing for more rigorous and broad evaluation of PVA hydrogels for disc replacement.

5. References

1. O. G. Ellis et al, J Oral Maxillofac Surg. 79(12):2448-2454 (2021)
2. K. M. Labus et al, J Mech Behav Biomed Mater. vol. 116, p. 104300 (2021)
3. J. P. Kuiper et al, Frontiers in Physics, vol 10, p. 928579, (2022)

ADVANCING VIRTUAL SURGICAL PLANNING OF MANDIBULAR RECONSTRUCTION USING GRADIENT-BASED OPTIMIZATION

Atabak Eghbal (1), Eitan Prisman (2), Antony Hodgson(3), Sidney Fels (1)

1, *Department of Electrical and Computer Engineering, University of British Columbia, Vancouver, Canada*

2, *Department of Surgery, University of British Columbia, Vancouver, Canada*

3, *Department of Mechanical Engineering, University of British Columbia, Vancouver, Canada*

1. Introduction

The mandible plays a vital role in the functional and aesthetic aspects of the jaw, allowing mastication and swallowing. Reconstruction of the resected mandibular defects with fibular free flaps is a complicated task. State-of-the-art approaches use shape descriptors to evaluate the surgical plan's geometrical aspects. [1]. In this study, we introduce a novel virtual surgical planning algorithm for mandibular reconstruction that takes advantage of convex optimization.

2. Materials and Methods

Using the ArtiSynth simulation platform [2] and MATLAB, we have created a two-way data acquisition interface workflow that collects reconstructed outcomes from ArtiSynth and uses an interior-point optimizer in MATLAB to optimize the reconstruction parameters. In this regard, we have introduced five geometrical shape descriptors/ objective functions, including (1) the angle between the resected faces of the mandible and fibula segments, Eq.1 (2) the projection distance between two resected faces, Figure.1b (3) the closest distance between reference polygon (resected face of either mandible or fibula) and the projected polygon, Figure.1d (4) the area overlap [3] between reference polygon and projected polygon, Figure.1c

$$C = \max \left(\min \left(\frac{\langle \vec{n}_1, \vec{n}_2 \rangle}{|n_1| |n_2|}, 1 \right), -1 \right) \quad (1)$$

3. Results

The objective of this study was to maximize the polygonal overlap of the resected faces of the mandible with the side faces of the fibular segment, Figure.1e. Our algorithm achieved 81.5% overlap on the Ramus side, and 85.1% on the body side.

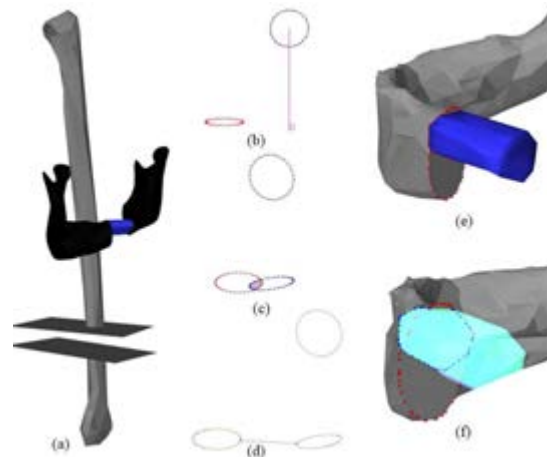


Figure 1: Objectives considered in the virtual surgical planning of mandibular reconstruction.

4. Discussion and Conclusions

The proposed novel framework addressed the area overlap of the corresponding mandible and fibula faces and achieved stable automated planning similar to the surgeons' reconstruction plans. We plan to extend the model by considering facial expression and dental implantation factors in the objectives.

5. Acknowledgments:

We want to thank Dr. John Lloyd for his discussions and comments.

6. References

1. Nakao, Megumi et al. "Volumetric fibular transfer planning with shape-based indicators in mandibular reconstruction." IEEE JBHI vol. 19,2 (2015): 581-9.
2. Lloyd, John E. et al. "ArtiSynth: A Fast Interactive Biomechanical Modeling Toolkit Combining Multibody and Finite Element Simulation." (2012).
3. Weiler, Kevin, and Peter Atherton. "Hidden surface removal using polygon area sorting." ACM SIGGRAPH computer graphics 11.2 (1977): 214-222.



A FINITE ELEMENT PROCEDURE FOR OPTIMAL ANNULOPLASTY RING SIZE ESTIMATION IN MITRAL VALVES WITH BARLOW'S DISEASE

Victorien Prot (1*), Hans Martin Aguilera (1), Robert Persson (2), Rune Haaverstad (2), Bjørn Skallerud (1), Stig Urheim(2)

1. Department of Structural Engineering, Faculty of Engineering Science, The Norwegian University of Science and Technology, Trondheim, Norway; 2. Department of Heart Disease, Haukeland University Hospital, Bergen, Norway

*corresponding author - victorien.prot@ntnu.no; tel: +47 73550872; Materialteknisk, 3-107, Gløshaugen, Richard Birkelands vei 1a, 7491 Trondheim, Norway.

1. Introduction

The mitral valve (MV) ensures unidirectional blood flow between the left atrium (LA) and left ventricle. Barlow's Disease (BD) affects the entire MV apparatus causing back flow into the LA [1]. Standard annuloplasty procedures lead to a significant annular area reduction and demand excision of excessive leaflet tissue. The objective was to predict the required mitral annular area reduction in selected Barlow patients to achieve sufficient coaptation without leaflet excision using finite element (FE) analyses.

2. Materials and Methods

Three-dimensional echocardiography was used to create patient-specific models of MV with BD. Six patients were studied post-operatively

in a finite element framework, to quantify the optimal coaptation area index (coaptation area to leaflet area ratio). For the patient-specific finite element analyses, realistic papillary muscle and annular motions are incorporated, also for the FE annuloplasty analyses [2]. The annuloplasty ring size is reduced moderately until the optimal coaptation area index is achieved for each patient.

3. Results

The mean mitral annular area at end diastole was reduced by 60% post-operatively, resulting in a post-operative coaptation area index of 20%. To achieve the same coaptation area index with moderate annular reductions and no leaflet resection, the annular reduction was 30%. This is illustrated in Figure 1.

4. Discussion and Conclusions

In silico analysis by 3D echocardiography have shown that an annuloplasty ring leading to moderate annular reduction secures the same leaflet coaptation area index in the selected patients compared with post-operative findings.

5. References

1. Anyanwu AC, Adams DH Semin. Thorac. Cardiovasc. Surg.; 19(2):90-96 (2007).
2. Aguilera HM, Urheim S, Persson RM, Haaverstad R, Skallerud B, Prot V. 2022 Journal of Biomechanics; 142:111226 (2022).

Acknowledgements:

This study was partially funded by the Trond Mohn Foundation (TMS2019TMT09).

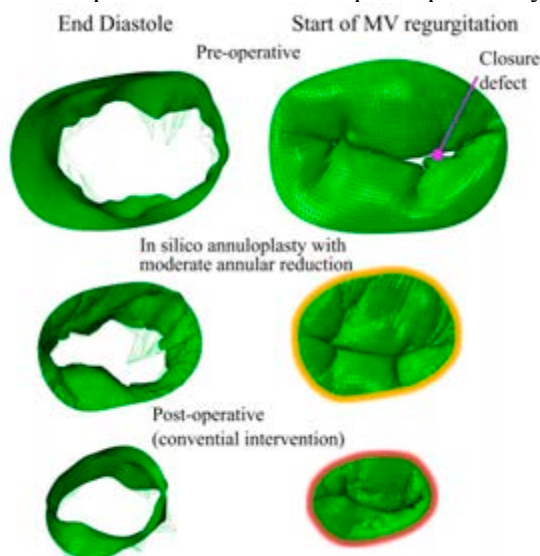


Figure 1: FE analysis of moderate annular reductions versus conventional annuloplasty rings



CONTROLLED COMPARISON OF SIMULATED HEMODYNAMICS ACROSS TRICUSPID AND BICUSPID AORTIC VALVES

Alexander D. Kaiser (1,2), Rohan Shad (3), Nicole Schiavone (4),
William Hiesinger (5), Alison L. Marsden (1,2,6)

1. Institute for Computational & Mathematical Engineering, Stanford University, USA;
2. Department of Pediatrics (Cardiology), Stanford University, USA;
3. Department of Cardiothoracic Surgery, University of Pennsylvania, USA;
4. Department of Mechanical Engineering, Stanford University, USA;
5. Department of Cardiothoracic Surgery, Stanford University, USA;
6. Department of Bioengineering, Stanford University, USA

Correspondence: alexdkaiser@stanford.edu

1. Introduction

Bicuspid aortic valve is the most common congenital heart defect, affecting 1–2% of the global population. Patients with bicuspid valves frequently develop dilation and aneurysms of the ascending aorta. Genetics and hemodynamics are both believed to play a role in causing dilation, but the precise cause of dilation remains under debate [1].

2. Materials and Methods

With fluid-structure interaction simulations using the immersed boundary method, we conducted a controlled comparison of the hemodynamics associated with multiple valve phenotypes. Using newly developed techniques we call design-based elasticity [2], we constructed models of a tricuspid aortic valve and bicuspid valves with left/right (LR), right/non (RN) and non/left (NL) coronary cusp fusion [3]. To isolate the effect of leaflet fusion phenotype, we performed simulations in a single, healthy patient-specific geometry.

3. Results

Simulations reveal dramatically different flow patterns through tri-leaflet and multiple phenotypes of bicuspid aortic valves depending on the location of cusp fusion. The tri-leaflet valves showed relatively uniform forward flow and little backflow during systole. The bicuspid cases showed elevated circulation and backflow. Further, with LR fusion the jets impact the vessel wall from the outer side of the root to the outer side of the distal ascending

aorta. With RN fusion, the jets impact the vessel wall primarily on the outside of the distal ascending aorta.

4. Discussion and Conclusions

With LR and RN cusp fusion, jets impact the vessel walls at locations generally known to be correlated with dilation with each phenotype, suggesting that hemodynamics may play a role in creating localized dilation. These results add evidence to a longstanding debate on the cause of ascending aortic aneurysms.

5. References

1. Verma S, Siu SC. *New England Journal of Medicine*. 370 (2014): 1920-1929.
2. Kaiser AD, et al. *Biomechanics and Modeling in Mechanobiology*. 20.6 (2021): 2413-2435.
3. Kaiser AD, et al. *Annals of Biomedical Engineering*. 50.9 (2022): 1053-1072.

Acknowledgements:

ADK was supported in part by a Grant from the National Heart, Lung and Blood Institute (Grant #1T32HL098049). ADK and ALM were supported in part by the National Science Foundation SSI (Grant #1663671). ADK and NS were supported in part by American Heart Association Transformational Project Award (Grant #19TPA34910000). RS was supported in part by the American Heart Association Postdoctoral Fellowship Award (Grant #834986). NS was supported in part by the Stanford Bio-X Bowes Fellowship.



INTEGRATION OF UNCERTAINTY QUANTIFICATION TO ADVANCE COMPUTATIONAL MODELS IN VASCULAR BIOMECHANICS

Lucas H. Timmins (1,2), Caleb C. Berggren (1), David Jiang (1), Y.F. Jack Wang (1),
Jake A. Bergquist (1,2,3), Lindsay C. Rupp (1,2,3), Zexin Liu (2,4),
Rob S. MacLeod (1,2,3), Akil Narayan (2,4)

1. Department of Biomedical Engineering, University of Utah, USA; 2. Scientific Computing and Imaging Institute, University of Utah, USA; 3. Nora Eccles Cardiovascular Research and Training Institute, University of Utah, USA 4. Department of Mathematics, University of Utah, USA

corresponding author: Lucas H. Timmins, Ph.D.; lucas.timmins@utah.edu

1. Introduction

Computational models of the cardiovascular system are increasingly being integrated into clinical decision-making, surgical planning, and medical device design. As model results have the potential to influence clinical outcomes, there is a need to provide confidence in model predictions. However, model confidence is marred by *uncertainties* through unaccounted variability in model input(s). Herein, we leveraged advancement in computational uncertainty quantification (UQ) to evaluate the influence of material property variability on the predicted coronary artery biomechanical environment.

2. Materials and Methods

An integrated UQ-finite element (FE) modeling framework was developed utilizing the UQ software, *UncertainSCI*, and the FE software, *FEBio* [1,2]. Using data from layer-specific mechanical testing of human non-atherosclerotic coronary artery tissue [3], probability density functions (PDFs) were created for each material coefficient, 10 in total, within a structurally-motivated strain energy function (SEF) [3]. A tensorial distribution was created from the 10 PDFs across orders 1 through 5, sampling the entire coefficient space. A multi-layered, axisymmetric quarter-cylinder model of a coronary artery subjected to *in vivo* loading was created and a forward-FE batch-processing scheme was developed to iterate through SEF coefficient combinations. A parameter-to-model-output emulator was constructed in *UncertainSCI* to describe the relationship between SEF coefficients (inputs) and FE-predicted stresses (outputs).

3. Results

The number of parameter combinations ranged from 21 (order 1) to >3,000 (order 5). Evaluation of the relative error for the 1st and 3rd principal stresses indicated order 2 was sufficient (errors <1%) and captured dominant uncertainty modes. Examining 1st principal stress distributions indicated that model variations decreased through layer thickness (Fig. 1), and the greatest dispersion was observed in the adventitia. Further, the stiffness of the anisotropic component in the adventitia was the dominant coefficient in driving predicted stress values.

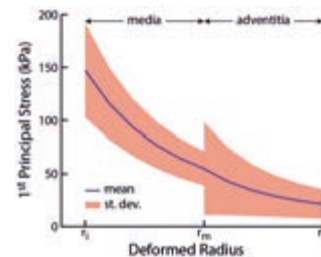


Figure 1: 1st principal stress distribution at order 2.

4. Discussion and Conclusions

Herein, we leveraged UQ techniques to understand the influence of material parameter variability on predicted coronary artery biomechanics. Future application to patient-specific models would promote model confidence and potential clinical adoption.

5. References

1. Narayan A et al., CompSciRN; (preprint).
2. Maas S et al., J Biomech Eng; (2012).
3. Holzapfel G et al., AJP-Heart Circ Physio (2005).

Acknowledgements: We thank the NIH (HL-150608, EB-02912) for providing support.

PATIENT-SPECIFIC SIMULATION OF MITRAL VALVE REPAIR IN HUMANS WITH MITRAL REGURGITATION

Natalie T. Simonian (1), Hao Liu (1), Sneha Vakamudi (2), Mark J. Pirwitz (2), Alison M. Pouch (3), Joseph H. Gorman, III (3), Robert C. Gorman (3), Michael S. Sacks (1)

1. The University of Texas at Austin, Austin, TX, USA; 2. Ascension Texas Cardiovascular, Austin, TX, USA; 3. The University of Pennsylvania, Philadelphia, PA, USA

Corresponding author: Michael Sacks, msacks@oden.utexas.edu, 201 E 24th St. Stop C0200 Austin, TX 78712

1. Introduction

Mitral valve (MV) repair techniques for regurgitation, such as surgical undersized ring annuloplasty (URA) or transcatheter edge-to-edge repair (TEER) have demonstrated significantly lower mortality than MV replacement. However, their long-term outcomes remain suboptimal or contradictory [1, 2]. Pre-clinical optimization is complicated by the heterogeneity of the patients' pre-operative states and the complexity of the repair configurations. We thus developed a patient-specific MV computational model based strictly on standard of care pre-operative imaging data to quantitatively predict the post-operative MV functional state.

2. Materials and Methods

First, we developed a finite-element model of the full patient-specific MV apparatus. To inform the subannular structure, we quantified the MV chordae tendinae (MVCT) origins and leaflet insertion distributions from 5 CT-imaged excised human hearts. Next, we segmented the patient-specific end-diastolic (ED) and end-systolic (ES) MV leaflets and identifiable MVCT origins from pre-operative 3D echocardiography images. Using a triangulated mesh of the ED leaflets with shell elements, the ED to ES annular and MVCT origin displacements as boundary conditions, and established material models for human MVCT and MV leaflets [3, 4], we simulated MV closure in Abaqus 6.14 and iteratively updated the leaflet and MVCT pre-strains to minimize the l^2 -norm between the simulated and target ES geometries. With this fully calibrated MV model, we simulated URA or TEER by modifying the annular displacement or applying 3D MitraClip models to predict the patient-specific post-operative state.

3. Results

In both the URA and TEER models, the post-operative geometry was predicted to within 1 mm of the target, and the circumferential and radial strain fields demonstrated both global and local correspondence (Fig. 1).

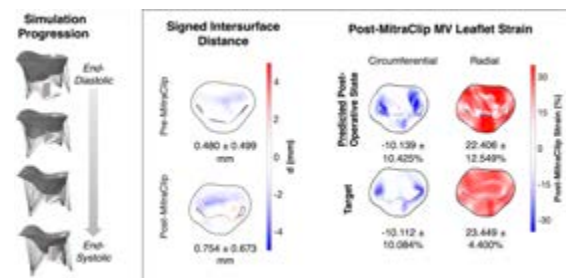


Figure 1: The TEER simulation progression and geometry and strain field predictions, demonstrating close agreement with the target.

4. Discussion and Conclusions

Such studies are crucial since outcomes of MV repair remain unpredictable, yet quantitative, patient-specific repair optimization techniques are profoundly limited. We were able to develop an anatomically faithful patient-specific model of the full MV apparatus to predict post-operative outcomes *from pre-operative clinical data alone*, and thus lay the foundation for quantitative surgical planning, tailored patient selection, and ultimately, a more durable repair.

5. References

1. Fernandez FG, et al. Ann Thorac Surg. 2019 Dec;108(6):1625-1632.
2. Obadia JF, et al. N Engl J Med. 2018 Dec 13;379(24):2297-2306.
3. Zuo K, et al. J Mech Behav Biomed Mater. 2016 Sep;62:607-618.
4. Narang H, et al. Ann Biomed Eng. 2021 Dec;49(12):3711-3723.



PRE-OPERATIVE PLANNING OF PIPELINE™ EMBOLIZATION DEVICE SIZING USING FINITE ELEMENT METHOD

Reza Abdollahi (1,2), Amirali Shahi (1, 2), Daniela Iancu (2), Simon Lessard (2,3), Gilles Soulez (1,2),

1. Université de Montréal, Canada; 2. Centre de recherche du Centre hospitalier de l'Université de Montréal, Canada 3. ETS, Canada

Corresponding author: Gilles Soulez, gilles.soulez.med@sss.gouv.qc.ca

1. Introduction

With progress in biomedical science, Flow Diverter (FD) devices are proposed as a non-invasive alternative to open surgery to treat complex intracranial aneurysms. The FD treatment is the endovascular deployment of a closed-mesh self-expanding stent at the level of the aneurysm neck to induce thrombotic occlusion while preserving the patency of side arteries. Hence, the use of FD is a promising procedure superior to traditional procedures in treating complex ICA with specific indications [1]. This work aims to represent a pre-operative planning technique that will assist physicians in predicting the outcome of the Pipeline™ Embolization Device (PED; Covidien, Irvine, California) on a patient-specific model through biomechanical interactions.

2. Materials and Methods

A patient-specific model of the internal carotid aneurysm was selected for this study which was treated by PED (4.5*16). The intended patient vascular anatomy has several tortuosities, as illustrated in Fig. 1. The compression, insertion and expansion of an FD were simulated using the finite element method. The morphological characteristics of the artery lumen are an essential factor for FD apposition (e. g. the lumen diameters at the FD site change between 3.20 and 4.65 mm). Therefore, studying biomechanical contact forces between FD and the vascular wall is necessary.

3. Results

The result for the virtual FD deployment stage is demonstrated in Fig. 1, which is a red sign indication of proper contact pressure between FD and the parent artery. The vascular wall in

contact by FD is divided into three regions: distal landing point zone, aneurysm neck and proximal zone, in which the FD lengths in every area are 4, 4.75, and 11.75 mm, respectively. The related force in every site is about 2.98, 2.18, and 5.88 N, respectively. Afterwards, the final length of the deployed virtual FD was compared with the last length of the real FD from postoperative angiograms of the patient follow-ups. The error for the length of deployment FD from the virtual model and the postoperative results is about 0.49 percent.

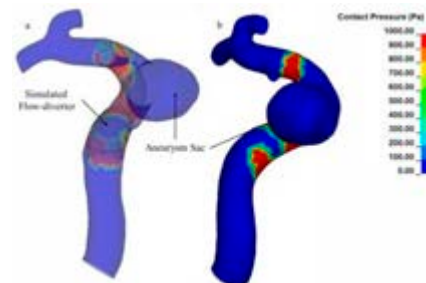


Figure 1: Contact pressure distribution on the vascular wall. (a) Transparent view of vascular with deployed simulated FD. (b) Proper apposition zones indicated in red

4. Discussion and Conclusions

This study was a step forward in demonstrating that computational biomechanical simulations of endovascular procedures can support physicians in planning treatment strategies.

5. References

1. Limbucci N et al., Neurosurgery. 2020;86(1);S85-S94

Acknowledgements:

The authors would like to thank the Siemens Healthineers for providing financial support to this project.



A MODEL OF HEART FAILURE PATIENTS FOR THE GENERATION OF AN IN-SILICO COHORT

Hamed Moradi (1), Frans van de Vosse (1), Wouter Huberts (1) (2)

1. Department of Biomedical Engineering, Eindhoven University of Technology, the Netherlands;

2. CARIM School for Cardiovascular Diseases, Maastricht University, the Netherlands

1. Introduction

Implementing a pulmonary artery pressure sensor (PAPS) and continuous pressure monitoring improves patient management and significantly reduces HF patients' hospitalization rates [1]. The utility of PAPS is compromised by thrombus formation, device detachment, and migration. Therefore, precise device design and efficacy evaluation are of paramount importance. The use of virtual patient cohorts based on realistic cardiovascular models can help the verification and validation of the sensor because model parameter variations can create a large number of virtual patients that cover a wide variety of patients' phenotypes [2], something that can hardly be achieved in real clinical trials.

The aim of this study was to develop and validate a model of an HF patient that realistically mimics the hemodynamics in the pulmonary both with and without a sensor implanted and can serve as the basis for a virtual cohort generator.

2. Materials and Methods

To create the model, a 3D geometry of the pulmonary artery was coupled to a 0D lumped parameter model, which enables us to have a realistic simulation of PAPS. The 0D model estimates the human cardiovascular system's physiological flow and pressure waveforms at the boundaries of the 3D domain, w. In contrast, the model gives a detailed picture of the local pressure and velocity fields around the PAPS. The parameters of the left and right ventricles' lumped model are changed to simulate the sick heart and the resulting pulmonary hypertensive situation.

3. Results

Validation of the simulated hemodynamics and the PAP sensor with literature and experiments showed a good alignment with them. For the evaluation of the PAPS, the output of interest can be listed as the pressure at the sensor's location, wall shear stress, the net force on the sensor, and the flow distribution through the side branches of PA.

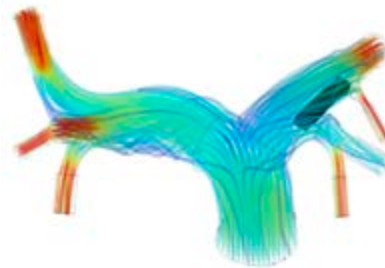


Figure 1: Results of PA with sensors

4. Discussion and Conclusions

The developed model enables us to investigate all physiological and non-physiological parameters in cardiovascular patients and devices. Moreover, it can now be used to generate realistic virtual patient cohorts.

5. References

1. Virani, Salim S., et al. "Heart disease and stroke statistics—2020 update: a report from the American Heart Association." *Circulation* 141.9 (2020): e139-e596.
2. Niederer, S. A., et al. "Creation and application of virtual patient cohorts of heart models." *Philosophical Transactions of the Royal Society A* 378.2173 (2020): 20190558.

Acknowledgements:

We acknowledge the European Union's Horizon 2020 research and innovation programme (grant agreement No 101017578) for their financial support

FINITE ELEMENT MODELLING OF RESPIRATORS INTERACTING WITH THE SOFT TISSUES OF THE FACE

Bethany Keenan¹ and Sam Evans¹

*1. School of Engineering / Cardiff University Brain Research Imaging Centre (CUBRIC),
Cardiff University, Wales, UK*

1. Introduction

Poor fit of respiratory personal protective equipment (PPE) can lead to leakage, discomfort or facial injuries. Current head models are rigid and do not account for the large deformation that occurs to the soft tissue whilst wearing a filtering facepiece (FFP3) respirator. Computational modelling offers the possibility of greater insights into the mechanics of respirator fit and allows estimation of tissue strains beneath the skin surface. This is the first study to date to utilise MRI techniques to measure the facial soft tissue deformation with different types of respiratory PPE.

2. Materials and Methods

A typical FFP3 bifold respirator was modelled using the FEBio finite element package (www.FEBio.org). Dimensions were obtained by direct measurement and the respirator mesh was constructed in GMsh (GMsh.info) and imported into FEBio Studio. A rigid head form based on the small ISO head form was modelled; the surface mesh was down-sampled using MeshLab (www.MeshLab.net). An MR Safety evaluation was performed on all respirators [1]. Subject-specific 3D deformable models were derived from high-resolution 3D magnetic resonance imaging (MRI) data. Digital volume correlation was used to extract the soft tissue deformation and measure the strain.

3. Results

Ten participants were recruited for this study (mean age 30.8yrs, height 1.70m and weight 72.3kg). Up to 10mm of deformation observed in cheek soft tissue. Max Green Lagrange strains of up to 0.4 observed when participant is wearing a respirator (Figure 1). The respirator can sit in multiple different positions on the face, some of which permit leakage. This

corroborates the importance of reproducing the respirator position after a fit test. The curvature of the face is important for a flexible mask and leaks are likely to occur in flat or concave areas such as under the chin, the cheeks and of course on either side of the nose. Correctly bending an aluminium nose strip to obtain a proper seal in this area is difficult, both in the model and in real life; over-bending is likely to be required to compensate for spring back of the metal strip.

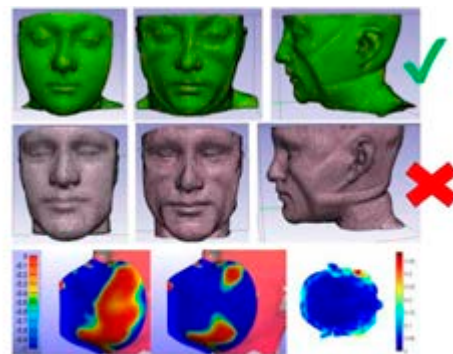


Figure 1 – Top to bottom - Resulting 3D model of participant with a good fit mask; poorly fitted mask; and FE contact pressure during inhalation and exhalation with strain map from full field MR data

4. Discussion and Conclusions

Modelling respiratory PPE is challenging due to large deformations and instability. However, it gives valuable insights into the mechanics of mask fitting and the causes of leaks and discomfort. It also has the potential to allow simulation and preclinical testing so that the design of masks can be optimised to fit many different faces without expensive, time consuming trial and error testing.

5. References

[1] Keenan et al. MRI Safety throughout Covid19. Clin Radiol (2022)

6. Acknowledgements

The authors would like to thank UKRI / EPSRC (EP/V045563/1) for providing financial support to this project.

MODEL-BASED SIMULATIONS OF THE INSERTION OF TENSOR THREADS IN PATIENT-SPECIFIC FACE: A PROOF OF CONCEPT

Marie-Charlotte Picard (1), Pascal Perrier (2), Mohammad Nazari (1, 3), Yohan Payan (1)

1. Univ. Grenoble Alpes, CNRS, Grenoble INP, TIMC, 38000 Grenoble, France

2. Univ. Grenoble Alpes, CNRS, Grenoble INP, GIPSA-lab, 38000 Grenoble, France

3. School of Mechanical Engineering, University of Tehran, Tehran, Iran

1. Introduction

Facial paralysis is associated with the loss of motricity of facial muscles, inducing face sagging under the effect of gravity, with aesthetic and functional consequences. In order to compensate for the sagging, surgeons have proposed a clinical procedure consisting of inserting and anchoring biodegradable tensor threads under the skin of the face, in order to restore tension to the sagging areas. This study allowed the realization of a proof of concept of a software tool that uses simulations with a Finite Element (FE) biomechanical model of the face [1] in order for the surgeons to (1) predict the behavior of the face after the addition of tensor threads and (2) visualize preoperatively in real-time the postoperative aesthetic appearance of the patient's face using reduced order models (ROM) [2].

2. Materials and Methods

Patient-specific FE face models are generated by registering a reference Face model using the Elastix library (fig. 1).

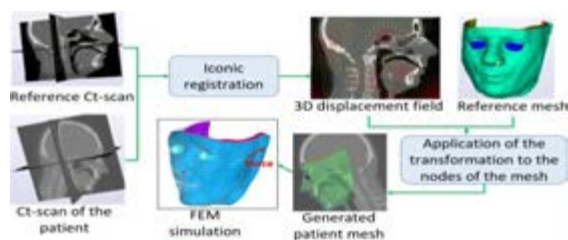


Figure 1: Patient-specific mesh generation

The mesh is composed of four layers, which represent skin, dermis, hypodermis and muscles, modeled by hyperelastic materials. An FE replica of the thread is inserted in the third layer of the FE face model and contacts between thread (that includes a set of hollow cones) and facial tissue are modeled. Nodal forces are then applied at the tip of the thread to simulate its

traction (fig. 1) and the lifting of facial tissue. A ROM is then built from a set of selected FE simulations of the impact of the applied force on the facial tissue shape, using the StaticRomBuilder software of Ansys®.

3. Results

An interactive software has been developed using the CamiTK library (cami.tk.imag.fr), in order for the clinician to (1) build the patient-specific biomechanical face model, (2) insert the tensor thread (position and rotation) in the model, (3) generate the corresponding ROM and (4) test and display in real-time the shape of the face resulting from tractions with the tensor threads (fig. 2).

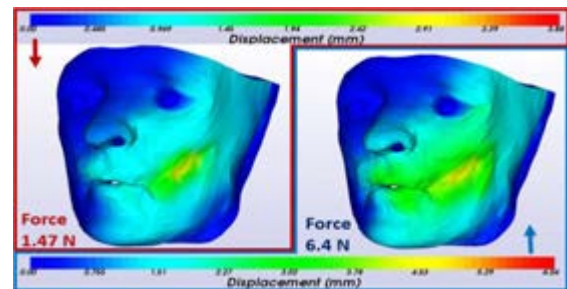


Figure 2: Simulated face appearance after tensile thread traction of two forces imposed by the user.

4. Discussion and Conclusions

We have demonstrated the feasibility of a software that allows surgeons to evaluate for each patient the extent to which the position of the threads can compensate for facial lifting.

5. References

1. Nazari, M. A. et al. (2011). Shaping by stiffening: a modeling study for lips. *Motor control*, 15(1), 141-16
2. Cueto, E., & Chinesta, F. (2014). Real time simulation for computational surgery: a review. *Advanced Modeling and Simulation in Engineering Sciences*, 1(1), 1-18

FACIAL BEHAVIOR RECOGNITION AND REHABILITATION USING 3D BIOMECHANICAL FEATURES AND DEEP LEARNING APPROACH

Duc-Phong NGUYEN (1), Marie-Christine HO BA THO (1), Tien-Tuan DAO (2)

1. Université de technologie de Compiègne, CNRS, Biomechanics and Bioengineering, France;
2. Univ. Lille, CNRS, Centrale Lille, UMR 9013 - LaMcube - Laboratoire de Mécanique, France

1. Introduction

Facial palsy patients or patients under facial transplantation have facial dysfunctionalities and abnormal facial motion due to altered facial muscle functions and nerve damage [1]. The restoration of normal and symmetrical facial expressions is essential to improve the quality of life and social interactions for involved patients. Current traditional facial rehabilitation has mainly been based on a mirror approach to monitor the visual qualitative feedback from the rehabilitation exercise [2]. However, the use of these systems in clinical routine practice still remains challenging in terms of guiding patients to practice rehabilitation exercises. The objectives of the research are to develop innovative engineering solutions toward a next-generation computer-aided decision support system for facial analysis and rehabilitation.

2. Materials and Methods

Four main contributions were provided.

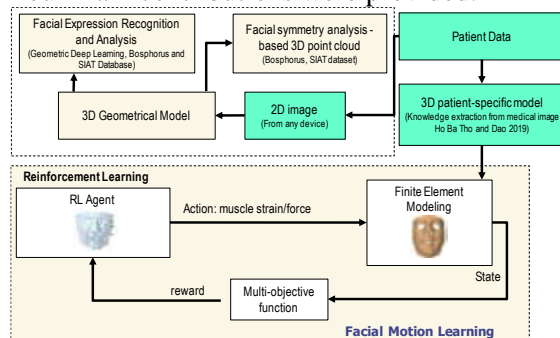


Figure 1: DDPG agent coupled with finite element model of the face for facial motion learning.

Firstly, a patient-specific 3D face model was fast reconstructed from a single 2D image using deep learning to learn the parameters of the 3D Morphable model. Secondly, the 3D face model will be recognized in terms of facial expressions using geometric deep learning directly on the 3D point set. Thirdly, the face symmetry was also analyzed based on novel descriptors

extracted from the geometric deep learning model. And finally, a novel modeling workflow was proposed for learning facial motion by coupling reinforcement learning and finite element modeling for facial motion learning and prediction.

3. Results

The outcomes of 3D face reconstruction, facial behavior recognition, and symmetry analysis could provide external information for estimating the severity of facial palsy patients. Because of that, rehabilitation exercises could be planned. And finally, our workflow for learning facial motion could provide the best facial mimic visualization to be achieved.



Figure 3: Face animation for symmetry (above) and smile (below)-oriented motion.

4. Discussion and Conclusions

The present study framework for facial behavior recognition and rehabilitation. This could provide both internal information (e.g. muscle excitation) and external visualization of facial mimics. As perspectives, this study will be extended for facial palsy and facial transplantation patients to optimize the functional rehabilitation program.

5. References

1. Robinson et al. *Operative Techniques in Otolaryngology-Head and Neck Surgery* 23.4 (2012): 288-296.
2. Nguyen et al. *Computer Methods and Programs in Biomedicine* 200 (2021): 105846.

Acknowledgements:

This work was financially supported by Sorbonne Center for Artificial Intelligence (SCAI).



PREDICTING THE RISK OF FRACTURE OF OSTEOSYNTHESIS PLATES

Charles Savoldelli (1, 2), Mohamed Syahmi Shaik (1), Yannick Tillier (1)

1. Mines Paris - PSL, France; 2. CHU-Nice, France

1. Introduction

The case of a partially edentulous patient who underwent orthognathic surgery is presented. A fracture of a right double plate was observed several weeks after surgery (Fig. 1, right). The objective of this work is to demonstrate whether it is possible to predict the risk of postoperative fracture of osteosynthesis plates using finite element (FE) modeling.

2. Materials and Methods

Fortunately, a CT scan of the patient had been performed prior to surgery. The 3D images were sent to Materialise Medical (Leuven, Belgium), for image segmentation and surgical planning. This allowed them to provide mesh files of the patient's facial structure and of the custom osteosynthesis plates used for the surgery. All meshed objects (ramus, mandible, maxilla, teeth, plates) were imported into the FE model Forge® NxT 3.2 (Transvalor, Sophia Antipolis, France). They were placed in contact with their neighbors and were considered as linear elastic and compressible materials in first approximation. The material data were taken from the literature [1].

Two different methods to get the desired jaw clenching movement for the simulations were used: (i) a set of muscle forces (masseter, temporalis and medial pterygoid) gradually increased up to 200 N along x , y and z axes respectively, resulting in an upward displacement of the mandible [2] and (ii) an upward displacement of a translation tool under the mandible. The calculations were arbitrarily stopped after a maximum imposed displacement of 0.016 mm, the forces becoming too high beyond that (teeth are already in contact at the beginning).

Two kinds of boundary conditions to simulate plate fixation (representative of a consolidated

state after healing) were evaluated: (i) with screws inside drilled bones (perfect contact) or (ii) without screws through a condition of bilateral sticking contact at the interface between the plate and the bone (Fig. 1, left).

3. Results

Not considering screws in the simulation does not allow the computations to converge. Screws tend to stabilize the system while increasing the contact surfaces and thus the computation times. Only the cases with screws were then analyzed. To push under the mandible allows the calculation to converge much faster than using a set of muscular forces, while also being much easier to define. The results show that the von Mises stress levels are higher at the plates, differently on the left and on right sides, with the highest values on the right plate (22 MPa vs 13 MPa), i.e. the side where the patient is partially edentulous, and furthermore in the area where the plate broke after surgery.

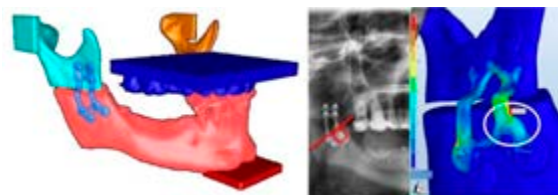


Figure 1: Finite element model (left) and von Mises stress distribution in the plate failure area (right).

4. Discussion and Conclusions

The surgical planning tools currently used in maxillofacial surgery are mainly based on geometric data. This study shows that the mechanical aspects should not be neglected.

5. References

1. Savoldelli C et al., Sci Rep. 11(1):8755 (2021)
2. Savoldelli C et al., IJOMS, 41(12) :1474-1482 (2012)



SIMULATION OF THE MECHANICAL BEHAVIOUR OF DIFFERENT PLATING SYSTEMS BRIDGING A SEGMENTAL BONE DEFECT

Guillaume Dubois (1,2)*, Philippe Rouch (1), Thomas Schouman (1,3)

1. Institut de Biomécanique Humaine Georges Charpak, Arts et Métiers Institute of Technology, Paris, France; 2. Materialise, Malakoff, France; 3. Médecine Sorbonne Université, AP-HP, Hôpital Pitié-Salpêtrière, Service de Chirurgie Maxillo-Faciale, Paris, France

*Corresponding author. Tel. : +33 1 44 24 63 64. E-mail address: Guillaume.DUBOIS@ensam.eu

1. Introduction

Mandibular segmental bone defects can generate severe functional impairments having strong consequences on the quality of life of patients. In most situations, their surgical reconstruction involves implants bridging the defect that are fixed by osteosynthesis screws [1]. Different plating strategies can be used, among which none is clearly established as superior [2]. The objective of this work is to compare the mechanical behaviour of different plating systems using Finite Element (FE) models to better understand the parameters affecting the efficiency of bone anchorage and support the choice of an optimal solution.

2. Materials and Methods

The chosen configuration for this study was a sheep hemi-mandible with an 18 mm segmental defect located between molars and incisors reconstructed by an implant stabilized with osteosynthesis screws. This FE model reproducing conditions of mechanical tests done previously was meshed using tetrahedral quadratic solid elements (Figure 1). A damage law was considered for cortical bone. A configuration with compression screws and another with locking screws were prepared. Before the application of a vertical load in the incisal area, the pretension generated by screw tightening was simulated.

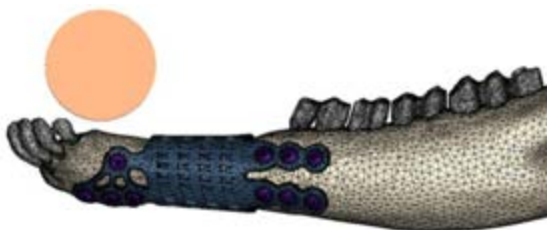


Figure 1: Lateral view of the FE model

Overall stiffness curves were plotted. Von Mises stress patterns in bone, implant and screws were compared and the Strain Energy Density (SED) was computed in bone regions surrounding every screw.

3. Results

In the model with locking screws, overall stiffness decreased monotonically as load was increasing. In the model with compression screws, stiffness was lower, but the decrease was preceded by an increase. Local damage was observed in bone already after screw tightening. Bone damage and SED heterogeneity were lower in the locking model. For both configurations, bone anchorage loss initiated before the implant stress became excessive.

4. Discussion and Conclusions

Our model included the pretension generated by tightening of screws, which is rarely considered in published studies [3]. This had a major impact on the results, both on bone induced damage and stiffness of the reconstructed mandible. The bone damage law allowed to simulate the load limit for each configuration and the progression of bone anchorage loss. Our results showed superiority of the locking system but also its dependency on a very accurate surgical execution.

5. References

1. Mehta RP, Deschler DG. Curr Opin Otolaryngol Head Neck Surg. 12:288-293 (2004).
2. Robey AB, Spann ML, McAuliff TM, Meza JL, Hollins RR, Johnson PJ. Plast Reconstr Surg. 122:1733-1738 (2008).
3. Bujtár P, Simonovics J, Váradi K, Sándor GKB, Avery CME. J Craniomaxillofac Surg. 42:855-862 (2014).



INFANT SKULL FRACTURE PREDICTION AND SUTURE MORPHOLOGY ANALYSIS

Siyuan Chen¹, Svein Kleiven¹, Xiaogai Li¹

1. Division of Neuronic Engineering, Department of Biomedical Engineering and Health Systems, KTH – Royal Institute of Technology, Huddinge, 14152 Sweden

1. Introduction

Anatomical details and mechanical properties of infants' skulls vary substantially from adults. This study contains two major parts. First, we implemented ductile and anisotropic mechanical properties of infant skulls using a unidirectional fiber composite model with progressive damage, which is then incorporated into CT-based subject-specific infant finite element head models at various ages to investigate infant fractures. Child skull fractures are often related to sutures and anatomical details of infant sutures distinguish across subjects like a "fingerprint", and this motivates the second part of this work. We performed a systematic investigation of suture morphology based on CT head images of over sixty infants.

2. Materials and Methods

The subject-specific FE head models employed in this study were developed by Li [1,2] based on the geometrical reconstruction of computerized tomography (CT) images (Fig. 1). Then the model's validation with the advanced damage model is conducted, including the three-point bending test, the global performance of the low-height drop test, and the validation of actual fracture cases.

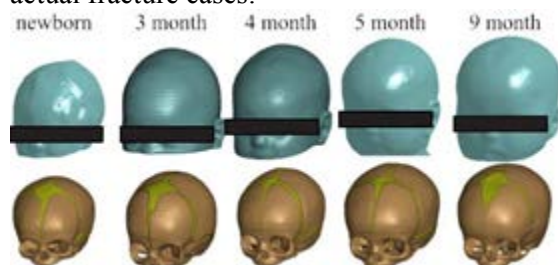


Figure 1: Generated infant FE model of various age.

From a collected database, head CT scans of 69 infants aged between 2 and 3 months without

obvious head injury or pathology were authorized.

The morphology study of the suture was conducted through principal component analysis (PCA). PCA is a commonly used method for representing data on an orthogonal basis with much fewer dimensions. The suture in each subject included 800 3D landmarks which were examined to create PCA, and the relevant principle component impact was analyzed as well.

3. Results

The simulation results show that the current model is capable of reproducing the infant skull fractures observed in the experiments, and the simulation predicts a skull fracture begins near the sutures and then travels back to the impact site or the ossification center. Results from parametric impact locations show that the infant skull bones are prone to fracture along lines parallel to the direction of trabecular fibers than along lines that run across them.

4. Discussion and Conclusions

The prediction fractures from the model agree with experimental findings. The primary cause of infant skull fracture is a failure in the direction perpendicular to the fiber direction.

5. References

1. Li, X., Sandler, H. and Kleiven, S. Biomechanics and modeling in mechanobiology, 2017 16(3), pp.823-840.
2. Li, X., Sandler, H., & Kleiven, S. Forensic science international, 2019, 294, 173-182.

Acknowledgements:

Swedish Research Council Grants n°2016-04203, n°2020-04724, n°2020-04496



PREDICTION OF REAL-LIFE SKULL FRACTURE PATTERNS USING SUBJECT-SPECIFIC FE HEAD MODELS

Natalia Lindgren (1), Mikkel J. Henningsen (2), Christina Jacobsen (2), Chiara Villa (2), Svein Kleiven (1), Xiaogai Li (1)

1. Division of Neuronic Engineering, KTH Royal Institute of Technology, Sweden;

2. Department of Forensic Medicine, University of Copenhagen, Denmark

1. Introduction

Thousands of people suffer from traumatic brain injuries every year [1]. Severe intra- and extracranial injuries often develop following skull fractures due to high-energy trauma. To study the biomechanics of head injuries, Finite Element (FE) analysis has shown to be a valuable tool and efforts have been made to characterize cranial bone material properties to predict skull injury and fracture risk [2-3]. However, injury assessment tools for predicting skull fracture risk are not well established yet. In this study, a material model for cranial bone is suggested for predicting fracture in fall accidents. The model was evaluated against a set of real-life fall accidents that were reconstructed using subject-specific FE head models.

2. Materials and Methods

An isotropic strain-rate dependent failure material model for cortical bone and diploë was established based on available LS-DYNA library material formulations. Cortical bone and diploë were evaluated against uniaxial tension tests and skullcap blunt indentation loading experiments [4-5]. The diploë was assumed to be significantly weaker and less stiff than the cortical bone layers.

Geometries of the head models were derived from CT images of the selected forensic cases with documented skull fractures. The anatomically detailed subject-specific head models were morphed from a previously developed head model using an image-registration based approach [6-7].

To derive input head kinematics, accident reconstructions using full-scale personalized FE Human Body Models (HBMs) under gravity loading were performed for all cases.

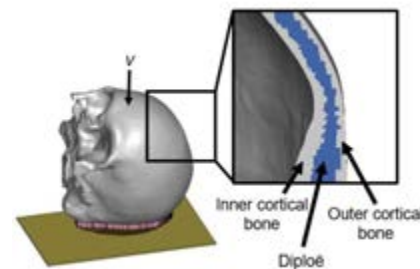


Figure 1: Simulation setup and cranial constituents.

3. Results

Linear, through-thickness skull fractures were predicted in all simulated impact cases. The fractures propagated in a direction comparable to what was observed in the real-life forensic cases. The model showed to be sensitive to impact velocity and direction, impact point and moment of inertia.

4. Discussion and Conclusions

In this study, the feasibility of using subject-specific head FE models to predict skull fracture has been demonstrated. A procedure by which occurrences of skull fracture can be reconstructed using computational engineering techniques, while capturing morphological variations among subjects, has been outlined.

5. References

1. Coronado V et al., Morbidity and Mortality Weekly Report; 60:1-32 (2011).
2. Kegel D et al., Journ of Mech Behav of Biomedical Materials; V100 (2019).
3. Barbosa et al., Biology; 267:9 (2020).
4. Wood J., Journ of Biomech, 4:1-12 (1971)
5. Gunnarsson A. et al, Army Research Lab (2021)
6. Li X. et al., Front in Bioen and Biote, V9 (2021)
7. Li X. et al., Biom and Mod in Mech, V20 (2021)

Acknowledgements:

This study was partly financed by Vinnova (no. 2019-03386) and Swedish Research Council (VR) (no. 2020-04724 and 2020-04496).



A TIERED VALIDATION APPROACH OF A PATIENT SPECIFIC HEART-VALVE MODEL

Nils Götzen (1), Tahir Turgut (1), Omar Zakala (1), Vincent Bouwman (1), Deniz Oztürk (2), Wojciech Zietak (2), Chiara Catalano (3), Salvatore Pasta (3,4)

1. 4RealSim Services BV, Netherlands; 2. capvidia B.V., Belgium; 3. University of Palermo, Italy; 4. IRCCS ISMETT, Italy

1. Introduction

Demonstrating adequate model credibility is a crucial requirement for allowing in-silico methods to become an integral part in the medical device development process. Recently, significant advances in developing a regulatory framework for in-silico methods were made, while also several international research organizations [1,4], FDA [2,3], and the EU funding program [5] are supporting these developments actively. We present a VVUQ framework for a Sapien-3 TAVI patient-specific in-silico model, which follows a tiered & hierarchical validation approach and complies largely with relevant standards.

2. Materials and Methods

The development & VVUQ of the in-silico model is organized in sequential and parallel phases (Figure 1): (I) Sapien-3 device FEM-model is developed and undergoes its own VVUQ program, focussing on structural performance parameters, such as in-vitro radial stent-frame stiffness and leaflet deformation; afterwards (II) FSI capability is added to the device model, which also is going through a verification, in-vitro validation & UQ phase. In parallel (III) a patient-specific FEM model of the left-ventricle/aortic-valve/aortic-arch is developed and combined with FSI capabilities (IV). This model will be calibrated, verified, and validated against a pre-TAVI scenario using a 20-patient sub-cohort of a larger patient group. Finally, the patient-specific FSI model is combine with the Sapien-3 FEM model to simulate the deployment process and acute clinical performance by evaluating pressure gradients, regurgitation fractions, flow-pattern etc considering a large patient cohort of about 100 subjects. At all development stages, UQ and uncertainty propagation will be considered using appropriate methods able to deal with complex and long-running simulations.

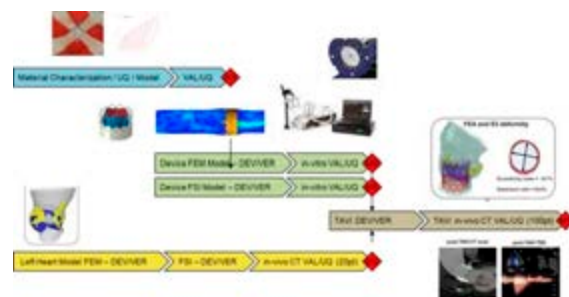


Figure 1

3. Results and Discussion

We present work-in-progress results and focus on the first stages of the program. Sapien-3 in-vitro FEM & FSI validation & UQ results will be presented together with the first patient-modelling results (Figure 2).

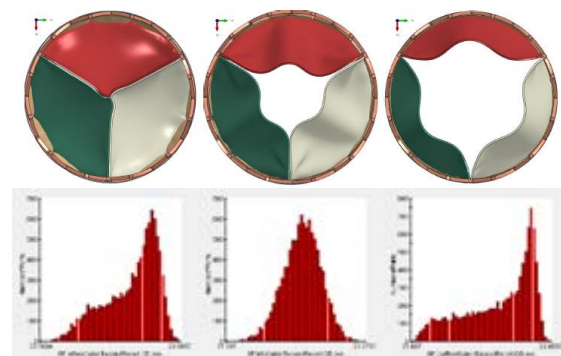


Figure 2

4. References

1. ASME V&V 40 - 2018
2. Tina Morrison (2018). How Simulation Can Transform Regulatory Pathways.
3. FDA (2021). FDA-2021-D-0980.
4. Viceconti et al., (2021). DOI: /10.1016/j.ymeth.2020.01.011
5. EU Horizon 2020. SC1-DTH-06-2020

Acknowledgements:

The authors would like to thank the Horizon 2020 (Grant no: 101017523) for providing financial support to this project.



VERIFICATION AND VALIDATION OF TRANSCATHETER HEART VALVE IMPLANTATION IN A VIRTUAL HUMAN COHORT

Chiara Catalano (1), Zahalka Omar (2), Turgut Tahir (2), Götzen Nils (2), Salvatore Pasta (1,3),

1. University of Palermo, Italy; 2. 4RealSim, Netherlands; 3. IRCCS ISMETT, Italy

1. Introduction

Assessing computational modelling credibility is relevant for developing safe and reliable in-silico clinical trials for testing medical devices. This study shows an example of the framework applied for verification and validation (VV) in transcatheter aortic valve implantation (TAVI) using current regulatory standards.

2. Materials and Methods

A master VV plan was developed according to ASME VV40. The intended use of patient-specific modelling was to simulate the acute/short term behaviour of SAPIEN 3 device in humans. The context of use (COU) and the model risk assessment (relevant parameter changes <1%) were defined. The VV of the TAVI simulation is based on hierarchical approach including the analysis of both the device and the patient-specific model. The model form, the model input, the comparator, testing conditions and assessment output comparison were defined.

The VV analysis was developed for a group of n.20 patients underwent TAVI with the SAPIEN 3 Ultra THV (Edwards Lifesciences, USA). Clinical data and imaging data were collected before and after TAVI. For all patients, ECG-gated CT scans were collected at systolic and diastolic cardiac phases. This was performed for both pre and post-TAVI procedure.

Semiautomatic thresholding was used to reconstruct the aortic wall while fully-automatic segmentation was done for the calcific plaques. Native valve leaflets were segmented using anatomic landmarks and surface modelling as done previously [1]. Different meshing approaches and element type were investigated. An inverse method was developed to determine material properties in a patient-specific fashion.

3. Results and Discussion

Model verification was performed for each structural level and included the discretization error (DE), numerical code verification (NCV) and numerical solver errors (NSE). Rigor assessment was based on the relative error (RE). Optimal element size was calculated using the convergence index, with errors kept <1% in all cases. Triangular and tetrahedral shell elements were better than quadrilateral and brick elements (eg, RE=0.76% for S3 vs RE=1.25% for S4 for the aortic wall). Similarly, prismatic elements were optimal for native valve leaflet modelling than structured and unstructured solid elements. For NCV, the LaPlace law was used as analytical solution to verify the aortic wall model solution. For the native valve leaflets, the stress analysis of native valve leaflet was verified against that of the analytical solution of the cantilever beam (RE=0.77%). For NSE, the influence of penalty factor, mass scaling and other solver parameters were evaluated and kept with RE<1%.

Both the pre- and post-TAVI validation was performed. For pre-TAVI, the orifice area of stenotic valve leaflet and aortic wall strain were used for validation. For post-TAVI, the model output parameters were the effective orifice area, peak maximum gradient and paravalvular leakage as measured by both echocardiography and post-TAVI CT imaging. For the pre-TAVI scenario, the relative errors between model output and clinical data were in the range of 0.08% to 5.86% (2.78% ± 4.50%) for the n.20 patients.

5. References

1. Pasta et al, Artificial Organs, 2017 Sep;41(9):E92-E102

Acknowledgements:

The authors would like to thank the Horizon 2020 (Grant no: 101017523) for providing financial support to this project.

HOW LARGE SHOULD A VESSEL WALL TEST SPECIMEN BE?

Joey Wolffs¹, Marta Alloisio², T.Christian Gasser^{2,3}

1.Eindhoven University of Technology, The Netherlands; 2.KTH Royal Institute of Technology, Sweden; 3.University of Southern Denmark, Denmark;

1. Introduction

Abdominal Aortic Aneurysm (AAA) remain a leading cause of disability and death worldwide [1], and its treatment is a major health care challenge with enormous socioeconomic impact. No medication is known to prevent AAA from rupture, the success in slowing-down AAA growth is moderate [2], and it remains difficult to predict AAA patients who require treatment. Whilst the biomechanical AAA rupture risk assessment showed promising results [3,4], it critically depends on information from experimental tissue characterization, data that remains to be inconsistent, see Fig. 1.

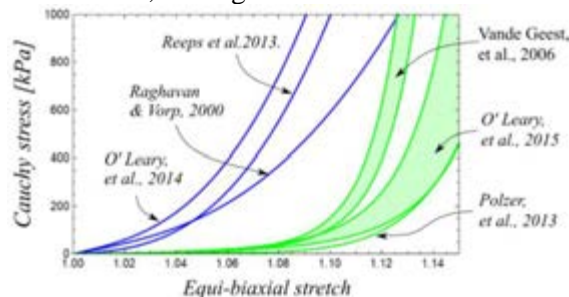


Figure 1: Stress-strain properties of the AAA wall at equi-biaxial tensions, as predicted by parameters acquired through simple tensile testing (blue) and biaxial tensile testing (green). Image taken from [5]

2. Materials and Methods

We followed the hypothesis that different test specimen dimensions are the underlying cause of the remarkable difference between the properties acquired by simple tensile testing and biaxial tensile testing of vascular tissue, see Figure 1. In total 15 porcine aorta samples of different dimensions have been tested at simple tension, and the acquired data was then consistently postprocessed. Specimens were tested along the circumferential and axial vessel directions, and Finite Element Method (FEM) models of the test specimens have been used to explore the implications of specimen dimensions.

3. Results

Fig. 2 illustrates the decrease of the tissue stiffness at decreasing width of the test specimen, a trend also underlined by results from FEM simulations.

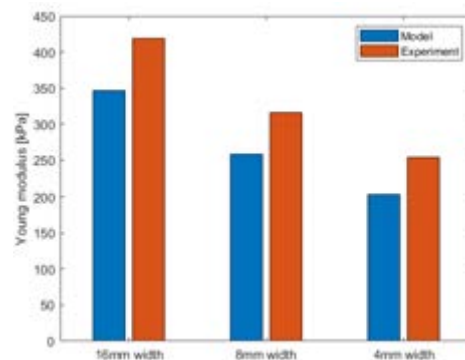


Figure 2: Tissue stiffens at 37.5% deformation as a function of the width of the test specimen. Red: Experimental tissue properties in axial direction. Blue: Results with an isotropic FEM model.

4. Discussion and Conclusions

The preparation of test specimens induces mechanical trauma, an effect that has not attracted much attention in the community. Our results indicate that aorta wall samples should have a width of appr. 2.0cm to acquire representative tissue properties. Simple tension specimens are used to be thinner, which might explain the difference seen in Fig. 1.

5. References

1. J Gollidge, Nat. Reviews Cardiology 16, 2019.
2. TP Singh, et al. Eur. J. Vasc. Endovasc. Surg. 64, 2022.
3. L Kubicek, et al. Eur. J. Vasc. Endovasc. Surg. 58, e306-e307.
4. TP Singh, et al. J. Am. Heart Assoc. 10, e019772.
5. TC Gasser, et al. Int. J. Nume. Meth. Biomed. Engrg, e3587, 2021.

Acknowledgements:

Financial support through the project grant No 2020-04447 from the Swedish Research Council.

C⁴BIO IN DEPTH: PROPAGATION OF VARIABILITIES AND UNCERTAINTIES IN PORCINE AORTA UNIAXIAL TENSILE TESTING

Heleen Fehervary (1,2), Klaas Vander Linden (1), Nele Famaey (1,2)

1. *Biomechanics, Dpt. Mechanical Engineering, KU Leuven, Belgium;*
2. *FIBER, KU Leuven Core Facility for Biomechanical Experimentation, Belgium*

1. Introduction

The lack of testing standards for biological tissue testing not only complicates the comparison of test results among different research groups, but also the assessment of data quality required for the regulation of in silico medicine. C⁴Bio is a community challenge aiming to address this problem by developing consensus testing protocols and reducing the variability currently present in testing protocols and results [1]. The results of the first and second test campaign show a large variability in the resulting stretch-stress curves within and between research groups worldwide. The goal of this abstract is to improve our understanding of the variabilities and uncertainties present throughout the complete testing protocol and their propagation into the final test results.

2. Materials and Methods

Experimental stretch-stress curves as obtained in the C⁴Bio test campaign on uniaxial tensile testing of porcine aorta were reproduced analytically. A typical fiber-reinforced hyperelastic material model was assumed, and uncertainty and variability were included on the material parameters, stretch range and sample dimensions. This was done by fitting probability density functions to the experimental data of the synthetic (for uncertainty) and biological (for variability) samples of the second test round of the C⁴Bio campaign. Per created stretch-stress curve, the used input parameter was a superposition of the ground truth value and a measurement uncertainty, both sampled from the stochastic distributions. By repeating the process for 100 virtual samples, a stochastic distribution of the results was obtained.

The uncertainties and variabilities present in the simulation were altered to get an understanding of their effect on the results.

3. Results

As an example, Fig. 1 shows a scatterplot relating the sample thickness to the tangent modulus of the stretch-stress curve, for the actual experimental data of the campaign (left), and for the simulated results (right). On the right, the blue dots show a simulation where only uncertainty was considered, the red dots when only variability was considered, and then the superposition of both.

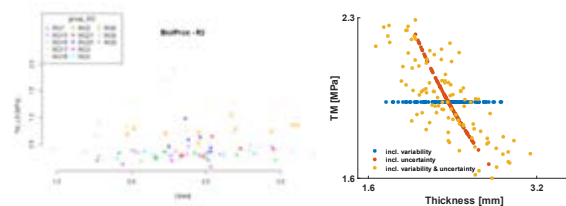


Figure 1: Scatter-plots relating sample thickness to tangent modulus.

4. Discussion and Conclusions

The results visualize how a combination of uncertainty and variability leads to great dispersion in the resulting output. Though this is expected, quantitative methods like these help us to improve our understanding of the effect of uncertainties and variabilities present in uniaxial tensile testing of biological tissues. Standardized (synthetic) materials with low variability are needed to fully appreciate the effect of a consensus methodology in terms of reduction of uncertainty.

5. References

1. <http://c4bio.eu>

Acknowledgements:

We thank all the participants of the C⁴Bio test campaign (see [1] for a complete list). This work was supported by a KU Leuven research project (C3-3E190409) and a junior postdoctoral mandate of Research Foundation-Flanders (FWO/12ZC820N).



VALIDATION OF FSI SIMULATIONS AGAINST A COMPLIANT AORTIC PHANTOM IN A HYBRID MOCK CIRCULATORY LOOP

Francesco Bardi (1,2,3), Emanuele Gasparotti (1), Emanuele Vignali (1), Miquel Aguirre (2), Stéphane Avril (2), Simona Celi (1)

1. BioCardioLab, Fondazione Toscana "G. Monasterio", Italy; 2. MINES Saint-Étienne, France 3. PrediSurge, France

1. Introduction

In the last decade, personalised computational fluid dynamics (CFD) models have been investigated as a tool to improve the understanding and clinical outcome of several cardiovascular diseases. In order to increase the credibility of CFD, a rigorous *in-vitro* validation process is required. In this study we use a novel Hybrid Mock Circulatory Loop (HMCL) to replicate physiological conditions in a flexible thoracic aortic phantom to validate a Fluid Structure Interaction (FSI) simulation.

2. Materials and Methods

The HMCL used for the experiment is described in [1,2] and is shown schematically in Fig 1. The principle is to set the boundary conditions in the same way as in a FSI simulation. A piston pump imposes a physiological flow rate at the inlet of the 3D compliant printed model. The outlets are connected to Hybrid-Units that are able to replicate the Windkessel effect. In order to track the deformation of the phantom, a camera system is synchronized with the piston pump. The FSI simulation was set up in CRIMSON. The fluid flow and the wall deformations were modelled using the coupled momentum method. The same material properties of the phantom, the same inlet flow rate and Windkessel parameters were used as boundary conditions. Moreover, in the FSI, the connections to the Hybrid Units were included as additional resistors and inductors. Three cardiac cycles were sufficient to achieve convergence.

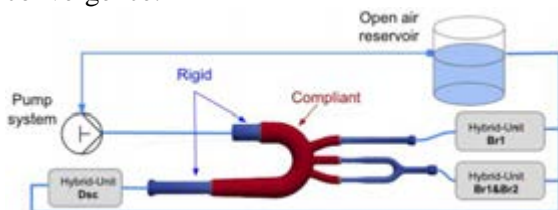


Figure 1: experimental setup.

3. Results

A comparison between the measured flow rates at the outlets and the results of the numerical simulation is shown in Fig. 2a. Similarly, in Fig 2b the diameter variation at the middle section of the aortic root is shown.

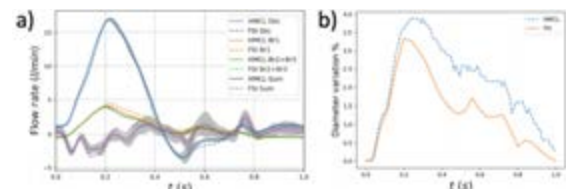


Figure 2: Flow rates (a) and diameter variation (b) comparison between experimental data and FSI results.

4. Discussion and Conclusions

Overall, a good agreement was found between the experimental and the numerical results. However, a detailed analysis of the results shows some differences. More specifically, the root mean squared error of the flow rate at Br1 was 0.2 l/min and the diameter variation was underestimated after the systolic peak. These discrepancies could be attributed to the fact that the wall is modelled as a linear elastic membrane. For these reasons, as a future development it would be worth to adopt an ALE [3] approach using more realistic material properties.

5. References

1. Bardi F. et al., IEEE TBME, 2022.
2. Vignali E. et al, ASAIO, 2022.
3. Campobasso R. et al., CVET, 2018.

Acknowledgements:

MeDiTaTe Project has received funding from the European Union's Horizon 2020 research and innovation programme under Grant Agreement 859836.



MATERIAL CHARACTERIZATION OF HETEROGENEOUS ATHEROSCLEROTIC ARTERIES

Su Guvenir Torun (1), Ali Akyildiz (1, 2)

1. Department of Biomedical Engineering, Erasmus Medical Center, the Netherlands

2. Department of Biomechanical Engineering, Delft University of Technology, the Netherlands

1. Introduction

Atherosclerotic plaque rupture in coronary and carotid arteries is a major trigger of myocardial infarct and stroke. High levels of pressure-induced mechanical stresses in plaques were hypothesized to correlate with plaque rupture [1]. Using correct material properties in the stress analyses is of critical importance for accurate stress prediction. We have recently developed a mechanical testing / computational modelling framework to acquire the component-wise mechanical properties of atherosclerotic arteries. We used our approach to obtain the heterogeneous material properties of atherosclerotic coronaries and carotids.

2. Materials and Methods

Atherosclerotic human carotids (n=5) and coronaries (n=5) were tested in 37°C PBS filled inflation testing setup. At each pressure step, the arteries were scanned with a high frequency ultrasound (US) system (Vevo 2100) and the acquired US radiofrequency data were processed by a cross-correlation technique for full-field plaque deformation measurements [2]. The multicomponent atherosclerotic artery compositions were obtained with a high field (7 Tesla) pre-clinical MRI system. The plaque components (fibrous intima, lipid core, arterial wall and calcification) of 23 plaque cross sections were segmented on US registered MR images, to create multi-component, 2-D, plane strain FE models (ABAQUS, ver. 2016) as Yeoh solids. Then, these models were used in the inverse finite element modeling (iFEM) approach, where the fibrous intima and arterial wall Yeoh constants (C1, C2, and C3) were iteratively predicted by the Deep Partitioning Tree Bayesian Optimization (DPTBO) [3], by minimizing the difference between the computed and experimentally measured plaque displacements.

3. Results

The optimization scheme of the iFEM reached the global minimum with a mean error of 3.8% in 133 iterations on average. The uniqueness of the results were confirmed with the inverted Gaussian Process (GP) model trained during the iFEM protocol. The Yeoh material constants obtained for the coronaries and carotids are shown in Figure 1.

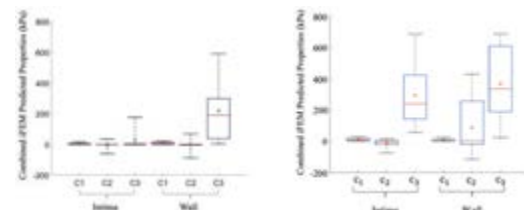


Figure 1: Yeoh material constants (C1, C2, and C3) determined for coronary (left) and carotid (right) atherosclerotic intima and wall.

4. Discussion and Conclusions

The developed iFEM approach successfully predicted component-wise material properties of intact atherosclerotic human carotids and coronaries ex-vivo under physiological-like loading conditions. The approach has the potential for in-vivo application.

5. References

1. Cheng et al., Circulation, 88: 1179-1187, 1993
2. Hansen et al., IEEE Trans. Med Im., 28.6:872-880, 2009.
3. Torun et al., IEEE Trans. Microw. Theory, 67:2128, 2019

Acknowledgements:

The authors would like to thank the European Commission's Horizon 2020 Research and Innovation Program under the Marie Skłodowska-Curie grant agreement #749283.

THE INFLUENCE OF GEOMETRICAL MEASUREMENTS ON MATERIAL PROPERTIES

John J.E. Mulvihill* (1), Michael T. Walsh (1), and Darragh R Walsh (2)

1. *Bernal Institute, University of Limerick, Ireland*; 2. *Holst Centre, TNO, Netherlands*.

*Corresponding Author: john.mulvihill@ul.ie

1. Introduction

There are no accepted standardised methods to mechanically characterise soft biological tissue. As biological tissue has inherent variabilities between person-to-person it is imperative we standardise the methods we use to properly compare and contrast studies and tissues. Furthermore, with access to human tissue being limited it is important that we come to an agreement on these methods.

There are an array of parameters and procedures that need to be decided upon, but none is more important than how we measure and calculate the geometrical parameters of the tissue being tested. As geometrical parameters are included in the equations for both Stress and Strain (i.e. width, thickness, and length) there is a need to understand how large a different varying this parameter may make. In this study we will show a variety of methods used across a range of tissues and the importance of using digital image-based methods for accurate and consistent measurements of geometry.

2. Materials and Methods

Mechanical Testing: a number of mechanical tests will be used from uniaxial and biaxial to pressure diameter across a variety of tissue types (i.e. atherosclerotic plaque, dura mater, urethra, aorta etc.). **Geometrical Testing:** a variety of methods will be shown such as vernier callipers, digital image processing, application of ink for image processing. **Finite Element (FE) Analysis:** Some aspects of this work will illustrate the effect of altered geometrical properties on the results of an FE model [1].

3. Results

The influence on tensile stress as a result of measurement technique ranged from 3.3% to 29.6% biological tissue [2]. Further, the gauge

length to width ratio altered the results of FE models between 6-16% by choosing an incorrect gauge length [1].

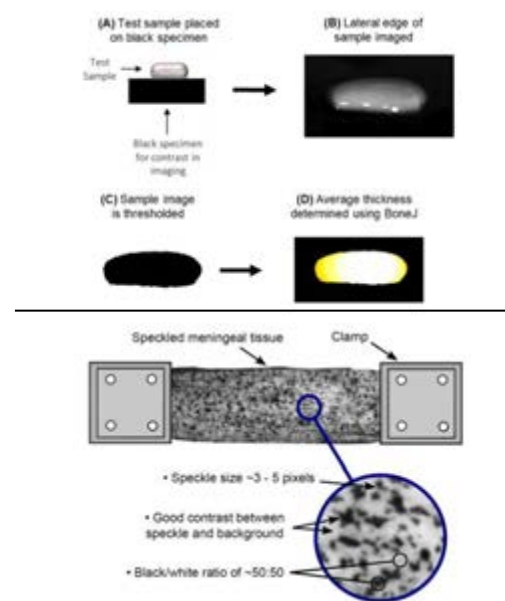


Figure 1: (Top) Digital image-based measurement of geometry prior to testing for the calculation of area. (Bottom) method of applying ink for digital image correlation for calculating local strain.

4. Discussion and Conclusions

We demonstrate the importance of accurately measuring the geometrical parameters of the tissue before and during testing. We show the accuracy and repeatability of digital-based measurements to remove user bias.

5. References

1. Mulvihill, J.J.E and Walsh, M.T. *BMMB*. 2012;12(5):975-985.
2. O'Leary, S., et al., *J. of Biomechanics* 2012;46(11):1955-60

Acknowledgements:

The authors would like to thank the Irish Research Council and Marie Curie Actions for providing financial support to this project.



VALIDATING THE MECHANICAL RESPONSE OF A MULTISCALE MODEL OF A KNITTED HERNIA IMPLANT

Baptiste Pierrat (1), Alice Siegel (2), Anicet Le Ruyet (2)

1. Mines Saint-Étienne, Univ Jean Monnet, INSERM, U 1059 Sainbiose, 42023 Saint-Étienne, France;
2. Medtronic – Sofradim Production, Trévoux, France

1. Introduction

Abdominal wall hernia (AWH) is a protrusion of the abdominal cavity contents through a defect in the abdominal wall. AWH repair is one of the most common surgeries worldwide and the use of mesh to reinforce the AW has become standard of care. Despite tremendous progress in the treatment, complications remain and reported recurrence rates are still high, up to 15-30% [1].

These meshes have been extensively modelled and characterized at a global scale, assuming a continuous medium [2]. However, such approaches cannot be used to relate a specific knitting pattern to a given mechanical response, which would be a significant step to manufacture implants with pre-defined mechanical behaviours. In this study, a knitted mesh was modelled at the yarn scale using the finite element (FE) method and validated at both local (yarn) and global (mesh) scales using an original optical measurement technique combined with mechanical tests.

2. Materials and Methods

A FE model of a single unit cell of the mesh was developed in LS-DYNA, featuring individual yarns and their contacts (Figure 1a). It was submitted to strip biaxial loading using periodic boundary conditions. The homogenised lineic force vs strain response was extracted from the model, together with local yarn kinematics.

Strip biaxial tensile experiments were performed on samples of the same mesh at a quasi-static rate. A speckle pattern was sprayed on the yarns using an airbrush. The specimens were backlit, and two cameras were used to capture stereo images, together with global tensile force and displacement. Post-processing and validation of the model was performed both at the homogenised scale and the yarn scale, using an original digital image correlation technique allowing local strain and curvature measurements of individual yarns (Figure 1b).

3. Results

Both experiments and FE model of the mesh generated a non-linear, anisotropic behaviour. Discrepancies between global numerical and experimental responses were explained by qualitative and quantitative comparisons at the yarn scale, and related to specific assumptions in the FE model (e.g. reference configuration).

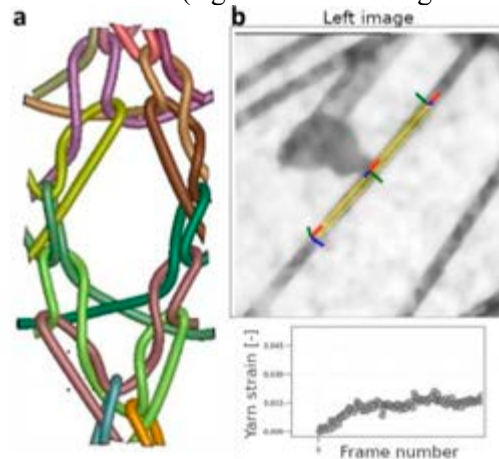


Figure 1: FE model of a unit cell of the mesh (a) and yarn-scale digital image correlation technique (b).

4. Discussion and Conclusions

Yarn scale results show that strains do not distribute evenly among the yarns, suggesting a strong reordering of the network under load. This results in a complex link between structure and function, which can only be apprehended by such multi scale approaches.

This study provides promising results to better understand how the load is transferred from the abdominal wall to individual yarns, depending on the knitting pattern. It is the first step towards the design of optimized meshes specifically adapted to their mechanical environment to better accommodate the physiology of the abdominal wall.

5. References

1. Parker et al. BJS Open, 5(2), 2021.
2. Röhrnbauer and Mazza, JMBBM, 29:7-19, 2014.



APPROACHING HUMAN GROUND RESIDUALS IN THE ANYBODY MODELING SYSTEM

Simon Auer (1), Franz Süß (1,2), Lukas Reinker (1,2), Sebastian Dendorfer (1,2)

1. Laboratory for Biomechanics, Ostbayerische Technische Hochschule (OTH) Regensburg, Germany; 2. Regensburg Center of Biomedical Engineering, OTH and University Regensburg, Germany

1. Introduction

Musculoskeletal models are sensitive to the given kinematics and the modelled boundary conditions and include forces acting on the hip to balance inaccuracies. In the AnyBody Modeling System (AMS) they are referred to as "Human-Ground-Residuals" (HGR). Although artificial forces like the HGR are necessary for numerical stability, they affect the models' actual results. Usually, the HGR are rather small and should not exceed 5% of the "net external force" [1]. Nevertheless, studies found HGR of about 70 %BW for gait movement simulations [2]. Therefore, this study aims to evaluate HGR minimization options of the AMS.

2. Materials and Methods

For this study, a counter-movement jump of one subject was recorded at 240 Hz using a marker-based (MMC) and an inertial (IMC) motion capture system. using two force plates recorded ground reaction forces (GRF) at 980 Hz. Kinematic data was used for a full-body inverse dynamics analysis with the AMS (v. 7.3). For MMC-driven models the measured GRF (mGRF) were used as well as the GRF predicted (pGRF) by the AMS. IMC-driven models only used pGRF. To minimize the HGR, one approach was to lower the kinematic low-pass filter's cut-off frequency (COF) from 12.5 Hz to 7.5 Hz. Another approach was to perform an optimization for the pGRF detection height and velocity limit using Python (v 3.7). Four configurations were investigated: MMC data with mGRF and COF at 12.5 Hz, IMC data with pGRF at 12.5 Hz COF, MMC data with optimized pGRF and 7.5 Hz COF and IMC data with optimized pGRF and 7.5 Hz COF.

3. Results

Out of the four models, the MMC-mGRF revealed the highest maximum HGR at 62 %BW (26.1% net external force) (Fig. 1a). The lowest maximum HGR appeared in the

optimized IMC-pGRF model with 17 %BW (7.6%) (Fig. 1d). In the IMC-pGRF they were at a 37% BW (13.5%) and in the optimized MMC-pGRF at 27 %BW (11.5%).

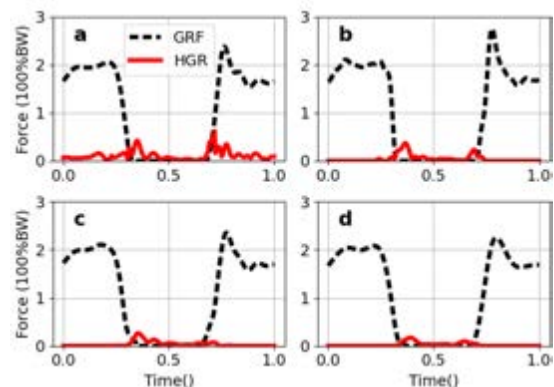


Figure 1: Resulting GRF (black) vs. resulting HGR (red) for (a) MMC, mGRF, COF=12.5 Hz, (b) IMC, pGRF, COF=12.5 Hz, (c) MMC, pGRF opt, COF=7.5Hz (d) IMC, pGRF opt, COF=7.5 Hz.

4. Discussion and Conclusions

The results show that a lower COF for the kinematic filter and optimized pGRF parameters can minimize the maximum HGR considerably. They also show that manually set pGRF parameters might be error-prone and that the COF of the kinematic filter should be chosen carefully to keep important kinematic information while decreasing HGR. Although the HGR are minimized by the presented approaches, they are still over the proposed 5% of the net external force [2]. Additionally, it is important to mention that the HGR are highest, when the model loses ground contact or regains it. And although the usage of pGRF bears the risk that the HGR are transferred to the pGRF without actually being minimized, the pGRF here match the mGRF quite well.

5. References

1. Hicks JL, Uchida TK, Seth A, Rajagopal A, Delp SL; J Biomed Eng;137(2):p.020905 (2015).
2. Ojeda J, Martinez-Reina J, Mayo J; Multibody Syst Dyn;37(3):291-309 (2016)



COMPARISON OF TWO MODELS TO PREDICT VERTEBRAL FAILURE LOADS ON THE SAME EXPERIMENTAL DATASET

V. Allard (1, 2), C. Heidsieck (3), F. Bermond (2), C. Confavreux (1, 4), C. Travert (3,5), L. Gajny, 3, W. Skalli (3), D. Mitton (2), H. Follet (1)

1. Univ Lyon, UCBL, INSERM, LYOS 1033, France; 2. Univ Lyon, Univ. Eiffel, UCBL, LBMC UMR_T 9406, France; 3. Arts et Métiers Institute of Technologie, Institut de Biomécanique Humaine Georges Charpak, France ; 4. Service de rhumatologie Sud, Hospices Civils de Lyon, France, 5 CHU Pitié Salpêtrière France

1. Introduction

Models in literature are numerous but have been rarely applied on the same experimental datasets, restraining comparison between models [1]. Clinical use of finite element analysis requires a well-defined process. Consequently, this study compared two models of vertebral bodies including endplates, on the same experimental dataset and evaluated the intra-operator influence on the segmentation.

2. Materials and Methods

The experiments were obtained in a previous study [2]. The main characteristics are reminded below. Twenty-eight vertebrae were extracted from eleven donors (5 males and 6 females, 61-87 y.o.). L1-L3 vertebral bodies with endplates were resected at the pedicles, loaded to failure on the anterior part with PMMA embedded supports. Samples were scanned with a QCT scanner ICT 256 (Philips Healthcare; 120 kV, 1489 mA/s), at 0.39 x 0.39 x 0.33 mm resolution with a calibration phantom (QRM-ESP, QRM GmbH, Germany).

Two FE models were considered in this study: ENSAM' model [2]: after semi-automatic segmentation of the scan, hexahedron mesh was created using a mesh deformation technique preserving mesh quality and topologic consistency. Each element was assigned a density from calibrated CT, which was then converted into Young's modulus via the relationship from [3]. The experimental conditions were simulated using Ansys with a linear resolution. Failure load criterion was when 1 cm³ of contiguous elements reached a 1.5% strain.

Lyon's model developed by LYOS and LBMC [4]: A 1 mm³ quadratic tetrahedron mesh was created after manual segmentation. Specific density was assigned to each element and converted to Young's modulus using the relationship from [3]. Perfectly elasto-plastic

law with a yield strain of 0.7% was computed, using a failure criterion of 1.9% of total strain (Ansys) to acquire failure load.

3. Results

ENSAM and Lyon Model results are strongly correlated ($R^2=0.91$). Comparison to the experiments is in (Table 1), in terms of accuracy (mean of the difference between simulated and experimental failure load) precision (SD of this difference) and correlation.

	Mean (N)	SD (N)	R ²
ENSAM' model	216	340	0.96
Lyon's model	523	482	0.92

Table 1: difference between simulated and experimental failure load as mean and standard deviation, and determination coefficient

4. Discussion and Conclusions

Both models considered the same dataset and boundary conditions. While both results were close to experimental results, differences in performance could result from differences in segmentation process, mesh (hexahedral vs tetrahedral), material representation and failure criteria. Linear analysis did not decrease model accuracy. Comparison of the processes allows the verification and validation of the models which should be done to further strengthen the reliability of models for clinical application

5. References

1. Shileo and Taddei, 2021, Current Osteoporosis Reports 19, 1–11.
2. Choise et al. 2018, *J Mechanical Behavior of Biomedical Materials*, 87, pp. 190–196.
3. Kopperdahl et al. 2002, *Journal of Orthopaedic Research*, 20(4), pp. 801–8054.
4. Allard et al. 2021, *Comput Methods Biomech Biomed Engin*.doi.org/10.1080/10255842.2021.1978758

Acknowledgement.

The authors thank the ParisTech BiomecAM chair (COVEA and Société Générale) for their financial support



DEVELOPMENT OF A MODEL OF THE ABDOMINAL WALL: SENSITIVITY ANALYSIS AND EVALUATION OF THE PERFORMANCE

Arthur Jourdan¹ – Anicet Le Ruyet¹ – Alice Siegel¹ – Rohit Dhume² – Mark Palmer²

1. Medtronic Surgical Innovations, Hernia & Wound Management – Trévoux, France;

2. Medtronic Corporate Core Technologies, MN, USA

1. Introduction

Abdominal wall hernia (AWH) is a protrusion of the abdominal cavity contents through a defect in the abdominal wall. AWH repair is one of the most common surgeries worldwide. The use of warp-knitted textile meshes to reinforce the abdominal wall in hernia prevention and repair has shown improved clinical outcomes regarding recurrence rate and quality of life. The recurrence rate, however, still remains high¹, partly due to a lack of knowledge regarding the mechanics of hernia mesh-soft tissue interactions. Numerical models have the potential to provide deeper insights into the mechanical response of the repaired abdominal wall. The objective of this work was to analyze the sensitivity of a finite element (FE) model of the abdominal wall and to evaluate its performance with a goal of supporting upcoming clinical trials and guiding future device designs.

2. Materials and Methods

Model geometry was derived from human cadaver measurements and medical images. The finite element model was parametrized so that it could represent various patient profiles: BMI, muscle and connective tissue thickness, material properties, contacts, intra-abdominal pressure (IAP) and muscle contractility. Two different loading scenarios were simulated: (1) passive inflation of the abdominal cavity to represent, e.g., breathing, and (2) inflation followed by muscular contraction to simulate the Valsalva maneuver. Two designs of experiments (DOE) studies were conducted on both passive and active simulation to assess the contribution of each parameter on several model responses (e.g., shape, muscles displacement and stretch, force on midline). A comparison of the range of each response with experimental data corridors has been conducted.

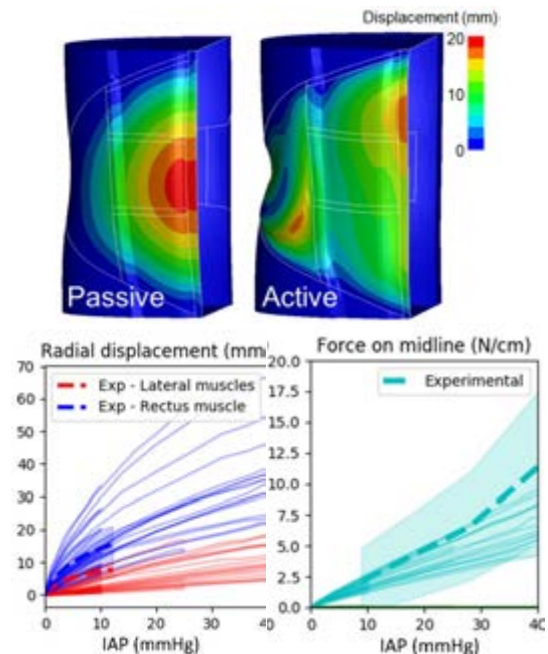


Figure 1: AW mode response w/o activation (above), Passive model predictions and experimental data vs. imposed IAP

3. Results

IAP was the most influential factor for breathing activities. Maximum tensile stress and muscle thickness were driving the response of the active simulations, in accordance with the literature. The mechanical properties of the connective tissue were the main contributors to the behavior of the medial part of the AW. The internal oblique muscle had a preponderant role on the passive response of the three lateral muscles. The overall model predictions were in good agreement with the experimental data (Figure 1).

4. Discussion and Conclusions

This work provides essential evidence for the verification and validation (V&V) of the model for future regulatory submissions. Next steps will be to include hernia meshes in the FE model to simulate the repaired abdominal walls.

5. References

1. S G Parker et al. BJS Open, Vol. 5, Issue 2, 2021

A VERIFICATION FRAMEWORK FOR FINITE ELEMENT MODELS TO PREDICT WEAR IN JOINT REPLACEMENTS

**Cristina Curreli (1,2)*, Sylwia Huebner (2), Santhosh Kumar Murugadass (3), Marc Horner (4)
and Marco Viceconti (1,2)**

1. Department of Industrial Engineering, Alma Mater Studiorum - University of Bologna, Italy;
2. Medical Technology Lab, IRCCS Istituto Ortopedico Rizzoli, Bologna, Italy;
3. Ansys Inc., Bengaluru, India; 4. Ansys Inc., Evanston, IL, USA.

* Correspondence details: cristina.curreli@unibo.it

1. Introduction

The finite element (FE) method is a powerful numerical technique used to predict the damage process in various medical devices, including joint replacements [1]. One of the first steps that should be performed before applying this computational technique to real-world problems is to assess the predictive capability of the models through verification and validation. A framework that can be used to establish the credibility of physics-based models for medical device applications was recently published [2]; however, “how to” instructions for modellers are lacking in the literature. The aim of this work is to present a methodology that can be used to verify FE wear models. To demonstrate the procedure's validity, a total knee replacement (TKR) model is used as a case study.

2. Materials and Methods

The FE wear model of the TKR was developed using the software Ansys and a three-dimensional geometry of a left knee implant (Zimmer Natural Knee II). The numerical wear simulations utilized Archard's Law to calculate surface wear. The boundary conditions (BCs) simulated the loading and kinematic conditions described in the ISO 14243–3:2014 standard for ten wear cycles (Fig 1.a). The verification workflow consists of code and calculation verification. Typical code verification analyses were conducted using Software Quality Assurance procedures and benchmark test cases to identify possible errors in the code and numerical algorithms. Calculation verification tests were specifically adapted to FE wear simulations, including time step and mesh size convergence analyses, kinematic consistency and sensitivity tests on contact and wear parameters.

3. Results

Three output quantities were considered for this study: volume loss, wear depth and contact pressure (Fig 1.b) in the medial and lateral contact side of the polyethylene tibial insert (TI). The results from the code verification tests showed that the source code and the implemented algorithms could be used to accurately reproduce benchmark solutions. Time step and mesh sensitivities studies showed different convergence trends depending on the selected quantity of interest. Coefficients of variation less than 8% were found for the predicted total wear volume by varying contact and wear solver parameters.

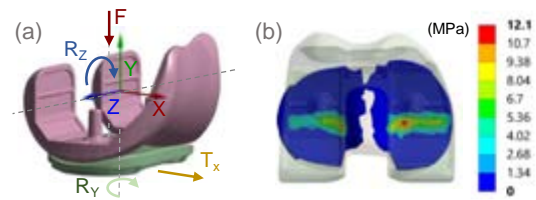


Figure 1: BCs defined for the FE model (a), predicted contact pressure map on the TI surface (b).

4. Discussion and Conclusions

This study proposes a verification framework to identify and quantify possible numerical errors in FE wear models outlining the importance of defining acceptable criteria based on the specific context of use. The proposed methodology can be used in the context of regulatory acceptability for the adoption of the modelling technique in clinical practice.

5. References

1. Viceconti et al, Ann Biomed Eng, 2021.
2. ASME Standard Subcommittee V&V 40, 2018.

Acknowledgements:

This study was supported by the H2020 ISW project (grant ID 101016503).



DESIGNING AND TESTING AN IMPLANTABLE SENSOR WITH IN-SILICO TECHNIQUES

Axel Seeger¹, Ingmar Stade¹, Ran Romberg¹, Jan Brüning², Leonid Goubergrits², Malte Rolf-Pissarczyk³, Michele Terzano³, Gerhard A. Holzapfel³ and Andreas Arndt¹

1. BIOTRONIK SE & Co. KG, 2. Charité-Universitätsmedizin Berlin, 3. Graz University of Technology

1. Introduction

Haemodynamic monitoring of heart failure (HF) patients with an implantable wireless pulmonary artery pressure sensor (PAPS) has been shown to reduce hospitalisation rate and improve patients' quality of life. Using the hemodynamic information acquired by the sensor physicians can optimize pharmacological treatment even without signs and symptoms of worsening HF.

We report on in silico methods used for design and testing of a PAPS with respect to potential adverse events such as device migration and vessel perforation.

2. Materials and Methods

Potential adverse events were defined using clinical evidence with similar devices and risk analysis techniques. Engineering metrics were derived which determine the probability of occurrence of the clinical adverse events. Device migration is connected to the axial retention force applied by the implant's fixation elements and disturbance forces such as gravitational, acceleration and fluid dynamic forces. Vessel perforation is determined by the radial contact force the fixation elements exert on the vessel wall.

We developed a computational model to investigate the interaction between implant and vessel comprising a structural mechanics model of the fixations and vessel. For the fixation elements we used a model for shape memory alloys. The vessel was modelled by generic geometries and subject-specific geometries. Subject-specific geometries (N=103) were obtained by segmentation of available CT scans of porcine and ovine animal models as well as humans. Constitutive properties of the vessel were assessed by experimental mechanical analysis of harvested vessel specimen for the 3 species.

The experimental data were used to fit a Holzapfel-Gasser-Ogden model. An explicit FEM solver is used to solve these nonlinear mechanical problems.

3. Results

We developed a method for virtual implantation of the sensor into the PA by inserting the sensor in crimped state within an implantation catheter and releasing the self-expandable fixation in the target implantation region. Average and peak contact force, contact pressure, contact length and axial retention force were determined during simulations.



Figure 1: PAPS in the pulmonary artery.

4. Discussion and Conclusions

Variations in device design, vessel geometries and material characteristics lead to an alteration of the output variables and provide a basis for conducting a sensitivity analysis in the next step. In a further step, we will perform experiments both in vitro and in vivo to validate the computational models. The validated models will then be used for iterative device design in virtual cohorts.

Acknowledgements: This project has received funding from the European Union's Horizon 2020 research and innovation programme under grant agreement N° 101017578.

ANALYSIS OF PATHOLOGICAL SKULL GROWTH PATTERNS

Maya Geoffroy (1,2,3), Maxime Taverne (2), Pierre-marc François (3) Roman Hossein Khonsari (2), Sebastien Laporte (1)

1. Arts et Métiers, IBHGC, France; 2. Hôpital Necker – Enfants Malades, France; 3. Bone 3D, France

1. Introduction

Craniosynostosis are rare diseases caused by the premature fusion of a cranial suture. The premature fusion of the metopic suture leads to trigonocephalies. The restrained cranial growth leads to a keel-shaped forehead. Metopic ridges are sometimes considered as mild cases with a premature metopic fusion, a mid-frontal ridge but a normal skull shape [1].

Morphology studies [2] only focus on geometries at certain timestep. Other methods are necessary to quantify the restrained and compensatory growth in trigonocephalies and confirm the normal growth of metopic ridges. Therefore, the aim of this study is to analyse the different growth trends of trigonocephalies (T), metopic ridge patients (M), and normal patients (N).

2. Materials and Methods

All trigonocephaly and metopic ridge patients evaluated at Necker Hospital between 2004 and 2012 were included. A control dataset was also developed. The CT scans were manually segmented, registered using a non-rigid iterative closest point algorithm and aligned in R [3] using a Procrust superimposition without scaling. A Two-block Partial Least Square (2B-PLS) analysis was conducted using the 3D geometries and the logged ages.

The results were analysed by comparing the shape score evolution in the three populations and extracting colormaps of the differences of skull shapes. The age period was chosen to include patients in all three populations.

3. Results

86 trigonocephalies, 18 metopic ridges and 74 controls from 3 to 14 months old were included. As expected, growth was more important before 7 months of age and decrease rapidly. Growth curves were similar for the three populations but metopic ridge skulls were smaller.

Growth is the most important in the mid-frontal and occipital areas for metopic ridges and controls, while trigonocephalies have a regular frontal growth (Fig. 1).

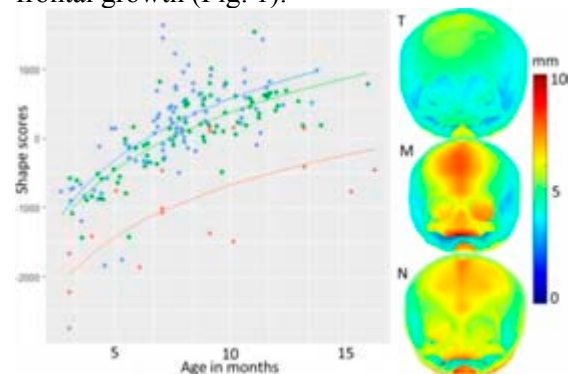


Figure 1: Growth curves (left) and 3 month old skulls with mapped distance differences between 3 and 7 months (right)

4. Discussion and Conclusions

In conclusion, this growth model leads to a clinical classification: metopic ridges are a variation of normality and growth in trigonocephalies is abnormally homothetic with a constant severity at the forehead.

The number of metopic ridges included was limited as there is no clinical reason to perform CT-scans. Increasing the dataset could be challenging but possible with collaborations. Finite element models could use statistical growth models for validation and help understand the anatomical risk factors leading to the differences in shape between metopic ridges and trigonocephalies.

5. References

1. Birgfeld C et al., J Craniofac Surg; 24:178-85 (2013)
2. Cho MJ et al., J Cranio-Maxillofacial Surg; 44:1259-65 (2016)
3. Bunn A; Vol.10 R Foundation for Statistical Computing. 11-18 (2017).

Acknowledgements:

Maya Geoffroy's PhD is funded by BONE 3D.

SPATIO-TEMPORAL ATLAS OF THE 3D BONE DENSITY DISTRIBUTION IN THE PROXIMAL FEMUR

Alice Dudle (1), Stefan Klein (2), Philippe Zysset (1)

1. ARTORG Center for Biomedical Engineering Research, University of Berne, Switzerland
2. Department of Radiology & Nuclear Medicine, Erasmus MC, Rotterdam, the Netherlands

1. Introduction

Osteoporosis induces a loss of bone mass with age, which results in a reduced bone strength and an increased risk of fragility fractures. The current diagnosis focuses on the average bone mineral density (BMD) obtained from 2D dual-energy x-ray absorptiometry (DXA) scans. Yet, little is known about the evolution of BMD distribution with age and its effect on bone strength. A first 2D spatio-temporal atlas of the proximal femur was developed by Farzi et al. [1] based on DXA scans. Using a similar approach, we propose a 3D atlas of the proximal femur based on quantitative computed tomography (QCT) scans.

2. Materials and Methods

129 QCT scans were collected by the Forensic Institute at the University of Bern. The dataset covered a wide age range (20-85 years), with an average of 49 years. A calibration phantom was included in the scan table and used to convert the CT intensities into BMD. All 258 proximal femurs were segmented semi-automatically and resampled to an isotropic resolution of 3 mm. Right femurs were flipped to match the orientation of left femurs, before registering all of them non-rigidly to a common shape template. Once all femurs were aligned, a voxel-wise quantile regression was computed, assuming a linear relationship between age and BMD. The median curves were then used to obtain the evolution of the BMD distribution.

3. Results

The median BMD distributions at age 20, 40, 60 and 80 are illustrated in Figure 1 for a coronal slice. We observe a significant (p -value < 0.01) decrease of the trabecular BMD values in the inter-trochanteric area, but no significant change in the cortical region. The relative BMD changes are summarized in Table 1 for three regions outlined in Figure 1.

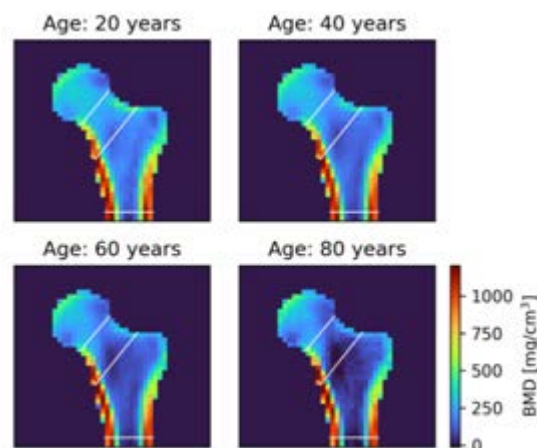


Figure 1: Median BMD distribution.

Table 1: BMD change in the proximal femur.

	BMD / year	BMD / 20 years
Fem. head	- 0.3 %	- 6.8 %
Fem. neck	- 0.6 %	- 11.1 %
Petrochant.	- 0.3 %	- 6.4 %

4. Discussion and Conclusions

The spatio-temporal atlas shows a BMD decrease in line with previous findings [1, 2]. While a 2D atlas only shows the projected density distribution, a 3D atlas contains the full spatial BMD distribution and can be used to estimate the evolution of bone strength with age, using finite element analysis models. Future work will refine the atlas with additional data, by allowing for non-linear BMD evolution and investigating the effect of gender and BMI.

5. References

1. Farzi M et al., IEEE Trans Med Imaging; 39(5):1359–68 (2020).
2. Keaveny T et al., JBMR; 25(5):994-1001 (2010).

Acknowledgements:

The authors thank the Forensic Institute for collecting the CT scans. This project was funded by a Synergia grant from the Swiss National Science Foundation (SNSF-183584).



EFFECT OF LABRUM SIZE ON CARTILAGE MECHANICS IN HIPS WITH CAM FEMOROACETABULAR IMPINGEMENT SYNDROME

Luke Hudson^{1,2}, Travis Maak³, Andrew Anderson^{1,2,3}, Gerard Ateshian⁴, Jeffrey Weiss^{1,2,3}

1. Department of Biomedical Engineering, University of Utah, Salt Lake City, United States

2. Scientific Computing and Imaging Institute (SCI Institute), Salt Lake City, United States

3. Department of Orthopaedics, University of Utah, Salt Lake City, United States

4. Department of Mechanical Engineering, Columbia University, New York City, United States

1. Introduction

In the presence of cam-type femoroacetabular impingement syndrome in the hip (FAIS), secondary labral tears are often observed, disrupting normal mechanical function and making labral repair a primary component of arthroscopic surgery [1]. An undersized labrum is thought to be an indication for labral reconstruction or augmentation with the rationale that an undersized labrum will result in higher cartilage contact stresses. However, there are no supporting biomechanical or clinical data [2]. The objective of this study was to assess the influence of labral size on the mechanical environment in the FAIS hip during walking using finite element (FE) modeling.

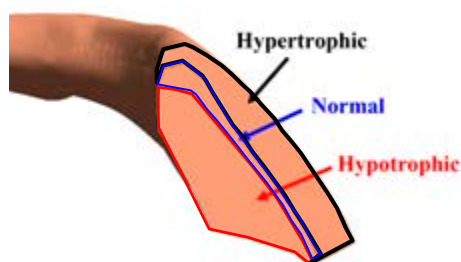


Figure 1: Cross-section view of the three labrum morphologies.

2. Materials and Methods

A patient-specific FE model of a hip with FAI was used. We examined three clinical morphologies: (1) an anatomically normal labrum, (2) hypotrophic labrum (<3mm in average thickness), and (3) hypertrophic labrum (>4mm in average thickness) (Fig. 1) [2,3]. Cartilage layers were represented as anisotropic hyperelastic materials with a continuous ellipsoidal fiber distribution of collagen fibers through the thickness. The labrum was modeled as transversely isotropic material with

circumferentially oriented fibers. Patient-specific kinematics from skin-marker motion tracking during gait and joint reaction forces collected by Bergmann et al. were incorporated into the finite-element models. All models were analyzed in FEBio (www.febio.org).

3. Results

A larger labrum resulted in greater load transfer across the labral surface throughout the gait cycle, but it did not produce any measurable changes in contact pressure at heel-strike. Small differences in 1st principal tensile strain were observed between the three cases, with the hypotrophic labrum model exhibiting the largest tensile strain within the same region for the cartilage (25.6%), followed by the hypertrophic (24.3%) and normal (20.2%) cases. Similarly, the max shear stress at the osteochondral interface was slightly higher for the hypotrophic labrum (13.1 MPa) followed by the hypertrophic (12.8 MPa) and normal (12.2 MPa) labra.

4. Discussion and Conclusions

These findings indicate that regardless of labral size within the cam-type hip, the mechanical loading on the acetabular cartilage is largely unchanged [4]. In the context of clinical interventions, this suggests that reconstruction of undersized labra may be unnecessary during arthroscopic surgery to correct FAI morphology.

5. References

1. Buzin SD, Orthop Res Rev 2022;14:121-132;
2. Ejnisman L, Clin Sports Med 2011;30(2):317-329;
3. Nwachukwu BU, Hip Int 2019;29(2):198-203;
4. Todd JN, Clin Orthop Relat Res 2022; 480(3):02-15

Acknowledgments: NIH #R01AR077636



QUANTIFICATION OF BONE MICROSTRUCTURE USING CLINICAL CT

Harry van Lenthe

KU Leuven, Belgium

Quantification of bone microstructure provides information about the structural integrity and quality of bone tissue. This information can be used to diagnose and monitor bone diseases such as osteoporosis and to evaluate the effectiveness of therapies for these conditions. Additionally, it can be used to study the effects of aging and other factors on bone tissue.

Accurate and unambiguous quantification of bone microstructure requires high-resolution three-dimensional imaging and, in the case of *in vivo* clinical applications, a low radiation dose combined with short acquisition time. High-resolution peripheral quantitative computed tomography (HR-pQCT) is currently considered the best technique for the quantification of bone microstructure. This imaging technique uses X-rays to non-invasively capture detailed three-dimensional images of bone tissue at a microscopic level. HR-pQCT is capable of providing information on bone mineral density, bone volume fraction, and bone microarchitecture. Additionally, it has been validated in several clinical trials, and has been used to study the effects of various diseases and treatments on bone microstructure.

Over the last years we have successfully explored the use of cone-beam computed tomography (CBCT), which combines fast scanning with of a large field of FOV at a high resolution and low radiation dose as an alternative to HRpQCT. We demonstrated that CBCT is able to quantify bone microstructural parameters with high accuracy. Proper reconstruction as well as adaptive segmentation proved to be key elements to quantify bone microstructural parameters, because they enabled segmentation of not completely homogeneous images [1].

A relatively new CT imaging modality is Photon Counting CT (PCCT). Whereas conventional energy-integrating CTs have scintillators that convert X-ray photons into

visible light, the PCCT detector material directly converts X-ray photons into an electrical signal. Therefore, individual pulses can be counted and by setting according thresholds, electronic noise can be cancelled out. Along with a reduced radiation dose, this greatly improves the contrast-to-noise ratio and spatial resolution [2].

With the aim to determine feasibility and accuracy of PCCT, we recently used PCCT (NAEOTOM Alpha, Siemens Healthineers) at an in-plane resolution of 0.17 mm and slice thickness of 0.1 mm to scan a cadaveric human wrist as well as five tibial plateaus. After scanning the wrist the eight carpal bones were removed and scanned *ex vivo* with μ CT (Skyscan 1272, Bruker), at an isotropic voxel size of 20 μ m. The medial plateaus were scanned with HRpQCT (XtremeCT II, Scanco).

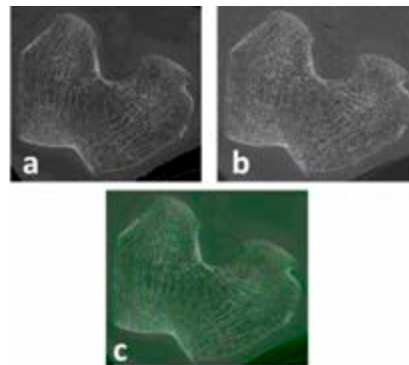


Figure 1: Cross-sectional image of the distal femur, scanned using PCCT (a) and HR-pQCT (b); c. overlay of the two images.

PCCT appears promising given the good qualitative agreement with HRpQCT (Fig. 1). Detailed analyses to evaluate the accuracy and precision of PCCT in the wrist and in the knee are ongoing.

References

1. Mys *et al.*, 2019, *J. Bone Miner. Res.* 34: 867-874.
2. Willeminck *et al.*, *Radiology* 289: 293-312, 2018.



THE APPLICATION OF HR-PQCT AND ADVANCED COMPUTATIONAL METHODS TO ASSESS PATIENT-SPECIFIC SKELETAL MECHANOBIOLOGY AND HEALTH

Danielle Whittier (1,2)

1. Institute for Biomechanics, ETH Zurich, Switzerland, 2. Osteoporosis University Clinic, Inselspital, Bern University Hospital, Switzerland.

Current clinical assessment of skeletal health relies on dual-energy x-ray absorptiometry, a two-dimensional imaging modality that provides a measure of areal bone mineral density (aBMD) [1]. Although aBMD is a reasonable surrogate for bone strength [2], it has diagnostic limitations for diseases such as osteoporosis, as bone strength is also dependent on bone structure at the macro- and micro-scale. High-resolution peripheral quantitative computed tomography (HR-pQCT) is an emerging imaging modality that can overcome these limitations as it is capable of providing novel information about bone microarchitecture *in vivo* at high resolutions, providing a snapshot of overall skeletal health [3].

The remarkable ability to resolve trabecular and cortical architecture with up to 61 μm resolution has advanced our understanding of the role bone microarchitecture plays in skeletal fragility [4]. When combined with micro finite element modelling, it is possible to obtain patient-specific biomechanical properties, allowing more direct measures of an individual's bone strength [5]. Further, time-lapse HR-pQCT imaging combined with computational techniques can be used to assess dynamic changes in local bone morphology, providing insight into patient-specific bone adaptation over time [6,7]. These computational techniques have allowed the development of numerous tools to assess patient-specific bone integrity, estimate fracture risk, and investigate mechanical changes during aging or fracture healing [4].

This session will showcase recent applications of HR-pQCT for patient-specific assessment of

skeletal health with focus on the development of computational techniques used to assess mechanical adaptation of bone microarchitecture on a patient-specific level, and finally highlight the insights gained from these techniques that may help future clinical decision-making.

References

1. Lorentzon M and Cummings SR. *J Intern Med.* 2015; 277(6):650-61.
2. Cheng XG, et al. *Bone.* 1997; 20(3):213-8
3. Boutroy S et al. *J Clin Endocrinol Metab.* 2005; 90(12):6508-15
4. van den Bergh JP, et al. *Osteoporos Int.* 2021; 32(8):1465-1485
5. Whittier DE et al. *Osteoporos Int.* 2020; Sep;31(9):1607-1627.
6. Walle M et al. *Front Bioeng Biotechnol.* 2021; 25:9:677985
7. Collins CJ et al. *Sci Rep.* 2022; 26;12(1):17960

Acknowledgements

I would like to thank members of the Laboratory for Bone Biomechanics at ETH Zurich and members of the Osteoporosis Centre at Inselspital, Bern University for their contributions. Further I would like to acknowledge financial support from the Natural Sciences and Engineering Research Council of Canada (PDF-557420-2021)

Thinking About Bone Loss on the ISS- An 18-month Perspective

Fernandez P.¹, Gordienko K.², Locrelle H.¹, Linossier M.¹, Lau P.³, Rittweger J.³, Vassilieva G.², Vico L.¹

¹ INSERM, U1059 – SAINBIOSE, Laboratory of Osteoarticular Tissue Biology, University of Lyon, France

² Russian Federation State Scientific Centre - Institute of Biomedical Problems of the Russian Academy of Sciences, Russia

³ Institute of Aerospace Medicine, German Aerospace Centre, Germany

Introduction

Prolonged exposure to the microgravity environment is known to elevate the rate of bone resorption in astronauts.^{1,2} Despite various forms of exercise countermeasures to regulate this rate of loss, the effect on bone continues to pose a significant challenge for both the present and future of long-duration spaceflight. While international space agencies continue to work towards developing a lunar habitat and eventually the colonisation of Mars, the unresolved consequences of spaceflight physiology on bone need to be understood so that effective countermeasures can be developed. For this reason, a longitudinal study (EDOS-2) examining the change in bone geometry and bone architecture is underway with a focus on determining reversibility, the quantity of deterioration, and identifying factors associated with intra-individual responses to spaceflight.

Materials and methods

8 male participants (48.11±6.05 years) had their volumetric BMD and microarchitecture parameters measured at the non-dominant distal radius and tibia using HRpQCT imaging (Xtreme CT, SCANCO Medical). Pre-flight measurements were taken at (1 or 2 months pre-flight, or at both time points) for a baseline reference and followed up for 1.5 years after landing. Post-flight measurements were obtained at the following time points: 1 day (R+1); 14 days (R+14), 3 months (R+90); 6 months (R+180); 12 months (R+360); and 18 months (R+540).

Results and discussion

Preliminary results demonstrated a decrease in cortical volumetric BMD from baseline values in both the distal radius and tibia upon return, with more pronounced differences in the tibia (Fig. 1). In addition, these values were also below pre-flight levels even 18-months later (Fig. 1). Cortical porosity levels followed a similar trend with elevated levels upon return and no signs of recovery to pre-flight values (Fig. 2). These preliminary results are consistent with a one-year longitudinal follow-up^{1,2} and further highlight that a return to baseline levels is currently not observed even after 18-months.

Fig. 1 Tibial Cortical Volumetric BMD

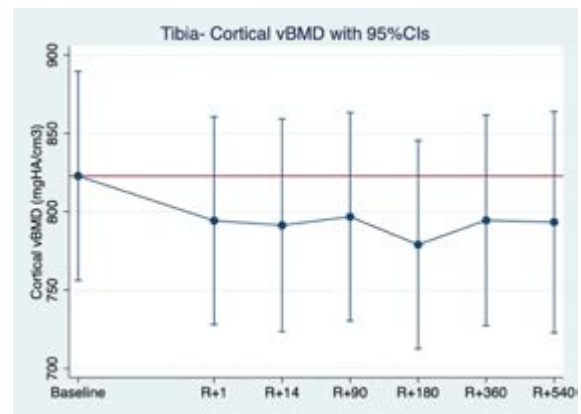
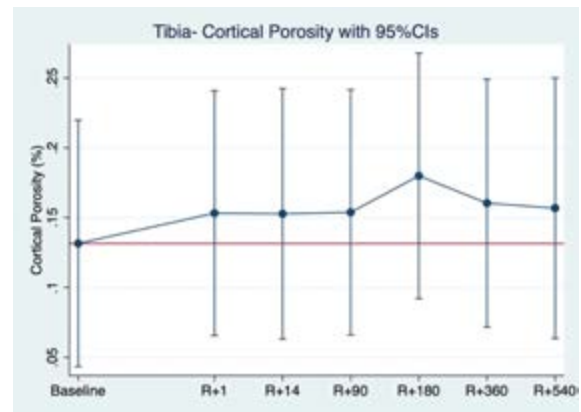


Fig. 2 Tibial Cortical Porosity



Conclusion

Preliminary data examining spaceflight effects on bone currently shows no signs of a return to baseline values even after 18-months.

Acknowledgements

We want to thank our partners at IMBP for their tremendous help and support. We would like to also extend our gratitude and appreciation to all the cosmonauts that took the time to participate and continue to do so in this study.

References

- [1] Vico L. et al., JBMR. 32:2010-2021, 2017
- [2] Gabel L. et al., BJSM. 54 : 196-203, 2021

CT-FREE NeRF VOLUME RECONSTRUCTION FROM SPARSE INTRA-OPERATIVE FLUOROSCOPY FOR SURGICAL NAVIGATION

Marcus Tatum, Geb W. Thomas, and Donald D. Anderson

University of Iowa, Iowa City, Iowa USA

1. Introduction

The use of fluoroscopy to track bones and/or bone fragments during orthopedic surgery can challenge a surgeon's ability to interpret the 3D pose of any but the simplest of bony anatomy. A novel biomechanical guidance system (BGS) for markerless intra-operative bone tracking that seamlessly integrates into the surgical setting was recently developed [1]. It utilizes 3D models from pre-operative CT, via 3D-to-2D registration methods, to update object poses based on 2D fluoroscopic images. However, in many cases where the BGS could be used, pre-operative CT images may be unavailable. Here we introduce a CT-free method to enable BGS use that leverages neural radiance fields (NeRF) to generate a continuous volumetric scene [2,3] from sparse intra-operative fluoroscopy.

2. Materials and Methods

For proof of concept, digitally reconstructed radiographs (DRRs) were created from pelvic CT data to serve as a stand-in for intra-operative fluoroscopy. DRRs and virtual C-arm positions were fed into an existing NeRF scene reconstruction system [2,3] (Figure 1). System

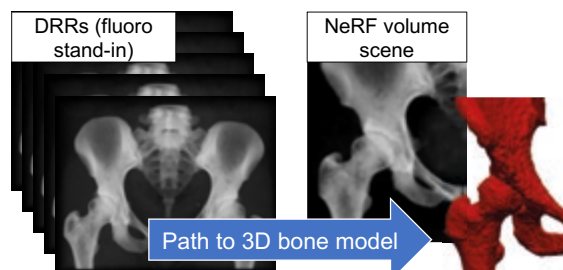


Figure 1. Procedure for generating 3D bone models from source fluoroscopy images (DRRs for present study).

training was allowed to proceed for up to 5 minutes. Bones were then segmented from the volumetric scene using commercial software. The accuracy of NeRF-derived segmentations was evaluated by comparison to gold-standard CT segmentation. The number of input DRRs was varied to study how this parameter

influences reconstructions. Sets of 12, 24, 36, and 72 images were acquired at regular intervals on two planar circular paths around the volume.

3. Results

Volume reconstructions were readily obtained using the NeRF scene reconstruction system. RMS errors of the NeRF-derived segmentations ranged from 1.14mm for 72 DRRs to 2.92mm when only 12 DRRs were used (Figure 2).

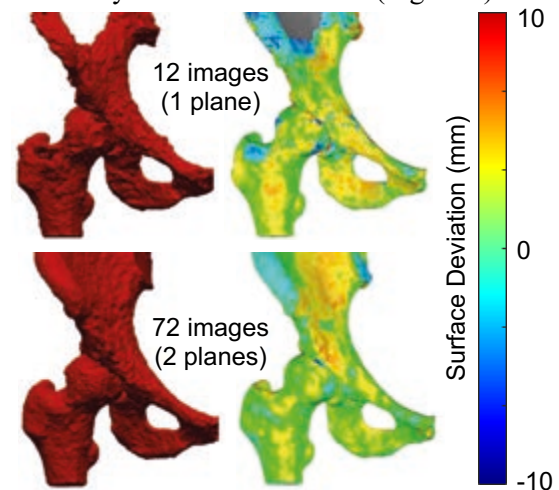


Figure 2. Segmentations of the pelvis are shown to the left, with corresponding surface deviation maps on the right. The top row is for the case of 12 DRR images, while the bottom row is for 72 DRR images

4. Discussion and Conclusions

CT-free NeRF volume reconstruction from sparse intra-operative fluoroscopy shows great promise for use in surgical navigation.

5. References

1. Willey MC, et al. J Orthop Res. 2022 Jun 7. doi: 10.1002/jor.25393. Epub ahead of print.
2. Mildenhall B, et al. ECCV 2020 conference: <https://arxiv.org/abs/2003.08934>.
3. Müller T, et al. CVPR 2022 conference: <https://arxiv.org/abs/2201.05989>.

Acknowledgements: This project was funded under grant #R18 HS025353 from the U.S. Agency for Healthcare Research and Quality.



STRESS DISTRIBUTION ANALYSIS IN THE LUMBAR FACET JOINT AFTER AN ARTHRODESIS OR AN ARTHROPLASTY

François Zot (1), Estelle Ben Brahim (2), Yann Ledoux (3), Michel Mesnard (3),
Cécile Swennen (2), Simon Teyssédou (2), Abdollah Yassine Moufid (2),
Arnaud Germaneau (1), Tanguy Vendevre (1, 2)

1. Institut Pprime, UPR 3346 CNRS – Université de Poitiers – ISAE ENSMA, Poitiers; 2. Department of Orthopaedic Surgery and Traumatology, University Hospital, Poitiers; 3. Institut de Mécanique et d'Ingénierie, UMR 5295 CNRS – Université de Bordeaux, Bordeaux, France

1. Introduction

Degenerative discopathies of the lumbar spine are frequent and disabling (low back pain, radiculalgia, etc.). Surgical arthrodesis procedures have provided a relevant response to this problem [1]. The significant hindsight of these techniques has revealed mechanical complications in the medium and long terms. This can be explained by the transfer of stress from the treated disc to the adjacent levels [2]. From this observation, a new approach to treat disc disease has emerged: arthroplasty, the advantage being the preservation of physiological mobility. The objective of this work was to study the stress distribution in the facet joint during physiological loadings after an arthrodesis or an arthroplasty.

2. Materials and Methods

To create the model, geometries were extracted from the segmented image of the CT scan of a human lumbar spine (L4-S1, male, 77 years old). Finite Element (FE) analysis was performed using Ansys (Ansys Mechanical Software, version 2022R1). Three models constituted of linear tetrahedral elements were developed: a first one corresponding to an intact spine was used as a reference; for the second and third models, one disc was replaced respectively by an arthroplasty prosthesis and by an arthrodesis implant. Articular cartilages were modelled between the facet joints of each level and homogenous bone material was assumed for vertebrae. Frictionless contact conditions were imposed between the facet joints, and perfect contacts (totally fixed) were imposed between every other bodies.

Loading was imposed by applying pure moments on the superior vertebra (+/- 5 Nm) for extension and axial rotation movements. The inferior part of the sacrum was fixed.

3. Results

The FE models showed that arthroplasty does not seem to modify the stress at the adjacent level in comparison with the intact spine, but the stress level was increased at the treated spinal unit (SU). Also, arthrodesis removes the stress at the operated level, but the stress was increased in the adjacent SU (Fig. 1).

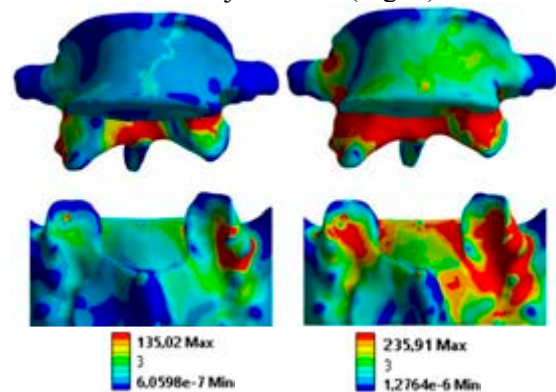


Figure 1: Stress distributions for the adjacent level: arthroplasty (left) and arthrodesis (right)

4. Discussion and Conclusion

This study provided data on the stress distribution in the facet joints by comparison of mechanical effects linked to an arthroplasty or an arthrodesis. This preliminary stress analysis revealed the advantage of arthroplasty compared to arthrodesis in the better stress distribution along the spine.

5. References

1. Tarpada SP, Morris MT, Burton DA. 2017. Spinal fusion surgery: A historical perspective. *Journal of Orthopaedics*. 14(1):134–136
2. Lee J, Park Y-S. 2016. Proximal Junctional Kyphosis: Diagnosis, Pathogenesis, and Treatment. *Asian Spine J*. 10(3):593.

Acknowledgements

The authors would like to thank the Nouvelle-Aquitaine region for its financial support.

COMBINED IMAGING, DEFORMATION AND REGISTRATION METHODOLOGY FOR PREDICTING RESPIRATOR FITTING

Silvia Caggiari^{1*}, Bethany Keenan², Dan L. Bader¹, Sam L. Evans², Peter R. Worsley¹

1. School of Health Sciences, University of Southampton, United Kingdom

2. School of Engineering, Cardiff University, United Kingdom

* Dr Silvia Caggiari, Clinical Academic Facility, School of Health Sciences, University Hospital Southampton, SO16 6YD, Email: Silvia.Caggiari@soton.ac.uk

1. Introduction

Respirators have been critical to protect healthcare workers and their patients from the transmission of COVID-19. However, these respirators are characterised by a limited range of size and geometry and are associated with fitting issues [1]. There is a paucity of technologies to support the fitting of these devices. However, Computer Aided Design analysis and registration has been used for other devices e.g., prosthetic sockets [2]. This study aims to corroborate a methodology of assessing FFP3 fitting against magnetic resonance imaging (MRI) in healthy individuals.

2. Materials and Methods

Eight volunteers were recruited, with institutional ethical approval. Their facial geometry pre- and post-respirator application was captured using MRI, and micro-focus computed tomography (μ CT) was used to image the internal geometry of the respirator. A methodology was implemented within the python module Ampscan [3] to automatically align, deform and register the internal geometry of the respirator onto the face geometry of each participant and predict its fitting (Fig. 1). The MRI data pre- and post-respirator application were used to estimate the soft tissue indentation and corroborate a sensitivity analysis on a deformation factor for the Ampscan module. The optimal respirator deformation was used to predict fitting against the participant's facial anthropometrics.



Figure 1: Schematic depicting the Ampscan workflow

3. Results

Results revealed a high degree of indentation of the respirator on the facial soft tissues (mean= 4.59 ± 0.93 mm). They also showed that the percentage of respirator area which provided an adequate seal ranged between 63% and 71%. When these values were compared against the facial anthropometrics, a statistically significant association ($p < 0.05$) was found against the bio-ocular width and the 1/3 lower facial height of the participants.

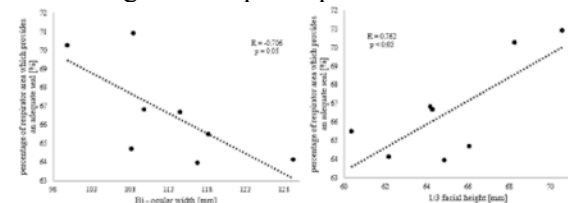


Figure 2: Relationship between an adequate seal [%] and bi-ocular width (left) and facial height (right).

4. Discussion and Conclusions

Intelligent algorithms are increasingly being developed to characterise the interactions at the face-respirator interface. The present study demonstrated corroboration against known tissue deformations estimated using MRI. The development of fitting platforms could be used to support respirator selection.

5. References

1. TUC. Personal protective equipment and women. 2017.
2. Dickinson AS et al., J Rehabil Res Dev. 2016;53(2):207-18
3. Steer JW et al. J Open Source Softw. 2020;5:2060

Acknowledgements:

The authors would like to acknowledge the European and Physical Science Research Council (EPSRC) (Grant no: EP/V045563/1) for providing financial support to this project.

CORNEAL MECHANICS FOR THE EARLY DETECTION OF THE KERATOCONUS

Chloé Giraudet (1,2), Jérôme Diaz (2), Patrick Le Tallec (1,2), Jean-Marc Allain (1,2)

1. LMS, CNRS, Ecole Polytechnique, Institut Polytechnique de Paris, France;
2. Inria, France

1. Introduction

Cornea is a front part of the eye providing two thirds of its optical power through its lens shape. In keratoconus disease, the cornea shape is progressively altered to become conical, leading to optical aberration [1]. A late detection imposes a surgery, explaining the need of early diagnosis. However, keratoconus origin is not clearly determined [2]: it is associated both a cornea thinning and a decrease of the mechanical properties. Still, it is not clear which effect is the driving one.

We propose a numerical approach to try to answer this question and help in the early detection of the keratoconus.

2. Materials and Methods

We combined a multiscale model with a patient-geometry (see Fig.1) to simulate the mechanical response of corneas under pressure. The cornea behavior contains an isotropic contribution (matrix), and an anisotropic part (collagen lamellae). We use experimental observations [3,4,5] to determine the different mechanical parameters of a healthy cornea.

The keratoconus origin is studied by using first the geometry of keratoconic cornea with reference mechanical parameters, and second the geometry of healthy cornea with altered mechanical parameters. We compared the evolution with pressure of cornea curvature [6].

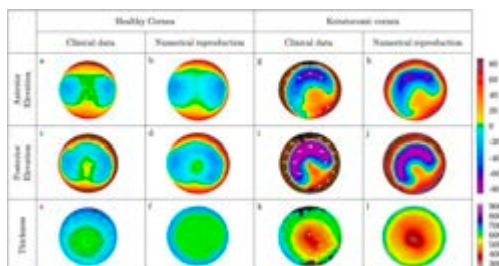


Figure 1: Elevation and thickness maps of healthy and keratoconic cornea (clinical and numerical reproduction, anterior and posterior). Scales in μm

3. Results

Mechanical properties of the cornea appear to be mainly controlled by the collagen response, and in particular its prestretch.

Keratoconic variations in SimK cannot be reproduced without changing the mechanical parameters, whatever the initial geometry. At the same time, changing the mechanical parameters is sufficient to recover the keratoconus response, even for a healthy geometry. We can also compute the full elevation maps, showing a cornea similar to a keratoconus at a very early stage.

4. Discussion and Conclusions

Our work shows that the keratoconic response is primary controlled by a weakening of the mechanical parameters. More precisely, it is the collagen stiffness which seems the most critical parameter. However, our modeling approach is very sensitive to few critical parameters, which are difficult to measure experimentally.

5. References

1. M.-R. Sedaghat et al., *OPHTH.* Volume 12 (2018) 1383–1390. doi: 10.2147/OPHTH.S169266
2. H. Najmi, *Int J Ophthalmol.* 12 (2019) 1775–1781. doi: 10.18240/ijo.2019.11.17
3. H. Aghamohammadzadeh et al., *Structure.* 12 (2004) 249–256. doi: 10.1016/j.str.2004.01.002
4. M. Winkler et al., *Investigative Ophthalmology & Visual Science.* 54 (2013) 7293. doi: 10.1167/iovs.13-13150
5. A. Elsheikh et al., *Journal of The Royal Society Interface.* 2 (2005) 177–185. doi: 10.1098/rsif.2005.0034
6. C.W. McMonnies et al., *Cornea.* 29 (2010) 764–770. doi: 10.1097/ICO.0b013e3181ca2b75

Acknowledgements:

We thank A. Pandolfi for the 3D mesh code, K. M. Meek and S. Hayes for the X-ray experimental data, and J. Knoeri and V. Borderie for clinical maps.

COMPUTATIONAL MODELING FOR CEREBRAL VASCULOPATHY IN EARLY CHILDHOOD IN SICKLE CELL DISEASE.

Weiqiang Liu (1), Lazaros Papamanolis (1), Christian Kassasseya (2), Suzanne Verlhac (3), Nour Bekezziz (2), Kim-Anh Nguyen-Peyre (2), Pablo Bartolucci (2), Irène Vignon-Clémentel (1)

1. Inria, Saclay Île-De-France, France; 2. Team Pirene, IMRB INSERM U955, Henri-Mondor Hospital and UPEC University, France; 3. Hospital Robert-Debré AP-HP, France

1. Introduction

Sickle cell disease (SCD) is an inherited disease associated with abnormal red blood cells. SCD-related cerebral vasculopathy (CV) appearing especially in young patients from 2 to 5 years old can lead to ischemic stroke, [1]. The main risk factors for developing CV are anemia and high arterial velocities in the distal part of internal carotid artery (ICA). Such high velocities are clinically evaluated by the time-mean of maximum velocity (TMMV) measured by Doppler ultrasound [2]. We investigate the hemodynamics differences in SCD patients across age based on CFD 3D-0D simulations.

2. Materials and Methods

The ICA with cerebral branches is segmented from MRA images, as shown in Fig.1. 3D blood flow simulations with mean inlet flow rate 5 mL/s are performed for 15 patients: 5 patients under 5 years old (UF), 5 patients from 5-18 years old (OF), and 5 adult patients (AD). TMMV and averaged Dean number are calculated in different arterial regions of ICA.

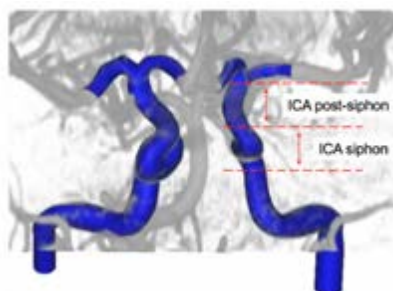


Fig 1: Patient-specific ICA model (blue) embedded in angiography data (grey).

3. Results

TMMV values in the OF and AD groups are significantly lower (Student's t test) compared to the UF group in both the siphon (Fig. 2A) and post-siphon regions (Fig. 2B). TMMV values are strongly correlated with Dean number, with

higher correlation coefficients in the UF and OF groups than those of the AD group (Fig. 3).

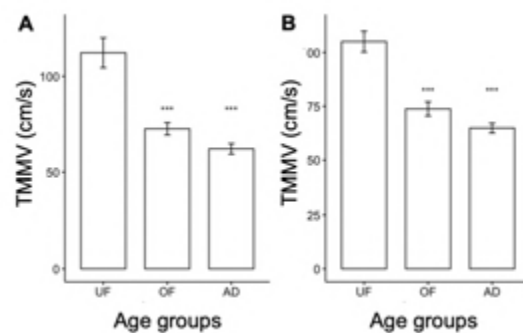


Figure 2: TMMV results per age group in two arterial segments: A. siphon region, B. post-siphon region. (***: p-value < 0.001)

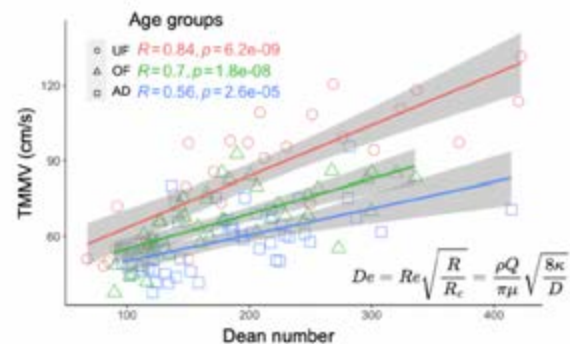


Figure 3: TMMV correlation with Dean number.

4. Discussion and Conclusions

For a given flow rate, patients under 5 years old reach higher TMMV values compared to older patients (Fig. 2), explaining their higher risk of stroke. TMMV is strongly related with Dean number: high flow rate (Q), large curvature (κ), and small diameter (D) contribute together to generate high blood flow velocity. These results could lead to a better understanding of the pathophysiological mechanisms of CV.

5. References

- Gibbons, et al. NEJM. 330.20 (1994)
- Bernaudin, et al. Am. J. Hematol. 117.4 (2011)



3D FE MODELING OF THE LATERAL SEMICIRCULAR CANAL OF THE INNER EAR

Manon Blaise (1), Daniel Baumgartner (1), Anne Charpiot (1,2)

1. University of Strasbourg, ICube Laboratory UMR 7357, France

2. University of Strasbourg, University Hospital, ENT Department, France

1. Introduction

In vivo experiments on the movements of fluids and thin membranes of the inner ear remain out of reach due to the fragility of the samples and the invasiveness of the procedures. Yet, understanding these mechanisms would greatly assist specialists to diagnose and treat the onset of vertigo related to this peripheral sensor. To this end, we present the construction of a 3D finite element (FE) model of a part of the posterior labyrinth involved in the balance system: the lateral semicircular canal (SCC) with its gelatinous portion of interest, the cupula. The head acceleration sensor is based on the movement and thus the mechanical behavior of the cupula. This model was run to simulate a clinical routine. Comparisons with and without taking into account the fluidic compartment that surrounds the membranes were performed to verify the relevance of modeling this perilymphatic space, which has never been considered in other models [1-3].

2. Methods

The inner ear labyrinth is a complex structure that includes a membranous labyrinth inserted in a slightly larger bony labyrinth. Both are filled with waterlike fluids, endolymph and perilymph respectively. Special attention was given to the dimensions of the structures, so that the inner membranous part was built from a previous model based on MRI slices of a patient [4] and the outer bony part was then built following the atlas of Veillon et al. [5]. The whole continuously mesh results in 162,806 elements with 134,908 tetrahedra and 27,898 shell trias (Altair HyperWorksTM; Fig. 1). Among them, 125,190 tetrahedra are fluid elements. As an hydrogel, the cupula follows a viscoelastic behavior [1]. An axial head rotation at a speed of $\pi \text{ rad.s}^{-1}$ followed by an abrupt interruption in 100 ms was imposed to the

model (with and without the perilymph part) to simulate a baseline clinical examination.

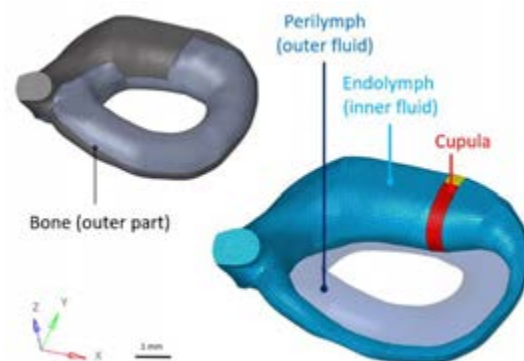


Figure 1: FE model of the lateral SCC: outer (top left) and inner (bottom right) labyrinth where the perilymphatic part appears by transparency.

3. Results

This model enhances a previous 3D model of a slice of the lateral SCC that includes the perilymph where the transversal displacement at the location of the sensory cells is of $48 \mu\text{m}$ [6]. Initial model validation uses the time it takes for the cupula to return to its resting position (time constant $T=6 \text{ s}$, [1]).

4. Discussion and Conclusions

To the best of our knowledge, this is the first 3D FE mesh of a SCC of the inner ear that models the boundary conditions of the membranous labyrinth, i.e. the perilymphatic compartment. This approach is necessary to simulate the modulations of inner ear fluids volume and pressure that occur in vestibular disorders such as endolymphatic hydrops.

5. References

1. Selva P et al., J Vestib Res; 19:95-110 (2009).
2. Shen S et al., Biophys J; 118:729-741 (2020).
3. Goyens J, Hear Res; 396:108071 (2020).
4. Chaney HV et al., J Transl Sci; 5(6):1-6 (2019).
5. Veillon F et al., Lavoisier Msp; vol. 1 (2014).
6. Blaise M et al., ESB 2022 conference; 2022.



TRANSVERSE FLOWS IN MODELS OF THE COCHLEAR DUCT VALIDATED BY 3D MICRO PARTICLE IMAGE VELOCIMETRY

Noëlle C. Harte (1,2), Guillaume P. R. Lajoinie (3), Michel Versluis (3), Marco D. Caversaccio (1,2), Dominik Obrist (1), and Wilhelm Wimmer (1,2)

1. University of Bern, ARTORG Center, Switzerland, 2. Bern University Hospital, Department of Otolaryngology, Head and Neck Surgery, Switzerland 3. University of Twente, Physics of Fluids group, MESA+ Institute for Nanotechnology, Technical Medical (TechMed) Center, The Netherlands

1. Introduction

The cochlea is a tiny, fluid-filled spiral structure in the inner ear that hosts our hearing sense. The current understanding of cochlear mechanics is incomplete, and the physiological role of the geometry remains unclear. We aim to investigate the influence of the cochlear geometry (i.e., curvature and torsion) on transverse flow arising during our hearing process. We analysed transverse flows under oscillating stimulation and compared results from computational fluid dynamics (CFD) with 3D micro particle image velocimetry (μ PIV).

2. Materials and Methods

We applied CFD to solve the Navier-Stokes equations for incompressible flow in simplified models, which feature torsion and curvature similar to human cochleae. To validate the computational results, we performed 3D laser μ PIV measurements in real-scale models (2 mm channel diameter). In our measurements, the laser scan rate was set to 100-600 Hz and a high-speed camera recorded images at a frame rate of 20-60 kfps. The spatial imaging resolution was $5 \times 5 \times 15 \mu\text{m}^3$. Axial velocity profiles, transverse flow patterns and magnitudes, and net motions were studied for different stimulation frequencies (0.125-512 Hz in simulations and 5-30 Hz in experiment).

3. Results and Discussion

The 3D μ PIV proved to be a promising tool to validate the CFD results, even in such small structures. We compared different analysis methods to reconstruct the transverse velocities, and the stroboscopic and dynamic approaches yielded the best results.

We obtained the following results from CFD and the PIV analysis: Curvature and torsion lead to different flow phenomena such as Dean cells

and saddle flow structures. Despite their small magnitudes, these transverse flow patterns were clearly identified in the PIV analysis for low oscillation frequencies (5, 10 Hz). We found that the effect of curvature decreased for higher Womersley numbers in the CFD result. Transverse velocities arising because of torsion, on the other hand, increased to more than 15 percent of the main flow magnitude. This is interesting because torsion was mostly neglected in previous cochlear studies. Furthermore, particles experience a net motion, which we validated using the stroboscopic approach. For example, the particles follow the streamlines of Dean cells in curved and helical ducts (Fig. 1). The observed net particle motion may provide new insight into biomedical mass transport in the inner ear.

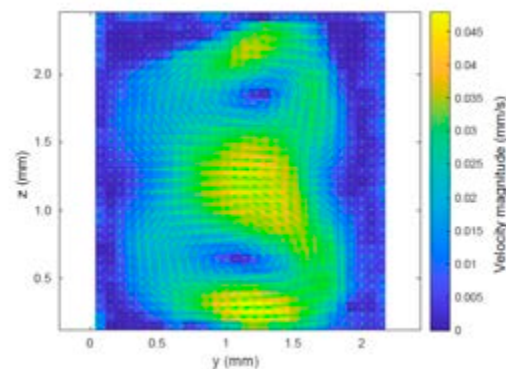


Figure 1: Dean cells as found by μ PIV.

Acknowledgements:

The authors would like to thank the Swiss National Science Foundation (Grant No. 205321_200850) and the 4TU Precision Medicine program supported by High Tech for a Sustainable Future for providing financial support to this project. We further thank the Burgergemeinde Bern, the Saly Frommer Foundation, and the FRIDERICUS Foundation for supporting the project.



A CORRECTED EJECTION FRACTION MEASURE CAN BETTER REPRESENT CARDIAC FUNCTION AND PREDICT OUTCOMES

Wei Xuan Chan (1,2), Amit Kaura (2), Yu Zheng (3), Anoop Shah (3),
Jamil Mayet (2), Choon Hwai Yap(1)

1. Dept of Bioengineering, Imperial College London, UK; 2. BHF Centre of Research Excellence, Imperial College London, UK; 3. National Heart and Lung Institute, Imperial College London, UK, 4. Dept of Biomedical Engineering, National University of Singapore, Singapore, 5. London School of Hygiene and Tropical Medicine, UK.

1. Introduction

During heart failure (HF), a wide range of remodelling of the cardiac geometry can occur [1]. The Ejection Fraction (EF) is a widely used measure for evaluating cardiac health and contractility function during HF, due to good prognostic and treatment indicating capabilities. However, geometric changes to the ventricle during remodelling is known to skew EF's representation of cardiac function [2], for example, during HF preserved EF (HFpEF), EF appears normal even though the heart is failing. We propose here a corrected EF (the EF_c) to resolve this, and show that it has improved prognosis properties for re-hospitalization.

2. Materials and Methods

The proposed EF_c is effectively equivalent to calculating the EF at the mid-wall layer rather than at the endocardial surface. EF_c can be obtained by applying a correction factor to EF computed from routine echo wall thicknesses and inner diameter measurements. A numerical model to calculate the conversion of myocardial strain to stroke volume was used to evaluate EF and EF_c's ability to represent cardiac function. Their ability to predict risk of heart failure admissions was evaluated via Cox-proportional regression models on a retrospective study population of 2752 individuals admitted with a request of a troponin test.

3. Results

Left ventricle (LV) hypertrophy increased EF while LV dilation decreased EF without a change to myocardial strain, but EF_c remained constant across such geometric changes. This was because radial displacements naturally elevated endocardial strain and caused deviation from overall LV strain, and this

deviation is geometry dependent. EF_c could statistically distinguish HFpEF patients from non-HF patients while EF could not. Both low EF and low EF_c were associated with high HF readmissions risks, but in the cohort with normal EF range (EF \geq 50%), predictive models using EF_c were significantly more accurate in predicting HF readmissions within 3 years, with ROC analysis showing 18.6% lower errors, and Net Classification Index (NRI) analysis showing 12.2% higher true positive and 16.6% lower false negative.

4. Discussion and Conclusions

Our study explained the mechanism for why EF can no longer effectively indicate cardiac function when the cardiac geometry changes during HF remodelling. Our modelling shows that our proposed corrected factor, the EF_c, could resolve this shortcoming, and we showed that this new measure have stronger prognosis values for predicting HF re-admissions, particularly for the group where EF appears normal. This is due to its ability to distinguish HFpEF from normal in this cohort. Since EF_c can be easily computed using existing echo measurements, it should be easy to implement clinically. Moving forward, we plan to test EF_c prognosis and drug indication capabilities in a larger dataset.

5. References

1. Katz DH, et al., Am J Cardiol 112, 1158-1164 (2013).
2. MacIver DH, et al. IJC Heart & Vasc. 7, 113-118 (2015).

Acknowledgements:

Funding is provided by BHF Centre of Research Excellence (RE/18/4/34215), BHF fellowships (FS/20/18/34972 and FS/19/17/34172).



INLET ASYMMETRY IN ACOMA ARTERY ANEURYSMS: COMPUTATIONAL VERSUS CLINICAL APPROACH

Sudhir B J (1,2), B.S.V. Patnaik (2), Santhosh K. Kannath (1), Shine S R (3)

1. Department of Neurosurgery, Sree Chitra Tirunal Institute for Medical Sciences & Technology Trivandrum, India; 2. Department of Applied Mechanics, Indian Institute of Technology, Madras, India; 3. Dept of Aerospace Engineering, Indian Institute of Space Science and Technology, Trivandrum, India

1. Introduction

Anterior communicating artery (ACOMA) aneurysms are difficult to treat surgically. The unique H-configuration with two inlets and two outlets warrants control over four blood vessels for safe surgical clipping. This configuration varies between individuals with asymmetric inlets and outlets [1]. Neurosurgeons decide on the side of surgical approach depending on the dominant inlet (A1 segment). Asymmetry of inlets is considered a predisposition to the development and rupture of such aneurysms [2]. We investigate the influence of asymmetric inlets on ACOMA in an attempt to decipher the pathogenesis and haemodynamic behaviour of ACOMA aneurysms.

2. Materials and Methods

A model of the part of the circle of Willis, with symmetric A1 inlets, the ACOMA and the outlets (A2 segments) is generated. The diameter of one of the inlets is progressively reduced and CFD studies are undertaken. Patient-specific ACOMA aneurysm models are generated from angiography images and classified into two groups with symmetric and asymmetric inlets. CFD studies are performed using Ansys Fluent by using patient-specific pulsatile inlet velocity. The haemodynamic characteristics predicted by the generic and patient-specific models are analysed.

3. Results

In the ideal geometric model, flow is cancelled in the ACOMA. As the constriction of one inlet A1 artery is increased, the flow through the ACOMA increases progressively from the dominant A1 to maintain a constant mass flow rate in the outlet A2 arteries. Higher velocity profiles are observed at the upper wall of the ACOMA at peak systole suggesting higher

haemodynamic stress. Wall shear stress (WSS) and its gradient increase at the contralateral upper region of ACOMA. Simulations performed on patient-specific models reveal a higher relative residence time (RRT), WSS divergence and oscillatory shear index (OSI) among aneurysms with asymmetric A1 inlets compared to co-dominant A1 inlets. Asymmetric inlet was associated with rupture status.

4. Discussion and Conclusions

ACOMA aneurysms evolve in response to haemodynamic stresses on the ACOMA and the ACOMA-A2 junction [3]. CFD studies have the potential to reinforce clinical decisions on surgical management by providing crucial haemodynamic information and rupture status prediction.

5. References

1. J. Shatri, S. Cerkezi, et al., Anatomical variations and dimensions of arteries in the anterior part of the circle of willis, *Folia Morphologica* 78 (2) (2019) 259–266.
2. Rinaldo, L., McCutcheon, et al. 2017. Relationship of A1 segment hypoplasia to anterior communicating artery aneurysm morphology and risk factors for aneurysm formation. *Journal of Neurosurgery* JNS 127, 89 – 95.
3. Cebal JR, Castro MA, Burgess JE, Pergolizzi RS, Sheridan MJ, Putman CM. Characterization of cerebral aneurysms for assessing risk of rupture by using patient-specific computational hemodynamics models. *AJNR Am J Neuroradiol.* 2005 Nov-Dec;26(10):2550-9.

Acknowledgements:

This work was supported by the Science and Engineering Research Board, Government of India, under the Scientific and Useful Profound Research Advancement (SUPRA) scheme (Grant No. SPR/2020/000298).



CLINICAL RISK ASSESSMENT AND MITIGATION OF POST-TAVR THROMBOGENICITY IN BAV USING IN SILICO MODELING

Salwa Anam (1), Kyle Baylous (1), Brandon Kovarovic (1), Ashraf Hamdan (2), Rami-Haj-Ali (3), Danny Bluestein (1)

1. Department of Biomedical Engineering, Stony Brook University, U.S.A.; 2. Department of Cardiology, Rabin Medical Center, Israel; 3. School of Mechanical Engineering, Faculty of Engineering, Tel-Aviv University, Israel

1. Introduction

Thrombotic events are persistent complications, associated with transcatheter aortic valve replacement (TAVR) procedure, which is a lifesaving treatment option for patients with severe aortic stenosis (AS). Flow-induced thrombotic events ensue from prolonged exposure of platelets to cyclic shear stress, which increases the risk of thrombus formation. Post-TAVR paravalvular leakage (PVL) increases these risks, and have a higher incidence in bicuspid aortic valve (BAV) patients. They were not approved for TAVR by the FDA until recently, due to the inherent mismatch between the TAVR device and BAV anatomy. As BAV patients tend to develop AS at an earlier age, the number of young TAVR candidates is projected to rise. TAV design optimization for improved hemodynamics can reduce TAVR associated thrombotic events [1]. The goal of this study is to use BAV patient-specific modeling to analyze the effect of PVL flow and TAV leaflet design on thrombogenicity, and mitigate them using valve design optimization.

2. Materials and Methods

Patient-specific finite elements model reconstruction and TAVR simulation of 3 anonymized BAV patients were conducted with both older (originally received by these patients) and newer generation self-expandable devices (Medtronic plc., MN). Computational fluid dynamics (CFD) analysis was then performed to assess PVL degree, location, and quantify stress accumulation (SA) on platelets flowing through the miniscule PVL channels during diastole. SA values of large population of flowing platelets were then compared between the older and newer devices for each case. In order to analyze the thrombotic potential of different TAV leaflet designs, 9 parametric valve geometries were developed.

Valve parameter optimization was performed in order to improve the hemodynamics using fluid structure interaction simulations. The risk of thrombogenicity associated with different designs was analyzed.

3. Results

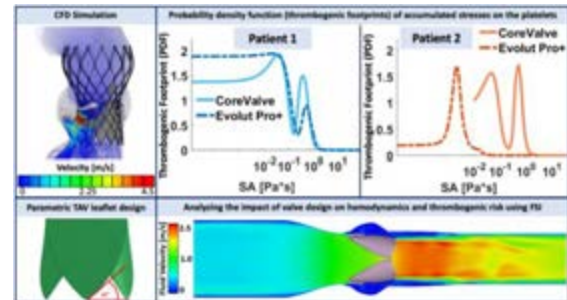


Figure 1: (Top row) CFD simulations comparing thrombotic footprints in older and newer generation cases in BAV; (Bottom row) hemodynamics analysis of a parametric valve model. In all the patients, newer generation device was associated with lower PVL and thrombotic potential. In patient 1 and 2 older generation device cases showed higher SA (Figure 1).

4. Discussion and Conclusions

Current study implements in-silico modeling techniques to assess the risk of PVL flow-induced thrombogenicity in complex BAV patient anatomies and analyze the impact of TAV leaflet designs on hemodynamics and associated risk of thrombogenicity, addressing an unmet clinical need and gaps in previous studies. This highlights the utility of utilizing advanced and meticulous in-silico modeling techniques for mitigating life-threatening post-TAVR clinical complications.

5. References

1. Kovarovic, B., et al. (2022) ASME. J Biomech Eng.; 144(6): 061008

Acknowledgements:

Funding-NIH-NIBIB U01EB026414 (DB).
Industry Partners: ANSYS, Simulia LHP



COMPLIANCE-MATCHING AORTIC GRAFT: COMPUTATIONAL MODELING AND MULTI-PARAMETER OPTIMIZATION

Georgios Rovas, Vasiliki Bikia, Nikolaos Stergiopoulos

École Polytechnique Fédérale de Lausanne (EPFL), Switzerland

Corresponding author: Georgios Rovas (georgios.rovas@epfl.ch)

1. Introduction

Synthetic vascular grafts have been widely used in clinical practice for more than 50 years. Despite their success, they remain significantly less compliant than the native aorta; a phenomenon commonly called compliance-mismatch. The reduction in compliance causes serious post-operative complications, including hypertension and myocardial hypertrophy.

2. Materials and Methods

To overcome this phenomenon, we designed a novel aortic graft consisting of a standard graft and a flexible nickel titanium outer layer. We simulated the multi-layer design using a finite element method (FEM), for which we derived the properties of the materials experimentally. We fabricated a prototype graft and measured its diameter in vitro, in a hydraulic circuit at different levels of pressure. Then, we validated the FEM model by comparison of the pressure-diameter curve with the experimental data.

Our goal was for our design to reach a predefined value of compliance at 100 mmHg that corresponds to the aortic compliance of a healthy adult. By utilizing the validated model, we performed multi-parameter optimization with a gradient descent method. We selected the design parameters with major impact on compliance, and we used a 6-dimensional Box-Behnken design. The optimization process was completely automated with minimal user input.

3. Results

The FEM model predicted the internal diameter of the novel graft with a $RMSE = 0.033$ mm over the expected pressure range (50-180 mmHg). This resulted in a $RMSE = 0.02$ mm² mmHg⁻¹ in the estimation of the area compliance over the

same pressure range. The prediction accuracy was additionally evaluated by linear regression analysis (Fig. 1). The optimization showed no further improvement after 9 cycles, resulting in an optimal compliance of 0.8 mm² mmHg⁻¹ at 100 mmHg.

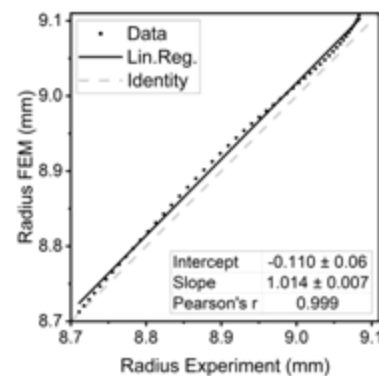


Figure 1. Linear regression analysis between the FEM-predicted graft radius and the experimental value at 50-200 mmHg of internal pressure. Reported values \pm 95% confidence intervals.

4. Discussion

To the best of our knowledge, there are no other aortic grafts with matching compliance to healthy human aortas, while maintaining the durability of commercial grafts. Consequently, our graft could potentially reduce the post-operative complications that are partly caused by the excessive stiffness of the existing grafts [1, 2]. The optimization procedure could also be used to produce grafts that optimally suit the compliance of each individual patient.

5. References

1. C. Spadaccio et al., *Journal of Cardiovascular Translational Research*. 9, 334–342 (2016).
2. B. Lucereau et al., *European Journal of Vascular and Endovascular Surgery*. 60, 773–779 (2020).



CT-BASED COMPUTATIONAL FLUID DYNAMICS ANALYSIS OF THE LEFT VENTRICLE ANEURYSM HEMODYNAMICS AFTER SURGERY

Leonid Goubergrits (1), Lukas Obermeier (1), Katharina Vellguth (1), Moritz Wiegand (1), Olena Nemchyna (2), Adriano Schlieff (1), Jan Bruening (1), Titus Kuehne (1), Christoph Knosalla (2), Natalia Solowjowa (2)

1. Institute of Computer-Assisted Cardiovascular Medicine, Charité-Universitätsmedizin Berlin, Germany; 2. Department of Cardiothoracic and Vascular Surgery, German Heart Center Berlin, Germany

1. Introduction

Surgical restoration of the left ventricular (LV) aneurysms aims to restore physiologic LV function and shape by volume reduction. Our purpose is to integrate the cardiac computed tomography (CCT) based analysis of LV hemodynamics by using computational fluid dynamics (CFD) in clinical decision making and treatment planning.

2. Materials and Methods

CCT data of 10 patients (mean age: 59 ± 12.3 years, 3 females, mean BSA: 1.88 ± 0.23 m²) before and after surgical reconstruction procedure were acquired using a dual-source multi-slice spiral CT scanner (Somatom Definition Flash, Siemens Healthcare GmbH, Germany) with a spatial resolution of 0.5 mm x 0.5 mm x 0.7 mm. One heart cycle was always resolved by 10 phases. These data were used to reconstruct end-diastolic and end-systolic LV anatomy using the visualization software ZIB-AMIRA. Finally reconstructed geometries were used to analyse anatomical changes due to the treatment and to simulate intracardiac flow by using prescribed motion CFD with a commercial solver STAR CCM+ according to the earlier developed pipeline [1].

3. Results

After treatment the NYHA class improved from 3 ± 0.45 to 1.3 ± 0.47 , whereas mitral valve regurgitation reduced from 1.1 ± 0.87 degree to 0.5 ± 0.52 . The end-diastolic volume reduced significantly from 228 ± 76.4 ml to 136 ± 37.0 ml. The stroke volume reduced no significant from 60 ± 21.9 ml to 56 ± 16.5 ml thus meaning significant increase in ejection fraction. We found individual changes in the LV shape (e.g. sphericity index), contractility patterns, mitral

valve opening area, peak-diastolic inflow and peak-systolic outflow rates. These are all parameters, which affect the intracardiac flow. In most cases a recovered E-wave blood flow with the mitral valve inflow jets, which forms a distinct vortex ring and penetrate to the apex in diastole was found. Thus, this flow results in an improved washout after the surgery (see fig. 01).

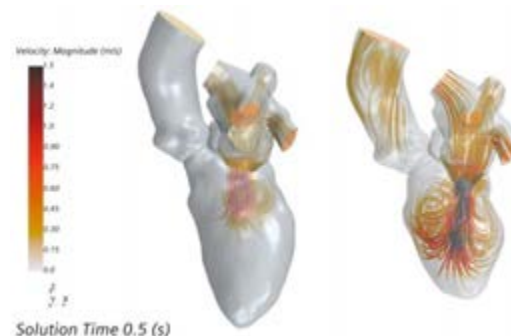


Figure 1: Exemplary change of the LV flow after the surgery (filling phase).

4. Discussion and Conclusions

The proposed CCT-based CFD analysis of intracardiac flow allows to quantify the hemodynamic impact of the LV surgical restoration. The method can be applied to routine CCT data of common quality and represents a fair balance between model accuracy and computational as well as human expenses.

5. References

1. Obermeier L et al. Front Cardiovasc Med.;9:828556 (2022).

Acknowledgements:

The authors would like to thank the DFG for the funding of the grant (Nr. 465178743 SPP2311).



COMPUTED FFR BASED ON WINDKESSEL MODELS WITH DIFFERENT NUMBER OF ELEMENTS

M. Fernandes (1,2), C.F. Castro (1,2), L.C. Sousa (1,2), C.C. António (1,2), S.I.S. Pinto (1,2)

1. *Engineering Faculty of University of Porto, Rua Dr. Roberto Frias, s/n, 4200-465 Porto, Portugal;*
2. *Institute of Science and Innovation in Mechanical and Industrial Engineering (LAETA-INEGI), Rua Dr. Roberto Frias, 400, 4200-465 Porto, Portugal*

1. Introduction

Cardiovascular diseases (CVDs) are the main cause of death in advanced countries. Atherosclerosis is a CVD that limits blood flow circulation in arteries - stenosis. The Fractional Flow Reserve (FFR) is a parameter to guide clinical decisions regarding revascularization procedures in coronaries. The main goal of the present work is to calculate the FFR specific to the patient through hemodynamic simulations. This value will be compared with the invasive FFR measured in the hospital. The computed FFR will be determined by imposing Windkessel models with a different number of elements (3, 5, or 7). The one giving the most accurate FFR and the lowest computational time should be used for clinical applications.

2. Materials and Methods

The 3D geometry of the patient case was obtained through Mimics® software. Then, this geometry was imported to ANSYS® for hemodynamic simulations. A tetrahedral mesh was considered: Path Independent Method. Rigid walls of the artery were taken into account. Results considering deformable or rigid walls are very similar (max. difference of 2%) [1]. At the inlet of the artery, a Womersley velocity profile was assumed, depending on the pulsatile time and the artery radius. Different Windkessel models for outlet boundary conditions were considered in different simulations: models with 3, 5, or 7 elements. Blood has complex properties and should be considered a viscoelastic fluid in numerical simulations. From the literature, the sPTT model is the one that best characterizes blood [2,3]. There are no studies in literature considering, simultaneously, viscoelasticity of blood and Windkessel model, for simulations.

3. Results

The patient under study is 63 years-old male with 40% stenosis in the left anterior descending artery. Table 1 shows the computed FFR considering Windkessel models of 3 and 5 elements, and the invasive FFR obtained in the hospital center, for this patient case.

Table 1: Computed and Invasive FFR for a patient

Computed FFR		Invasive FFR	Relative Error
3-elements	0.910	0.930	2.15%
5-elements	0.925		0.53%
7-elements	in achievement		in achievement

4. Discussion and Conclusions

The relative error considering the Windkessel model of 5 elements is much lower than the one of 3 parameters. Since the computational time is practically the same (1h30 – Workstation Desktop Intel Core i9 Extreme Processor units 4 × 3.0 GHz and 64 GB RAM.), the model of 5 elements should be used for hemodynamic simulations, since it is more complete regarding coronary characterization. Although not included in Table 1, the 7-elements model is being implemented and is nearly tested. In a near future, the validation must be done with many patient cases with different stenosis.

5. References

1. Miranda E et al., *Comput Methods Biomech Biomed Engin*; 24(13):1488-1503 (2021).
2. Pinto SIS et al., *Int J Non Linear Mech*; 123(6): 103477 (2020).
3. Campo-Deaño L et al., *Biomicrofluidics*; 7(3):034102–034111 (2013).

Acknowledgements:

Authors gratefully acknowledge the financial support of FCT (Portugal) regarding the R&D Project “PTDC/EMD-EMD/0980/2020”; and institutions FEUP, INEGI, FMUP, CHVNG/E.



PARTIAL HEPATECTOMY HEMODYNAMICS DIGITAL TWIN: A SENSITIVITY ANALYSIS STUDY

Lorenzo Sala (1), Nicolas Golse (2,3), Alexandre Joosten (2,3),
Eric Vibert (2,3), Irene Vignon-Clementel (1)

1. Inria Saclay, France; 2. Université Paris-Saclay, France;
3. Inserm Physiopathogénèse et traitement des maladie du foie, France

1. Introduction

Liver surgery is one of the only curative treatments for primary or secondary liver tumours. Partial hepatectomy is a partial resection of the liver allowing for tumour removal. The main risk of hepatectomy is the occurrence of Post-Hepatectomy Liver Failure, which may occur due to post-operative portal hypertension (PHT) [1]. This abstract presents a global sensitivity analysis (SA) study of a mathematical model simulating the hemodynamics response to partial hepatectomy to better understand the main drivers of the clinical outputs of interest.

2. Materials and Methods

Recently a lumped-parameter model of the cardiovascular system was proposed to simulate the whole-body hemodynamics before and after a partial hepatectomy and evaluate the risk of PHT due to this surgery [2]. The input parameters of this mathematical model \mathcal{M} considered for the SA study proposed are:

- the heart elastances of the right atrium and left ventricle ($E_{a,RA}, E_{b,RA}, E_{a,LV}, E_{b,LV}$);
- the resistances to the flow within the portal vein, hepatic artery, hepatic vein, total digestive organs, and other organs ($R_{pv}, R_{ha}, R_{hv}, R_{DO}, R_{OO}$, respectively);
- the fraction of the total liver mass to be resected during the surgery (H_{px}).

Motivated by the clinical needs to evaluate the patient state during hepatectomy, the pre-operative (pre-hpx) and post-operative (post-hpx) quantities of interest for this study are: (i) the portal vein pressure (P_{pv}), (ii) the portocaval gradient (PCG) that is the pressure difference between the portal vein and the vena cava, (iii) the systemic arterial pressure (MAP), (iv) the cardiac output (CO), and (v) the blood flows in the hepatic artery (Q_{ha}) and (vi) in the portal vein (Q_{pv}). While performing the SA using the Sobol indices method, the model

outputs required to be constrained to physiological ranges. Thus, an innovative approach [3] that exploits the features of the polynomial chaos expansion method has been applied to generate a metamodel \mathcal{M}_{pce} , reducing the overall computational cost to complete a physiological global SA.

3. Results

Fig. 1 shows the most sensitive parameters (red), the fairly sensitive parameters (pink) and the insensitive parameters (white) to the studied quantities of interest.

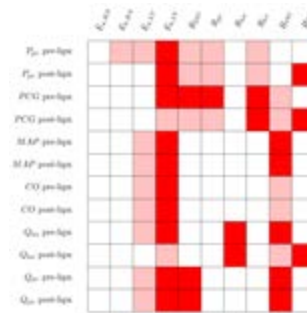


Figure 1: Sensitive (red), fairly sensitive (pink) and insensitive (white) input parameters for each quantity of interest suggested by the SA performed with the surrogate model \mathcal{M}_{pce} .

4. Discussion and Conclusions

The results suggest which parameters are more important for this hemodynamic model targeting surgical actions, identifying which measurements can be negligible (e.g. Q_{ha}) and which require good accuracy (e.g. Q_{pv}) to provide solid predictions. Moreover, these outcomes give new insights on how to improve the calibration of some model parameters to be more patient-specific.

5. References

1. Allard MA et al., *Annals of surgery*; 2013.
2. Golse N et al., *Journal of Hepatology*; 2021
3. Sala L et al., *Annals of Biomedical Engineering*; to appear. DOI:10.1007/s10439-022-03098-6.

Acknowledgements of funding support:

European Research Council under the European Union's Horizon 2020 research and innovation program (Grant no: 864313).



FINITE ELEMENT STUDY OF STRAINS AROUND SACRAL AND HEEL PRESSURE ULCERS WITH A NEW BI-LAYER DRESSING

Nolwenn Fougeron (1), Nathanaël Connesson (1), Grégory Chagnon (1), Thierry Alonso (1), Laurent Pasquinet (3), Stéphane Auguste (3), Antoine Perrier (1, 2), Yohan Payan (1)

1. Univ. Grenoble Alpes, CNRS, UMR 5525, VetAgro Sup, Grenoble INP, TIMC, 38000 Grenoble, France, 2. Service de Diabétologie, AP-HP, 75004 Paris, France, 3. Urgo Research, Innovation & Development, 21300, Chenôve, France

1. Introduction

Pressure Ulcers (PU) are soft tissues wounds occurring after a detrimental external loading. Maximal shear strains are considered as a mechanical biomarker to estimate the risks for PU [1]. These strains can be computed with Finite Element Models (FEM). It is common to use dressings to protect and improve the environment around the wound but the mechanical impact of such devices has been poorly investigated. In this work, FEM of the heel and sacrum are used to numerically evaluate the ability of a new Urgo RID bi-layer dressing to reduce soft tissues internal strains.

2. Materials and Methods

FEM of the sacrum and the heel regions were designed from medical images of one healthy volunteer. Both models included a fat and a skin layer. Achille's tendon and muscles were added for the heel. Bones were not included in the models since they were supposed to be rigid.

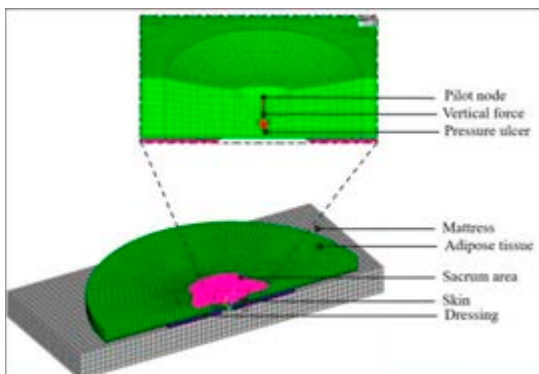


Figure 1: FEM of the sacrum region with a PU.

To simulate a PU, a 30.0 mm cylinder, 1.3 mm deep, was removed from the soft tissues, below bony prominences (see figure 1 for an axis-symmetrical model of the sacrum). Hyperelastic constitutive equations were used to model the

tissues with a stiffening around the PU. Materials constitutive behaviours were optimised according to literature experimental cadaveric tests. The dressing was composed of a compressible honeycombed material with a hole under the bony prominences. A second layer, the compress, consisted in an orthotropic linear elastic material. The dressing was glued to the skin and a vertical force equivalent to 47 % and 6 % of the subject weight was applied to the sacrum and the heel respectively. A mattress with a linear elastic material was used as a support in both models.

3. Results

The dressing reduced the strains under the bony prominences in models with and without PU. Volumes of “healthy” tissues, i.e. under 50 % strains [1], were also larger in all models when the dressing was used.

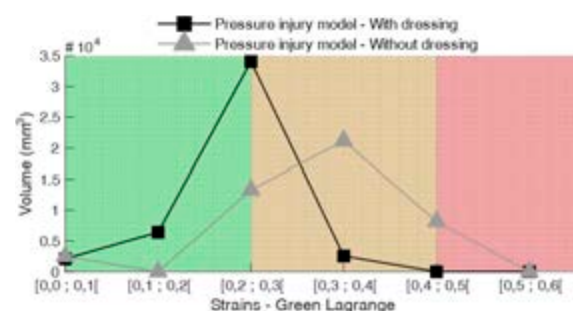


Figure 2: Strains distributions in the sacrum models.

4. Discussion and Conclusions

New concepts of dressings such as the Urgo bi-layer dressing, may provide more than a proper biochemical environment: they can also create mechanical conditions that alleviate the tissues.

5. References

- [1] K. K. Ceelen *et al.*, *J. Biomech.*, 41:3399–3404, (2008),



IN SILICO OPTIMIZATION OF HELMET MATERIAL PROPERTIES FOR TRAUMATIC BRAIN INJURY MITIGATION

Vincent Varanges(1)(2), Pezhman Eghbali(1), Pierre-Etienne Bourban(2), Dominique Pioletti(1)

1. Laboratory of Biomechanical Orthopedics, Ecole Polytechnique Fédérale de Lausanne (EPFL), Lausanne, Switzerland.

2. Laboratory for Processing of Advanced Composites (LPAC) Ecole Polytechnique Fédérale de Lausanne (EPFL), Lausanne, Switzerland

1. Introduction

Despite the generalized use of helmets [1], the traumatic brain injuries (TBI) are still prevailing in high-speed sports. This situation stresses the need to develop new helmet materials taking into account injury metrics such as the Brain Injury Criteria (BrIC) [2]. The proposed numerical model aims at optimizing material properties in order to reduce BrIC values for different impact scenarios.

2. Materials and Methods

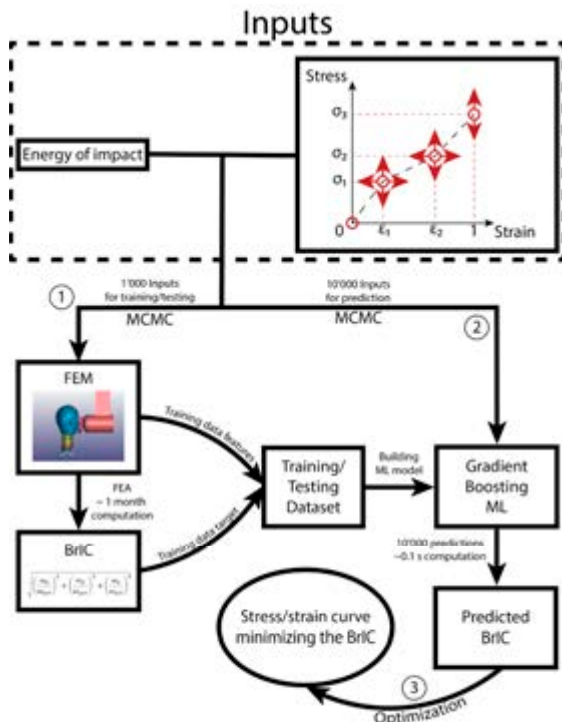


Figure 1: Flowchart of the optimization method

This study used the open-source FE model from Biocore LLC including a Hybrid III head and neck dummy, a protection and a pendulum impactor [3]. This model is simulating the kinematic data of the headform under a pendulum impact at a given energy.

The compressive stress/strain curve of the material's protection was simplified into five parameters ($\sigma_{1,2,3}, \epsilon_{1,2}$). Sampling of the model's inputs was performed with the Markov Chain Monte Carlo (MCMC) method which were then injected into the FEM. Optimization of the gradient boosting ML model was performed by minimizing the mean absolute error of predicted BrIC values (see Fig.1).

3. Results

The model's evaluation parameters resulted in an R^2 of 0.99 and a mean absolute error of 0.01. The optimized stress/strain curves according to the BrIC are displayed in green in Fig.2.

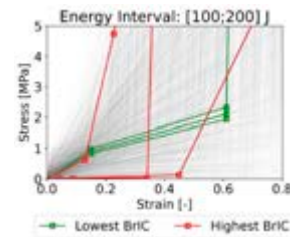


Figure 2: Ideal stress strain curves for impact ranging from 100 to 200 Joules

4. Discussion and Conclusions

The model showed strong capabilities to define material properties enhancing the protection against TBI according to the BrIC. The optimized stress-strain curves lead to a BrIC of 0.11 whereas it reaches 0.48 for standard materials such as EPS-foam. Other criteria were also studied the same way such as HIC or RIC.

5. References

[1] Niemann, S. et al., 2020, BFU; [2] Takhounts, E. G. et al., 2013, Stapp Car Crash Journal.;[3] Giudice, J. S et al., 2019, Ann Biomed Eng

Acknowledgements:

This study utilized model licensed from Biomechanics Consulting and Research, LC (Biocore), model derived therefrom, or both.



WHAT ARE THE INFLUENCE OF ANATOMICAL VARIABILITIES ON SKULL-BRAIN BEHAVIOR? A NUMERICAL APPROACH.

Pierre-Marc François (1), Baptiste Sandoz (1), Philippe Decq (1,2), Sébastien Laporte (1)

1. *Institut de Biomécanique Humaine Georges Charpak, Arts et Metiers Institute of Technology, France*; 2. *Service de neurochirurgie, hôpital Beaujon (AP-HP) France*

1. Introduction

Concussion is a common head injury in contact sports, but its pathophysiology is not fully understood. The objective of the present study is to use a Finite Element Analysis to investigate of the influence of geometry on brain injury risk for a frontal impact.

2. Materials and Methods

The Parameterized Finite Element Model of the Head developed in our laboratory is designed of shell elements to model the scalp, the skull, the falx cerebri and the tentorium cerebelli, and tetra elements for the brain, the blood in the main sinus and the cerebrospinal fluid in the ventricles. The bridging veins were modelled with spring elements (Fig. 1).

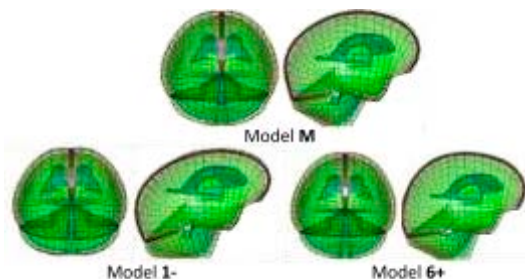


Figure 1: Elements models obtained for the mean geometry (M), the modes 1 & 6 (1- and 6+)

Mechanical behaviours of all the anatomical structures are homogeneous and linear elastic (Table 1). A tied interface between the brain and the skull was used to model their interaction.

A Principal Component Analysis, performed on a database of 40 intra-cranial surfaces reconstructed from CT-scan data, was used to define anatomical variations. The first 6 modes were extracted (85% of variance) to build 13 models: a mean one (M) and, for each mode N, two models representing the geometric variations at plus (N+) or minus (N-) three standard deviations.

The frontal impact N°37 from the study of Nahum et al. [2] was simulated. Frontal, parietal and occipital maximal pressures, as well as in the posterior fossa, were recorded [2].

Table 1: Mechanical Properties of the anatomical structures.

Structures	Young Modulus	Poisson Coefficient
Falx & Tentorium	31.5 MPa	0.45
Skull	15 GPa	0.2
Ventricular System	80 kPa	0.495
Brain	670 kPa	0.495

3. Results

The pressures computed for each model are of the same order of magnitude as those measured experimentally [2]. The Model M is always closest to the maximal reference pressures. The anatomical variabilities have an impact on the measured pressures. For example, Mode 1, which mainly describes a variation in the volume the skull, showed an increase between 1- and 1+ increases of 200% for frontal pressure, 50% for occipital pressure and 40% for parietal pressure.

4. Discussion and Conclusions

The proposed parametric study allowed performing a first investigation of the influence of the geometry on the brain mechanical behaviour. However, these results need to be analysed qualitatively because of the simplifying assumptions that have been made.

A more in-depth statistical study, coupled with this type of modelling, should make it possible to identify the anatomies that are most at risk.

5. References

1. François PM, et al., CMBBE, 23:sup1, S113-S114, 2020.
2. Nahum, et al., 21st Stapp Car Crash Conference, 1977.



MUSCULOSKELETAL MODELING OF RUSSIAN BAR PORTER'S TO ASSESS THEIR SPINAL LOADS DURING A PERFORMANCE

Pierre Schmidt (1, 2), Marion Cossin (2), Gerald Parent (3), Anne-Laure Ménard (3),
Michel Behr (4), Wei Wei (4), Eric Wagnac (1)

1. *École de technologie supérieure, Canada*; 2. *CRITAC-École nationale de cirque, Canada*;
3. *INÉDI-Cégep régional de Lanaudière à Terrebonne, Canada*; 4. *Université Gustave Eiffel, France*

1. Introduction

The Russian bar is a circus discipline performed by two porters, who balance a flexible bar on their shoulders, and one flyer, who jumps onto the bar to perform acrobatics (Fig. 1). The porters soften his landing and give an extra push by bending their chest and knees. As the bar rests on one shoulder only, an asymmetrical load is applied to the back of the porters, which in the long run could lead to back pain and/or injury [1]. The objective of this study is to (1) develop and validate a computer model of the porters' dynamic movement and (2) evaluate the asymmetric loads applied on the porters' lumbar spine.



Figure 1: Russian bar performance showing the two porters, the flyer and the flexibility of the bar

2. Materials and Methods

After obtaining the approval of the ethics committees of École de technologie supérieure and École nationale du cirque, three artists were recruited. The data acquisition included motion capture (Optitrack, Natural Point, USA), back muscles electromyographic activity (EMG Trigno system, Delsys, CA) and ground reaction forces (AccuGait force plate, A-Tech Instruments, USA) of semi-static and dynamic movements of the artists. A full body-lumbar-spine model [2] was scaled and adapted to the porters' movements and validated with collected data using the open-source software OpenSim (version 4.4). The EMG and ground reaction forces (GRF) acquisition were used

only to validate the model. However, due to the displacement of the porters during the performance, it was impossible to measure GRF for all the exercises. Thus, GRF used as input for the model were estimated using an actuator-based method [3]. The forces on the porters' shoulders were also estimated from the deflection of the bar, according to experimental force vs deflection curves. Finally, the loads on the lumbar spine were estimated using static optimization and joint reaction analysis with OpenSim [2].

3. Results

The actuator-based method estimated GRF within 4% of the force plate measurements. A linear relationship was found between the bar deflection and supporting forces. Forces applied to the porters' shoulder reached up to 1300N. Used as inputs for the static optimization and joint reaction analysis, the unilateral shoulder forces resulted in a strong activation of the left-sided trunk muscles.

4. Discussion and Conclusions

Our preliminary results demonstrate the relevance of this model to assess changes in lumbar loading during a Russian bar performance. They also highlight the intensity of the asymmetric loading experienced by the porters during their performance. This study is the first to quantify load on Russian bar artists. The current model will be used to optimize the porters' techniques and to develop new Russian bar devices that would help prevent back pain or injury.

5. References

1. Marras et al., *The Spine Journal*, 4(1), 64-75. (2004).
2. Beaucauge-Gauvreau et al., *Computer Methods in Biomechanics and Biomedical Engineering*, 22(5), 451-464. (2019)
3. Skals, S. et al., *Multibody System Dynamics*, 39(3), 175-195. (2017)



BRAIN RESPONSES TO FOOTBALL IMPACTS IN REGIONS OF INTEREST: REFINEMENT OF A FINITE ELEMENT HEAD MODEL

Véronique Bouvette^{1,2}, Yvan Petit^{1,2}, Samuel Guay^{2,3}, Sophie-Andrée Vinet^{2,3}, Louis DeBeaumont^{2,3}, Eric Wagnac^{1,2}

1. *École de technologie supérieure, Mechanical Engineering; Montréal, Canada* ; 2. *CIUSS Nord-de-l'île-de-Montreal, Research Center, Montréal, Canada*; 3. *University of Montréal, Psychology Department, Montréal, Canada.*

1. Introduction

Football athletes are exposed to a high rate of repetitive head impacts. As more studies shed light on brain changes and neurological deficits associated with repetitive head impacts in specific regions of the brain over the course of a game or a season [1][2], it has become critical to evaluate brain tissue responses to impact in regions of interest (ROIs).

This study aims to refine the head model of THUMS [3], an opensource finite element model (FEM) of a male human body originally dedicated to vehicle collisions, to better represent brain ROIs of a population of collegiate Canadian football players and validate its use for simulating impact scenarios observed on the field.

2. Materials and Methods

Magnetic resonance imaging (MRI) data of collegiate Canadian football players were obtained on a 3-T Siemens MAGNETOM Prisma MRI scanner using a high-resolution 32-channel head coil. ROIs true MRI volumes were then assessed by a neuroimaging expert. Average volumes of ROIs relative to the total encephalic volume were used for FEM segmentation specific to the group. ROIs include corpus callosum (CC), cingulate cortex (Cg), motor cortex (mC), thalamus (Th) and basal ganglia (BG). Geometric segmentation of THUMS was validated by the same MRI expert responsible of evaluating true MRI volumes. Head impact simulations described by Ji et al. [4] were applied to our refined THUMS FEM and brain responses (maximal principal strain (MPS), strain rate and pressure) were compared to responses from other FEM already used to evaluate brain injuries in contact sports: DSNM, SIMon and WSUHIM head FEMs. THUMS

FEM was compared using available kinematic inputs in the range of Ji et al. (2013) study. Four impacts were computed with a combination of 66 g of linear acceleration, 4405 and 6998 rad/s² of rotational acceleration and azimuth and elevation at both 0° and 45°. Kinematics were applied at FEM centre of gravity.

3. Results

The comparison to other head FEMs shows that THUMS stress and strain cerebrum responses are in the range of values previously computed for similar kinematic inputs. Disparities across FEMs is still evident which enhance the importance of linking FEMs responses to true tissue changes.

Table 1: Ranges (Min-Max) of brain tissue responses for THUMS and comparative study

FEM	MPS	Strain rate (1/s)	Pressure (kPa)
SIMon	0.00 - 0.33	0.4 - 53.5	0.4 - 46.3
WSUBIM	0.00 - 1.83	0.0 - 512.7	0.0 - 257.0
DSNM	0.00 - 0.39	0.4 - 45.6	1.4 - 120.7
THUMS	0.00 - 0.85	0.02 - 87.5	0 - 104

4. Discussion and Conclusions

THUMS FEM uses same material properties across cerebrum. Next step would be to evaluate the effect of grey and white matter material differentiation. The end goal is to compare cumulation of FEM responses weighted for time between impacts to brain changes on MRI using on-field kinematics as input on a refine and segmented version of the THUMS.

5. References

1. Montenegro et al., J Neurotrauma (2017).
2. Stamm et al., J Neurotrauma (2015).
3. Toyota (2021).
4. Ji et al., CMBBE (2013).

Analysis of the effectiveness of foam headguards to protect against mTBI in rugby

Una Prendergast¹, Lucia Pérez Del Olmo¹, Theo Farrell¹, Sandra Ganly², Mark Ganly², Tahar Kechadi³, Brian Caulfield³, Aisling Ní Annaidh¹ and Michael D. Gilchrist¹

1. School of Mechanical & Materials Engineering, University College Dublin, Belfield, Dublin 4, Ireland
2. Contego Sports Ltd., Galway, Ireland
3. Insight Centre for Data Analytics, University College Dublin, Belfield, Dublin 4, Ireland

Objective: We hypothesise that a foam headguard will attenuate accelerations and mTBI indicators sustained by a rugby player if their head impacts the ground.

Materials and Methods: Broadcast video footage of a dataset of professional rugby head impact events were analysed to identify various unprotected head-ground impact scenarios. These were reconstructed using three-dimensional finite element models, with and without an energy absorbing foam headguard and accounting for friction at the ground-head and head-helmet interfaces. Three-dimensional computational modelling with the UCD Brain Trauma Model [1-3] were used for accident reconstruction purposes. Linear and angular accelerations, and stress/strain within the brain were quantified while wearing and not wearing a headguard for all five types of head-ground impacts.

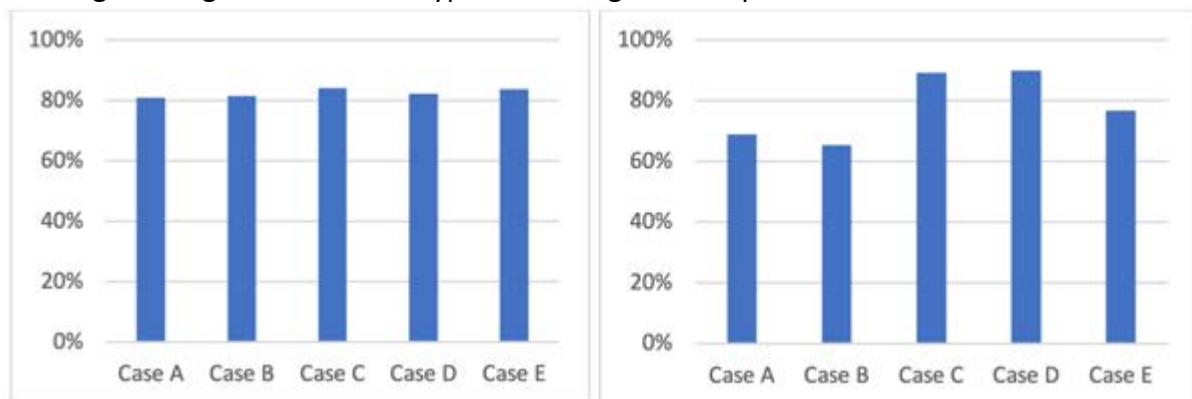


Figure 1: Percentage reduction of peak linear acceleration (left figure) and peak angular acceleration (right figure) when wearing headguard.

Results: In all cases, the level of acceleration reduced when the headguard was worn. The reduction varied between 60-90%, with Case D, namely a back-of-head ground impact scenario, corresponding to when the greatest level of protection is afforded by wearing a headguard. Von Mises stress and maximum principal strain for this case were also reduced by over 60% (not shown).

Discussion and Conclusions: This set of 5 reconstructed rugby tackle impact events confirm that a headguard can indeed provide a clear and quantifiable level of head protection against injury if worn while playing a contact sport such as rugby. Depending on the particular ground impact situation sustained by a person, and the ground compliance, the level of attenuation that will be associated with wearing a headguard can be as much as 90% less than what would be sustained if a headguard is not worn.



PREDICTION OF BRAIN AND CERVICAL LOADING IN A SNOWBOARDING BACKWARD FALLS TO EVALUATE HELMETS

Nicolas Bailly (1), Dorian Salin (3), Wei Wei (1)

1. Aix Marseille Univ, Univ Gustave Eiffel, LBA, Marseille, France; 3. Hexagon, Wissous, France

1. Introduction

Snowboarding backward fall is one of the most common crash scenarios leading to brain injury on ski slopes [1]. To design effective protection against those injuries, it is critical to understand the injury mechanism. Previous work reproduced hundreds of crashes scenarios using the fast and robust multibody simulation method, highlighting a large range of head impact conditions but with no information on local brain loadings nor on the effect of helmet [1]. The use of human finite element (FE) models would enable to access that information. However, it is too costly and time consuming to reproduce hundreds of impact scenarios and thus inoperable to evaluate and design protections against a wide range of crashes. Recent advance in Reduced Order Model (ROM) technique have enable the prediction of finite element modelling results in real-time. The purpose of this study was to propose and evaluate a method coupling a finite element Human model with a ROM technique from ODYSSEE [2] to provide real-time analysis of the snowboarding backward fall and to evaluate one commercially available helmet.

2. Materials and Methods

The range of normal and tangential impact velocity and of head impact angle (α) relative to the ground, were extracted from the 324 multibody reconstructions of snowboarding backward fall [1]. A Montecarlo method was used to define a design of experiments with 9 impact conditions covering the range of those 3 parameters. These impact conditions were reproduced, with or without helmet using the THUMS v5.03 M-50 FE human model [3] impacting a modelled snow ground [1]. Three additional impact scenarios, randomly chosen were also reproduced using the FE Model with and without helmet for validation. The head accelerations, maximal principal strain (MPS) in the brain as well as the loading force in the cervical vertebrae of the first 9 simulations were

extracted and used to create a ROM in ODYSSEE and to predict those of the 3 other scenarios simulated. The MPS, and vertebral loading curves predicted by the ROM were compared to those obtained by the FE simulations. The ROM was then used to predict brain and vertebral loading with or without helmet in the hundreds of crashes scenarios identified in the multibody study [1].

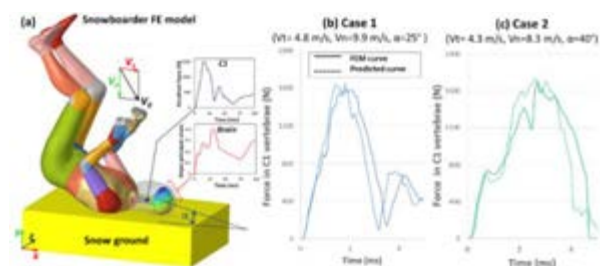


Figure 1: (a) FE model setup and (b)-(c) examples of comparison between the force in C1 vertebra measured in the FEM and predicted by the ROM.

3. Results

Figure 1 presents comparison between the force measure in the C1 vertebra of the THUMS model and that predicted by the ROM in the 2 of the tested impact conditions. The ROM closely predict in real time the force curve in C1 (R2 of 79.8, 88 and 82) as well as the MPS strain in the brain (R2 of 84.8, 79.7 and 88.0). In the 324 identified snowboarding crashes [1], the ROM predicted that the helmet did reduce head linear acceleration, on average, but not the MPS in the brain.

4. Discussion and Conclusions

The use of Reduced Order Modelling methods was adequate to predict tissue-level loadings of the THUMS model during a snowboarding backward fall. This work is a proof of concept that the methodology could be used on detailed biomechanical model, and open up numerical design and evaluation of protective devices.

5. References

1. Bailly et al., Scand. J. Med. Sci. Sports, 2017
2. Kayvantash, Automotive CAE companion, 2019
3. M. Iwamoto et al. Traffic injury prevention, 2015



INVARIANT KINEMATIC CONSEQUENCES OF MUSCULAR ANTICIPATION DURING LANDING AND DROP-JUMPING

Romain Bechet (1), Romain Tisserand (1), Laetitia Fradet (1), Floren Colloud (2)

(1) Institut Pprime, UPR 3346, CNRS – University of Poitiers, France, (2) Institut de Biomécanique Humaine Georges Charpak, Arts et Métiers Institute of Technology, Paris, France

romain.tisserand@univ-poitiers.fr

1. Introduction

When humans execute voluntary movements, their Central Nervous System (CNS) programs muscular anticipation to coordinate joint rotations according to the constraints of the task [1]. In motor tasks with large momentum, such as landing or drop-jumping, the muscular anticipation serves two key purposes: protect the skeletal system [2] and adjust the lower-limb muscles stiffness to modulate energy dissipation or restitution depending on the task [3]. Because the kinematic consequences of the muscular anticipation have been poorly described, the objective of the study was to characterize the evolution of lower-limb joint angles during the anticipation phase to clarify how they contribute to both protect the skeletal system and perform the movement.

2. Materials and Methods

10 young healthy subjects (5 females, 25 years old) *landed* and *drop-jumped* from a 30 cm elevated platform on two force plates recording the 3D ground reaction forces (GRF) at 2000 Hz. The best trial (out of three) was analysed for each subject in each condition: the lowest vertical GRF peak for *landing* and the shortest contact time for *drop-jumping*. The 3D trajectories of 64 reflective markers placed on anatomical landmarks were recorded by 19 infrared cameras at 200 Hz. The knee and ankle sagittal angles were computed with an individualized full-body musculoskeletal model [4] during the 100 ms preceding ground contact (*i.e.* when the vertical GRF exceeded 20 N). The influence of the condition on the angle was tested with a paired t-test using Statistical Parametric Mapping for each joint.

3. Results

In all subjects, only the knee joint flexed before

ground contact (-47 ± 15 ms). No difference was observed between conditions (Fig. 1).

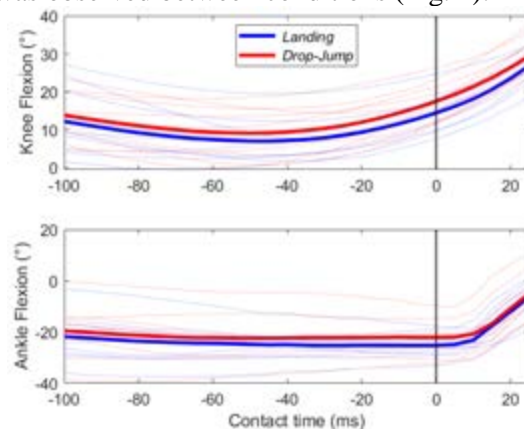


Fig. 1: Knee and Ankle flexion angle for each condition. Vertical lines indicate ground contact.

4. Discussion and Conclusions

Contrary to the ankle, the anticipated knee flexion suggests that the knee flexors are recruited to initiate the joint rotation before it is accelerated by the ground contact. This may protect the knee from extending too much and/or lowering the whole-body center of mass to enable upper-body adjustment and maintain balance. The absence of difference across joint angles between conditions suggests that this anticipatory motor command is conservatively used by the CNS to protect the skeletal system.

5. References

1. Kawato M. *Curr Opin Neurobiol.* 1999; 9(6):718–727.
2. DeMers M et al., *J Biomech.* 2017;52:17–23.
3. Bechet et al., *Comp Met in Biomech*, (accepted)
4. Raabe ME et al., *J Biomech.* 2016; 49(7):1238–1243

Acknowledgements:

This work was funded by the Region Nouvelle-Aquitaine and PPrime laboratory (France).



Clustering of knee osteoarthritis patients based on kinematic data using k-means algorithm

Zahra Bensaddek (1), Nicola Hagemeister (2), Alix Cagnin (3), Nathalie J Bureau (1), Nathaly Gaudreault (4), Madeleine Durand (1), Manon Choinière (1), Karim Loulou (5), Youssef Ouakrim (5), Neila Mezghani (5)

1. Université de Montréal, Canada; 2. École de technologie supérieure, Canada; 3. Emovi, Canada; 4. Université de Sherbrooke, Canada; 5. Université TÉLUQ, Canada

1. Introduction

The significant variability in biomechanical profiles is largely known, both in healthy and knee osteoarthritis (OA) individuals. Clustering techniques have been used to identify kinematic phenotypes in healthy people and in patients awaiting total knee arthroplasty^{1,2}. However, little is known on such phenotypes in mid- to late-stage knee OA. This study aimed at identifying knee OA patients' phenotypes based on kinematic data and assess their differences in terms of socio-demographic data and patient-reported outcomes.

2. Materials and Methods

This study was conducted on 291 patients (64.9% of women) with confirmed radiographic knee OA using Kellgren-Lawrence grading ≥ 2 (i.e., KL2, KL3, or KL4)³. For each patient, three-dimensional (3D) knee kinematics (i.e., flexion / extension; varus / valgus; external / internal tibial rotation) were captured on both knees using a knee kinesiology exam using the KneeKG® system (Emovi Inc., Canada)⁴. The Knee Injury and Osteoarthritis Outcome Score (KOOS) pain subscale was used to assess pain levels. The optimal number of phenotypes (i.e., clusters) within the kinematic data set has been determined based on the Elbow method. A K-Means algorithm was then used to identify the different clusters and a phenotype per cluster were obtained by averaging the kinematic data set in each one. Intraclass correlation coefficient (ICC) was calculated for each cluster and in each plane of movement. Statistical parametric mapping (SPM) was used to assess differences between the identified clusters in terms of 3D kinematics during a gait. ANOVAs and post-hoc analyses were performed to assess between-cluster differences and to characterize them in terms of age, body mass index (BMI), and pain scores.

3. Results

Five clusters were identified from a total of 439 knees. SPM analysis showed that each cluster significantly differ ($p < 0.05$) from the four others for at least 80% of the gait cycle in two different planes of movement. ICCs were higher for the varus/valgus patterns ($0.56 < ICC < 0.78$), compared to values for ext./int. rotation ($0.48 < ICC < 0.54$) and flexion/extension ($0.39 < ICC < 0.56$). In addition to their significant kinematic differences, clusters also differed on other characteristics. One cluster (i.e., C5) differed from all four others in terms of women/men distribution. Patients from this cluster also reported significantly lower KOOS pain scores and higher proportion of KL4 grades, suggesting more pain and advanced OA compared to patients from all other clusters (all $p \leq 0.02$). Another cluster (i.e., C4) gathered significantly younger patients (i.e., 58.9 years vs other clusters > 64.3 ; all $p < 0.001$).

4. Discussion and Conclusions

This study successfully identified distinct phenotypes in knee OA patients based on kinematic profiles. Since these phenotypes also differ in patient characteristics, this novel analysis may constitute the first step towards the development of more tailored therapeutic approaches based on each phenotype compared to the generic standard of care.

5. References

1. Mezghani et al., *Appl. Sci.* **2021**, *11*(24), 120542.
2. Young-Shand et al., *J Orthop Res.* 2022
3. Kellgren, *Ann. rheum. Dis.* (1957). 1, 16, 494.
4. Lustig et al., *Knee Surg Sports Traum Arthrosc.* 2012 *20*(4):633-8.

Acknowledgements:

This study has been financed by the Québec Minister of Economy, and Emovi inc and the the Canada Research Chair on Biomedical Data Mining (950-231214).

DIGITAL SINGLE-LIMB STANCE ASSESSMENT BASED ON A 3-DIMENSIONAL KINEMATIC ALGORITHM

Yu Yuan Lee¹, Lena Fennen¹, Rosemary Dubbeldam¹

¹ University of Münster, Institute for Sport Science, Department of Movement Science, Germany

1. Introduction

Single Limb Stance Test (SLST) is a reliable movement tests for assessing fall risk and balance [1]. We aim to automate the SLST assessment process by developing a marker-based rating algorithm based on Balance Error Scoring System (BESS) [2].

2. Materials and Methods

19 healthy young adults (Age 25 ± 5 years, 10 male, 9 female) and 9 young adults with chronic ankle instability (Age 25 ± 6 years, 6 male, 3 female) were included.

The Qualisys motion capture system was used to record full body segment motions. The participants performed the SLST with both eyes-closed and eyes-open for 60 seconds. Each participant performed two trials of each condition on each limb. Only the second non-dominant (healthy) or impaired (patients) limb SLST trial was analysed. The BESS (table 1) was assessed for each trial by 3 persons and each participant's balance was classified as good, moderate, or bad. MATLAB[®] was used to build the kinematic rating algorithm based on the BESS items. The algorithm used the marker positions of toe, fore foot, hind foot, thigh, trunk, and wrist segments to calculate the balance errors in the BESS items. A paired t-test was used to study the relationship between human and digital BESS assessment.

Table 1: Balance Error Scoring System (BESS)

1. Lifting forefoot or heel
2. Moving the upper body more than 30 degrees of flexion or abduction
3. Stepping, stumbling, or falling
4. Arm movement
5. Remaining out of the test position for more than 5 seconds
6. Eye close count (not applicable in 3D segment motion capture system)

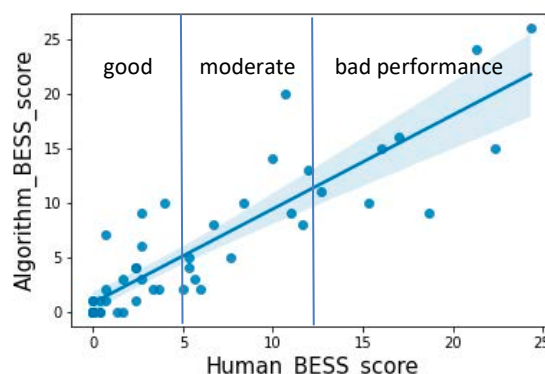


Figure 1: The comparison of BESS score between the rating algorithm and human assessors.

3. Results

49 trials including 26 eyes-closed and 23 eye-open SLSTs were analysed. Among them, 60% demonstrated good, 24% moderate, and 16% bad performance, corresponding to a BESS of <5 , 5-12 or >12 respectively. The BESS score assessed by the algorithm is highly correlated to the human assessed BESS score ($r = 0.88$, $p = 0.001$). The Root Mean Square Error between the assessments is 2.1.

4. Discussion and Conclusions

The marker-based rating algorithm can efficiently and objectively assess SLST performance. The algorithm is repeatable and more accurate in small movement assessment than the subjective human observations. Furthermore, the algorithm can be further deployed in 2-dimensional video-based motion capture system to provide a low-cost solution for the assessment of fall risk and balance.

5. References

1. Drusini, A. G et al (2002). Aging clinical and experimental research, 14(1), 42-46.
2. Rienmann, B. L et al (1999). Journal of sport rehabilitation, 8(2), 71-82

Acknowledgements

We would like to thank V. Lima, A. Radetzky and O. Ojomo for their assessment of the BESS.

UNIQUE TIBIOFEMORAL GEOMETRIC FEATURES AFFECT SIMULATED KNEE MECHANICS IN YOUNG FEMALE ATHLETES

Mitchell GA Wheatley (1), Andrew D Pearle (1), Danyal H Nawabi (1), Thomas L Wickiewicz (1), Bruce D Beynon (2), Carl W Imhauser (1)

1. Hospital for Special Surgery, USA; 2. University of Vermont, USA

1. Introduction

Young, female athletes are at elevated risk of non-contact ACL injury compared to males. Multiple, unique, sex-specific geometric features of the tibiofemoral joint as measured via 2D imaging are associated with increased risk of ACL injury in females [1]. Yet, the relationship between 3D tibiofemoral geometry in high-risk female athletes and knee mechanics is unknown. The first objective of this study is to characterize 3D tibiofemoral geometry in a subset of young, female athletes via statistical shape modeling. The second is to determine whether tibiofemoral geometry is related to ACL force and to knee kinematics.

2. Materials and Methods

We selected MRI data of knees from 20 young, female athletes (Age: 17.3 ± 1.5 years) from a larger dataset. Tibiofemoral cartilage and bone were segmented using an automated algorithm [2]. We manually segmented the menisci and identified ligament insertions and origins from the MRI scans. To accomplish our first objective, we used principal component analysis of tibiofemoral geometries to identify the directions of maximum variation (principal components, PCs). To accomplish our second objective, we integrated the 20 subject-specific knee geometries into an established computational modeling pipeline [3] to predict ACL force and tibiofemoral kinematics. We simulated a clinical pivoting exam via serially applied compressive (100 N), valgus (8 Nm), and anterior (30 N) loads at 15° of flexion. We compared PC scores to ACL force and knee kinematics using simple linear regression ($\alpha = 0.05$) and reported the p-value and coefficient of determination (R^2).

3. Results

Regarding objective one, the first 13 PCs accounted for 91.7% of the variations in tibiofemoral geometry. The fourth principal component (PC4) explained 6.3% of tibiofemoral variation and described shape

differences in lateral tibial plateau slope, lateral tibial plateau anterior position, lateral femoral condyle size, and lateral tibial spine height and anterior-posterior (AP) offset. Regarding objective two, PC4 scores positively correlated with both maximum ACL force (R^2 : 0.39, $p < 0.01$) (Figure 1) and coupled translations and internal tibial rotation (ITR) with valgus loading (R^2 : 0.49, $p < 0.001$). Greater ACL force at the peak applied loads and increased ITR were associated with greater lateral tibial plateau slope, lateral femoral condyle size, and lateral tibial spine height and decreased AP tibial spine offset.

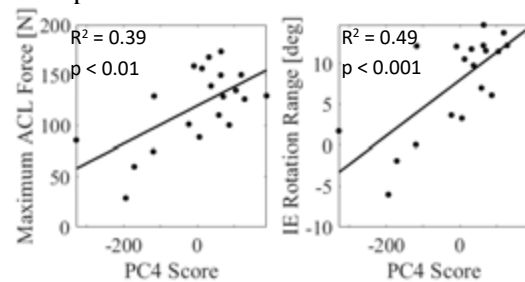


Figure 1: ACL force at peak applied load vs PC4 scores of the 20 female knees (left). ITR range vs PC4 scores (right).

4. Discussion and Conclusions

Our statistically augmented computational modeling pipeline may enable development of holistic, sex-specific, mechanics-based screening tools for ACL injury and clinical treatments for knee trauma that target unique combinations of geometric risk factors for ACL injury in females to help address sex-based disparities in orthopaedic care. Our most important finding was that multiple geometric variations captured in PC4 of our 3D shape analysis were associated with ACL force and coupled ITR. Thus, risk mitigations strategies or surgical treatments limiting coupled ITR with valgus loading may be critical to reduce risk of ACL injury in young female athletes.

5. References

1. Sturnick D et al., AJSM (2012).
2. Gatti A, Maly M, Magn Reson Mater Phy (2021).
3. Kia M et al. J Biomech Eng (2016).



TOWARD A PHYSICAL HUMAN THORAX SURROGATE DEDICATED TO BLUNT BALLISTIC IMPACTS BASED ON FE SIMULATIONS

M. Chaufer ^{*}(1), R. Delille (2), B. Bourel (2), C. Marechal (2), F. Lauro (2), O. Mauzac (3), S. Roth (1)

1. *Interdisciplinary Laboratory Carnot of Bourgogne, site UTBM, UMR 6303, CNRS / Univ. Bourgogne Franche-Comté (UBFC), 90010 Belfort, France;*
2. *Laboratory LAMIH UMR 8201 CNRS, Univ. Polytechnique Hauts-de-France, 59313 Valenciennes, France;*
3. *French Ministry of Interior, CREL/SAELSI, Place Beauveau, Paris, France*

**Corresponding author, e-mail address: martin.chaufer@utbm.fr*

1. Introduction

In the framework of biomechanics, the use of numerical procedures can help understanding complex phenomena which cannot be analyzed with experimental setups. Indeed, experimental data on human cadavers lead to complex ethical issues that can be overcome when using biofidelic models. The use of such models has shown their wide interests especially for the evaluation of protective devices like body armors. The difficulty of such development remains in the characterization and modeling of body armors. Thus, this study proposes to simplify the structure of an existing biofidelic FE model of human thorax. Once validated, this new simplified FE model will be a basis for building his physical twin, which will be used for protection assessment.

2. Materials and Methods

This study focuses on the development of a simplified FE model based on HUByx FE model [1]. As the structure of both bones and cartilage in HUByx was not easily manufacturable, simplifications were needed. Previous work proposed homogenizing the cortical and trabecular parts of both bones and cartilage [2]. In addition, the geometry of the spine was also simplified, resulting in a FE model named SurHUByx for Surrogate Hermaphrodite Universal Body YX. In terms of material properties, the objective was to implement manufacturable human substitute material properties able to reproduce correctly the behaviour of the thorax. All the simplifications can be appreciated by comparing HUByx and SurHUByx in Figure 1.

3. Results

The simplified geometry of the SurHUByx FE model showed consistent anthropometry with experimental data [3]. SurHUByx FE model with his new material properties showed consistent behavior with Bir et al. corridors [4].

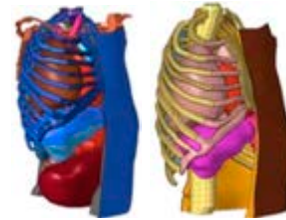


Figure 1: Structural and anthropometrical simplifications between initial HUByx (left) and SurHUByx FE model (right)

4. Discussion and Conclusions

In order to implement material laws and properties from manufacturable human substitute materials in SurHUByx FE model, anthropometrical, structural, and geometrical simplifications were conducted. Validation process of this new simplified model provided satisfying results. This study was the first step in the design of SurHUByx, the physical twin of SurHUByx FE model.

5. References

1. Roth et al., CMPB, 160:170-110, (2013).
2. Chaufer et al., 27th ESB Congress, 2022. p.293
3. O. Mayeur, Ph.D. thesis, (2013).
4. Bir et al., J. Biomech, 37:73-7, (2004).

Acknowledgements:

This work was conducted in a Ph.D thesis framework supported by the “Direction Générale de l’Armement”. The authors also thank the French Ministry of Interior for their financial support.

ROBUST AND TIME-EFFECTIVE MODELING OF CEREBROSPINAL FLUID FOR IMPACT BIOMECHANICS

Claire Bruna-Rosso^{1*}, Nabih Fezai¹, Marie-Hélène Beauséjour²

1. Laboratoire de Biomécanique Appliquée, Aix-Marseille Univ., Gustave Eiffel Univ. France; 2. Ecole de Technologie Supérieure, Montréal, Canada.

*Corresponding author: claire.bruna-rosso@univ-eiffel.fr

1. Introduction

Traumatic spinal cord injuries (TSCI) are a critical condition that may have dramatic consequences. However, the underlying mechanisms are still widely unknown. Several studies have investigated TSCI through numerical modeling [1,2] which allows to circumvent the complexity of direct observation. One of the numerical challenges is to model the Cerebro-Spinal Fluid (CSF) without giving rise to unaffordable computing times. To do so, Smoothed Particle Hydrodynamic (SPH) is a promising method [3,4]. In this context, a hybrid Finite Element (FE) – SPH model was developed and validated to investigate the behavior of the spinal cord (SC) under a contusion [5].

2. Materials and Methods

The model was developed within the Altair Hyperworks framework. Fig. 1 illustrates the various components. The geometry and mechanical properties of the SC and dura mater reproduce the one of Persson et al. [5] for validation purposes. Pia mater properties were taken from Fradet et al. [6]. Two simulations were performed, one with the CSF, and one without.

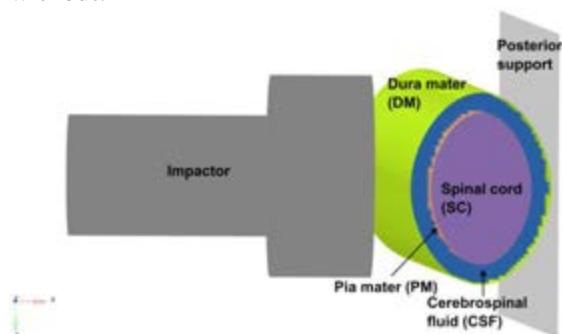


Figure 2: FEM-SPH model reproducing the experiment of Persson et al. [5]

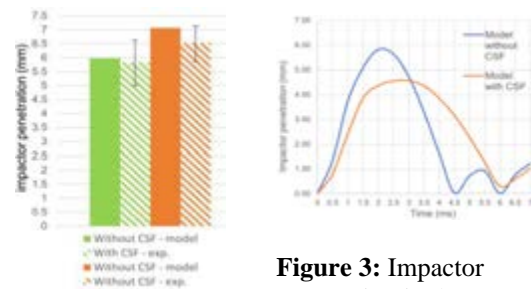


Figure 1: Max. impactor penetration: model vs. experimental [5]

Figure 3: Impactor penetration in the SC

3. Results

The model was able to reproduce the experimental results reported in [5]: impactor penetration in the spinal cord and meninges complex, both with and without CSF (Fig 2.). The model also predicts a lower penetration of the impactor within the SC with the CSF (Fig. 3).

4. Discussion and Conclusions

The model reproduced the impactor penetration in the spinal canal within reasonable computing times (36h, 8 cores 4.6GB @ 3.1 GHz). It also showed the energy absorption due to the CSF which has a protective effect on the spinal cord. Future works will aim at analyzing the effect of denticulate ligaments and tissue mechanical parameters on TSCIs.

5. References

- Bailly N et al. *Clinic Biomech*;74:58-65 (2020)
- Beauséjour MH et al. *Comput Meth Biomech Biomed Eng*; 12 (2019)
- Rycman A et al. *Num Meth Biomed Eng*; 38(3):e3570 (2021)
- Arhptsov K and Marom G. *J Neurotrauma*; 38(15):2176-2185 (2021).
- Persson C. et al. *J Neurosurg Spine*. 10(4):315-323 (2009).
- Fradet L. et al. *Adv Mech Eng*; 8(8): 1- 8 (2016)



THE BENEFITS OF AERO HANDLEBARS ON AERODYNAMIC IN CYCLISTS USING COMPUTATIONAL FLUID DYNAMICS METHODS

Mojtaba Ghasemi (1), Daniel Curnier (2, 3), Maxime Caru (1,2,3), Jean-Yves Trépanier (1), Delphine Périé (1)

1. Department of Mechanical Engineering, Polytechnique Montreal, Canada; 2. Sainte-Justine University Health Center, Research Center, Canada; 3. School of Kinesiology and Physical Activity Sciences, Faculty of Medicine, University of Montreal, Canada

1. Introduction

Aerodynamic drag is the most considerable resistive force cyclists experience, and its reduction is critical to improving cycling performance. Adopting the time trial position (TTP) represents a notable improvement for cycling aerodynamic performance. Aero handlebars are designed to enable the cyclist to adopt a more aerodynamic TTP. However, it is unclear to what realistic extent the aero handlebar configuration affects the aerodynamics and physiological functioning. Thus this study aimed to investigate the effect of aero handlebar alterations on gas exchange parameters and aerodynamics of TTP.

2. Materials and Methods

Seven male competitive cyclists and triathletes performed submaximal tests on a cycle ergometer at six different TTPs. Oxygen uptake, respiratory exchange ratio, minute ventilation and tidal volume were collected. Using the computational fluid dynamics (CFD) method, the detailed airflow patterns around the cyclist were investigated. The transition shear stress transport (SST) $k-\omega$ model was opted to solve the 3D steady Reynolds averaged Navier-Stokes equations (3D RANS). The semi-implicit method for pressure linked equations (SIMPLE) algorithm was used for pressure-velocity coupling with second-order discretization schemes. Pressure interpolation was second order. Gradients were computed with the least-squares cell-based method [1]. The governing equations were solved iteratively, while convergence was monitored. Convergence was obtained when residuals reached less than 10^{-5} .

3. Results

The results were analyzed in terms of drag area, velocity and pressure distributions around the cyclist, surface pressure coefficient and wall shear stress magnitude. It was revealed that

varying the aero handlebar position significantly influences aerodynamic performance, while maximal values of all the gas exchange variables remained unchanged. Compared to the cyclist's preferred TTP, the frontal area, drag coefficient and drag area were reduced by 4.1%, 4.6% and 8.5%, respectively, when lowering the handlebar position by 5 cm, which overcomes the metabolic costs.

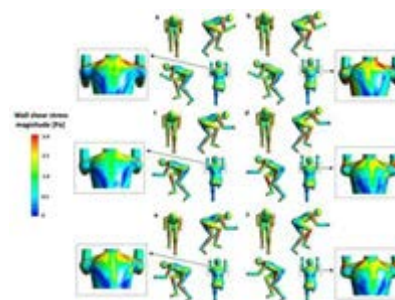


Figure 1: Front, sides and top views of the wall shear stress magnitude on the cyclist's body. (a) time trial position (TTP) 30° up; (b) TTP 30° and 5 cm up; (c) TTP 5 cm down; (d) TTP 5 cm up; (e) preferred TTP; (f) TTP 5 cm forward.

4. Discussion and Conclusions

TTP 5 cm down exhibited the least value of the drag area. This reduction will likely outweigh the insignificant increase in metabolic costs at the investigated cycling intensity. Results indicated that in the positions with the elevated handlebar, the low-pressure areas at the shoulders and bottom of the cyclist body are more significant, leading to a higher CD.

5. References

1. Defraeye, T., Blocken, B., & Carmeliet, J. (2010a). CFD analysis of convective heat transfer at the surfaces of a cube immersed in a turbulent boundary layer. *Int J Heat Mass Transf*, 53(1), 297-308

Acknowledgements:

We thank all participants for their energy



ACTIVE NECK MUSCULAR REACTION DEPENDING ON THE SURROUNDING ENVIRONMENT

María González-García (1,2), Baptiste Sandoz (3), Steffen Peldschus (2), Jens Weber (1)

1. Volkswagen AG, Germany; 2. Ludwig Maximilian University, Germany; 3. Arts et Métiers Institute of Technology, France

(maria.gonzalez.garcia@volkswagen.de, Group Innovation, Volkswagen AG, Berliner Ring 2, 38440 Wolfsburg, Germany)

1. Introduction

Since the introduction of advanced driver assistance systems in the car fleet, such as automatic emergency braking or evasive steering assist, the behaviour of occupants during the pre-crash phase of an actual collision has become increasingly important in vehicle safety. Factors such as the position or muscular state of the occupant can influence the interaction with the restraint safety systems.

In this study, the closed-loop feedback muscle control of a finite element (FE) active human body model (AHBM) has been improved to reproduce lateral neck flexion kinematics as a function of the surrounding environment, based on experimental data from ten volunteers. In this way, the model behaves differently when moving inwards or outwards inside the vehicle.

2. Materials and Methods

Ten male volunteers close to 50th percentile (175 ± 6 cm, 77 ± 5 kg) participated in a sled experiment, in which they were seated on a rigid surface. The sled was accelerated to their left. Four different pulses were applied and in total they underwent 30 trials [1]. The protocol was approved by the French Ethics Committee CPP IDF VII 15-018.

The investigations presented here focus on one of these four pulses, which consists of a maximum acceleration phase of 0.3 g of one second duration and a symmetrical deceleration phase. Five of the volunteers were also subjected to this pulse while a side structure was placed to their right in 6 trials, representing the vehicle door and window in order to investigate the effect of the environment on the volunteers' behaviour.

The volunteers were securely fastened by a thigh belt and the pelvis motion was limited by a lateral support.

The upper body kinematics were recorded by an on-sled high-speed camera (50 fps).

In a second step, the setup was modelled in the Visual Performance Solution FE software. The THUMS TUC-VW AHBM [2] was positioned on the sled according to the posture of the volunteers. This model includes 600 1D muscles. The activation of the stretched muscles is controlled to maintain their initial length. Additionally, the model has been further improved to laterally activate the neck musculature based on the distance to the surrounding and the head acceleration.

3. Results

The lateral movement of the five volunteers' head to the right was significantly reduced when the side structure was in place compared to when there was no side structure ($p < 0.01$).

The maximum lateral movement of the AHBM head was reduced by approximately 150 mm with the side structure compared to the movement without it.

4. Discussion and Conclusions

The results have shown the influence of the environment on the neuromuscular behaviour of the volunteers.

Furthermore, the enhanced AHBM is capable of showing similar kinematic behaviour as the volunteers depending on the presence or absence of the side structure.

5. References

1. Sandoz B et al., IRCOBI Conference (2018).
2. Davidsson J et al., OSCCAR EU Project (2021)

EFFECT OF SEATBELTS ON SEATED PEDESTRIAN IMPACTS

Daniel Grindle¹, Costin Untaroiu¹

1. Virginia Tech, United States

1. Introduction

Pedestrians who use wheelchairs (seated pedestrians) report 36% - 75% higher mortality rates than standing pedestrians in car-to-pedestrian collisions (CPCs) [1]. A previous computational impact study [2] reported that the head and brain had the highest risk of injury in CPCs but no studies have investigated ways to reduce these injury risks. The wheelchair seatbelt has been reported to reduce head injury risks in tip over events [3]. The goal of this study is to investigate the effectiveness of the seatbelt in simulated CPCs.

2. Materials and Methods

A finite element model of an ultralight manual wheelchair model was developed from CAD data and material properties with online databases. The Global Human Body Model Consortium (GHBMC) male detailed 50th percentile occupant model (M50-O) was selected as the seated pedestrian and placed in the wheelchair. The seated pedestrian was impacted by two simplified, validated vehicles [4], a family car (FCR) and sports utility vehicle (SUV). The pedestrian was positioned laterally to the vehicle at the centreline. Vehicles travelled at 40 km/h with a 1 g ($g=9.81 \text{ m/s}^2$) deceleration pulse (Fig. 1). The vehicle impacts were run with and without a wheelchair seatbelt model. The injury outcomes of interest were the AIS+3 injury risks at the head (He), brain (Br), neck (Ne), thorax (Th), abdomen (Ab), and pelvis (Pe) [2].

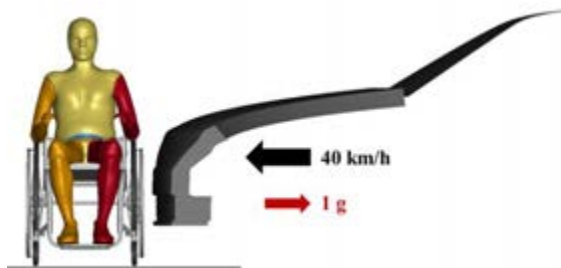
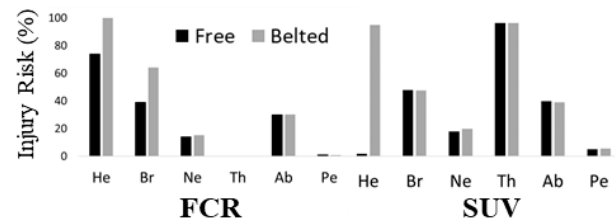


Figure 1: Seated pedestrian impact scenario with FCR

3. Results

The belted pedestrian reported larger risks of head injury with both vehicles and larger brain injury risks only with the FCR (Fig. 2). The remaining injury metrics were mostly unchanged.

Figure 2: Seated pedestrian injury outcomes free and belted



4. Discussion and Conclusions

The use of a wheelchair seatbelt reported to increase the risk of head and brain injury in CPC scenarios. Future work should examine additional impact conditions and different human anthropometries to expand the breadth of this investigation before use recommendations can be made.

5. References

1. Kraemer, J., et al., BMJ Open; 2015; 5(11):
2. Grindle, D., et al., Comput Methods Biomech Biomed Eng, 2022: p. 1-14.
3. Fast, A., et al., Am J Phys Med Rehabil, 1997. 76(5): p. 370-7.
4. EURONCAP, 2019

Acknowledgements:

We thank the Global Human Body Models Consortium, LLC (GHBMC) for providing their M50-OS model used in this study.



ATHLETE 3D MOTION FROM VIDEO: APPLICATION TO INJURY PREVENTION IN ON-FIELD AND OFF-FIELD ENVIRONMENTS

Ciaran Simms (1), Clara Mercadal (2), Euan Reid (3); Richard Blythman (4), Chao Liu (5), Jorge Gonzalez (6), Aljosa Smolic (7)

Centre for Biomedical Engineering, School of Engineering, Trinity College Dublin, Ireland

1. Introduction

Injury is an inevitable consequence of most professional sports, especially contact sports. Injuries arise from unsafe movements, on and off pitch. Multi-camera marker (eg Vicon) and markerless (eg SIMI) systems are the gold standard for athlete kinematic tracking to understand injury prevention, but these are available only for certain elite athletes. Tracking athlete kinematics using one or more handheld cameras holds promise for much more widespread use. This paper presents approaches to tracking athlete collisions on-pitch using three calibrated mobile cameras as well as tracking rehabilitation motion using a single camera.

2. Materials and Methods

On-pitch scenario: we staged low-severity rugby ruck collisions recorded with three spatially calibrated cameras. The 2D human joint positions were inferred using open-source software [1]. Camera calibration (MATLAB tool) combined with using algebraic triangulation allowed for these 2D poses to be lifted to 3D space, centred on the pelvis position.

Off-pitch scenarios, we used eight volunteer athletes to perform common strength & rehabilitation exercises (squats, counter movement jumps (CMJs) and Romanian deadlifts (RDLs)) in a Vicon motion capture environment (eight infra red cameras), where we also recorded the athlete movements using various mobile devices (mobile phones and tablets) in a range of positions in an arc around the athlete. Detectron2 was applied for 2D key point detection [2] together with Stridedformer [3] to predict 3D pose. Knee joint and torso angle changes were assessed by comparison with the Vicon outputs.

3. Results

Sample on-field kinematic results are shown in Figure 1. Sample error measures are shown for the rehabilitation exercises in Table 1 for a camera at 20 degrees from the side and 3m distance from the athletes.



Figure 1: Staged rugby ruck still, 2D keypoint overlay and 3D reconstruction.

Subject	Squat (x9)	RDL(x5)	CMJ(x5)
MEAN	6.5	6.1	6.4
STD	3.2	2.5	2.1

Table 1: Knee joint angle error metrics for squats, RDLs and CMJs.

4. Discussion and Conclusions

The on-pitch tracking using three calibrated cameras is successful up to the point of occlusion, and this approach can be used together with Kinopose [4] to initialise multibody dynamics simulations to estimate collision forces from video [5].

The accuracy of the single camera tracking of common rehabilitation exercises shows significant promise as a means to quantify, though further evaluation is needed.

5. References

1. Cao *et al.*, IEEE Mach Learning, 2019
2. Lo & Girshick, Facebook 2019
3. Li *et al.*, CVPR, 2022.
4. Gildea *et al.*, CVPR 2022
5. Reid *et al.* IRCOBI 2022.

Acknowledgements: Enterprise Ireland & Science Foundation Ireland

DETECTING MUSCLE FATIGUE IN SURFACE EMG DATA THROUGH TOPOLOGICAL DATA ANALYSIS

Allyson Clarke (1), Benjamin Wheatley (1), Chulhyun Ahn (2)

1. Bucknell University, USA; 2. Geisinger Commonwealth SoM, USA

1. Introduction

Estimating the degree of muscle fatigue from surface electromyography (sEMG) recordings has great implications for rehabilitation and sports science. Various linear and nonlinear signal processing methods have been employed in characterizing muscle fatigue from sEMG data.[1, 2] However, endeavors to capitalize on the topological properties of sEMG are in their incipient stages. This study explores the feasibility of using topological data analysis (TDA) as a robust measure of muscle fatigue.

2. Materials and Methods

A total of 31 subjects (ages 19-54, 15 M, 16 F) completed muscle fatigue data collection trials using sEMG. With the hand fixed to a custom rig that included a force sensor attached to the index finger, an sEMG sensor (Delsys, Inc.) was placed on the subject's first dorsal interosseus muscle (Fig. 1A). Subjects were instructed to perform finger abduction at maximum voluntary contraction (MVC). After 2 minutes of rest, subjects were instructed to maintain 50% of their MVC for 5 minutes to ensure muscle fatigue. As a traditional analysis, the sEMG data was segmented into 15 second intervals, and the evolution of median frequency (MDF) was computed from power spectrum of sEMG via fast Fourier transform. As for the TDA of sEMG, graph networks were created for each of the 15 second intervals via visibility algorithm, and then expanded to simplicial chains by equating maximal cliques with simplices.[3] The total number of simplices in the chain served as the topological characterizer of the sEMG time series.

3. Results

Fourteen (n=14) trials were selected for analysis from the greater pool that exhibited constant force values over time. The linear analysis revealed a statistically significant, inverse

nonlinear relationship between MDF and time interval ($p < 0.001$, $R^2 = 0.28$) (Fig. 1B). Average MDF decreased from 104 Hz to 58.9 Hz. The TDA revealed a statistically significant, linear relationship between the number of simplices and time interval ($p < 0.001$, $R^2 = 0.31$) (Fig. 1B). Average number of simplices increased from 2,020 to 3,110.

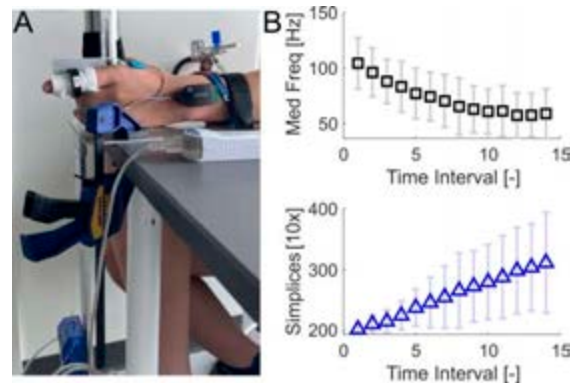


Figure 1: A) Experimental setup to isolate FDI muscle. B) Average MDF (top) and average number of simplices (bottom) as a function of time interval from 20-220 sec (standard deviation bars).

4. Discussion and Conclusions

Compared to the MDF-vs-time interval relationship ($R^2 = 0.28$), the number of simplices-vs-time interval relationship exhibited a more linear correlation ($R^2 = 0.31$) based on visual inspection. This result suggests the number of simplices is not only associated with the degree of muscle fatigue, but may exhibit a stronger correlation than traditionally employed approaches such as MDF. Introducing additional machine learning algorithms drawing on TDA for representing muscle fatigue could further increase the impact and accessibility of this work.

5. References

1. Cifrek et al., *Clin Biomech*, (24) 2009.
2. Rampichini et al., *Entropy*, (22) 2020.
3. Chutani et al., *Chaos*, (30) 2020.

SIMULATIONS OF DYSFUNCTIONAL NEURO-MUSCULAR MECHANISMS EXPLAIN GRADUAL SPASTIC GAIT CHANGES

Christian Lassmann (1), Winfried Ilg (1), Daniel F.B. Haeufle (1,2)

1. Hertie Institute for Clinical Brain Research, University of Tübingen, Germany;
 2. Institute for Modelling and Simulation of Biomechanical Systems, University of Stuttgart, Germany

1. Introduction

Spastic gait is a leading symptom in Hereditary Spastic Paraplegia (HSP) type 4 (SPG4). Due to a length-dependent axonal degeneration in the cortico-spinal tract progressing hyperreflexia, muscle weakness, and spasticity of lower extremities occur. Even before the manifestation of spastic gait, in the prodromal phase, axonal degeneration leads to subtle gait changes [1,2]. These gait changes are related to disease severity in prodromal and early-to-moderate manifest SPG4 subjects.

We hypothesize that disease-specific dysfunctional neuro-muscular mechanisms, such as hyperreflexia and muscle weakness, explain these severity-related gait changes of prodromal and early-to-moderate manifest SPG4 subjects.

2. Materials and Methods

To reproduce subtle gait changes, we used a neuro-muscular model of human walking. We introduced neuro-muscular dysfunction by gradually increasing sensory-motor reflex sensitivity based on increased velocity feedback and gradually increasing muscle weakness by reducing the maximum isometric force in seven muscles per leg.

3. Results

The increased simulated velocity feedback gain (hyperreflexia) produced gradual muscular and kinematic changes that are comparable to the subtle gait changes found in prodromal and early manifest SPG4 subjects. Muscle weakness did not lead to characteristic changes, however, in combination with hyperreflexia we found a toe-gait pattern characteristic of the severe phase of SPG4.

4. Discussion and Conclusions

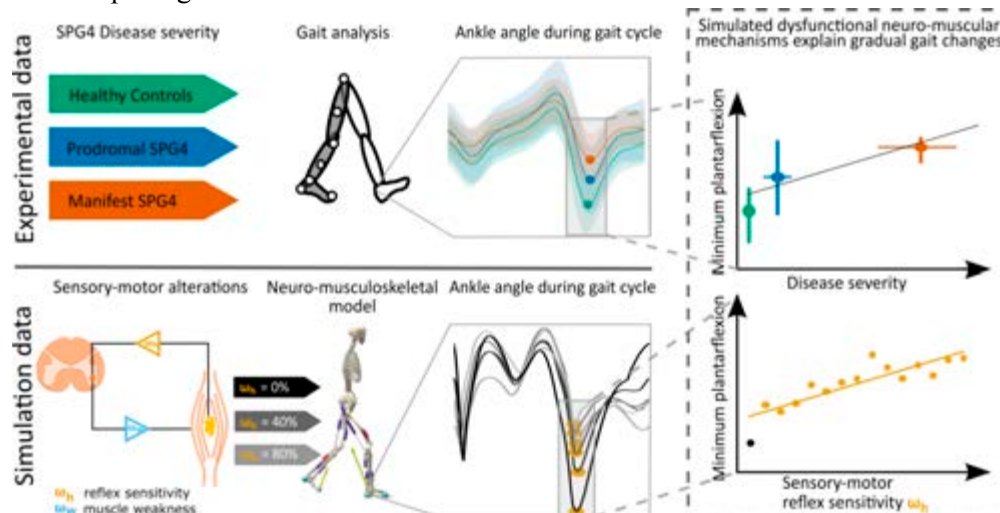
The gradual alteration of sensory-motor reflex sensitivity to predict kinematic and muscular changes of prodromal SPG4 subjects, allows us to identify neuro-muscular changes and link them to gait as a directly accessible performance marker. These insights may help to design future therapeutic interventions.

5. References

- Rattay et al., Brain. 2022; doi:10.1093/brain/awac15.
- Lassmann et al. Movement Disorders. 2022; doi:10.1002/mds.29199.

6. Acknowledgement

In collaboration with T. Rattay and L. Schoels





EMG-DRIVEN ESTIMATION OF MUSCLE MOMENTS REVISITED THROUGH INTEGRATION OF INTERMUSCULAR COHERENCE

Emilie Mathieu (1)*, Sylvain Crémoux (2), David Gasq (3,4), Philippe Pudlo (1)**, David Amarantini (4)**

1. Univ. Polytechnique Hauts-de-France, LAMIH, CNRS, UMR 8201, Valenciennes, France ;

2. Centre de Recherche Cerveau et Cognition, Université de Toulouse, UPS, Toulouse, France ;

3. Explorations Fonctionnelles Physiologiques, CHU Toulouse, Toulouse, France ;

4. ToNIC, Toulouse NeuroImaging Center, Université de Toulouse, Inserm, UPS, France.

* Corresponding author: UPHF, Campus Mont Houy 59313 Valenciennes, France; emilie.mathieu@uphf.fr.

** Co-last authors

1. Introduction

The accurate estimation of mechanical efforts developed by the muscles involved in motor action is of great interest in biomechanics and all related fields. Despite a number of existing (neuro)musculoskeletal models, neural strategies are still poorly exploited while they can contribute to improve estimations of muscle efforts [1]. Neural strategies can be quantified with intermuscular coherence (IMC), i.e., the frequency correlation between two electromyographic (EMG) signals [2]. The aim of the present study is to integrate IMC into an EMG-driven neuromusculoskeletal model to improve the estimation of muscle moments.

2. Materials and Methods

Surface EMG and 3D kinematics of the right upper limb were recorded on 24 healthy subjects performing 10 self-paced in-plane full elbow extensions. The elbow net joint torque was calculated with inverse dynamics. IMC was calculated between the pairs of elbow extensors and flexors [3]. IMC results were used to split each recorded EMG signal into independent and common components further used as input data in an EMG-driven minmax optimization-based musculoskeletal model inspired by [4] and generalized to the upper limb. Estimation of muscle moments and related cocontraction index were compared to those obtained with the same model [4] without integration of IMC.

3. Results

The tracking of elbow net torque calculated with inverse dynamics is similar for both

models, but the optimization doesn't converge for 4 subjects without integration of IMC. Furthermore, the estimations are more physiologically realistic with IMC: the antagonist moments are not neglected while, without IMC, they are zeroed over more than half of the movement for some subjects.

The cocontraction index calculated between agonist and antagonist muscle moments was significantly higher at ~7-37% ($p < 0.001$) and lower at ~77-83% ($p < 0.001$) and ~97-100% ($p = 0.02$) of the extension movement with IMC than without.

4. Discussion and Conclusions

In line with the view that it is necessary to consider neural strategies for consistently improving the estimation of muscle efforts, our results provide strong evidence that the determination of independent and common neural component through IMC improves the physiological interpretation of muscle moments estimation and related metrics. This finding pleads for the integration of IMC in musculoskeletal models to obtain more realistic and interpretable estimates of muscle moments in both healthy and clinical populations.

5. References

- [1] C. Pizzolato et al., J. Biomech., vol. 48, no. 14, pp. 3929–3936, 2015.
- [2] S. Kattla and M. M. Lowery, Exp. Brain Res., vol. 202, no. 1, pp. 89–99, 2010.
- [3] J. Bigot et al., NeuroImage, vol. 55, no. 4, pp. 1504–1518, 2011.
- [4] D. Amarantini and L. Martin, J. Biomech., vol. 37, no. 9, pp. 1393–1404, 2004.

LEARNING WITH MUSCLES: BENEFITS OF MUSCLE-ACTUATED MOTION IN ROBOTICS AND BIOLOGY

Isabell Wochner* (1), Pierre Schumacher* (2,3), Georg Martius (2), Syn Schmitt (1), Daniel F.B. Haeufle (1,3)

1. Institute for Modelling and Simulation of Biomechanical Systems, University of Stuttgart, Germany;
2. Max Planck Institute for Intelligent Systems, Tübingen, Germany;
3. Hertie-Institute for Clinical Brain Research, University of Tübingen, Germany

Correspondence: Isabell Wochner, isabell.wochner@simtech.uni-stuttgart.de

1. Introduction

Humans have the remarkable ability to learn complex and challenging tasks as well as move in uncertain and unstable environments. There is evidence that we do so by relying on our specific biomechanical structure including the nonlinear muscle dynamics. This structure provides inherent stability and simplifies the control by acting as a low-level zero-delay feedback system [1]. However, so far, no research has been conducted to investigate whether muscle actuators also facilitate *learning* in terms of data-efficiency and robustness. Here, we close this gap by applying learning methods to show the benefits of muscle actuators for a wide range of tasks [2].

2. Materials and Methods

We used optimal control and reinforcement learning to learn a wide range of different anthropomorphic tasks, including point-reaching, hitting a ball, squatting, hopping and high-jumping. For each of these tasks, we compared two different actuator morphologies: 1. A Hill-type muscle model with nonlinear activation dynamics and the nonlinear force-length-velocity relation, as well as 2. idealized torque actuators acting directly on the joints.

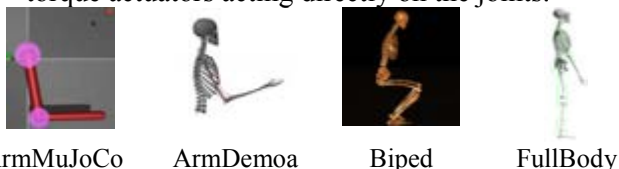


Table 1: Models used to learn different tasks.

3. Results

We showed that muscle-actuated models are in general able to learn more efficiently compared to torque-actuated models. This is shown

exemplarily for point-reaching in Fig. 1. Secondly, we show that the muscle-actuated motions are able to better resist force perturbations e.g. unknown weight lifting or force pushes that were not present during learning.

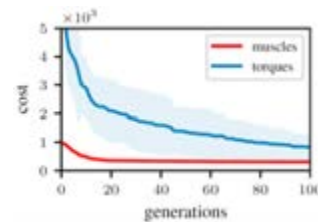


Figure 1: Cost value for point-reaching comparing learning of muscle and torque-actuated motion.

4. Discussion and Conclusions

We showed that using muscle-actuated models, we can learn more efficiently in all tasks except for extreme motions where a strong force application without a trade-off for stability is enforced. This data-efficiency can be exploited for real robotic systems, e.g. wearable rehabilitation devices by using soft robotic actuators (artificial muscles).

5. References

1. Brown, I. E. et al., (1995). Preflexes-programmable high-gain zero-delay intrinsic responses of perturbed musculoskeletal systems. Soc. Neuroscience
2. Wochner, I., et al., Learning with Muscles: Benefits for Data-Efficiency and Robustness in Anthropomorphic Tasks. CoRL 2022.

Acknowledgements:

This work was supported by the DFG under Germany's Excellence Strategy - EXC 2075 - 390740016 (SimTech). We thank the International Max Planck Research School for Intelligent Systems for supporting all authors.



FEMUR STRENGTH ASSESSMENT BY MERGING FE MODELING WITH CT IMAGES FOR HIP FRACTURE RISK PREDICTION

Cristina Falcinelli (1)

1. Department of Engineering and Geology, University "G. D'Annunzio" Chieti-Pescara, Italy

1. Introduction

Osteoporosis compromises femur strength increasing the fracture risk. While fracture is considered a critical endpoint, the success of the bone mineral density (BMD) used to estimate the femoral fracture risk in clinical practice is modest since BMD does not account for mechanical determinants that concur to fracture. Patient-specific modeling of the femur through Computed Tomography (CT)-based Finite Element (FE) models, an established procedure in computational bone biomechanics research [1], has been proposed to overcome BMD limitations. The ultimate aim is to bring these models to clinical practice. This work aims to verify if the femur strength derived from a validated subject-specific CT-based FE modelling procedure can improve the classification of osteoporotic fractures over BMD measurements in three clinical studies.

2. Materials and Methods

Cross-sectional study on proximal femur fracture: 22 proximal femur fractures, 33 controls, all osteopenic or osteoporotic (women). Prospective study on proximal femur fracture: 21 women and 13 men on which proximal femur fractures were prospectively observed, as well as 45 (women) and 26 (men) age-matched controls. Cross-sectional study on prevalent osteoporotic fractures: 35 women with prevalent osteoporotic fracture, 40 BMD-matched controls. CT-based FE strength estimates: femur FE models were generated from CT [2]. Femur strength was evaluated in a wide range of stance and fall loading directions mimicking the in-vivo variability of hip reactions. For each loading direction, femur strength was defined as the load inducing on the femoral neck surface a $\varepsilon_{\max} > \varepsilon_{\lim}$ (0.73% tensile, 1.04% compressive limit). The minimum strength among all stance (FE_s) and fall configurations (FE_f) was considered for patient

classification. Statistics: FE_s, FE_f, and BMD were tested to discriminate groups of fractures from controls and individually classify cases at risk through logistic regressions to derive Area under ROC Curve (AUC).

3. Results

Cross-sectional study on femur fractures: FE_s and FE_f showed higher group differences (33%, $p < 0.001$, vs. 12% for BMD, $p = 0.01$) and a better fracture classification (AUC=0.88 vs. 0.71 for BMD). Prospective study on proximal femur fracture: only FE_s was robust to load identification on proximal femur geometry. In women, FE_s showed slightly higher group differences (19%, $p < 0.001$, vs. 15% for BMD, $p = 0.004$), and a higher classification of fracture cases (AUC=0.78 vs. 0.72 for BMD). In men, FE_s showed non-significant differences, while BMD could discriminate groups and classify fractures (AUC=0.76). Cross-sectional study on prevalent osteoporotic fractures: fractures and controls were BMD-matched by study design. FE_s was 5% lower in fracture cases (differences not significant, $p = 0.32$).

4. Discussion and Conclusions

CT-based femur FE strength estimates add complementary value to the BMD in identifying cases at risk of fracture. A gender difference in FE predictive ability was found. Site-specific use of femur FE models was found to be a key factor. Finally, a wide range of loading conditions that enables specific bone weakness features to be captured (e.g., bending and torsional stress states) improves the performance of the FE model.

5. References

1. Falcinelli C et al., Comput Methods Biomech Biomed Engin; 23(14):1138-1161 (2020).
2. Falcinelli C et al., Bone; 67:71-80 (2014).

THE BONE STRENGTH (BOS) SCORE: PREDICTING FRACTURE RISK IN PATIENTS WITH FEMORAL METASTASES USING A PATIENT-SPECIFIC FINITE ELEMENT MODEL

Esther Tanck (1), Yvette van der Linden (2), Nico Verdonschot (1,3), Edwin Dierselhuis (4), Paulien Westhoff (5), Florieke Eggermont (1)

1. Orthopaedic Research Lab, Radboud university medical center, Nijmegen, The Netherlands;
2. Department of Radiotherapy, Leiden University Medical Center, Leiden, The Netherlands;
3. Laboratory of Biomechanical Engineering, University of Twente, Enschede, The Netherlands;
4. Department of Orthopaedics, Radboud university medical center, Nijmegen, The Netherlands;
5. Department of Radiation Oncology, Radboud university medical center, Nijmegen, The Netherlands

Patients with advanced cancer and femoral bone metastases can have an increased fracture risk. Patients with an expected low fracture risk are generally treated with radiotherapy to relieve pain, whereas patients with an expected high fracture risk are considered for prophylactic stabilizing surgery. However, fracture risk assessment is challenging when using the currently available methods. Therefore, we developed a patient-specific non-linear isotropic finite element (FE) model for fracture risk assessment of patients with femoral bone metastases [1-4] (Fig. 1, central part).

We validated the FE model *in vitro* using cadaveric femurs of which the bone strength was determined using mechanical experiments. We showed that the FE model could predict bone strength in cadaveric femurs with simulated lytic metastatic lesions [1,2]. Next, in two patient studies, we showed that our fracture risk assessments were more accurate than the current Dutch clinical guidelines (30 mm cortical involvement; sensitivity: 100% vs. 86%, specificity: 74% vs. 42%, PPV: 39% vs. 19%, and NPV: 100% vs. 95%) [3,4].

In December 2019, we started a pilot for clinical implementation of the BOne Strength (BOS) score, which aims to be an easy-to-use objective score based on the FE outcomes (Fig. 1). It can help physicians to determine the best treatment together with the patient. In this presentation an overview of our work is presented.

References

- 1) Tanck E. et al., Bone. 45:777-783, 2009; 2) Derikx L. et al., J Bone Joint Surg Br. 94:1135-1142, 2012; 3) Eggermont F. et al., Bone Joint Res. 7:430-439, 2018; 4) Eggermont F. et al, Bone. 130:115101, 2020.

Acknowledgements:

Financial support: Dutch Research Council NWO-STW (NPG.06778), Fonds NutsOhra (1102-071), Furlong Research Charitable Foundation, the Dutch Cancer Society (KUN 2012-5591), Betaalbaar Beter 2018, and Innovatiefonds Zorgverzekeraars (dossier 3919). Participating hospitals: Radboudumc, LUMC Leiden, RIF Leeuwarden and Verbeeten Instituut Tilburg; The Netherlands.



Figure 1: BOS workflow. The radiotherapy planning QCT scan is digitally sent, together with some general patient information such as body weight, to our research lab. The CT scan is used to generate the FE model, on which an axial load is simulated until failure. The BOS score is calculated by normalizing bone strength by body weight. Subsequently, a report is returned, which can be used to determine the best treatment for patients..



PREDICTION OF HIP STRENGTH FROM CLINICAL DATA. WHAT IS NEXT?

B. Helgason^{1,2}, A. Baker¹, I. Fleps^{1,9}, V. S. Cheong², D. Jha^{1,2}, A. Fung¹, A. D. Praveen², E. Bliven^{1,3}, P. Guy³, P. A. Crompton³, H. Palsson⁴, S. Sigurdsson⁶, V. Gudnason⁶, P. Bjornsson⁴, Thor Aspelund⁴, L. Grassi⁷, L. M. Ellingsen⁴, K. A. Greene⁵, A. A. Weaver⁵, H. Isaksson⁷, S. Väänänen⁸, N. Hong¹⁰, Y. Rhee¹⁰, S. Ferguson^{1,2}.

1. ETH-Zurich, CH; 2. Singapore ETH Centre, SG; 3. University of British Columbia, CA; 4. University of Iceland, IS; 5. Wake Forest University, USA. 6. The Icelandic Heart Association, IS; 7. Lund University, SE; 8. University of Eastern Finland, FI. 9. University of Boston, USA. 10. Yonsei University College of Medicine, KOR.

1. Introduction

Despite the lack of sensitivity and specificity of DXA-derived areal bone mineral density (aBMD), in terms of identifying individuals at risk of hip fractures, aBMD has proven to be resilient against attempts from the bone-mechanics field to replace it with biomarkers derived from Finite Element Models (FEMs). In this presentation, we will provide an overview of our current work in this area and provide insight into potential future trends in assessing hip fracture risk in clinical cohorts using FEMs.

2. Materials and Methods

We recently developed an automatic segmentation method [1] for building QCT based FEMs of the proximal femur and used it for modelling 4800 subjects in the AGES Reykjavik cohort (Fig. 1). Fracture classification of the FEMs and aBMD was compared at a 7-year follow-up from baseline using ROC analysis (AUC).

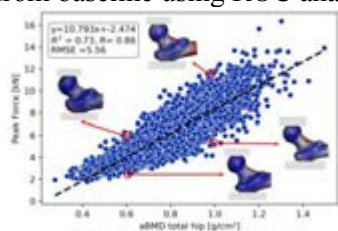


Fig. 1: FEM derived femoral strength vs. aBMD for 4800 left femurs from the AGES cohort.

The use of database models for building 3D FEMs of the proximal femur based on 2D DXA images is gaining interest in our field. With a paired QCT-3D DXA comparison, we are studying how to best utilize the DXA data for this purpose (Fig. 2). Finally, we have extended the capability of our pipeline for building biofidelic FEMs [2] to accommodate both QCT and DXA input. We are currently using this technology for assessing the efficacy of various strategies for preventing hip fractures (Fig. 3).

3. Results

After adjusting for sex and age we found QCT FEM-derived femoral strength to be better at classifying hip fractures in the AGES cohort than aBMD (AUC of 0.80 vs. 0.77, statistically

significant). Our study on a commercially available technology for building DXA derived FEMs, indicates a good match in whole bone volume and bone mass but matching femoral strength for QCT and DXA-derived FEMs may require adaption of the DXA derived data.

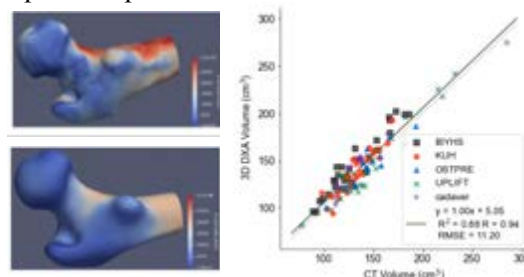


Fig. 2: Paired QCT FEM (above-left) vs. 3D DXA FEM (below-left) built using the 3D Shaper commercial software. Paired QCT vs. 3D DXA analysis of whole bone volume for 112 bones (right).

4. Discussion and Conclusions

Our results support the conclusions of other research groups that QCT FEM derived strength is, at best, only marginally better at classifying hip fractures than aBMD. Some loss of accuracy is to be expected for DXA derived FEMs of the proximal femur compared to CT derived FEMs. However, it may be possible to compensate for this loss through biofidelic representations of soft tissue and adjacent skeletal structures.



Figure 3: Biofidelic FEM for quantifying the efficacy of biomaterial-based femoral augmentation.

5. References

1. P. Bjornsson et al., Comp Meth in Biomech and Biomed Eng: Imag & Vis, 1-13 (2022).
2. I. Fleps et al. Bone, 154:116219 (2022).

Acknowledgements:

PHRT grants 325 and 430, ETH Domain, Switzerland. Future Health Technologies programme, National Research Foundation, Prime Minister's Office, Singapore.



PRACTICAL CONSIDERATIONS FOR THE USE OF 3D DXA-BASED FE ANALYSIS FOR THE ESTIMATION OF FEMORAL STRENGTH

Yvan Gugler (1), Emmanuel Biver (2), Kurt Lippuner (3),
Serge Ferrari (2), Philippe Zysset (1)

1. ARTORG Center for Biomedical Engineering Research, University of Bern, Switzerland

2. Division of Bone Diseases, Geneva University Hospitals and Faculty of Medicine, Switzerland

3. Department of Osteoporosis, Bern University Hospital and University of Bern, Switzerland

Corresponding author: Yvan Gugler; yvan.gugler@unibe.ch

1. Introduction

QCT-based FE analysis has proven to outperform DXA-based areal bone mineral density (aBMD) for the estimation of femoral strength. However, QCT images are not readily available and expensive. 3D DXA [1] is a technology that uses statistical shape and appearance models to reconstruct CT-like 3D images from planar DXA. 3D DXA may have the potential to replace QCT as input for FE analysis. Yet, many open questions remain to be answered, in order to evaluate the suitability of the technology for clinical use.

2. Materials and Methods

Repeated DXA measurements were performed on 38 individuals (age 60.4 ± 13.1 years) at Inselspital Bern. 3D DXA images were reconstructed using the software 3D Shaper (3D Shaper Medical, Barcelona, Spain), totaling 80 3D DXA images. These images were processed using a previously validated FE pipeline for the computation of femoral strength in a side-fall configuration. Short-term precision errors for femoral neck (FN) aBMD and 3D DXA-based strength were computed according to [2].

In addition, 3D DXA images were reconstructed from DXA for 827 women (age range: 62.74 to 76.65; mean: 69.96 ± 2.96 years) from the Geneva Retirees Cohort with 3D Shaper and FE femoral strength was computed. We computed linear regression of FN aBMD and femoral strength versus age. Moreover, we applied strength-based treatment thresholds [3] to compare the classification between 3D DXA-based strength and DXA-based T-scores.

3. Results

The short-term precision error for FN aBMD was 8.3 mg/cm^2 (CV: 0.64%). The error for 3D DXA-based strength was 174 N (CV: 2.51%). Linear regression indicates an age-related decrease of aBMD of 3.0 mg/cm^2 resp. strength

of 61.1 N per year. Figure 1 depicts the categorization of individuals following DXA- and strength-based treatment thresholds suggested by [3]. A large fraction of osteopenic individuals appears to have fragile bone strength.

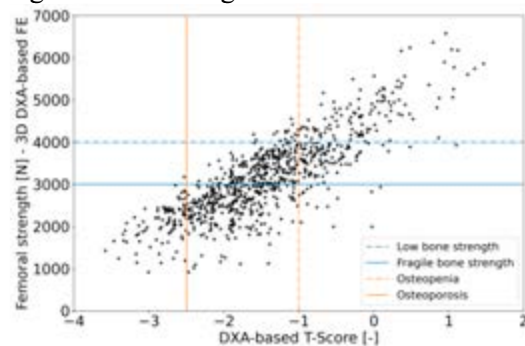


Figure 1: 3D DXA-based strength vs. T-score with interventional thresholds for low and fragile bone strength [3] and DXA-based thresholds.

4. Discussion and Conclusions

Relative precision errors are higher for 3D DXA-based strength computations than for FN aBMD.

Nevertheless, using 3D DXA-based FE strength values instead of aBMD may give interesting insight as many individuals with osteopenia, in fact, appear to have fragile bone strength.

5. References

1. Humbert L et al., IEEE Trans Med Imaging (2017); 36(1):27-38.
2. Glüer CC et al., Osteoporosis Int (1995); 5:262-270
3. Kopperdahl DL et al.; Journal of Bone and Mineral Research (2014) 29(3):570-580

Acknowledgements: The authors thank Dr. Ludovic Humbert for the help with 3D Shaper and the Swiss National Science Foundation (grant no: 183584) for provision of financial support.

PHANTOMLESS CT CALIBRATION INCREASES STRATIFICATION ACCURACY IN A FEMORAL FRACTURE COHORT

Carla Winsor¹, Xinshan Li^{2,3}, Perry J. Pickhardt¹, Heidi Ploeg⁴

1. University of Wisconsin-Madison, USA; 2. University of Sheffield, UK; 3. Insigneo Institute for in silico Medicine, UK; 4. Queen's University, CAN

1. Introduction

CT-based patient-specific femoral fragility fracture finite element modelling is sensitive to mechanical properties. Phantomless CT calibration (phantomless) has been developed to enable the processing and analysis of clinical cohorts lacking phantom-based densitometric CT calibration (phantom-based) information. One public domain method for phantomless CT calibration has been verified and validated by our group [1]. This method has yet to be examined in the context of CT-based patient-specific model of a femoral fragility fracture cohort. The aim of this study is to determine if phantomless CT calibration can be used in place of phantom-based CT calibration.

2. Materials and Methods

26 female prefracture patients and 26 sex and age matched controls were identified from a larger cohort retrospectively collected from routine virtual colonoscopy exams [2]. Clinical scanning parameters were: 120 kVp, 1.25 mm slice thickness, 0.625 mm slice increment, variable current, and standard reconstruction kernels. All scans were captured on GE Lightspeed CT scanners. An offline calibration scan was captured of a femoral density phantom at matching CT acquisition and reconstruction parameters [1]. Patient-specific phantomless calibrations were derived from air, aortic blood, and skeletal muscle using a previously published method [1]. Two material models were set up for each patient: (1) phantomless [1] and (2) phantom-based. Finite element models and simulations were set-up to be consistent with prior studies [1, 3, 4]. The fracture/control stratification accuracy were assessed using the area under the receiver operating characteristic curve, using minimum fall strength and mean tissue segmentation CT Number (HU: Hounsfield Unit) respectively as classifiers.

Power tests were conducted to determine minimum sample sizes.

3. Results

Fracture/control stratification accuracy was 0.02 higher for phantomless derived minimum fall strength than phantom-based. Of the tissues, blood both had the highest stratification accuracy, 0.76, and met the minimum sample size required for statistical power.

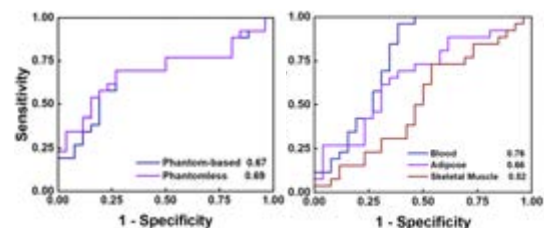


Figure 1: Fracture/control stratification accuracy for: (left) phantom-based, and phantomless derived minimum fall strength; and (right) mean CT Number (HU) for blood, adipose, and skeletal muscle.

4. Discussion and Conclusions

Fracture/control stratification accuracy results are consistent with Michalski et al. 2021 [5]. One factor in the increase in fracture/control stratification accuracy with phantomless CT calibration may be the high stratification accuracy of blood. Phantomless calibration continues to show promise for enabling the analyses of patient CT scans captured without phantom-based CT calibration information.

5. References

1. Winsor et al. Bone 143:115759 (2021).
2. Lee SJ et al. Am J of Roent. 209:2,395(2017).
3. Qasim M. et al. Osteoporos Int. 27:2815 (2016).
4. Altai Z. et al. Clin. Biomech. 68:137 (2019).
5. Michalski A. et al. Osteoporos Int. 32:1639 (2021).

Acknowledgements:

The authors thank the Whitaker Foundation for financial support.

ADVANCES IN EXPERIMENTAL AND COMPUTATIONAL SIMULATION OF TKA MECHANICS DURING ADLS

Chadd W Clary (1), Yashar A Behnam (1), Ahilan Anantha Krisnan (1)

1. University of Denver, Center for Orthopaedic Biomechanics, USA

2155 E Wesley Ave, Room 279, Denver, CO, 80120, USA, email: chadd.clary@du.edu

1. Introduction

Development of total knee arthroplasty (TKA) requires *in vitro* simulation of *in vivo* tibiofemoral (TF) and patellofemoral (PF) joint loading for pre-clinical evaluation of knee kinematics and stability. Advancements in finite element (FE) modelling have led to improved tools to predict knee mechanics and are commonly used during pre-clinical testing of TKA designs. The purpose of this study was to develop a novel experimental simulator to evaluate knee mechanics with load-control of both TF and PF joints and to experimentally validate a complementary FE model.

2. Materials and Methods

A servo-hydraulic 6-DoF VIVO joint simulator was retrofit with a secondary actuator to enable whole joint loading (Fig. 1). A corresponding dynamic FE model of the simulator was developed in Abaqus Explicit, including the bones and implants modelled with a pressure-overclosure contact relationship and friction ($\mu=0.04$). The quadriceps and patella tendons were modelled as fibre-reinforced membranes and the VIVO actuators with connector elements [1].

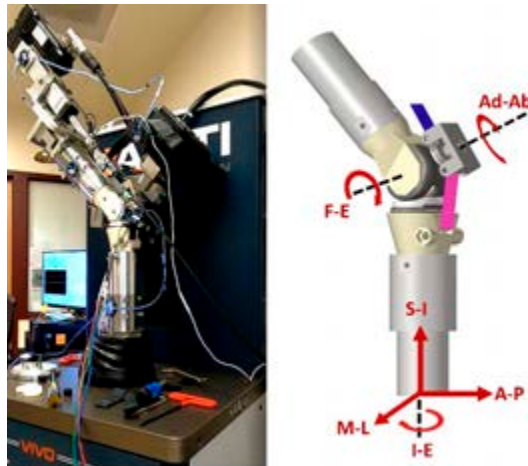


Figure 1: Simulator (left) and FE model (right).

The FE model was used to develop loading conditions that replicated *in vivo* activities of daily living (ADL) kinematics measured during dynamic fluoroscopy of the same implant system [2]. The experimental boundary conditions were evaluated on a cohort of 12 cadaveric knees.

3. Results

Verification testing demonstrated root mean square errors (RMSE) between the model and experiment kinematics ranging from 0.3 to 1.6 mm and 0.4° to 1.7° for TF predictions, and from 0.7 to 1.3 mm and 0.8° to 1.7° for PF predictions. Cadaveric simulations recreated the target condylar translations observed from fluoroscopy, with RMSEs ranging from 0.3 to 4.3 mm for the medial and lateral condyles during gait, stair descent, and sit-to-stand activities.

4. Discussion and Conclusions

Standardized boundary conditions historically used to evaluate implant mechanics are not always appropriate for modern implant designs and surgical techniques. The combined experimental and computational framework developed in this study enables implant-specific and patient-specific simulation in pre-clinical TKA testing.

5. References

1. Fitzpatrick C, et al. Comput Methods Biomech Biomed Engin. 2014;17(4)
2. List R et al. PLoS One. 2017;12(10):1-13

Acknowledgements:

The authors would like to thank Depuy Synthes Joint Reconstruction for providing financial support to this project.



ACETABULAR CUP ORIENTATION DURING GAIT: VARIATION AND IMPLICATIONS FOR HIP REPLACEMENT DEVICE TESTING

Alison Jones (1), Lee Etchels (1), Philip Conaghan (2,3), Graham Isaac (1), Sophie Williams (1), Ruth Wilcox (1)

1. Leeds Institute of Medical and Biological Engineering, University of Leeds, UK 2. Leeds Institute of Rheumatic and Musculoskeletal Medicine, University of Leeds, UK 3. National Institute for Health and Care Research (NIHR) Leeds Biomedical Research Centre, UK

1. Introduction

Standard hip replacement testing conditions represent averaged gait loading profiles and simplified relative movement of the joint. These simplifications are more significant when testing under separating conditions, where the head-liner contact location moves on to the liner rim. The aim of this work was to quantify the movement of the acetabular cup during swing phase of gait, the person-to-person variation in that movement and assess the implications for testing of hip replacement devices under separating conditions.

2. Materials and Methods

Pelvic angles and ground reaction forces during gait were taken from 30 participants (15 male, 15 female) from a cohort of people with symptomatic hip pain at Chapel Allerton Hospital, Leeds. Their native acetabular orientation (within the pelvis) was measured from three-dimensional supine MRI of the pelvis and hip joints. Dynamic acetabular cup orientation during gait was calculated by assuming an initial cup implantation position and applying the movement of the pelvis. Subject-specific cup orientations were recorded for two points in the gait cycle: toe-off and heel-strike, marking the start and end of swing phase. The calculation was performed for 1) a cup implantation position aligned with the native acetabular position of that patient, and 2) a position consistent across all patients (45° inclination angle, 18° version angle). The latter aided the separation of patient specific anatomy effects and patient specific effects.

3. Results and discussion

There was greater variation in inclination angle from native anatomy (Fig.1A) than from pelvic movement during gait (Fig.1B). Overall those inclination angles are well represented by the current ISO14242-4 testing (i.e. a static 65° inclination). In contrast, the cup version angles

were poorly represented by that test (i.e. a static 0° version). The vast majority of version angles before and after swing phase were greater than zero, reaching a maximum of 40° (at heel-strike, for one patient). There was an increase in version during swing phase for the majority of patients (29/30); a mean increase of 5.6° (-4 to 11°).

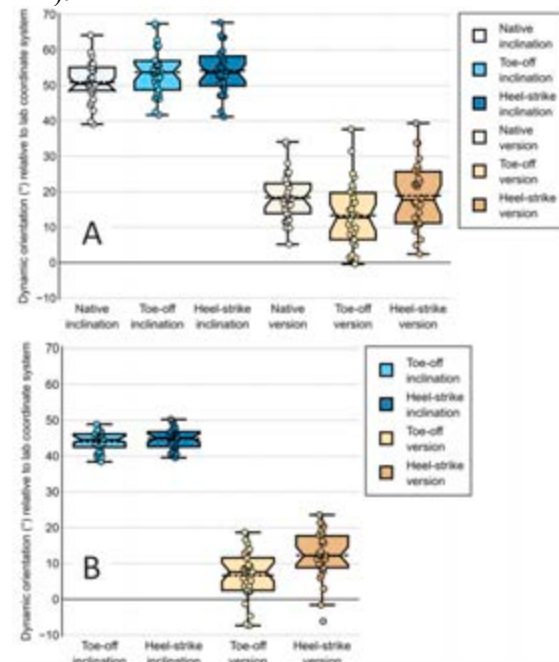


Fig. 1: Box plot of acetabular cup inclination and version angles at toe-off and heel-strike of gait, for A) an implantation position matching the native acetabular and B) a universal implantation position.

4. Conclusions

Testing with larger acetabular cup version angles and an increase in that angle during swing phase may impact the separation and rim loading patterns, and therefore severity of damage, that occurs.

Acknowledgements:

Financial support provided by EPSRC (EP/N02480X/1, EP/W003139/1) and NIHR through Leeds Biomedical Research Centre.



TESTING THA DESIGNS UNDER FEMORAL HEAD TO LINER RIM CONTACT CONDITIONS – USING COMPUTATIONAL MODELLING TO SUPPORT AND DEVELOP THE METHODOLOGY

Lee Etchels (1), Ruth Wilcox (1), Alison Jones (1)

1. Leeds Institute of Medical and Biological Engineering, University of Leeds, UK

1. Introduction

Pre-clinical hip replacement testing under separation conditions forces the contact to the liner rim during swing phase. Separation is generated by a passive spring that provides a lateral misalignment force. The separations are dependent on the loading, implant design and size, and liner orientation. Understanding the kinematics prior to experimental testing can aid planning and introduce edge loading considerations earlier in the design cycle. Understanding the liner stress-strain state can aid the interpretation of the experimental results and ongoing design refinement.

2. Materials and Methods

PyEL [1]: An open-source rigid static python tool estimates the maximum separation, and resulting liner contact location, for different designs, component orientations, and loading scenarios. Validated against experimental test data and static implicit and dynamic explicit finite element (FE) models.

Dynamic Explicit FE: Model of 36mm metal-on-polyethylene bearing (Fig. 1). ISO 14242:4 test conditions. Mass-scaling and mesh refinement analysis allowed for 0.075mm rim elements and <1h run times. Sensitivity of rim plastic strain to the spring damping coefficient and experimental fixture mass was investigated (range 0 – 2Ns/mm and 0.5 – 5kg) to capture potential effects of different simulator setups.

3. Results

PyEL: The experimental tests were overdamped and therefore the static solution maximum separations matched well ($\pm \sim 0.3$ mm). PyEL underestimated the peak rim load as the head moved back into the cup more slowly at heel strike in the dynamic models.

Dynamic Explicit FE: The plastic strain variation across the range of inputs considered

was similar to changing the swing phase load from 70N to ~ 200 N. Increased damping or mass resulted in an increase in the peak plastic strain (range 0.15 – 0.19).

4. Discussion and Conclusions

Computational models can aid in device design earlier in the development cycle, and provide additional insights behind the results seen from experimental testing. The static PyEL model can be used to select test cases and gauge the effect of uncertainty in the simulator inputs. The dynamic Explicit FE showed sensitivity to the mass and damping, and these factors should be described when reporting results, however this modelling approach was needed to capture peak rim loading and therefore potential liner damage.

5. References

1. Etchels, L. et al., J. Biomech.; 95 (2019).

Acknowledgements:

The authors would like to thank the EPSRC (Grant no's: EP/N02480X/1, EP/W003139/1) for providing financial support to this project.

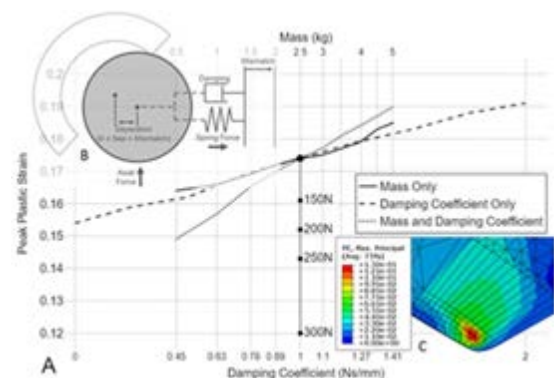


Figure 1: (A) Peak absolute principal plastic strain for the variations in fixture mass, spring damping coefficient, and swing phase load. (B) Schematic of the test methodology. (C) Plastic strain at liner rim, showing subsurface concentration.



IMPACT OF FEMORAL DEFECT SIZE ON PRIMARY STABILITY OF TAPERED SPLINED REVISION HIP STEM

Lin Wang, Richard Patnelli, Oliver Coultrup

DePuy Synthes, Leeds, UK

1. Introduction

Tapered splined titanium stems (TSTSs) have shown excellent survival and reliable clinical results in cementless hip revision surgery where proximal bone is often compromised. Nevertheless, effects of defect size on the axial and torsional stability of TSTS, which are critical for bone on-growth and long-term success, are not well documented. In addition, the few published studies all rely on resource-intensive benchtop or cadaveric testing. Hence, the present study investigated multi-strike stem insertion and post-seating torsional resistance in the cases of intact and defected bones, by utilising a cost-efficient “digital twin” [1].

2. Materials and Methods

Explicit Finite Element Analysis (FEA) coupled with an adaptive meshing technique was used to simulate highly non-linear contacts and material deformations. A 26x235mm 2.5° taper TSTS (which features an innovative design by hybridising primary straight splines with secondary angled splines [1]) is anchored into a pre-reamed elastic-plastic 20PCF polyurethane foam block through multiple impactions (hammer mass = 0.7kg; initial speed = 5m/s), as shown in Figure 1a. Proximal portions of the blocks were removed by 30% and 50% of the full taper engagement length, representing Paprosky type 1 and 3a defects. For benchmarking purpose, rotation of five-degrees along the axial axis was applied to the stem which had been fully seated quasi-statically (Figure 1b), to evaluate the torsional stability.

3. Results

Based on the insertion FEA, only 4 hammer strikes were required for the stem to be fully seated (defined as stem progression < 0.5 mm for any given strike) into the intact foam block with a cumulative progression of 7.5 mm. However, as for 30% and 50% bone defects,

numbers of strikes required for full-seating were doubled (8 strikes) and more than quadrupled (17 strikes); while the progressions increased to 14.6 mm and 29.1 mm (Figure 1c), respectively. Moreover, the peak insertion forces were predicted to be 2801 N, 4238 N and 5327 N; while peak torques were 27.2 Nm, 32.8 Nm and 39.1 Nm, according to the stem torsion FEA with 0%, 30% and 50% bone loss.

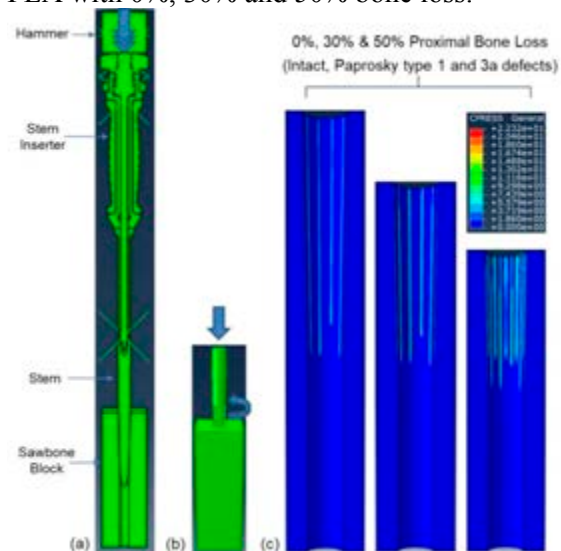


Figure 1: Illustration of stem insertion (a) and torsion (b) FEA models; Contact pressure (MPa) results of stem-bone interface when fully seated (c).

4. Discussion and Conclusions

Femoral defect size plays a key role in the intraoperative progression, bony engagement and primary stability of TSTS. Noticeably, the stems travel further for larger defects, indicating that the surgeon must be careful to select the appropriate stem length based on the patient presentation. The novel in-silico technique may offer an effective and efficient platform to evaluate patient, surgical and design factors.

5. References

1. Wang, L., Digital Twin: Investigating Effects of Spline Designs on Revision Hip Stem Seating, WCB2022, Taipei, Taiwan.



ON THE INFLUENCE OF INCORRECT IDEALIZED JOINT AXES TO THE DESIGN PROCESS OF ORTHOSES

Patrick Steck (1), David Scherb (1), Harald Völkl (1), Jörg Miehling (1), Sandro Wartzack (1)

1. Friedrich-Alexander-Universität Erlangen-Nürnberg, Engineering Design, Germany

1. Introduction

According to the analysis of the Global Burden of Disease (GBD) approximately 1.71 billion people worldwide suffer from musculoskeletal disorders [1]. For the treatment of gait pathologies so-called ankle foot orthoses (AFO) are used in the field of rehabilitation and physiotherapy [2]. Therefore, precise information about the individual joint axes position for each patient are necessary. This contribution illustrates what happens if an idealized axis is applied on a structural analysis of orthoses. Furthermore, it is shown that 3D scanning methods can provide similarly good results in the determination of joint axes like high-cost (magnetic resonance) or radiation-risk (computed tomography) methods.

2. Methods

Since the strip light projection (SLP) method is not conventionally used for moving objects, a set of fixtures are designed and manufactured to fix the foot and lower leg during imaging. In order to determine the precision and accuracy 10 measurements are made. After that, the tessellated 3D model is transformed into a B-Rep model. Finally, a transient structural analysis is applied to determine the impact of position idealization on the reaction forces of an ankle foot orthosis. For constraints and loads, the approach according to [3] is chosen and the material is assumed to be isotropic and linear-elastic.

3. Results

Figure 1 shows foot-flat load curves of a generic orthotic design space with real and idealized ankle axis position. Both the axial reaction forces and the bending due to a moment are significantly higher for the idealized joint axis. While the axial loads in both cases remain approximately constant over the complete load

phase, the bending moments show an exponential course.

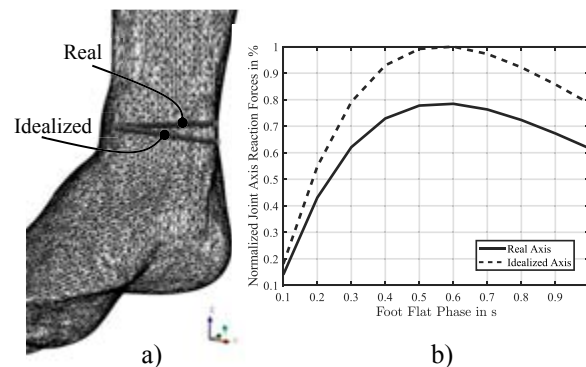


Figure 1: a) Different ankle joint axes orientation b) Normalized loads on the ankle joint during the foot flat phase.

4. Discussion and Conclusions

Since the reaction forces on the ankle joint are overestimated when the idealized axis is used, lower safety factors can be assumed for the design of orthoses. In musculoskeletal simulation the axis should be modified to match the measured orientation. Furthermore, the presented results can open up additional potential for lightweight design.

5. References

- Sebbag, E. et al.: The world-wide burden of musculoskeletal diseases. In. Annals of the Rheumatic Diseases Bd. 78 (2019) Nr. 6
- Kirby, K. A.: Subtalar joint axis location and rotational equilibrium theory of foot function. J. o. the American Podiatric Medical Association Bd. 91 (2001) Nr. 9
- Galica, A. M. et al.: Hallux valgus and plantar pressure loading: the Framingham foot study. J. o. foot and ankle research Bd. 6 (2013)

Acknowledgements:

The authors gratefully acknowledge the German Research Foundation (DFG) (Grant no: WA 2913/43-1 and MI 2608/2-1) for providing financial support to this project.

3D ULTRASOUND-BASED MECHANICAL AND GEOMETRICAL ANALYSIS OF ABDOMINAL AORTIC ANEURYSMS

Esther Maas (1,2), Arjet Nievergeld (1,2), Judith Fonken (1,2), Mirunalini Thirugnanasambandam (1), Marc van Sambeek (1,2), Richard Lopata (1)

1. Eindhoven University of Technology, Netherlands; 2. Catharina Hospital Eindhoven, Netherlands

1. Introduction

An abdominal aortic aneurysm (AAA), a local dilatation of the aorta, is a progressive condition. Between patients, there is a large variety in the advancement of the disease, with differences in growth rates and diameter at which the AAA ruptures [1-2].

In this study, these differences between patients were investigated by analyzing 3D geometrical and mechanical parameters of AAAs in a longitudinal study using time-resolved 3D ultrasound (3D+t US), providing insight in mutual relationships of these parameters, and correlations with diameter and growth.

2. Materials and Methods

For 178 patients, 3D+t US AAA images were obtained. All patients had ≥ 3 follow-up 2D-US based diameter measurements (d_{2D}), from which the growth after the 3D+t US acquisition was obtained. A fully automated analysis tool was developed to (Fig. 1a):

1. Segment the aortic wall on all time frames.
2. Determine the contours \perp to the centerline (CL), maximal diameter (d_{3D}) and volume (V_{60}) in a 60mm region around d_{3D} .
3. Calculate compliance (C) and distensibility (D) of the AAA, based on the volumes, diameter-time curves and pulse pressure.

The acquired volumes and diameters were compared to the available computed tomography (CT) scans (N = 30). Relationships between parameters were explored with Spearman correlation, and parameters' predictive value for growth were investigated.

3. Results

The automatic segmentations, successful for 172 of 178 patients, show good correspondence to CT (median SI 0.92). Diameters are slightly underestimated (Fig. 1b), but the range in differences is similar to d_{2D} (10 and 9 mm).

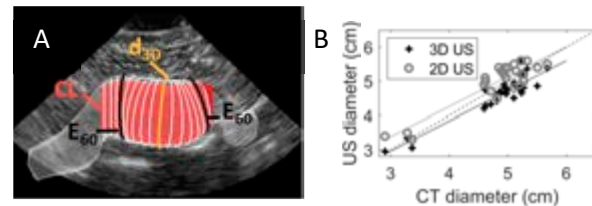


Figure 1: A: US (red) and CT (white) geometry, centerline CL , perpendicular slices (white), maximal diameter d_{3D} and edges E_{60} of the 60mm region. B: US and CT based maximal AAA diameters.

A decrease in D with increasing diameter ($p < 0.05$) and blood pressure ($p < 0.0001$) was observed. Furthermore, growth is related to d_{2D} and d_{3D} , V_{60} , and C ($p < 0.005$). C has a better predictive value for growth than the established relation with diameter [1,3] (Fig 2).

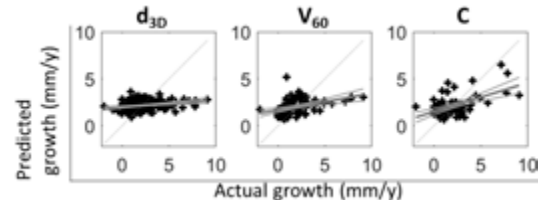


Figure 2: growth prediction based on d_{3D} , V_{60} and C .

4. Discussion and Conclusions

A tool to automatically determine 3D mechanical and geometrical AAA parameters from US images had been developed, validated, and applied to a large patient group. With this, compliance has been identified as a potential growth predictor. This is a step towards more patient-specific treatment of AAAs.

5. References

1. Brady AR et al., *Circulation*; 110(1):16-21 (2004)
2. Nicholls SC et al., *J Vasc Surg*; 28(5):884-8 (1998)
3. Schouten O et al., *Eur J Vasc Endovasc Surg*, 32(1):21-6 (2006)

Acknowledgements:

The authors would like to thank the European Research Council (Grant no: 757958) for providing financial support to this project.

A 3D PREOPERATIVE PLANNING TOOL FOR SELECTIVE CLAMPING DURING PARTIAL NEPHRECTOMY

Saar Vermijs (1,2,3), Pieter De Backer (1,2,4,5), Pieter De Visschere (6), Alexandre Mottrie (4,7), Charles Van Praet (2,5), Karel Decaestecker (2,5,8), Charlotte Debbaut (1,3)

1. IBiTech-Biommeda, Ghent University, Belgium; 2. Dept. of Human Structure and Repair, Ghent University, Belgium; 3. CRIG, Belgium; 4. ORSI Academy, Belgium; 5. Dept. of Urology, Ghent University Hospital, Belgium; 6. Dept. of Radiology and Nuclear Medicine, Ghent University Hospital, Belgium; 7. Dept. of Urology, OLV Aalst, Belgium; 8. Dept. of Urology, AZ Maria Middelaes, Belgium

1. Introduction

During (robot-assisted) partial nephrectomy (RAPN) the so-called ‘trifecta’ should be reached: (i) negative surgical margins, (ii) minimal injury to the healthy renal parenchyma and (iii) avoiding complications [1]. Selective clamping (SC) facilitates the trade-off between the last two goals by minimizing both ischemic time and blood loss [2]. Here, an in-house developed 3D preoperative planning tool to determine the optimal clamping position is presented and tested against intraoperative imaging data.

2. Materials and Methods

Retrospectively, 25 patients who underwent RAPN with SC at Ghent University Hospital were included. Four-phase CT-scans (à blanc, arterial, venous and excretory; pixel size ≤ 1 mm; slice thickness ≤ 1.5 mm) were collected and segmented in Mimics (Materialise, Belgium). Centerlines were calculated in the 3D segmented arterial tree (vmtk.org) to label the arterial branches. A region growing algorithm was executed within a voxelized bounding box around the parenchyma and tumor using labeled centerline points as initial seeds. This resulted in a 3D model indicating the kidney perfusion zones for each patient.

Next, the clamped selective arteries were identified on the retrospective surgical video and the indo-cyanine green (ICG) injections revealed their perfusion zones. This was compared to the calculated perfusion zones using two metrics based on scoring total overlap of perfusion zone contours on both tumor and parenchyma (metric 1) and the ratio of perfused/ischemic tissue at tumor level using a scoring grid (metric 2) (Fig 1).

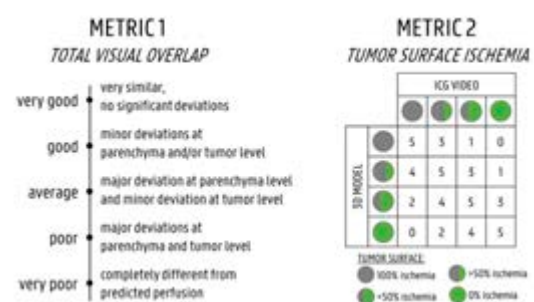


Figure 1: The perfusion zones derived from ICG contours were compared to the calculations. Overlap was evaluated using two metrics. Six urologists scored metric 1. The authors scored metric 2.

3. Results

Metric 1 resulted in an average score of 4.28 out of 5 on the proposed Likert scale (median: 5; range: 2-5; IQR: 4-5). Metric 2 resulted in an average score of 4.14 out of 5 (median: 5; range: 2-5; IQR: 3.5-5). Lower scores were observed in cases where the perfusion zone border was close to the tumor, as a small deviation in this area was penalized more severely.

4. Discussion and Conclusions

In this study, an in-house developed planning tool for SC during PN was validated. Note, however, that ICG was only visible on the kidney surface and therefore the inner perfusion zones could not be validated. Nonetheless, the results of this study are promising.

5. References

1. A.J. Hung et al. J Urol. 2013; 189(1):36-42
2. G. Di Lascio et al. C E J Urol. 2022; 75(1):14-27

Acknowledgements:

The authors would like to thank the six urologists for scoring metric 1 and Ipsen NV (Belgium) for financial support.



TOWARDS AN *IN-VIVO* MRI-PATHOLOGY TOOL TO DECODE PLACENTAL ABNORMALITIES

Romina Plitman-Mayo (1), Talia Harris (2), Elisha Goldstein (3), Ido Azuri (3), Michal Kovo (4), Simcha Yagel (5) & Michal Neeman (1)

1. Department of Immunology and Regenerative Biology, Weizmann Institute of Science, Israel; 2. Department of Chemical Research Support, Weizmann Institute of Science, Israel; 3. Department of Life Sciences Core Facilities, Weizmann Institute of Science; 4. Department of Obstetrics & Gynecology, Meir Medical Center, Israel; 5. Department of Obstetrics & Gynecology, Hadassah-Hebrew University Medical Center, Israel.

1. Introduction

Placental malfunctioning accounts for most of pregnancy complications [1]. However, placental *in vivo* and *ex vivo* imaging has proved to be extremely challenging due to its vascular complexity and pregnancy-related ethical constraints. This study aims to develop a proof-of-concept for the detection of placental complications using MRI and ML methods.

2. Materials and Methods

Delivered placental samples were scanned in a 15.2-T MRI scanner. Utilizing a 3-D Gradient Recalled Echo sequence, four sets of MRI images with 100 μ m isotropic resolution were acquired and from these images, magnetization transfer, T1 relaxivity, T2* relaxivity, and apparent diffusion were determined for each voxel. A digital biopsy of 186x186x186 pixels was taken and normalized, and the pixels were clustered by the unsupervised Fuzzy c means machine learning algorithm. A ground truth sub-set was semi-automatically generated. Each cluster was then characterized by the corresponding pathological features. As a preliminary step, each cluster was compared between healthy and gestational diabetes placentas.

3. Results

High-field MRI of post-partum placenta specimens reveals the pattern of villi organization. Figure 1(a) shows a representative slice of the magnetization transfer, T1 relaxivity, T2* relaxivity, and apparent diffusion images for a healthy placental sample, where red highlights the regions with high signal and blue with low. Figure 1(c) shows an example of a digital biopsy, a labelled slice

according to the different clusters, and a histogram of the labelled pixels. Figure 1(c) shows a representative slice, with the model-based and unbiased clustering aligned with its corresponding histological section for annotation purposes.

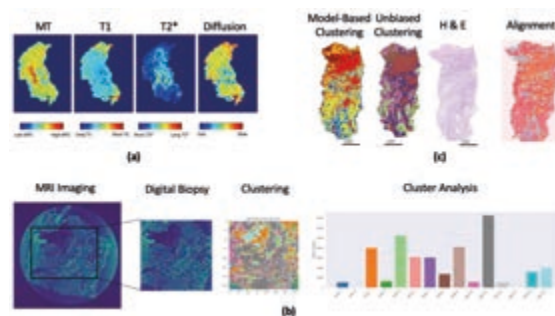


Figure 1: (a) Four sets of MRI images; (b) Overall project approach; (c) Generation of the ground truth.

4. Discussion and Conclusions

MRI has the potential to become an invaluable tool in pregnancy management and early diagnosis of pregnancy complications. The combination of multiple contrast mechanisms together with machine learning techniques can reveal the richness of pathological information and shed light on the antenatal environment that can affect pregnancy outcome. This study demonstrates the capabilities of MRI in the determination of placental micro structure and detection of pathologies.

5. References

1. Benirschke K, Burton GJ, Baergen RN (2012). Springer, Sixth edition.

Acknowledgements:

This study is partially funded by ISF and Minerva Foundation research grants.



EFFECT OF YAWNING ON CSF AND BLOOD FLOW THROUGH THE NECK

Adam Martinac, Robert Lloyd, Stean Waters, Lynne Bilston

1. Neuroscience Research Australia, Australia

1. Introduction

Research into yawning has received little attention, despite being a common behaviour amongst most mammals, amphibians, and reptiles [1]. Yet, beyond simple characterisation, investigation into the mechanics of yawning is limited [2]. The purpose of this study is to investigate the effect of respiration on the flow of neurofluids during yawning. By observing neurofluid movement through the C3 vertebra, using sagittal real time and phase contrast scans, we expect that the flow will be driven by differences between spinal and cranial pressures and not only a cranial fluid volume balance.

2. Materials and Methods

MRI data was collected using a 3T Philips IngeniaTX. During the scans, the subjects were supine and were shown video clips of people and animals yawning to induce contagious yawns. The scans collected included anatomical scans of the head-neck region, and real time phase contrast MRI scans to measure blood and CSF flow during yawning and quiet breathing using real-time-PC-MRI protocols. Respiratory motion was also recorded concurrently with the MRI scans using a respiratory monitoring band, placed on the sternum, measuring thorax displacement.

3. Results

Figure 1 shows typical data obtained from the MRI scans and respiration band in a representative subject during periods of normal breathing and yawning. We collected data on CSF and blood flow (carotid and vertebral arteries and the internal jugular vein (IJV)). The most pronounced changes in neurofluid flow were noticed during the sharp inspiration, “gaping”, and sharp exhalation. IJV and CSF flow were found to both move caudally during inspiration and rostrally during expiration.

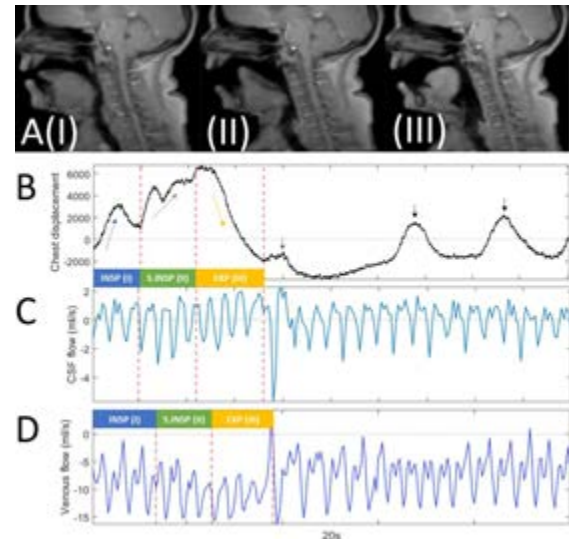


Figure 1: (A) Time lapse of 1 yawn. Multiple vertical dashed lines indicate end of yawn phases. (I) Start of yawn, tongue retracts, and inspiration begins (blue box). (II) Sharp inspiration (green box). (III) Sharp exhalation (yellow box). (B) Chest displacement. Blue arrow after yawn is a swallow and black arrows are normal breaths. (C) CSF flow through C3. (D) Venous blood flow through C3. Scan was taken separately from B and C.

4. Discussion and Conclusions

Our findings are in line with recent investigations into a holistic view of cranial and spinal respiratory CSF flow [3], where cervical CSF flow directions during respiratory manoeuvres (coughs and sniffs) depend on the difference between spinal and cranial pressures.

5. References

1. Baenninger, R. *Psychon Bull Rev* 4, 198–207 (1997).
2. Guggisberg, A. G., Mathis, J., Schnider, A., & Hess, C. W. (2010). *Neuroscience and Biobehavioral Reviews*, 34, 1267-1276.
3. Lloyd RA, Butler JE, Gandevia SC, et al. *J Physiol*. 2020;598(24):5789-5805.

Acknowledgements:

The authors would like to thank the NHMRC for providing financial support for this project (NHMRC Investigator Grant #APP1172988 (RG183247)), and the Australian Government for providing an RTP Scholarship.



TOWARDS MECHANICAL CHARACTERIZATION OF BOTH AAA WALL AND INTRALUMINAL THROMBUS USING 3D+t ULTRASOUND

Arjet H.M. Nievergeld(1,2), Judith H.C. Fonken(1,2), Esther J. Maas(1,2), Marc R.H.M. van Sambeek(1,2) and Richard G.P. Lopata(1)

1. Dept of Biomedical Engineering, Eindhoven University of Technology, Eindhoven, the Netherlands;
2. Catharina hospital Eindhoven, Eindhoven, the Netherlands;

1. Introduction

An abdominal aortic aneurysm (AAA) is a localized dilatation of the aorta, which in case of rupture has a mortality rate of 80%. Current clinical guidelines of intervention are based on AAA diameter, which has been proven to be an inadequate criterion. Biomechanical models can improve rupture risk prediction in a more patient-specific way, using e.g. CT or ultrasound (US) imaging [1, 2]. US is safer compared to CT and adds temporal information for mechanical characterization of the AAA. It is hypothesized that the intraluminal thrombus (ILT) lowers the wall stress and therefore should be included in rupture risk assessment [3]. The objective of this study is to show feasibility to use the acquired time-varying geometry of the lumen and vessel wall for mechanical characterization of both ILT and AAA wall, for future patient-specific modelling of the AAA, including ILT.

2. Materials and Methods

An in-house developed semi-automatic segmentation method was used to segment the lumen, ILT, and vessel wall out of 3D+t US images. Despite the low contrast, the lumen diameter-time curve showed a clear blood pressure induced pulsatility in 22 out of 26 patients (Figure 1). Those diameter-time curves were used to calculate the ILT systolic-diastolic volume change, and both lumen and vessel distensibility [4].

3. Results

The ILT volume change (median -0.57%) was within the IQR range of Kontopodis et al. [5]. The median distensibility of the lumen (5.9 MPa⁻¹) and vessel wall (2.8 MPa⁻¹) are lower than the ones found in Molacek et al. (lumen 12 - 30 MPa⁻¹, vessel 5 - 13 MPa⁻¹) [4].

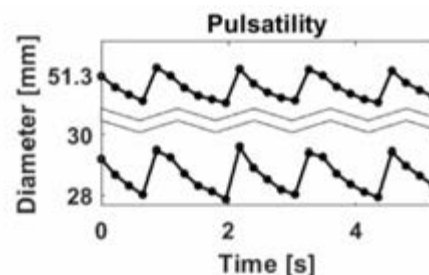


Figure 1: Example diameter-time curve of vessel (upper curve) and lumen (lower curve) for mechanical characterization

4. Discussion and Conclusions

The compressibility was in agreement with literature showing that ILT can be considered as incompressible. The under-estimation in distensibility might result from the low frame rate of (3D+t) US (3.2-7.3 Hz), since this might cause an under-estimation in systolic diameter and over-estimation of the diastolic diameter (Figure 1). Despite this limitation, a higher distensibility was found for the lumen, compared to the vessel. This observation is in agreement with Molacek et al. [5]. Future research will focus on incorporating these mechanical properties in personalized biomechanical models to improve AAA rupture risk assessment.

5. References

1. Van Disseldorp et al, Eur J Vasc Endovasc Surg, 59: 81-91, 2020
2. Kok et al, J Vasc Surg 61: 1175-1185, 2015
3. Domonkos et al. , Int. Angiol.38: 39-45, 2019
4. Molacek et al. Ann Vasc Surg 2011;25:1036-1042
5. Kontopodis et al. Theor Biol Med Model. 2013;10(1):1-9

Acknowledgements:

This work was supported by e/MTIC MEDICAID project.



A BETTER UNDERSTANDING OF ABDOMINAL WALL BEHAVIOUR IN VIVO USING DYNAMIC MRI AND PRESSURE MEASUREMENTS

Victoria JOPPIN¹, Catherine MASSON¹, Arthur JOURDAN¹, Stanislas Rapacchi³,
David BENDAHAN³, Thierry BEGE^{1,2}

1. Aix Marseille Université, Université Gustave Eiffel, LBA, Marseille France

2. Aix Marseille Université, Department of Surgery North Hospital, APHM, Marseille, France

3. Aix Marseille Université, CNRS, CRMBM UMR 7339, Marseille France

1. Introduction

A better understanding of the biomechanical behaviour of the anterolateral abdominal wall might be helpful in order to prevent pathologies such as hernias and improve the corresponding management. The objective of the present study was to assess the relationship between mechanical loading, intra-abdominal pressure (IAP) and the induced response of the abdominal wall through different solicitations so as to describe the behaviour of the healthy abdominal wall *in vivo*.

2. Materials and Methods

A 2 stage experiment was conducted with twenty healthy subjects who were asked to perform audio-guided activities i.e. breathing, coughing and Valsalva maneuver. During the first part of the study, 3T MRI was used to record the kinematic behaviour of the abdominal wall in a transverse plane. During the second step, subjects swallowed a Smartpill® pressure sensor to measure IAP throughout the same exercises as previously described [1], [2].

3. Results

The evolution of IAP is studied as a function of different metrics obtained from MRI images post-processing, such as the radial displacement of abdominal muscles as illustrated figure 1. The average maximum IAP is 12.1, 57.8 and 53.7 mmHg for breathing, coughing and Valsalva maneuver respectively. The average maximum radial displacement is obtained during breathing, with a higher value for rectus abdominis than for lateral muscles (17.9 mm, versus 10.5 mm). Unlike breathing, lateral muscles move mainly inwards during coughing and Valsalva maneuver, while the direction of movement of the rectus abdominis depends on

the individual. The Pearson linear correlation coefficient between temporal evolution of IAP and radial displacement is stronger for lateral muscles than for rectus abdominis, especially for stresses involving muscle contraction.

Intra abdominal pressure and MRI radial displacement, volunteer 1

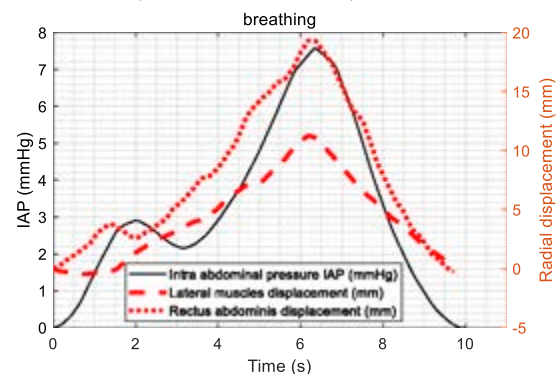


Figure 1 Intra-abdominal pressure (IAP) and radial displacement of abdominal muscles during a breathing exercise performed by a healthy subject.

4. Discussion and Conclusions

This study brings new quantitative data in accordance with results from other studies [3], [4] which allow a mechanical characterization of the abdominal wall by combining the *in vivo* study of both the stresses and their effects on the abdominal cavity.

5. References

- [1] Soucasse *et al*, *Med Eng Phys*, Jun. 2022, doi: 10.1016/j.medengphy.2022.103813.
- [2] Jourdan *et al*, *NMR in Biomedicine*, vol. 34, no. 4, p. e4470, 2021, doi: 10.1002/nbm.4470.
- [3] Cobb *et al*, *Journal of Surgical Research*, vol. 129, Dec. 2005, doi: 0.1016/j.jss.2005.06.015.
- [4] P. Neumann *et al*, *Int Urogynecol J*, vol. 13, no. 2, Apr. 2002, doi: 10.1007/s001920200027.



NEW INSIGHTS INTO NANOSCALE ORGANIZATION OF DENTIN

MC. Riou^{a,b,c}, J. Pérez^d, A. Martin^e, A. Nicolay^f, T. Reiss^e, BPJ Fournier^{a,b,c}, M. de la Dure-Molla^{a,b,g}, E. Vennat^e

^a Université Paris-Cité, Dental Faculty, Paris, France ; ^b Dental Department, Reference Center for Oral and Dental Rare Diseases (ORARES), AP-HP, Rothschild, Paris, France ; ^c Centre de Recherche des Cordeliers, UMR_S_1138, Molecular Oral Pathophysiology, Université Paris-Cité, INSERM, Sorbonne Université, Paris, France; ^d Synchrotron SOLEIL, Saint-Aubin, France ; ^e Université Paris-Saclay, CentraleSupélec, ENS Paris-Saclay, CNRS, LMPS – Laboratoire de Mécanique Paris-Saclay, Gif-sur-Yvette, France; ^f Mines Paris, PSL-Research University, CEMEF-Centre de mise en forme des matériaux, Sophia-Antipolis, France; ^g Université Paris-Cité, Molecular and Physiopathological basis of osteochondrodysplasia, INSERM UMR_S1163 - IHU Imagine

1. Introduction

Dentin is the main tissue of the tooth, located between the enamel and the pulpal cavity. Dentin displays a hierarchical organization with microscale porosities surrounded by a dense mineral collar (peritubular dentin, PTD) called tubules, embedded in a matrix of intertubular dentin (ITD). At the nanoscale, the ITD matrix is made up of an entanglement of collagen fibrils (roughly 100nm diameter) and mineral platelets (roughly 5nm thick). X-Ray ptychotomography (PXCT), a recent nanotomography technique, has already been used by Zanette et al. [1] to analyze the dentin nanostructure, reaching a resolution of about 160nm, superior to the collagen fibril diameter. We present here a new PXCT study with a resolution of 50nm.

2. Materials and Methods

Two healthy teeth were examined, one permanent and one primary. The samples were cut and polished to the micron using classical techniques. Cylindrical samples of roughly 20 microns in height and 20 microns in diameter were extracted, with a first step of coarse micromachining using a Plasma FIB-SEM (Fera3, Tecscan), followed by the extraction and fixation of the sample on the pin, using a Gallium FIB-SEM (Helios 660, FEI).

The PXCT experiments were performed at Synchrotron Soleil on the SWING beamline [2]. A coherent X-ray beam with an energy of 8 keV was focused ahead of the sample position, resulting in a 4 μm probe size. For each tomographic projection, about 500 diffraction patterns were recorded with an exposure time of 0.1 s each by scanning the sample with a step size of 1 μm . This procedure was repeated for about 600 evenly spaced angular positions of the sample which rotated over 180°.

3. Results

Our observations confirm the presence of lateral branches surrounded by a dense collar linking tubules together and a fibrillar mesh globally located in planes perpendicular to the tubule main axis in agreement with the literature. We could also distinguish local heterogeneities in this organization: the interface between ITD and PTD exhibits fibrils oriented along the tubule main axis and there are local differences in mineral density that cannot be seen on averaged/global estimations. More strikingly, the collagen fibrils 3D organization in intertubular dentin can also be observed (Fig. 1), a direct consequence of the very high achieved resolution.

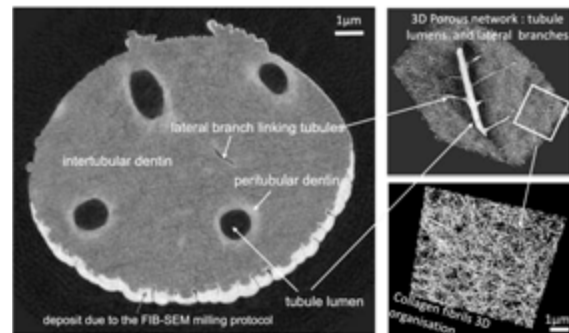


Figure 1: 3D images on the permanent tooth

5. References

1. Zanette I et al., Sci Rep; 5(1), 1-4 (2015).
2. Engblom, et al., J. Euspen's 20th International Conference & Exhibition, (2020).

Acknowledgements:

This research was supported by INSERM/APHP Interface grant (BPJF) and the "Filière Tête-Cou" (Ultradents project). We acknowledge Synchrotron SOLEIL for providing beamtime through proposal 20220699.

SENSITIVITY ANALYSIS AND PARAMETER IDENTIFICATION OF BLOOD FLOW MODELS

Moctar Ndiaye (1), Patricia Cathalifaud (1), Michel Fournié (2), Jean-Pierre Raymond (2), Mokhtar Zagzoule (1)

1. IMFT Toulouse 3, France; 2. IMT Toulouse 3, France

1. Introduction

Our aim is to estimate hemodynamics parameters based on PC-MRI blood flow measurements. We consider a 1d blood flow model for the Circle of Willis (CoW) with Windkessel elements for the peripheral circulation. The model depends on 52 parameters (geometrical properties and Young modulus of the arteries, resistances and compliances of the Windkessel elements), and on time periodic inflow conditions. Our model output (OM1) consists of noisy synthetic flow rates of the 6 outflow boundaries of the CoW, at 32 times/period. The Sensibility Analysis (SA) is performed either with the above 1d model or with the corresponding 0d model.

2. Methods

Our 1d model is a quasilinear hyperbolic system. For the space discretization we use a Discontinuous Galerkin Method with numerical fluxes of high order obtained by solving generalized Riemann problems. For the time discretization, we use the second order Adams-Bashforth method.

To select influential parameters, the SA is done with either outputs corresponding to the inflow pressure or the outflow flow rate of each artery (OM2) or with OM1. We compute the Global Sobol Indices (for the 0d model, with the method in [1] for multivariate outputs) and the sensitivity indices based on the Fischer Information Matrix for the 1d model.

The parameter estimation is done with a Gauss-Newton algorithm and a parameter selection at each iteration, based on the condition number of the Fischer Information Matrix.

3. Results

The Global and Local Sensibility Analysis showed that, for OM1, only the 12 peripheral resistances can be estimated (among the 52 uncertain parameters of our model), see Fig. 1.

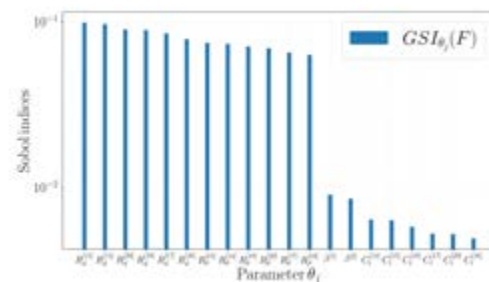


Figure 1: The Global Sobol Indices of the OM1.

Starting from initial guesses with relative errors varying from 15% to 70% for OM1, peripheral resistances are recovered with relative errors varying from 1% to 10%, see Fig. 2.

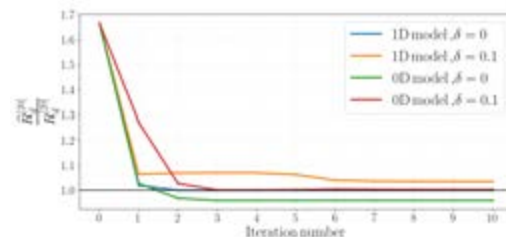


Figure 2: R_d^{20} for the 0d and 1d models with a level noise of δ ($\delta=0.1$ corresponds to 10% of noise).

4. Discussion and Conclusions

Our results confirm that the 0d model can be used for estimating parameters of the CoW [2]. The local and Global Sensitivity indices allow to select the measurements needed to estimate a given parameter.

5. References

1. Xu L. et al., Appl. Math. Model. 66(2019), 592-610.
2. Lal R. et al., Ann. Biom. Eng. 45(2017), 1-18.

Acknowledgements:

The authors would like to thank the French National Research Agency (ANR project HANUMAN 18-CE45-0014-01) for providing financial support to this project.



IDENTIFICATION OF PATIENT-SPECIFIC LEFT VENTRICLE STIFFNESS USING MRI-BASED FEM AND VFM

Mehdi Ghafarinatanzi (1), Delphine Perie (1, 2)

1. Polytechnique Montréal, Canada; 2. Sainte-Justine University Health Center, Montreal, Canada.

1. Introduction

Myocardial function depends significantly on its material properties. Changes in material properties are an important determinant of myocardial dysfunction and even the heart failure. Cardiac magnetic resonance (CMR) tissue tracking methods are a non-invasive imaging technic that allows the measurement of stiffness. Finite element (FE)-based inversion methods that iteratively convert displacement data to stiffness information [1] were not robust when operating on the heart complex geometry. The virtual fields method (VFM) has been introduced as an alternative to FEM inverse that directly uses full image data [2].

2. Materials and Methods

First, the strain field from the measured actual CMR data for the patient-specific left ventricle (LV) were reconstructed. The strain fields are approximated by using the first-order polynomial interpolation functions in brick (8-node) and wedge (6-node) elements. The final FE LV mesh was created by using 2048 element, fitting to the endocardial and epicardial surfaces of the LV at each cardiac phase. The principle of virtual work was required to build up a cost function using the squared residual between strain energy and external work produced by cardiac pressure, Fig 1. Two material parameters, which are coupled in nonlinear Ogden hyperelastic law were determined by minimizing the energy function.

3. Results

In a case study of leukemia cancer survivors with doxorubicin treatment, who were separated into three risk groups: standard risk (SR), high risk (HR), and high risk with dexrazoxane (HR-dex) [3], the stiffness parameters were estimated to be compared between groups. The nonlinear relation between the parameters in hyperelastic law, between

patient-specific groups, revealed changes in the identifiability of the inverse method.

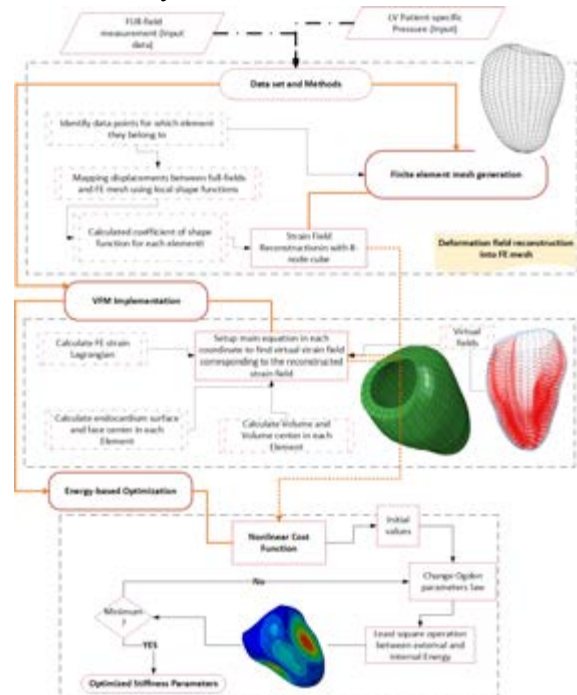


Figure 1: Inverse framework including FE mesh generation, VFM implementation, and optimization.

4. Discussion and Conclusions

The estimated shear modulus values for three groups were affected significantly in presence of large displacements from CMR acquisition. Given the inverse framework, we successfully applied VFM for the reconstructed patient's LV and assessed the identifiability of hyperelastic parameters.

5. References

1. Wang Y. 2012 conference: Springer; 2009. p. 705-14 Doctoral dissertation, Auckland.
2. Avril S et al., Experimental Mechanics; 48(4):381-402 (2008).
3. Aissou, M., F. Cheriet, et al. Canadian Journal of Cardiology; 2016; 32(10): S299-S300.

Acknowledgements:

The authors would like to thank Polytechnique Montreal for providing the financial support.



FROM AUTOMATED AND DATA-DRIVEN MODELLING TO MANUFACTURING OF MECHANO-ACOUSTIC PHANTOM-TWINS

Nataliya Perevoshchikova (1), Christian Langton (1), Ben Liyou (1), Kevin Mattheus Moerman (2), Stefanie Feih (1), Rod Barrett (1), David Lloyd (1), Laurent Frossard (1)

1. Griffith Centre of Biomedical and Rehabilitation Engineering, Griffith University, Australia;
2. Biomechanics Research Centre, National University of Ireland, Ireland

1. Introduction

This study outlines a framework to create a mechano-acoustic transfemoral amputation residuum (TFAR) phantom-twin using patient-specific, automated and data-driven computational modelling and manufacturing.

2. Materials and Methods



Figure 1: TFAR phantom-twin built using SimuLimb, showing the femur (grey), muscle (maroon), and skin and fat (green) volume regions.

The framework involves: (a) creating a patient-specific soft tissue (muscle, fat, skin) TFAR model with volume and surface meshes (Fig. 1); (b) 3D printing soft tissue moulds and femur geometry with Polymaker Polysmooth PVB (Voron24r2 350) and 3DXtech Simubone (Ultimaker S5 Pro), respectively; (c) property testing of representative polymer materials (Pinkysil[®], Dragon Skin[™], Ecoflex[™] 10 and 30); (d) fitting hyperelastic material parameters using analytical and iterative inverse finite element analysis (iFEA) with friction (benchmarking FEBio, v3, University of Utah, USA, and Dassault Systèmes Abaqus Simulia v2022); (e) selecting polymers to best represent soft tissues based on their shear moduli in (d); (f) manufacturing TFAR phantoms by casting selected polymers into the moulds around the femur and (g) verifying the TFAR soft tissue phantom layers with DAU (dynamic anatomical ultrasonography).

3. Results and Discussion

Compression tests were repeated five times and were found to be highly consistent for each material. The iFEA fitting with the first order

reduced polynomial of the Ogden material model resulted in an excellent approximation of experimental mechanics up to 25% compression including friction effects (Fig. 2). The iFEA fitted shear moduli of Ecoflex[™] 10 ($\mu=18$ kPa), Ecoflex[™] 30 ($\mu=32$ kPa) and Dragon Skin[™] ($\mu=110$ kPa) fell within the reported range of human skin, fat, and muscle, while Pinkysil was too stiff ($\mu=190$ kPa). Ecoflex[™] 30 and Dragon Skin[™] were used for muscle and skin+fat volumes to manufacture the TFAR phantom. The selected polymers with interlayers can mimic human tissues' acoustic properties.

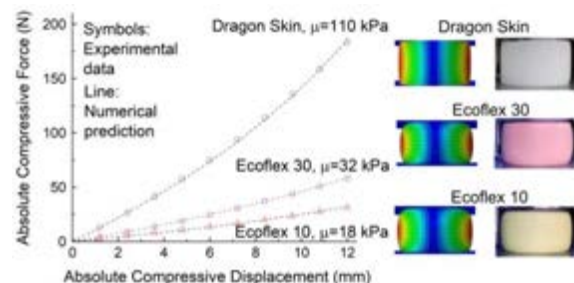


Figure 2: Comparison of force-displacement curves with hyperelastic material parameters from iFEA. Friction effects during simulation are highlighted.

4. Conclusion

This work reports on the current state-of-the-art patient-specific and data-driven computational framework for automated designs of moulds to manufacture TFAR phantom-twins. Fitted hyperelastic material constants enabled the optimum phantom material selection. The validated mechano-acoustic digital phantom-twin enables establishment and evaluation of computational analyses and design approaches.

Funding:

DoD RESTORE Award W81XWH2110215-DM190659 and the Bionics Queensland Challenge 2021 Major Prize – Mobility.



COMBINING 4D ULTRASOUND AND MODIFIED VIRTUAL FIELDS TO REGIONALLY CHARACTERIZE ABDOMINAL AORTIC ANEURYSMS

Mirunalini Thirugnanasambandam (1), Esther J Maas (1,2), Arjet HM Nievergeld (1,2),
Marc RHM van Sambeek (1,2), Stephane Avril (3), Richard GP Lopata (1)

1. Eindhoven University of Technology, the Netherlands;

2. Catharina Hospital Eindhoven, the Netherlands; 3. Ecole des MINES Saint-Etienne, France

1. Introduction

Use of personalized mechanical properties of abdominal aortic aneurysms (AAA) in biomechanical analyses significantly improves the accuracy of patient-specific rupture risk indices. In this study, we harness the capability of 4D ultrasound (US) to estimate wall motion, and use it in combination with a novel inverse method based on the principle of virtual work, to evaluate patient-specific material parameters.

2. Materials and Methods

4D-US images were acquired in AAA patients over 5-10 cardiac cycles at a rate of 4-8 volumes/second. End diastolic images of the AAAs were segmented, and the inner- and outer walls were tracked over time using the 3D speckle tracking algorithm. The resulting pointclouds were fitted with B-spline grids at systolic and diastolic configurations. By minimizing the distance between neighbouring knots in the systolic and diastolic grids, the two geometries were co-registered, and the displacement fields of the inner- and outer walls were evaluated. Displacement of all the nodes in the bulk of the AAA wall were estimated by interpolating between the displacement vectors of their inner- and outerwall neighbors. Post-unsupervised discretized spline smoothing, the deformation field was used as input for the modified virtual fields method (mVFM) [1]. mVFM uses the principle of virtual work-based cost function to iteratively optimize the material parameters. In addition, a technique to automatically choose the appropriate virtual fields was embedded within mVFM to realize the iterative nature of the optimization protocol. Three different regions were defined in each AAA, and the corresponding values of material model parameters were estimated using the 4DUS+mVFM framework.

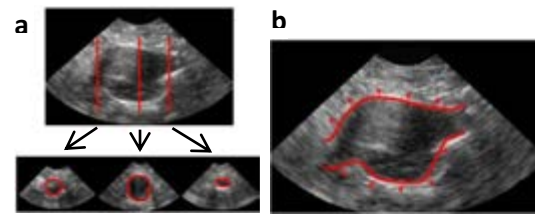


Figure 1a: Automatic segmentation of US images.
b. Speckle tracking of the inner wall of AAA

3. Results

Using an uncoupled Neo-Hookean material model with an initial guess of $c_{10}=1.24 \cdot 10^6$ Pa, the predicted material parameter values converged within three iterations when global patient-specific values of c_{10} were sought, and within ten iterations when local values of c_{10} were sought.

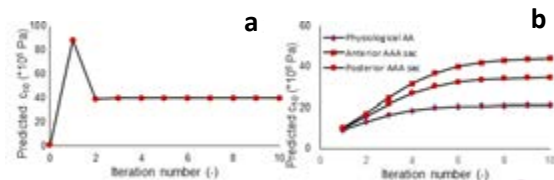


Figure 2: Prediction of **a.** global and **b.** local values of material model parameters using mVFM.

4. Discussion and Conclusions

mVFM was successfully implemented using AAA deformation fields obtained from routine US images. The anterior AAA sac and the healthy abdominal aorta had the highest and lowest shear modulus respectively. As a next step, the use of more sophisticated material models within the mVFM framework will be evaluated.

5. References

1. Mei Y et al. J Elast, 145, 265-194 (2021).

Acknowledgements:

The authors would like to thank NWO (VIDI 17533) for financially supporting this project.



BIOMECHANICAL CHARACTERIZATION OF YOUNG HUMAN CORNEA USING CLEAR LENTICULES

Malavika H Nambiar (1), Liechti Layko (1), Harald Studer (2), Abhijit Sinha Roy (3),
Theo G. Seiler (4), Philippe Büchler (1)

1. University of Bern, Switzerland; 2. Optimo Medical AG, Switzerland; 3. Narayana Nethralaya Eye
Clinic, India; 4. Institut für Refraktive und Ophtho-Chirurgie (IROC), Switzerland

1. Introduction

In surgical refractive interventions, over-correction or under-correction still occurs in 10-15 % of cases. Improved outcomes could be achieved by incorporating patient-specific corneal biomechanics into surgical planning. As a first step, this study mechanically characterizes and numerically simulates corneal lenticules harvested from patients during the refractive intervention, Corneal Lenticule Extraction for Advanced Refractive Correction (CLEAR).

2. Materials and Methods

Five human corneal lenticules were obtained post-surgery and mechanically tested in uniaxial extension in a hydration-preserving media. The tissue of length ~ 4.5 mm was pre-stretched and preconditioned with 5 cycles of 10 % strain. The loading speed was 0.75 % /s. The last cycle of force-displacement data was recorded for analysis. Since the lenticules have a non-uniform thickness, a patient-specific finite element model was used to identify their mechanical properties. The patient-specific morphology of the lenticule and its specific geometry in conjunction with surgical parameters such as the “ablation” profile and the surgical depth were reconstructed, based on clinical data. A finite element mesh of the lenticules was then reconstructed using the softwares GMSH and Python. These numerical models were implemented with orthogonal collagen fibers according to published x-ray scattering measurements [1]. In addition, in and out of plane fiber dispersion was also accounted for. The material behavior was described using the HGO material model [2]. The material parameters that best reproduce the experimental force/displacement were obtained by parameter estimation using Bayesian optimization.

3. Results

The estimated material parameters ($C10 = 24\text{kPa}$, $k1 = 6.1\text{ MPa}$, $k2 = 35.9$, $k_i = k_o = 0.45$) agree well with the experimental data (Fig.1) and represent a promising material model for young patients of a certain age group (25-35 y) and with correction up to -4.5 D without astigmatism.

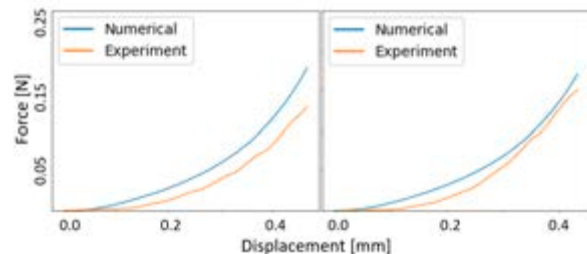


Figure 1: Experimental and numerical results of the material model on two representative patient cases.

4. Discussion and Conclusions

In the future, these parameters will be used with pre-operative morphologic clinical data of the same patients to simulate postsurgical corrections and compare with the post-operative clinical data. If the surgery can be successfully simulated, such a material model can be used to compare the outcomes of different refractive interventions such as PRK, LASIK and CLEAR, providing a predictive tool for surgeons. The main limitation of the current characterization is that it is only performed on 5 patients and that the lenticules represent only the most anterior part of the cornea. Still, this provides a unique approach to quantify the properties of young patients.

5. References

1. Hayes et al, J. The Anatomical Record, 2007.
2. Holzapfel G.A. et al, J Elasticity, vol. 6, 2000.

6. Acknowledgements:

“The authors thank the SNSF (Grant no: IZLIZ3_182975) for providing financial support to this project”.



MACHINE LEARNING-ASSISTED FINITE ELEMENT MODELING OF ADDITIVELY MANUFACTURED META-BIOMATERIALS

Alexander Meynen (1), Eline Kolken (2), Michiel Mulier (1,3), Amir Zadpoor (2),
Lennart Scheys (1,3)

1. Institute for Orthopaedic Research and Training, Department of Development and Regeneration,
KU Leuven, Belgium

2. Department of Biomechanical Engineering, Delft University of Technology, Netherlands

3. Division of Orthopaedics, University Hospitals Leuven, Belgium

1. Introduction

The mechanical characterization of porous lattice structures is rapidly becoming a crucial component throughout the development of novel medical device concepts, including, but not limited to, novel functional graded implant designs for orthopedics. Finite element (FE) simulations are a valid alternative to time-consuming, expensive, and challenging experimental tests. Despite recent research efforts, state-of-the-art FE modeling approaches of porous lattice structures are increasingly complex while their accuracy is still limited. A critical condition for increasing accuracy is the identification of correct model parameters. This study proposes a machine learning-based strategy for the identification of model parameters, such as material parameters and model boundary conditions, targeting accurate simulations of the mechanical macro-scale behavior of porous lattice structures.

2. Materials and Methods

An artificial neural network model was developed and trained using synthetic input data from a fully automated FE modeling workflow. The model was tested using real experimental force-displacement data as input for the neural network. Predicted model parameters were then used in a FE simulation and compared to the qualitative and quantitative experimental data.

3. Results

Our results show that the proposed strategy can identify model parameters so that the derived FE simulation matches the experimental results well, outperforming the accuracy of state-of-the-art FE models (Fig 1).

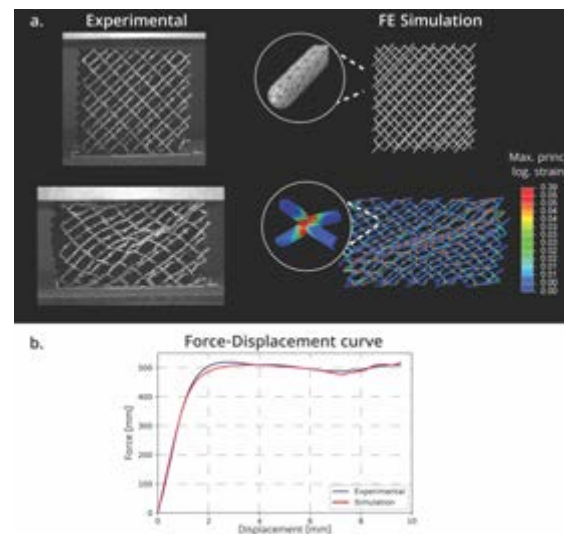


Figure 1: The experimental data and neural network was used to generate a finite element model. The simulated deformation behavior is very similar to the experimental result, as shown in (a), with maximal strain found near strut connections. The force-displacement curves (b) show almost perfect agreement between experiments and simulation.

4. Discussion and Conclusions

This study presents a novel machine-learning based parameter identification method to accurately simulate the behavior of porous lattice structures. This approach thus provides an alternative to trial-and-error-based and optimization-based inverse methods. As such it can potentially accelerate the use of finite element simulations as a tool in the evaluation of additive manufactured parts during their development.

Acknowledgements: The research for this paper was supported by the PROSPEROS project, funded by the Interreg VAFlanders – The Netherlands program, CCI grant no. 2014TC16RFCB046; A.M. is a SB PhD fellow at FWO (Research Foundation – Flanders) grant no. 1SB3819N.

A MACHINE LEARNING METHOD TO INVESTIGATE EFFECT OF STRUCTURE ON MECHANICAL BEHAVIOR OF OPTIC NERVE AXONS

Yik Tung Tracy Ling (1), Thao D. Nguyen

Department of Mechanical Engineering, Johns Hopkins University, Baltimore, Maryland, USA

1. Introduction

Previous inflation tests using digital volume correlation (DVC) measured the strain field caused by an increase in intraocular pressure (IOP) in the astrocytic lamina (AL) of the mouse optic nerve head.¹ It is currently not feasible to measure the strain response in the axonal compartments, which may be important to understanding the pattern of optic axon loss in glaucoma. The objective of the study is to develop a computational modeling framework to: 1) estimate the strains in the axonal compartments using eye-specific models of the mouse AL and DVC measurements from inflation tests, and 2) study the effect of the AL network structure on the strain response of the axonal compartments using machine learning.

2. Materials and Methods

An unmyelinated optic nerve section of a 6-month old GFP-GLT1 mouse was immunolabeled for GFAP and stained for actin (Fig. 1a).² The non-GFAP and non-actin regions in the acquired confocal image were segmented as axonal compartments (ACs). A finite element model (FEM) was created using the GFAP, actin and AC labels in Gibbon Toolbox (Fig. 1b). Displacements were applied on side surfaces using the averaged boundary displacements measured by DVC for inflation from 10-20 mmHg for 14 mouse eyes. A pressure of 20 mmHg was applied on the anterior surface to simulate IOP loading of the inflation test (Fig. 1c). A compressible Neo-Hookean model was used for the materials. The structure of the axonal compartments were measured, including area, aspect ratio, orientation, and location. The effect of structure on simulated strain were cross-trained using Gaussian Process Regression (GPR) with a squared exponential kernel.

3. Results and Discussion

The average strain computed for the AL processes agreed with the inflation test results. The converged GPR model ($R^2=0.64$, Fig. 1e)

showed that the maximum principal strain in the axonal compartments increased with larger axonal compartments (Fig. 1d). Axons aligned horizontal to the nasal-temporal axis experienced lower strain than those that are vertically aligned (Fig. 1f). A greater density of actin in the surrounding processes reduced the maximum principal strain in the axonal compartments. FEM simulation and machine learning of AL strains may help predict susceptibility to pressure-induced degeneration. We will next to study the strain response in the eyes of glaucoma mouse models.

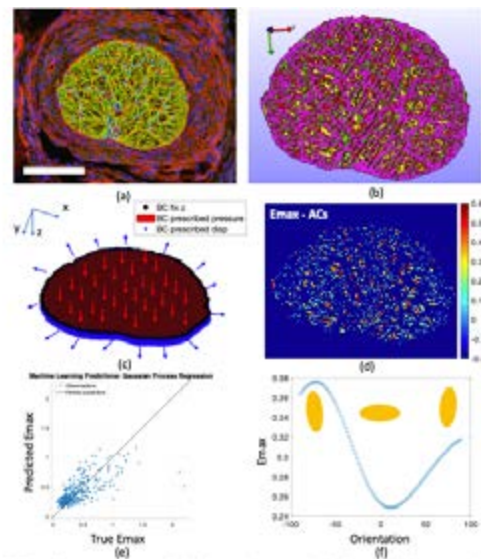


Fig. 1 Effect of structure on pressured-induced strain response in ACs, showing (a) image acquired from the unmyelinated region of a mouse optic nerve that was labeled for GFAP (green), actin (red). Non-actin and non-GFAP labelled regions were marked as axonal compartments. (b) The actin (red), GFAP (green), overlapping actin and GFAP (purple) and axonal area (yellow) were converted to a finite element model using Gibbon toolbox. (c) Pressure was applied on the anterior surface to simulate increase in IOP, and nodal displacements were applied on the side surface using experimentally averaged results from previous inflation study. (d) resulting strain response in the ACs from FEBIO 3.0 (e) Converged GPR model was cross-trained with 7 structural properties to predict maximum principal strain (Emax) in ACs. (f) GPR showed that axons that are more aligned with nasal temporal axis experienced lower strain compared to those that are vertically aligned. Scale bar = 100 μ m.

4. References

1. Korneva, A. et al., *J. R. Soc. Interface* **17**, 20200708 (2020).
2. Ling, Y.T.T. et al. *Invest. Ophthalmol. Vis. Sci.* **61**, 14 (2020).

Acknowledgements:

This work was funded by NIH EY02120 and EY01765, and the Croucher Foundation.

BRIDGING TISSUE-SCALE MULTI-PHYSICS TO ORGAN-SCALE BIOMECHANICS THROUGH MULTI-FIDELITY MACHINE LEARNING

Seyed Shayan Sajjadinia* (1), Bruno Carpentieri (1), Gerhard A. Holzapfel (2,3)

1. Faculty of Computer Science, Free University of Bozen-Bolzano, Italy; 2. Institute of Biomechanics, Graz University of Technology, Austria; 3. Department of Structural Engineering, Norwegian University of Science and Technology, Norway

*Corresponding author: e-mail: ssajjadinia@unibz.it

1. Introduction

Supervised machine learning is able to find every possible mapping between different but related datasets and can therefore be used as a scale-bridging approach by providing data samples from different scales. But in the context of computational biomechanics, generating high-fidelity (HF) data at the tissue scale (TS) might be straightforward (due to the simplified geometry), but collecting samples at the organ scale (OS) can be too expensive. This work aims to address this using a multi-fidelity machine learning (MFML) algorithm to bridge the scales, but without having to be trained on the expensive HF OS samples.

2. Materials and Methods

The proposed method is based on our recent MFML research [1], which defines the LF model by simplifying the multi-physics equations of the HF model. However, here we improve the generalizability of the trained to large-scale data, in particular through data augmentation, where the new pointwise data are interpolated. In order to empirically test the functionality of the proposed method (as shown in Fig. 1), the TS multi-physics data are created to train an MFML model with an advanced

cartilage model [2], which is then applied to an OS geometry [3] for the large-scale simulation of cartilage multi-physics.

3. Results

The machine learning model is successfully implemented on the numerical TS data with a regular hardware setup. It enables the generation of complex multi-physics data in the OS articular cartilage models for further analysis.

4. Discussion and Conclusion

While a biomechanical OS model that contains complex multi-physics TS equations may need weeks of implementation, this approach yields equivalent results in less than a day (including dataset generation and model training) that can be generalized to other similar biomechanical models.

5. References

1. Sajjadinia SS et al., *Comput Biol Med*; 148: 105699 (2022).
2. Sajjadinia SS et al., *J. Mech. Behav. Biomed. Mater*; 114: 104203 (2021).
3. Erdemir A, *J. Knee Surg*; 29(2):107–116 (2016).

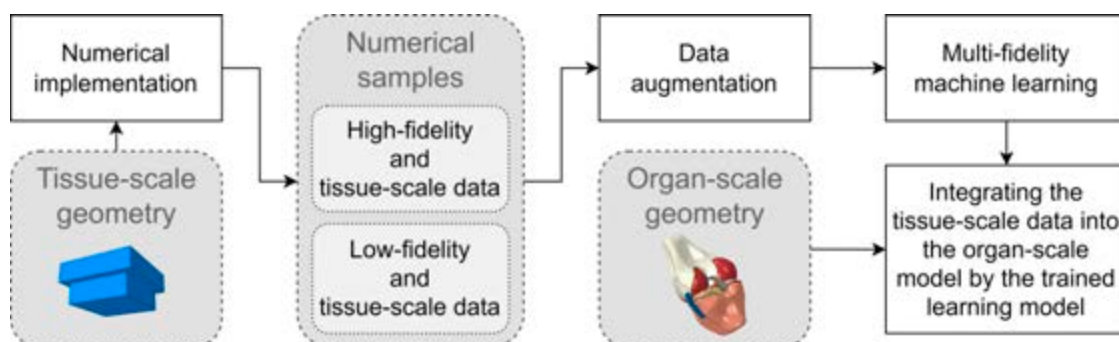


Figure 1. Workflow of the proposed method of multi-fidelity machine learning

MACHINE LEARNING BASED DESIGN OF TRIPLY-PERIODIC MINIMAL SURFACE SCAFFOLDS FOR BONE TISSUE ENGINEERING

D'Andrea Luca (1), Ibrahimi Silvia (1), Gastaldi Dario (1),
Rivolta Massimo W. (2), Vena Pasquale (1)

1. Politecnico di Milano, Italy; 2. Università degli Studi di Milano, Italy

1. Introduction

Triply-Periodic Minimal Surfaces (TPMS) geometries represent a valid strategy to generate scaffolds for bone tissue engineering [1]. Finite Element Modeling (FEM) and image analysis can be used to estimate the mechanical properties and the morphometrical features, respectively. Additionally, Machine Learning (ML) techniques offer optimization algorithms which are particularly effective when dealing with large datasets [2]. In this study, we have first generated a large dataset using in-silico analysis and then a ML approach has been employed to predict the input parameters for optimal scaffold design.

2. Materials and Methods

Three TPMS, namely diamond, gyroid and IWP, were implemented in Matlab to obtain stacks of binary images from analytical formulation (Eq. 1):

$$f_1 = f_D(b, \delta) \quad f_2 = f_G(b, \delta) \quad f_3 = f_I(b, \delta) \quad (1)$$

where b and δ are the two input parameters. The voxel discretization of the images were used as hexahedral mesh to perform the homogenization process. The 3D stacks of images were analyzed through ImageJ to assess the morphometrical features. The total number of outputs of the simulations was 38. All the results have been stored in a dataset used to train a ML algorithm. In particular, the dataset was divided in training set (60%), validation set (30%) and test set (10%). The greedy algorithm was adopted to select the minimum number of features necessary to obtain the best prediction of the properties. A linear regression model and a multinomial logistic regression were used to predict the two input parameters and the input geometry, respectively.

3. Results

Combining different values of b and δ parameters, 1279 scaffold geometries were tested, spanning a range of porosity from 2% to 99%. The features selected by the greedy algorithm are the index of permeability, the standard deviation of the trabecular thickness, the Poisson coefficient, the maximum and median ellipsoid factor. The multinomial logistic regression returned the correct geometry with a precision of 88.1% (diamond), 96.3% (gyroid) and 100% (IWP). As representative example, the worst case of a gyroid scaffold generated from the estimated input parameters (\hat{b} and $\hat{\delta}$) is reported in Figure 1.

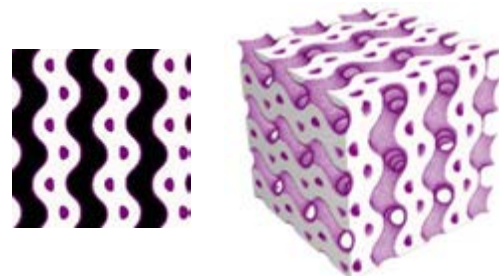


Figure 1: 2D slice and 3D scaffold obtained using \hat{b} and $\hat{\delta}$. The over-amount of material present in the predicted structure is highlighted in purple.

4. Discussion and Conclusions

Although the greedy algorithm returned the features corresponding to the best performance, some values of such features, such as the ellipsoidal factor, are not easily accessible in the design process. Therefore, although a higher error is expected, a combined approach between user-defined features and the ones selected by the greedy algorithm is preferred.

5. References

1. Naveen Kumar M. et al., Computer-Aided Design and Applications 18 (4) (2020)
2. Zheng X. et al., Journal of Materials Science 53 (14) (2018)

EMG-BASED IDENTIFICATION OF ADL GRASP TYPES WITH A DEEP-LEARNING APPROACH FOR PROSTHETIC USE

Marta C. Mora (1), María L. Morató (1), José V. García-Ortiz (1), Joaquín Cerdá-Boluda (2)

1. Dept. of Mechanical Engineering and Construction, Universitat Jaume I, Spain;
2. Dept. of Electronic Engineering, Universitat Politècnica de València, Spain

1. Introduction

Advanced anthropomorphic hand prostheses are a reality. However, their use is limited due to their cost (20 k\$ - 100 k\$) and their lack of functionality and comfort [1], directly related to the control performance. A capital problem is the difficulty of communicating the user with the hand in a natural way. A real-time proper interpretation of the user's intention is essential. Commonly, this information is obtained from Human-Machine Interface (HMI) signals and their processing through deep-learning (DL) methods [2]. They have been used for gesture classification or for detecting a few grasp types (3 in [3]) with performances around 80%. Still, these works don't identify some basic grasps used by the human hand in Activities of Daily Living (ADL) [4], which are necessary for prostheses. This work focuses on detecting the main ADL grasp types [4] based on EMG data and a DL approach. A simple architecture is used with promising results.

2. Materials and Methods

An artificial neural network (ANN) has been trained in Matlab for posture classification with a 2-layer feedforward architecture with 150 neurons in the hidden layer, already used in previous authors' works. EMG data from 9 ADL hand postures (*pulp pinch*, *lateral pinch*, *diagonal volar grip*, *cylindrical grip*, *extension grip*, *tripod pinch*, *spherical grip*, *hook*, *rest*, see Fig.1) have been gathered from the Ninapro Dataset 5 and the Myo Armband, an EMG-based HMI. The Ninapro data are used in the training phase and the Myo data (10 healthy right-handed subjects) in the validation phase. Raw signals are processed to extract relevant information (descriptors) using a 52-sample window with an overlap of 47. Eight time-domain descriptors have been computed (mean absolute value MAV, zero crossing, slope sign

changes, waveform length, skewness, root mean square RMS, integrated EMG, Hjorth parameters) to identify those providing better classification results (RMS error).



Figure 1: ADL Grasping postures (except *rest*).

3. Results

The best results have been obtained using only 2 descriptors, MAV and Skewness, as inputs to the ANN. The mean percentage of success in the recognition was 73.04%, higher than results reported in the literature with less postures. Most of the grasp types obtained around a 70% of success, with better results for *lateral pinch* (75.3%) and the *rest* posture (90%).

4. Discussion and Conclusions

The results indicate that this DL approach can enhance functionality of current prostheses. Future work will imply the implementation of this technique in real-time on a low-cost hand prosthesis.

5. References

1. Smail LC et al, *Disabil Rehabil-Assi*; 16(8): 821-830 (2021).
2. Calado A et al, *ICARSC conf: IEEE*; 2019 p.1-6.
3. Batzianoulis I et al, *J NeuroEngineering Rehabil*; 15, 57 (2018).
4. Vergara M et al, *J Hand Therapy* 27:225-34(2014)

Acknowledgements:

The authors thank the Spanish Ministry (Grant no: PID2020-118021RB-100) and University Jaume I (Grant no: UJI-B2022-48) for the financial support to this work.



COMPUTING TRANSVALVULAR PRESSURE GRADIENT USING DEEP-LEARNING FROM SEGMENTED IMAGE DATA

Pavlo Yevtushenko (1), Leonid Goubergrits (1,3), Marie Schafstedde (1,2,3), Titus Kuehne(1,2)

1. Charité-Universitätsmedizin Berlin, Germany; 2. German Heart Center Berlin, Germany; 3. Berlin Institute of Health, Germany

1. Introduction

The transvalvular pressure gradient (TPG) is a critical hemodynamic parameter for the diagnosis and treatment decision of patients with aortic valve disease (AVD) [1]. In this work, we propose a deep learning (DL) based method to compute patient-specific TPG from medical image data. Compared to computational fluid dynamics (CFD)-based methods, which are usually proposed, the DL-method provides results much faster and requires very little computational power, thereby being potentially more suited for a clinical use.

2. Materials and Methods

A total of 267 peak-systolic CFD simulations were performed using aortic geometries segmented from computed tomography (CT) data of 103 AVD patients (Figure 1).

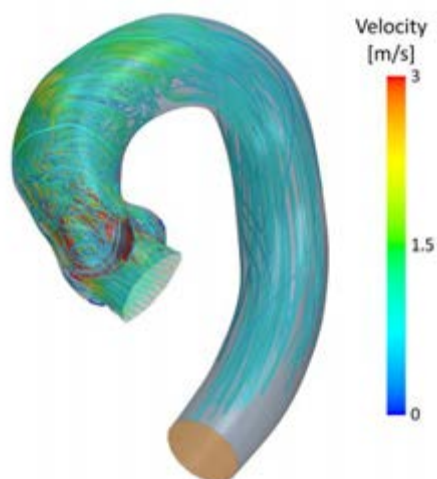


Figure 1: Streamlines in the aorta based on a patient-specific numerical flow simulation

This simulation data was then used to train a recurrent neural network to compute TPG from segmented image data. The DL-computed

TPG values were compared against CFD-computed TPG values on a separate test dataset (n=23) to assess the accuracy of the DL method.

3. Results

CFD- and DL-computed TPG values agreed well for the test-cases with an R^2 of 0.98. Furthermore, an equivalence test indicated statistical equivalency of both methods within a margin of ± 5 mmHg.

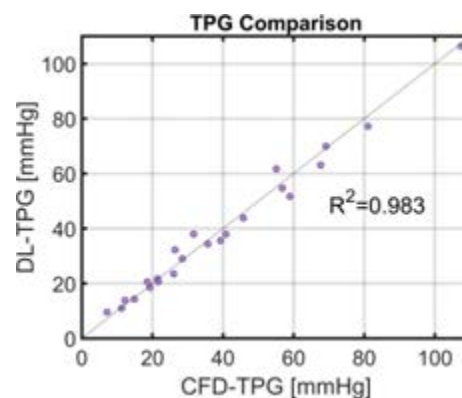


Figure 2: Comparison of DL- and CFD-based TPG values for 23 test cases

4. Discussion and Conclusions

The DL-based computation of patient-specific TPG appears to be a viable alternative to CFD-based methods with the benefit of requiring substantially less computational power. However, the network currently uses manually segmented image data and is therefore not suited for a clinical application yet. Further work towards an automated segmentation algorithm that provides segmented image data from raw clinical data as an input to the network is required.

5. References

1. A. Kanwar, J. J. Thaden, and V. T. Nkomo, "Management of Patients With Aortic Valve Stenosis", *Mayo Clin Proc*, vol. 93, no. 4, pp. 488-508, Apr 2018.



A HYBRID AGENT-BASED MODEL TO UNRAVEL THE MECHANISMS OF VISCERAL LEISHMANIASIS PROGRESSION AND RELAPSE

Margot Passier (1), Luka Verrest (2), Alwin D.R. Huitema (2), Thomas P.C. Dorlo (2,3)

1. Eindhoven University of Technology, The Netherlands; 2. Netherlands Cancer Institute, The Netherlands; 3. Uppsala University, Sweden

Correspondence details: m.m.passier@tue.nl

1. Introduction

Visceral Leishmaniasis (VL) is a severe tropical parasitic disease. Following initially successful treatment, unfortunately, a subset of patients suffers from unpredictable disease relapse, characterized by parasite recrudescence. This is still an urgent problem [1]. Relapse prevention requires in depth knowledge of the underlying mechanisms, which are yet poorly understood. Here, a pharmacokinetic-pharmacodynamic model linked to an agent-based model (PKPD-ABM) was developed to gain more insight into the relapse mechanisms.

2. Materials and Methods

The model focused on VL in the liver and consisted of hepatocytes, Kupffer cells, T-lymphocytes and blood derived macrophages. At each time-step, these cells (agents) interacted on a 2D grid by performing actions based on rules and probabilities (model parameters motivated by literature). We implemented two scenarios for parasite proliferation: linear and logistic. Resulting from intracellular parasite growth, macrophages burst when the number of parasites exceeded carrying capacity. Treatment was implemented by adapting the model parameters over time depending on the drug concentration per time step, determined by a linked set of differential equations. The model parameters were fitted on *in vitro* and haematological patient data. To investigate possible causes for relapse, we conducted *in silico* experiments.

3. Results

After fitting the parameters, we compared simulated parasite growth with histology. The resulting growth patterns (cluster formations) very closely resembled real within-patient VL growth. Additionally, we observed that

exhausted T-lymphocytes were vital in maintaining the infected cores.

Interestingly, we found that insufficient parasite clearance and subsequent regrowth of parasites could be caused by underexposure to drugs or logistic parasitic growth. Even with sufficient drug exposure, logistic parasite growth led to recrudescence, yielding up to 8 times more parasites than underexposed patients (Fig. 1).

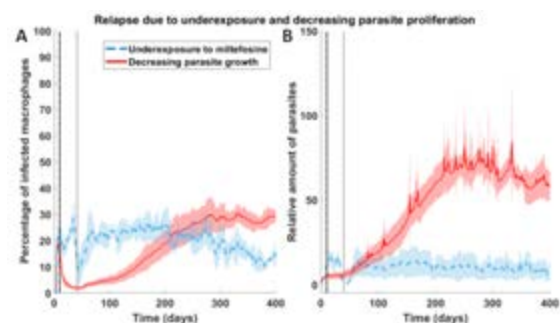


Figure 1: Simulated relapse due to drug underexposure (blue, dashed) or logistic parasite proliferation (red, solid). The solid and dashed lines represent the average results, while the shaded areas represent the standard deviation. The black and grey vertical lines indicate the start and end of treatment, respectively. The model predicts a strong relapse especially in case of logistic parasite proliferation.

4. Discussion and Conclusions

The developed PKPD-ABM well recapitulates parasitic growth patterns in VL progression. Our results identified intracellular logistic parasite growth as a possible key factor in VL relapse. Future studies will aim at validating our findings and investigating how mechanics affect intracellular parasite growth and related bursting of the infected macrophages.

5. References

1. Verrest L et al., Clin. Infect. Dis.;73(5): 775-782 (2021).



QUANTIFYING THE IMPACT OF SYNTHETIC DATA IN MARKERLESS MOTION CAPTURE

Tylan Templin (1), Travis Eliason (1), Kase Saylor (1), Omar Medjaouri (1), Daniel P. Nicoletta (1)

1. Southwest Research Institute, United States

1. Introduction

With advances in computer vision and artificial intelligence, neural network-based markerless motion capture systems have begun to demonstrate promising accuracy compared to marker-based tracking [1]. However, these markerless systems require hand labeling training images, which is manually intensive and potentially error prone. The need for a diverse set of training images that can be automatically labeled in large quantities with high accuracy to further improve pose estimation has led to the creation of synthetic datasets [2]. The purpose of this study is to evaluate the utility of incorporating synthetic data into the training of a markerless system.

2. Materials and Methods

Two custom convolutional neural networks (CNN) were trained to detect a set of 49 anatomical landmarks on subjects of interest. The first network (Base) was trained with publicly available hand-labeled pose datasets (50k images) and a custom training dataset where video images were automatically labelled using Vicon and OpenSim processed data (50k images) [3]. The second network (Base+Synthetic) also included a custom dataset (50k images) generated using the Infinity AI API [4]. To evaluate the performance of both markerless motion capture systems, synchronized video from 8 video cameras was captured along with Vicon marker-based data from 9 subjects who performed 3 repetitions of 4 movements (counter movement jump (CMJ), squat, left and right single leg jump (SLJ)). 2D keypoint detections were used to generate 3D locations using an outlier-aware triangulation algorithm. Subject kinematic data was determined via scaling and inverse kinematics in OpenSim [5] for both the markerless and Vicon data. Quantitative performance was evaluated using

root mean square error (RMSE) between the markerless and marker-based motion capture derived lower body kinematic data. Average RMSE for each movement was calculated across hip, knee, and ankle angles.

3. Results

Both markerless systems demonstrated a high degree of agreement with the Vicon derived data with average RMSE values less than 8 degrees (Fig 1). The Base+Synthetic condition showed an average of 22% less error than the Base condition relative to the Vicon measurements.

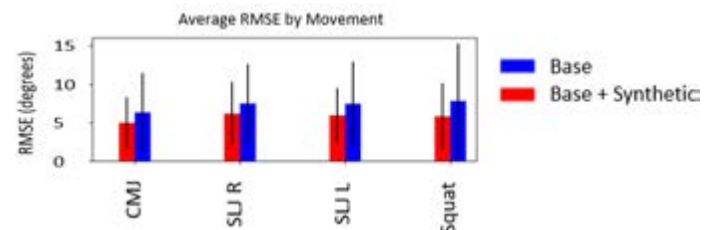


Figure 1: Comparison of Average RMSE between Base and Base+Synthetic Markerless Kinematics.

4. Discussion and Conclusions

We demonstrated that a synthetic dataset of human movement can be used to augment training of a markerless motion capture system to improve accuracy. Future development of synthetic data should focus on including backgrounds and movements that are poorly represented in other datasets to increase overall reliability and robustness.

5. References

1. Kanko et al., J. Biomech., 127 (2021).
2. Weitz et al., arXiv:2110.01330, 2021.
3. Eliason et al., ISB Proceedings, 2019.
4. <https://infinity.ai/api>
5. Delp et al., IEEE Bio Eng 200754(11):1940-50

Acknowledgements:

This work was supported by the SwRI Internal Research and Development program.



TOWARDS BIOMECHANICAL ANALYSIS IN WORKPLACE ERGONOMICS USING MARKER-LESS MOTION CAPTURE

Jindong Jiang (1,2), Wafa Skalli (1), Saman Vafadar (1), Marc Khalifé (1), Ali Siadat (2),
Laurent Gajny (1)

1. Arts et Métiers Institute of Technology, Institut de Biomécanique Humaine Georges Charpak, France

2. Arts et Métiers Institute of Technology, Laboratoire de Conception Fabrication Commande, France

1. Introduction

Workplace lift task analysis benefits from 3D biomechanical motion capture [1, 2]. Advances in computer vision pave the way for practical marker-less applications in ergonomics [1–3]. However, these systems require further evaluation in terms of joint center localization due to occlusion from lifted objects.

In this work, an AI-based markerless approach is proposed and evaluated for box lifting/lowering motions.

2. Materials and Methods

12 subjects (24.2±2.3 years, 172.4±10.1 cm, 65.9±14.7 kg) participated in the experiment (Ethical committee approval CPP 06036, Paris VI). 57 markers were attached to the subject by a surgeon. Biplanar X-Rays were taken to get the accurate 3D location of joint centers in marker sets coordinate systems. Subjects were asked to lift a cardboard box onto a table and then move it down. 2 systems simultaneously captured the motion: a marker-based reference system (Vicon, UK) and a marker-less system with 4 digital cameras [4]. The collected dataset contained over 180K multi-view RGB frames and corresponding 3D coordinates of 17 key points. All faces of the subjects were blurred on these images to protect the subject's privacy, using Gaussian Blur.

A neural network of learnable triangulation [5] was trained/evaluated on the dataset (see Fig.1). 6 subjects were randomly selected as the training set and the rest were in the test set. MPJPE (Mean Per Joint Position Error) was used for evaluation.

3. Results

An average MPJPE of 12.7mm (SD:10.8mm) was achieved in 3D joint position estimation on the test set. The anatomical keypoints with the largest MPJPE were L4/L5 (20.6± 9.0mm) and

hips (16.2±9.7mm). The errors of other key points were around or less than 15.0mm.



Figure 1: Example images in the dataset with the keypoints projected on two camera views

4. Discussion and Conclusions

The neural network trained for lifting/lowering can achieve performances comparable to that obtained on other motions like walking [4]. Moreover, face blurring does not have significant impacts on keypoint localization but can enable easier data sharing. Therefore, further kinematic analysis can be developed and evaluated for workplace ergonomics assessment. One limitation of this study is that the collected data does not reflect the industrial environment but they have the potential for generating synthetic data.

5. References

1. Plantard, P. et al., DHM and Posturography. pp. 673–682. Elsevier (2019)
2. Mehrizi, R. et al., IEEE Trans. Hum.-Mach. Syst. 49, 85–94 (2019)
3. Li, L. et al., J. Biomech. 113, 110086 (2020).
4. Vafadar, S. et al., Gait Posture. 86, 70–76 (2021).
5. Iskakov, et al., ICCV. pp. 7717–7726. (2019)

Acknowledgements:

The authors deeply thank Fondation Arts et Métiers for its support, and Floren Colloud, Hélène Pillet for their advice.

ADAPTIVE ISOKINETICS AND MULTICHANNEL HIGH-DENSITY ELECTROMYOGRAPHY FOR TRANSTIBIAL AMPUTATION

Usha Kuruganti, Jacqueline Gaudet and Victoria Chester

Andrew and Marjorie McCain Human Performance Laboratory, Faculty of Kinesiology, University of New Brunswick, Canada

1. Introduction

Transtibial amputation significantly impacts mobility and function and increases the risk of developing secondary complications. Prosthesis users can benefit from strength training using isokinetic dynamometers (1). Surface electromyography (EMG) can provide insight regarding muscle function. Multichannel high-density EMG (HDEMG) recordings are promising for prosthesis users (2). The purpose of this work was to examine HDEMG parameters during slow, moderate and fast isokinetic knee extension for both non-affected and amputated legs to assess strength and neuromuscular function.

2. Materials and Methods

Ten able-bodied individuals (4 males and 6 females, mean age = 38.4 ± 18.4 years old and two individuals with transtibial amputation (22-year-old male, 77-year-old female) participated in this study. HDEMG were recorded from the rectus femoris during slow, moderate and fast isokinetic knee extensions. Spatial distribution was estimated using the Root Mean Square (RMS) EMG signals for each of the 64 electrode grid locations from which 2D maps were developed (Figure 1). Alterations in muscle heterogeneity and pattern were estimated using the coefficient of variation (CV) and modified entropy.

3. Results

Both prosthesis users demonstrated reduced strength on their affected side compared to their sound side across all speeds. Prosthesis users showed differences in muscle activity in the affected leg compared to the sound leg, however the male prosthesis user showed higher EMG activity in his non-affected leg while the older female prosthesis user demonstrated lower EMG activity in her non-affected leg across all

speeds. Differences in modified entropy and CV in the rectus femoris of the affected side suggested altered muscle heterogeneity compared to the sound side for both users.

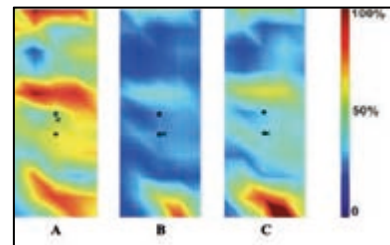


Figure 1: Sample spatial muscle activation maps of rectus femoris from prosthesis user during: A) 60°/sec; B) 90°/sec; C) 120°/sec contractions.

4. Discussion and Conclusions

This study showed that HDEMG can be used successfully with isokinetic dynamometry for those with transtibial amputation. Spatial parameters indicated that prosthesis users demonstrated strength and muscle activity differences between their non-affected and amputated leg across speeds. Age and the nature of amputation may explain individual differences. Results showed that isokinetic strength testing combined with HDEMG is a viable option of strength assessment for prosthesis users. Future studies should investigate the impact of targeted training on strength and HDEMG parameters for improved rehabilitation.

5. References

1. Pedrinelli A et al., *Prosthetics and Orthotics International.*; 26(3):195-205 (2002).
2. Kuruganti U et al., *Front Med Technol*; 3, 690285 doi: 10.3389/fmedt. (2021).

Acknowledgements:

The authors would like to thank the Natural Sciences and Engineering Research Council for providing financial support to this project.

BEST IMU SENSOR PLACEMENT TO PREDICT JOINT KINEMATICS AND KINETICS DURING GAIT USING A RANDOM FOREST MODEL

Shima Mohammadi Moghadam (1), Ted Yeung (1) and Julie Choisne (1)

1. The Auckland Bioengineering Institute, the University of Auckland, New Zealand

1. Introduction

To date, a combination of Inertial Measurement Units (IMUs) and Machine Learning (ML) techniques has been used in many studies to predict gait time series (joint kinematics and kinetics) [1]. However, the optimal IMU placement for predicting joints' kinematics and kinetics has not been investigated. This study investigates how the number and location of IMU sensors affect the performance of a Random Forest (RF) model to predict joints' kinematics and kinetics during gait.

2. Materials and Methods

Twenty healthy volunteers (11F, 27 ± 5 yrs, 1.70 ± 0.70 m, 66 ± 10 kg) were asked to walk over-ground for a minimum of 16 trials. Marker trajectories from a 12-camera optical motion capture system (Vicon), 7 IMUs (Vicon iMeasureU), and 3 GR plates (Bertec, OH) were synchronised. Pelvis, hip, knee, and ankle kinematics and kinetics were computed using a MAP-client [2] scaled OpenSim model (gait 2392) using marker trajectories and GRFs. Acceleration and angular velocity from IMUs in different positions (a combination of the pelvis, thigh, shank, and foot IMUs) were used for feature extraction by Tsfresh [3]. For each IMUs' combination, the following steps were followed: 1) Top ten relevant features for each target (joint angles and moments) were used as input in an RF model and 2) A leave-one-out analysis was used to evaluate the performance of the RF models. Data analysis consisted of root mean square error (RMSE) calculation.

3. Results

Average RMSE was calculated between OpenSim computed, and RF predicted joint angles and moments for each IMU combination (Figure 1). The average RMSEs for all IMU combinations are in the same range. In the case of using only one IMU, the lowest prediction

errors are related to foot IMU for both joints' kinematics and kinetics prediction.

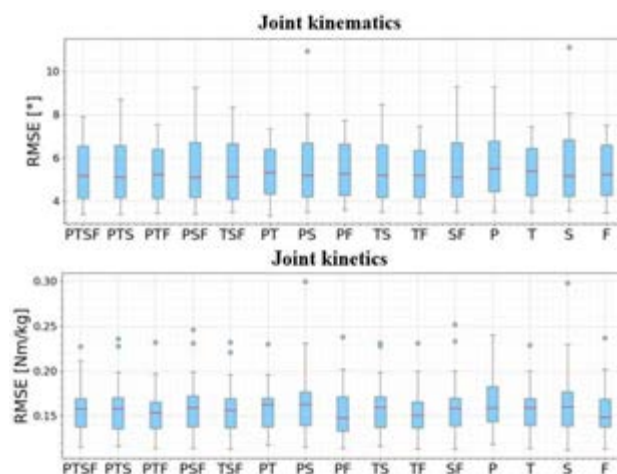


Figure 1: Joint kinematics and kinetics RMSE for different IMU placements. P stands for the pelvis, T for the thigh, S for the shank, and F for the foot.

4. Discussion and Conclusions

This study suggests that using IMUs on each foot combined with an RF model is as accurate as using 7 IMUs with an average RMSE of 5.34 degrees for kinematics and 0.154 Nm/kg for joint moments. Future studies will examine the impact of using different features and window size on the RF model performance.

5. References

- [1] Gurchiek, R.D., Sensors, 2019. 19(23): p. 5227.
- [2] Zhang, J., et al., International Symposium on Biomedical Simulation. 2014. Springer
- [3] Christ, M., et al., Neurocomputing, 2018. 307 : p. 72-77.

Acknowledgements

We would like to acknowledge the Health Research Council of NZ and the Science for Technological Innovation NZ for funding this study.

Shima Mohammadi Moghadam,
smoh433@aucklanduni.ac.nz



MODELING THE BIAxIAL MECHANICAL BEHAVIOR OF THE BRONCHIAL TREE

Samaneh Sattari (1), Crystal A. Mariano (1), Mona Eskandari (1,2,3)

1. Department of Mechanical Engineering, University of California, Riverside, CA, USA

2. Department of Bioengineering, University of California, Riverside, CA, USA

3. BREATHE Center, School of Medicine, University of California, Riverside, CA, USA

1. Introduction

The COVID-19 pandemic has recently reinvigorated advancements in pulmonary mechanics research. Understanding the structure-material-function relationships of pulmonary airways is critical to understanding how remodeling corresponds to health versus disease onset and progression [1]. Previous airway models often utilize linear, isotropic, and homogenous assumptions due to the lack of comprehensive experimental data [2]. To address this knowledge gap, we present a new constitutive airway model informed by multiple biaxial loading conditions, characteristic of the various regions of the bronchial tree. This nonlinear, heterogenous, and anisotropic representation of the airways provides a foundation to construct predictive computational tools of pulmonary disease and improve our understanding of lung mechanics.

2. Materials and Methods

Airways were dissected from seven porcine lungs and categorized by three regions (trachea, large and small bronchi) based on their inner diameters [3]. 126 soft tissue specimens were tested using planar biaxial loading, preconditioned to 60% strain following multiple displacement ratio protocols, including 1:1 (circumferential:axial), 1:0.75, 1:0.5, 0.5:1, 0.75:1, where digital image correlation tracked the strains. Hyperfit was used to evaluate the fit of Fung, Holzapfel, and four-fiber family (FFF) models to the simultaneous fit of the five loading scenarios using the coefficient of determination R^2 [4]. Anisotropic models were only considered given the strong directional preference of airway tissue [5].

3. Results

The FFF model best described the simultaneous

experimental loading profiles with $R^2 > 0.9$ compared to Fung and Holzapfel models (Figure 1).

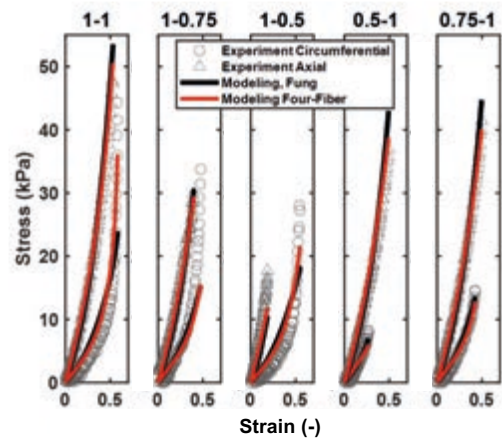


Figure 1: Representative specimen's experimental data model fit to the Fung and FFF models.

4. Discussion and Conclusions

We present a constitutive model based on simultaneous biaxial tensile experimental protocols for the proximal and distal airway tree for the first time. The superior performance of four-fiber family model compared to Fung and Holzapfel is reported, which agrees with findings for the arterial wall [6]. The parameters yielded by this structurally motivated phenomenological model can aid the development of predictive pulmonary models, as well as bioinspired airway stent designs.

5. References

1. Ganjeh MM et al. *Curr Opin Physiol.* 2021;22.
2. Zhao J et al. *Phys Fluids.* 2021;33.
3. Sattari S et al. *Acta Biomater.* 2022;in press.
4. Schroeder F et al. *JMBBM.* 2018;78.
5. Sattari S, Eskandari M. *JMBBM.* 2020;110.
6. Ferruzzi J et al. *J R Soc Interface.* 2011;8.



MULTISCALE RESPIRATORY MECHANICS: LUNG MODELING AND APPLICATIONS TO MECHANICAL VENTILATION

Daniel E. Hurtado (1,2), Nivaldo Avilés-Rojas (1,2) Felipe Concha (1)

1. Department of Structural and Geotechnical Engineering, School of Engineering, Pontificia Universidad Católica de Chile

2. Institute for Biological and Medical Engineering, Schools of Engineering, Medicine, and Biological Sciences, Pontificia Universidad Católica de Chile, Chile

1. Introduction

The high prevalence of chronic respiratory diseases together with the death toll taken by the Covid-19 pandemic have increased the need of new tools to improve the management of respiratory diseases. Computational lung models arise as promising, as they offer a flexible platform for personalized treatment. However, current organ models may not be predictive enough, as they lack of a direct connection between morphological features at the alveolar level with whole-organ behaviour.

2. Materials and Methods

We present a poromechanical multiscale framework based on two-scale homogenization techniques. To this end, we separate scales using asymptotic expansions for the displacement and porosity fields. Using symmetry arguments and collecting terms we arrive at fine-scale and coarse-scale problems. The fine-scale problem is solved using a TKD micromechanical model [1]. Once the fine-scale response is computed, we average its stress fields to inform the coarse-scale constitutive model. The governing equations derived from linear momentum balance and mass balance are solved using a non-linear finite element scheme on patient-informed lung geometries [2].

3. Results

Whole-lung finite-element simulations were carried out on anatomical lung geometries. Figure 1 shows the lung response to a pressure-controlled ventilatory mode, where airway pressure on the cross-section of main airways is prescribed. The resulting flow and volume curves show a dependence on the TKD material porosity (f_0), where an increase of porosity results in higher airflow and lung volumes.

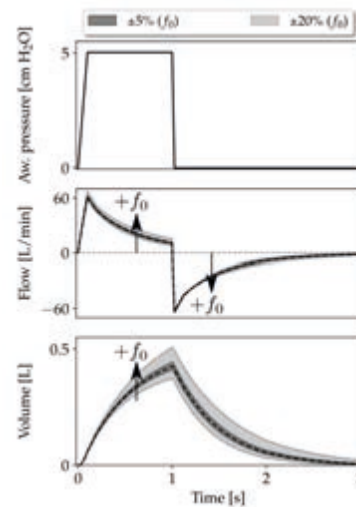


Figure 1: Parameter sensitivity analysis: effect of tissue porosity on the mechanical response of a ventilated lung under pressure-controlled ventilation mode.

4. Discussion and Conclusions

Our results show that lung compliance is modulated both by the parenchyma tissue porosity and by the alveolar wall. The effect of these morphological parameters on the organ mechanical response is consistent with clinical observations on lungs with emphysema and fibrosis.

5. References

- Concha, F., & Hurtado, D. E. (2020). J Mech Phys Solids, 145, 104147.
- Avilés-Rojas, N., & Hurtado, D. E. (2022). Whole-lung finite-element models for mechanical ventilation and respiratory research applications. Front Phys, 13, 984286.

Acknowledgements:

Authors acknowledge the support of ANID Chile through grant FONDECYT Regular 1220465 and BECAS DOCTORADO NACIONAL 21212320.°

MULTI-SCALE MODELING OF THE LUNG PARENCHYMA

Mahdi Manochehrtayebi (1, 2), Aline Bel-Brunon (3), Marin Genet (1, 2)

1. LMS, École Polytechnique/IPP/CNRS, France; 2. M_{EDISIM} team, INRIA, France; 3. LaMCoS, INSA-Lyon/CNRS, France

1. Introduction

To better understand the link between the macroscopic behavior of the lung parenchyma and its microscopic geometrical and mechanical features, we aim to develop a micromechanical model and compare its global response to the response of a poroelastic behavior law [1].

2. Materials and Methods

We propose a microscopic model for the lung parenchyma, based on which we can study the stress and the strain at the microscopic scale and compare their average values to the ones from the macroscopic model.

Based on microscopic images of the lung parenchyma, we proposed a hexagonal geometry in 2D for the alveolar walls, see Figure 1.

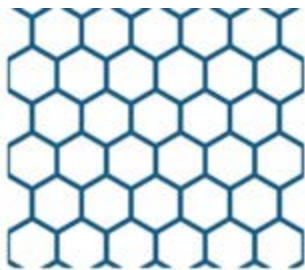


Figure 1: Generic microstructure used for the lung parenchyma.

Thanks to an augmented variational formulation based on [2], we can apply various loadings, such as macroscopic strain, macroscopic stress, pore pressure, and/or surface tension. In order to compare the responses of both models, we linearized them and matched the material parameters of the linearized models.

3. Results

The response of both macroscopic and microscopic models to an internal pressure load is shown in Figure 2. As the macroscopic model parameters have been adapted to the global

response of the microscopic model in the linear setting, the stress-strain curves match for small strains.

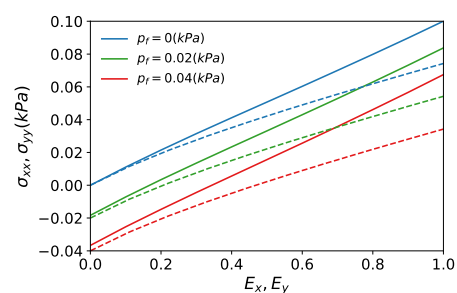


Figure 2: Macroscopic stress-strain responses of the macroscopic and microscopic models, subjected to internal pressure. (Dashed lines are related to the macroscopic model.)

4. Discussion and Conclusions

We have also studied the effect of applying both macroscopic strain and internal pressure on both models, and we have observed coupling between strain and pressure in the microscopic model, while they are decoupled in the macroscopic model. We are aiming to develop a reduced model of the microscopic model, in order to perform organ scale simulations based on the behavior described by the microscopic model.

5. References

- [1] Patte, Genet, Chapelle, A quasi-static poromechanical model of the lungs, *Biomech. Model. Mechanobiol.*, 2022.
- [2] Álvarez-Barrientos, Hurtado, Genet, Pressure-driven micro-poro-mechanics: a variational framework for modeling the response of porous materials, *Int. J. Eng. Sci.*, 2021.

Acknowledgments:

This study was funded by ANR-19-CE45-0007.



MATERIALS SIMPLIFICATION IN TRACHEO-STENT ANALYSIS

João Brites Pinto (1), Jairson C. Dinis (1), Carlos A. Campos (1), Mário S. Correia (1,3),
Henrique Almeida (1,4), Helder Cordeiro (5), Salvato Feijó (6), Rui B. Ruben (1,2)

1. ESTG, Polytechnic of Leiria, Portugal; 2. CDRsp, Polytechnic of Leiria, Portugal; 3. CEMMPRE,
University of Coimbra, Portugal; 4. CIIC, Polytechnic of Leiria, Portugal; 5. Moldes RP, Portugal; 6.
Centro Hospitalar de Leiria, Portugal

1. Introduction

Tracheal stenosis leads to breathe difficulties. In these cases, stents are a common procedure. However, silicone stents have some performance limitations related with implant migration, development of granulation tissue and accumulation of secretions. To understand stents performance is useful to define a computational model, in order to simulate full swallowing movement. However, this is a complex computational analysis, due to large displacements and materials definition that include airway cartilage rings, annular ligaments and smooth muscle. Based on homogenization techniques, equivalent material properties were obtained, trying to reduce analysis complexity.

2. Materials and Methods

Based on material properties obtained experimentally by Teng et al. [1], an asymptotic homogenization technique was applied in order to define equivalent material properties.

3. Results

Swallowing movement analysis is a very complex computational analysis, due to large displacements involved. And this is one movement that can create stent migration and granulation. Considering all materials (cartilage rings, annular ligaments and smooth muscle) as shown in Fig. 1, Abaqus software takes more than 6 hours in a Xeon E3-1240v6 3.70GHz 8MB computer, in a full swallowing analysis. In addition, implant is considered a shell without studs. With equivalent properties obtained with homogenization a significant reduction is obtained, for the same swallowing analysis. Comparing the most important result for migration and granulation, is concluded that contact results between stent and trachea are

almost the same, for homogenized and full materials analysis. In Fig. 2 is possible to observe that contact stress between stent and trachea is similar when considering equivalent material, in all swallowing sequence.

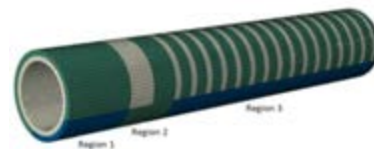


Figure 1: Materials at tracheal airway system: muscle (blue), ligament (white) and cartilage (green). 3 regions homogenized are also defined.

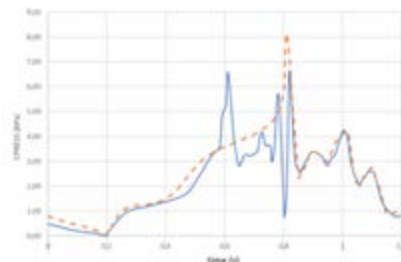


Figure 2: Contact stress in interface. Blue for full material and dash orange for equivalent materials.

4. Discussion and Conclusions

With this work, material simplification is possible to use more complex stent analysis and include studs, instead of a simple shell stent model.

5. References

1. Teng et al, J Biomech, 45:1717-1723 (2012).

Acknowledgements:

This work was financially supported by project PTDC/CTM-CTM/39713/2017-POCI-01-247-FEDER-039713 funded by Agência Nacional de Inovação, S.A. PT2020-SII&DT-Copromoção by FEDER funds through COMPETE2020-Programa Operacional Competitividade e Internacionalização (POCI).



TREATMENT OF SUPRASYSTEMIC PULMONARY ARTERY HYPERTENSION: GEOMETRIC MULTISCALE AND REDUCED MODELS OF THE POTTS SHUNT

S. Pant (1), A. Sizarov (2), A. Knepper (1), G. Gossard (3), A. Noferi (3), Y. Boudjemline (4), I.E. Vignon-Clementel (4)

1 Faculty of Science and Engineering, Swansea University, Swansea, United Kingdom. 2 Department of Pediatrics, Maastricht University Medical Centre, Maastricht, The Netherlands. 3 Inria, Saclay Ile-de-France, Palaiseau, France. 4 Cardiac Catheterization Laboratories, Sidra Heart Center, Sidra Medicine, Doha, Qatar

1. Introduction

The Potts shunt (PS) is an anastomosis that connects the left pulmonary artery to the descending aorta. It has been proposed as a potential palliative treatment of drug-resistant suprasystemic pulmonary arterial hypertension (PAH) [1]. A geometric multiscale (GMS) model is developed here to study the changes in both local and global haemodynamics induced by the Potts shunt [2]. GMS model parameters are estimated to reproduce the pre-operative measurements of a patient with suprasystemic idiopathic PAH, treated with a PS percutaneously [3]. Validation is based on post-operative measurements.

2. Materials and Methods

For GMS parameter estimation, a standalone fast-to-run reduced model, a lumped parameter model (LPM), was generated by representing the 3D regions with lumped equivalents. The LPM components were estimated by a regression analysis on the results of a few GMS model simulations. For the lumped shunt model, it was found that the inertial losses could be ignored relative to the viscous losses. Depending on the 3D region, the pressure loss could be neglected or not in the LPM.

3. Results and Conclusions

The GMS models indicate the following changes induced by the PS: (i) the PS of a sufficiently large diameter is effective in equalising the pressures in the pulmonary arteries and the aorta; (ii) the left ventricle (LV) output decreases while the right ventricle (RV) output increases; (iii) even though the LV output decreases, the flow to the supra-aortic branches and hence the superior vena cava increases; (iv) while even though the RV output

increases, the flow to both the peripheral pulmonary arteries (and hence veins) decreases as the increased flow in the main pulmonary artery is diverted through the left pulmonary artery towards the PS; (v) the LV ejection fraction decreases while the RV ejection fraction increases; and (vi) the LV workload decreases while that of the RV increases. The analysis of shunt diameters shows that higher diameters increase the shunt flow and decrease the pressure gradient. The 3D features show that the jet from the shunt impinges strongly on the descending aorta wall, leading to high forces, abnormally high wall shear stresses, and high pressures.

In conclusion, while the PS of a sufficiently large diameter is effective in reducing pulmonary artery pressures, it also leads to increased LV afterload and hence, decreased LV output and worsened LV ejection fraction. It leads to an increased workload for the RV despite the lower afterload. For PS suitability, these considerations need to be assessed individually for each patient.

5. References

- [1] Grady RM. And Eghtesady P. *The Annals of thoracic surgery* 2016; 10194:1539–1543.
- [2] Pant et al. *Biomechanics and Modeling in Mechanobiology* 2022; 21(2): 471-511.
- [3] Boudjemline et al. *Canadian Journal of Cardiology* 2017; 33.9:1188–1196.

Acknowledgements of funding support:

EPSRC Grant Number EP/R010811/1 and the European Research Council (ERC) under the European Union's Horizon 2020 research and innovation program (Grant No. 864313).

CMBBE 2023

18th International Symposium on Computer Methods
in Biomechanics and Biomedical Engineering

3 - 5 May 2023, Paris, France



Arts et Métiers Institute of Technology

Institut de Biomécanique Humaine
Georges Charpak

155 boulevard de l'Hôpital 75013
Paris France

www.cmbbe-symposium.com

TACKLING SUBJECT SPECIFICITY IN MSK DISORDERS ANALYSIS: METHODOLOGICAL CHALLENGES AND RECENT ADVANCES.

Wafa Skalli (1), Laurent Gajny (1), Helene Pillet (1), Ayman Assi (1-2)

1. *Arts et Métiers Institute of Technology, Institut de Biomécanique Humaine Georges Charpak, France*

2. *Faculty of Medicine, Saint-Joseph University, Beirut, Lebanon*

Musculoskeletal disorders are extremely complex to understand because they involve several systems that interact together: the skeleton (bone and joints system) can be in a given posture and can move thanks to muscular system, that act under the control of neurocontrol system (NCS). This control is affected by the proprioceptive sensors that are widely distributed in the body (skin, ears, ligaments, ...). Disorders can result from alterations of components of each of these systems, and compensation strategies are settled to maintain an as acceptable as possible posture and motion for a given individual. Such compensations may change local overloading that can result, because of the mechanobiology of the tissues, into alterations in geometry or material properties of the musculoskeletal system.

Research communities in musculoskeletal modeling have long been compartmentalized: For skeleton, researchers have developed more and more efficient finite element bone and joint models, with progress in taking into account subject-specific geometry and material properties of tissues from medical images: however, quantification of subject specific loads, that is crucial, is still a real issue. Researchers from motion analysis consider more and more sophisticated musculoskeletal models, with the aim to quantify intersegmental and interarticular loads. However, the transition from skin markers

measurements to internal subject-specific skeleton still raises significant methodological issues, because of the well-known soft tissue artefacts, and because of the scaling approaches that only grossly represent the geometry of a given patient and its body inertial parameters. As for clinical investigation of musculoskeletal disorders, it is still mainly based on static medical images and clinical examination, while functional assessment is still omitted. This talk presents some recent methodological advances to fuse data resulting from complementary examinations in order to progress into filling the gaps and provide clinically relevant data from the combination of various approaches.

Acknowledgements:

Authors The authors would like to thank the ParisTech foundation BiomecAM chair program for subject specific musculoskeletal modelling, with the support of COVEA, and the franco-lebanese joint research program PHC CEDRE 2022 PROJET N° 46556SG for providing financial support to this project”.



QUANTITATIVE FUNCTIONAL ASSESSMENT IN THE SETTING OF ADULT SPINAL DEFORMITY USING SUBJECT-SPECIFIC 3D MUSCULOSKELETAL DATA

Ayman Assi (1,2), Rami El Rachkidi (1), Guillaume Rebeyrat (2), Hélène Pillet (2), Virginie Lafage (3), Wafa Skalli (2)

1. Faculty of Medicine, St-Joseph University, Beirut, Lebanon

2. Institut de Biomécanique Humaine Georges Charpak, Arts et Métiers, Paris, France

3. Orthopaedics Surgery, Lenox Hill Hospital, New York, USA

Background

Adult Spinal Deformity (ASD) consists of alterations of the lumbar or thoracolumbar spine [1], leading to compensatory mechanisms in the pelvis, lower limbs, trunk and head [2]. Clinical assessment is usually based on full X-rays in standing position. Compensatory mechanisms can have severe consequences, causing increased back pain, muscle fatigue, joints degeneration, and a limitation of numerous daily life activities such as walking. Clinicians rely mostly on health-related quality of life (HRQoL) questionnaires for the assessment of deformity repercussions on functionality. Since these techniques lack objectivity and quantification, the aim of our research is to evaluate ASD function using subject-specific 3D musculoskeletal models during daily life activities.

Recent Advances

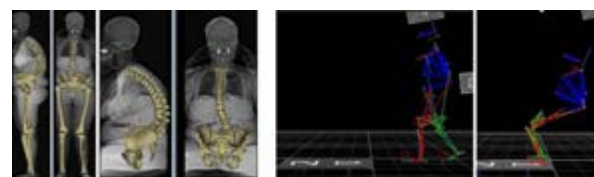
We have enrolled more than 120 ASD patients and 70 controls who underwent 3D motion analysis for several daily life activities such as: walking at self-selected speed and fast speed, sitting and standing movement and stairs climbing. The kinematics of the trunk, pelvis and lower limbs were calculated as well as segmental spine motion [3, 4]. Biplanar X-rays were performed in both standing and sitting positions, while the reflective markers were kept in place, with subsequent 3D reconstructions of skeletal segments and calculation of classic radiographic parameters. Image registration techniques were applied in order to calculate subject-specific postural radiographic parameters during movement. All subjects filled HRQoL questionnaires. Patients are followed 3 months and 2 years after surgery or medical treatment.

The findings to date show that quantitative functional assessment in the setting of ASD are

better related to HRQoL outcomes than radiographic parameters [5]. Moreover, movement patterns differ between patients depending on the type of spinal deformity: patients with sagittal malalignment have more altered gait with different compensatory mechanisms [6, 7]. Subject-specific image registration techniques showed that some patients have altered balance during gait and are more prone to falls [8]. Some patients use different spinopelvic strategies to acquire a balanced sitting position [9, 10]. Moreover, this research contributed to better understand the hip-spine syndrome in these patients [11, 12].

Future directions

Using 3D subject-specific musculoskeletal models during movement help in better understanding of orthopedic pathologies and to choose the optimal treatment in patients and to improve their quality of life.



Data acquisition in static (standing and sitting) and during motion for ASD and controls.

References

1. Schwab F, et al (2005) Spine;
2. Dubousset J (1994) Pediatr Spine;
3. Leardini A, et al (2011) Clin Biomech;
4. Davis RB, et al (1991) Hum Mov Sci;
5. Saliby RM, et al (2020) Gait Posture;
6. Kawkabani G, et al (2021) Gait Posture;
7. Semaan K, et al (2022) Eur Spine;
8. Rebeyrat G, et al (2021) Eur Spine;
9. Saad E, et al (2021) Frontiers;
10. El Rachkidi R, et al (2022) Cureus;
11. Mekhael M, et al (2021) Eur Spine;
12. Rebeyrat G, et al (2022) Gait Posture;

CMBBE 2023

18th International Symposium on Computer Methods
in Biomechanics and Biomedical Engineering

3 - 5 May 2023, Paris, France



Arts et Métiers Institute of Technology

Institut de Biomécanique Humaine

Georges Charpak

155 boulevard de l'Hôpital 75013
Paris France

www.cmbbe-symposium.com

SUBJECT-SPECIFIC KINEMATIC MODELLING OF THE SPINE AND LOWER LIMBS BASED ON STANDING BIPLANAR RADIOGRAPHY FOR 3D MOVEMENT ANALYSIS

L. Scheys^{1,2}, T. Overbergh¹, P. Severijns¹, B. Peeters¹, E. Beaucage-Gauvreau¹, T. Ackermans¹, D. Al Otti¹, D. Monari¹, S. Ghijssels^{1,2}, F. Staes³, S. Schelfaut^{1,2}, L. Moke^{1,2}

(1) Institute for Orthopaedic Research and Training (IORT), Department of Development and Regeneration, KU Leuven, Belgium; (2) Division of Orthopaedics, University Hospitals Leuven, Belgium; (3) Research Group for Musculoskeletal Rehabilitation, Department of Rehabilitation Sciences, KU Leuven, Belgium

1. Introduction

Still to date, rescaling generic models based on specific anatomic landmarks is the most common approach to define biomechanical models for inverse kinematics. Nevertheless, this procedure introduces errors in calculated kinematics associated with: (1) the identification of a minimum of three reliable anatomical landmarks per body segment with respect to the chosen kinematic trackers, whether skin-mounted markers, inertial measurement units, or others (2) inaccuracies in the axes of the segmental coordinate frames that define the cardan angle decomposition of the kinematic tracker signals into physiologically relevant degrees of freedom. Previous studies already reported that these errors can be importantly inflated in case of structural deformities of pathologic locomotor systems, such as aberrant femoral torsion in cerebral palsy or spinal deformities in adolescents or adults. On the other hand, these errors can also exceed the expected impact on a specific kinematic outcome measure in studies involving healthy individuals, e.g., when studying secondary degrees of freedom with typically smaller degrees of freedom.

In these cases, medical imaging has been suggested as a possible data source for the definition of subject-specific kinematic models. Due to their relatively wide availability in clinical settings as well as their large, three-dimensional field-of-view, computed tomography and magnetic resonance imaging have been mostly used. Nevertheless, these modalities typically involve unloaded, supine patient positioning which might impede their

validity as a reference position to define kinematic models used to study loaded, upright standing motor tasks. Furthermore, their cost, scanning time and invasive character might further limit their applicability.

More recently, kinematic modeling based on biplanar, upright standing radiographs has been introduced to overcome the above limitations. In this lecture we will thereto introduce subject-specific kinematic modeling pipelines based on biplanar radiography for the spine and lower limbs.

2. Materials and Methods

We documented the accuracy and reliability of two subject-specific kinematic modeling pipelines based on biplanar radiography for the spine and lower limbs, respectively. Furthermore, we investigated their application potential for two specific research applications: (1) the analysis of spinal kinematics in subjects with adult spinal deformity and (2) out-of-sagittal plane hip kinematics in healthy subjects during highly dynamic motor tasks.

3. Results

Our results demonstrate that these novel modeling pipelines allow to further improve the reliability of three-dimensional movement analysis and thus expands the application field of research based on such data.

4. Discussion and Conclusions

Future work should focus on further automating the presented modeling pipelines as well as their integration in full musculoskeletal models and simulations.



PATIENT-SPECIFIC CERVICAL SPINE MUSCULOSKELETAL MODEL FROM REDUCED IMAGE ACQUISITION

Christophe Muth-seng (1), Sébastien Laporte (1), Jean-Yves Le Coz (1), Maxim Van den Abbeele (1), Maxime Huneidi (2), Olivier Gille (2), Wafa Skalli (1)

1. Institut de Biomécanique Humaine George Charpak, Arts et Métiers Institute of Technology, France,
2. Groupe hospitalier Pellegrin, CHU de Bordeaux, France

1. Introduction

For both clinical and sports applications, cervical spinal loads can be estimated via subject-specific musculoskeletal models (SSMM) [1]. They can be built by combining MRI with biplanar X-ray (BPXR) data. However, while BPXR could be routinely used, using MRI acquisition is less convenient, and time-consuming. An approach to generate such models via generic template deformation appeared promising for the lower limb [2]. The aim of the study is to adapt this approach for cervical spine load estimation and evaluate its performance.

2. Materials and Methods

Low dose BPXR (EOS imaging, France) and MRI acquisition (Philips, Netherlands) were collected for 6 asymptomatic subjects and 15 neck pain patients planned for cervical surgery, which were approved according to CPP N° 2010/113 and N° 2014/89. For all subjects, elastic registration of MRI-based muscles (in lying position) was performed onto the 3D reconstruction of spine and head-neck envelope from the BPXR (in standing position). This process yielded a reference SSMM from a Full image DataSet (FDS). The FDS models of the 6 asymptomatic subjects were averaged to obtain a generic template. The template was then deformed onto the head-neck reconstruction of a given patient from BPXR only, yielding a Reduced DataSet (RDS) model. RDS models were further adjusted using muscle contours from up to 4 MRI slices, yielding Partially Reduced DataSets (PRDS1-4) models. For each model, C3C7 spinal loads in neutral standing position were assessed with a proprioception-based model [1] and the agreement between modelling methods were analysed for all 21 subjects with the Bland-Altman approach [3].

3. Results

Spinal anteroposterior load was estimated at 25.2 N (SD: 11.7) via the FDS approach. Errors of the RDS approach were relatively low, averaging -1.3 (SD: 4.8) N. Adding MRI slices only had a marginal effect, slightly reducing the bias but not the limits of agreement (Figure 1). Similar observations could be made for spinal compression and moments.

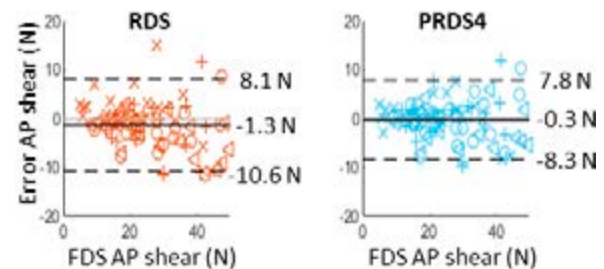


Figure 1: Bland-Altman plots for spinal anteroposterior shear of FDS method with RDS and PRDS4 methods

4. Discussion and Conclusions

Though the Full Data Set remains necessary for fine assessment, a reasonably simplified approach from BPXR only could facilitate large scale spinal loads estimation particularly in clinical routine or in sports biomechanics. Work is in progress to improve the modelling approach for a larger range of applications.

5. References

1. Van den Abbeele M et al., Clin. Biomech. 2018;51:58-66.
2. Dubois G et al., CMBBE. 2016; 19:1592-98.
3. Bland & Altman, Lancet, 1986; 1(8476):307-10.

Acknowledgements: BiomecAM chair of Fondation ParisTech and COVEA for funding this work, and staff of Pellegrin and Francheville Hospitals for patient data collection.

DETERMINANTS OF KNEE JOINT LOADING IN MEDIAL KNEE OA: INSIGHTS FROM POPULATION-BASED MODELING APPROACHES

Miel Willems (1), Bryce A. Killen (1), Giacomo Di Raimondo (1), Ilse Jonkers (1)
 1. KU Leuven, Movement Science Department, Belgium

1. Introduction

The use of 3D Mocap combined with musculoskeletal modelling and dynamic simulations, has opened the avenue of studying joint loading in patients with Osteoarthritis (OA). Furthermore, advances in medical imaging techniques that allow highly detailed visualization and segmentation of soft tissues including cartilage surface geometry, can now be integrated into highly personalised musculoskeletal models. Despite increasing the level of patient-specificity, this approach is at the expense of high (operator) cost not sustainable for use in routine clinical screening applications. In this presentation, we will present how population-based modelling approaches, in particular statistical shape modelling, can be exploited to understand the impact of anatomical variation on the knee joint loading landscape.

2. Materials and Methods

A workflow was developed to include population-specific tibiofemoral joint geometry in state-of-the-art musculoskeletal models. Geometries were based on a previously published statistical shape model [1], defined based on MRI-images collected in 524 subjects. More specific, articular surface geometry and alignment of the tibiofemoral joint were incorporated in the 6DOF Lenhart model [2] to create models representing the 8 main modes of variation (± 3 std). Dynamic gait simulations were then generated for each model using control and OA-specific gait patterns. Variations in peak medial compartmental forces were evaluated in function of the anatomical variation defined by the statistical shape model.

3. Results

Variation in peak medial compartment loading was highly dependent on the individual PCAs. Variations up to 1,5 BW were found mainly for

mode 2 (tibial rotations), whereas only minimal variation was observed for mode 3 and 8, being anterior-posterior translation of the tibia and joint space narrowing respectively. Interestingly, the first mode of variation (frontal plane alignment), that explained 21,7 % of variation in the tibiofemoral geometry, resulted only in a moderate change in medial compartment forces of 0,5 BW.

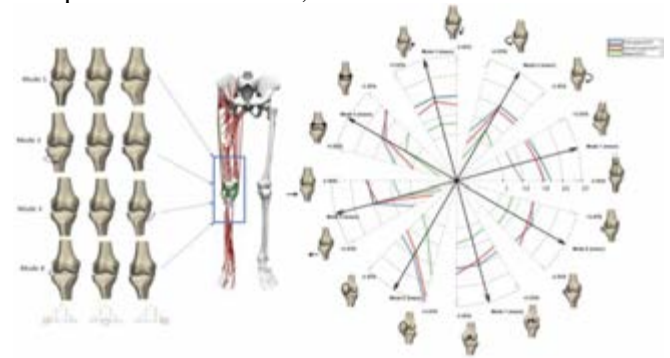


Figure 1: Population-based variation in medial knee compartmental loading during gait.

4. Discussion and Conclusions

Population-based approaches allow identification of relevant anatomical features that explain variability in tibiofemoral joint anatomy and relate these to changes in knee joint loading. Combined with low fidelity data (e.g. radiographs), statistical shape-based approaches may alleviate the need for high fidelity – and costly – imaging modalities to personalise the knee joint loading landscape for use in more routine clinical screening applications.

5. References

1. Van Dijck et al., *Comp Meth Biomech Biomed Engin.*,21(9):568-78, 2018
2. Lenhart et al., *Ann Biomed Eng*, 43(11): 2675-85, 2015

Acknowledgements:

Authors acknowledge financial support through Research Fund Flanders (G0E4521N and 1SC9922N).



A 3D SUBJECT-SPECIFIC MUSCULOSKELETAL MODEL TO CALCULATE MUSCLE LENGTHS DURING WALKING

Guillaume Rebeyrat (1), Ayman Assi (1,2), Rami Rachkidi (2), H el ene Pillet (1), Wafa Skalli (1)

1. Institut de Biom ecanique Humaine Georges Charpak, Arts et M etiers ParisTech, Paris, France;

2. Faculty of Medicine, University of Saint-Joseph in Beirut, Lebanon.

1. Introduction

The computation of muscle lengths during walking is essential for a better understanding of musculoskeletal pathologies and treatment decision-making. Several methods exist in the literature to compute these lengths variation, however, models used for such studies remain generic or poorly personalized. The aim was to develop a 3D subject-specific musculoskeletal model using patient's anatomy, and to validate the results to existing models.

2. Materials and Methods

26 controls (49±13) and 28 patients with adult spinal deformity (ASD, 55±21y.o.) underwent bi-planar X-rays and gait analysis from which 3D skeletal reconstructions, body envelop, and 3D walking kinematics were extracted.

Muscles were obtained, in standing static position by applying a non-linear transformation of a generic musculoskeletal model (based on MRI of an adult subject), while taking into account both the subject-specific 3D bones and body envelop [1]. Subject-specific muscle paths were obtained as the centre of each muscle contour on the generic MRI slice of the generic model. Subject-specific insertion points of the muscles were computed with the 3D skeletal reconstructions, using prior anatomical identification of insertions on cadaveric skeletal segments. Subject-specific skeletal segments, muscle paths, and insertions were registered during the subject's gait, while using a soft tissue artefact reduction method based on FEM [2]. Then, muscle lengths were obtained during the gait cycle.

Variation of muscle lengths during gait were compared to those obtained by an OpenSim model scaled to each subject [3]. RMSE between the two lengths (in %) and statistical parametric mapping (SPM) method were used to compare five muscles length variation between both models: adductor magnus, gluteus

medius, iliacus, gastrocnemius medius and rectus femoris.

3. Results

The RMSE of muscle lengths across patients and controls varied from 1.5 (gastrocnemius) and 8.5% (gluteus) with a median of 3.5% (adductor). SPM showed no differences between the two models except for the gluteus at the beginning and the end of the gait cycle.

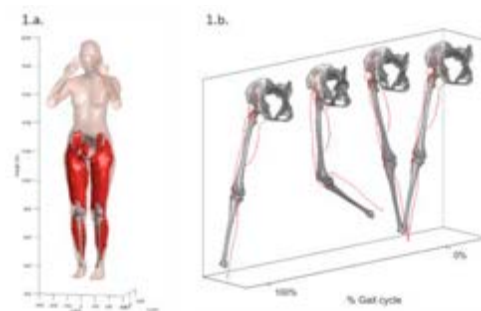


Figure 1: (a) Generic musculoskeletal model scaled on a subject. (b) Evolution of the five studied muscles during the gait cycle of a subject.

4. Discussion and Conclusions

A new subject-specific musculoskeletal model has been developed to calculate muscle lengths during gait in control adults and ASD patients. While differences remain moderate, they could be higher with higher bone deformities. Work in progress to compare muscle lengths during gait between children controls and cerebral palsy patients.

5. References

- [1] Hausselle J et al., CMBBE; 17(5):480-7 (2014).
- [2] Lahkar BK et al. J Biomech. 122:110464 (2021).
- [3] Hoy MG et al., J Biomech.; 23(2):157-69 (1990).

Acknowledgements:

The authors would like to thank the BiomecAM chair and Franco-Lebanese PHC C edre program for providing financial support to this project.

DECREASING RECTUS FEMORIS ACTIVITY CAN DECREASE KNEE LOADS IN PEOPLE WITH INCREASED FEMORAL ANTEVERSION

Basilio Gonçalves (1), Willi Koller (1), Arnold Baca (1), Hans Kainz (1)

1. Centre for Sport Science and University Sports, University of Vienna, Austria

1. Introduction

Excessive femoral anteversion can lead to hip and knee pain and, in some cases, osteoarthritis [1,2]. Individuals with femoral anteversion angle (AVA) 30° above reference values (12°) walk with increased hip and knee joint contact forces (JCF) largely due to increased hip flexor and knee extensor muscle forces [3]. Musculoskeletal simulations have shown potential to inform gait retraining by determining the potential of individual muscles to alter joint loading [4]. The aim of this study was to investigate how different in-silico muscle coordination strategies with decreased rectus femoris (RF) muscle activity alters JCF in an individual with increased AVA.

2. Materials and Methods

We used publicly available data including full body kinematics and ground reaction forces from a healthy adult male walking at a speed of 1.25 m/s [4]. Using a MATLAB tool [5], we created two OpenSim models [6] with reference (12°) and increased (42°) AVA. Using static optimisation, we calculated muscles forces, which were then used to estimate hip, and knee JCF [7]. Muscle inhibition was simulated by increasing the penalty weight of the RF muscle from 0 (no inhibition) to 1000 (maximum inhibition) in the objective function that minimises muscle activation. We investigated the relationship (r^2) between the impulse generated by JCF and RF muscle forces to determine if decreases in RF force were associated with decreases in JCF. Overall, 6 walking trials for two models were simulated over 5 different inhibition levels.

3. Results

Compared to the reference model, increased AVA led to greater hip (25-38%) and knee (23-65%) peak JCF. Using the model with increased AVA, inhibition of RF led to only moderate 7 to 9% reductions in the first peak of hip JCF and 0 to 2% increases in the second peak of hip JCF (Figure 1). On the other hand, inhibition of RF muscle led to large reductions both in the first (14 to 30%) and

second (9 to 21%) peaks of knee JCF. We observed no association between the impulse of RF and hip JCF ($r^2 = 0.141$) but very strong association between impulse of RF and knee JCF ($r^2=0.999$).

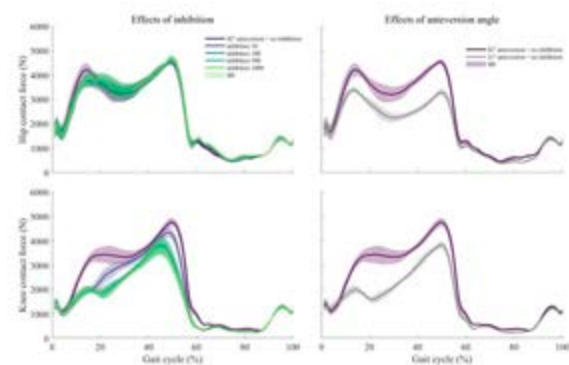


Figure 1. Effects of RF inhibition and femoral AVA on hip and knee JCF.

4. Discussion and Conclusions

We showed that in individuals with increased AVA, RF muscle forces have a large influence on knee but not hip JCF. Given the association between increased femoral anteversion and knee pain [2], gait retraining targeting inhibition of RF muscle has potential to reduce knee loading and improve symptoms. In the future we will investigate if gait retraining (e.g. with real-time feedback) can reduce RF activity and therefore knee loads in people with increased AVA.

5. References

- [1] T. Terjesen *et al.*, *Acta Orthop. Scand.*, 53, 4, 571–575, (1982)
- [2] D. G. Eckhoff *et al.*, *Clin. Orthop. Relat. Res.*, 302, 64–8, (1994) [Online]. Available: <http://www.ncbi.nlm.nih.gov/pubmed/8168324>
- [3] H. Kainz and G. T. Mindler, *PRE-PRINT*, 1–25, (2022)
- [4] S. D. Uhlich *et al.*, *Sci. Rep.*, 12, 1, (2022)
- [5] L. Modenese *et al.*, *Gait Posture*, 88, 318–321, (2021)
- [6] A. Rajagopal *et al.*, *IEEE Trans. Biomed. Eng.*, 63, 10, 2068–2079, (2016)
- [7] K. M. Steele *et al.*, *Gait Posture*, 35, 4, 556–560, (2012)



PIPELINES FOR MODEL AND DIGITAL TWIN PERSONALIZATION IN PULMONARY HYPERTENSION

Prashanna Khwaounjoo (1)*, Behdad Shaarbafebrahimi (1)*, Finbar Argus (1), Ho-Fung Chan (1), Atefeh Rahimi (1), Alys R. Clark (1), Martyn P. Nash (1), Merryn H. Tawhai (1)

1. Auckland Bioengineering Institute, University of Auckland, Auckland, New Zealand *Joint first authors

1. Introduction

Pulmonary hypertension (PH) has multiple aetiologies and can be difficult to diagnose and differentiate. Personalised digital twin models for patients with PH that explore the interactions between the heart and lungs can help improve diagnosis and treatment options. Here, we present an overview of patient-specific modelling pathways and biomarkers for a specific phenotype of PH, chronic thromboembolic pulmonary hypertension (CTEPH).

2. Materials and Methods

Comprehensive data including dual-energy computed tomography pulmonary angiogram (CTPA), and haemodynamic data of CTEPH patients (n=8) was obtained from the Alfred Hospital in Melbourne, Australia.

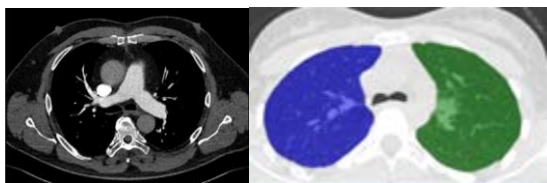


Figure 1: Example CTPA image and right/left lung segmentation using Pulmonary ToolKit.

An anatomical model of the entire pulmonary vasculature was used to understand the global pathology typical of CTEPH [1]. Dual-energy CTPA was segmented (Fig 1) using the Pulmonary ToolKit. Voxel intensities were mapped to terminal branches of the vascular tree and then summed together and normalised by the cardiac output. These values were then differentiated from the expected baseline (healthy) values to predict under and over-perfused regions/subsegments.

3. Results

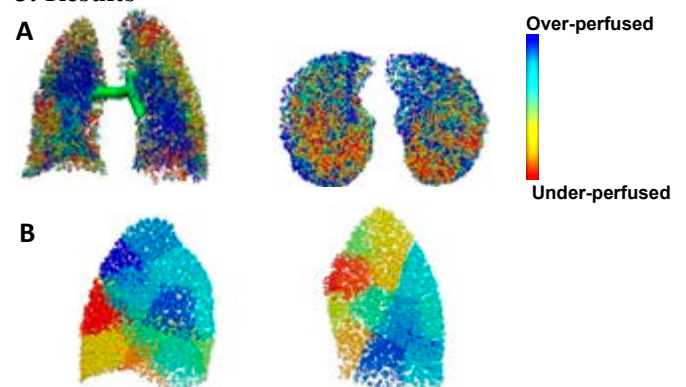


Figure 2: Pulmonary modelling: A: Lung perfusion, coronal and sagittal view respectively (colour indicates level of perfusion) B: Segmentation, right and left lung respectively (colours indicates segments).

Preliminary results show the outputs provide an accurate discernment of perfusion variance (Fig 2) observed in the lung regions. The under-perfused segments corresponded to the clots observed in the CTPA.

4. Discussion and Conclusions

Overall, the spatial perfusion estimates provide pertinent information to enable clinicians to make better-informed diagnostic decisions. Computational modelling enables estimations of the extent of remodelling and proximal disease in CTEPH. This information has the potential to expand/improve on predicting response to treatment by providing a non-invasive risk assessment prior to surgery.

5. References

1. Ebrahimi BS, et al. *A computational model of contributors to pulmonary hypertensive disease: impacts of whole lung and focal disease distributions*. *Pulm Circ*. 2021 Nov

Acknowledgements:

The authors would like to thank the Ministry of Business, Innovation and Employment (Catalyst Grant) for providing financial support to this 12 Labours Exemplar Project 1.



TRUNCATION STRATEGIES FOR PERSONALIZED CFD MODELS OF SELECTIVE LIVER RADIOEMBOLIZATION

Tim Bomberna (1,2), Saar Vermijs (1,2), Chris Verslype (3), Lawrence Bonne (4), Geert Maleux (4,5) and Charlotte Debbaut (1,2)

1. IBItech-Biommeda, UGent, Belgium; 2. Cancer Research Institute Ghent, Belgium; 3. Department of Clinical Digestive Oncology, University Hospitals Leuven, Belgium; 4. Department of Radiology, University Hospitals Leuven, Belgium; 5. Department of Imaging & Pathology, KU Leuven, Belgium

Corresponding author: Tim.Bomberna@UGent.be

1. Introduction

Computational fluid dynamics (CFD) models are increasingly being used to better understand blood flow and drug transport in the circulatory system. For hepatocellular carcinoma, CFD modelling of arterially injected radioactive microparticles might aid in patient-specific treatment decision-making. However, CFD models of particle distribution can be computationally costly. Previously, we showed that we can truncate the CFD geometry assuming that microparticles distribute proportional to the flow distribution (FD) downstream of the catheter tip [1]. Here, we want to evaluate (1) this assumption for selective injection in the right hepatic artery (HA) and (2) the possibility of truncating upstream bifurcations.

2. Materials and Methods

The patient-specific hepatic arterial network was simplified from 48 (Geometry 1, Fig. 1A) to 17 outlets (Geometry 2, Fig. 1B) [1]. Additionally, since the catheter tip is in the RHA, the left HA was truncated entirely, and the proper HA was shortened until a length of 8 cm before the catheter tip, leading to a 3rd geometry of 6 outlets (Geometry 2U, Fig. 1C). The catheter and arterial lumens of the geometries were meshed in Fluent Meshing (Ansys, USA) using tetrahedral bulk elements and prism elements near the walls. Using Fluent (Ansys, USA), a multiphysics approach was employed to model both blood (ρ : 1060 kg/m³) and microparticle (diameter: 40 μ m, ρ : 1600 kg/m³) flow. At the inlets, a time-dependent waveform was applied; at the outlets, outflow fractions were prescribed according to the tissue volume each outlet perfused [1]. The outlet-

specific particle distribution at all 48 outlets was compared between Geometries 1-2 and 2-2U to evaluate downstream and upstream truncation, respectively; and between Geometry 1 and the FD to evaluate the need for particle modelling.

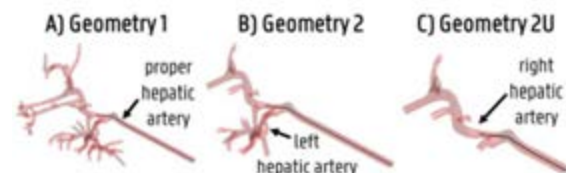


Figure 1: Successive down- and upstream truncation of Geometry 1 leads to Geometry 2, 2U.

3. Results

The median and 95-percentile differences in outlet-specific (particle) distribution are 1.5% and 13% between Geometry 1 and the FD; 0.3% and 3.8% between Geometry 1-2; and 0.015% and 0.16% between Geometry 2-2U.

4. Discussion and Conclusions

The results show that the FD is not an accurate surrogate of the particle distribution. However, by assuming that particles distribute according to the FD downstream of truncated outlets, the 95-percentile error can be reduced from 13% to 3.8%. Furthermore, this geometry can be truncated upstream of the catheter tip, which barely impacts the particle distribution. Hence, successive down- and upstream truncation is a more reliable simplification strategy than only modelling the FD, but still induces a certain error. Future work should focus on validating this surrogate model for multiple patient-specific geometries.

5. References

1. Bomberna T, et al., *Front. Bioeng. Biotechnol.*; 10:914979.



PREDICTION OF RIGHT VENTRICLE PRESSURE FOLLOWING PULMONARY ENDARTERECTOMY USING A DIGITAL TWIN

Finbar Argus (1), Behdad Shaarbafebrahimi (1), Prashanna Khwaounjoo(1), Ho-Fung Chan (1), Stephen Creamer (1), Atefeh Rahimi (1), Alys Clark (1), David Nickerson (1), Soroush Safaei (1), Peter Hunter (1), Merryyn Tawhai (1), Martyn Nash (1)

1. Auckland Bioengineering Institute, University of Auckland, New Zealand;

1. Introduction

Pulmonary Endarterectomy (PEA) is a common treatment for chronic thromboembolic pulmonary hypertension (CTEPH), however, the efficacy of the treatment is variable due to disease severity, heart condition, pulmonary heterogeneity, and patient specific autonomic nervous system (ANS) dynamics. Obtaining an estimate of the decrease in right ventricle pressure due to surgery would better inform clinicians and aid them in deciding the optimal treatment strategy.

2. Materials and Methods

Dual-energy computed tomography pulmonary angiogram (CTPA) (see Figure 1), and haemodynamic data of CTEPH patients (n=8) were obtained from the Alfred Hospital in Melbourne, Australia.



Figure 1: CTPA image showing left (right side of image) pulmonary artery branching.

This CT data was used to generate a high-fidelity frequency domain model of the pulmonary system [1]. An efficient low-fidelity lumped parameter model of the closed loop circulatory system [2] was then calibrated to the impedances of the high-fidelity pulmonary system model and clinical measurements of echocardiogram volume, ECG inter-peak timings, and brachial-cuff pressure. The pulmonary system compartment of the low-fidelity model was then recalibrated to the high-fidelity model after removal of the blood clot. This model was then

simulated to give estimates and standard deviations of post-operative right ventricle pressure, as well as changes in oxygen perfusion to different regions of tissue.

3. Results

This method allows the prediction of the decrease in right ventricle pressure due to PEA treatment of patients with CTEPH (see Figure 2).

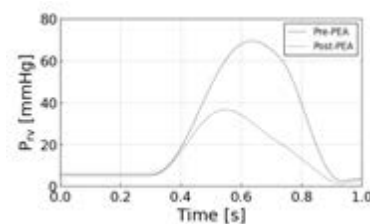


Figure 2: Simulated right ventricle pressure pre- and post-pulmonary endarterectomy.

4. Discussion and Conclusions

Model-based prediction of the response to treatment has the potential to reduce inter- and intra-clinician variability and improve patient care by optimising treatment selection. This approach takes into account patient specific pulmonary, cardiovascular, and ANS dynamics to give a clinically useful prediction of post-PEA right ventricle pressure.

5. References

1. Clark, Alys Rachel, and M. H. Tawhai. "Temporal and spatial heterogeneity..." The ANZIAM Journal 59.4 (2018): 562-580.
2. Argus, Finbar, et al. "Automated model calibration..." Frontiers in Physiology 13 (2022).

Acknowledgements:

The authors would like to thank the Ministry of Business, Innovation and Employment (Catalyst Grant) for providing financial support to this 12 Labours project (Exemplar Project 1 and Platform 1).



EFFICIENT PARAMETER ESTIMATION IN CARDIAC MODELS BASED ON PHYSICS-INFORMED NEURAL NETWORKS

Federica Caforio(1,2), Francesco Regazzoni(3), Stefano Pagani(3), Alfio Quarteroni(3,4), Gernot Plank(2) and Gundolf Haase(1)

1. *Institute of Mathematics and Scientific Computing, NAWI Graz, University of Graz, Austria;*
2. *Gottfried Schatz Research Center: Division of Biophysics, Medical University of Graz, Austria;*
3. *MOX, Department of Mathematics, Politecnico di Milano, Italy;*
4. *Institute of Mathematics, EPFL, Switzerland (Professor Emeritus)*

1. Introduction

The development of biophysical models, e.g. of the cardiovascular system [1], is rapidly advancing in the research community. However, accurate, multiphysics mathematical models are computationally expensive and their personalisation involves fine calibration of a large number of parameters, challenging their clinical translation.

2. Materials and Methods

In this talk a novel methodology is proposed, relying on the integration of physics-informed neural networks (PINNs) methodologies [2] with high-resolution three-dimensional cardiac biomechanical models, to generate robust and effective surrogate reduced-order models capable of reconstructing displacement fields and estimating patient-specific biophysical properties. The proposed learning algorithm encodes information from displacement data, that can be routinely acquired in the clinical setting, and combines it with the physics of the problem, represented by a mathematical model based on partial differential equations, to regularise it and improve its convergence properties.

3. Results

Several benchmarks will be presented to show the accuracy and robustness of the proposed method and its great potential to enable the robust and effective identification of patient-specific physical properties. As an example, in Figure 1 PINNs are implemented for parameter

estimation in cardiac biomechanics (inflation experiment). Observations are represented by *in silico* displacement and stress data at random locations based on the solution of a finite element model of the cardiac function.

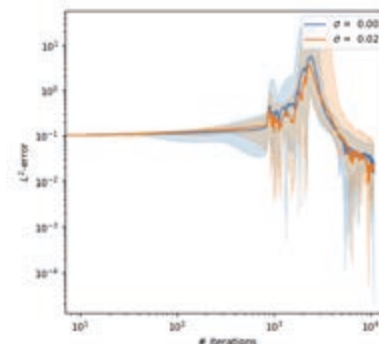


Figure 1: L^2 -error on the estimation of the passive stiffness considering noise-free or data corrupted by Gaussian white noise with standard deviation σ . Results of 10 training processes. The solid line depicts the geometric mean; the shaded region is the area spanned by the trajectories.

4. Discussion and Conclusions

This methodology paves the way for the robust and effective identification of patient-specific physical properties in biomechanical models.

5. References

1. Quarteroni A, et al., Cambridge Monogr. Appl. Comput. Math., Cambridge Univ. Press (2019)
2. Raissi M et al., J. Comp. Phys. 378: 686–707 (2019)



HUMAN BODY IMAGING TOWARD THE DEVELOPMENT OF FULL BODY SCAFFOLDS FOR PERSONALISED DIGITAL TWINS

Alexander Dixon* (1), Robin Laven (1), Thiranjya Prasad Babarenda Gamage (1), and Poul Nielsen (1) (2)

1. *Auckland Bioengineering Institute, New Zealand*; 2. *Department of Engineering Science, University of Auckland, New Zealand*

*Corresponding author email: alex.dixon@auckland.ac.nz

1. Introduction

The development of personalised healthcare models to facilitate home-based healthcare will enable new strategies for treating chronic disease. Such personalised models that incorporate the physiological systems of the human body (digital twins) require a common 3D coordinate system in which different organ systems can be positioned and linked together.

A common coordinate system for the human body requires a dataset of accurate whole-body geometries sufficient to characterise the population variation. Camera-based 3D reconstruction of the external geometry of the body, that is the skin surface, offers a relatively cheap and quick method to measure the body shape of many individuals.

2. Materials and Methods

A prototype camera-based human body imaging system was developed for measuring the external geometry of many individuals in static poses and dynamic poses. This system consisted of 10 depth cameras (Intel D415) mounted on a pentagonal antiprism frame (Fig. 1). Cameras were controlled using custom python software that allowed 3D recordings of individuals at 30 frames per second for >1 min. A custom inward facing camera calibration using a 3D calibration target gave reprojection error < 1 pixel [1]. Full body reconstructions were performed using rigid geometric transformations of point clouds from all camera views.

3. Results

The imaging system captured coloured 3D data of the skin surface of individuals in static poses

(Fig. 1) as well as recordings of body movements during dynamic poses.



Figure 1: 3D reconstruction of adult male in a static T-pose within virtual model of the body imaging system frame.

4. Discussion and Conclusions

This imaging system provides a platform for the development of techniques for fitting full body scaffolds. We aim to image up to 400 adults in various poses to provide a robust dataset from which to establish a common fiducial coordinate system for positioning and linking organ systems in personalised digital twins.

5. References

1. R. Laven et al. IJCV. 2022. High Precision Calibration of Multi-View Stereo Systems with Imperfect 3D Targets (in review).

Acknowledgements:

The authors would like to thank the New Zealand Ministry of Business, Innovation and Employment 12 Labours grant for providing financial support to this project.



HOW DOES KNEE ORTHOSIS MODELLING INFLUENCE THE PREDICTION OF CONTACT FORCES?

Sacha Guitteny (1), Rachid Aissaoui (2), Raphaël Dumas (1)

1. Univ Lyon, Univ Gustave Eiffel, Univ Claude Bernard Lyon 1, LBMC UMR_T9406, France ; 2. Laboratoire de recherche en Imagerie et Orthopédie, Dépt génie des systèmes, ETS, Canada

1. Introduction

Valgus knee orthoses are recommended to improve the quality of life of osteoarthritic (OA) patients and to postpone the arthroplasty. Tibio-femoral (TF) contact forces are important measure for the follow up of OA and the assessment of the orthosis efficiency. Musculo-skeletal models have been developed but, generally, without modelling the orthosis or adding a simple external moment [1]. This study investigates how modelling the interaction between the orthosis and the lower limb modifies the prediction of TF contact forces.

2. Materials and Methods

Sixteen patients with severe medial OA wore a personalised 3D printed orthosis (Evoke, OssKin) with a 4mm medial and 5° abduction correction during four weeks before the test. All patients completed the consent form approved by the institutional Ethics Committees.

Low dose biplane x-rays (EOS) were acquired in five weight-bearing squat postures (0°, 15°, 30°, 45°, 70° knee flexion) on an AMTI force plate with and without wearing the orthosis.

A lower limb model with 5 joint degrees of freedom and 43 muscles lines of action was scaled, adapted, and positioned to match the patients' bone geometries (TF contact points) and posture obtained from the biplane x-rays. Musculo-tendon and contact forces were computed via static optimization.

The orthosis medial force F_z^i and the abduction moment M_x^i were computed from the soft tissue stiffness (K_{tz}^i , K_{rx}^i) [2,3] of each segment i ($i=2,3$ for tibia and femur respectively):

$$\begin{cases} F_z^i \\ M_x^i \end{cases} = \begin{cases} K_{tz}^i * (u - u_0) \\ K_{rx}^i * (\vartheta - \vartheta_0) \end{cases} \quad (1)$$

Three orthosis modelling have been studied: *Personalized* with correction $(u_0, \vartheta_0) =$

$(-4mm, -5^\circ)$ applied at standing posture and orthosis movement (u, ϑ) measured in the other biplane x-rays, *Theoretical* without considering orthosis movement between posture, i.e. $(u, \vartheta) = (0,0)$. *None* without modelling any orthosis loads, i.e. (u_0, ϑ_0) also fixed to 0.

3. Results

Personalized medial force F_z^2 on tibia tends to decrease, from -12N at 0° to -7.2N at 70° and abduction moment M_x^2 varies between -1.5 and -6.1Nm along knee flexion (Fig.1a). Implementing any orthosis forces and moments reveals medial unloading, around 30% at 15° and 30° (Fig.1b). No change in the contact force appears when the orthosis is not modelled.

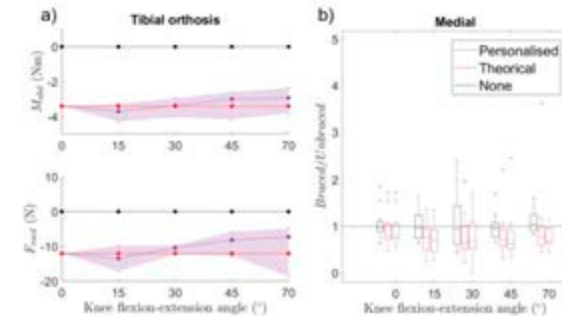


Figure 1: Evolution of (a) F_z^2 , M_x^2 on tibia and (b) medial TF contact load ratio without / with orthosis.

4. Discussion and Conclusion

The theoretical abduction moment of -3.4Nm is similar to literature values [4]. No differences in TF contact force have been found between the *Personalized* and *Theoretical* orthosis modelling even if the loads computed from the orthosis movement varied between patients.

5. References

1. Moyer RF et al., Osteoarthritis Cartilage 23(2): 178-188 (2015).
2. Guitteny S et al., J Biomech 134: 110987 (2022).
3. Shafiei M and Behzadipour S, J Mech Robot 12(1): 011007 (2020).
4. Brandon SC et al., Knee 26(3):564-577 (2019).

KNEE IMPLANT WEAR PREDICTION IS SENSITIVE TO CHOICE OF FORCE OR DISPLACEMENT CONTROL

Michael Dreyer (1,2), Bernhard Weisse (2), William R. Taylor (1)

1. ETH Zurich, Switzerland; 2. Empa, Switzerland

Corresponding author: William R. Taylor, bt@ethz.ch

1. Introduction

Polyethylene wear in knee implants is commonly investigated using ISO 14243 wear tests in force-controlled (FC) or displacement-controlled (DC) setups. As an alternative to the ISO input data, we recently presented “Stan” [1], who exhibits representative in vivo joint level loads and kinematics based on data from load-sensing implants and video-fluoroscopy [2]. Here, we (1.) developed and validated a computational wear prediction algorithm and (2.) compared wear for the ISO and Stan conditions in both FC and DC configuration using simulation and laboratory testing.

2. Materials and Methods

We developed finite-element models of the ISO FC and DC wear tests of the same knee implant Stan’s data was obtained from. Stan’s (FC, DC) load and motion curves for walking were also applied to otherwise identical copies of the ISO models for a direct comparison. Polyethylene inlay wear and creep was predicted for 5 million cycles using a cross-shear and contact-pressure dependent wear model [3] and a compressive creep model. For validation of the models, two groups of three specimens each were tested on a six-station knee simulator for 5 million cycles. One group was subjected to the ISO FC boundary conditions and the other to Stan’s kinematics in DC mode. Wear was measured gravimetrically. The effective loads and kinematics of the implants were also recorded.

3. Results

Experimentally, wear of the DC Stan condition was 2.7 times higher than for the FC ISO condition (Fig. 1, right). For the corresponding simulations (Fig. 1, left), the DC CAMS model matched the experiment closely, while the FC ISO model drastically overpredicted wear.

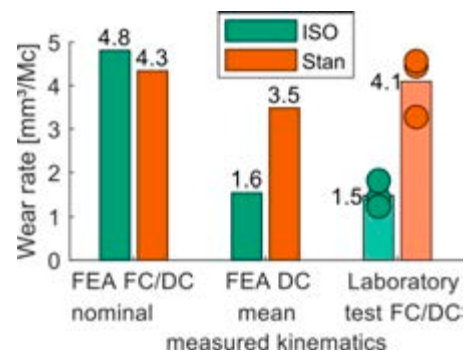


Figure 1: Gravimetric wear rate for simulations (left, middle) and laboratory wear test (right).

To investigate whether this mismatch was due to differences in FC and DC method or because of poor modelling of wear, we performed additional simulation where the effective kinematics measured on the knee simulator machine were applied in DC mode for both ISO and Stan. Now, there was good agreement for Stan as well as for ISO (Fig. 1, middle), which had been in FC mode in the initial simulation

4. Discussion and Conclusions

The comparison between the lab tests and the simulations using DC control served to validate our wear prediction algorithm. The large mismatch between the FC ISO experiment and simulation resulted from different resulting kinematics, and thus contact mechanics, in each. This shows that wear simulation is sensitive to small variations contact mechanics.

5. References

1. Dreyer MJ et al., J Biomech 141:111171 (2022).
2. Taylor WR et al., J Biomech 65:32-39 (2017).
3. Dreyer MJ et al., Tribol Lett 70(4):119

Acknowledgements:

We thank Zimmer Biomet for access to data and performing the laboratory wear test.



GEOMETRIC MRI-DERIVED BIOMARKERS AS PREDICTORS OF JOINT MECHANIC CHANGES AFTER PARTIAL MENISCECTOMY

Brett Steineman (1), Erin Leatherman (2), Thomas Santner (3), Joshua Leadem (4), Madison Lang (4), Kate Lindsey (4), Erin Argentieri (1), Amanda Wach (1), Kalle Chastain (1), Ashley Pekmezian (1), Matthew Koff (1), Amy Lerner (4), Scott Rodeo (1), Suzanne Maher (1)

1. Hospital for Special Surgery, USA; 2. Kenyon College, USA; 3. The Ohio State University, USA;
4. University of Rochester, USA

1. Introduction

Partial meniscectomies (PMs) are common treatments, but results vary. Some PM patients develop rapid degeneration within 6-12 months postop, where forces across the knee joint is implicated to drive variability [1,2]. Our objective was to identify knee factors that drive variability in force redistribution after PM due to: (i) PM volume removed, (ii) MRI-extracted geometric variables, and (iii) meniscal and cartilage properties. We hypothesized that PM volume would be a key predictive factor.

2. Materials and Methods

MRIs were acquired of four knees (3 cadaveric, and one volunteer) in an unloaded and a 50% bodyweight loaded condition [3,4]. Menisci and cartilage surfaces were segmented from unloaded scans and finite element models were created to replicate the loaded MRI condition. A 'small' and 'large' PM were created in the posterior medial meniscus. A total of 50 geometric parameters were measured to identify variables associated with force through the medial meniscus. A maximin space-filling design was constructed using material property ranges from the literature to create 70 simulation scenarios [2]. A fitted Gaussian process predictor model was used and the root mean squared prediction error (RMSPE) for all knee-specific variables were calculated [5]. A sensitivity analysis was performed to determine which variables were related to variability in model outputs.

3. Results

The percent load through the medial meniscus decreased from intact by 29% (range: 0-55%) for small PMs and 58% (range: 18-82%) for large PMs. Models with the smallest RMSPE included the intact geometry variables of the 'tibial medial-lateral width' and the 'medial

tibial surface covered by the meniscus', which were used for the modified sensitivity analysis. Variance ratios indicated that PM volume removed together with the two geometry variables were responsible for 96% the main effect variation in output. Material properties were related to smaller variations (up to 2%).

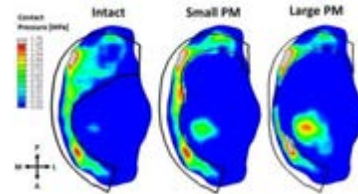


Figure 1: Contact pressure of loaded MRI simulation for intact, small PM, and large PM.

4. Discussion and Conclusions

We rejected our hypothesis that PM volume alone predicts joint force redistribution. Instead, the combination of PM volume removed AND tibial geometric variables together were predictive of the change in force distribution after PM. Material properties had minimal effects on force distribution. Knee geometry and the volume of meniscus removed are key predictors of the redistribution of joint forces after PM during simulated standing. This data will be used to enable MRI-derived predictions of biomechanical changes caused by planned PMs, prior to surgery, which will aid clinicians in predicting prognosis.

5. References

- [1] Souza et al., *Knee Surg Sports Traumatol Arthrosc* 2015
- [2] Guo et al., *J Orthop Res* 2017
- [3] Wang et al., *J Biomech* 2015
- [4] Maher et al., *J Orthop Res* 2017
- [5] Santner TJ et al., 2018.

Acknowledgements:

The authors would like to thank the National Institutes of Health (NIH 5R01AR075523) for providing financial support to this project.



STATISTICAL SHAPE MODELING-BASED WORKFLOW FOR PATIENT-SPECIFIC PLANNING OF TIBIAL FRACTURE FIXATION

Jet Moolenaar (1, 2), Nazli Tümer (1)*, Sara Checa (2)*

1. Department of Biomechanical Engineering, Delft University of Technology (TU Delft), Netherlands; 2. Berlin Institute of Health at Charité, Universitätsmedizin Berlin, Julius Wolff Institute, Germany; *equal contributions

1. Introduction

Tibial fracture healing complications occur frequently with reported non-union rates up to 23% [1]. Preoperative patient-specific finite element (FE) modelling of fracture fixation may help to minimize these complications. However, the development of such models requires labor-intensive work including (manual) segmentations of bones from medical images, which makes them unpractical for clinical applications. This study aims to establish a (semi-)automated pipeline for the development of three-dimensional (3D) patient-specific FE models of long bone fractures based on two-dimensional (2D) X-ray images.

2. Materials and Methods

An overview of the proposed pipeline is depicted in Figure 1. Accordingly, a parametric statistical shape model (SSM) of the tibia was developed based on computed tomography (CT) scans of subjects without tibial fractures. Using the model, shape parameters were correlated to patient-characteristics, including sex, age, weight and stature of the subjects, using multi-linear regression. Methodologies were developed to (1) morph the SSM of the tibia to two orthogonal X-rays of a previously unseen fractured tibia to estimate its 3D shape, and to (2) automatically introduce the fracture lines as detected on the X-rays into the tibia model. Using the automatically created geometries, FE models of stabilized fractures

are developed in Abaqus and used to investigate strains within the callus under post-operative physiological loading conditions. The pipeline was tested on two patient cases and the strains obtained from the FE models within the fracture region were compared to strains reported in the literature.

3. Results

An SSM of the tibia was developed based on CT scans of 25 subjects (15 male, age = 60 ± 5.5 & 10 female, age = 51 ± 7.1). The first five shape modes captured 90% of the total shape variation in the studied population. Significant correlations were found between the first shape mode, which described shape changes in the tibial length, and patient sex and stature. FE analysis of the stabilized fracture showed inter-fragmentary strains between 2% and 10%.

4. Discussion and Conclusions

SSM results were in accordance with previously developed models [2] and patient-specific FE analysis results demonstrated strains in a range reported for optimal bone formation [3]. Future work will focus on fully automating the suggested workflow.

5. References

- [1] S. Stewart, 2019, doi: 10.5704/MOJ.1907.001.
- [2] N. Tümer et al., 2019, doi: 10.1111/joa.12900.
- [3] S. Perren, 1989, doi: 10.3928/0147-7447-19890101-06.

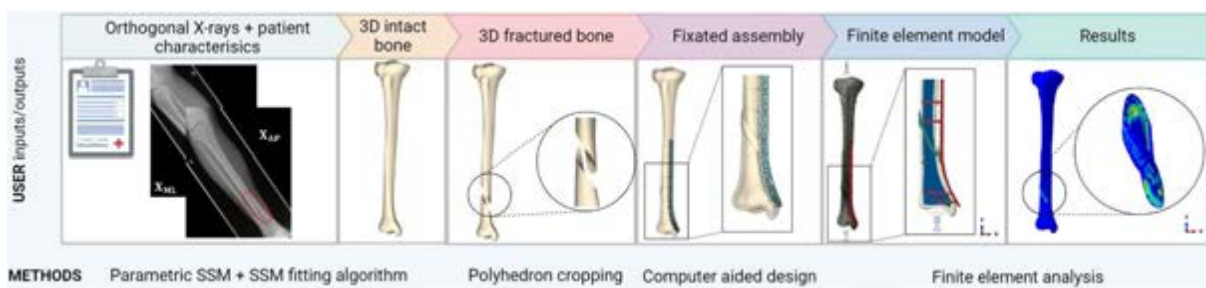


Figure 1: Proposed computational pipeline for patient-specific planning of tibial fracture fixation



COMBINED SHAPE MODEL OF THE LOWER LIMB IN A PAEDIATRIC POPULATION PROVIDES ACCURATE BONE SHAPE ESTIMATION

Laura Carman (1), Thor F. Besier (1), Julie Choisne (1)

1. Auckland Bioengineering Institute, The University of Auckland, New Zealand

1. Introduction

The skeletal anatomy of children differs significantly from adults, yet musculoskeletal models were mainly developed from adult datasets. Subject-specific models from medical imaging are costly and time-consuming [1]. Ideally, we would scale musculoskeletal models using an atlas built from a population of paediatric bones that captures morphological variation of the growing skeleton. The aims of this study were to: 1) characterise lower limb bone shape variation in a typically developed paediatric population aged 4 to 18 years old and 2) evaluate bone shape prediction error using a combined shape model.

2. Materials and Methods

Post-mortem CT scans of 333 children (137 F, Age: 12 ± 5 Y, H: 148 ± 24 cm, M: 49 ± 22 kg) [2] were obtained from the Victorian Institute of Forensic Medicine (Australia). The pelvis, femurs, and tibias/fibulas were segmented. Each bone was non-rigidly registered and fitted to a template mesh, using radial basis functions to achieve nodal correspondence. Each pelvis, femur, and tibia/fibula were then rigidly aligned to a selected template case with a neutral pose. The bones were then combined and the shape model was characterized using principal component analysis [2]. The predictive power of the shape model was assessed with a leave one out (LOO) analysis using height, ASIS width, femur length, and tibial length [2].

3. Results

The first 3 principal components (PCs) captured 92.5%, 2.07%, and 0.53% of the variation in the dataset (Figure 1). The first PC described combined size and shape variation and the second and third PCs described shape variation and the aspect ratio of the long bones. The results from the LOO analysis gave an average RMSE of 2.94 ± 0.83 mm and Dice score of 0.8.

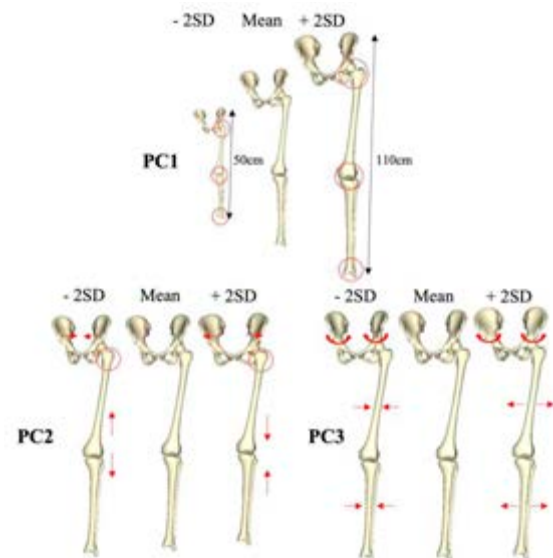


Figure 1: First 3 PCs of the combined statistical shape model. Red annotation indicate main changes in shape

4. Discussion and Conclusions

This unique dataset characterises morphological variation in lower limb bones in a paediatric population aged from 4 to 18 years. It allows for prediction of new bone shapes with lower errors than typical scaling for use in clinical settings and musculoskeletal modelling. Future work will add articulation to the model for incorporation into the MAP client for building personalised OpenSim models.

5. References

1. Scheys L. et al. Gait Posture, 2011; 33: 158-164
2. Carman L. et al. Sci. report. 2022; 12 (3251)

Acknowledgements:

Data from the VIFM made this research possible. The authors would like to thank the University of Auckland doctoral scholarship, the Health Research Council of NZ, the Friedlander Foundation and the Aotearoa Foundation for providing financial support to this project.



3D RECONSTRUCTION OF THE PAEDIATRIC HIP: A COMPARISON OF DIFFERENT METHODS

Claudio Vergari (1*), Xavier du Cluzel de Remaurin (1,2), Nejib Khouri (2), Laurent Gajny (1), Samuel Georges (2), Alina Badina (2)

1. *École Nationale Supérieure d'Arts et Métiers, IBHGC-Institut de Biomécanique Humaine Georges Charpak, Paris, France*; 2. *Service de Chirurgie Orthopédique Pédiatrique, Université Paris Cité, AP-HP, Hôpital Necker- Enfants Malades, Paris, France*

*corresponding author: c.vergari@gmail.com

1. Introduction

Hip dysplasia is a deformity of the pelvis which can cause pain and loss of function. Its surgical treatment is a complex procedure, especially in the paediatric population. It mainly consists of a pelvic osteotomy which aims to reorient the acetabulum towards a physiological orientation. Patient-specific surgical cutting guides can be employed to precisely reorient the acetabulum, but the planification of the reorientation angles is often qualitative and based on the surgeon's experience. This is in part due to the lack of consensus on the method to determine the acetabulum's orientation.

In this work, we compared the reliability of three methods which were recently described in the literature [1-3] and which provided sufficient information to reproduce them.

2. Materials and Methods

Seventeen patients (34 hips, patients between 7 and 16 years old) were included: 9 had an indication for surgery to correct dysplasia while 8 had healthy hips. Patients underwent CT scan (max slice thickness: 1.3 mm) and 3D reconstruction of the pelvis (D2P, 3D Systems). The superior anterior iliac spines and pubic tubercles were manually digitized to build the anterior pelvic plane (APP).

Furthermore, the acetabula were digitized. Then, a vector representing the orientation of the acetabulum was built according to three methods. The first method uses the overall normal vector of the acetabular surface to represent the acetabulum [1]. For the second method, the acetabular rim was automatically extracted and its tangential plane was defined; the normal to this plane was the acetabular vector [2]. For the third method, this tangential plane was translated every 0.5 mm towards the acetabulum and an ellipse was fitted to the

intersection between each plane and the acetabular surface. A vector was defined by least-square fit to the sequence of the midpoints of these ellipses [3]. The orientations of the three vectors were expressed in terms of inclination, version and tilt relative to the APP. Manual digitization was repeated twice by three experienced operators. Intraclass correlation coefficients and inter-operator uncertainty (in terms of 2*standard deviation) were computed.

3. Results

Results are reported in Table 1. No difference was observed between healthy and pathological hips.

Table 1: ICC and inter-operator uncertainty.

Method	Angle	ICC	Uncertainty
[1]	Inclination	0.89	3.6 °
	Version	0.95	4.1 °
	Tilt	0.91	5.9 °
[2]	Inclination	0.95	1.7 °
	Version	0.99	1.4 °
	Tilt	0.98	2.1 °
[3]	Inclination	0.52	6.2 °
	Version	0.87	5.1 °
	Tilt	0.85	8.6 °

4. Discussion and Conclusions

The three methods can be implemented using the same manual digitization, and different processing. The method described in [2] resulted in lower uncertainty, and similar ICC as [1]. Further studies should focus on the surgical outcome concerning hip function, when using the characterization method in [2].

5. References

- Peterson JB et al., Clin Orthop Relat Res; 473:2489-94 (2015)
- Zhang et al., PLoS One ; 12 :e0172297 (2017).
- Jóźwiak M et al., Dev Med Child Neurol; 63:608-13 (2021).

SUBJECT SPECIFIC MODELING FOR SURGERY COMPLICATIONS ANALYSIS: A PRELIMINARY CASE REPORT

Raphaël Badaoui (1), Léonard Chatelain (2,3), Emanuelle Ferrero (2,3), Virginie Lafage (4), Wafa Skalli (2)

1. *Université Gustave Eiffel, France*; 2. *Arts et Metiers Institute of Technology, France*; 3. *Hôpital Européen Georges Pompidou, France*; 4. *Lennox Hill Hospital, USA*

1. Introduction

Lumbar spine surgery mechanical complications include implant failure, screw loosening and early adjacent disc degeneration [1]. Finite element models (FEM) allow better understanding underlying mechanisms, providing they are patient specific, particularly for geometry and loads. The aim of this study is to explore the ability of a FEM to explain the mechanical complications of lumbar spine surgery. A preliminary study on a single, selected case was conducted.

2. Materials and Methods

A lumbar spine nonlinear FEM was used. It included the lumbar vertebrae, the intervertebral discs and ligaments, with surface contacts in the facet joints. The model with a mean geometry was extensively evaluated with regard to in vitro experiments in flexion, extension, lateral bending and torsion.

A 72-years-old female patient was considered. She had a L3-L5 laminectomy and a three-level rod-screws fixation. A proximal disc failure with a L2-L3 stenosis required reoperation.

The L3-L5 FEM was used in three configurations : 1/ reference mean geometry and 280 N compressive load with lever arm of 24 mm (Mean L1 lever arm for people aged 60 and over [2]); 2/ Subject specific geometry (*GEOM*) was built from medical images (Sagittal X-Rays and CT-Scans) using a mesh deformation technique, with the same compressive load 3/ because of the patient postural trouble, a worst case scenario considered an increased lever arm of 47 mm [3] (*GEOM+LEVARM*). Stress in the adjacent disc fibers (L2-L3) and in the implant were considered.

3. Results

with regard to the reference, changing the conditions yielded an increase in disc fibers loads, from 2.8 N to 4.2 N (*GEOM*) and 6.4 N (*GEOM+LEVARM*). Maximum Von Mises stress increased from 11 MPa to 23 MPa (*GEOM*) and 173 MPa (*GEOM+LEVARM*).

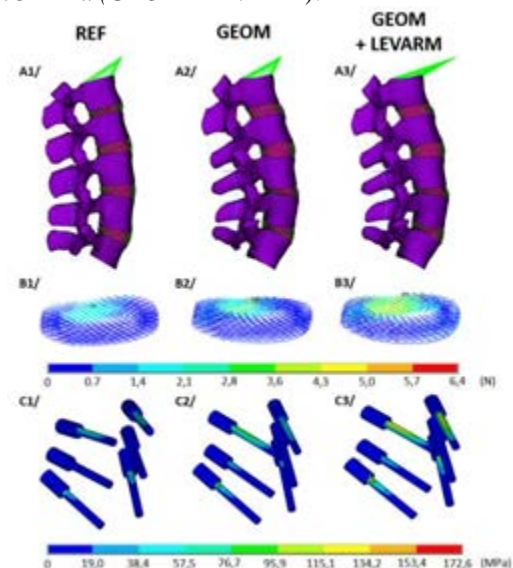


Figure 1: FEM (A), Fibers loads in L2-L3 disc in N (B), Von Mises stress in the screws in MPa (C).

4. Discussion and Conclusions

This study only concerns a case report and cannot be generalized. However it highlights the importance of taking into account both subject specific geometry and subject specific loads when considering clinical use of models to investigate surgery complications. Work is in progress on a cohort of patients.

5. References

1. Katonis P et al. Clin Orthop Relat Res. 2003.
2. Vialle R et al. J Bone Joint Surg Am. 2005.
3. Heidsieck C et al. Osteoporos Int. 2022.

Acknowledgements:

The authors thank Skairos company for its support.

FACET JOINT CAPSULAR LIGAMENT RESPONSE UNDER SIMPLE LOADING MODES FOR COMPUTATIONAL MODEL VALIDATION

Gwennyth Carroll (1), Martine McGregor (1), Duane Cronin (1), Stewart McLachlin (1)

1. Mechanical and Mechatronics Engineering, University of Waterloo, Canada

1. Introduction

Cervical spine facet joints (FJ) experience complex kinematics and are implicated in neck injury [1]. There has been extensive research at the macroscopic level into FJ capsular ligaments (CL). However, CLs are anisotropic, nonlinear, viscoelastic structures that respond to various loads and there is currently a lack of experimental data, limiting the ability to validate computational models [2]. The goal of this study was to experimentally examine the facet joint CL under different modes of loading and rates and compare to a state-of-the-art computational cervical spine model [3].

2. Materials and Methods

Six unilateral FJs were isolated and fixed in cement. Samples were loaded in displacement control using a six-degrees-of-freedom force and motion simulator (AMTI VIVO). Each sample was loaded at 0.1 mm/s and 10 mm/s for 5 or 10 sinusoidal cycles in joint distraction (JD), anterior-posterior translation (AP) and lateral translation (LT). Force and displacement were recorded at 100 or 1000 Hz for the slow and fast rates respectively. Average force vs displacement curves for each rate and mode of loading were found using ArcGen [4].

The C4-C5 facet joint was isolated from the model [3] and run in LS-Dyna v9.2. Displacement-prescribed loading was applied in the local joint coordinate system in JD, AP and LT at 0.1 mm/s and 10 mm/s to replicate the experiment. Force and displacement of the rigid facet joint endplate were extracted and compared to experiment curves.

3. Results

Experimental displacement graphs showed the simulator performed well in matching the input for both slow/fast rates. After an initial decrease in force, peak force between cycles was

repeatable. In each load case, samples were displaced beyond the ligament toe region. Figure 1 shows a representative force and displacement vs time graph. Initial assessment relative to the model indicates good agreement in JD, but less so with AP and LT though further investigation is needed.

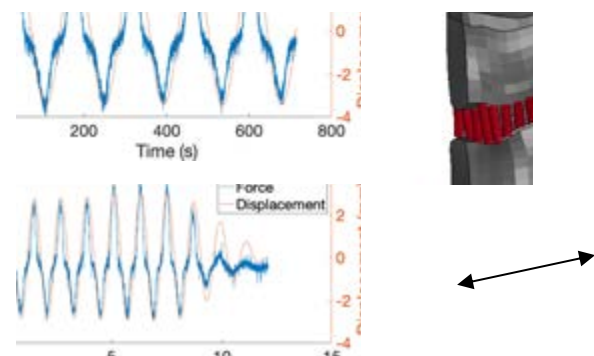


Figure 1: Representative experimental force and displacement vs time graphs for LT at 0.1 mm/s (top) and 10 mm/s (bottom); LT load condition applied to model (right).

4. Discussion and Conclusions

This study provides new experimental data needed to better understand the response of the CL under different loading modes and rates. This data will be used to validate and enhance the CL response of the model [3].

5. References

1. Jaumard N, et al. Journal of Biomechanical Engineering. 133 (2011)
2. Fice J, et al. Annals of Biomedical Engineering. 39(8) (2011)
3. Barker JB, et al. ASME J Biomech Eng. 139 (2017)
4. Hartlen D, Cronin, D. Frontiers in Bioeng and Biotech. 10 (2022)

Acknowledgements:

We would like to thank Dr Renan Fernandes for assistance with tissue sample preparation.



QUASI-AUTOMATIC GEOMETRIC AND STRUCTURAL QUANTITATIVE ANALYSIS OF FRACTURED VERTEBRAS

Lucas Le Gallo (1), Mourad Ould-Slimane (2), Camille Damade (3) Marc-Antoine Rousseau (4),
Cécile Heidsieck (1) Olivier Gille (3), Wafa Skalli (1)

1. Institut de Biomécanique Humaine Georges Charpak, France; 2. Hôpital Charles Nicolle, CHU de Rouen, France; 3. Hôpital Pellegrin Tripode, CHU de Bordeaux, France ; 4. Hôpital Bichât-Beaujon, APHP, France

1. Introduction

Thoracolumbar vertebral fractures present a wide range of localization and severity. When necessary, the surgical strategy (implant type, combination) is drawn from the observation of Computed Tomography (CT-scan) imagery. Clinical classification could help in the decision but are limited in practice [1]. The aim of this study is to propose a process for quantitative characterization of fractured vertebrae (FV), both on geometry and on bone quality.

2. Materials and Methods

Non-calibrated CT-scan data of 53 patients were collected from routine clinical exams. They included both the FV and at least one adjacent non-fractured vertebra (NFV). An existing database of 56 in vitro CT-scan of NFV was used as a reference. A two-step process was considered. First, a previously validated semi-automatic method was used for 3D reconstruction from CT-scan, both for FV and NFV (adapted from [2]). Geometric parameters, such as wedgings or height loss, were computed with regard to the patient's adjacent NFV and NFV database. Then, the 3D reconstruction was used for automatic hexahedral mesh generation, with a consistent topology (adapted from [3]). The patient specific adjacent NFV allowed to associate each element to a reference density value, in order to quantify the FV structural alteration (mean density of cortical and spongy bone and density distribution cortical/spongy).

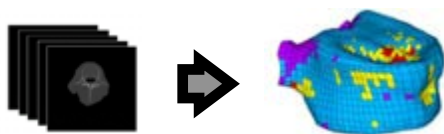


Figure 1: Example of finite element mesh obtained from CT-scan data processing.

3. Results

The process appeared robust and successfully ran for all the 295 vertebrae included, with a mean time of 7 min per vertebra.

Geometry of FV presented significantly abnormal wedgings, especially in the sagittal plane. Height loss in the anterior part was respectively higher than 10% in 83% of the FV and higher than 20% in 50%.

For structural results, the ratio of cortical / spongy bone mean density was found lower in FV compared to their associated reference NFV in 85% of cases (similar 13% and higher 2%).

4. Discussion and Conclusions

Limitations are related to the number of FV (53) which did not cover the high variability of VF. However the process appeared robust and rapid, allowing for large scale analysis with clinical routine CT. Moreover, non-calibrated data were used, while a calibration phantom would allow to translate density into bone material properties. However, as the aim is to perform analysis in clinical routine, the proposed process allowed phantomless quantification of bone alteration. Semi-automatic computation of morphologic and structural parameters could help clinician assess fracture severity and pave the way for a quantitative clinical classification.

5. References

1. Curfs I et al, Int J Spine Surg. (2020).
2. Le Pennec G et al., CMBBE (2014).
3. Travert C, thesis (2012)

Acknowledgements:

The authors would like to thank Stryker/Vexim for providing financial support to this project.

EXAMINING IMPLEMENTATION OF THE FACET JOINT CAPSULAR LIGAMENT IN A COMPUTATIONAL HUMAN BODY MODEL

Gwennyth Carroll (1), Miguel Corrales (1), Stewart McLachlin (1), Duane Cronin (1)

1. Mechanical and Mechatronics Engineering, University of Waterloo, Canada

1. Introduction

Cervical spine facet joints (FJ) experience complex kinematics and are implicated in neck injuries suffered in automotive impacts [1]. Computational human body models can help understand and predict tissue response under different loading conditions [2]. However, current models use simplified representations of the facet joint, limiting tissue-level injury assessment. For example, the Global Human Body Model Consortium (GHBMC) uses tension-only elements characterized in joint tension to represent the complex behaviour of the capsular ligament (CL) [3]. The goal of this study was to examine the current and potential implementations of the CL to improve the response under different modes of loading.

2. Materials and Methods

The C4-C5 facet joint was isolated from the GHBMC head and neck model and run in LS-DYNA v9.2. Constant velocity load conditions in joint tension and shear were applied to the superior facet pillar in the global coordinate system at 3 rates (2 mm/s, 60 mm/s and 1000 mm/s). Force and displacement of the C4 facet rigid body endplate were extracted and compared to experimental data by Mattucci [4]. Additional tension-only elements (diagonal elements) were added at opposing angles to the original CL elements to alter the shear response (Figure 1), while material inputs were updated to maintain the tension response.

3. Results

In joint tension, the current implementation closely follows experimental data at 2 and 1000 mm/s (Figure 1). In joint shear, individual tension-only elements were found to decrease in length or remain unchanged during initial joint displacement, carrying no load. Elements were also found to penetrate the cartilage during joint tension and shear. Adding diagonal elements

engaged the capsular ligament earlier in joint shear but did not affect the joint tension response.

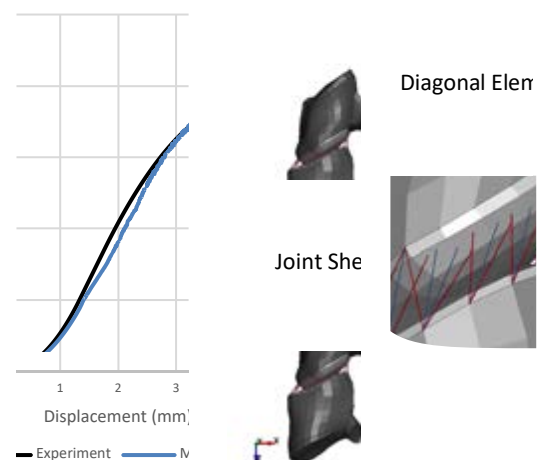


Figure 1 comparing F vs d of experiment and model in tension at 2 mm/s (left). Model showing loading direction and highlighting original (blue) and diagonal (red) elements (right).

4. Discussion and Conclusions

While the model behaves well in joint tension, not all of the CL elements were engaged in shear loading, and the CL elements lacked interaction with the bony anatomy. There is currently a lack of experimental data representing different loading conditions, limiting validation of computational models. Future research will aim to generate experimental data for model validation and alternate CL element formulations in the FE model.

5. References

1. Jaumard N, et al. Journal of Biomechanical Engineering. 133 (2011)
2. Stemper B, et al. Med Biol Eng Computing. 42 (2004)
3. Barker JB, et al. ASME J Biomech Eng. 139 (2017)
4. Mattucci S, and Cronin D. JMBBM. (2015)



DO ASSUMED PROBABILITY DISTRIBUTIONS OF ARTERY MODEL PARAMETERS MATTER DURING SENSITIVITY ANALYSIS?

Friederike Schäfer*, Jacob Sturdy, Leif Rune Hellevik

Norwegian University of Science and Technology (NTNU), Norway

* Department of Structural Engineering, Division of Biomechanics, NTNU, Trondheim Norway,
friederike.e.schaefer@ntnu.no

1. Introduction

Arterial stiffness is an acknowledged biomarker of cardiovascular health [1]. However, local arterial stiffness cannot be measured in vivo. We seek to combine non-invasive measurements and a numerical model to estimate local arterial stiffness through an inverse methodology. To ensure that during the inverse problem solving the parameter describing arterial stiffness can be identified, the forward problem needs to be investigated in terms of input sensitivities. To propagate uncertainties through a numerical model, assumptions on the underlying input parameter distributions need to be made. As distributional uncertainties affect the robustness of sensitivity measures [2], we investigate the influence of these distributional assumptions on the sensitivity structure of artery models.

2. Materials and Methods

We consider the common carotid artery (CCA) as a 1D-model, depicted in Fig. 1. Wall mechanics are described by the linear elastic tube law relating the pressure in the vessel to its cross-sectional area. A physiological flow rate and waveform is prescribed at the inlet and a 3-element Windkessel model mimics the outlet.

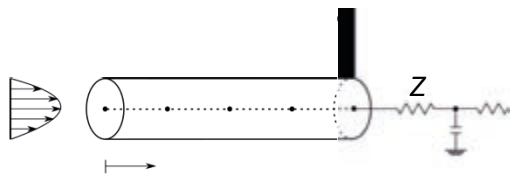


Figure 1: Representation of the 1D-model of the CCA including a 3-element Windkessel model with arterial impedance Z , compliance C , resistance R .

To quantify the uncertainty due to biological variations, polynomial chaos is applied. A total of eight model parameters are considered as uncertain. The uncertain parameter distributions are assumed as either uniform, normal and lognormal, or distributions fit to experimental

data. In a sensitivity analysis, the sensitivity structure of the 1D-artery model is compared to assess the influence of the choice of parameter distributions.

3. Results

The time-averaged variability and sensitivity indices of the pressure, flow and distension at the artery's midpoint show that the Young's modulus, wall thickness, and lumen radius are relatively important. Fluid properties, density and viscosity, total arterial resistance and the Poisson ratio have sensitivity values of approximately zero. The relative importance of input parameters is the same for both uniform and normal input distributions, but the magnitudes of sensitivity indices differ.

4. Discussion and Conclusions

A high sensitivity value for the Young's modulus suggests that this parameter can be inferred in the inverse problem. Model output variance seems to be independent from variations in the fluid properties, the total arterial resistance, and the Poisson ratio such that they can be fixed to reference values. Uncertainty propagation of fitted parameter distributions are yet to be conducted and compared. Further assessment is needed since the sensitivity indices' magnitude depends on the distribution.

5. References

1. Laurent et al., Eur Heart J; 27(21), 2588-2605 (2006).
2. Hart and Gremaud, SIAM/ASA J Uncertain Quantif, 7(4), 1224–1244 (2019).

Acknowledgements:

The authors would like to thank the Polish National Science Center GRIEG programme, (Grant no: UMO-2019/34/H/ST8/00624) for providing financial support to this project.



PRESCRIBED-MOTION AND QUASI-STEADY CFD OF HEART HEMODYNAMICS – VALIDATION STUDY WITH 4D FLOW MRI

Lukas Obermeier (1), Katharina Vellguth (1), Jan Brüning (1), Leonid Goubergrits (1)

1. Institute for Computer-Assisted Cardiovascular Medicine, Charité - Universitätsmedizin Berlin, Germany

Correspondence: Lukas Obermeier, lukas.obermeier@charite.de

1. Introduction

Left ventricular (LV) hemodynamics are hypothesized to serve as indicator for the manifestation of diseases in early states and are associated with e.g., ventricular remodeling [1]. Computational fluid dynamics (CFD) can complement medical imaging methods for in-depth flow analysis and may be a valuable resource to estimate interventional outcomes pre-operatively [2]. Besides addressing complexity and time-intensity of image-based LV-CFD approaches, extensive validation of these models is required to enable transfers to the clinic. In this study, we compare the computed hemodynamics of two CFD approaches of different fidelity level to 4D flow MRI data of three healthy patients to investigate the usability of each method.

2. Materials and Methods

MRI data of three healthy subjects was acquired in a 1.5T MR scanner. The LV geometrics were segmented from cine-short axis, end-diastolic whole heart, and a rotational sequence for the mitral valve (MV). 4D flow data was acquired in a three-chamber view, as well as for the whole volumetric LV cavity. The segmentations were used as boundary conditions (BCs) for the two CFD approaches developed earlier [2,3]. In the first method (high fidelity), the LV motion is prescribed as BC in an Arbitrary-Lagrangian-Eulerian manner. The whole cardiac cycle is computed. The second approach (low fidelity) is based on a quasi-steady setup, where the ventricular volume change is modelled via a volume flux BC at the LV. In this method, focus is laid on the diastolic phase and the diastolic inflowing jet. Both approaches incorporate a 3D stiff MV.

3. Results

Preliminary CFD results show the diastolic inflowing jets in both approaches to be of similar orientation and velocity as the 4D flow MRI measurements. Likewise, the formation of ring vortices around the MV leaflet tips is found in the prescribed-motion and the quasi-steady setup, as well as in the 4D flow data. In early diastole, pressure drops over the MV behave alike in both approaches with minor differences (± 1 mmHg). Towards late diastole, the flow field in the quasi-steady approach starts deviating from the prescribed-motion approach and the 4D flow MRI data. The systolic flow field of latter two both show blood form all LV regions rushing to the LVOT. The quasi-steady approach is computed 4-5 times faster.

4. Discussion and Conclusions

Both approaches deliver consistent results to 4D flow MRI to some extent. The quasi-steady approach delivers reasonable results in early diastole, the prescribed-motion approach for the entire cardiac cycle with the downside of being computationally more expensive. In-depth analyses are still outstanding to further clarify potentials and limitations of each method.

5. References

1. Pedrizzetti G et al.; Nat Rev Cardiol. 2014; 11:545–53.
2. Vellguth K et al.; Int J Comput Assist RadiolSurg. 2018; 13:1795–805.
3. Obermeier L et al., Front Cardiovasc Med. 2022; 9:828556.

Acknowledgements:

The authors would like to thank the DFG for the funding of this project (Nr. 465178743, SPP2311).



NON-INVASIVE LEFT VENTRICULAR HEMODYNAMICS ANALYSIS IN ALL SURVIVORS DURING EXERCISE

Agathe Bedoux (1), Daniel Curnier (2), Maja Krajinovic (2), Caroline Laverdière (2), Daniel Sinnett (2), Delphine Périé (1)

1. Polytechnique Montréal, Canada; 2. Université de Montréal, Canada

1. Introduction

Acute Lymphoblastic Leukemia (ALL) survivors have a higher risk of developing heart failure due to treatment cardiotoxicity [1]. A non-invasive analysis of the left ventricular hemodynamics during exercise may help to identify biomarkers of induced cardiomyopathies during the early stages, and thus allow for a better and personalised follow-up.

2. Materials and Methods

Forty-two ALL survivors were classified into three groups depending on their risk of developing heart failure: standard risk (SR), high risk (HR), and high risk with cardioprotective agent (HRdex) [1]. Each participant did a complete transthoracic echocardiographic assessment (Vivid 9 machine, GE Medical Systems, Milwaukee, Wisconsin) in order to compute the E/A ratio. Participants underwent maximal cardio-pulmonary exercise testing (CPET) with incremental stress loads using a cycle ergometer (Oxycon Pro, Jaeger), going from 0W to maximum stress (150-225W). Heart rate, diastolic and systolic aortic pressure and cardiac output were monitored using a cardiac hemodynamic monitoring (PhysioFlow, Manatec Biomedical).

These four hemodynamic parameters at rest, as well as reverse-optimised inputs previously obtained in our lab, were used as inputs for the CircAdapt model [3], a lumped model of the heart and circulation. A total of six inputs were available for each patient: left ventricle stiffness and contractility, arteriovenous pressure drop, heart rate, cardiac output, and mean aortic pressure. The E/A ratio and the systolic and diastolic aortic pressures were used to reverse optimise three most impacting inputs on three outputs: blood speeds at the mitral and aortic valve, and aortic pressure. Then, the personalised CircAdapt model was used to simulate exercise using the hemodynamic parameters monitored during CPET.

3. Results

No significant differences were observed between groups, however, the increase of peak blood speeds at the aortic valve with increased stress was higher in the HRdex group than both SR and HR groups. More disparity was found in the HR group at higher loads and blood speed at the aortic valve stopped increasing at loads higher than 100W in this group (Figure 1).

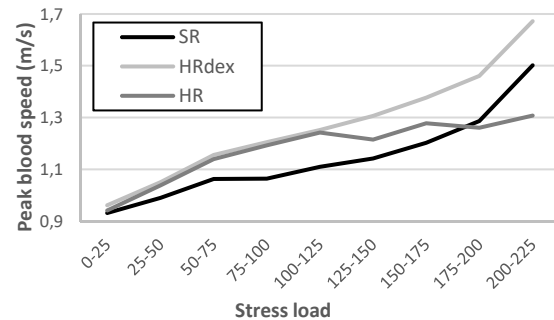


Figure 1: Evolution of peak blood speed at the aortic valve during incremental stress testing.

4. Discussion and Conclusions

For HR patients, the risk of cardiomyopathies is estimated at 35-40% [1], which could explain the disparity observed in HR group, as well as the lower mean peak blood velocities at the aortic valve in this group at higher loads. Thus, this approach allowed to detect subtle changes in left ventricle hemodynamics in ALL survivors during stress loading.

5. References

1. Marcoux S, et al. The PETALE study: Late adverse effects and biomarkers in childhood acute lymphoblastic leukemia survivors. *Pediatric blood & cancer*. 2017;64(6):1-8.
2. Walmsley J et al. Fast Simulation of Mechanical Heterogeneity in the Electrically Asynchronous Heart Using the MultiPatch Module. *PLoS Comput Biol* 2015;11:e1004284.

Acknowledgements:

We thank FRQNT, Polytechnique Montréal and researchers from the PETALE study.



HIGH RESOLUTION SIMULATION OF BASILAR ARTERY INFARCT AND FLOW WITHIN THE CIRCLE OF WILLIS

Jon W. S. McCullough (1), Ioannis Zacharoudiou (1), Sharp Lo (1), Peter V. Coveney (1, 2)

1. University College London, UK; 2. University of Amsterdam, Netherlands

Corresponding author: j.mccullough@ucl.ac.uk

1. Introduction

On a global scale, cerebro- and cardiovascular diseases have long been one of the leading causes of death and disability and its prevalence appears to be increasing in more recent times. Understanding potential biomarkers and risk factors will help to identify individuals potentially at risk of suffering an ischemic stroke. In this work, we have used high resolution 3D fluid simulations to examine the redistribution of flow within circle of Willis (COW) geometries in the immediate aftermath of a stroke due to a blockage of the basilar artery.

2. Materials and Methods

In our work, we have used the open-source HemeLB code [1]. HemeLB is built upon the lattice Boltzmann method and allows for highly scalable studies of macroscopic blood flow in complex and sparse vascular domains. Simulations were conducted on SuperMUC-NG at Leibniz Supercomputing Centre.

To represent a stroke in the basilar artery, we modified a healthy heartbeat profile to one with the flow reducing or ceasing over the remainder of the simulation. All simulations were conducted over a total period of 3 heartbeats. The impact of such changes were evaluated by comparing the flow at the cerebral arteries leaving the COW over this duration to that observed with a healthy flow profile. To reflect some of the variation in the COW structure within the population, we repeat these tests on a complete COW and domains where posterior communicating arteries are absent.

3. Results

In Figure 1, it is illustrated how the flow in the left and right posterior cerebral arteries (LPCA, RPCA) is significantly reduced as a result of the basilar infarct.

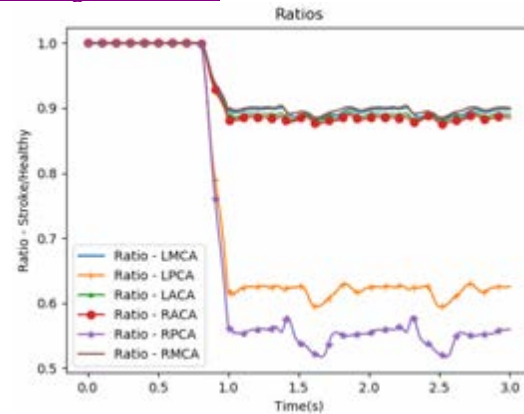


Figure 1: Ratio of observed flow rates leaving the COW between the stroke case 1 and healthy flow.

4. Discussion and Conclusions

We particularly observed that, due to the choice of infarct in the basilar artery, outflow from the posterior cerebral arteries was reduced by the largest amount - up to approximately 70% in some cases. As COW physiology can vary significantly between individuals, our results highlight how a nominally identical stroke can cause very different stroke outcomes.

5. References

1. <https://github.com/hemelb-codes>

Acknowledgements:

We acknowledge funding from European Commission CompBioMed Centre of Excellence (Grant No. 675451 and 823712); UK Engineering and Physical Sciences Research Council for 'UK Consortium on Mesoscale Engineering Sciences (UKCOMES)' (Grant No. EP/R029598/1); MRC for a Medical Bioinformatics grant (MR/L016311/1), and special funding from the UCL Provost. This work was supported by computing time on SuperMUC-NG (LRZ).



ABSTRACT FOR CMBBE 2023: NUMERICAL INVESTIGATION OF RELATIONS BETWEEN TURBULENCE AND HEMOLYSIS IN VENTRICULAR ASSISTANCE DEVICE

Louis MARCEL (1), Mathieu SPECKLIN (1), Andrea MARES (2) Antonio GIL (2), Roberto NAVARRO (2), Pedro QUINTERO (2), Smaine KOUIDRI (1)

1. Arts et Metiers Institute of Technology, CNAM, LIFSE, HESAM University, 75013 Paris, France;
2. CMT-Motores Térmicos, Universitat Politècnica de València, Camí de Vera, s/n, 46022 Valencia, Spain;

1. Introduction

Since a few decades, statistics present concerning figures regarding the amount of patient on the active waiting list for heart transplant compared to the number of potential donors. In this context, engineers and clinicians developed Ventricular Assistance Devices (VADs) to paliate this issue. However these devices are the source of mechanical red-blood cell's damage: Hemolysis. This phenomenon is numerically investigated in this study for a commercial device: the HVAD.

2. Materials and Methods

Blood in our case can be considered Newtonian with a viscosity $\mu=3,5\text{ mPa}\cdot\text{s}$ and incompressible with a constant density $\rho=1060\text{ kg/m}^3$. The fluid behavior is governed by the steady Navier-Stokes equations. In order to quantify mechanical blood damage we introduce the Hemolysis Index (HI) defined by [1]:

$$HI(\%) = \frac{\Delta Hb}{Hb} \times 100 = C \times t^\alpha \times \tau_{ss}^\beta$$

With Hb being the plasma's concentration in hemoglobin, t the time of exposure of a fluid particle to a shear stress τ_{ss} . We proceed to the definition of $Hb' = Hb^{1/\alpha}$ to resolve [2]:

$$\frac{\partial Hb'}{\partial t} + V \cdot \nabla (Hb') = (HB \cdot C \cdot \tau_{ss}^\beta)^{1/\alpha}$$

A RANS approach was adopted, using a $k-\epsilon$ turbulence model. Indeed, in the model's equation, we can express the dissipation of turbulent kinetic energy as a spatial variation of the local shear stress, suggesting that HI is depending on the quantity ϵ . If we refer to the transport equation for the turbulent kinetic energy we have [3]:

$$\frac{\partial \overline{v_j k}}{\partial x_j} = P_k + D_k - \epsilon$$

with ϵ its dissipation and can be written as:

$$\epsilon = -v \frac{\partial v'_i}{\partial x_j} \frac{\partial v'_i}{\partial x_j} = v'_i \frac{\partial \tau'_{ij}}{\partial x_j}$$

This results highlights that the mean value of the unsteady component of the shear stress is proportionnal to a spatial integration of ϵ .

3. Results

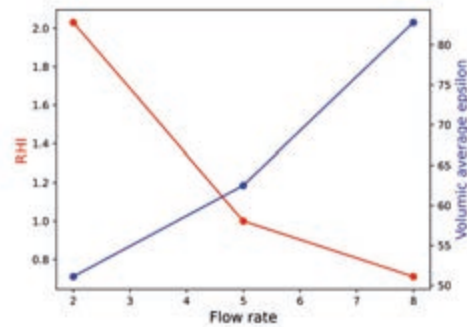


Figure 1: Volumic Average of ϵ in the pump at different flow rates and Relative HI (RHI) comparing the of HI flow rates to nominal flow rate (5l/min).

HI is expected to decrease with an increasing flow rate because residence time decreases. However, if volumic ϵ is increasing with flow rate like shown in Figure 1, shear stress is increasing also, meaning there may be an optimal flow rate generating a minimum of hemolysis.

5. References

1. Garon A et al. Artificial organs 28 11 (2004): 1016-25 .
2. Prasanna H, et al., journal of biomachanical engineering 2015, Vol. 137 094501/1-10
3. Lars D, Fluid Mechanics, turbulent flow and turbulence modeling, August 2020

THE EFFECT OF BLOOD FLOW RATE ON ARTERIAL REFLECTIVE PHOTOPLETHYSMOGRAPHY

Georgios Rovas, Vasiliki Bikia, Nikolaos Stergiopoulos

École Polytechnique Fédérale de Lausanne (EPFL), Switzerland

Corresponding author: Georgios Rovas (georgios.rovas@epfl.ch)

1. Introduction

The popularity of devices that utilize photoplethysmography (PPG) for health monitoring is constantly increasing. The variations in light attenuation due to the pulsatile blood volume changes in the illuminated tissue consist the major determinant of the PPG signal. However, there are other factors that affect the measured signal. We aimed to elucidate and quantify the contribution of one of them, the blood flow rate, on reflective PPG over peripheral arteries.

2. Materials and Methods

We examined the dependence of the reflected radiant flux on the percentage of erythrocytes that are aligned with the direction of blood flow. To achieve that, we performed Monte-Carlo simulations of photons in an inhomogeneous medium (Fig. 1), which consisted of dispersed erythrocytes in blood plasma with physiological values of hematocrit. We derived the optical properties of the components at the wavelengths of interest from the literature. We varied the

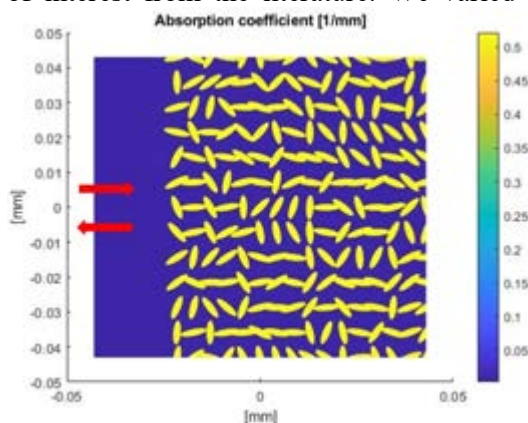


Figure 1. Example of a distribution of the absorption coefficient in the inhomogeneous medium, in the case of randomly aligned erythrocytes. The arrows indicate the directions of illumination and measurement.

ratio of aligned erythrocytes and measured the reflected flux.

Consequently, we designed a custom infrared PPG probe with a wavelength of 830 nm. With this probe, we measured the PPG signal on an elastic artery model, which was filled with porcine blood. By imposing varying levels of blood flow rate in the model, we could quantify the dependence of PPG on blood flow rate.

3. Results

The reflected flux was proportional to the ratio of aligned erythrocytes with a good approximation ($R^2 = 0.95$, RMSE = 65 mW). When we disregarded ratios over 60%, which are not expected in arteries, the approximation error reduced (RMSE = 41 mW). The measured PPG was approximated ($R^2 = 0.99$) by a non-linear function of the flow rate Q : $PPG \propto \sqrt{Q}/(c + \sqrt{Q})$.

4. Discussion

The dependence of PPG on the blood flow rate has been indicated [1], but not thoroughly investigated. Our experimental results agree with the reported ratio of aligned erythrocytes as a function of the flow rate, as measured in vitro [2]. Further research could allow the correction of reflective PPG to reduce the influence of blood flow rate. This could potentially increase the accuracy of health monitoring devices that are based on PPG, especially those that aim on non-invasive blood pressure estimation.

5. References

1. A. V. Moço et al., Scientific Reports. 8, 8501 (2018).
2. M. Bitbol, D. Quemada, Biorheology. 22, 31–42 (1985).

TOWARDS THE COMPUTATIONAL DEVELOPMENT OF AN IDEAL EXTERNAL SUPPORT FOR THE ROSS PROCEDURE

Thibault Vervenne (1), Lauranne Maes (1), Filip Rega (2), Nele Famaey (1)

1. Biomechanics, Mechanical Engineering Department, KU Leuven, Leuven, Belgium;
2. Cardiac Surgery, Department of Cardiovascular Sciences, KU Leuven, Leuven, Belgium

1. Introduction

In the Ross procedure, a pulmonary artery is placed in aortic position, as a so-called autograft. Dilatation is a common adverse effect leading to failure, due to the inability of the autograft to adapt to a high pressure environment. Textile mesh wrapping can stabilize this dilatation, but causes stress-shielding on the longer term. Computational modelling can predict the outcomes of an artery exposed to different pressure levels, and as such help to derive the optimal properties of such a textile reinforcement in the Ross procedure.

2. Materials and Methods

Considering an isotropic thin-walled cylinder and Laplace's law, the circumferential stress $\sigma_{\theta\theta}$ in an arterial wall can be written as

$$\frac{P}{h/r} = \sigma_{\theta\theta} = 2C_{10}\lambda_{\theta}^2 - p, \quad (1)$$

whereby the stretch $\lambda_{\theta} = \frac{r}{R}$ assumes an unloaded reference radius R . The Lagrange multiplier p enforces incompressibility. Model parameters representative for the Ross procedure were taken from [1]. Pulmonary pressure P is chosen as baseline homeostatic state of the tissue. An artery can remodel after an acute pressure increase through mass turnover of its constituents. Mass deposition or removal over time t is driven by a deviation from homeostatic stress to as

$$\rho(t) = \rho(t-1) + \dot{\rho}(\Delta\sigma_{\theta\theta}), \quad (2)$$

in turn leading to a change in wall thickness.

3. Results

On the one hand, Fig. 1 depicts benign arterial remodelling for three different applied pressure increases, considering the initial homeostatic pulmonary state of the tissue. In case of benign adaptation, smooth muscle cells are able to recruit enough collagen fibers, and wall thickness will increase to restore the

homeostatic stress. On the other hand however, if the sudden pressure jump leads to a critical overstretch and excessive stress deviation, the tissue cannot restore and maladaptation occurs. Tissue damage will decrease wall thickness, leading to long-term dilation and failure.

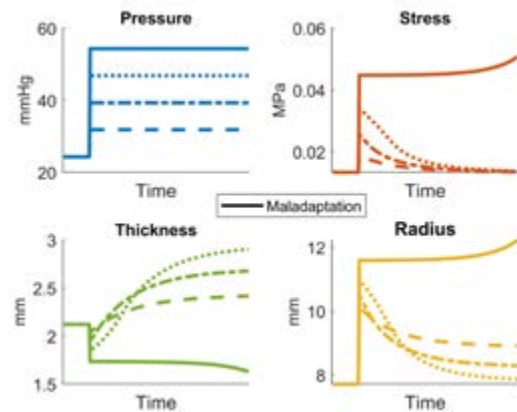


Figure 1: Simulated outcomes of a pulmonary artery exposed to different pressure levels.

4. Discussion and Conclusions

The different curves show how benign adaptation through collagen production is possible only up to a certain pressure increase. Computational analysis can help to define that tipping point. Future work will incorporate an external support into the model, which will allow us to determine textile properties that can avoid maladaptation, even for higher aortic pressures. To then also restore the homeostatic state and prevent stress-shielding, the same theoretical framework will help us to find the optimal biomechanical environment for the Ross procedure, using a biodegradable textile.

5. References

1. Maes L et al., CMBE22 conference; 2022. p. 579-582.

Acknowledgements:

This work was supported by a doctoral grant from the Research Foundation Flanders (FWO) (SB1SE2123N).



A MATHEMATICAL MODEL OF HIPSC CARDIOMYOCYTES IN ISCHEMIA/REPERFUSION

Mohamadamin Forouzandehmehr(1), Michelangelo Paci(1), Jari Hyttinen(1), Jussi Koivumäki(1)

1. BioMediTech, Faculty of Medicine and Health Technology, Tampere University, Finland

1. Introduction

Ischemic Heart disease (IHD) represents the first cause of death globally [1]. Human induced pluripotent stem cell-derived cardiomyocytes (hiPSC-CMs) provide unparalleled opportunities to research ischemia/reperfusion pathophysiology [2]. We have developed a metabolite-sensitive computational model of hiPSC-CMs to investigate I/R mechanisms.

2. Materials and Methods

We have developed an ODE-based whole-cell hiPSC-CM model integrating a reparametrized metabolite-sensitive SERCA model [3] and contractile element [4] into Paci2020 [5] model of hiPSC-CMs electrophysiology. The values of MgATP, MgADP, and pH in ischemia were obtained from [4].

3. Results

Our model could capture the ischemic-induced Ca^{2+} transient (CaT) plateau abnormalities in agreement with experimental data [2] concurrent with early afterdepolarizations (Fig. 1 A-C). The model also simulated the cardioprotective effect of I_{Ks} activation [6] as it significantly abolishes the CaT abnormalities and the consequent aftercontractions (Fig. 1D).

4. Discussion and Conclusions

We propose a computational model linking the I/R-induced temporal change of metabolites to cell-level outputs to identify the ionic, subcellular, and interorganellar mechanisms at play in ischemia and reperfusion. Incorporating electro-mechano-energetic coupling in cardiac mathematical models can lead to a higher deep-phenotyping and drug-screening potentials and a better understanding of the mechanism of I/R-induced arrhythmia. This model can be employed to test different I/R treatment strategies and drug-induced simulations.

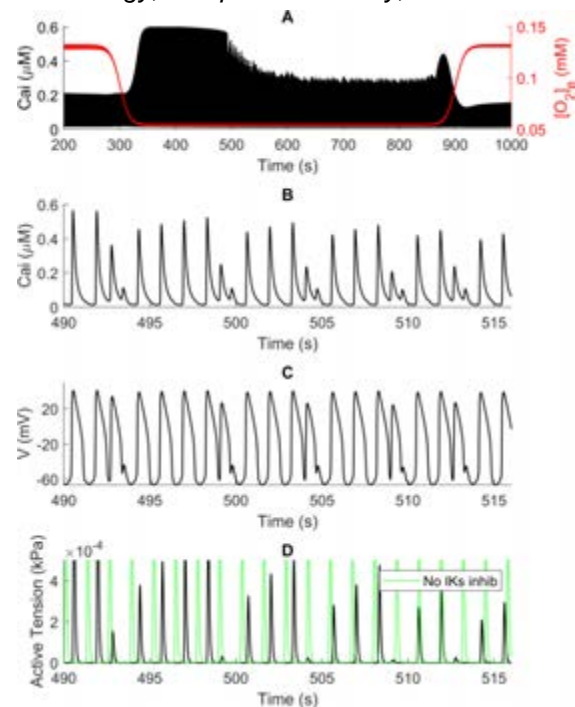


Figure 1: Ca^{2+} transients (CaT) in ischemia/reperfusion (A), developed CaT abnormalities (B), early afterdepolarizations in ischemic phase (C), active tensions in ischemia compared with no I_{Ks} blockade condition (D).

5. References

1. Nowbar AN, et al., Circ. Cardiovasc. Qual. Outcomes. 12 (2019)
2. Gaballah M, et al., Cells. 11 (2022).
3. Tran K, et al., Biophys. J. 96 (2009)
4. Tran K, et al., Biophys. J. 98 (2010)
5. Paci M, et al., Biophys. J. (2020)
6. Guo X, et al., PLoS One. 7 (2012)

Acknowledgements:

MF was supported by the graduate school of Faculty of Medicine and Health Technology, Tampere University. MP was supported by the Finnish Cultural Foundation (decision 210813). JTK was supported by Academy of Finland and Finnish Foundation for Cardiovascular Research (grant number 200101).



DATA-DRIVEN COMPUTATION OF GROWTH PATTERNS. APPLICATION TO HEART MORPHOGENESIS.

Jose J Muñoz (1,2,3), Cécilia Olivesi (1)

1. Universitat Politècnica de Catalunya, Spain; 2. Centre Internacional de Mètodes Numèrics en Enginyeria (CIMNE); 3. Institut de Matemàtiques de la UPC (IMTech)

1. Introduction

At the state of embryo, the heart has the form of a tube. During its elongation, it is constrained by the thorax to buckle - almost always in the same direction - and obtained its final helix shape during embryogenesis (see Fig. 1). However, heart malformations due to congenital anomalies are numerous and ubiquitous: 97% of heart loopings are oriented rightward and 20% of heart anomalies in children are caused by abnormal looping.

Some mutants, such as the *greb11*, may cause defects in growth patterns and consequently aberrant shapes which may have fatal consequences during embryogenesis.

In this work we present an algorithm to detect deficiencies in growth distributions from a series of microscopy images.

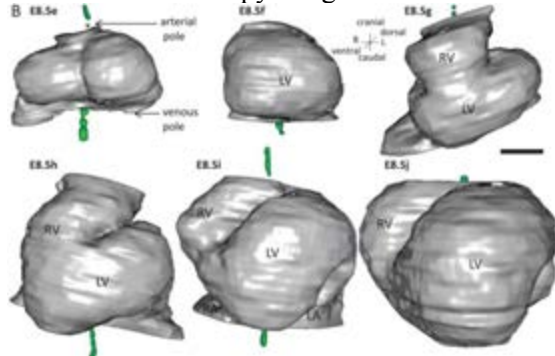


Figure 1: 3D reconstructions of heart shapes from HREM images at each stage of heart looping [1].

2. Materials and Methods

From a set of experimental position \mathbf{x}_{exp} , we aim to compute an equilibrated close deformed field \mathbf{x} , resulting from a growth pattern $\mathbf{F}_g = \gamma \mathbf{I}$, which is determined by a spatially dependent growth factor γ . Mathematically, we solve

$$\begin{aligned} \min_{\gamma} \|\mathbf{x} - \mathbf{x}_{exp}\|^2 + \beta \|\gamma\|^2 \\ \text{s.t. } \nabla \cdot \boldsymbol{\sigma} = 0 \end{aligned} \quad (1)$$

where $\boldsymbol{\sigma} = \mathbf{j}^{-1} \mathbf{F} \mathbf{S} \mathbf{F}^T$ is the Cauchy stress tensor, \mathbf{S} the second Piola stress tensor, and $\mathbf{F} = \mathbf{F}_e \mathbf{F}_g$ is the

deformation gradient, decomposed in its elastic (\mathbf{F}_e) and growth ($\mathbf{F}_g = \gamma \mathbf{I}$) components, and $\mathbf{j} = \det(\mathbf{F})$. The optimality conditions of this minimisation problem can be re-casted as the solution of the following system of equations:

$$\begin{aligned} \nabla J + \mathbf{K}^T \boldsymbol{\lambda} &= 0 \\ \mathbf{g}(\mathbf{x}, \gamma) &= 0 \\ \beta(\gamma - 1) + \mathbf{G}^T \boldsymbol{\lambda} &= 0 \end{aligned} \quad (2)$$

where J is here objective functional in (1), $\mathbf{g}(\mathbf{x}, \gamma)$ is the FE discretisation of the static equilibrium $\nabla \cdot \boldsymbol{\sigma} = \mathbf{0}$, $\mathbf{G} = \nabla_{\gamma} \mathbf{g}$, and $\mathbf{K} = \nabla_{\boldsymbol{\lambda}} \mathbf{g}$.

3. Results, discussion and Conclusions

The analysis of the method and accuracy as a function of imposed boundary conditions and regularisation parameter β will be discussed. We have simulated the heart by directly applying an experimentally measured growth pattern $\gamma(\mathbf{x})$ and compared this solution with the experimental measurements.

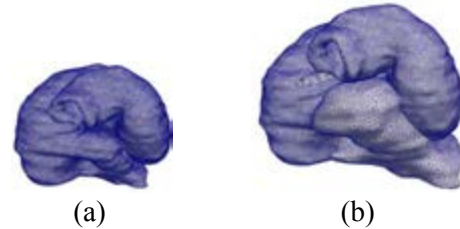


Figure 2. Growth pattern of control heart between stage E9.5 (a) and E10.5 (b).

4. References

1. JF Le Garrec, JN Dominguez, A Desgrange, KD Ivanovitch, E Raphaël, JA Bangham, M Torres, E Coen, TJ Mohun, SM Meilhac (2017). A predictive model of asymmetric morphogenesis from 3D reconstructions of mouse heart looping dynamics *eLife* 6:e28951.
2. Manuel K. Rausch, Martin Genet, Jay D. Humphrey, An augmented iterative method for identifying a stress-free reference configuration in image-based biomechanical modeling, *J Biomechanics*, 58: 227-231, 2017.

Acknowledgements:

This work has been financially supported by the Spanish Ministry of Science and Innovation under grant PID2020-116141GB-I00.



FLUID STRUCTURE INTERACTION MODELING OF AORTIC VALVES USING THE LATTICE BOLTZMANN AND FEM METHODS

Adi Morany (1), Ricardo Gomez Bardon (2), Brandon Kovarovic (3), Ashraf Hamdan (4), Danny Bluestein (3), Rami Haj-Ali (1,3)

1. School of Mechanical Engineering, Tel Aviv University, Tel Aviv, Israel 2. Dassault Systemes España, SIMULIA, Madrid, Spain 3. Department of Biomedical Engineering, Stony Brook University, Stony Brook, NY, USA 4. Department of Cardiology, Rabin Medical Center, Petach Tikva, Israel

Corresponding author: Prof. Rami Haj-Ali, rami98@tau.ac.il

1. Introduction

This study introduces a new coupled fluid-structure interaction (FSI) co-modeling approach using the Lattice Boltzmann (LBM) and the FE methods. The suitability of the proposed LBM-FE approach was examined, including structural and hemodynamic parameters for the biomechanical behavior of compliant aortic valves (AVs). Towards that goal, LBM-FE FSI models were generated for healthy tri and bi-cuspid aortic valves (TAV, BAV) for normal and stenotic valves with calcified and fibrocalcific.

2. Materials and Methods

The parametric geometry adopted for the AV describes a 3D geometry of TAV [1,2] and is extended for calcific and fibrocalcific BAVs [3]. The heterogeneous tissue structure is also considered. Toward that goal, the XFlow commercial code was utilized for the CFD fluid part using LBM approach. Representative FSI test cases utilizing LBM-FE approach of healthy and pathological compliant valves were investigated using realistic normotensive physiological pressure profiles. FSI partitioned approach was used using XFlow and Abaqus (Dassault Systemes, Simulia, Providence, RI) solvers.

3. Results

Fig. 1 presents the flow velocity field evolution using FSI LBM-FE at systole peak for the different models. Moreover, the paravalvular leakage (PVL) and thrombogenic footprint after transcatheter aortic valve (TAVR) deployment.

4. Discussion and Conclusions

The TAV orifice area at the peak systole was calculated (3.38 cm^2) with the max velocity (1.0 m/s). It corresponds adequately with the published range of values from the literature. The predicted maximal principal stresses along the surface of the leaflets were also calculated. The wall shear stress has a high value around the leaflets' coaptation region and gradually decreases towards the belly. Similarly, the calcific and fibrocalcific BAV models are examined as a test case of pathological valves. We show that the LBM-FE FSI approach can predict the flow and structural responses of TAVs, and handles irregular geometries such as BAV and AV-related diseases.

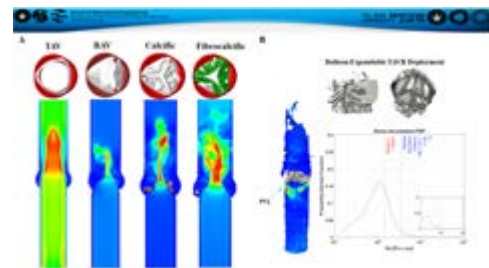


Figure 1: FSI models using coupled LBM-FE: (A) Velocity at systole peak (B) PVL and thrombogenic footprint after TAVR deployment.

5. References

1. Haj-Ali et al. J. Biomech., 2012
2. Morany et al. Ann. Biomed. Eng., 2021
3. Karnibad et al. Biomed. Phys. Eng. Express, 2022

Acknowledgements:

Author Adi Morany acknowledges the support of PBC Israeli Council for Higher Education. This study was funded by a National Institutes of Health grant: Bioengineering Research Partnerships (U01) under Grant No. EB026414.



AN OVERVIEW OF THE STRUCTURE AND MECHANICS OF PASSIVE MUSCLE ACROSS DIFFERENT LENGTH SCALES

Ciaran Simms

Centre for Biomedical Engineering, School of Engineering, Trinity College Dublin, Ireland

1. Introduction

Skeletal muscle accounts for almost half of bodyweight in humans. The principal purpose of skeletal muscle is to develop contractile forces to facilitate motion. However, the passive properties of muscle tissue play a significant role in many applications, including impact, surgical simulation, training and rehabilitation. Passive muscle stress is orders of magnitude lower than active stress physiological stretches, but passive properties dominate in some circumstances and recent findings show passive muscle contribute almost half of the spinal flexion moment demand [1].

2. Materials and Methods

This paper presents an overview of the structure and mechanics of passive muscle across different length scales. The hierarchical structure of skeletal muscle is first presented, emphasising the interconnectedness of the muscle fibres and the collagen fibres in the extracellular matrix (ECM) as well as differences between species.

The value of different imaging modalities is introduced, including the seminal work by Purslow and colleagues using SEM [2] as well as more recent work by Bilston and colleagues using diffusion tensor imaging [3].

The nonlinearity of the elastic response and the significant anisotropy are presented. The now well-known tension compression asymmetry is then discussed [4], including its presence across a number of different species [5] and its relationship at different length scales. Recent work has shown that the tension compression asymmetry is strongly amplified by the ECM [65]. Further recent work applying biaxial testing has been emphasising the importance of the ECM [7].

Computational models of skeletal muscle at different length scales have been proposed, eg [8], and these are used in various applications, including automotive safety. However, models struggle to replicate the range of experimental observations. A relatively simple model has been found to replicate many of the tension compression and anisotropic properties [9], and recent geometric models have been developed to predict muscle architecture and arbitrary muscle lengths [10].

A particularly important feature of the mechanics of skeletal muscle is the internal fluid pressure, and the relationship between this and the tensile stress in the collagen environs of the ECM, as shown by recent work [11].

3. Discussion and Conclusions

Much remains to be understood about passive skeletal muscle. Computational models are powerful tools but most models of skeletal muscle are developed for a specific application and do not have broad validity. Material constants are often derived by fitting to experimental data and validating against limited loading conditions. However, muscle in vivo experiences complex loading involving tension, compression, and shearing and no current model captures all the experimentally observed phenomena.

5. References

1. Zwambag & Brown, JBiomechanics 2020.
2. Trotter & Purslow, JMorphology 1992.
3. Bilston et al, J Appl Phys 2019
4. Gindre et al JMBBM 2013
5. Mohammadkhah et al JMBBM 2018.
6. Bol et al ActaBiomat, 2020
7. Wheatley et al, Frontiers Physiology 2020
8. Roehrle et al, Biomech Mod Mechano 2017.
9. Valentin & Simms, JBiomechanics 2020
10. Schenk et al JBiomechanics 2020
11. Sleboda & Thomas, PNAS 2019



THE MECHANICAL ROLE OF EXTRACELLULAR MATRIX: FROM SKELETAL MUSCLE FIBER TO MUSCLE COMPARTMENTS

Filiz Ates

Institute of Structural Mechanics and Dynamics in Aerospace Engineering, University of Stuttgart, Germany

1. Introduction

The extracellular matrix (ECM) is studied as the mechanical support of tissues and organs. In activatable tissues, such as skeletal muscles, this aspect is not enough. A key hereby is to understand how the ECM mechanically interacts within and around activatable tissues i.e. contractile elements. Understanding this interaction and relating it with the joint function that muscle facilitates would help reveal mechanisms of aging, tissue remodelling, exercise, or progression of diseases such as cerebral palsy (CP). Furthermore, with validated and data-informed computational models generated using this understanding, we can simulate the impact of ECM alterations on human locomotion.

The earlier work in frog muscles indicated force transmission through sarcolemma [1]. In the present work, we aim to discuss (i) the impact of force transmission through fascial connective tissues at muscle and compartment level and their implications in CP, and (ii) the preliminary findings on ECM interactions at fibre level.

2. Materials and Methods

By reaching the target muscle's tendon during surgical operations, semitendinosus muscle isometric forces were measured at various knee joint angle positions. For active measurements, muscles were supramaximally stimulated with skin electrodes using a current source. Fibre level measurements were performed on rat extensor digitorum longus muscle fibres.

3. Results

The intraoperative experiments on patients with CP showed that muscle force production was elevated when the neighbouring muscles are also active [e.g. 2-4]. We found that the mechanics of semitendinosus muscle did not represent the knee joint restriction observed in CP when activated solely. Interestingly, if semitendinosus is co-activated with synergistic and even with antagonistic muscles their forces

at the tendon increase. This characteristic is found to be similar to the anticipated contracture behaviour at the compartment level. At the fibre level, the preliminary results showed that the absence of endomysium between two neighbouring fibres changes the shape of the passive and active force-length characteristics of the fibre dramatically.

4. Discussion and Conclusions

Direct force measurements are rare and provide invaluable information on in vivo muscle mechanics at the muscle and compartment level. The series of data on hamstring muscles indicate the importance of ECM interactions in particular for diseased muscles. Therefore, they should be considered during treatment [e.g. 5]. The fibre level experiments, on the other hand, indicate that the mechanical interactions through ECM occur at every scale. Hence, the force-transmitting elements between sarcomere and ECM and their overall impact on force production should further be investigated.

5. References

1. Street, S.F., *J Cell Physiol*, 114(3):346-64 (1983)
2. Kaya C.S., et al. *Journal of the Mechanical Behavior of Biomedical Materials* 77, 78-84 (2018).
3. Ates F., et al, *Human Movement Science*, 57: 103-110 (2018).
4. Yucesoy C.A., et al. *J Electromyography and Kinesiology* 36, 49-55 (2017).
5. Ates F., Yucesoy C.A, *J Mechanical Behavior of Biomedical Materials* 84, 208-216 (2018).

Acknowledgments:

This research was partially funded by the Bundesministerium für Bildung und Forschung (BMBF, Federal Ministry of Education and Research) through the project "3DFoot", grant number 01EC1907B, by Deutsche Forschungsgemeinschaft (DFG, German Research Foundation), grant number 465195108, and University of Stuttgart, 2022 Terra Incognita, grant number 82899031.



MULTISCALE EXPERIMENTS AND MODELLING OF SKELETAL MUSCLES

Markus Böl (1), Kay Leichenring (1), Ramachandra Kuravi (4) Alexander E. Ehret (2,3)

1. Institute of Mechanics and Adaptionics, Technische Universität Braunschweig, Braunschweig D-38106, Germany; 2. Empa, Swiss Federal Laboratories for Materials Science and Technology, Überlandstrasse 129, CH-8600, Dübendorf; 3. ETH Zurich, Institute for Mechanical Systems, Leonhardstrasse 21, CH-8092, Zürich, Switzerland; Engineering Division, Lawrence Berkeley National Lab, Berkeley, CA

1. Introduction

Skeletal muscle tissues consist of interconnected contractile and structural proteins, membranes and other extracellular matrix components (ECMs) that enable active and passive load transfer. Over the past few decades, it has been confirmed that muscles are essentially controlled by their micro- and nanoscale structures. In short, skeletal muscle tissue exhibits a three-dimensional and highly hierarchical architecture in which muscle fibres and the ECM interact to generate active forces and resist external loads. While the muscle fibres generate active forces during contraction, the ECM, as connective tissue, connects the muscle components and transmits loads across multiple size scales. Skeletal muscle tissue is characterised by varying degrees of complexity, exhibiting partly isotropic and strongly anisotropic mechanical properties [6].

Computational multi-scale modelling of skeletal muscle tissue can help to understand the processes taking place during active and passive loadings and is particularly challenging due to the composition, complex spatial distribution and orientation of its components and their respective internal hierarchical structure, which together contribute to the overall movement, force generation, and gait stabilisation properties of skeletal muscle. On the other hand, the multiscale experiments required for such a model are also a major challenge, especially at the micro level.

In this presentation, multiscale experiments at micro and macro level will be presented. At the micro level, the mechanical properties of muscle fibres [1-2] and the ECM [3] are characterised. For this purpose, different deformation states will be presented and discussed. At the macro level, experimental

investigations at the tissue [3, 6-7] and organ level [7-8] are presented. Through the investigations on the different scales, it is possible to view phenomena such as the tension/compression asymmetry (TCA) under the light of the different scales and thus better understand them.

The data generated from the experimental investigations is valuable information for the identification of model parameters as well as for the validation of a corresponding muscle scale model [4-5].

2. References

- [1] M. Böl, R. Iyer, J. Dittmann, M. Garcés-Schröder, A. Dietzel, , Acta Biomater, 92, 277-289, 2019.
- [2] M. Böl, R. Iyer, M. Garcés-Schröder, S. Kohn, A. Dietzel, J Mech Behav Biomed Mater, 101, 104001, 2020.
- [3] S. Kohn, K. Leichenring, R. Kuravi, A. E. Ehret, M. Böl, Acta Biomater, 122, 249-262, 2021.
- [4] R. Kuravi, K. Leichenring, R. Trostorf, E. Morales-Orcajo, M. Böl, A. E. Ehret, J Mech Behav Biomed Mater, 117, 104375, 2021.
- [5] R. Kuravi, K. Leichenring, M. Böl, A. E. Ehret, J Mech Behav Biomed Mater, 113, 104109, 2021.
- [6] M. Böl, A. E. Ehret, K. Leichenring, C. Weichert, R. Kruse, Acta Biomater, 10, 3225-3234, 2014.
- [7] K. Leichenring, A. Viswanathan, S. Kutschke, T. Siebert, M. Böl, Acta Biomater, 134, 453-465, 2021.
- [8] M. Böl, K. Leichenring, C. Weichert, M. Sturmat, P. Schenk, R. Blickhan, T. Siebert, Biomechanics and Modeling in Mechanobiology, 12, 1205-1220, 2013.
- [9] M. Böl, K. Leichenring, M. Ernst, C. Wick, R. Blickhan, T. Siebert, Journal of the Mechanical Behavior of Biomedical Materials, 51, 25-39, 2015.



A POROELASTIC FRAMEWORK TO REPRODUCE THE APPARENT VISCOELASTIC BEHAVIOUR OF MUSCLE UNDER COMPRESSION

Thomas Lavigne (1,2), Giuseppe Sciumè (2), Sébastien Laporte (3), Hélène Pillet (1), Stéphane Urcun (1,2,3) Benjamin Wheatley (3) and P-Y. Rohan (1)

(1) IBHGC, ENSAM, Paris, France (2) I2M, ENSAM, Univ. of Bordeaux, CNRS, Bordeaux INP, INRAE, Talence, France (3) Institute for Computational Engineering Sciences, Department of Engineering Sciences, Université du Luxembourg, Luxembourg (4) Department of Mechanical Engineering, Bucknell University, USA

1. Introduction

Wound healing and prevention of chronic wounds are challenging issues in public health. Wounds result from prolonged, repetitive mechanical loads. A biomechanical approach to evaluate the soft tissue injury risk could be a solution towards a personalized estimate of this risk. Current approaches however often ignore the detailed biomechanical properties of compressed soft tissues and in particular muscle. In the literature, attempts to characterize muscle tissue generally assume a viscoelastic formulation, ignoring the underlying physical mechanisms that give rise to the time dependent stress-strain behaviour. Porous media models represent a promising approach. The aim of this study was to investigate the capability of poroelasticity to reproduce the apparent viscoelastic behaviour of muscle tissue under confined compression.

2. Methods

Experimental stress-time relaxation curves of $N=31$ cylindrical tibialis anterior porcine muscle samples previously tested in confined compression and previously reported in (Vaidya and Wheatley, 2020) were numerically reproduced. A poro-elastic axisymmetric finite element model was developed in ABAQUS (Figure 1(a)). A one to one calibration was performed to fit the assumed quasi-incompressible, isotropic, poro-elastic constitutive model. The calibration procedure was gradient-based and the cost function was defined as the weighted sum of the peak stress error, the normalized Root Mean Square Error and the error on the derivative of the stress-time curve during the last 50s.

3. Results

The peak stress, characteristic relaxation time and consolidated state were recovered for most of the samples (normalized RMS Error $\leq 0,03$).

The toe-region of the curve did not follow the experimental curves. The stress-relaxation curve predicted by the poro-elastic model is given in Figure 1(b) for the average case.

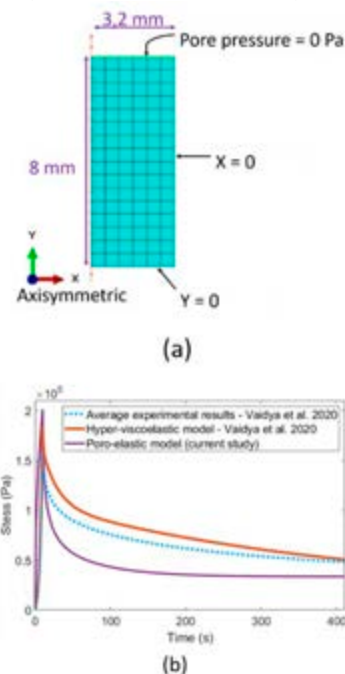


Figure 1: (a) FE model (b) Stress-relaxation curves

4. Discussion

The strength of the proposed model of this contribution is its fewer number of variables with respect to visco-hyperelastic models generally assumed in the literature. This contribution provides an important step toward a mechanistic interpretation of passive muscle tissue under going compression in the context of prevention of chronic wounds. Poroelasticity also represents a promising approach for integrating multiscale/multiphysics data to probe biologically relevant phenomena at a smaller scale.

References

Vaidya, A.J., Wheatley, B.B., 2020. JMBBM. <https://doi.org/10.1016/j.jmbbm.2019.103526>



ACTIVE RUPTURE MODELING OF THE MUSCULOTENDINOUS COMPLEX WITH DISCRETE ELEMENT METHOD.

Anthony ROUX (1,2), Jennyfer LECOMPTE (1), Ivan IORDANOFF (2), Sébastien LAPORTE (1)

1. *Institut de Biomécanique Humaine Georges Charpak, Arts et Metiers Institute of Technology, France*; 2. *Service de neurochirurgie, hôpital Beaujon (AP-HP) France*

1. Introduction

Tears of the muscle-tendon complex (MTC) are common sports-related injuries. The biomechanical mechanisms leading to such injuries are still not well understood [1]. This study focuses on the development of a MTC model using the discrete element method (DEM) and its use to analyse MTC failure.

2. Materials and Methods

2.1 Development of the Elastic Model

The MTC's model was developed in DEM with GranOO software. Mechanical properties of MTC were addressed thanks to literature values. The model was evaluated against traction tests [2].

2.2 Development of the Contractible Model

Contractibility properties were added to the mechanical properties of the muscle fibers in order to reproduce a behaviour of macroscopic muscle contraction. This model was then compared with data from the literature [3].

2.3 Development of the Rupture Model

Strain failure criteria for all elements of the TCM model were used, mechanical parameters were either extracted from the literature or fixed for the different anatomical structures. The failure model was then evaluated with *ex-vivo* tests [4].

2.4 Simulation of eccentric MTC injury

Muscle activation was then combined with a pull-to-failure test to observe the MTC tear. The lower part of the MTC was fixed and a linear displacement was applied to the upper part. Initially, the same force/length relationship was applied simultaneously to all muscle fibres.

2.4 Data Analysis – MTC injury

The force/displacement curve as well as the location of the failure, its mechanisms and the structures involved, were analyzed. A focus on

the stresses inside each discrete element was also performed to detect the stress concentration areas.

3. Results and Discussion

Delamination of muscle fibers was observed near the myotendinous junction (MTJ) (Figure 1). The concentration of stresses, near the MTJ, reveals that this region will be subjected to high forces and thus rupture. One reason is the gradient in mechanical properties between the muscle (soft) and the tendon (rigid). The numerical results are in agreement with the literature (80% rupture at the MTJ, [5]) and with *ex-vivo* tests [4]. A first important delamination is observed, and then a second rupture highlights the global delamination of the MTJ with a tearing of the muscle fibers.

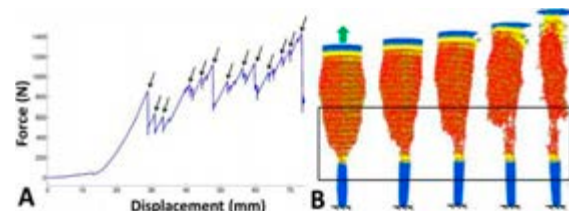


Figure 1: A. Force/displacement curve of the MTC during an active tensile test until rupture. B. Rupture of the MTC during an active tensile test.

4. Conclusion

The DEM is a promising method for modeling the tear of the MTC. In the longer term, the objective would be to prevent injuries based on a personalized DEM model.

5. References

1. Uchiyama Y et al., Sports Med Arthrosc Rehabil Ther Technol, 3, 20, 2011
2. Roux A et al., J. Biomech, 49, 252-258, 2016.
3. Roux A et al., CMBBE, 24, 1184-94, 2020.
4. Roux A et al., CMBBE, 18 sup1, 2046-47, 2015.
5. Ilaslan H et al, Skeletal Radiology, 36(6), 503-507, 2007.



SKELETAL MUSCLE FINITE ELEMENT MODELING: ADAPTATION FROM CARDIAC TISSUE ACTIVATION LAWS

Najoua Assila^{1,2,3}, Mickaël Begon^{2,3}, Sonia Duprey^{1,3}

1. Univ Lyon, Univ Gustave Eiffel, Univ Claude Bernard Lyon 1, LBMC UMR T_9406, F-69622 Lyon, France; 2. University of Montréal, Canada; 3. Associated International Laboratory EVASYM

Correspondence: sonia.duprey@univ-lyon1.fr

1. Introduction

When exploring joint pathomechanisms through human body modelling, 3D active muscles are essential. Yet, finite-element models of volumetric active skeletal muscles are seldom [1], [2]. Models of heart contraction have been implemented to trigger tissue deformation with an electrical potential [3]. As cardiac and skeletal muscles have similar contraction mechanisms [4], these constitutive laws might be extrapolated to the latter. Thus, the objective of this study was to validate that cardiac laws could yield physiological skeletal muscle behaviour reproducing the Hill force-length relationship [5].

2. Materials and Methods

Isometric contractions were simulated using a cylindrical muscle volume with a tetrahedral meshing. A 3D hyperelastic, anisotropic, quasi-incompressible, activated law was implemented using MAT295 in the explicit finite-element solver LS-Dyna®. Particularly, the passive component was modelled as a fibre-reinforced isotropic matrix. The contractile behaviour was modelled through a relationship between calcium concentration and fibre tension [6]. As calcium concentration is correlated with the muscle excitation intensity [7], the latter was used to drive muscle contraction.

The volume elements were at their optimal lengths when the muscle was at rest (l_0). To evaluate its passive force, the muscle was first stretched up to $1.5 l_0$. Then, maximal isometric contractions were simulated by first shortening or stretching the muscle within $[0.5 l_0, 1.5 l_0]$, before fully activating it. The passive force was subtracted from the force measured at the

muscle's extremities to evaluate the active force-length relationship.

3. Results

The predicted force fits reasonably well the Hill model (Fig. 1). Yet, as the muscle stretched, the active force decreased slower than expected.

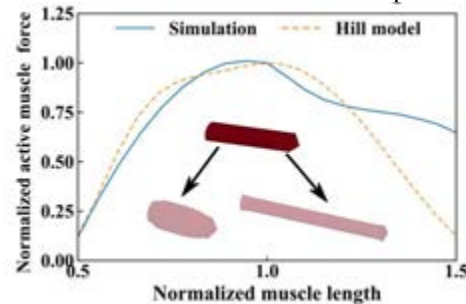


Figure 1: Active force-length relationship predicted through simulation compared to the Hill model.

4. Discussion and Conclusions

The divergence observed when the muscle was stretched could be explained by the parameters chosen for the passive component of the constitutive law as they can vary greatly. Nevertheless, the obtained results indicate that this approach could be implemented to study muscle strain during dynamic tasks using an electromyography-driven approach.

5. References

1. Vogt F et al., ISBMS 2006 conference: Springer; 2006. p. 19-28.
2. Péan F et al., *Comput Methods Biomech Biomed Eng*; 22(7): 740-751 (2019).
3. Zhang Y et al., *Front Physiol*; 11: 158 (2020).
4. Adams RJ and Schwartz A., *Chest*; 78(1): 123-139 (1980).
5. Zajac FE, *Crit Rev Biomed Eng*; 17(4):359-411 (1989).
6. Guccione JM et al., *J Biomech Eng*; 115(1): 82-90 (1993).
7. van Zandwijk JP et al., *Biol Cybern*; 75(5): 409-417 (1996).

COMBINED EXPERIMENTAL AND NUMERICAL STUDIES IN DENTAL BIOMECHANICS

Christoph Bourauel

Oral Technology, University Hospital Bonn, Germany

1. Introduction

In this review the significant progress in dental biomechanics within the past 30 years will be outlined with the help of selected examples in the field of orthodontics, periodontics and dental implantology. The spectrum ranges from idealised numerical models of tooth movement to patient-specific models and clinical studies to validate the results. The finite element analyses are supplemented by experimental investigations in specially developed measurement setups.

2. Examples from Dental Biomechanics

2.1 Orthodontic Tooth Movement

During orthodontic therapy teeth are moved through the alveolar bone due to bone remodelling. The biomechanical and biophysical background is rather complex and control of tooth movement needs a deep understanding of the interrelations. We developed simplified models using bone remodelling algorithms to predict tooth movement and validated the models using clinical results [1]. The results show that the strains in the periodontal ligament (PDL) seem to be the mechanical key stimulus to correctly predict orthodontic tooth movement (OTM).



Figure 1: Simplified FE model of a canine with PDL and surrounding bone (left) and result of a simulated canine retraction (right).

2.2 Material Parameters of the PDL

The biophysical and biochemical processes within the PDL are key factors not only for OTM but for a large number of further processes [2]. However the PDL has an extremely complex structure with fibres, vessels, nerves, cells and a fluid phase. Consequently a full constitutive law of the PDL must include nonlinear, time-dependent and multi-phasic components, which is still not yet solved. This part of the presentation covers experimental, theoretical as

well as clinical studies in this relevant field. A pronounced nonlinearity and time dependency of the PDL could be proven [3,4].



Figure 2: A collection of human, pig and rat tooth models (left) and a specialised device to measure intra-oral force/deflection characteristics (right).

2.3 Periodontally Compromised Teeth

The studies presented above were used to develop models to analyse the loading of the tooth supporting structures in periodontally compromised dentition during OTM. The results helped to make recommendations for orthodontists to better select appropriate devices [5].



Figure 3: Clinical situation of a patient suffering from periodontitis (left), FE model (right).

3. Discussion and Conclusions

The examples above show that the biomechanical models can help to improve the understanding of the complex clinical situations.

4. References

1. Bourauel C et al., J Orofac Orthop. 1999; 60(2): 136-51.
2. Basdra EK, Komposch G. Eur J Orthod. 1997; 19(6):615-2.
3. Poppe M et al., J Orofac Orthop. 2002;63(5): 358-70.
4. Keilig L et al., Ann Anat. 2016;206:80-8.
5. Baghdadi D et al., J Orofac Orthop. 2019;80(4): 184-193.

Acknowledgements:

The author wishes to thank Prof. Dr. Reimann, Prof. Dr. Hasan, Dr. Keilig and an endless list of doctoral students for their long-term support. Partial financial support by DFG, BMBF and Medical Faculty of Bonn is greatly appreciated.

CLINICAL AND NUMERICAL STUDY OF A LONG-TERM ORTHODONTIC TREATMENT

Gauthier Dot (1,2), Florent Goussard (3), Raphael Licha (4,5), Vittorio Sansalone (4,5)

1. UFR Odontologie, Université Paris Cité, Paris, France; 2. AP-HP, Hôpital Pitié Salpêtrière, Service de Médecine Bucco-Dentaire, Paris, France; 3. CR2P, UMR 7207, MNHN, CNRS, Sorbonne Université, Paris, France; 4. Univ Paris Est Créteil, CNRS, MSME, F-94010, Créteil, France; 5. Univ Gustave Eiffel, MSME, F-77474, Marne-la-Vallée, France

vittorio.sansalone@u-pec.fr

1. Introduction

A critical issue in the development of Finite Element Analysis (FEA) of orthodontic tooth movement (OTM) concerns the availability of suitable clinical data. The goal of this paper is to present a novel clinical protocol to accurately track OTM in three-dimensions (3D) that may provide clinical data to support FEA [1]. We will discuss our results from the perspective of a modeling-supported approach to orthodontics.

2. Materials and Methods

Clinical procedure. This study concerns the recoil of the upper canines of one 28-year-old patient. After avulsion of first premolars, Temporary Anchorage Devices (TADs) and an individualized lingual device (ILD) were placed in the maxilla, and connected through Ni-Ti springs (Fig.1A). The whole treatment lasted about 7 months.

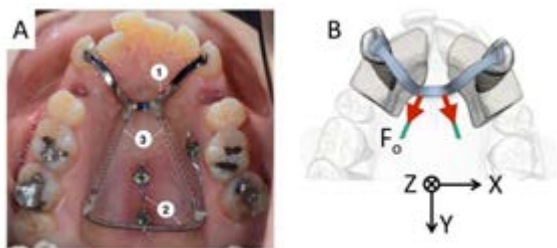


Figure 1: A: Intra-oral occlusal view of the ILD (1), TADs (2) and Ni-Ti springs (3). B: FEA model.

Data acquisition and 3D models. A cone beam computed tomography (CBCT) scan was taken at the beginning of the treatment. An intra-oral scan (IOS) was taken at each monthly appointment of the patient. Initial CBCT and IOSs were combined to obtain 3D models of the canines at each step (T_i , $i=0..7$) of the treatment.

FEA. A simplified 3D model was created based on the CBCT/IOS at T_0 , and imported into

Comsol Multiphysics software for FEA (see Fig. 1B). As a first step, all the materials were considered linearly elastic, except the alveolar bone for which a Zener viscoelastic model was used in order to allow irreversible OTM. The characteristic time of this model was calibrated with respect to the clinically measured recoil. Two loading conditions were tested, either applying only the orthodontic forces ($F_0=100$ cN) along the axes of the Ni-Ti springs or also adding a force $F_+=80$ cN along the Z axis.

3. Results

Fig. 2 shows the time course of the recoil (U_Y) and intrusion (U_Z) observed in clinics and computed by FEA for the left canine.

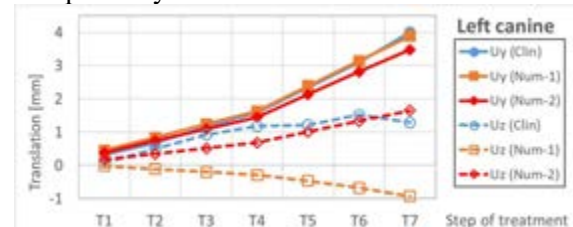


Figure 2: OTM of left canine: clinical data (Clin) and FEA results (Num-1: F_0 ; Num-2: F_0 and F_+).

4. Discussion and Conclusions

The proposed 3D tracking procedure could support FEA but requires a higher degree of automation. Deep learning models could help to automatize model construction [2].

FEA was fairly able to reproduce clinical OTM when adding vertical forces, that may be related to functional forces, to the orthodontic forces. This shows the major difficulty to obtain the full force system experienced by the teeth.

5. References

- Dot G et al. J Biomech; 129:110760 (2021).
- Dot G et al. Eur Radiol; 32(6):3639–3648 (2022).



HOW THE TRIM LINE DESIGN OF ORTHODONTIC ALIGNERS AFFECTS THEIR BIOMECHANICAL BEHAVIOR

Tarek Elshazly (1), Christoph Bourauel (1), Damiano Salvatori (2), Ludger Keilig (1)

1. Oral Technology Department, University Hospital Bonn, Bonn, Germany

2. Institut Straumann AG, Basel, Switzerland

1. Introduction

Due to the complexity of teeth movement by orthodontic aligners, use of finite element analysis (FEA) may facilitate understanding their biomechanical behavior [1]. The aim of current numerical study is to use a FE model to investigate effect of the trim line design of aligners on the force delivery and stress distribution onto tooth and the periodontal ligaments (PDL).

2. Materials and Methods

In 3-Matic software, a 3D model of upper jaw was imported and the central incisor (Tooth 11) was separated to be movable. Aligners with different thicknesses (0.3, 0.4, 0.5, and 0.6 mm) and different trim line designs (Fig. 1) were modelled, similar to Elshazly et al. [2]. The models were then exported to Marc/Mentat FE software package. The bone and the PDL of Tooth 11 were designed (Fig. 2). 10-noded tetrahedral elements were designated to aligners elements, while 4-noded tetrahedral elements were designated to the teeth and the cast. Material parameters were selected as shown in Table 1. A touching frictionless contact mode was specified between the aligner and the tooth surfaces, with an interference closure of (-0.04). The forces generated at a 0.2 mm facio-lingual bodily movement of the Tooth 11 were calculated.

Table 1: Material parameters of all structures..

Structure	Young's Modulus (MPa)	Poisson's ratio
Aligner	1800	0.3
Teeth	80000	0.3
Bone	2000	0.25
PDL	0.1	0.35

3. Results

The initial generated forces were in the range of 0.5 – 1.5 N, compatible with the reported ideal

orthodontic movement (0.5 -1.0 N) [3]. Forces increased with thickness and extension of the trim line.

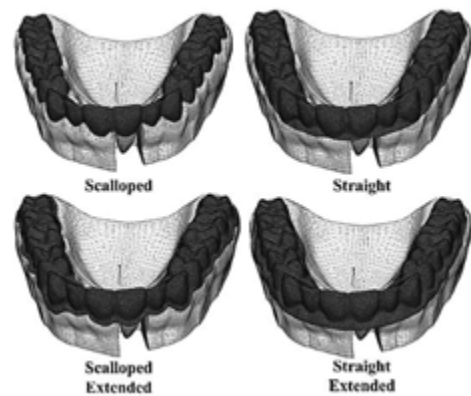


Figure 1: Different trim line designs of aligner.

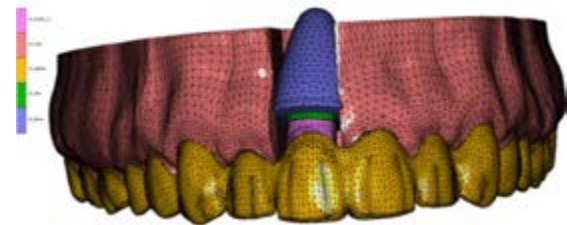


Figure 2: A finite element model of an upper jaw, an aligner, and a moveable central incisor with its PDL and Bone.

4. Discussion and Conclusions

The straight trim line showed higher forces than the scalloped, and better force distribution pattern, applying more forces at the gingival one third, closer to centre of resistance.

5. References

1. Elshazly TM et al., Clin. Oral Investig. (2022).
2. Elshazly TM et al., J. Dent. (2022).
3. Proffit WR, St. Louis. Mosby. Inc. (2000)

Acknowledgements:

This work was partially funded by Institut Straumann AG, Basel, Switzerland.

FINITE ELEMENT MODELLING OF CANTILEVER SINGLE-RETAINER RESIN-BONDED FIXED DENTAL PROSTHESES

Philippe Boitelle (1,2), Elisa Caussin (1), Irena Sailer (3), Jean-Pierre Attal (1), Aurélie Benoit (1)

1. *URB2i, Faculty of Dental Surgery, Université Paris Cité, France*; 2. *Oral rehabilitation Department, Faculty of Dental Surgery, University of Lille, Lille University Hospital Center, France*; 3. *Division of Fixed Prosthodontics and Biomaterials, University Clinic of Dental Medicine, University of Geneva, Switzerland*

1. Introduction

Among resin-bonded fixed dental prostheses (RBFDP), ceramic cantilever single-retainer is considered as a valuable treatment option in the posterior region [1]. This aesthetic and non-invasive approach depicts an actual alternative to implants. A minimal preparation involves a variety of clinical configurations. The finite element model (FEM) is an interesting tool, from a mechanical point of view, to optimise the design of RBFDPs to resist delamination prostheses or fracture in the connector regions and secondary caries [2].

The objective of our study is (1) to draw clinical recommendations from a simple 2D FEM and (2) to improve RBFDP design by the use of more realistic 3D FEM, then (3) to validate by experimental data.

2. Materials and Methods

Simplified 2D finite element models of RBFDPs were created with COMSOL Multiphysics (V6.0) to analyse stress distribution in the adhesive layer and in the prosthesis. The influence of parameters such as the length and the thickness of the retainer or the bonding length along the loading axis was evaluated (Fig. 1a).

A 3D FEM of a RBFDP on a left mandibular molar was created in Abaqus (Dassault Systems) from clinical data (intraoral scan, cone-beam computed tomography). Various software programs were used to create the geometries: inLab Model (Dentsply Sirona) for the prosthesis; 3D Slicer and Meshmixer for segmentation and smoothing of dentin and Catia for part repositioning. The adhesive layer was not modelled. All materials were considered homogeneous, linear elastic in both models. 2 designs of RBFDP associated with 2 constitutive materials and adhesive systems

were mechanically loaded in a computer-controlled masticator with thermal cycles (Fig. 1b).

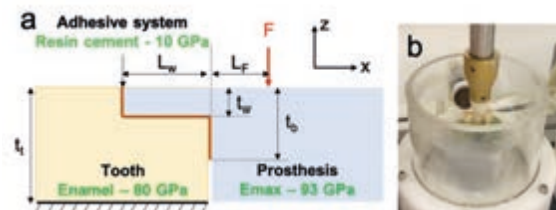


Figure 1: a) Simplified 2D FEM and b) Thermomechanical loading of a RBFDP

3. Results

The 2D model shows results in accordance with the mechanical theory of bending beams. In particular, the dimensioning factor for the connector is not its section but its width times the square of the bonding length along the force direction. The 3D FEM shows stress concentration in the connector region as expected. One design of lithium disilicate RBFDP did not fail after simulated mastication whereas mechanical failure was observed in the 3 other groups by debonding.

4. Discussion and Conclusions

The simple 2D models were sufficient to draw clinical recommendations and showed the need to consider the orientation of occlusal forces for connector design. The 3D RBFDP FEM was personalised according to clinical data. Adhesive system should be added in the model to correlate with experimental data showing mostly debonding.

5. References

1. Yazigi et al, J Dentistry, 116:103907, 2022.
2. Chen et al, J Prosthetic Dentistry, in press, 2022.



BIOMECHANICAL SIMULATION OF HAEMOSTATIC SPONGES USED FOR SINUS LIFT PROCEDURE

Nathalia Soar (1), Caio de Oliveira Cafiero (1), Cédric Laurent (1), Pascale Royer (2), Simon Le Floc'h (2), Chrystelle Po (3), Nadia Bahlouli (3), Cédric Mauprivez (4), Halima Kerdjoudj (4), Adrien Baldit (1)

1. LEM3-UMR-7239, CNRS – Univ. de Lorraine - Arts et Métiers ParisTech, France; 2. LMGC, Univ. Montpellier, CNRS, Montpellier, France; 3. Laboratoire ICube, CNRS UMR 7357, Strasbourg, France; 4. BIOS, Univ. de Reims Champagne Ardenne, EA 4691 Reims, France.

Corresponding author: Adrien Baldit, adrien.baldit@univ-lorraine.fr

1. Introduction

The objective of this study is to provide a geometrical model that describes the morphological behavior of haemostatic gelatin-based sponges under the effect of hydration following the sinus lift surgery [1]. For this purpose, a finite element model was developed to simulate conditions close to clinical ones and experimentally reproduced by Okley et al. [2].

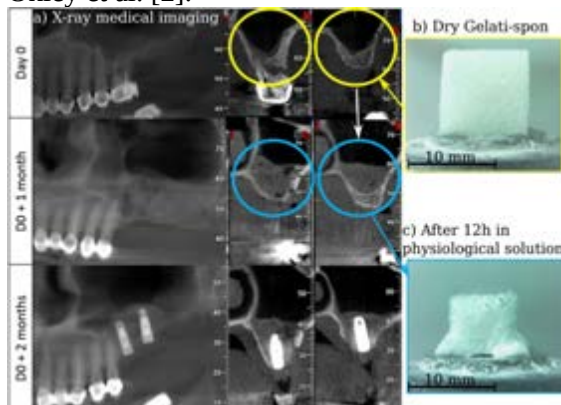


Figure 1: Sinus lift X-ray monitoring with in yellow the defect to fill and in blue the newly formed bone after one-month implantation. b) side view of a dry haemostatic sponge (Gelita-spon) and c) its state after 12 hours within physiological fluid. The final objective is to build a patient specific tool to predict how much initial sponge volume is required to promote the bone formation and support the dental implants once mineralized.

2. Materials and Methods

Modelling such a shrinking within physiological conditions rises many issues involving hydro-chemo-mechanical couplings. Aiming a fast answer to the clinical demand, the morphological effects of hydration on haemostatic sponges has been modelled through a thermo-stress problem [3] with Abaqus where the temperature variation represented the sponge hydration. Gelita-spon

sponge being cubic ($10 \times 10 \times 10 \text{ mm}^3$), only one fourth has been used with a mesh size of 1mm leading to 250 linear hexahedral temperature-displacement coupled elements (C3D8H).

3. Results

An optimisation loop has been set with Python to reach the set of parameters fitting the experiments presented in Fig 2.

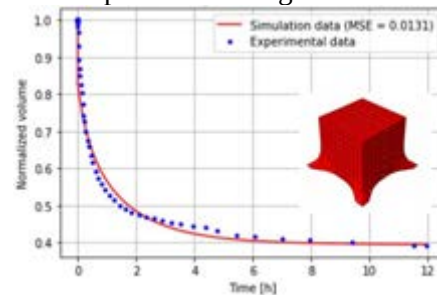


Figure 2: Simulation results (red line) fitting experimental data (blue dots) in terms of normalized volume as function of time.

The associated final geometries (one example in Fig 2) are close to experiments Fig 1c.

4. Discussion and Conclusions

The results are satisfactory for an extend to the patient specific geometry, i.e. sinus cavity. Although, mesh refinement led to convergence issues due to excessive deformations. Besides, the analogy with thermomechanics is far from reality and microstructural analyses are under progress to be coupled with poromechanical simulation.

5. References

1. Sohn D.-S. et al., J Oral Maxillofac Surg, 68:1327–33, 2010.
2. Okley S. et al., Comput Methods Biomech Biomed Engin, 23(sup1):S206–S208, 2020.
3. Banks D., Acque Sotteranee - Italian Journal of Groundwater, 2012, 1

Acknowledgements:

The authors would like to thank the CNRS MoTiV grant and the FLI IMCOLL grant for providing financial support to this project.



Calibration of traction-separation laws for the adhesive layer of indirect dental restorations

Yannick Yasothan (1), Nicolas Schmitt (1), Jan Neggers (1) Elsa Vennat (1)

1. *Université Paris-Saclay, CentraleSupélec, ENS Paris-Saclay, CNRS, LMPS - Laboratoire de Mécanique Paris-Saclay, 91190, Gif-sur-Yvette*

1. Introduction

Nearly 2.3 billion people are affected by caries worldwide [1]. Indirect Dental Restoration (IDR) is a treatment that removes the affected part and fills the cavity by bonding a dental prosthesis. Despite many advances, this treatment is still prone to a mechanical failure that initiates in the adhesive layer. Using numerical simulations allowed us to identify the optimal parameters minimizing the mechanical stresses endured by the IDRs [2]. However, the critical part of the IDRs, the adhesive layer, is always approximated by an elastic behavior. If the numerical results are too far from reality, this description may need to be revised to size the RDIs. This work aims to calibrate more accurate constitutive laws, named Traction-Separation Laws (TSLs), of this layer by Integrated-Digital Image Correlation (I-DIC).

2. Materials and Methods

MMMB tests [3] were conducted on small notched samples (35 mm x 4.2 mm x 1.9 mm) composed of two ceramic beams bonded with a dental adhesive. Images are taken during the tests to identify the parameters of the law.

These tests will allow identifying the parameters of the TSLs. However, before calibration, it is essential to identify the position of the crack front because the parameters sought are sensitive to it. However, there is no convention on this position's detection method. Since this position will be used to calibrate TSLs by I-DIC, it is best to identify it by I-DIC.

After identifying these positions, the calibration of the TSLs is performed. The TSLs describe a mixed-mode I/II behavior where the only two

variables are the stiffness and the toughness; the other parameters are fixed according to considerations of their sensitivity to the results.

3. Results

The calibrated TSLs describe the behavior of the adhesive layer.

4. Discussion and Conclusions

The modeling choices are justified and are sufficient to describe the complex behavior of IDRs.

The identified parameters present a high variability that the uncertainties cannot explain. This variability is probably due to the sensitivity of the TSL parameters to the materials, the bonding process, and the storage conditions.

The next step would be to implement these laws in IDR optimization simulations to see if a more accurate description of the critical part behavior influences their results.

5. References

1. James SL et al., *The Lancet*; 392(10159):1789-1858 (2018).
2. Shindo K et al., *Comput Aided Des Appl*; 19(3):426-448 (2022).
3. Kolluri NVVRM et al., *J Phys D: Appl Phys*; 44(3) (2011).



Joseph Ackerman(1), Chiara Bernard (2), Massimiliano Fraldi (2), Ludovico Mori (1), Martine Ben Amar (1)

1. LPENS & Sorbonne University Paris, France; 2 Università Federico due, Napoli Italy ;

1. Introduction

Phenotypical heterogeneity constitutes a trend of tumours that strongly impacts their growth and stability as well as possible therapies. Among the biological models that take this aspect into account the Cancer Stem Cell model [2], which assumes the tumor population to be composed of stem cells and differentiated cells explains many characteristics of tumour evolution as the spontaneous collapse of a tumour or the relapse after treatments. Another cellular population concerns the immune cells as fibroblasts and T cells that cancer cells modify to maintain the tumour integrity. Active and aggressive cells can either proliferate or be inactivated according to numerous signaling pathways and their physical description requires a spatio-dynamical study [2] with parameters to be estimated. In addition, the stochasticity inherent to the cancer population may modify the theoretical prediction. I will present first a dynamical model, eventually stochastic [3] which will be transformed to include space variation controlled by friction and cell-cell density interactions.

2. Methods

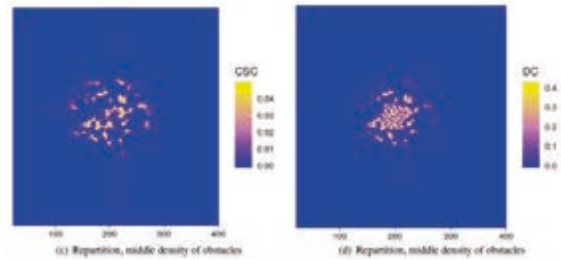
The formalism has been explained in previous publications [2] and rests on the mixture model with a fluid friction. Basically, we are faced to a system of nonlinear partial differential equations for each cell density (ϕ_i) and each chemical signal (c_i) acting on the cell evolution.. When the tumour involves different active cell types, a first step will focus on the dynamics leading to a non-linear dynamical system which reminds ecologic models. It is possible to detect the fixed points of the dynamics, their stability versus perturbations as their behaviour when stochasticity and drug treatments are included. Such study evaluates the phenotypic transformation of all cells including immune cells and may explain the weakness of the immune system inside the tumour and the

immediate micro-environnement. Then the spatial environment is introduced leading to a system of partial differential equation mixing cell and biochemical concentration:

$$\begin{cases} \partial_t \phi_i + \nabla \cdot \mathbf{j}_i = 0 \\ \nabla \mu_i = (\sum_j D_j \phi_j^{-1} + D_0 \phi_0^{-1} - \alpha_{ij}) \nabla \phi_i - \epsilon^2 \nabla (\nabla^2 \phi_i) \\ \mathbf{v}_i = -M \phi_i (1 - \phi_i) \nabla (\mu_i - \epsilon^2 \nabla^2 \phi_i) \\ \partial_t c_j = D_c \nabla^2 c_j - d_{ij} c_j \phi_i \end{cases}$$

for cells (i) and chemical (j).

3. Results



Examples of CSC population in a stochastic environment published in [1]

5. References

1. Olmeda F M, Ben Amar M, Sci. Reports 9,15607 (2019)
2. Ackermann J, Ben Amar M., Joanny J.F Phys. Reports 927 (7), 1-30, (2021)
3. Mori L, Ben Amar M, preprint ENS

Acknowledgements:

MBA acknowledges the financial support from ITMO Cancer of Aviesan within the framework of the 2021-2030 Cancer Control Strategy, on funds administrated by Inserm (PCSI 2021, MCMP 2022)

MICROMECHANICAL ANALYSIS OF THE EFFECTIVE STIFFNESS OF POROELASTIC BIOLOGICAL COMPOSITES

Laura Miller (1), Raimondo Penta (1)

1. School of Mathematics & Statistics, University of Glasgow, UK.

Within this work we investigate the role that the microstructure of a poroelastic material has on the resulting elastic parameters.

We are considering the effect that multiple elastic and fluid phases at the same scale (LMRP model [1]) have on the estimation of the materials elastic parameters when compared with a standard poroelastic approach.

We present a summary of both the LMRP model and the comparable standard poroelastic approach both derived via the asymptotic homogenization approach.

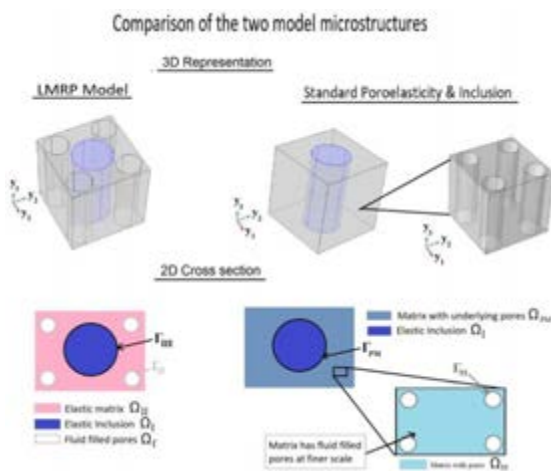


Figure 1: Comparison of the microstructures of both approaches highlighting the direct same scale approach of LMRP and the two-step approach of previous models.

We provide the 3D periodic cell problems with associated boundary loads that are required to be solved to obtain the effective elasticity tensor for both model setups. We then perform a 2D reduction of the cell problems, again presenting the 2D boundary loads that are required to solve the problems numerically.

The results of our numerical simulations show that whenever investigating a poroelastic

composite material with porosity exceeding 5% then the LMRP model should be considered more appropriate in incorporating the structural details in the Young's moduli E_1 and E_3 and the shear C_{44} .

Whenever the porosity exceeds 20% it should also be used to investigate the shear C_{66} . We find that for materials with less than 5% porosity that the voids are so small that a standard poroelastic approach or the LMRP model produce the same results.

We conclude by focussing on relevant biological applications such as myocardial infarction, where the cardiac myocytes die and become replaced by fibrous collagen matrix.

In this case we could perform a parametric analysis where the inclusion volume fraction and geometry are changed to simulate the loss of myocytes and the replacement with fibrous collagen matrix scar tissue.

References

1. Miller, L., Penta, R. Continuum Mechanics and Thermodynamics, 32, 1533-1557 (2020).

Acknowledgements:

L.M. is funded by EPSRC with Project Number EP/N509668/1, and RP is partially funded by EPSRC Grants EP/S030875/1 and EP/T017899/1.



A 3D IMAGE-BASED MATHEMATICAL MODEL COUPLING TUMOUR GROWTH TO MICROCIRCULATION TRANSPORT

Hani Cheikh Sleiman (1), Simon Walker-Samuel (2), Rebecca J Shipley (1)

1. Department of Mechanical Engineering, University College London, London UK;
2. Centre for Advanced Biomedical Imaging, University College London, London UK

1. Introduction

Numerical modelling of tumour growth and its response to different therapeutic regimens is pivotal for optimising therapy delivery and evaluating outcomes. The vascular architecture is critical in determining how nutrients and drugs are delivered. Despite this, it is rare that 3D blood network structures derived from real-world imaging datasets are used as inputs to mathematical models to predict tumour growth dynamics.

In this work, we couple a 3D multiphase tumour growth model to a microcirculation model using realistic microvasculature volume datasets.

2. Materials and Methods

The tumour environment is treated as a porous medium and assumes a viscous fluid analogy for the different cell populations [1,2]; where the non-deformable extracellular matrix (ECM) constitutes the solid scaffold and where the porosity is saturated by the tumour cells (TC), host cells (HC) and the interstitial fluid (IF).

Blood flow in the microcirculation is described using Stokes flow [3], applied to a real-world network geometry extracted using high-resolution optical imaging, segmentation and skeletonisation. A special attention is dedicated to generating the multi-domain 3D volumetric conform mesh while preserving the network morphology.

3. Results

The meshing pipeline results in having a three-domain volumetric mesh i.e. the tumour, the surrounding tissue and the morphologically preserved vascular domain (Fig. 1).

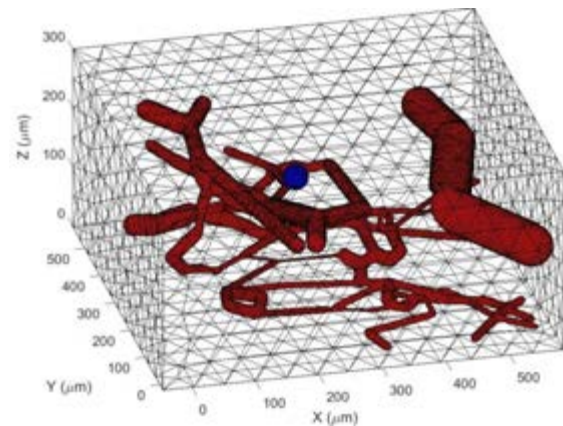


Figure 1: An example three-domain conform mesh representing the tumour (blue), the host tissue and the morphologically preserved vasculature (red).

Through several illustrative examples, we show the potential of the two-model framework to reproduce important aspects of heterogeneous tumour processes, such as response to local oxygen gradients and drug treatments delivered through the vasculature.

4. Discussion and Conclusions

The coupling of the two models enables studying the local mass transport from a realistic vascular domain to the tumour environment. This was possible due to the development of a meshing pipeline that allows the representation of image-acquired blood networks on a finite element mesh.

5. References

1. Urcun S et al., PLoS One. 16(7):e0254512 (2021)
2. Sciumè G et al., Physical Biology. (2014).
3. d'Esposito A, Sweeney P et al. Nat Biomed Eng. 10:773-787 (2018)

A FUNCTIONALLY GRADED ANISOTROPIC FRACTIONAL POROELASTIC MODEL TO SHADE LIGHT ON LUBRICATION MECHANISMS OF THE HUMAN MENISCUS DURING LOADING

Sachin Gunda (1), Sundararajan Natarajan (1), Olga Barrera (2, 3)

1. Indian Institute of Technology Madras, India; 2. Oxford Brookes University, United Kingdom; 3. University of Oxford, United Kingdom

1. Introduction

Experimental evidence shows that the permeability, hence the fluid flow rate, inside the meniscal tissue is not constant in time and space. This behaviour is described by a poroelastic model in which non-integer order derivatives rule the pore pressure diffusion equation [1]. This paper focuses on coupling “anomalous” transport phenomena with mechanics in a porous solid within the theory of anisotropic poroelasticity. We verified the model and ran consolidation problems and compared results with analytical solutions and experimental values. Moreover, we show results of a knee patient-specific FEM model in dynamic conditions and study the lubrication mechanisms in the knee joint.

2. Materials and Methods

Fractional poroelasticity in time is used to model the material behaviour. In Fractional poroelasticity, Biot’s theory is used along with Fractional Darcy’s law given by eq. (1) [1]:

$$J = \lambda \, {}_0D_t^\beta \nabla p \quad (1)$$

where J denotes the flux, λ is the permeability, p is the pore pressure and ${}_0D_t^\beta$ denotes the fractional derivative in time.

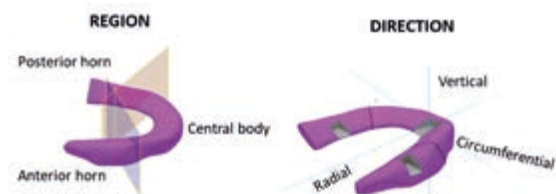


Figure 1: Regions and orientations in the meniscus

Material properties along different orientations and different regions of the meniscus were found from confined creep experiments using optimisation techniques in MATLAB. The

fractional poroelastic model is implemented using UMATHT in Abaqus.

3. Results

Using the properties obtained from the experiments, confined compression tests were simulated along different orientations. The displacement vs time result is shown in Fig. 2, which shows the transversely isotropic nature of the material.

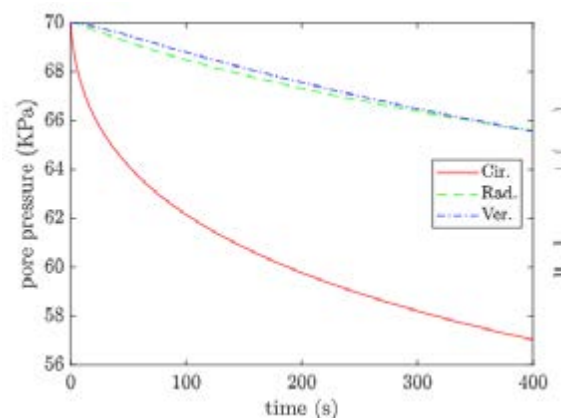


Figure 2: Pore pressure evolution during confined compression for different orientations

4. Discussion and Conclusions

Results show the transversely isotropic nature of the meniscus. Using the Abaqus subroutine of fractional poroelasticity along with the obtained material properties, the tissue level function of the whole meniscus in load bearing and lubrication will be studied.

5. References

1. Bulle R. et al., Applied Sciences, 11(20), 9405 (2021).

Acknowledgements: O.B. would like to acknowledge MSCA-IF-2017, MetaBioMec, Grant agreement ID: 796405.

DIGITAL FUNCTIONAL IMAGING AT MICROSCALE: OSTEOSARCOMA MICROENVIRONMENT AND TREATMENT RESISTANCE

Pauline Assemat (1), Anne Gomez-Brouchet (2), Anthony Mancini (1), Romain Alis (1), Michel Quintard (1), Pascal Swider (1)

1. *Institut de Mécanique des Fluides de Toulouse, France*; 2. *CRCT, CHU de Toulouse, France*

1. Introduction

Osteosarcoma (OST) is a malignant primary bone tumor that mainly affects children and young adults. It is characterized by the anarchic production of bone by tumor cells. The high genomic complexity of OST has not allowed the identification of recurrent therapeutic molecular targets or specific treatment resistance biomarkers. This genomic complexity leads to an intra tumoral and inter individual heterogeneity [1] which can be explored at different scales: metabolomic, molecular, tissue or macroscopic scales. OST components are moreover subject structural and fluid mechanical effects adding supplementary complexity in the understanding tumor microenvironment.

Using porous media theory, we developed a new digital functional imaging technique to explore mechanical and transport properties of tissue from histological and immunohistological human data. We found correlations between elastic properties, convective properties and cell distribution into the microenvironment depending upon treatment response and we highlighted the impact on neo-formed bone microarchitecture.

2. Materials and Methods

We propose a consistent upscaling method to characterize the mechanical properties of tumoral microenvironment which is a strongly heterogeneous porous medium. The core is a sequential grid-block approach [2] after applying dedicated image segmentations. The methodology is adapted to large size binarized images (50000px*50000px) extracted from histological and immunohistological slices obtained in clinical routines. Interstitial fluid flow and elastic models are explored. Piecewise constant equivalent parameters such as

tissular permeabilities and stiffness coefficients are determined with reliability.

3. Results

On a cohort of 4 patients, it was found that chemotherapy was more efficient in lacy-like neo-formed bone regions compared to trabecular-like neo-formed bone regions with areas of good response matching with a decreasing number of residual cells and a decreasing local tissue permeability and stiffness (fig 1).

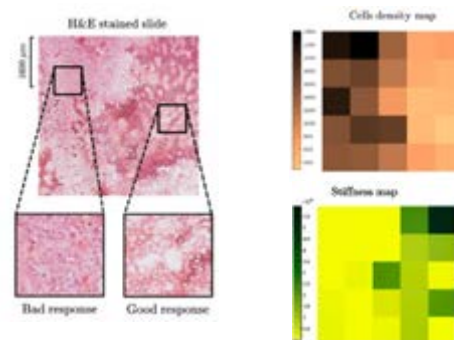


Figure 1: OST histological section, cell density map (bad response to treatment corresponds to high cell density) and stiffness map.

4. Discussion and Conclusions

We have developed an innovative approach based on heterogeneous porous media theory and based on data from clinical setting to explore tumoral microenvironment properties.

This new *in silico* functional imaging technique, is generic and could be adapted for different physics and other cancers.

5. References

1. Gomez-Brouchet et al, Cancers 2021.
2. Durlafsky. Water Res. Research, 1991.

Acknowledgments: INCa, Cancéropole GSO.



MALIGNANT TRANSFORMATION OF LOW GRADE ASTROCYTOMAS: IMAGING-INFORMED MODELLING

Meryem Abbad Andaloussi(1,2), Stéphane Urcun(1), Andreas Husch(2), Isabel Fernandes Arroteia (3), Giuseppe Sciumè(4), Stéphane P.A. Bordas(1, 5), Frank Hertel(1,3)

1. *Department of Engineering Sciences, Faculté des Sciences, de la Technologie et de Médecine, Université du Luxembourg, Campus Belval, Luxembourg.*
2. *Luxembourg Centre for Systems Biomedicine, Université du Luxembourg, Campus Belval, Luxembourg.*
3. *Service National de Neurochirurgie, Centre Hospitalier de Luxembourg, Luxembourg.*
4. *Université de Bordeaux, France.*
5. *Clyde Visiting Fellow, Department of Mechanical Engineering, The University of Utah, Salt Lake City, Utah, United States.*

1. Introduction

Low grade glioma (LGG) are tumours in the central nervous system that are defined by the WHO as grade 2 tumours. In particular, low grade astrocytoma (LGA) tumours are characterized by a mutant IDH and 1p/19q non codeleted chromosomes. Even after resection surgery, the tumour is expected to recur showing a more aggressive behaviour. This process, MT, is generally defined by clinicians as a newly acquired contrast uptake in Medical Resonance Imaging (MRI) throughout the evolution of the disease. On a micro-environment level, the role of stiffened extra-cellular matrix (ECM) in the invasiveness of grade 4 astrocytoma IDH mutant cells was investigated. The cells were not only more invasive in a stiff substrate, but they also showed signalling representative of primary high grade tumours. These findings were later consolidated by an in vivo comparison between recurrent grade 4 astrocytoma IDH mutant tumour and a glioblastoma [1].

2. Materials and Methods

We introduce a novel mathematical model to assess MT of grade 2 to grade 3 astrocytoma [2]. The brain is considered as a porous medium where the tumour is defined as one fluid phase of the porosity. The model is initialized and calibrated using data from the same patient at two different timepoints. This patient-specific approach helps segmenting the tumour region throughout the disease along with nutrient and cellularity parameters from MRIs of the patient [3].

3. Results

MT is defined by the model as the region with less access to nutrient overlaid with regions of high intracranial pressure (ICP). The patient malignantly transformed region is compared to the model prediction: the model is capable of correlating the region that is more likely to be malignantly transformed 540 days earlier.

4. Discussion and Conclusions

In order to test the robustness of the model, more patients are needed. For each patient, perfusion MR sequences are needed to consider the change in nutrients uptake throughout the disease evolution.

5. References

1. Miroshnikova, ... (2016). Tissue mechanics promote IDH1-dependent HIF1 α -tenascin C feedback to regulate glioblastoma aggression. *Nature cell biology*, 18(12), 1336-1345.
2. Sciumè, ... (2014). A tumor growth model with deformable ECM. *Physical biology*, 11(6), 065004.
3. van der Voort, S. R., ... (2020). WHO 2016 subtyping and automated segmentation of glioma using multi-task deep learning. arXiv preprint arXiv:2010.04425.

Acknowledgements:

MAA was supported by the Institute of Advanced Studies (IAS) of the University of Luxembourg, project U-AGR-6046-00-B. SU thanks the Agence Nationale de la Recherche (ANR) (France) and the Fond National de la Recherche (FNR) (Luxembourg) joint grant number ANR-21-CE45-0025-01.



DIGITAL TWINNING OF THE CELLULAR CAPSULE TECHNOLOGY: A POROMECHANICAL APPROACH

Giuseppe Sciumè (1), Pierre Nassoy (2), Stéphane Urcun (3)

1. University of Bordeaux, France; 2. Optics Institute of Bordeaux, France; 3. University of Luxembourg, Luxembourg.

1. Introduction

During tumor growth, tumor cells may move locally in the proximity of the primary tumor by invading the host tissue and/or enter within the circulatory system and form metastases in other organs. Talking about motion is talking about physics which has a primary role in the evolution of cancer [1]. Hence, one of the big challenges of cancer research is today to understand the couplings between biological factors and cancer physics for the development of novel physics inspired therapies. To face this challenge experimental approaches, which are the high road, can be even more effective when coupled with relevant biophysical mathematical models which allow us to better interpret results and also to improve and to well engineer the experiments which sometimes are designed with a certain dose of heurism.

2. Materials and Methods

Experimental-numerical approaches may be used to study different facets of cancer phenomenology. In this contribution we present recent *in vitro-in silico* studies aiming at quantifying the coupled role that hypoxia and mechanical stress have in the growth dynamics of a spheroid. During tumor growth *in vivo* the malignant mass deforms the host tissue inducing a significant mechanical interaction with the stroma. This physiological condition can be mimicked *in vitro* by culturing spheroids in confined conditions. One smart way is to encapsulate spheroids within alginate capsules; these last are deformed once the spheroid has filled the whole intra-capsular space (confluence). Hence, by imaging and measuring this deformation one can retrieve by inverse analysis the interaction stress between the spheroid and the inner wall of the capsule. This is the working principle of the Cellular Capsule Technology (CCT) [2]. We present here some results of the joint research activity between

LP2N and I2M aiming at the digital twinning of CCT and CCT derived protocols [3, 4].

3. Results

Between these results we will emphasize in particular those of a recent paper [4] where we show that a modeling approach accounting for the triphasic nature of the spheroid (extracellular matrix, tumor cells and interstitial fluid) offers a new perspective of analysis revealing that the pressure retrieved experimentally cannot be interpreted as a direct picture of the pressure sustained by the tumor cells and, as such, cannot therefore be used to quantify the critical pressure which induces stress-induced phenotype switch in tumor cells. The proposed multiphase reactive poromechanical model was cross-validated. Parameter sensitivity analyses on the digital twin revealed that the main parameters determining the encapsulated growth configuration are different from those driving growth in free condition, confirming that radically different phenomena are at play.

4. Discussion and Conclusions

These results have demonstrated that multiphase reactive poromechanics is an exceptional theoretical framework to attain an in-depth understanding of CCT experiments, to confirm their hypotheses and to further improve their design.

5. References

1. Nia HT et al.(2020) Science, 370(6516): eaaz0868
2. Alessandri K. et al. (2013) PNAS, 110(37): 14843-8
3. Le Maout V. et al. (2020) Science Advances, 6 (13), pp. eaaz7130
4. Urcun S. et al. (2021) Plos One 16(7): e0254512



UNDERSTANDING HOW TRANSPORT IN ORGAN VASCULAR TREES REFLECT THEIR ARCHITECTURE

Jérôme Kowalski (1), Lorenzo Sala (1), Jules Dichamp (1), Irene Vignon-Clementel (1)

1. Inria (Saclay IdF), France

1. Introduction

Partial liver resection (or partial hepatectomy) is a liver surgery performed in the treatment of major liver diseases or in liver partial transplantation. In some cases, the patients suffer from post-operative liver disorders due to the reaction of the vascular system to the radical change in mass of the liver. To understand this behaviour, surgeons perform the injection of a fluorescent contrast agent (indocyanine green) pre- and post-operation which helps in the imaging of blood flow in the liver input vessels. More generally, in the study of dynamic imaging of organs, certain regions of interest are evaluated by their time characteristics.

We here present an *in-silico* model of vascular trees (VT) accounting for the differences in geometry and hemodynamic behaviours of organs to understand the transformation induced by such trees on an input concentration profile.

2. Materials and Methods

Every VT is here described geometrically as a binary tree with an asymmetry parameter $\gamma \in [0,1]$ and a power-law index p [1]. They are constitutive parameters of the tree, change from one organ to the other and can be recovered from the literature [2].

The approach lies on three points:

- construction of a binary tree;
- solve for 0D stationary hemodynamics;
- inject a species to be transported.

A resistive model is chosen for the equivalent impedances of the vessels. A uniform pressure field is applied in the capillaries (leaves of the tree). The species is transported from the input vessel in a piecewise constant hemodynamic field. It exits the tree in the organ as a sum of delayed functions weighted by a relative quantity provided by the hemodynamic distribution and the power conservation law (parameter p , [1]). The family of delays given

by each branch creates a probabilistic distribution of the transit time. Interesting statistics are extracted from the time distribution, such as the mean transit time ($\bar{\tau}$), the time of maximum output (τ_{max}) and the first and third quartiles ($Q_{1/4}$, $Q_{3/4}$).

3. Results

The transit time distributions of the main vascular inputs of the liver are computed with different geometry parameters and compared to the analytical solution of simpler cases. The characteristic features of the delay distribution (plotted in Fig. 1.) give insights on the geometric properties of different VT.

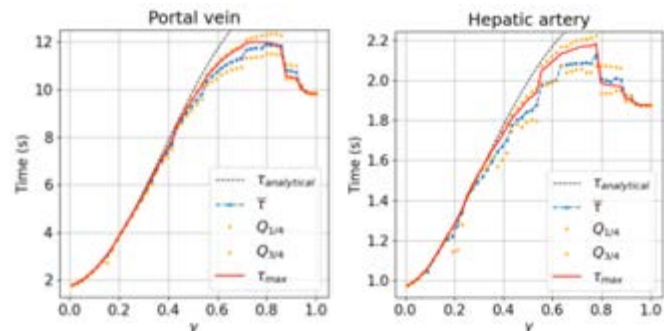


Figure 1: Variations of the characteristic times of the two hepatic input VT with the parameter γ .

4. Discussion and Conclusions

This approach helps to understand the simple mechanisms behind the transformation of the shape of a concentration profile when flowing through a VT. It also gives the foundations to study abnormal modifications of the vasculature of any organ, as in the case of liver regeneration following a partial hepatectomy.

5. References

1. Zamir, J. theor. Biol., (1999).
2. Debbaut C. et al., TBME (2012).

Acknowledgements of funding support:

European Research Council under the European Union's Horizon 2020 research and innovation program (Grant no: 864313).

BIOMECHANICAL MODELLING OF FETAL HEART WITH AORTIC STENOSIS TO PREDICT INTERVENTION EFFECTIVENESS

Laura Green (1), Wei Xuan Chan (1), Andreas Tulzer (2), Gerald Tulzer (2), Choon Hwai Yap(1)

1. Dept of Bioengineering, Imperial College London, UK; 2. Children's Heart Centre Linz, Austria.

1. Introduction

Fetal hearts can encounter abnormalities during mid-gestation, causing progressions to congenital heart malformations by birth. For example, fetal aortic stenosis with specific abnormalities such as bidirectional systolic transverse arch flow and left-to-right foramen ovale flow can progress to hypoplastic left heart syndrome (HLHS) by birth. This abnormality is thus known as evolving HLHS (eHLHS). In this case, the catheter based fetal aortic valvuloplasty (FAV) intervention can resolve the stenosis, and reduce the risk of the progression to malformation from 72% [1] to 32% [2]. However, we do not understand the biomechanical impact of disease and intervention well, and our ability to predict outcomes and select appropriate patients for intervention is poor. Here, we perform 3D echo-based finite element (FE) modelling of fetal hearts to improve understanding. We show that the back-computed myocardial contractility can predict fetal heart's response to FAV.

2. Materials and Methods

FE modelling of normal fetal hearts and those with eHLHS before and after FAV were performed. An optimization algorithm carefully matches model characteristics to scanned parameters to allow patient specificity. Post interventional conditions were simulated with pre-intervention data to predict outcomes.

3. Results

Fetal aortic stenosis results in reduced strains, stroke volumes and mitral regurgitation. Back-computation of myocardial contractility during patient-specific matching with FE modelling showed that diseased hearts had lower contractility, and that hearts with higher contractility responded positively to FAV intervention and became biventricular at birth, while those with lower contractility did not respond and progressed to univentricular malformations. Simulations showed that FAV intervention normalizes LV and left atria (LA) pressure, but the introduction of aortic regurgitation (AR), from the valvuloplasty, can prevent LA depressurization.

4. Discussion and Conclusions

Our model elucidated the biomechanics of eHLHS and FAV and showed that contractility can be used to predict if the fetal heart would respond to intervention. Contractility cannot be clinically measured, and this demonstrates the importance of modelling. To counter AR, future development of fetal transcatheter valve replacement could be useful.

5. References

1. MäKikallio, *Circulation* 113: 1401-1405 (2006).
2. Tulzer, *Ultrasound in Obstetrics & Gynecology*, 59(5):633-41 (2021).

Acknowledgements:

Imperial College startup funds (PI: Yap).

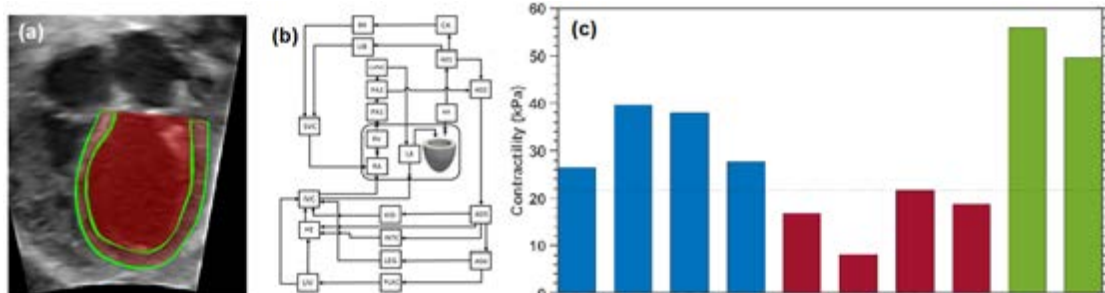


Fig 1. (a) Reconstruction of LV from 4D echo and (b) FE simulation coupled with fetal lumped parameter model. (c) Back-computed myocardial contractility, which could distinguish hearts that respond to intervention and those that do not.

CORRELATIVE ANALYSIS OF HIGHLY RESOLVED AAA WALL COMPOSITION AND STRAIN IN MICE

Achim Hegner (1), Hannah L. Cebull (2), Christopher Blase (1), Craig J. Goergen (2), Andreas Wittek (1)

1. Frankfurt University of Applied Sciences, Germany; 2. Purdue University, USA

1. Introduction

Abdominal aortic aneurysms (AAA) and dissections are degenerative diseases of the aortic wall with characteristic changes in wall microstructure, composition and elastic properties. *In vivo* full field strain measurement can provide (non invasive) information on the deformation of the aneurysmal wall, which is closely related to the elastic tissue properties. In this study, the *in vivo* strain distributions in a AAA mouse model were determined for different AAA wall regions and compared to the tissue composition, identified by histological staining.

2. Materials and Methods

Aneurysm formation was induced in five *apoE*^{-/-} mice by angiotensin-II infusion. The 3D *in vivo* wall strain was determined from 4D ultrasound imaging by use of the direct deformation estimation approach (DDE). The AAA wall composition at two positions in each aorta was analyzed from histological sections stained with Movat pentachrome (Fig. 1). [1]

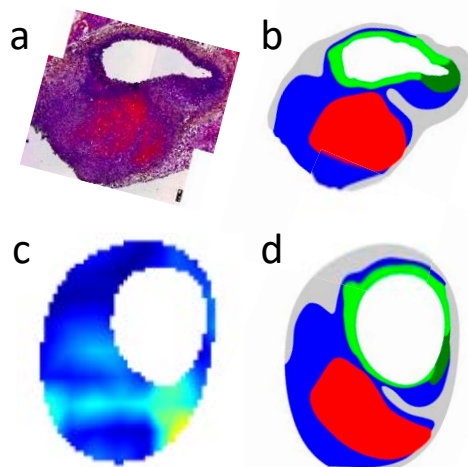


Figure 1: Workflow for the registration of *ex vivo* histological (a) and *in vivo* strain (c) data. FE model created from the histology segmentation: b) undeformed reference configuration, d) deformed configuration.

The different components of the aneurysms were manually segmented in the histological images: regions containing elastin with and without thrombus attachment, fragmented elastin, and thrombus with and without red blood cells (RBCs). Finite element (FE) models were built from the individual contours of the histological segmentations (corresponding to an unloaded configuration). The inner and outer contours of the aortic wall of each histological section were registered onto the inner and outer contour of the aortic wall from *in vivo* ultrasound imaging (deformed configuration). The strains within the different tissue regions were analyzed.

3. Results

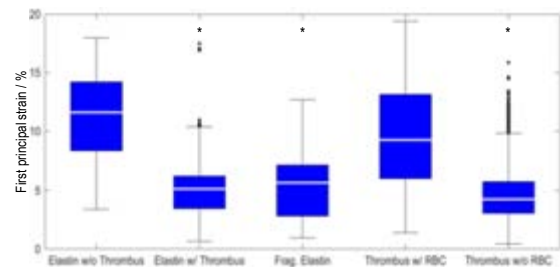


Figure 2: Strains in different wall regions ($p < 0.05$).

3D strain in the media was significantly reduced in wall regions with thrombus attachment and where the elastic lamellae were fragmented.

4. Discussion and Conclusions

In vivo strain analysis is sensitive to wall composition: strain amplitude as well as heterogeneity of the strain distribution depend on wall composition. Interestingly, thrombus with RBCs displayed relatively high strain values compared to other stiffer regions, suggesting that the size, composition, and age of intramural thrombus influence aortic dissection kinematics.

5. References

- Cebull HL et al., J Biomech Eng. 2019; 141(6): 060907 (8 pages).



THE RELATIONSHIP BETWEEN EMOTION AND INTERNET GAMING DISORDER: A MODEL MEDIATED BY HEART RATE VARIABILITY

Tsai-Chieh Lai (1), Hung-Ming Chi (2), Tzu-Chien Hsiao (1,2)

1. Institute of Biomedical Engineering, College of Electrical and Computer Engineering, National Yang Ming Chiao Tung University, Taiwan, ROC; 2. Department of Computer Science, College of Computer Science, National Yang Ming Chiao Tung University, Taiwan, ROC

1. Introduction

The individual with Internet gaming disorder (IGD) shows playing online games excessively and difficulty in self-control, which may negatively impact their emotional expressions, interpersonal relations, academic performance, or physical and mental health. Compared to baseline durations, IGD users exhibit significantly reduced high-frequency heart rate variability (HRV) during gaming [1]. However, the mediators among psychological features, physiological responses, and the risk of IGD remain unclear. This aim of this study is to investigate the HRV as the mediator between the risk of IGD and emotions with and without abdominal breathing (AB) training.

2. Materials and Methods

48 participants from the campus, Taiwan, were classified into low-risk IGD (LIGD) and high-risk IGD (HIGD) groups by the Chen Internet addiction scale (CIAS: cut-off point > 63) [2] and IGD questionnaire (cut-off point > 4) [3]. The experimental procedure consists of trial I, iso-volume maneuver [4] (as AB training, 5 min), and trial II. Each trial contains a baseline (6 min), playing an easy car racing game (7 min), playing a hard car racing game (7 min), and rest (6 min). After playing, participants fill in the Self-Assessment Manikin (emotional valence and arousal) and emotional questionnaire (anger, sadness, disgust, fear, happiness, and surprise feeling). The impedance cardiography (ICG, AESCULON, Osypka, Germany) with a sampling rate of 200 Hz was recorded during the experiment. The ICG signal was used to calculate the RR intervals of heartbeat and then transform to the frequency domain of HRV. The normalized high frequency (nHF) during baseline was subtracted from the nHF during gaming to obtain Δ nHF, the change in the parasympathetic nervous system.

The linear regression analysis was used to investigate the relation between CIAS and emotions. The mediation analysis [5] was applied to examine whether Δ nHF mediated the relationship between CIAS and emotions.

3. Results

Participants were classified into 30 LIGD (23 ± 2 years old; 26 males) and 18 HIGD (22 ± 3 years old; 15 males). The Δ nHF is negatively related to CIAS ($r = -0.53, p < 0.05$), happiness ($r = -0.55, p < 0.05$), and emotional valence ($r = -0.59, p < 0.05$). The mediation model showed that the indirect effect was significant, Δ nHF mediated the relation between CIAS and happiness during the trial I. Another mediation model showed that Δ nHF also mediated the relationship between CIAS and emotional valence during the trial I.

4. Discussion and Conclusions

The Δ nHF is the mediator between the risk of IGD and emotions (happiness and emotional valence) in the HIGD group. This study provides the initial evidence about the mechanism between IGD and emotion, which may offer to predict the risk of IGD in the future.

5. References

1. Hong SJ et al., *Front Psychiatry*, 9:429 (2018).
2. Chen SH et al., *Chin J of Psychology*, 45:279–294 (2003).
3. Petry NM et al., *Addiction*, 109(9):1399–1406 (2014).
4. Chen YC, & Hsiao TC, *IFMBE Proceedings* 45; 2015. p. 419–422
5. Shrout PE, Bolger N. *Psychol methods*, 7(4):422 (2002).

Acknowledgements:

This work was supported by the Taiwan Ministry of Science and Technology (Grant no: MOST109-2221-E009-117-MY3).



THE EFFECT OF DRIVING PRESSURE ON LUNG COMPLIANCE IN PRONE AND SUPINE POSITION IN PATIENTS WITH ARDS

Sjeng Quicken (1), Tycho Maas (1), Linda Veldmeijer (1)

1. Department of Biomedical Engineering, Eindhoven University of Technology, the Netherlands

E-mail: j.a.c.quicken@tue.nl

1. Introduction

Acute respiratory distress syndrome (ARDS) is characterized by severe respiratory failure and alterations in pulmonary mechanics. Mechanical ventilation (MV), although necessary, can initiate or aggravate lung injury. This ventilator-induced lung injury (VILI) is due to alveolar collapse and hyperdistention [1]. To minimize VILI, lung-protective ventilation is advised: low tidal volumes (V_T 4-6ml/kg) with high positive end-expiratory pressure (PEEP). Placing a patient in prone position (PP) could further minimize VILI by increasing the homogeneity of ventilation and improve oxygenation [1]. Driving pressure (ΔP), as a marker of strain, is found to be correlated with outcome in ARDS [1]. Therefore, the effect of ΔP on lung compliance is studied in prone and supine position (SP) in a respiratory computer model with two degrees of ARDS severity.

2. Materials and Methods

A geometry consisting of lung lobes and large airways was generated based on a single CT scan. The smaller airways of the geometry were automatically generated by a modified lobefilling algorithm as proposed in [3]. The terminal airways were modelled by lumped-parameter acinar models [4], with an intrapleural pressure prescribed at each acinar element. Supine and prone intrapleural pressure distributions were estimated from [5] and [6]. ARDS was modelled as a randomly distributed reduction in acinar compliance for 50% (moderate ARDS) and 90% (severe ARDS) of the acini. Ventilation settings were set to values typical for ARDS ventilation, with the total lung compliance and V_T calculated for a range of driving pressures.

3. Results

Total lung compliance is lower for a higher severity of ARDS. Lower ΔP responds to higher compliance in PP than SP for both 50% and 90%, while for higher ΔP this effect is reversed. An adequate V_T was reached for the moderate ARDS case in both SP and PP. In the severe ARDS case, adequate V_T was not achieved with the used ventilation settings (Figure 1).

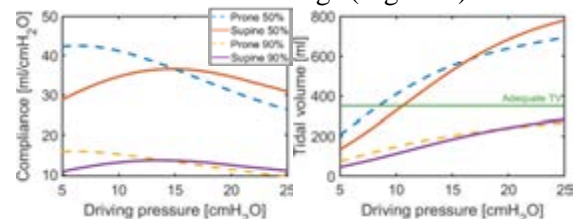


Figure 1: Total lung compliance (left) and V_T (right) for moderate and severe ARDS

4. Discussion and Conclusions

Our results suggest that with lower ΔP , lung compliance is higher in PP. However, if higher values for ΔP are needed to reach adequate values for V_T , the compliance in PP can become lower than in SP. Our results present a potential mechanism as to why a patient may not benefit from PP. Further research, using multiple ventilation settings, lung geometries and ARDS severities, are needed to further substantiate these findings.

5. References

1. Slutsky AS et al., N Engl J Med 369:2126-2136 (2013).
2. Guérin C et al., Intensive Care Med 46:2385–2396 (2020).
3. Tawhai et al., Ann Biomed Eng, 28:793–802 (2000)
4. Ismail et al., Int J Numer Method Biomed Eng, 29:1285–1305 (2013)
5. Kumaresan et al., Anesthesiology. 128:1187–1192 (2018)
6. Tawhai et al., J Appl Physiol, 107:912–920 (2009)



IN SILICO PNEUMATIC SIMULATIONS OF PATIENTS VENTILATED WITH A NEW NON-INVASIVE CLOSED-LOOP BREATHING CIRCUIT

A. Formaggio (1,2), M. De Luca (1,2), G. Putame (1,2), S. Borrelli (1,2), A. L. Audenino (1,2) and M. Terzini (1,2)

1. Department of Mechanical and Aerospace Engineering, Politecnico di Torino, Torino (Italy)

2. Polito^{BIO}Med Lab, Politecnico di Torino, Torino (Italy)

1. Introduction

CPAP (continuous positive airway pressure) therapy, widely used during the COVID-19 pandemic, is traditionally delivered in an open-configuration. A new non-invasive ventilation system was proposed [1], working in a closed-loop circuit, able to reduce the oxygen consumption, and the viral load dispersion in the environment. In this study, an *in silico* testbench was developed, and experimentally validated, aimed at the optimization of the system parameters (e.g., circuit layout, working pressure regulation, patient-specific therapy).

2. Materials and Methods

The patient and the closed-loop system were reproduced as a lumped circuit model (Figure 1) in Simscape (Mathworks). A blower imposes CPAP at the patient interface through a PID control, while a simulated muscles action generates the patient's breathing.

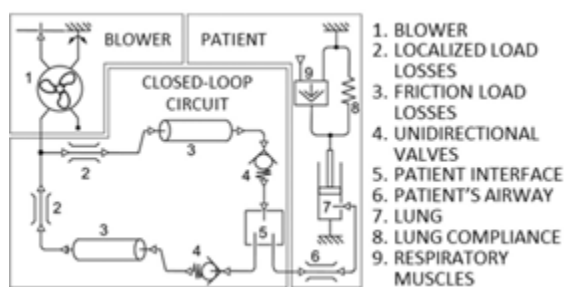


Figure 1: Schematics of the closed-loop circuit.

To validate the lumped model, the entire system was assembled *in vitro* using commercial components and connected to a lung simulator (TestChest® V3, Organix GmbH, CH). Both healthy [2] and pathologic patient conditions [3] were simulated at different therapy pressures. The flow through the patient's airway and the pressure at the patient interface were recorded and compared, computing the R^2 coefficient

through linear regression with the 45-degree line (which corresponds to a perfect overlap).

3. Results

In all tested conditions the *in silico* pneumatic model was able to capture the *in vitro* behaviour (Figure 2), with promising performance in determining both flows ($R^2 = 0.85 \div 0.95$) and pressures ($R^2 = 0.89 \div 0.94$).

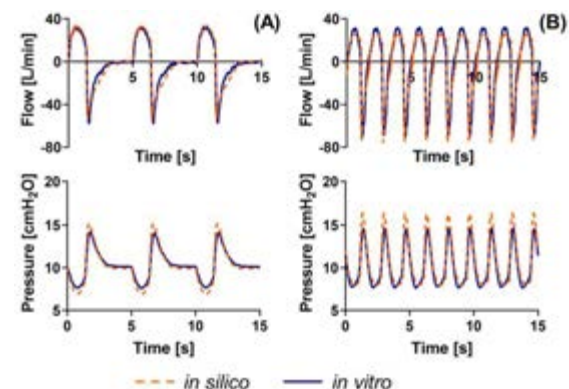


Figure 2: Representative flow and pressure curves (CPAP = 10 cmH₂O) as a function of time for the healthy (A) and COVID-19 (B) conditions.

4. Discussion and Conclusions

The developed model succeeded in reproducing CPAP therapy delivered to patients, ranging from healthy to pathologic, and constitutes an *in silico* testbench, able to investigate and optimize non-invasive ventilation circuits.

5. References

1. M. Cavaglià et al. *Artif. Organs*, 2021, 45(7): 754-761
2. J.M. Arnal et al. *Respir. Care*, 2018, 63(2): 158-168.
3. L. Gattinoni et al. *Am. J. Respir. Crit. Care Med*, 2020, 201(10): 1299-1300

Acknowledgements:

Research supported by DIVOC (INFRA-P2).



MICROMOBILITY AND GAP OPENING IN THE IMPLANT/ABUTMENT INTERFACE FOR DENTAL IMPLANTS – A SYSTEMATIC ANALYSIS

Ludger Keilig (1,2), Christin Cosse (1), Martina Wylezalek (1),
Helmut Stark (2), Christoph Bourauel (1)

1. Oral Technology, Medical Faculty, University of Bonn, Germany; 2. Department of Prosthetic Dentistry, Preclinical Education and Materials Science, Medical Faculty, University of Bonn, Germany

1. Introduction

The design of the interface between dental implants and abutments plays a crucial role for the stability of the connection between these components. Gaps due to micromotion between implant and abutment might allow fluids or bacteria to reach the inside of the implant, which might in turn have a negative influence on the implant survival [1,2]. It was the aim of this study to investigate micromobility and gap opening of three different interface designs under different loading conditions.

2. Materials and Methods

In a previous study [3], we modelled different interface designs based on a commercial implant (7 mm length, 3.7 mm diameter). From these models, we chose three different geometries: conical (15 °), flat and stepped connection (see Fig. 1). All models were available with four different index designs.

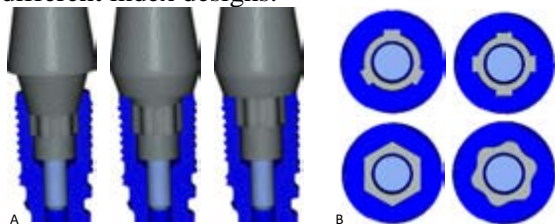


Figure 1: (A) Investigated connection designs and (B) different index shapes used as rotation stops.

In a first part, the abutments were loaded directly with a central point of force application, or with a lateral offset of 1 mm and 5 mm, respectively, in an angle of 30 ° to the implant/abutment axis. In a second part, the transversal direction of load application was varied in steps of 15 ° relative to the symmetry axis of the index shapes. In a third part, an idealised segment of mandibular bone was modelled, and an implant-supported 3-unit bridge (tooth 34 to 36) was inserted (Fig. 2) for each of the 12 connection variants. Load was applied on either the

mesial, central or distal unit of the bridge. We applied a force of 500 N in an angle of 30 ° to the implant/abutment axis in all simulations. We determined the relative movement between implant and abutment as well as measured the width of any opening gaps.

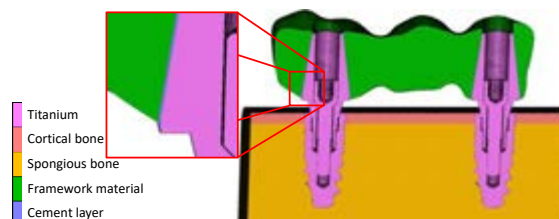


Figure 2: Cut through the cemented 3-unit bridge.

3. Results

Conical and flat connection geometry showed a different movement pattern. Conical connections reduced the gap opening (conical: 23 µm, flat: 69 µm) but increased crown movement (conical: 610 µm, flat: 140 µm). Lateral offset added a rotation around the implant axis, but did not increase the gap opening. The bridge model reduced the mobility of the loaded abutment on the cost of the unloaded abutment.

4. Discussion and Conclusions

Our current study showed that micromobility determined in idealised conditions reflected the behaviour under more complex and clinically realistic loading conditions. In all simulations, the conical connections showed compared to the flat connection a reduced gap opening at the cost of an increased abutment/crown mobility.

5. References

1. Liu Y. and Wang J., Arch Oral Biol, 83:153-160 (2017).
2. Tallarico M. et al, J Prosthodont Res, 61:233–241 (2017).
3. Wylezalek M., Doctoral Thesis, Univ. Bonn (2020).

REAL-TIME FINITE ELEMENT ASSESSEMENT OF DENTAL IMPLANT REHABILITATION TREATMENT PERFORMANCE

Mohsen Nakhaei(1), Manon Sterba(1), Laurent Badih(1), Jean-Marc Foletti(2,3), Michel Behr(2)

1. Glad Medical SAS, Salon De Provence, France

2. Laboratoire de Biomécanique Appliquée UMR T24, Université Gustave Eiffel, Marseille, France

3. Assistance publique Hopitaux de Marseille, France

1. Introduction

Several studies have used FEM to predict the risk of implant and/or peri-implant bone failure, demonstrating its ability to evaluate treatment performance [1,2]. However, FEM clinical applicability is limited due to the computational time and numerical skills required to perform and interpret. The aim of this study is to develop a real-time method for evaluating the performance and safety of a complete implant-supported dental rehabilitation treatment that would support the selection of the most appropriate treatment plan for each patient.

2. Materials and Methods

In the context of the Medscope® project, a user-friendly software interface was developed (Fig. 1-a), to be used by clinical practitioners.

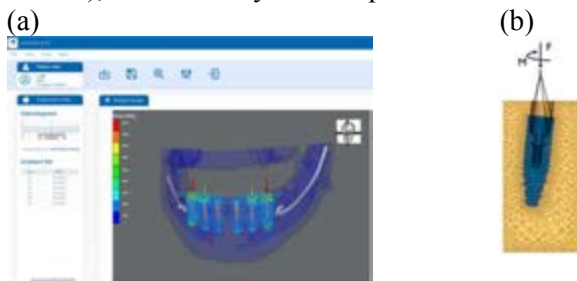


Figure 1. (a) Medscope®'s user interface (b) Bone implant unit (BIU)

The proposed methodology consists of the following steps. 1) Extraction of patient-specific mechanical properties using CBCT imaging. 2) Application of the load on the superstructure and calculation of the resulting load on each implant. The superstructure was modeled as 3D bar elements under a total force of 500 N with an angle of 25° to the implant axis, based on previous studies [3]. 3) Automatic creation of the FEM for each implant and the surrounding bone (referred to as the bone implant unit (BIU)), (Fig. 1-b). The contact between implant and bone was modelled as continuous mesh to simulate secondary stability and may be set as sliding contact to simulate primary stability condition.

FE calculations for each BIU were run in parallel using an implicit solver (Optistruct®, Altair, USA). 4) Calculation of two scores indicating the treatment quality: Bone safety index (BSI), based on the maximum averaged von Mises stress (VMS) measured on cortical and trabecular bone relative to their damage thresholds (80 MPa and 40 MPa, respectively [4]) and implant loading ratio (ILR) that indicate how the loading is distributed between the BIUs in a treatment (i.e. ILR=100% means equal maximum stress for all BIUs). Based on this method, two treatment plans were evaluated: a fixed full bridge supported by 6 and 4 implants (All-on-six and All-on-Four, respectively).

3. Results

The calculation time for each treatment was 4 minutes. Similar maximum bone stresses at the distal implants were observed for the two treatments. Higher ILR was observed for the All-on-Four treatment compared to the All-on-six one indicating a better stress distribution in the first case (Table 1).

Treatment	Max. VMS [MPa]	Min. BIS [%]	ILR [%]
All-on-Six	12.5	80	10
All-on-Four	16.9	73	20

Table 1: Associated indexes for the two treatments

4. Discussion and Conclusions

The results were in good agreement with the experimental observations, such that distal implants absorb the largest amount of the force [5]. The combination of these indexes supports the choice of All-on-four treatment for the patient. The presented method allowed a fully automated reduced-time FE analysis which could be applied to help surgeons in validating and improving their treatment plan.

5. References

1. Dogru et al. J Mech Med Biol, 18.02, 2018.
2. Jiménez, et al. Dental materials 36.7, 2022.
3. Doğan, et al. Clin. Implant Dent. Relat., 2014.
4. Lacroix, D. et al, M.P.B.M., pp. 303-336, 2021.
5. Duyck, et al. Clin. Oral Implants Res, 11.5, 2000.



BIOMECHANICAL EVALUATION OF NARROW TMJ IMPLANT

Rajdeep Ghosh (1), Anoushka Gupta (1), Abir Dutta (2), Garima Khandelwal (3), Ajoy Roychoudhury (3), Sudipto Mukherjee (1), Anoop Chawla (1), Kaushik Mukherjee (1)

1. Department of Mechanical Engineering; Indian Institute of Technology Delhi, India; 2. Department of Ortho and MSK Science, Division of Surgery & Interventional Sci; Faculty of Medical Sciences, University College London, UK; 3. Department of Oral and Maxillofacial Surgery; Centre for Dental Education and Research, All India Institute of Medical Sciences Delhi, India

1. Introduction

Despite the short-term success, parameters responsible for the long-term durability of a mandibular prosthesis used to reconstruct the temporomandibular joint (TMJ) are not fully understood. Although several *in silico* studies [1-3] investigated the stress-strain behaviour around a TMJ prosthesis, most of these studies used a generalized TMJ implant along with simplified loading conditions and mandibular material properties. The present investigation focuses on the biomechanical evaluation of a patient-specific reconstructed mandible with a commercial narrow mandibular implant under the physiological mastication cycle [4].

2. Materials and Methods

A patient-specific model of an intact mandible and a narrow (size = 45 mm) TMJ implant (Zimmer Biomet Microfixation System, Jacksonville, FL, USA) were reconstructed separately from CT-scan datasets. Cylindrical screws were modelled and further virtually implanted within the mandible and implant. Region-specific orthotropic material properties [4] were assigned to cortical bone, while teeth, implants (Co-Cr alloy), and screws (Ti alloy) were modelled with isotropic material properties. Models were simulated under the right molar biting condition [4]. All the interfaces were assumed to be bonded.

3. Results

Under the contralateral occlusion, higher principal tensile strain were observed around the reconstructed side (left) of the mandible as compared to the intact one (Fig. 1c). The highest von Mises stresses developed in the mandibular prosthesis (~280.28 MPa) as well as the screws (~685.30 MPa) were, however, found to be lower than the average yield strength. The

screws in the inferior portion of the implant experienced higher stresses as compared to those in the superior part.

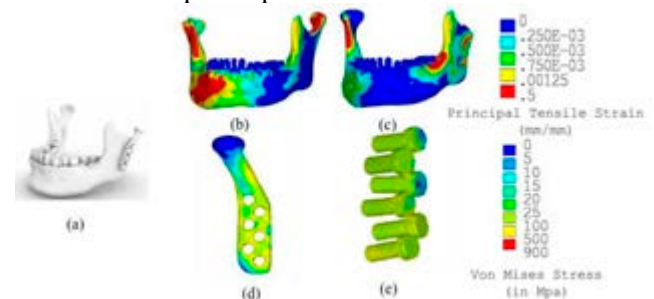


Figure 1: (a)implanted mandible; principal tensile strain distribution in (b) intact mandible and (c) reconstructed mandible; von Mises stress in (d) mandibular prosthesis and (e) mandibular screws

4. Discussion and Conclusions

Although the peak stress observed around the prosthesis and screws were under safe yield limit, the high stresses developed towards the superior implant portion need to be minimized which warrants further design optimization of the prosthesis.

5. References

1. Kashi A et al., Journal of Dental Research; 89(3):241-245 (2010).
2. Bekcioglu B et al., Journal of Oral and Maxillofacial Surgery;75(11):2316-2322 (2017).
3. Pinheiro M et al., Scientific Reports ;11(1):14034 (2021).
4. Koriath TWP et al., American Journal of Physical Anthropology; 88(1):69-96 (1992).

Acknowledgements:

This work was supported by the Indo-German Science & Technology Centre (IGSTC), a bilateral institution of Government of India (DST) and Federal Government of Germany (BMBF), under grant no. IGSTC/Call 2020/add-bite/48/2021-22/260

Biomechanical Assessment of Multi-Rooted Root Analogue Implants

Mostafa Aldesoki (1), Ludger Keilig (1,2), Istabrak Dörsam (1,2), Christoph Bourauel (1)

1. Oral Technology, University Hospital Bonn, Germany; 2. Department of Prosthodontics, University Hospital Bonn, Germany

1. Introduction

Threaded implants (TI) have been successfully used for the replacement of missing teeth. Although TI have a high success rate for late implant placement, they still have certain limitations as immediate implants due to their standard design in terms of diameter and length compared to customised root-analogue implants (RAI) [1]. The benefits of RAI over TI are decreased number of surgeries, less initial bone loss, and uncomplicated placement [2]. The aim of this study was to compare the biomechanical behaviour of different RAIs experimentally and numerically to the conventional TIs.

2. Materials and Methods

A multi-rooted RAI model was designed based on tooth 47 obtained from cone-beam computed tomography (CBCT). RAIs were subdivided into four groups (two materials: titanium, zirconia; two manufacturing techniques: milling, 3D printing, each N = 5). RAIs and TIs (as control) were inserted into bone replacement blocks (Sawbones, Vashon, USA) and loaded up to 100 N in a customised biomechanical setup (hexapod measurement system, HexMeS) [3]. Furthermore, finite element (FE) models of the examined RAIs and TIs were generated and loaded with and without osseointegration in different directions (Figure 1).

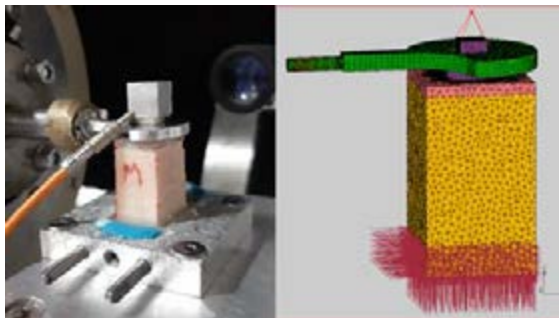


Figure 1: The experimental model (HexMeS, to the left) and the respective numerical model (right).

3. Results

In vitro measurements showed insignificant difference in the stability between the TIs and the RAIs. This could also be reproduced in the finite element simulations as shown in table 1. There were only minor differences between the various RAIs in both, experimental and numerical investigations.

Table 1: Displacement (Z) at Force = 50 N in μm

Group	TI	RAI	p value
Experimental (HexMeS)	47 ^A	53 ^A	<0.001*
Numerical (FEA)	57	52	<0.001*

Different superscript letters indicate a statistically significant difference within the same row. *Significant (p<0.05)

4. Discussion and Conclusions

RAIs showed promising biomechanical behaviour both, experimentally and numerically. TIs revealed a more predictable biomechanical behaviour compared to RAIs due to its standard design.

5. References

- Chen et al, J Prosthet Dent, 112:1088-1095, 2014.
- Mangano et al, Lasers Med Sci, 29:1321-1328, 2014.
- Keilig et al, Biomed Tech, 49:208-215, 2004.

Acknowledgements:

This work was supported by a grant from the German academic exchange service (DAAD, 2019/20, 57440921).

APPLICATION OF A NEW IMPLANT FOR DENTAL RESTORATION IN CASE OF STRONGLY DEGRADATED MANDIBULAR BONE

Cynthia Dreistadt, Victor Creuillot, Pawel Lipinski

Université de Lorraine, Laboratoire d'Etude des Microstructures et de Mécanique des Matériaux (LEM3), France

1. Introduction

Numerical simulation could help clinicians to study the effect of dental restoration by the implant system on the masticatory apparatus and test innovative concept in various situations such as strongly degraded mandibular bone. The aim of this study was to analyse the incidence of a new implant type on the peri implant bone and temporomandibular joints through a complete 3D finite element model of the mastication system.

2. Materials and Methods

Mandibular bone degradation was carried out numerically on the healthy model presented by Creuillot et al. [1] and validated by clinicians, see acknowledgments. Cortical and cancellous anisotropic bones were defined with various mechanical bone properties reproducing different classes of bone degradation. All-on-four prosthetic solution (fig 1a) with two types of implants (fig 1b) were considered; the classical straight implants and a new T-implant [2]. Mechanical load was applied by the muscular contractions as in [1] and results were analysed for a clenching force of 140N.



Figure 1: a) Representation of the 3D FEM model and b) implant systems tested.

3. Results

Occlusal states obtained were similar for all the simulations whatever the bone class. The distribution of occlusal forces was: 17% supported by each condyle and 66% by the implants. In the peri-implant zone, extreme values of stress are observed in the cortical bone

while major values of strain concern the cancellous bone near posterior implants, fig 2. These values increase with the decrease of bone quality. The critical values of strain energy density (SED) were generally observed on the peri-implant crest bone.

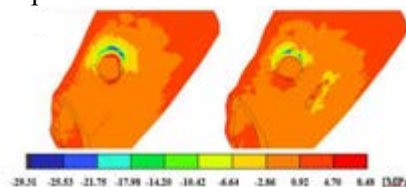


Figure 2: Comparison of stress fields in peri-implant zones for classic and novel implants

4. Discussion and Conclusions

Occlusal forces supported by the implants depend on the occlusion areas. The most loaded implant is close to the zone supporting maximal occlusal force. There is no risk of implant failure since the von Mises stress in the implant was much lower than the yield limit. A significative difference between the two implant systems, especially for specific strongly degraded bone was observed. For both implants types no damage risk was found considering Frost strain threshold [3]. However, moderate clenching force was considered here. In the case of bruxism or biting, occlusal forces could be much higher increasing risk of bone damage and implant loss.

5. References

1. Creuillot V, Dreistadt C, Kaliński KJ, Lipinski P, AISC, 2016; 414
2. M. Daas, K. Dada, WO 2014203149 A1 patent
3. Frost HM, Angle Orthod.,2004;74(1):3-15

Acknowledgements:

The authors would like to thank clinicians Drs M. Daas and K. Dada for precious advises and the critical evaluation of bone degradation considered in this work.



FINITE ELEMENT MODELING OF THE MASTICATORY SYSTEM: APPLICATION TO BRUXISM

Elodie Ehrmann (1,2), Sara Feghali (1,2), Marie Bernabeu (2), Yannick Tillier (1)

1. CEMEF Mines Paris - PSL, France; 2. CHU-Nice, France

1. Introduction

Bruxism is responsible for temporo-mandibular joint (TMJ) disorders and tooth wear [1]. This work is part of a larger project that aims to better understand the biomechanical impact of such a parafunction on the TMJ and teeth, by comparing two finite element models (FEMs) of the masticatory system of a patient, before and after an oral rehabilitation. Retrieving the geometry of the different tissues from medical images is relatively common. The originality of this work is to propose to use an extraoral device (Modjaw® [2]) to record the kinematic data of a patient and apply them, as a loading condition, to the FEMs.

2. Materials and Methods

A FEM corresponding to the situation before oral rehabilitation of a 37-year-old male patient with mild bruxism was created. Geometric data were obtained after the alignment of multimodal medical images (CBCT, MRI, 3D scan acquisition of a dental arch plaster model). The bones, the soft tissues, and the teeth were modelled (segmented and meshed with Mimics (Materialize®), and transferred to the FE analysis software FORGE (Transvalor®). Mechanical properties were assigned to each anatomical structure (all of which are considered linear elastic materials). Particular attention was paid to the application, as a loading condition, of the real kinematics of the patient. For this purpose, he was asked to perform 3s grinding movements (a right and then left latero-deviation). The Modjaw® medical device was used to record, as a function of time, the coordinates of 3 points denoted I, RC and LC on Fig. 1 and corresponding respectively to the inferior incisal edge point, and 2 points away from the right and left condyles. Three rigid objects were then created in the FEM and assigned the same coordinate evolutions to set the mandible in motion.

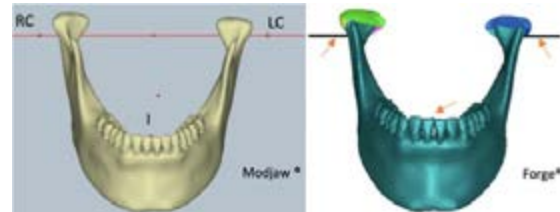


Figure 1: Application in Forge® of the boundary conditions recorded by Modjaw®

3. Results

The von Mises stress distribution, given by the FEM, on the teeth and in both joints during a grinding cycle was analysed and compared to the experimental contact areas given by the Modjaw® device (Fig. 2).

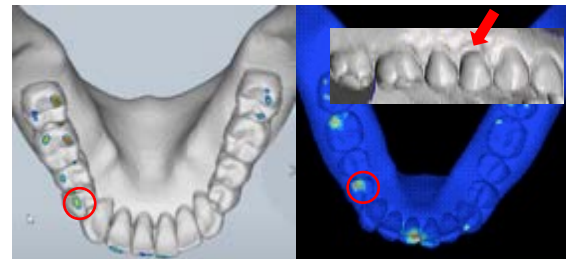


Figure 2: Right lateral excursion. Comparison of von Mises stress distribution (FEM, right) vs dental contact areas (Modjaw®, left). Teeth 44/14 in red.

4. Discussion and Conclusions

The similarities observed seem to confirm the accuracy of the chosen approach, although we can note a very high level of stress at the I-point used to move the mandible. It is interesting to note that tooth 44 at the neck of which a stress peak is observed numerically (red circles in Fig. 2) is slightly worn in the patient and that gingival recession was clinically observed on the facing tooth 14 (red arrow in Fig.2).

5. References

1. Guillot M et al., CRANIO®; 39(5):412-423 (2021).
2. Bapelle M et al., CRANIO®; 1-7 (Published online: 06 Nov 2021).



ANGIOGRAPHY-BASED COMPUTATIONAL FLUID DYNAMICS SIMULATIONS TO PREDICT MYOCARDIAL INFARCTION

Claudio Chiastra (1), Maurizio Lodi Rizzini (1), Alessandro Candreva (1,2), Takuya Mizukami (3),
Jean-Paul Aben (4), Carlos Collet (3), Diego Gallo (1), Umberto Morbiducci (1)

1. Dept. of Mechanical and Aerospace Engineering, Politecnico di Torino, Italy; 2. Dept. of Cardiology,
USZ, Switzerland; 3. Cardiovascular Center Aalst, Belgium; 4. Pie Medical Imaging BV, Netherlands

1. Introduction

Myocardial infarction (MI) is the most frequent cause of mortality in developed countries. Given the severity and high incidence of MI, the identification of predictive markers for this pathology is of paramount importance. Recently, hemodynamic features have been linked to the vulnerable transformation of atherosclerotic lesions and their rupture, which are mechanisms leading to MI [1]. In this context, we propose a computational workflow for the hemodynamic analysis of diseased coronary arteries in a standard clinical setting aiming to identify lesions culprit for future MI.

2. Materials and Methods

188 vessels were retrospectively selected considering patients suffering from acute MI who had (i) an angiography performed between 1 month and 5 years before the event, (ii) a mild lesion culprit for MI (future culprit, FC) at the baseline angiography and (iii) at least one additional lesion non-culprit for MI (non-future culprit, NFC) in the other major epicardial vessels [2]. The dataset included 80 FC and 108 NFC lesions. The computational workflow (Fig. 1) consisted of [2]: (i) 3D vessel reconstruction from angiography; (ii) transient computational fluid dynamics (CFD) analysis; (iii) computation of hemodynamic descriptors; (iv) statistical analysis. A near-wall hemodynamic analysis was performed by computing the time-averaged wall shear stress (TAWSS) and the topological shear variation index (TSVI), which measures the variability in the wall shear stress (WSS) contraction/expansion action exerted on the endothelium over the cardiac cycle [3]. Additionally, we tested the hypothesis that blood flow rotational energy, quantified in terms of enstrophy, may be a predictor of MI.

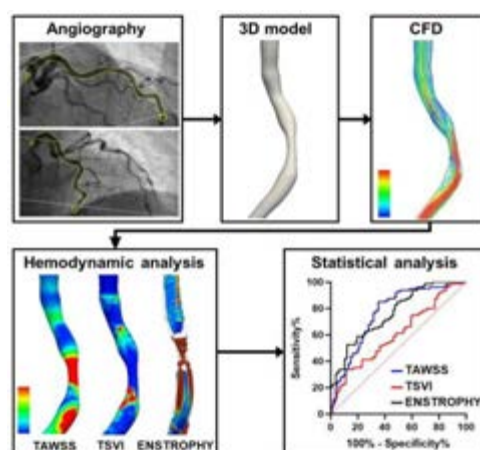


Figure 1: Computational workflow.

Results

~15 minutes per patient were required to obtain the WSS results using a prototype software for clinical use (CAAS Workstation, WSS tool, Pie Medical Imaging). The analysis of the ROC curves (Fig. 1) highlighted that TAWSS was a moderate MI predictor (AUC=0.61; 95%CI 0.53-0.69, $p=0.011$). Differently, both enstrophy (AUC=0.76, 95%CI 0.70-0.83, $p<0.001$) and TSVI (AUC=0.77; 95%CI 0.70-0.84, $p<0.001$) were strong MI predictors.

4. Discussion and Conclusions

The proposed approach based on hemodynamic analysis from standard angiographic images and CFD simulations proved to be effective in predicting lesions culprit for future MI with times compatible with the clinical practice (at least for the WSS analysis). Further clinical trials are recommended to enforce the promising results here presented and to translate this concept into clinical practice.

5. References

1. Kumar et al, J Am Coll Cardiol, 72:1926-35, 2018.
2. Candreva et al., Atherosclerosis, 342:38-35, 2022.
3. Mazzi et al., Ann Biomed Eng, 49:2606-21, 2021.

A DISCUSSION ON STRATEGIES FOR THE IN SILICO DEPLOYMENT OF LEFT ATRIAL APPENDAGE OCCLUDERS

Francesca Danielli (1), Benigno Marco Fanni (2), Emanuele Gasparotti (2), Lorenza Petrini (3), Giancarlo Pennati (1), Francesca Berti (1)

1. DCMC, Politecnico di Milano, Italy; 2. Fondazione Toscana Gabriele Monasterio, Massa, Italy; 3. DICA, Politecnico di Milano, Italy

1. Introduction

Left Atrial Appendage (LAA) occlusion (LAAO) with self-expandable devices is a percutaneous procedure used to prevent thrombus formation in patients with atrial fibrillation. Despite the demonstrated safety and efficacy, the intra-subject complexity and the inter-subject heterogeneity of the LAA hinder the device sizing and positioning, resulting in eventual postprocedural drawbacks, such as peri-device leakage [1]. Finite Element (FE) modeling represents an effective tool for investigating different implant scenarios, which can be exploited to guide pre-procedural planning. However, the limited literature on LAAO modeling [2] focuses on the device deployment without providing evidence of a thorough investigation of those anatomical and device-related features affecting the procedure outcome. This work aims at discussing the impact of different strategies on the simulation output of an LAA occluder deployment.

2. Materials and Methods

The CAD model of the Watchman FLX device (Boston Scientific) was obtained through high-fidelity CT imaging reconstruction, discretized with 1D elements, and validated following the pipeline in [3]. First, an accurate representation of the device, considering the PET fabric sewn to the device, conceived to occlude the LAA ostium, and the hooks allowing the anchoring to the tissue, was considered as a reference. Then, a simplified model was prepared (Fig. 1a). Different idealized parametric conduits were developed to clear from patient-specific aspects but mimicking LAA anatomical features affecting the deployment, in particular (Fig. 1b): i) the eccentricity of the LAA ostium, ii) the length of the landing zone, iii) the initial positioning of the crimped device, iv) the device nominal oversizing, v) the LAA wall stiffness.

A total of 64 different cases were simulated, considering the variability of the aforementioned features and the two device models. The procedural outcome was evaluated according to different indicators (e.g. device relative position to the ostium, maximum device diameter, device-wall distance). According to these results, the best modeling strategy was used for investigating patient-specific cases.

3. Results

Preliminary results showed a relevant impact of the accurate device modeling on the outcome (Fig. 1c). The use of the simplified conduit confirmed the crucial role of the introduced parameters on the device sizing and positioning.

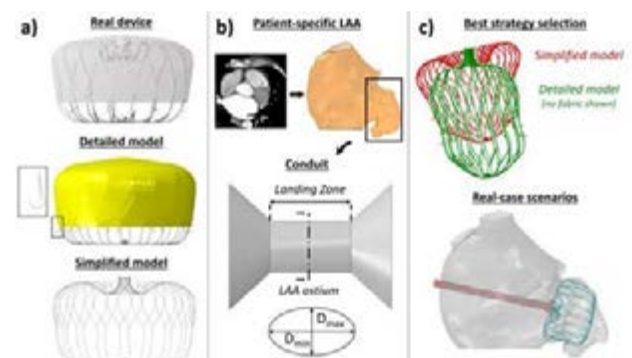


Figure 1: a) Device models; b) Idealized conduits; c) Deployment simulations.

4. Discussion and Conclusions

This study demonstrated the importance of using a proper modeling strategy for simulating the LAAO considering all those relevant anatomical features that may affect the final device positioning.

5. References

1. Hong et al., Sci Rep 12, (2022).
2. Bavo et al., J Cardiovasc Med Biol 14, (2020)
3. Zaccaria et al., Med Eng Phys 82, (2020)



NUMERICAL SIMULATIONS TO EVALUATE THE DEVICE-RELATED EFFECTS IN ATRIAL FIBRILLATION PATIENTS

Emanuele Gasparotti (1), Benigno Marco Fanni (1), Katia Capellini (1), Alberto Clemente (2), Sergio Berti (3) and Simona Celi (1)

1. BioCardioLab, Fondazione Toscana G. Monasterio, Italy; 2. Radiology Unit Fondazione Toscana G. Monasterio, Italy; 3. Adult Cardiology Unit, Fondazione Toscana G. Monasterio, Italy.

1. Introduction

The Left Atrial Appendage (LAA) is responsible for more than 90% of thrombi formation in patients with non-valvular Atrial Fibrillation (AF) [1]. To reduce the risk of cardioembolic events, LAA Occlusion (LAAO) is a recommended treatment for those patients unable to take anti-coagulation therapy [2]. However, Device-Related Thrombosis (DRT) after LAAO have an incidence ranging from 2% to 16% [3]. In this context, Computational Fluid Dynamics (CFD) is a powerful tool to assess the hemodynamics within LAA [4]. This study aims to investigate the effects of different LAAO devices on the hemodynamics at the left atrial face of the device.

2. Materials and Methods

Patient-specific LA models before and after LAAO were obtained from CT images. Patients with three different implanted devices were considered: Watchman, Watchman FLX and Amulet Amplatzer. The models were discretized with a tetrahedral mesh (1 mm average element size). CFD simulations were conducted in an AF scenario, using an inflow pressure condition of 8 mmHg at pulmonary veins and an outflow velocity profile at mitral valve. The mesh generation process and CFD simulations were performed in ANSA and ANSYS Fluent, respectively. CFD results were analysed in terms of pressure, velocity, and main hemodynamic indices: Time-Averaged Wall Shear Stress (TAWSS), Oscillatory Index (OSI), Endothelial Cell Activation Potential (ECAP), and Relative Residence Time (RRT).

3. Results

Significant differences were found for all parameters not only between pre- and post-LAAO but also among the different devices. Figure 1 depicts the velocity field from CFD

simulations of each patient after LAAO, showing the zones with high risk of DRT. It was possible to note that the LAAO performed for the first patient led to a greater reduction for ECAP and RRT values together with a minor area affected by OSI values closer to 0.5.

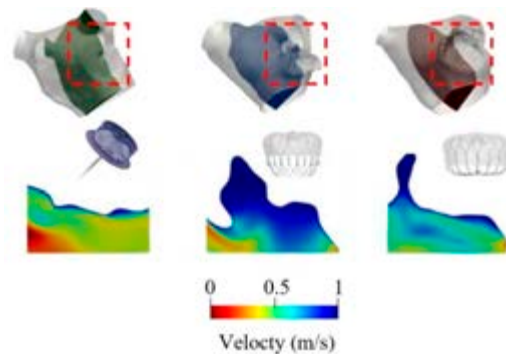


Figure 1: Detail of velocities after LAAO of the three analysed devices.

4. Discussion and Conclusions

The combined analysis of different hemodynamic indices in the pre- and post-LAAO conditions considering various type of devices revealed different effects on the hemodynamics. The residual presence of zones high ECAP and RRT associated with large OSI, that mean regions with low velocities and complex flow pattern, can suggest a non-negligible risk of DRT.

5. References

1. Holmes DR et al. J. Am. Coll. Cardiol. 2014.
2. Berti S et al. Appl. Sci. 2018. 11, 2228–2231.
3. Sedaghat A et al. Circ. Cardiovasc. Interv. 2021.
4. Fanni BM et al. Appl. Sci. 2020.

Acknowledgements:

This work was funded by the Italian Ministry of Health with the project “PLACE - Planning Laa Closures” (RF-2021-12375208).

ON THE IMPORTANCE OF THOROUGH IN SILICO DRUG-COATED BALLOON REPLICAS TO SIMULATE COATING TRANSFER

Efsthathios Stratakos (1), Luca Antonini (1), Gianluca Poletti (1), Francesca Berti (1), Lorenza Petrini (2), Giancarlo Pennati (1)

1. LaBS – Dept. of Chemistry, Materials and Chemical Engineering, Politecnico di Milano, Milan, Italy;
2. Dept. of Civil and Environmental Engineering, Politecnico di Milano, Milan, Italy

1. Introduction

Drug-Coated Balloons (DCBs) provide a promising minimally invasive solution to treat stenotic arteries, by advocating the leave-nothing-behind strategy and by offering the potential to deliver the drug-coating homogeneously on the lesion. This should act as a long-term, homogeneous, local drug source. However, recent animal studies revealed limited coating transfer [1]. Moreover, *in vitro* studies of DCBs suggested the Contact Pressure (CP) between the balloon and the endothelium to be the leading cause of the transfer [2]. Considering the above, this work suggests a detailed angioplasty balloon computational model aiming to predict the spatial distribution of CP during a DCB angioplasty.

2. Materials and Methods

A finite element model of an angioplasty balloon was implemented, taking into account the realistic, longitudinal non-uniform wall thickness and folding process. The folded balloon was then expanded in idealized human femoral artery models (cylinders with suitable wall stiffness), using explicit, quasi-static simulations. Various conditions were investigated (Table 1), to evaluate the CP spatial distribution for a wide range of Inflation Pressures (IPs).

Conditions	Value 1	Value 2	Value 3
<i>Oversizing (%)</i>	15	25	40
<i>Length (mm)</i>	20	40	100
<i>Friction</i>	0	0.3	0.8
<i>Positioning</i>	Concentric	Eccentric	Inclined
<i>Artery stiffness</i>	Healthy	Stiffening 1	Stiffening 2

Table 1: Balloon expansion simulation conditions.

3. Results

Figure 1 represents a 2D colour map of the CP on the arterial wall. The CP after full expansion (for IPs equal to 1.1-1.5 MPa) of the balloon

catheter reveals one order of magnitude lower values with respect to the concurrent IP. Furthermore, the distribution is highly heterogeneous, because the initial irregular contact formed linearly patterned contact zones, while the balloon's non-uniform thickness creates higher CP in the vessel's central part.

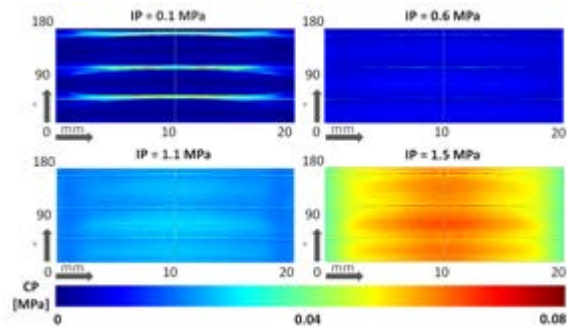


Figure 1: CP values among different IP maps. The x-axis represents the length and the y-axis the circumference.

4. Discussion and Conclusions

Conclusively, this study disclosed the highly irregular contact between the balloon and the artery, which is completely justified by the balloon's features, since a cylindrical geometry was adopted for the artery. To the best of the authors' knowledge, this is the first evidence and interpretation of systematic, heterogeneous CP developed during angioplasty, that could explain the animal studies observation with limited coating transfer.

5. References

1. A. R. Tzafiriri et al., Biomaterials, vol. 260, p. 120337, Nov. 2020
2. G. H. Chang et al. Sci Rep, vol. 9, no. 1, p. 6839, Dec. 2019

Acknowledgments:



This project has received funding from the European Union's Horizon 2020 research and innovation programme under the Marie Skłodowska-Curie grant agreement No 956470.



MACHINE LEARNING FOR FAST COMPUTATIONAL FLUID DYNAMICS CARDIOVASCULAR ASSESSMENT

Endrit Pajaziti, Raphael Sivera, Claudio Capelli, Silvia Schievano

UCL Institute of Cardiovascular Science & Great Ormond Street Hospital for Children, London, UK

1. Introduction

In cardiovascular disease, patient 3D imaging by magnetic resonance (MR)/ computed tomography provides clinicians with information on patient anatomical and physiological conditions. However, in congenital heart disease (CHD), lesions are often complex, and, in some cases, imaging alone fails to provide conclusive information. In the past 20-30 years, image-derived 3D modelling applications, such as computational fluid dynamics (CFD), have shown major advancements and successful use in CHD management. However, due to current software/hardware limitations, these applications have remained largely isolated to research settings. The aim of this study was to leverage machine learning (ML) to replicate conventional CFD modelling in much shorter times, and thus lower the adoption barrier for CFD in clinical practice.

2. Materials and Methods

3D MR data from 67 patients post-surgical repair of aortic coarctation were processed to create a statistical shape model (SSM, Deformetrica). Principal component analysis (PCA) was used to reduce the shape dimensionality and a population of 3,000 synthetic aortic anatomies was generated by randomly sampling the shape space. CFD (Fluent, Ansys Technologies) was performed on the 3,000 synthetic aortas to train/test the model. A deep neural network was set-up with shape PCA as inputs and pressure/velocity PCA scores from the CFD simulations as output [1].

3. Results

35 PCA modes were required to capture 99% of the shape variance in the population, whilst 20 modes were needed for 99% of pressure and 55 for 87% of velocity variance, respectively. Inference performed on 200 test shapes resulted in average errors of $6\pm 3\%$ and $4\pm 1\%$ for

pressure and velocity, respectively. The ML-based model performed CFD in ~ 0.075 seconds (4,000x faster than the solver).

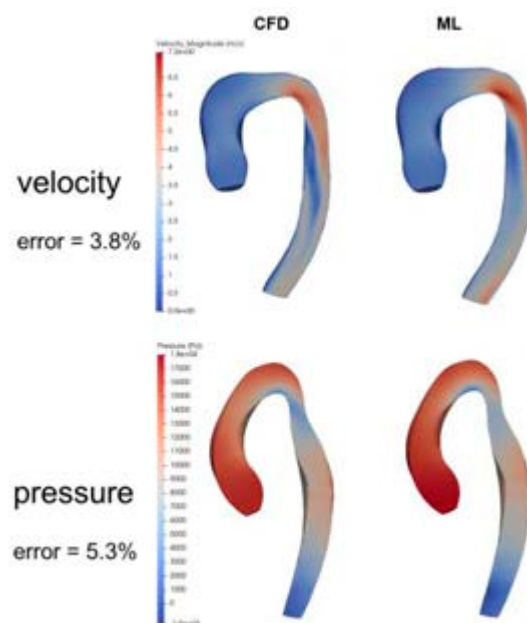


Figure: Example of velocity and pressure field distributions for those aortas with median errors for velocity and pressure, respectively.

4. Discussion and Conclusions

This study shows that results from conventional CFD simulations can be reproduced using ML at a much faster rate, in an automatic process, and with high accuracy. ML derived parameters can be used to extend 3D imaging and support diagnosis and management of CHD.

5. References

1. Liang L, Mao W, Sun W. Journal of Biomechanics. 2020;99.

Acknowledgements:

The work was supported by the BHF (PG/17/6/32797), EPSRC (EP/N02124X/1) and the ERC (ERC-2017-StG-757923).



DAMAGE MECHANICS OF BIOLOGICAL TISSUES IN RELATION TO VISCOELASTICITY: COMPUTATIONAL IMPLEMENTATION

Gerard A. Ateshian (1), Kimberly R. Kroupa (1), Courtney A. Petersen (1)
 Brandon K. Zimmeman (2), Steve A. Maas (3) Jeffrey A. Weiss (3)

1. Columbia University, USA; 2. Lawrence Livermore National Laboratory, USA;
 3. University of Utah, USA

1. Introduction

The objective of this study was to examine the theoretical foundations for the damage and failure mechanics of anisotropic biological tissues in relation to viscoelasticity, and to provide computational tools to model viscoelastic tissue damage and failure in the open-source finite element code FEBio [1].

2. Materials and Methods

Tissue damage occurs when strong bonds, such as covalent bonds in the solid matrix of a biological tissue, break in response to loading. This type of failure is described as elastic damage, under the idealizing assumption that strong bonds behave elastically. Viscoelasticity arises from three types of dissipative mechanisms: (1) Friction between molecules of the same species, which is represented by the tissue viscosity. (2) Friction between fluid and solid constituents of a porous medium, which is represented by the tissue hydraulic permeability. (3) Dissipative reactions arising from weak bonds breaking in response to loading, and reforming in a stress-free state, such as hydrogen bonds and other weak electrostatic bonds. When a viscoelastic tissue is subjected to loading, some of that load may be temporarily supported by those frictional and weak bond forces, reducing the amount of load supported by elastic strong bonds and thus, the extent of elastic damage sustained by those bonds. This protective effect depends on the characteristic time response of viscoelastic mechanisms in relation to the loading history.

3. Results

In a recent study, we fitted the tensile stress-relaxation response of an immature bovine articular cartilage sample from [2] to the reactive viscoelasticity framework [3]. Here,

we use this model to examine the tensile and damage response of immature bovine cartilage to a linearly ramping engineering strain from 0 to 60%, at strain rates varying from 0.01%/s to 1000%/s, by decade increments. A damage cumulative distribution function, which follows a Weibull distribution, was used, as reported in our earlier study of elastic damage [4]. All analyses were performed using FEBio (febio.org) [1]. The stress-strain response at all strain rates is shown in Fig. 1a and the failure stress versus strain rate is shown in Fig. 1b.

4. Discussion and Conclusions

The presentation of this study may better inform the biomechanics community on the topic of viscoelastic damage, providing the theoretical foundations and computational tools for addressing an important component of biological tissue mechanics, namely the topic of tissue failure under different loading conditions.

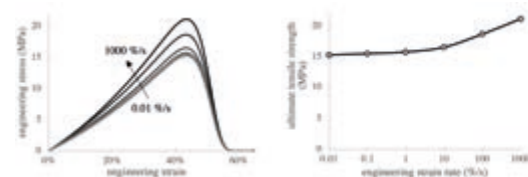


Fig. 1. FE simulation of viscoelastic damage response of immature bovine cartilage at various strain rates. Stress-strain and ultimate strength.

5. References

1. Maas SA, Ellis BJ, Ateshian GA, Weiss JA. *J Biomech Eng.* 2012;134(1):011005.
2. Park S, Ateshian GA. *J Biomech Eng.* 2006 Aug;128(4):623-30.
3. Ateshian GA, Petersen CA, Maas SA, Weiss JA. *J Biomech Eng.* 2023;145(1):011004
4. Nims RJ, Durney KM, Cigan AD, Dusséaux A, Hung CT, Ateshian GA. *Interface Focus.* 2016 Feb 6;6(1):20150063.

Acknowledgements: NIH R01 GM083925.



A MODULAR FRAMEWORK FOR STRONG 3D/0D COUPLING IN CARDIAC MECHANICS SIMULATIONS

Aaron L. Brown (1), Zinan Hu (1), Vijay Vedula (2), Alison L. Marsden (1)

1. Stanford University, USA; 2. Columbia University, USA

Corresponding author: Aaron Brown, abrown97@stanford.edu

1. Introduction

Due to the strong physical coupling between the heart and the blood circulation, accurate and efficient numerical coupling methods remain an active area of research [1,2,3]. In this work, we present an efficient, modular, strong coupling framework for coupling a 3D mechanical simulation of the heart (structure or fluid) to a 0D fluid model of the circulation.

2. Materials and Methods

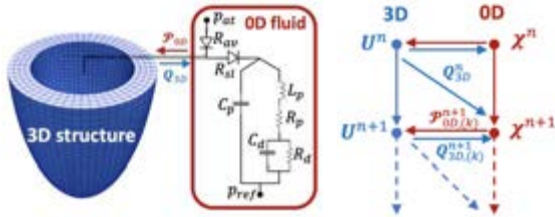


Figure 1: Left: Schematic showing an idealized left ventricle (3D structure) coupled to a lumped-parameter model of circulation (0D fluid). Right: Communication pattern in our coupling. \mathbf{U} are the 3D state variables and χ are the 0D state variables.

The 3D fluid or structure equations are discretized using finite element methods and integrated using the generalized-alpha method. The 0D fluid ODE system is integrated with RK4. Solving the coupled system in a monolithic fashion using Newton's method yields a linear system to be solved at each Newton iteration. We apply the Approximate Newton Method of [4] to solve this system in a modular manner. The resulting coupling framework involves communication of pressure \mathcal{P} and flow rate \mathcal{Q} between the 3D and 0D solvers each Newton iteration [5] (Fig. 1).

3. Results

Using our coupling, we obtain a realistic pressure-volume loop with no difficulty during the isovolumic phases (Fig. 2).

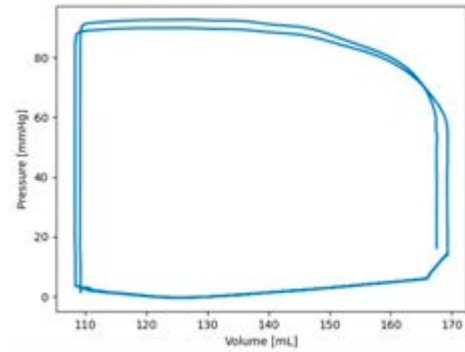


Figure 2: Pressure-volume loop obtained by coupling an idealized left ventricle with active stress to a 0D circulation model (see Fig. 1 left).

4. Discussion and Conclusions

Compared to an uncoupled 3D simulation, our coupling additionally requires evaluating the computationally cheap 0D solver each Newton iteration, a relatively small burden. In addition, our coupling method retains the quadratic convergence of Newton's method [4]. We do not require the additional volume constraint (for structure solver) and ad hoc stabilization found in the partitioned coupling strategies of [1,2,3]. Finally, we emphasize that the coupling applies equally well to a 3D fluid – 0D fluid system.

5. References

1. C.M. Augustin, et al., *Comp. Meth. App. Mech. and Eng.* 386, 114092 (2021).
2. F. Regazzoni, et al., *J. Comp. Phys.* 457, 111083 (2022).
3. F. Regazzoni, MOX report 17 (2022)
4. T.F. Chan, *SIAM journal on numerical analysis* 22(5), 904–913 (1985).
5. M.E. Moghadam et al., *J. Comp. Phys.* 244, 63–79 (2013).

Acknowledgements:

We thank the National Institutes of Health (R01HL129727) and the National Science Foundation (1663671) for grant funding for this project.



A SENSITIVITY-BASED STOCHASTIC FINITE ELEMENT FORMULATION FOR BIOLOGICAL SOFT MATTER MECHANICS

Georges Limbert (1, 2), Teja Melink (3), Jože Korelc (3)

1. University of Southampton, UK; 2. University of Cape Town, South Africa; 3. University of Ljubljana, Slovenia

1. Introduction

Integration of variability in predictive finite element models of biological soft matter is a fundamental aspect of biomedical engineering, particularly in the context of diverse populations. Sources of variability include biophysical and microstructural properties, boundary and loading conditions. For example, the skin features significant intra- and inter-individual variability which are essential in conditioning its broad range of biophysical behaviours [1]. Stochastic finite element (SFE) analyses are notoriously more complex to implement and computationally expensive than their deterministic counterparts [2]. It is therefore advantageous to develop general, efficient and modular methodologies to conduct such analyses, especially those that can capture *spatial* variations of random variables.

2. Materials and Methods

Here, it is proposed to represent stochastic fields using the Karhunen-Loève (KL) decomposition and calculate the stochastic response of the system using a second-order sensitivity analysis [2, 3] within a unified finite element environment. The numerical implementation is general and modular, valid for arbitrary kinematics and constitutive laws, making it particularly attractive to model biological soft tissues and their inherent heterogeneities. KL decomposition is computed via the formulation of a macro-element associated with a Fredholm integral equation of the second kind involving the covariance kernel of the stochastic field, and whose solution is obtained via standard Galerkin procedure.

3. Results

The SFE framework was assessed on various examples (**Figure 1**) by accounting for geometric and material stochastic fields (i.e.

random variables indexed by spatial position) on two-dimensional geometries, and solutions compared to Monte-Carlo simulations. An arc-length method was used to solve the geometrically and materially non-linear problems. On some problems, the gain in computational speed afforded by the stochastic framework is over four orders of magnitude.



Figure 1: Wrinkling plane strain finite element analysis of a soft neo-Hookean bi-layer structure where ground-state Young's moduli are stochastic fields (i.e. random variables indexed by spatial position). Cropped image of deformed configuration after application of a 25% compressive strain highlighting symmetry breaking in surface instability patterns.

4. Discussion and Conclusions

The ability of a perturbation approach to capture propagation of uncertainties in highly non-linear systems is inherently limited by the expansion order (here, second order). However, the use of automatic differentiation combined with optimisation of computer code means that extension of the SFE framework to higher orders is possible and should be explored in the future, as extension to three-dimensional geometries.

The numerical framework presented here provides an attractive platform to rapidly and statistically explore the influence of multiple factors on the physics of biological soft matter.

5. References

1. Limbert G. Proc Roy Soc A, 473:1-39 (2017).
2. Stefanou G. Comp Meth Appl Mech Eng, 198(9-12):1031-1051 (2009).
3. Melink T and Korelc J. Probabil Eng Mech, 37:7-15 (2014).



DIGITAL TWIN TO PREDICT VENTRICULAR TACHYCARDIAS

Carlijn Buck (1), Anouk de Lepper (2), Marcel van 't Veer (1,2), Wouter Huberts (2,3), Frans van de Vosse (2), Lukas Dekker (1,2)

1. Department of biomedical Engineering, Eindhoven University of Technology, Eindhoven, the Netherlands. 2. Department of Cardiology, Catharina Hospital, Eindhoven, the Netherlands; 3. Department of Biomedical Engineering, CARIM School for Cardiovascular Diseases, Maastricht University, Maastricht, the Netherlands

Corresponding Author: Carlijn Buck (c.m.a.buck@tue.nl)

1. Introduction

Survivors of myocardial infarction have an increased risk for scar-related ventricular tachycardia (VT): a heart rhythm disorders which may lead to sudden cardiac death. Current guidelines to identify patients at high risk prove to be insufficient and are solely based on symptoms and left ventricular ejection fraction. Better prediction of the occurrence of VT, will reduce mortality and morbidity. For this purpose, multiple, time-evolving aspects of the underlying pathophysiology should be part of the prediction model. Three different scientific approaches are available to estimate VT risk: (1) evidence-based medicine, (2) data-driven models, (3) mechanistic models. All approaches are derived from different fields (clinical, data science and biomedical engineering field respectively). The question arises which approach is most suitable to estimate VT risk.

2. Materials and Methods

Evidence-based medicine is mostly based on population studies. The individual patient, however often does not comply with the average study population. There is need to tailor treatments to the individual pathology.

Data-driven models, such as AI, can discover new unknown relationships without the need of any predefined knowledge. However, such models need large amount of clean and structured data, which is often not available. Additionally their black box nature makes interpretability and trustworthiness challenging.

Mechanistic models, which are based on known physics, are exceptional powerful in improving

our understanding and making predictions if the underlying mechanism are known. However, often the underlying physics are not known.

3. Results

A comprehensive overview of the current approaches and their application for VT prediction was made [1]. However, the true merit lies in combining all three approaches into one: a digital twin [1]. A digital twin is a virtual copy of your patient which integrates data-driven models and mechanistic models in a hybrid way. In this way, part of the model can be based on *a priori* knowledge and part of the model can be inferred from data.

4. Discussion and Conclusions

To optimize VT prediction, digital twins are needed which integrate patient-specific data in a hybrid way using data-driven and mechanistic modelling of the individual anatomical, mechanical and electrophysiological characteristics.

5. References

1. de Lepper, A. et al. (2022). From evidence-based medicine to digital twin technology for predicting ventricular tachycardia in ischaemic cardiomyopathy. *Journal of the Royal Society Interface*, 19(194), 20220317.

Acknowledgements:

This publication is part of the COMBAT-VT project (project no. 17983, www.combatvt.nl) of the research programme High Tech Systems and Materials which is partly financed by the Dutch Research Council and part of the Picasso project (reference no. TKI HTSM/20.0022) of the Eindhoven MedTech Innovation Center.



MECHANICAL BEHAVIOUR OF SOFT SPHERICAL TISSUE CONSTRUCTS IN MICROFLUIDIC CULTURE

Willy V. Bonneuil(1*), T. Christian Gasser(1), Shervin Bagheri(1)

1. Department of Engineering Mechanics, KTH Royal Institute of Technology, Stockholm, Sweden

*E-mail: bonneuil@kth.se

1. Introduction

Avascular organoids cultured under fluid flow achieved larger diameters and lower necrotic fractions [1,2,3]. The employed microfluidic setups varied in design, geometry, and rate and oscillatory nature of the applied fluid stimulus. The larger diameter increase, necrotic fraction reduction, and symmetry loss were observed in organoids cultured under fluid flow that was both high and oscillating. Candidate mechanical phenomena to explain these findings include convective mixing in the culture medium and deformation-induced convection inside the organoid. Here, we use multiphase mixture theory to interrogate the mechanical behaviour of deformable spherical multi-cellular tissue constructs (MCTC) cultured under microfluidic stimuli.

2. Materials and Methods

MCTCs were modelled as idealised spheres obeying biphasic theory. The solid phase was assumed to be linearly elastic under the small deformations involved. Fluid flow in the culture chamber was modelled with Stokes' equation. Molecular transport of oxygen and glucose were modelled with effective diffusivity for fibrous media, Michaelis-Menten kinetics, and advective terms as per the triphasic theory applied to cartilage [4]. Two groups of simulations were conducted in COMSOL Multiphysics: one on the role of mixing in the culture chamber where MCTCs were assumed rigid and porous, and one on mechanical fields in deformable porous MCTCs subjected to oscillatory loading. Their key result was the depth of tissue at which nutrient concentration decreased to zero.

3. Results

The necrotic fractions of brain organoids observed in microfluidic chambers [1,2] were

accurately reproduced in rigid MCTCs by varying the magnitude of the medium supply flow rate only. A high enough flow rate around the MCTCs maintained the concentration of nutrient at their rim equal to that in the bulk culture medium. The ranges of flow rates used in microfluidic culture and of permeabilities of hydrogels used to grow MCTCs pointed to no role for pressure-gradient-induced convection. However, the mechanical properties of spheroids, whose stiffness strongly depends on cell type and culture protocol [5], render deformation-induced convection plausible. Loading periods in microfluidic culture are typically 1-10 s. Simulations of hollow spheres with characteristic frequencies of that order, loaded from their cavity, showed a slight increase in oxygen concentration compared to purely diffusive cases.

4. Discussion and Conclusions

Microfluidic flow facilitates nutrient supply to the surface of MCTCs without inducing high shear stress. Whilst it appears to be the dominant mechanism for the increase of oxygen penetration depth, poroelastic deformation could have other effects on MCTC survival, such as via stress gradients. Current work aims to fully simulate soft porous MCTCs in culture by coupling Stokes' flow with poroelastic deformation.

5. References

1. A. Cho et al. *Nat Comm* 12:4730 (2021)
2. E. Berger et al. *Lab Chip* 18:3172 (2018)
3. K. Homan et al. *Nat Meth* 16:255-262 (2019)
4. R. Mauck et al. *J Biomech Eng* 125:602 (2003)
5. L. Guillaume et al. *Sci Rep* 9:6597 (2019)

Acknowledgements:

The authors acknowledge the support of Maria Tenje and Neeraj Katiyar.

THE APPARENT MODULUS OF TRABECULAR BONE: EXPERIMENTS VS MICROSTRUCTURAL FINITE ELEMENT MODELS

Trevor J. Cloete*, Claire V. Rampersadh, Gerald N. Nurick

Blast Impact and Survivability Research Unit (BISRU),

Department of Mechanical Engineering, University of Cape Town, Rondebosch, South Africa

*Correspondence Email: trevor.cloete@uct.ac.za

1. Introduction

Bone mineral density measurement via dual X-ray absorptiometry is the current best practice for osteoporosis (OP) diagnosis. However, recent research suggests more complex causes, including the microstructure and composition of trabecular bone [1]. A potential approach is patient specific microstructural finite element (FE) analysis of trabecular bone based on micro-computed tomography (μ -CT) images. While not currently clinically feasible due to radiation dose and scan duration limits that result in low resolutions ($>100 \mu\text{m}$) [1], foreseeable technological improvements, with finer resolutions ($<100 \mu\text{m}$), suggest it is prudent to develop sound μ -CT/FE analyses.

The voxel-based method (VBM) is regarded as best practice for FE predictions of the apparent modulus, although it is also computationally expensive as each bone voxel from a μ -CT scan is represented with a solid element, resulting in a large mesh [2]. A more efficient approach is the beam-shell method (BSM), where microstructural rods and plates are identified from a μ -CT scan and represented by FE beams and shells [3]. This paper compares VBM and BSM predictions to the measured apparent moduli for bovine trabecular bone.

2. Materials and Methods

In all, 110 cylindrical specimens ($D = 10 \text{ mm}$, $L = 7.5 \text{ mm}$) were machined from bovine humeri, μ -CT scanned at an $80 \mu\text{m}$ voxel resolution and tested in quasi-static compression to obtain the apparent moduli. An automated analysis cycle was developed which binarizes the μ -CT scans, creates VBM and BSM meshes, performs FE simulations and returns the apparent modulus. The cycle was validated by analysing regular lattices with

known responses. The cycle was then used to predict the apparent moduli of the trabecular bone specimens using an assumed Young's modulus $E = 1 \text{ GPa}$ and Poisson's ratio $\nu = 0.3$.

3. Results

Figure 1 shows selected numerical predictions vs experimental results for the bone specimens. Exact correlation was not expected as the true values of E and ν are unknown. Rather, the trends and scatter of the data are used to assess the performance of the methods.

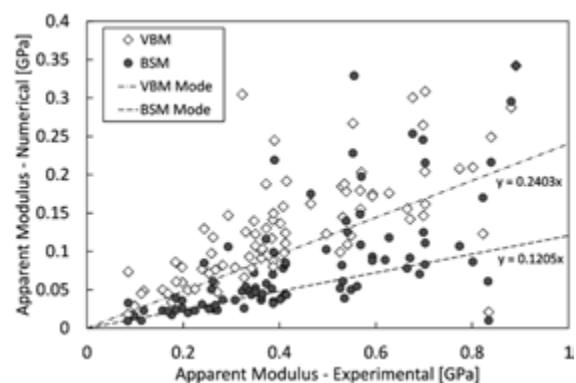


Figure 1: BSM and VBM simulation results.

4. Discussion and Conclusions

The BSM shows more general scatter although the VBM produces more extreme outliers. The BSM results imply a value of $E = 8.3 \text{ GPa}$, which is closer to published values [4] than the VBM result of $E = 4.2 \text{ GPa}$, i.e. the VBM appears over stiff. While still requiring more development, both the VBM and BSM show good potential for patient specific modelling to enhance OP diagnoses, although the BSM is significantly less resource intensive.

5. References

1. Molino G et al., Appl. Sci. 10: 9839 (2020).
2. Sabet FA et al., Interface Focus, 6 (1) (2016).
3. Vanderroost J et al. J. Biomech. 44 (8) (2011).
4. Rho RB et al., J. Biomech. 26(2) (1993).



WEAKLY SUPERVISED CONVOLUTIONAL NEURAL NETWORKS-BASED 3D RECONSTRUCTION FROM MEDICAL IMAGES GUIDED BY PARAMETRIC GEOMETRIC MODELS

Jean-Rassaire Fouefack (1), Guillaume Dardenne (1,2), Tinashe E.M Mutsvangwa (3,5), Bhushan Borotikar (4,5), Valérie Burdin (1,5)

1. LaTIM INSERM U1101, France ; 2. CHU de Brest, France ; 3. University Cape Town, South Africa ; 4. SCMIA, Pune, India ; 5. IMT Atlantique, France ;

1. Introduction

Patient-specific features used for surgical planning and custom implant design may require 3D reconstruction of the shape and pose of organs of interest from medical images. In this work, we propose a novel generative model-based deep convolutional autoencoder to reconstruct multiple organs in 3D from a 2D image. To this end, we combine a convolutional encoder network with a parametric geometric model that serves as a decoder [1,2].

2. Materials and Methods

To solve this challenging problem, we integrate a CNN-based encoder with a statistical model (pre-trained generative model)-based decoder and create synergy between them (Fig 1).

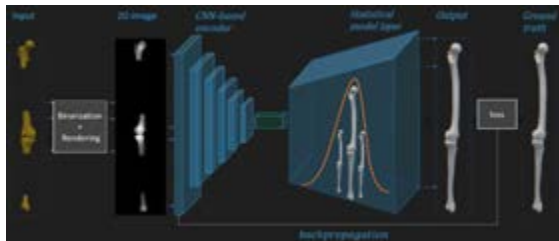


Figure 1: Our deep parametric geometric model-based autoencoder allows end-to-end learning of latent variables that encode meaningful information including shape and their relative spatial position as well as global spatial orientation.

A total of 49 non-pathological knee joints with variation in morphology and knee flexion were used to build a dynamic multi-object Gaussian process model (DMO-GPM) [2] of the knee. A total of 1000 3D geometry meshes were generated using the generative knee DMO-GPM. In order to obtain paired (2D and 3D) data, the 3D geometries were cropped, binarized and then rendered into 2D images (left of Figure 1). To train the network in a weakly supervised manner, the 49 real data were added

to the 1000 generated data and used together as labelled training data. The weakly trained network was tested on 15 unseen real data and the results were compared to those of Markov chain Monte Carlo (MCMC)-based fitting [3] to recover the 3D object corresponding to the 2D rendering.

3. Results

The reconstructions of the test dataset using our approach were compared to those of the MCMC-fitting. The surface-to-surface RMS errors were calculated between the reconstructed knee meshes and the ground truth. The errors of our network are smaller than those of the MCMC, with an average RMS error of $1.64 \pm 0.18 \text{ mm}$ for our approach versus $3.07 \pm 0.62 \text{ mm}$ for the MCMC.

4. Discussion and Conclusions

Our findings suggest that indeed, our model trained in weakly supervised manner is better suited for 3D reconstruction from partial data as it outperforms the MCMC sampling-based approach. One benefit of the approach is that it can be trained in a weakly supervised manner to reconstruct any type of partial data. This approach creates a methodological foundation for many applications.

5. References

1. Tewari et al., IEEE Trans Pattern Anal and Machine Intelligence; 42(2):357–370, 2018
2. Fouefack et al. MICCAI, 755–764, 2020
3. Fouefack et al, PhD manuscript, HAL Archive, 2021IMTA0240.tel-03506272

Acknowledgements: This work is granted by the FollowKnee project from French National Agency for Research (n°ANR-17-RHUS-0005). Jean-Rassaire Fouefack is now with ISEN Yncréa Ouest, Brest, France.

ADOLESCENT IDIOPATHIC SCOLIOSIS DETECTION USING SURFACE TOPOGRAPHY AND CONVOLUTIONAL NEURAL NETWORKS

Nada Mohamed (1), Mostafa Hassan (1), Qiwei Mei (2), Eric C. Parent (3), Lindsey Westover (1)

1. Department of Mechanical Engineering, University of Alberta, Canada; 2. Department of Civil and Environmental Engineering, University of Alberta, Canada; 3. Department of Physical Therapy, Faculty of Rehabilitation Medicine, University of Alberta, Canada

1. Introduction

Adolescent idiopathic scoliosis (AIS) is a three-dimensional torsional curvature of the spine, affecting up to 5% of the population[1]. Conventional scoliosis screening tools have low positive predictive values, involving unnecessary referrals and exposure to ionizing radiation from x-ray assessments[2]. The 3D markerless surface topography (ST) technique that quantifies the severity of trunk asymmetry can potentially be used as a scoliosis screening tool. However, differences in trunk asymmetries between individuals with scoliosis and typically developing individuals are not well characterised. This study aims to detect AIS from healthy adolescents using ST.

2. Methods

Surface torso scans of participants (10 -18 years) with AIS (n = 239) recruited from a scoliosis clinic and healthy volunteers (n = 89) who responded to the study ads. The AIS group was defined based on radiographic exams, with curves between 10° - 45°. Healthy volunteers were eligible if their Scoliometer test < 7°. ST analysis involved reflecting the torso's 3D geometry and aligning with the original torso by minimizing the distance between points. Deviations over the back surface between the torsos, as well as the depth differences were mapped onto 102 x 102 grids (figure 1). Using

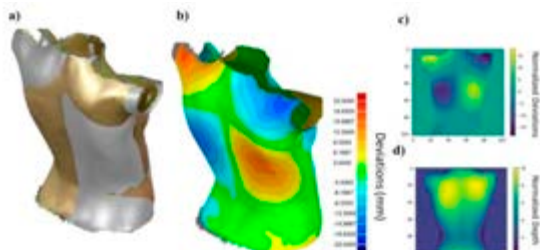


Figure 1: (a) alignment of original and reflected torso, (b) deviations map of 3D torso, (c) deviation map of back, (d) torso depth differences

the deviations and the depth as inputs, a convolution neural network (CNN) was developed to classify ST of healthy adolescents and those with AIS, using 60% of the data for training. The model was evaluated during training using the validation set (20%) and assessed following training using the testing set (20%). Classification results of the proposed model was compared to the ground truth.

3. Results

During the model training phase, the training and validation set obtained an accuracy (ACC) of 90% and 88%, respectively. Additionally, the classifications from the testing sets obtained an accuracy, sensitivity (SE), and specificity (SP) of 91%, 96%, and 78%, respectively (table 1). The positive likelihood ratio (PLR) of the testing set was 4.3. Likewise, A negative likelihood ratio (NLR) of 0.1 was also attained.

Table 1: Comparison between CNN and ground truth for (a) validation and (b) testing set

a)	AIS	Healthy	
CNN\Truth			
AIS	46 (96%)	6 (33%)	PLR=2.9
Healthy	2 (4%)	12 (67%)	NLR=0.1
	SE=96%	SP=67%	ACC=88%
b)	AIS	Healthy	
CNN\Truth			
AIS	46 (96%)	4 (22%)	PLR=4.3
Healthy	2 (4%)	14 (78%)	NLR=0.1
	SE=96%	SP=78%	ACC=91%

4. Conclusions

The proposed CNN predictive model to distinguish AIS from healthy individuals using ST showed promising results, achieving an accuracy of 91%.

5. References

1. Choudhry et al. (2016), Open Orthop. J, 10, 143-154.
2. Fong et al. (2010), Spine, 35(10), 1061-1071.

PREDICTING THE PREMORBID ANATOMY OF THE SCAPULA USING AUTOENCODERS

Osman Berk Satir (1), Pezhman Eghbali (2), Alexandre Terrier (2, 3), Fabio Becce (3), Patrick Goetti (3), Arnaud Meylan (3), Robin Diot (3), Philippe Büchler (1)

1. ARTORG Center for Biomedical Engineering Research, Switzerland; 2. Ecole Polytechnique Fédérale de Lausanne (EPFL), Switzerland; 3. Lausanne University Hospital (CHUV), Switzerland

1. Introduction

Total shoulder arthroplasty (TSA) is an increasingly common surgical procedure used to relieve pain and disability associated with glenohumeral osteoarthritis (OA). Accurate positioning of the glenoid implant is crucial for the long term-success of TSA. However, determining the proper glenoid implant positioning is challenging because OA significantly alters bone anatomy. In addition, since OA affects both shoulders, contralateral morphology cannot be relied upon. Therefore, the aim of this study was to develop an autoencoder-based approach to predict the premorbid anatomy of the scapula objectively.

2. Materials and Methods

Our dataset consisted of 60 healthy and 56 pathological segmented scapulae. 48 healthy and 44 pathological cases were used for training, and remaining cases for validation. An autoencoder was implemented with one encoder and two specific decoders for healthy and pathological cases. The goal of the encoder is to extract the latent features, and each decoder reconstructs the healthy and pathological anatomy, respectively. To predict the premorbid anatomy of a pathological scapula, we first extracted the latent features with the encoder and reconstructed the scapula with the decoder trained with healthy cases. This allows objective prediction of the premorbid anatomy, based on other healthy cases in the dataset.

3. Results

The anatomic reconstruction was adequate, with Dice overlaps between the inputs and outputs of the autoencoder of 92% and 93% for healthy and pathologic cases, respectively. Glenoid version, a key morphometric parameter, was used to evaluate the predictions.

An average difference of 5.4° between glenoid version of healthy and pathological cases was observed in the whole dataset (Fig. 1). In the validation dataset, the model increased the glenoid version of pathological cases by $3.0^\circ \pm 4.5^\circ$, which showed that glenoid version approached to the values of the healthy anatomy (Fig 1). The glenoid version of the pathologic cases and their premorbid prediction were also significantly different ($p=0.04$).

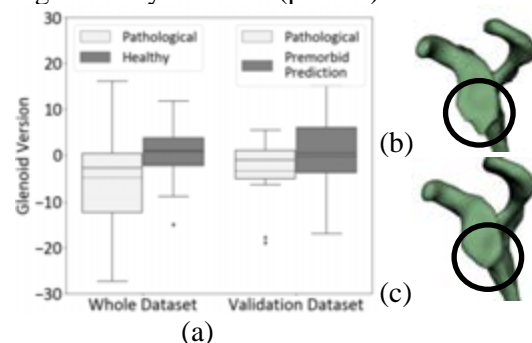


Figure 1: Boxplot comparing glenoid version between pathological and healthy scapulae of the whole dataset, as well as pathological cases and their premorbid prediction of the validation dataset (a). The 3D reconstruction of a pathological scapula (b) and its premorbid prediction (c).

4. Discussion and Conclusions

An approach to automatically predict the premorbid anatomy of pathological scapulae using deep learning was proposed. Initial results show that predictions are close to healthier anatomy, but there are still cases where improvements are marginal. More cases should be added to training to better capture population variability. In the future, this approach should help improve TSA planning by allowing correction of OA-induced glenoid deformities.

Acknowledgements:

This work is supported by the Swiss National Science Foundation (Grant no: 189972).

BAYESIAN NETWORK ANALYSIS OF ROTATOR CUFF MUSCLE DEGENERATIONS

Pezhman Eghbali (1), Osman Berk Satir (2), Fabio Becce (3), Patrick Goetti (3), Philippe Büchler (2), Dominique Pioletti (1), Alexandre Terrier (1, 3)

1. École Polytechnique Fédérale de Lausanne (EPFL), Switzerland; 2. ARTORG Center for Biomedical Engineering Research, Switzerland; 3. Lausanne University Hospital (CHUV), Switzerland;

1. Introduction

The 4 rotator cuff (RC) muscles, supraspinatus (SS), subscapularis (SC), infraspinatus (IS), and teres minor (TM), often present degeneration, which affects the outcome of total shoulder arthroplasty (TSA) [1]. Despite its importance, there is no systematic analysis of the effect of patients' variables on RC muscles degeneration. Hence, here we aimed to measure the effect of sex, age, weight, and height on RC muscles degeneration for four groups, normal shoulders without any sign of pathology as control (CTRL), cuff tear arthroplasty (CTA), primary (POA) and secondary osteoarthritis (SOA).

2. Materials and Methods

We considered 114 CTRL subjects (79 M), 63 CTA (13 M), 133 POA (46 M), and 16 SOA (16 M). We developed a Bayesian network to measure the effect of sex, age, weight, and height on muscle atrophy and fatty infiltration, of SS, SC, IS, TM, for CTRL, CTA, POA, SOA. Markov Chain Monte Carlo sampling with 4 chains and 1000 iterations estimated the posterior distribution. Muscle pre-morbid contours were automatically identified on a sagittal-oblique CT section [2] by deep learning [3], to quantify atrophy and fatty infiltration by image processing. We reported the effect as z-score of atrophy and fatty infiltration (of CTRL) by year, kg, cm, for age, weight, and height respectively.

3. Results

For atrophy, the average effect was not sex-dependent for the 4 groups. The age effect was different for males/females in some of the groups (> 0.1 difference in SS and TM of CTA, Fig. 1), and the weight effect was higher for females (0.03 in IS of CTA). The highest age effect on atrophy occurred in SS and TM

(> 0.12) for CTA-male subjects. Weight effect on atrophy was highest in IS for CTA-female subjects (0.04). Height did not affect atrophy. For fatty infiltration, the average effect was only sex-dependent in SS of POA subjects (0.74 fatty infiltration z-score higher for females), and the highest age effect difference was in IS and TM of CTA subjects (0.03). The age effect was highest in IS, SC, and TM (0.03) of CTA-male subjects. Weight and height did not affect fatty infiltration.

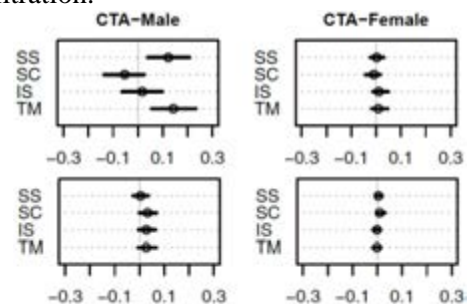


Figure 1: Atrophy (top) and fatty infiltration (bottom) per age (z-score/year, 89% CI) for males and females with CTA.

4. Discussion and Conclusions

The effect of age was dominant, compared to sex, weight, and height, and was higher for males than females and CTA than other groups. Our results mean that SS would be 18% more atrophied (on average) for a 60-year-old man with CTA than a 70-year-old man with CTA. Similarly, IS would be 4.5% more atrophied for females with each 10 extra kg. These results can be helpful for the preoperative planning of TSA.

5. References

1. McElvany et al., Am J Sports Med; (2015).
2. Terrier et al., J OSTR; (2016).
3. Taghizadeh et al., Eur Radiol; (2020).

Acknowledgements:

This work is supported by the Swiss National Science Foundation (Grant no: 189972).



DEEP LEARNING CARDIAC SEGMENTATION OF DUAL ULTRASOUND AND PHOTOACOUSTIC IMAGE DATA

Katherine A. Leyba (1), Hayley Chan (2), Olivia Loesch (1) Pierre Sicard (3) Craig J. Goergen (1)

1. Purdue University, United States; 2. Indiana University School of Medicine, United States;

3. Université de Montpellier, France

1. Introduction

Though methods exist to extract regions of interest (ROI) from the endo- and epicardial boundaries of the left ventricle (LV) via ultrasound (US) images [1], they are often time-consuming and cannot obtain functional information such as myocardial oxygen saturation (sO_2), a biomarker of cardiac disease. Photoacoustic imaging (PAI), however, can be used to noninvasively quantify sO_2 of tissue [2]. Here, we highlight the capability of deep learning methods to improve LV anterior wall analysis via segmentation of preclinical murine US and PAI images.

2. Materials and Methods

The dataset used in this study consists of long-axis US and PAI images (400 each) of murine cardiac LVs acquired by a Vevo 3100 LAZR-X system (FUJIFILM, VisualSonics) and manually segmented ground truth binary masks of the anterior myocardium via a custom MATLAB script each split into training (80%) and validation sets (20%). These images and masks served as input to a U-Net deep neural network [3] which generated predicted ROI masks and were compared to manual segmentation. Initial testing was achieved on a down sampled set of images (240 x 160 pixels) on a personal computer with an NVIDIA T500 using PyTorch. Following a similar approach as outlined above, we also identified and removed reverberation artifacts on a smaller set of 200 PAI images. Accuracy and dice score metrics were used to evaluate algorithm performance.

3. Results

An accuracy of 98.8% and dice score 0.864 were achieved for myocardium segmentation and an accuracy of 98.9% and dice score 0.936 were achieved during reverberation artifact segmentation in ~ 4.5 sec/image vs. ~ 45 sec/image manual segmentation.

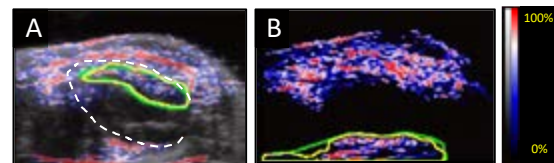


Figure 1: Ground truth (green) and predicted (yellow) ROIs on (A) an overlaid US and PAI image of the LV anterior myocardium and (B) PAI image around a deep reverberation artifact. Oxygenated (red) and deoxygenated (blue) regions are shown. White dashes outline the LV.

4. Discussion and Conclusions

Results revealed that training on overlaid US/PAI images using a U-Net neural network can be used to create ROIs of the anterior LV wall in murine cardiac datasets and remove unwanted artifacts. Limitations include a small delay between US and PAI acquisition time that may lead to registration errors. We plan to use this algorithm on Electrocardiogram-gated Kilohertz Visualization images with improved time resolution to determine if alignment issues and algorithm performance improves and run the algorithm on a cluster to provide segmentations on the order of milliseconds. This approach has the potential to improve estimation of cardiac function and tissue oxygenation from large US/PAI image data.

5. References

1. Potter E., Marwick T., *JACC Cardiovasc. Imaging*, 11(2 Pt. 1):260–274 (2018).
2. David H., *et al.*, *Front. in Cardiovasc. Med.*, 7: 615507 (2021).
3. Ronneberger O., *et al.*, CoRR, *arXiv*: 1505.04597 (2015).

Acknowledgements:

The authors thank the National Science Foundation Graduate Research Fellowship Program (grant number DGE-1842166), the Chateaubriand Fellowship, Fulbright Program, and FACE Foundation for supporting this work.



AUTOMATIC INTERPRETATION OF POINT-OF-CARE LUNG ULTRASOUND USING DEEP LEARNING

Bárbara Malainho (1,2,3), Catarina Rodrigues (1,2,3), Ana Cláudia Tonelli (4, 5), André Santanchè (6), Marco A. Carvalho-Filho (7), Jaime C. Fonseca (3), Sandro Queirós (1,2)

1. Life and Health Sciences Research Institute, School of Medicine, University of Minho, Braga, Portugal; 2. ICVS/3B's – PT Government Associate Laboratory, Portugal; 3. Algoritmi Center, School of Engineering, University of Minho, Guimarães, Portugal; 4. Department of General Internal Medicine, Hospital Clínicas de Porto Alegre, Brazil; 5. Department of Medicine, Unisinos University, São Leopoldo, Brazil; 6. Institute of Computing, University of Campinas, São Paulo, Brazil; 7. Univeristy Medical Center Groningen, University of Groningen, Groningen, The Netherlands.

1. Introduction

Point-of-care ultrasound (POCUS) is an imaging technique useful in emergency rooms for a rapid examination. While deep learning-based solutions have increased their presence in the medical imaging field, the usage of these methodologies in pulmonary POCUS remains underexplored.

2. Methodology

This work proposes a deep learning framework for the interpretation of lung POCUS videos, whose outputs are the finding(s) present in said videos, including: scattering only, A-lines, up to 3 B-lines, more than 3 B-lines, coalescent B-lines, consolidation, and pleural effusion. Based on a R2+1D convolutional neural network [1], a multi-label classification model is proposed, comprehending three key aspects: a label smoothing regularisation (LSR), a video-level inference routine (VL), and a dataset-specific post-processing (PP). Specifically, the training of the model was done with an LSR-based binary cross entropy loss. During inference, multiple overlapping clips from the same video are extracted and fed to the model, with the average predicted scores being used as the video-level result. The pipeline culminates with the PP block, that consists in a set of ad-hoc rules leveraging of the natural hierarchy and clinical significance of the ultrasound findings.

3. Results

A dataset of 3649 lung POCUS videos was curated and annotated by experts and used in the development of the algorithm. The results are summarized in Table 1. On the validation set, a

5-fold cross-validation was employed, with the test-set results reported as the average metric scores of the five trained models.

Table 1: F1-scores for the baseline model, and upon inclusion of each one of the proposed blocks

Set	LSR	VL	PP	F1 Macro	F1 Micro
Validation	-	-	-	0.6231	0.6634
	x	-	-	0.6302	0.6663
	x	x	-	0.6414	0.6775
	x	x	x	0.6481	0.6872
		(proposed)			
Test	x	x	x	0.6168	0.6694

4. Discussion and Conclusion

The effectiveness of the proposed framework was verified, with each block improving the model's performance over the baseline. A similar performance (albeit slightly lower) was observed for the test set, demonstrating the model's generalisation capabilities. Overall, the proposal provides strong results for a difficult clinical interpretation task, demonstrating its value as a promising asset for patient's triage and management.

5. References

1. D. Tran et al., IEEE/CVF Computer Vision and Pattern Recognition; 2018, p.6450-6459.

Acknowledgements:

The authors acknowledge the financial support provided by National funds, through the Foundation for Science and Technology (FCT, Portugal; PTDC/EMD-EMD/1140/2020 and UMINHO/BIM/2021/68), and the donation of a RTX A6000 GPU by NVIDIA (USA).

AUTOMATIC GENERATION OF MULTI-VIEW SYNTHETIC ECHOCARDIOGRAPHIC IMAGES

**João Freitas (1, 2, 3), João Gomes-Fonseca (1, 2), Jorge Correia-Pinto (1, 2),
Jaime C. Fonseca (3), Sandro Queirós (1, 2)**

1. Life and Health Sciences Research Institute (ICVS), School of Medicine, University of Minho, Braga 4710-057, Portugal; 2. ICVS/3B's – PT Government Associate Laboratory, Braga/Guimarães, Portugal; 3. Centro ALGORITMI, School of Engineering, University of Minho, Portugal.

1. Introduction

Echocardiography is essential for assessing cardiac anatomy and function, with an ever-growing number of algorithms being developed to assist physicians in the clinics. However, the lack of datasets containing spatially related images from multiple cardiac windows is limiting novel developments. Considering time and ethical concerns associated with acquiring and using real images, this work targets the synthetic generation of such a dataset.

2. Methodology

A pipeline for the automatic generation of synthetic echocardiographic images of multiple views is proposed, comprising three modules. The first comprehends the creation of variable, representative models of the heart anatomy, using 24 public whole-heart models [1]. The second comprises an ultrasound simulator, PLUS [2], capable of generating synthetic images from five cardiac views (apical 4- and 2-chambers, parasternal long- and short-axis, and subxiphoid). Here, each image's 3D pose is also extracted, which may be useful in developing algorithms to estimate image pose or inter-view relationship. The third module employs an image-to-image translation method, GLA-Net [3], to increase the synthetic images' realism.

3. Results

Two different datasets were created (Fig. 1): a synthetic 5-view dataset generated with the first two modules of the proposed pipeline and a 2-view dataset generated with the whole pipeline.

4. Discussion and Conclusion

The first two modules of the proposed pipeline can produce realistic images in terms of cardiac geometry and probe's spatial positioning.

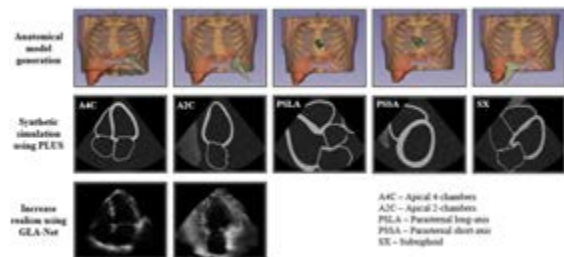


Figure 1: Example probe positioning and anatomical models (first row), respective synthetic image (second row) and realistic apical images (third row).

Nevertheless, the absence of the characteristic speckle noise and acoustic shadowing artifacts in the images encourages the use of the third module. In the present work, images from the EchoNet-Dynamic dataset [4] were used as target domain, which limited its application to the apical views. Notwithstanding, promising results were achieved. In the future, real images from parasternal and subxiphoid views must be gathered to ultimately create a 5-view realistic echocardiography dataset.

5. References

1. M. Strocchi et al., PloS ONE, vol. 15(6), p. e0235145, 2020.
2. A. Lasso et al., IEEE Transactions on Biomedical Engineering, vol. 61(10), pp. 2527–2537, 2014.
3. G. Yang et al., arXiv preprint:2111.10346, 2021.
4. D. Ouyang et al., Nature, vol. 580(7802), pp. 252–256, 2020.

Acknowledgements: The authors acknowledge the financial support provided by National funds, through the Foundation for Science and Technology (FCT, Portugal; PTDC/EMD-EMD/1140/2020), and the donation of a RTX A6000 GPU by NVIDIA (USA).



IN VIVO MEASUREMENT OF HUMAN BRAIN MATERIAL PROPERTIES UNDER QUASI-STATIC LOADING.

Nicholas Bennion (1), Stefano Zappalá (2,3), Matthew Potts (1), David Marshall (2), Sam L Evans (1)

1. School of Engineering, Cardiff University, United Kingdom; 2. School of Computer Science and Informatics, Cardiff University, United Kingdom; 3. Cardiff University Brain Research Imaging Centre (CUBRIC), Cardiff University, United Kingdom

Corresponding Author: Nicholas Bennion: bennionn@cardiff.ac.uk

1. Introduction

Computational modelling of the brain requires accurate representation of the tissues concerned. Due to the soft, biphasic nature of the tissue, mechanical testing has numerous challenges. This is significant for applications with low strain rates like neurosurgery, where redistribution of fluid is thought to be biomechanically important.

2. Materials and Methods

A finite element (FE) model was generated in FEBio, incorporating a spring element/fluid-structure interaction representation of the pia-arachnoid complex (PAC). The model was loaded to represent gravity in prone and supine positions. 105 models were computed using parameter values over broad initial estimates of the actual ranges. Inverse material parameter identification was performed by fitting a Gaussian Process Regression model to the input parameters and the similarity between the FE displacements and human ($n=8$) *in vivo* measurements under the same loading [1].

3. Results

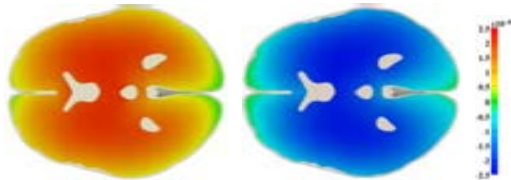


Figure 1: Transverse section displacement maps (m) for prone (left) and supine (right) simulations.

Results for the brain Ogden parameters, μ , α and k yielded values of 670 Pa, -19 and 148 kPa; values in the order of 1.2 MPa and 7.7 kPa were obtained for stiffness of the pia mater and out-of-plane tensile stiffness of the PAC

respectively. Positional brain shift was found to be non-rigid, with a small component of displacement within the PAC and deep brain ‘sagging’ up to 1mm (Figure 1). Material sensitivity was greatest with the bulk modulus and initial shear modulus.

4. Discussion and Conclusions

Material properties, in particular the bulk and shear moduli of the brain were found to support previously published mechanical testing data [2]. Sensitivity to the bulk modulus supports the argument that redistribution of fluid within the tissue is biomechanically important in such scenarios. To the best of our knowledge, this is the first study using *in vivo* human data and gravitational loading to estimate the material properties of intracranial tissues. In using a whole-volume human displacement field, it was possible to derive multiple parameters simultaneously, which can be challenging with traditional mechanical testing. The model and derived properties could now be applied in clinical applications, such as accounting for brain shift in stereotactic neurosurgery.

5. References

1. Zappala S, et al. Full-field MRI measurements of in-vivo positional brain shift reveal the significance of intra-cranial geometry and head orientation for stereotactic surgery. *Sci Rep-Uk*. 11(1): (2021)
2. Budday S, et al. Mechanical characterization of human brain tissue. *Acta Biomater*. 48, 319-340 (2017)

Acknowledgements:

This work was funded by the ESPRC as part of an iCase studentship with Renishaw Plc.



NUMERICAL SIMULATION FOR BRAIN CHARACTERISATION: ISOTROPIC AND ANISOTROPIC HYPERELASTIC MATERIAL

Wael ALLILICHE¹, Christine RENAUD¹, Jean-Michel CROS¹, Zhi-Qiang FENG¹

1. Université Paris-Saclay, Univ Evry, LMEE, Evry, 91020, France

1. Introduction

This study aims to characterise biological soft tissues within a suction test. Isotropic Yeoh and anisotropic four-fibre polyconvex hyperelastic constitutive laws are implemented in an in-house finite element code (FER) [1]. An axisymmetric model is used for the isotropic models, and a 3D model is made for anisotropic ones. The goal is to perform an inverse identification through experimental data.

2. Materials and Methods

2.1 Yeoh isotropic model: Yeoh is a three-parameter isotropic hyperelastic energy density according to the classical invariant I_1 [2]:

$$W = \sum_{i=1}^3 a_i (I_1 - 3)^i \quad (1)$$

2.2 Polyconvex anisotropic model: Polyconvex law is a quadratic polynomial form with nine parameters [3]. Six polyconvex invariants L_i contain all the information relative to the fibres' orientation:

$$W = a_1(L_1 - 1) + a_2(L_2 - 1) + a_3(L_3 - 1) + a_4(L_4 - 4) + a_5(L_5 - 4) + a_6(L_6 - 4) + a_7(L_1 - 1)^2 + a_8(L_2 - 1)^2 + a_9(L_3 - 1)^2 \quad (2)$$

2.3 Suction test: The data are collected in vivo from an adult brain tumour patient [4]. A negative pressure is applied with a suction tube. A camera measures the displacements of point M (Figure. 1) at each step of applied pressure.

2.5 Suction finite element model: Quasi-static pressure is applied negatively in the suction zone for suction simulation. The contact between the brain and the rigid tube is modelled by the bipotential method [2] with sliding conditions.

2.6 Parameters identification: A genetic algorithm from MATLAB is used to minimise the coefficient of determination " R^2 ". This coefficient is calculated from experimental data and simulation results.

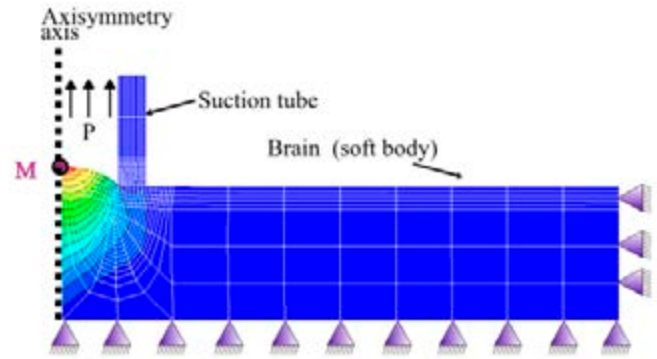


Figure 1: Axisymmetric model of suction.

3. Results

A parameter set is obtained for each hyperelastic law. Numerical solutions are compared to experimental data.

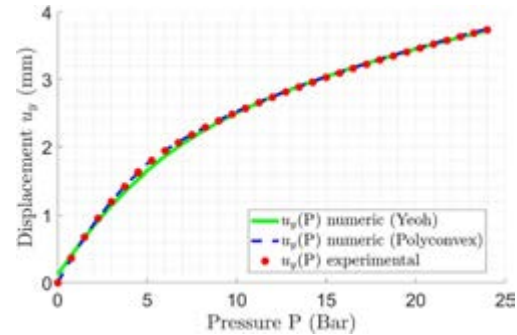


Figure 2: Point M displacement according to pressure.

4. Discussion and Conclusions

The brain material was defined by inverse identification of isotropic axisymmetric and anisotropic 3D models. Figure 2 shows that the polyconvex law is more accurate than Yeoh one. A sensitivity analysis will be performed to investigate the influence of each model parameter for the suction test.

5. References

1. Z.-Q. Feng et al., Int. J. Eng. Sci. 44(1-2) 113-126 (2006).
2. W. Alliliche et al., Com. Met. Img. Visu. Biomech. Biomed. Eng. II; 271-280 (2022).
3. W. Alliliche et al. CFM 2022 conference.
4. P Schiavone et al., Med Image Anal. 2009 Aug;13(4):673-8.

QUANTIFYING BRAIN CONNECTIVITY DURING RESTRICTED KNEE MOVEMENT

Rateb Katmah ⁽¹⁾, Herbert F. Jelinek ^(1,2,3), Abdul Aziz Hulleck ⁽¹⁾, Kinda Khalaf ^(1,2)

1. Department of Biomedical Engineering, Khalifa University of Science and Technology, Abu Dhabi, United Arab Emirates; 2. Health Engineering Innovation Center, Khalifa University of Science and Technology, Abu Dhabi, United Arab Emirates; 3. Biotechnology Center, Khalifa University of Science and Technology, Abu Dhabi, United Arab Emirates

1. Introduction

The human knee is the largest and among the most complex joints in the musculoskeletal system. Situated between the body's longest lever arms, the knee sustains high cyclical forces/moments, making it greatly susceptible to injury. The central nervous system (CNS) plays a role in the process due to neuromuscular control adaptation. The association between brain activity and accompanying gait anomalies post knee injury, recuperation, and recurring damage remain elusive [1]. This work aimed to investigate this association towards shedding light on the underlying functional adaptation mechanisms.

2. Materials and Methods

A multi-sensor headset system (PLUX, Lisbon, Portugal) with three EEG electrodes covering the sensorimotor and prefrontal regions, was used to monitor brain activity during gait with and without knee motion restriction. The complete experimental protocol is depicted in Fig. 1. Partial directed coherence (PDC) was applied on post-processed EEG data to estimate the time-dependent multivariate autoregressive (MVAR) coefficients which describe the information flow between the brain regions [2].

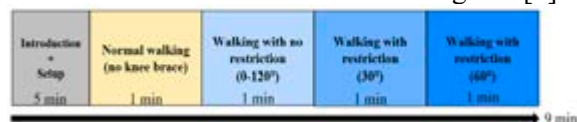


Figure 1: Experimental procedure during several conditions of knee restriction.

3. Results

The PDC maps reveal an increase and decrease in connectivity and information flow between various brain regions during the four

experimental conditions (as shown in Fig. 2). Fig. 3 shows significant variations in EEG connectivity networks between the experimental phases (for the no-brace phase, red represents a strong connection, whereas blue represents the other three knee brace phases).



Figure 2: The average PDC connectivity maps (a) no-brace phase, (b) range-of-motion phase, (c) knee restriction-at-30° phase, and (d) knee restriction-at-60° phase.

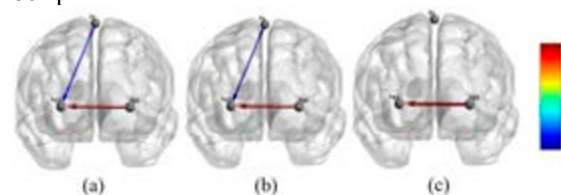


Figure 3: Significant connectivity between the phases (a) no-brace phase vs range-of-motion phase, (b) no-brace phase vs restriction-at-30° phase, (c) no-brace phase vs restriction-at-60° phase.

4. Discussion and Conclusions

PDC findings revealed that limited knee mobility decreased the information flow from left to right in the ventrolateral prefrontal cortex (vPFC), while enhancing the connection from the sensorimotor cortex to the right vPFC. This extends previous work suggesting a relevant CNS role, associated with visual processing and active explicit decision making, due to movement restriction.

5. References

1. E. R. Garwood, R. Tai, and G. Joshi, "The use of artificial intelligence in the evaluation of knee pathology," in SMR 2020, vol. 24, no. 01: TM Publishers pp. 021-029.
2. F. M. Al-Shargie, O. Hassanin, U. Tariq, and H. Al-Nashash, "EEG-Based Semantic Vigilance Level Classification Using Directed Connectivity Patterns and Graph Theory Analysis," IEEE Access, vol. 8, pp. 115941-115956, 2020.

TRANSCRANIAL DIRECT CURRENT STIMULATION FOR OCD PATIENTS: A FINITE ELEMENT STUDY USING PyAnsys

Julien Gosez (1), Karim El Houari (2), Michel Rochette (2), Sophie Collin (2), Wenfeng Ye (2), Arnaud Germaneau (3), Nematollah Jaafari (1), Nicolas Langbour (1), Prasanth Bokam (1), Ghina Harika Germaneau (1)

1. *Unité de Recherche Clinique, Poitiers, France*; 2. *Ansys, France*; 3. *Institut Pprime, CNRS, Université de Poitiers, France*

1. Introduction

The transcranial direct current stimulation (tDCS) shown to induce potent and long-lasting effects in obsessive-compulsive disorder (OCD) patients. However, some patients are resistant to the treatment, where there is still a gap clinically to understand this further. With the recent advancements in finite element methods, a computational tDCS pipeline using PyAnsys was used to study the brain activity in responders and non-responders OCD patients to find significant region of interest which better help the clinicians to improve the treatment for non-responders.

2. Methods

In the present study, 48 patients who suffered from OCD ($y_{bocs} \geq 21$) who took part in a clinical study of 105 days of tDCS treatment were chosen. YBOC scale had been measured at 14 days after the beginning of the trial. 16 of 48 patients responded to treatment and the rest are non-responders.

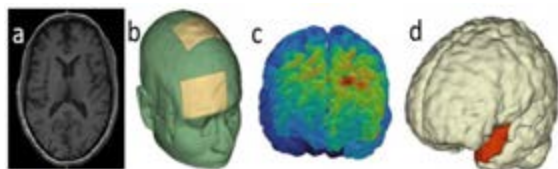


Figure 1: Automated tDCS model pipeline, (a) MRI images, (b) head model with electrodes placements, (c) simulations results and (d) statistical test for ROI.

We took subject's MRI data and segmented it using the SIMNIBS headreco procedure [1] to recover the anatomy of subjects' head (Fig. 1.a). We segmented skin, skull, csf, grey and white matter and applied the aal3 atlas [2] using CAT12 to recover regions of interest (ROIs) in the grey matter. We used a custom Python

programme to model electrodes by respecting their clinical position as describe in this paper [3]. We used PyMapdl package to perform a finite-elements simulation by applying current (2mA on the anode and -2mA on the cathode) between the modelled electrodes and sponge (Fig. 1.b).

3. Results

Fig. 1.c show finite-elements results. We computed mean of current density in every ROI to see correlation between responders and non-responders for 14 days. For that, we performed a Kruskal-Wallis test and ROI where p value were under 0.05 were considered significant. A post-hoc test has been performed to see if current density in responders were higher or lower than current density in non-responders.

4. Discussion and Conclusions

In the present study, we successfully developed a pipeline from MRI to simulations to compute current during tDCS session for each OCD patients. We see significant differences on left temporal pole and left superior temporal gyrus Fig. 1.d, with higher current density in non-responders. The scope of our future works includes two major parts, firstly to increase the number of patient data and to optimize the electrodes placement on patient specific MRI data to target the ROI which yield better response to tDCS treatment.

5. References

1. Nielsen J, Madsen K. *Neuroimage*, 2018, 174, 587-598.
2. Rolls E, Huang C. *Neuroimage*, 2020, 206, 116189.
3. Harika G, Heit D. *Brain Behav.* 2020; 10(7)e01648.



A PHYSICAL MULTIFIELD COMPUTATIONAL MODEL EXPLAINS THE ROLE OF DIFFERENT CELL TYPES IN CORTICAL FOLDING.

Mohammad Saeed Zarzor (1), Ingmar Blümcke (2), Silvia Budday (1)

1. Institute of Applied Mechanics, Friedrich-Alexander-University Erlangen-Nürnberg;
2. Neuropathological Institute, University Hospitals Erlangen, 91054 Erlangen, Germany

1. Introduction

The human brain is one of the most intriguing organs in our body. It undergoes a wide range of changes on both micro- and macroscopic scales during development, e.g., through neurogenesis at the cell scale and the formation of cortical folds at the tissue/organ scale. Different types of cells are generated, and each of these types plays an essential role in forming the brain. Neuroscientists have carefully assessed the pedigree relationship between different cell types. They have successfully investigated the behavior and role of each type on the microscopic scale. Still, the link between the changes on the microscopic scale and the formation of cortical folds on the macroscopic scale remains less well understood. From a mechanical point of view, mechanical forces generated as a result of cellular processes and brain growth play an important role in forming cortical morphology [1]. In this work, we mathematically link the changes on the microscopic scale with the forming cortical folds on the macroscopic scale.

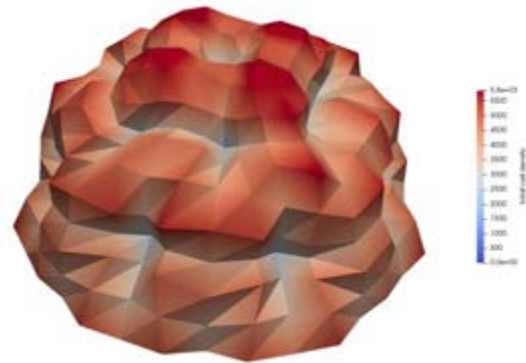
2. Materials and Methods

We establish a multifield computational model that couples multiple advection-diffusion equations (ADEs) with the theory of finite growth [2]. Each of the ADEs is formulated in such a way to mimic the biological behavior of a certain cell type, including cell proliferation, cell migration, and connectivity, Eq.1. We consider four cell types, i.e., radial glial cells, intermediate progenitor cells, outer radial glial cells, and neurons. Here, the differential growth of the cortex is controlled by the density of the neurons in the cortical layers.

$$\frac{j}{j} c + \dot{c} = -\nabla_x \cdot [\hat{v}(c, x) c - d^{cc}(x) \cdot \nabla_x c] + r_1^c(x, s) + r_2^c(x, s), \quad (1)$$

3. Results

Our results show how different cell types affect the formation of cortical folds. We observe, for instance, how a slight increase in the proliferation of radial glial cells during neurogenesis enormously increases the number of generated neurons and, thus, the complexity of cortical folds (Fig.1).



4. Discussion and Conclusions

The presented work not only allows us to better understand normal cortical folding but could also eventually help neuroscientists and clinicians to explore the reason behind abnormal cortical folding associated with diseases like epilepsy, which arise from disruptions in cellular development.

5. References

1. Budday S., et al., *Frontiers in cellular neuroscience*; 9:257 (2015).
2. Zarzor M.S., et al., *Brain Multiphysics*; 2, 100025 (2021).

Acknowledgements:

We gratefully acknowledge the funding by the Deutsche Forschungsgemeinschaft (DFG, German Research Foundation) through the grant BU 3728/1-1 to SB.



COMPUTATIONAL MODELING OF THE CEREBROSPINAL FLUID FLOW: EFFECT OF CILIA-INDUCED VELOCITY

Shunichi Ishida (1), Haruki Yoshida (1), Taiki Yamamoto (2), Takayuki Ishikawa (2), Yuichi Nagata (2), Kazuhito Takeuchi (2), Hironori Ueno (3), Yohsuke Imai (1)

1. Kobe University, Japan; 2. Nagoya University, Japan; 3. Aichi University of Education, Japan

1. Introduction

Ciliary motility disorders are known to cause hydrocephalus. The instantaneous velocity of cerebrospinal fluid (CSF) flow is dominated by artery pulsation, and it remains unclear why ciliary dysfunction results in hydrocephalus. In this study, we investigated the effects of cilia-induced surface velocity on CSF flow using computational fluid dynamics [1].

2. Materials and Methods

A geometric model of the human ventricles was constructed using medical imaging data. The CSF produced by the choroid plexus and cilia-induced surface velocity were given as the velocity boundary conditions at the ventricular walls. We developed healthy and ciliary-dysfunction models based on experimental data of cilia-induced velocity in healthy wild-type and *Dpcd*-knockout.

3. Results

We first investigated the intraventricular pressure of the healthy and ciliary-dysfunction models. There was almost no difference in pressure between two models (data not shown).

Next, we investigated the CSF exchange in the ventricles. Figure 1 shows how the newly produced CSF from the choroid plexus spreads into the ventricles after 5000 s in the healthy and ciliary-dysfunction models. The newly

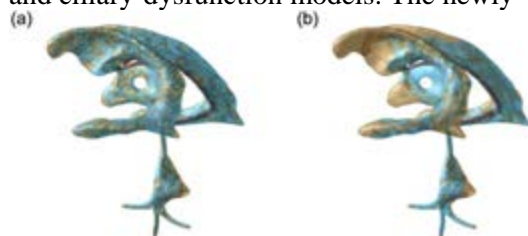


Figure 1: Spread of newly produced CSF (blue) from the choroid plexus into the ventricles after 5000 s, where the ventricles are initially filled with old CSF (brown): (a) healthy and (b) ciliary-dysfunction models.

produced CSF was greatly agitated and spread into all ventricles in the healthy model. However, in the ciliary-dysfunction model, it did not spread into the anterior and inferior horns of the lateral ventricles, and the anterior part of the third ventricle.

To evaluate the exchange ratio of the CSF locally, we divided the lateral ventricles into three regions: the anterior horn, body and inferior horn, as shown in figure 2a. The CSF exchange ratio after 1 h is shown in figure 2b. The local exchange ratio in the body of the lateral ventricles was the same for the healthy, ciliary-dysfunction, and no-cilia models. However, in the anterior and inferior horns, the no-cilia and ciliary-dysfunction models showed much lower exchange ratios than the healthy model.

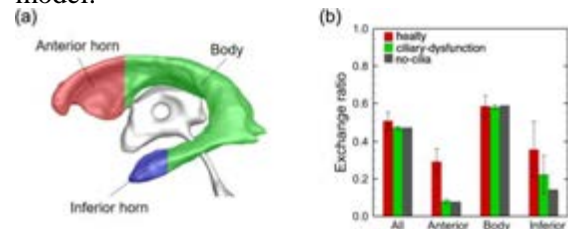


Figure 2: (a) The lateral ventricles are divided into three regions: anterior horn (red), body (green), and inferior horn (blue). (b) The exchange ratio in all ventricles, and the local exchange ratio in anterior horns, body and inferior horns of lateral ventricles after 1h.

4. Discussion and Conclusions

In this study, we numerically investigated the effects of the cilia-induced surface velocity on the intravascular pressure and CSF exchange in the cerebral ventricles for the healthy and ciliary-dysfunction models. The findings of this study suggest that a ciliary motility disorder could delay CSF exchange in the anterior and inferior horns of the lateral ventricles.

5. References

- Yoshida H et al., J. R. Soc. Interface, **19**:20220321 (2022).



SMOOTHED FINITE ELEMENT METHODS IN MODELLING AND SIMULATION OF ACTIVE CARDIAC CONTRACTION

Denisa Martonová (1)*, David Holz (1), Minh Tuan Duong (1,2), Sigrid Leyendecker (1)

1. Institute of Applied Dynamics, Friedrich-Alexander-Universität Erlangen-Nürnberg Germany;
2. School of Mechanical Engineering, Hanoi University of Science and Technology, Vietnam

*denisa.martonova@fau.de

1. Introduction

Smoothed finite element methods (S-FEMs) have been originally proposed by Liu and co-workers [1]. These methods combine the finite element method (FEM) and specific techniques from meshless methods, in particular strain smoothing over a designed smoothing domain (SD). The advantages and applications of S-FEMs are summarised e.g. in [2]. Briefly, S-FEM models are softer than their FEM counterparts using the same mesh, less sensitive to mesh distortion, able to overcome the volumetric locking problems and working well with triangular and tetrahedral meshes which can be generated automatically. Up to date, different S-FEMs have been implemented in biomechanical simulations for the growth of soft tissue, aortic valve opening or passive cardiac mechanics. In our work [3], node-based S-FEM (NS-FEM) is extended for the use in modelling and simulation of the active cardiac mechanics.

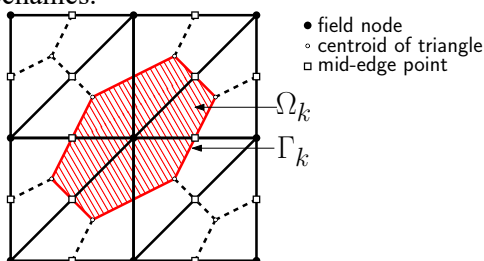


Figure 1: SDs in 2D for NS-FEM. In red, the SD around the node in the centre of the square is highlighted, from [3].

2. Materials and Methods

The basic idea of all S-FEMs is the strain smoothing over a specific SD, see exemplarily Figure 1 for a SD in 2D in NS-FEM. Initially, the domain Ω bounded by Γ is discretised into non-overlapping elements in the same way as in the FEM. Subsequently, it is subdivided into a finite number of non-overlapping SDs Ω_k with

boundary Γ_k . In the first numerical example, a homogenous 2D material representing a transversal cut through a healthy myocardium is considered. Additionally, myocardial infarction is modelled by reducing the active force in this region to zero. Secondly, an active contraction is induced in the fibre direction on a 3D geometry and the results produced by various S-FEMs are compared.

3. Results

The simulation results confirm that S-FEMs perform softer than linear FEM for both healthy and infarcted tissue samples. This is in agreement with the known softening effect of S-FEMs presented in previous works. We observe that, compared to FEM, NS-FEM is less computationally expensive considering the same number of degrees of freedom. Furthermore, even a coarse discretisation leads to nearly the same solution as FEM with a much finer mesh.

4. Discussion and Conclusions

The proposed method works well with automatically generated triangular and tetrahedral meshes. We conclude that S-FEMs are a promising tool for modelling of 3D cardiac active mechanics and electromechanics.

5. References

1. Liu et al, *Comput Mech*, 39:859-877, 2007.
2. Liu et al, *Front Struct Civ Eng*, 13: 456-477, 2019.
3. Martonová et al, *J. Biomech*, 115: 110153, 2021.

Acknowledgements:

The authors would like to gratefully acknowledge funding received through German Research Foundation (DFG) grant no. 496647562.

FASTER AND MORE RELIABLE SOLUTION ALGORITHMS FOR LARGE DEFORMATION FE MODELS

Sam Evans

School of Engineering, Cardiff University, UK

1. Introduction

Although finite elements are widely used for modelling large deformation, nonlinear problems, conventional solution algorithms remain slow, unreliable and frustrating, often requiring many attempts and extensive input from an expert user to reach a solution.

Conventional Newton-Raphson algorithms work well for mildly nonlinear problems but struggle with instabilities such as buckling or snap-through or where there are large strains. The size of the stiffness matrix increases as $O(N^2)$ so that the size of problem that can be solved is limited by available memory. One possible way to avoid these problems is direct solution of the nonlinear problem using conjugate gradient methods.

2. Methods

A nonlinear conjugate gradient algorithm was implemented in FEBio (the CG-Solid solver) using the Hager & Zhang CG_DESCENT algorithm [1] with a modified line search. Various preconditioners were implemented, based on the idea of using a single diagonal representing the compliance of each node. The challenge is to compute a reasonable approximation to the compliance without assembling the full stiffness matrix.

3. Results

Fig. 1 shows the solution time for models with different numbers of elements; it is clear that the CG-Solid solver is much faster and requires fewer timesteps than the usual BFGS solver. Fig. 2 shows a very large deformation model solved in a single time step, demonstrating the robustness of the CG-Solid solver.

4. Discussion and Conclusions

Nonlinear conjugate gradient algorithms are highly effective for certain types of problem but perform poorly where there are large differences in stiffness between degrees of

freedom, particularly in adjacent nodes such as when using quadratic elements. Then the less stiff nodes move faster, resulting in excessive element distortion and failure. A suitable preconditioner can greatly alleviate this problem and there are exciting opportunities for further development.

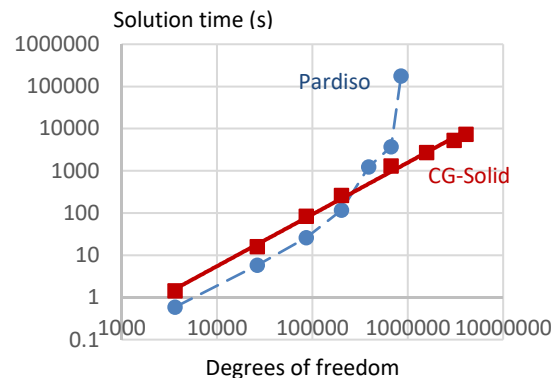


Figure 1: Solution time for different size models.

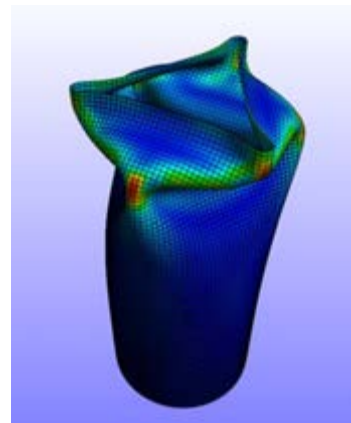


Figure 2: Yoshimura buckling of a tube, solved in a single time step.

5. References

- Hager, WW & Zhang H, SIAM J Optim. 16(1):170-192 (2005).

Acknowledgements: The assistance of Steve Maas in implementing the algorithms in FEBio is gratefully acknowledged.



UNIFIED POSITION-BASED DYNAMICS SOLVER FOR SURGICAL SIMULATION

Andrew Wilson (1), Jacob Moore, PhD (1), Harald Scheirich (1), Ganesh Sankaranarayanan, PhD (2), PhD, Rachel B. Clipp, PhD (1)

1. Kitware Inc., U.S.A; 2. University of Texas Southwestern Medical Center at Dallas, U.S.A.

1. Introduction

Virtual surgical simulation is a growing segment of medical simulation with unique needs for real-time accurate physics-based models. Surgical tools that interact and collide with multiple elements of a simulation, such as suture threads, other tools, tissues, and fluids, lead to complicated constraints. Solving each set of collisions individually can impact performance. A fully unified position-based dynamics (PBD) framework for real time surgical simulation was implemented in the open-source interactive Medical Simulation Toolkit (iMSTK) to address these limitations. The unified solver builds on the existing PBD model [1], [2] with rigid bodies [3] in iMSTK. The unified solver allows the simulation to capture the multiple two-way interactions and collisions associated with surgical simulations within a single constraint-based framework and linear solver. This method is robust and fast.

2. Materials and Methods

The PBD implementation [3] is composed of particles and constraints. Particles have positions, orientations, velocities, angular velocities, masses, and inertias. A constraint is a function of particle positions, orientations, or both yielding a single constraint value. Given a system of many constraints, these non-linear equations are linearized and iteratively solved to obtain positions and orientations for all constraints at zero. Because PBD is position based, the recalculation of these constraint values is computationally efficient, other systems would require expensive integrations of velocities or forces to produce new positions. iMSTK's existing semi-implicit rigid body solver was compared to the implicit unified solver to evaluate computational accuracy.

3. Results

The comparison of the two methods demonstrates that the unified solver produces more accurate and smoother forces, Fig. 1.

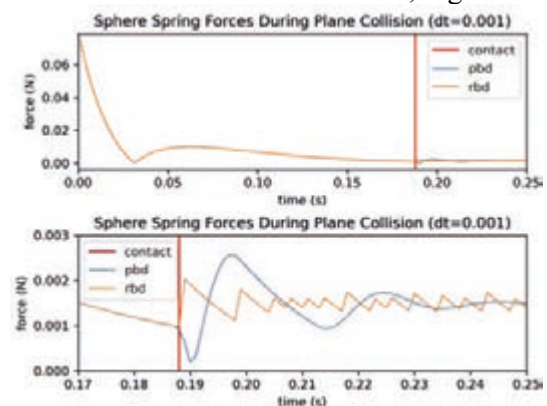


Figure 1: A critically damped spring attached to a rigid body contacting a deformable surface. Orange and blue represent velocity-based and position-based rigid body systems, respectively.

4. Discussion and Conclusions

This is the first implementation of PBD that includes rigid bodies in an open source surgical toolkit (iMSTK). This implementation is being used in simulation of tasks in a laparoscopic hiatal hernia procedure to represent complex two-way interactions and improve performance.

5. References

1. Muller M., Heidelberger B., et al. "Position based dynamics, J Vis Commun Image Represent, 18:2, p109-118, 2007.
2. Macklin M. Muller M., Chentanez N., XPBD: Position-Based Simulation of Compliant Constrained Dynamics; 2016.
3. Muller M., Macklin M., Chentanez N., et al., Proc. Of the ACM SIGGRAPH; 2020. 10(1-12).

Acknowledgements:

The authors would like to thank the NIH (Grant no: 1R01EB025247 and R01EB031808) for providing financial support to this project.



NUMERICAL SCHEME FOR DYNAMIC ELASTOGRAPHIC MEASUREMENTS ON THE CORNEA

Giulia Merlini (1), Jean-Marc Allain (1), Sébastien Imperiale (2)

1. LMS, Ecole Polytechnique, CNRS — Inria — Université Paris-Saclay, France ;

2. Inria — LMS, Ecole Polytechnique, CNRS — Université Paris-Saclay, France

1. Introduction

Dynamic elastography is a fundamental technique to study the local mechanical property of the tissues, such as cornea. It is based on in-vivo tracking of shear waves propagation as a result of a transient stimulation. In nearly incompressible materials, such as the cornea, the shear waves are 150 times slower than the compressional waves. The incompressibility and the double-scale of the phenomena make the FE approximation difficult. The objective of this study is to propose an efficient scheme to obtain a reliable modelling of transient elastography measurements applied to the cornea and to improve tissue characterization techniques.

2. Materials and Methods

The acoustic radiation force is a common mechanical stimulation to generate low-frequency shear waves. In order to model the resulting shear-wave propagation phenomenon, we propose a FE approximation with high-order spectral elements together with Mass Lumping approach. This allows to avoid the inversion of mass matrix at each time-step by computing an approximated value of the mass integrals with a numerical integration formula (Gauss-Lobatto rule) [1].

Incompressibility is a well-known problem in FE approximation with pure displacement method, due to locking, ill-conditioning of the stiffness matrix and incorrect pressures approximations. To overcome these limitations, we use a mixed formulation with the introduction of the pressure as a local variable defined on each element. The approximation of the displacement and the pressure field are performed with \mathbb{Q}_4 - \mathbb{Q}_2^{disc} elements as proposed in [2].

For the time discretization, the explicit leapfrog scheme shows high efficiency and second order accuracy. However, the time-step is strongly decreased by the velocity of the compressional wave [3]. In this study, we propose a strategy inspired by local time-stepping method. The contribution of pressure wave is computed explicitly in an inner loop. While maintaining stability and accuracy, we obtain a fully explicit algorithm that is more efficient in terms of CPU time compared to the standard LF scheme.

3. Results and Perspectives

We have performed simulations of elastic wave propagation on a homogeneous isotropic cornea with a CPU time of 75 minutes.

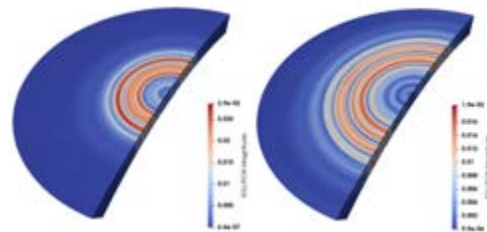


Figure 1: Left: $t = 2$. Right: $t = 3s$. Simulation with $\lambda/\mu = 500$ (Lamé parameters) and 2,5 MDoF.

In preliminary simulations we achieve a computational time three times lower, with a relative $L^2(\Omega)$ -error on the displacement of the order of 4% compared to the LF scheme. The natural extension of this work is to perform simulations taking into account the pre-stress state with a non-linear law and then integrate the model with the anisotropic behavior related to the lamellar structure of the cornea.

5. References

1. Cohen, G. C. (2002).
2. Bernardi, C., & Maday, Y. (1999).
3. Ye, W., Bel-Brunon, A., Catheline, S., Rochette, M., & Combescuré, A. (2017).



ONE DIMENSIONAL MODEL OF THE MICROVASCULAR NETWORK OF THE RETINA : APPLICATIONS TO MULTIPLES STENOSES

Laureline Julien * (1,2), Michel Paques (2,3), José-Maria Fullana (1)

1. Institut Jean le Rond d'Alembert, Sorbonne Université, Paris, France ; 2. Institut de la Vision, Paris, France ; 3. Centre d'Investigation Clinique 1423, Hôpital des Quinze-Vingts, INSERM, Sorbonne Université, Paris, France

* laureline.julien@dalembert.upmc.fr

1. Introduction

In cardiovascular disorders the microvascular network of the retina may undergo hemodynamics and morphological perturbations. The severity these disorders can produce a rapid alteration of the vision. Focal stenoses may affect the network according to their characteristics (severity, length). We propose a 1D patient-specific retina model of arterial microcirculation and to use it to study the hemodynamics impacts of focal stenoses. Our model is based on conservation laws, and on multimodal imaging. The model simulate the blood flow from the central retina artery to the terminal smallest arterioles.

2. Materials and Methods

The 1D microcirculatory model developed gives us the area and the flow rate deduced from Navier-Stokes equations integrated over the section [1]. The apparent viscosity takes into account the Fåhræus-Lindqvist effect [2]. The morphological data : vessel diameters, positions and lengths are extracted by segmentation of confocal Scanning Laser Ophthalmoscope and Adaptive Optics Ophthalmoscope images. Those data allow us to build the geometry imposed of the simulation. Doppler Ultrasound gives us quantitative data of flow rate $Q_{in}(t)$ that is imposed at the input of the network.

3. Results

The study case is a patient affected by a stenosis of the left carotid artery. We choose the network of the right eye as a healthy model. Blood flow in vessels resulting from the simulation is in Fig. 1. First, results for a

healthy patient are compared to data from the literature [3] and show comparable results in terms of magnitude and behaviour. Then, for the pathological simulations we applied a stenosis (Fig. 1). We perform simulations for different degrees, length and profiles of stenoses.

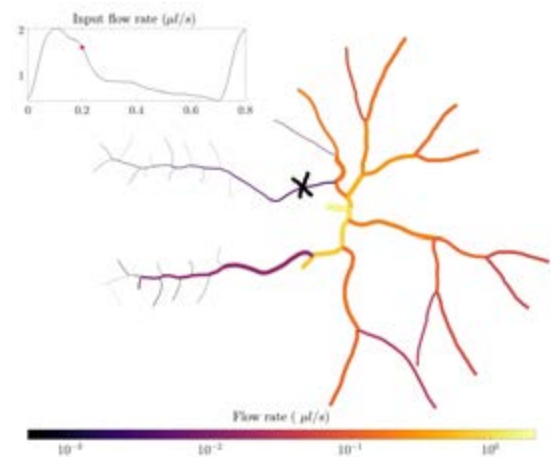


Figure 1: Flow rate snapshot obtained with the model without stenosis. Top-left : the flow $Q_{in}(t)$, red dot indicates the position on the cardiac cycle. The black cross is the position of the stenosis.

4. Discussion and Conclusions

We compare simulations with and without stenosis. Upstream of the stenosis differences are observed only after a certain degree of stenosis.

5. References

1. Ghigo A. et al., Journal of non-newtonian Fluid Mechanics. 253.36–49 (2018).
2. Fåhræus R, Lindqvist T. Journal of Physiology-Legacy Content. ; 96.3:562–568 (1931).
3. Causin P. et al., Biomechanics and Modeling in Mechanobiology ; 15.3:525-542 (2016)



PRESTRESSING ALGORITHMS FOR ARTERIAL WALL MECHANICS: ANALYSIS OF THE ROBUSTNESS AND UNIQUENESS

Klaas Vander Linden (1), Lauranne Maes (1), Nele Famaey (1)

1. Biomechanics Section, Mechanical engineering, KU Leuven, Belgium

1. Introduction

Simulations of arterial wall mechanics often use image-based data to define the *in vivo* geometry. However, this state is not stress-free, such that prestressing algorithms are required to ensure mechanical equilibrium given the corresponding *in vivo* boundary conditions [1]. This study investigates the robustness of a prestressing algorithm with a special focus on the uniqueness of the resulting transmural stress distribution.

2. Materials and Methods

We model the artery as an axisymmetric thick-walled cylinder with an inner radius of 15mm and thickness of 2mm corresponding to a diastolic configuration at 80mmHg. We consider a constrained incompressible mixture of an isotropic elastin matrix and two symmetrically oriented collagen fibre families. The diastolic configuration is prestressed according to [2, 3]. In short, the unstressed *in vivo* diastolic geometry is pressurized while a constant prestretch is assigned to collagen and an initial prestretch tensor $\mathbf{G}_e = \text{diag}(1/(g_{zz}g_{\theta\theta,init}), g_{\theta\theta,init}, g_{zz})$ is assigned to elastin, with g_{zz} a known constant axial prestretch and $g_{\theta\theta,init}$ the initial circumferential prestretch. Next, \mathbf{G}_e is updated iteratively by multiplying the tensor with the current deformation gradient with respect to the diastolic reference while holding the initially applied loading conditions. Once the diastolic geometry is obtained, the cylinder is loaded to a systolic pressure of 120mmHg.

3. Results

Fig 1. shows the transmural distribution of the circumferential Cauchy stress $\sigma_{\theta\theta}$ in the diastolic and systolic state (left) with the corresponding diameter (D) - pressure (P) relationships (right), for six different cases of $g_{\theta\theta,init}$ ranging from 0.5 to 2.0.

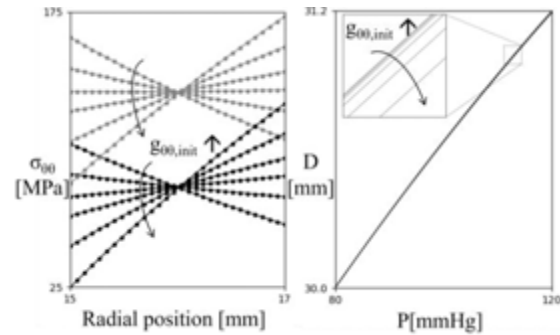


Figure 1: Left: transmural $\sigma_{\theta\theta}$ at diastole (black) and systole (gray) for different $g_{\theta\theta,init}$; Right: diameter-pressure relationships for different $g_{\theta\theta,init}$.

4. Discussion and Conclusions

The results show that a prestressed state of an *in vivo* geometry is not uniquely defined even though the corresponding $D(P)$ behaviour remains similar. The choice of $g_{\theta\theta,init}$ highly influences the maximal stress. This problem is valid for every prestressing algorithm that does not impose any prior assumption on the transmural prestress or stretch distribution. It has been suggested that the transmural stress gradient at vascular homeostasis is minimal, or that developmental prestretches are the highest at the luminal side [4]. As some of these assumptions are purely hypothetical or may only be valid for healthy tissue, more research is needed that links computational data with microstructural observations.

5. References

1. Weisbecker *et al.* Int. J. Numer. Meth. Biomed. Eng. 2014; 30:857–872
2. Famaey *et al.* ZAMM. 2018; 2239–2257
3. Bellini *et al.* Ann Biomed Eng 2014; 488–502
4. Cardamone *et al.* Biomech. Model. Mechanobiol. (2009) 8:431–446

Acknowledgements:

The authors would like to thank Research Foundation – Flanders (FWO) (Grants no: SB1SA9119N, 11A6519N) for providing financial support to this project.



NUMERICAL SIMULATION OF THE ONSET OF THE SECOND STAGE OF LABOR

Alice M. Collier (1), Ghaidaa A. Khalid (2), Mike D. Jones (3), Kristin Myers (4), and Antoine Jerusalem (1)

1. Department of Engineering Science, University of Oxford, UK; 2. College of Electrical Engineering Techniques, Middle Technical University, Iraq; 3. Cardiff School of Engineering, Cardiff University, UK; 4. Department of Mechanical Engineering, Columbia University, USA

1. Introduction

During vaginal labour, the fetal head moulds to accommodate the geometric constraints of the birth canal. By also causing change in the shape of the brain, excessive moulding can produce brain injuries and long-term sequelae [1]. While previous research focusing on fetal head moulding has predicted the moulding during the second stage (descent through the vaginal canal) [2], an in-silico model predicting the loading of the fetal brain has still not been proposed. This study proposes a finite element model of the fetal head and maternal canal environment, capable of predicting the stresses experienced by the fetal brain during the onset of the second stage of labour.

2. Materials and Methods

To simulate labour, a fetal head and a maternal finite element model were adapted from existing studies [3,4] to better represent the geometry of an at-term pregnancy at the onset of the second stage of labour.

A large amount of deformation occurring at the sutures during labour. As such, to prevent excessive distortion of elements, the folding of the sutures was modelled separately, and an energy equivalent suture constitutive model was used in the overall head model. All other material models were taken from the literature.

3. Results

Two labour scenarios were simulated and compared, the fetus presenting left-occiput-anterior (LOA) and left-occiput-posterior (LOP). The fetal head was displaced into the canal by imposing a trajectory.

The simulations for both configurations will be presented during this talk.

4. Discussion and Conclusions

Differences and peak deformation and stress can be observed between LOA and LOP, with minimum effect on the force required to displace the fetus or stretch of the maternal uterus. This and more detailed analysis will be presented in this talk, with data available in Ref. [5].

5. References

1. N. N. Rabelo et al., *Arq. Neuropsiquiatr.*, 75:180–8 (2017).
2. R. Moura et al., *Int. J. Numer. Meth. Biomed. Engng.*, 37:e3411 (2021).
3. G. A. Khalid et al., *Forensic Science International.*, 300:107-86 (2019).
4. A. R. Westervelt et al., *Journal of Biomedical Engineering.*, 139:051004-1–11 (2017).
5. A. M. Collier, G. A. Khalid, M. D. Jones, K. Myers and A. Jerusalem. In preparation.

Acknowledgements:

The authors would like to thank EPSRC for providing financial support to this project.



DEVELOPING A BIOMECHANICAL MODEL TO STUDY OASIS

Dulce Oliveira (1), Rita Moura (1), Catarina Rocha (2), Marco Parente (1),
Teresa Mascarenhas (3) and Renato Natal (1)

1. INEGI, LAETA, FEUP, Portugal; 2. FEUP, Portugal; 3. FMUP, LAETA, Portugal

1. Introduction

Most women who have a vaginal delivery will experience some type of injury to the perineum, with a laceration occurring in up to 80% of vaginal deliveries [1]. Currently, obstetric anal sphincter injuries (OASIS), defined as third- and fourth-degree tears, are less common, occurring in approximately 3% and 1% of deliveries, respectively. The most devastating complication of OASIS is anal incontinence, described as an involuntary loss of flatus, liquid or solid stool, which is a serious social and hygienic problem. This work will present some challenges in characterizing the anal sphincter and its insertion in a computational model that includes the pelvic floor and perineum.

2. Materials and Methods

A geometric model of the pelvic floor muscles and perineum was developed, including the region of the sphincter anal. The latter region has been fused to the pelvic floor muscles through a tie constraint that prevents relative motion between them. The anal sphincter was characterized using data from the literature (Table 1) [2].

Table 1: Anal sphincter characterization: average thickness in millimetres of the female anal sphincter muscles; and constitutive parameters of the Neo Hookean model. IAS: Internal Anal Sphincter. EAS: External Anal Sphincter.

Structure	IAS	EAS
Thickness	2.69 mm	5.75 mm
Constitutive parameters	$C_{10}=0.5$ MPa $D_1=0.0001$	$C_{10}=1.5$ MPa $D_1=0.001$

A vaginal delivery simulation was performed with a rigid foetal head in the vertex presentation and occipito-anterior position. The maximum principal stress and stretch were analysed in the pelvic structures and in a defined path between the EAS and the vaginal opening.

3. Results

The maximum principal stresses were observed in the urogenital hiatus. Relative to the perineal body, the maximum principal stress obtained was almost 75% lower. At the vaginal opening, the maximum principal stress was more than 80% lower than that measured at the urogenital hiatus, considering the instant of maximum perineal stretch. The maximum stretch of the perineal body was 2.5.

4. Discussion and Conclusions

The inclusion of the perineum in the biomechanical model is a step forward for the complete representation of maternal soft tissue. The inclusion of more structures allows increasingly reliable results to be achieved. However, it is necessary that the relationships between the different structures are well established. In this work we found that the stresses in the perineal body are much lower than the stresses recorded in the urogenital hiatus. One would expect high stresses in this region of the perineum body due to it being a structure prone to tearing during vaginal delivery. This behaviour may be due to inadequate modelling of the contact between the structures.

5. References

1. Fleming N et al., J Midwifery Women's Heal; 48(1):53-59 (2003).
2. Junior H, Ultra-sonografia transperineal como método de imagem para avaliação do canal anal e esfíncteres anais. MSc Thesis (1999).

Acknowledgements:

The authors acknowledge the support from Portuguese Foundation of Science under the Junior Researcher Contract CEECIND/01522/2020, the Grant SFRH/BD/05876/2021, and the funding of Project UIDB/50022/2020 cofinanced by NORTE2020, through FEDER.



FINITE ELEMENT MODELING OF CESAREAN SECTION SCARS

Adrienne K. Scott (1), Erin Louwagie (2), Kristin Myers (2), Michelle Oyen (1)

1. Washington University in St. Louis, United States; 2. Columbia University, United States

1. Introduction

Uterine rupture is an intrinsically biomechanical process associated with high maternal and fetal mortality [1]. A previous C-section is the main risk factor for uterine rupture in a subsequent pregnancy due to failure of the tissue at the scar region [1]. Although improved imaging methods allow for the evaluation of the scar tissue, there is currently no reliable model to predict uterine rupture. Finite element (FE) modeling of the uterus and scar tissue presents a promising method to further understand and predict uterine ruptures.

2. Materials and Methods

Modeled geometries of a uterus, cervix, C-section scar, and abdomen were generated in Solidworks. MRI images from an at-term pregnant patient were used to generate the uterus geometry [2]. All geometries were meshed with Hypermesh and were modeled as a nearly incompressible (Poisson's ratio=0.48) neo-Hookean elastic material. The Young's modulus (E) of the abdomen and the uterus were set to 100kPa, while the Young's modulus of the scar tissue was varied (50kPa, 100kPa, 200kPa). The boundary conditions and a physiological intrauterine pressure (2.6kPa [3]) were applied as shown in Fig. 1A. A finite element analysis was performed using FEBio to generate heat maps of 1st principal Lagrange strain and von Mises stress.

3. Results

The von Mises stress on the C-section scar was greater for sagittal scars in comparison to the transverse scar with the same stiffness (Fig 1B). As expected, the von Mises stress increased in the scar region with increasing scar stiffness, while the 1st principal Lagrange strain decreased (Fig. 1B). The models in which the scar tissue stiffness matched the stiffness of the uterus showed the expected null result and validated the boundary conditions.

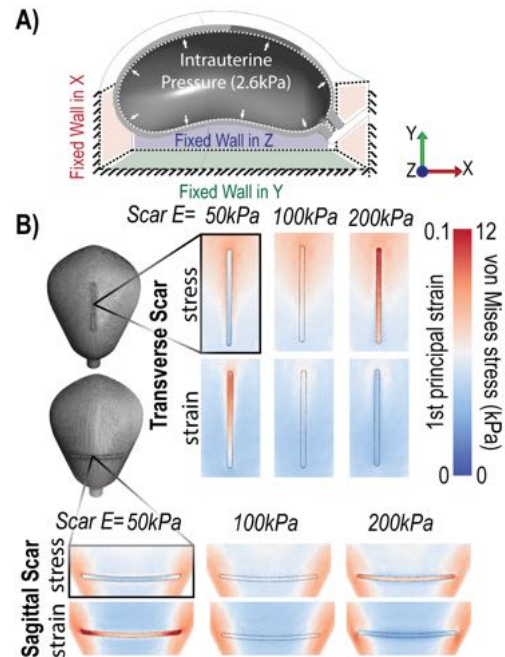


Figure 1: A) The abdomen walls were fixed in the X, Y, and Z direction and an intrauterine pressure was applied. B) Heat maps of von Mises stress and 1st principal Lagrange strain were generated.

4. Discussion and Conclusions

The modeled stress distributions confirmed clinical observations; there is an increased risk of uterine rupture in sagittal scars compared with low transverse scars. With further characterization of the mechanical properties of uterine scar, computational models could be a powerful tool for surgical planning.

5. References

1. Schepker N et al., Arch Gynecol Obstet.; 291: 1417-1423 (2015).
2. Rajasekharan D et al., Summer 2020 Undergrad Project- Late Pregnancy Uterus Model; (2020).
3. Wheeler ML, Oyen ML., Front Physiol; 11:524 (2020).

Acknowledgments:

The authors would like to acknowledge the NIH T32 Grant (T32 EB028092).



DEVELOPMENT AND CALIBRATION OF A BILAYER FETAL MEMBRANE MODEL USING EXPERIMENTAL DATA

Daniel Fidalgo (1), Kayvan Samimi (2), Emmanuel Contreras Guzman (2), Michelle Oyen (3), Helen Feltovich (4), Tim Hall (5), Melissa Skala (2), Dulce Oliveira (1), Kristin Myers (6)

1 LAETA, Portugal, 2 Morgridge Institute for Research, USA, 3 Washington University in St. Louis, USA, 4 Intermountain Health, USA, 5 University of Wisconsin, USA, 6 Columbia University, USA

1. Introduction

The fetal membrane is a complex structure, comprising two main layers: the amnion and the chorion [1,2]. They are separated by a spongy layer. The fetal membrane also comprises the decidua, which is in direct contact with the uterine wall [3]. The main goal of this work is to formulate a bilayer fetal membrane material model using experimental data from an inflation mechanical test carried on by the *Skala Lab* - Morgridge Institute for Research.

2. Materials and Methods

The inflation experimental data was performed by the *Skala Lab* - Morgridge Institute for Research. The peri-placental fetal membrane samples (amnion + chorion + part of the decidua) were harvested from c-section deliveries and each disk had a diameter of 6 cm. The inflation mechanical test has a clamping piece with 30 mm diameter opening and a fillet edge to avoid sharp edges. A 10 kPa/min pressure ramp was applied. Concerning the bilayer fetal membrane model (Figure 1), the amnion was characterized with a modified version of Buerzle-Mazza constitutive model ($\mu=2.4\text{MPa}$, $q=2.96$, $m_5=0.463$, $m_2=0.00228$, $m_3=41.12$, $m_4=1.27$, $N=32$, $\nu=0$), while the chorion ($E=1\text{MPa}$, $\nu=0.41$) and the decidua ($E=1\text{MPa}$, $\nu=0.49$) were characterized by elastin linear properties. The simulation of the inflation mechanical test was developed under the same conditions as the one by the *Skala Lab*.

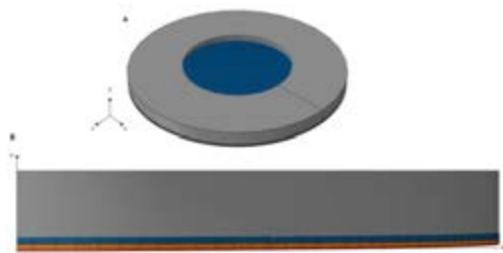


Figure 1: Finite element setup of the inflation mechanical test using the bilayer fetal membrane model; A: general view; B: detailed view (gray: clamping ring; blue: decidua; orange: chorion; red: chorion).

3. Results

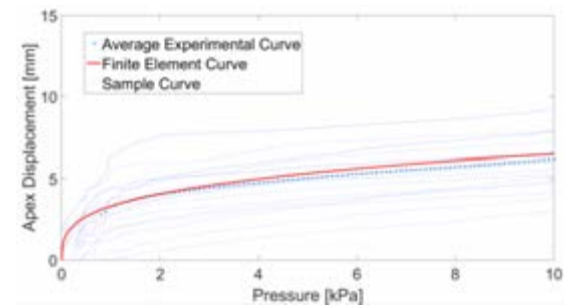


Figure 2: Calibration of the bilayer fetal membrane model using the experimental apex displacements.

4. Discussion and Conclusions

The maximum relative error (%) calculated between the experimental and the finite element curves of the apex displacement is lower than 5%, which indicates a good agreement between the experimental data and the mechanical outcomes of our model. This highlights the potential of our model to study several obstetrical factors, such as the premature rupture of the fetal membrane.

5. References

- [1] Buerzle et al, *JBiomech*, 46: 1777-1783, 2013;
- [2] Verbruggen et al, *PLoS ONE*, 12 (3): e0171588, 2017;
- [3] Tahan and Tahan et al, *Front. Med*, 1: 48, 2014.

Acknowledgments:

The authors truly acknowledge the support from the Portuguese Foundation for Science and Technology (FCT) under grant 2020.05400.BD, the *Skala Lab*, the Oyen lab at Wash U, and the Myers Lab at Columbia.



IMPACT OF PERINEAL STRUCTURES IN THE BIOMECHANICAL ANALYSIS OF CHILDBIRTH

Rita Moura (1), Dulce Oliveira (2), Marco Parente (3), Teresa Mascarenhas (4), Renato Natal (5)

1. INEGI-FEUP, Portugal; 2. INEGI, Portugal; 3. FEUP, Portugal; 4. FMUP, Portugal. 5. FEUP, Portugal.

1. Introduction

Childbirth trauma affects millions of women worldwide. The incidence of perineal trauma is over 85% in nulliparous women. Severe degrees of perineal trauma and levator ani injuries are associated with decreased women's quality of life [1]. Most biomechanical studies focus only on levator ani lesions and, despite being a widely discussed subject, childbirth trauma remains unpredictable [2]. This work aims to create a finite element model of the pelvic floor and perineum, to understand the impact of including the perineal structures in childbirth simulations and identify the most affected areas.

2. Materials and Methods

A geometric model of the pelvic floor muscles (levator ani and coccygeus) and perineum (perineal body, external anal sphincter, ischio-cavernosus, bulbospongiosus, superficial and deep transverse perineal muscles) was created (Fig. 1). The geometries were modelled in Rhinoceros[®] according to descriptions from literature and advice from obstetricians. Then, a finite element mesh consisting of C3D8H type elements was created in Abaqus[®], with different thicknesses defined between muscles.

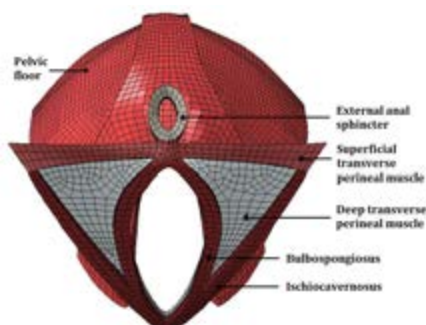


Figure 1: Finite element model of the pelvic floor muscles and perineum.

Two simulations of vaginal delivery with a rigid fetal head in the vertex presentation and occipito-anterior position were performed, with and without the inclusion of the perineum.

3. Results

The maximum principal stresses were measured in the urogenital hiatus in both simulations, which were 50.2% higher when the perineum is included, with a maximum stress of 17.83 N. For the instant of maximum perineal stretch, the maximum stress obtained in the vaginal opening was 3.40 N. The stresses were also measured in a path between the external anal sphincter and the vaginal opening, aiming to analyze the area of a possible perineal tear. The maximum stress obtained was 4.49 N. Furthermore, the maximum stretch of the perineal body was equal to 2.5.

4. Discussion and Conclusions

Childbirth computational models rarely include other structures than the levator ani muscle. Since the fetus is confined to a very limited space, the inclusion of anatomical structures that restrict fetal movement is crucial to correctly mimic its cardinal movements. In this work, the perineum was included in the finite element analysis of childbirth. The results between the simulation with and without the perineum showed major differences, indicating that its presence influences the results of childbirth simulations. The development of a complete representation of the maternal soft tissues is a need to achieve reliable outcomes.

5. References

1. Doumouchtsis, S. Springer, 2016.
2. Howard, D. et al. *Int Urogynecol J*, 27(12):1811–1815, 2016.

Acknowledgements:

The authors acknowledge the support from Portuguese Foundation of Science under the Grant SFRH/BD/05876/2021, the Junior Researcher Contract CEECIND/01522/2020, and the funding of Project UIDB/50022/2020 cofinanced by NORTE2020, through FEDER.



A FINITE ELEMENT MODEL OF PROLAPSE MESH INCLUDING FILAMENT-LEVEL INTERACTIONS

Madeline Hackett, BS (1), Teseo Schneider, PhD (2), Zachary Ferguson, BS (3) Daniele Panozzo, PhD (3), Denis Zorin, PhD (3), Pamela Moalli, MD (1) Steven Abramowitch, PhD (1)

1. University of Pittsburgh, USA; 2. University of Victoria, CA; 3. New York University, USA

Corresponding author: Madeline Hackett, mep118@pitt.edu

1. Introduction

Urogynecological mesh devices are used for the treatment of female pelvic organ prolapse and have been associated with high rates of complications. Recent data suggest that local tissue stress variations resulting from interactions between the device and the host are relevant [1]. In a step towards modeling such interactions, this study shows that experimental force measurement can be closely matched by a simulation model capturing individual filament geometry and their interactions through contact and friction forces.

2. Materials and Methods

Restorelle (Coloplast, Inc.) was chosen for its popularity in surgical prolapse repair procedures. The geometry of the device was acquired using a SkyScan 1272 microCT system. The images were thresholded to create a rough 3D geometry (3DSlicer, slicer.org). In Blender (blender.org; v.3.3.1), a series of circles were manually fit to each filament and lofted to create a smoothed geometry. The simulation mesh (104,906 tetrahedra) was generated using Houdini (sideFX, Inc.; v. 19.5) and fletwild [2]. The geometry of the ballhead was based on a CAD representation of that used in the experiment. The simulation was performed in PolyFEM, a finite element solver that incorporates a potential contact model in a robust and accurate high order elastodynamic FE simulation that does not suffer from intersections or inverted Jacobians [3,4,5]. Boundary conditions were assigned to match the experiment and a Neo-Hookean material model specific to polypropylene and steel was assigned to the device and ballhead, respectively. The contact force on the ballhead was plotted versus the displacement and compared to experimental results.

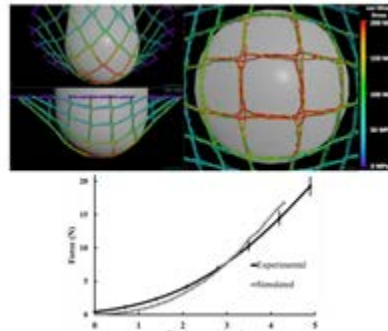


Figure 1: (Top) von Mises stresses in the mesh device as viewed from multiple perspectives. (Bottom) Resulting force-displacement curve compared with experimental data (mean±SD, n=4).

3. Results

Visually and quantitatively, the simulation matches the kinematics of the experiment well. Stresses are concentrated near the tip of the ballhead and along vertical and horizontal filaments with local heterogeneity (Figure 1). Contact forces match the general trends of the experimental data with the greatest deviations at smaller and larger displacements.

4. Discussion and Conclusions

Overall, this study demonstrated the feasibility of simulating a urogynecological textile device while incorporating filament-to-filament interactions. Future work will optimize performance and improve the material model to increase the simulation fidelity.

5. References

1. Knight *et al.*, 2018.
2. Hu *et al.*, *TOG*, 2020.
3. M. Li *et al.*, *par.nsf.gov*, v.39(4), p. 20, 2020.
4. Feola *et al.*, *Int Urogyn J*, v.24(4), p. 559, 2013.
5. Schneider *et al.*, PolyFEM, 2019.

Acknowledgements: NIH R01 HD097187-01, NSF 2053851, NSF 1835712



COMPUTATIONAL HOMOGENIZATION OF HISTOLOGICAL MICROSTRUCTURES IN HUMAN PROSTATE AND CANCER

Calum Anderson (1), Chara Ntala (2), Ali Ozel (1), Robert L Reuben (1), Yuhang Chen(1)

1. Heriot-Watt University, Institute of Mechanical, Process and Energy Engineering, United Kingdom
2. Western General Hospital, Department of Pathology, United Kingdom

1. Introduction

Human prostatic tissue exhibits complex mechanical behaviour due to its multiphasic, heterogeneous nature, with hierarchical microstructures involving multiple tissue constituents, all interconnected in complex networks. This study aims to establish a computational framework to quantify how microstructure changes in prostate under different pathophysiological conditions including cancer affect mechanical behaviours.

2. Materials and Methods

2D and 3D representative tissue microstructure models were reconstructed from high-resolution histology images. Tissue constituents in human prostate such as epithelial compartments, acinar lumens and stroma were modeled as hyperelastic materials, and collagen fibres in stromal tissue were also accounted for using the HGO model [1]. Fabric tensor analysis of different structures was performed in search of principle directions, before formulation of finite-element based homogenization using periodic boundary conditions [2] (Fig. 1) was employed to quantify the apparent properties of prostate tissue samples.

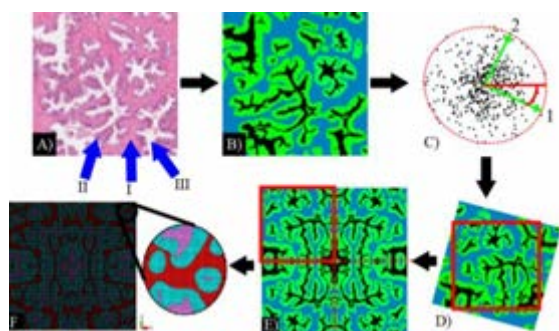


Fig 1. Modelling schematic. A) Raw histology image; B) segmented tissue constituents; C) tissue fabric tensor analysis - principal directions; D) rotating the RoI using principal directions; E) mirroring for perfectly orthotropic RVE; and F) finite element mesh. Arrows in (A) indicate; (i) stoma; (ii) epithelial compartments; (iii) acini.

3. Discussion and Conclusions

A strong correlation between the area fraction of the tissue constituents and their microstructural fabric tensor was observed. Results showed a significant anisotropy, both structural and mechanical, and tension-compression asymmetry of the apparent behaviours of the prostatic tissue, given rise by the critical role of collagen fibre network in the stromal tissue. The comparison study suggested a strong influence of stromal tissue in determining the apparent properties of normal tissue, and the epithelium-dominated behaviour in prostate cancer. The direction and degree of mechanical anisotropy was found to be closely linked to the structural anisotropy of the tissue, especially stromal anisotropy in normal prostatic tissue. This work presented a histology-based computational homogenization approach to quantify the apparent mechanical behaviours of human prostatic tissues, with the ultimate aim of assessing the structure-property-function relations in human glandular tissues and cancers.

4. References

- [1] T.C. Gasser, R.W. Ogden, and G.A. Holzapfel, *J R Soc Interface*, vol. 3, no. 6, pp. 15–35, Feb. 2005, doi: 10.1098/RSIF.2005.0073.
- [2] D. H. Pahr and P. K. Zysset, *Biomech Model Mechanobiol*, vol. 7, no. 6, pp. 463–476, Dec. 2008, doi: 10.1007/s10237-007-0109-7

Acknowledgements:

This work was funded by the Engineering and Physical Sciences Research Council (EPSRC) under grants nos. EP/K036939/1 and EP/N006089/1. This study is also supported by the EPSRC Doctoral Training Partnership (DTP) scholarship awarded to the first author.

VISCOELASTIC MATERIAL MODELS FOR PESSARY PROSTHETIC MODELLING

Kyra Wanuch (1), Alexandra Blokker, (2), Stewart McLachlin (1)

1. University of Waterloo, Canada; 2. Cosm Medical, Canada

1. Introduction

Pelvic organ prolapse (POP) is the descent of one or more pelvic organs (e.g., uterus, bladder, vaginal walls, rectum) [1]. Disordered pelvic floor function will affect 50% of all women in their lifetimes [2]. POP treatments include surgery, physiotherapy, or use of a removable gynaecological prosthetic, known as a pessary. Pessary fitting success is reported as low as 41% [3]. Computational models can potentially assist with understanding pessary biomechanics to improve ease of insertion and fit; however, appropriate material models are required. This study aimed to identify a viscoelastic material model for pessary manufacturing silicone.

2. Materials and Methods

To understand the material characteristics of pessary silicone, tension and compression tests were performed using Dogbone and cylinder test samples of pessary silicone. Experimental data was fit with a Mooney-Rivlin (MR) material model, see Eqn. 1 [4], by maximizing the coefficient of determination (R^2) between the model and experimental data.

$$\Psi = C_1(\bar{I}_1 - 3) + C_2(\bar{I}_2 - 3) + \frac{1}{2}K(\ln J)^2 \quad (1)$$

To ensure the material model characterizes the pessary behaviour, data from mechanical tests representing the ring with support pessary folding in half were compared to finite element (FE) models with the MR material. FE fold test models were created in FEBio, with TetGen, MMG Remesh, and mesh conversion used to generate the Tet10 mesh for four pessary sizes. Preliminary FEBio tests were done to confirm convergence and verify element quality.

3. Results

The MR material coefficients were determined as $C_1=0.6410$, $C_2=-0.1238$, and $K=51.3765$. Material scaling to fit the test data was needed

due to differences in the test samples and pessary silicone curing. Test data and FE results for the calibrated (size 5) and independent models (sizes 3,7 and 11) are shown in Fig. 1.

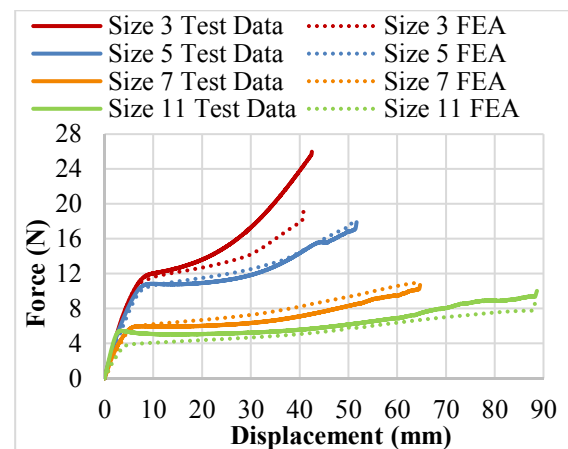


Figure 1: Pessary folding response comparison.

4. Discussion and Conclusions

There was excellent agreement in the force-displacement response for the independent FE fold models of different pessary sizes, apart from the peak folding of size 3. This demonstrates the efficacy of the material model identified. Future FE studies will use this material to improve understanding of pessaries.

5. References

1. M. Bureau and K.V Carlson, "Pelvic organ prolapse: A primer for urologists," *Can. Urol. Assoc J.*, vol. 11, no. 6, pp. 125–130, 2017.
2. V.W. Sung, and B.S. Hampton, "Epidemiology of pelvic floor dysfunction," *Obstet Gynecol Clin North Am.*, vol 36 no. 3, pp. 421-443, 2009.
3. C. Panman et al., "Predictors of unsuccessful pessary fitting in women with prolapse," *Int. Urog. J.*, vol 28 no. 2, pp. 307-313, 2017.
4. S. Maas, D. Rawlins, J. Weiss, and G. Ateshian, (2019). FEBio User Manual Version 2.9.

Acknowledgements:

The authors would like to thank Cosm Medical, and Mitacs Accelerate for funding support.



AN IN-SILICO MECHANICAL TEST TO STUDY CERVICAL LOADING IN PATIENTS AT LOW- AND HIGH-RISK FOR PRETERM BIRTH

Erin Louwagie (1), Mirella Mourad (2), Michael House (3), Ronald Wapner (2), Kristin Myers (1)

1. Columbia University, USA; 2. Columbia University Irving Medical Center, USA; 3. Tufts Medical Center, USA

Correspondence regarding this work should be addressed to Kristin Myers (kmm2233@cumc.columbia.edu)

1. Introduction

Preterm birth (PTB, delivery <37 weeks) globally occurs in 10% of pregnancies [1]. Despite its prevalence, PTB is difficult to predict and prevent [1,2]. Though sonographic cervical length is the current gold standard in PTB prediction, it cannot capture the mechanical integrity of the reproductive tissues that are essential to pregnancy [3]. In this work, we study proximal cervix loading in patients at high- and low-risk for PTB with parametric, patient-specific computational models.

2. Materials and Methods

Ultrasonic dimensions of the maternal uterus and cervix and *in-vivo* cervical aspiration stiffness (Pregnotia AG, Switzerland) were measured between 16-24 weeks gestation. Measurements were taken in two clinical patient cohorts, one at high-risk (by conventional sonographic cervical length) and one at low-risk for PTB (normal cervical length). Using our established parametric modeling methods [4], we built models of each patient's uterus, cervix, fetal membrane, and a supporting abdomen. We discretized models into elements (Hypermesh Altair, Troy, MI) and assigned all tissue material properties based on existing data, with a patient-specific cervical fiber stiffness determined through inverse finite element analysis (FEA) of the *in-vivo* aspiration procedure. Physiologically inspired loading, contact, and boundary conditions were applied, and FEA was run in FEBio Studio v1.3.0 for 16 patients from each cohort [5].

3. Results

Stretch magnitude is generally larger in the high-risk group than the low-risk group (Fig. 1). The patients from the high-risk group who delivered extremely preterm (<28 weeks) have

the largest 1st principal right stretches at the uterocervical junction and the lowest of all cervical stiffnesses by aspiration.

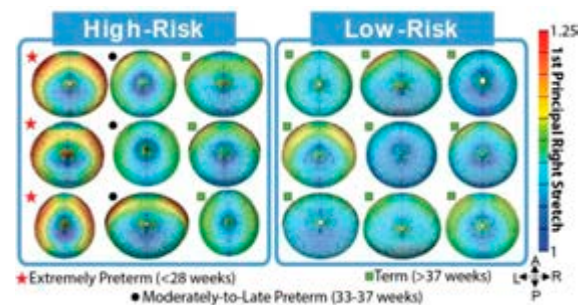


Figure 1: Heat maps of 1st principal stretch in the proximal cervix for a subset of subjects at high- and low-risk for PTB.

4. Discussion and Conclusions

The FEA results show a distinct stretch pattern in patients at high-risk for PTB. The increased stretch between the uterus and cervix found in patients destined to deliver extremely prematurely sheds light on the mechanisms by which the cervix may be prematurely dilated.

5. References

1. WHO, "Preterm birth", 2018.
2. Medley et al., *Cochrane DB Syst Rev*, 11, 2018.
3. Vink & Myers, *Best Pract Res Clin Ob*, 52:88-102, 2018.
4. Louwagie et al., *Plos One*, 16(1):e0242118, 2021.
5. Maas et al., *J Biomech Eng*, 134(1):011005, 2012.

Acknowledgements:

This work is supported by the Eunice Kennedy Shriver National Institute of Child Health & Human Development of the National Institutes of Health under award number 1R01HD091153-01. The content is solely the responsibility of the authors and does not necessarily represent the official views of the National Institutes of Health.



TOWARDS A NUMERICAL MODEL OF A TRAINING OBSTETRICAL DUMMY TO ENHANCE VACUUM ASSISTED DELIVERY

Yves Vallet (1), Charline Bertholdt (2,3), Rachid Rahouadj (1), Olivier Morel (2,3), Cédric Laurent (1)

1. CNRS UMR 7239 LEM3 - Université de Lorraine, Nancy, France ; 2. Université de Lorraine, CHRU-NANCY, Pôle de la femme, F-54000 Nancy, France ; 3. IADI INSERM U1254, Rue du Morvan, 54500, Vandoeuvre-lès-Nancy, France

Corresponding author: Yves Vallet, yves.vallet@univ-lorraine.fr

1. Introduction

Vacuum Assisted Delivery (VAD) has become the predominant strategy for operative vaginal delivery, with a high prevalence and rare associated complications [1], except pop-offs that could lead to a clinical failure of VAD, and damage at the level of maternal tissues. However, neither the best design of the vacuum extractor nor the best-suited clinical gesture to avoid such complications have been subjected to substantial research. Since a clinical trial-and-error approach is obviously unsafe, training dummies are commonly used to simulate VAD, while recent approaches tend to use numerical modelling through Finite Element (FE) simulations to understand and enhance the clinics of vaginal delivery [2]. However, the reliability of such simulations depend on their capacity to reproduce experimental data. The present work aims at comparing the extraction force required to perform a VAD on a training dummy with the force predicted by a FE numerical model, in order to propose a reliable simulation model for VAD.

2. Materials and Methods

A common training dummy (*Limbs&Things Ltd*) was mounted on a 3D platform force (*OR6-6-OP, A-tech*) while a practitioner performed a VAD using a Kiwi® vacuum cup. Forces were recorded as well as the clinical gesture (Fig.1.A). The geometries of training dummy were acquired by CT and reconstructed in order to build a FE mesh of the soft materials mimicking the maternal soft tissues. The midsection of these tissues were build and meshed with 5402 and 737 S4 elements respectively. The hyperelastic behaviour of the corresponding materials were identified by tensile tests, and the VAD was simulated in Abaqus-explicit assuming a rigid fetal head

going through the soft tissues (Fig. 1.B). Reaction force at the level of the fetal head was measured and compared to experimental forces.

3. Results

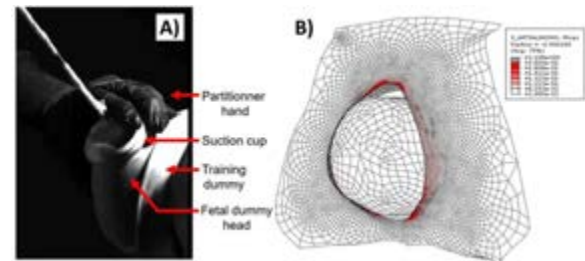


Figure 1: Experimental acquisition on training dummy B) Simulation of the fetal head extraction and associated stress field in soft tissues.

Typical experimental maximal extraction forces were in the range 46.2-85.3 N while the simulated maxim force was equal to 80.8 N considering the head/soft tissue friction coefficient as an adjustable parameter to be identified, and evaluated at 0.2.

4. Discussion and Conclusions

To the best of our knowledge, this study is the first attempt to measure VAD extraction forces and to propose a FE numerical model able to satisfyingly reproduce these experimental data. This model will be used in forthcoming studies to improve VAD gesture as well as vacuum cup geometries.

5. References

1. Baskett, T.F. Operative Vaginal Delivery 56, 3–10. (2019)
2. Silva, M.E.T. et al, J. Biomechanics 48, 1600–1605. (2015)

Acknowledgements:

The authors acknowledge the imaging facilities of CHU of Nancy for the CT imaging of training dummy, as well as the CERAH of Woippy for the acquisition of extraction force.

Computational modeling of cervical support during human pregnancy: implications for the treatment of cervical insufficiency.

Abigail Laughlin¹ Kristin Myers¹, Devon Campbell², Michael House^{3,4}

¹Mechanical Engineering, Columbia University, New York, NY, USA

²Prodct LLC, Lexington, MA, USA

³Obstetrics and Gynecology, Tufts Medical Center, Boston, MA, USA

⁴Cx Therapeutics, Lowell, MA, USA

Abstract:

Preterm birth is a severe complication of pregnancy. Preterm birth refers to pregnancies that deliver before 37 weeks of gestational age. Cervical insufficiency is a significant cause of preterm birth. In normal pregnancy, the cervix remains closed as the fetus grows. However, in cases of cervical insufficiency, painless cervical dilation occurs, resulting in preterm birth.

Cervical insufficiency is caused by structural failure of the cervix. As the fetus grows, multiple cervical stresses act to dilate the cervix. Variables that influence the stress state include the weight of the fetal sac; the distention of the uterus associated with fetal growth; the anatomic geometry; the variation in cervical microstructure; and the adhesion properties of the fetal membrane on the cervical surface. Stresses acting to dilate the cervix are counterbalanced by the strength of fibrous cervical tissue. When the cervical stresses overcome the strength of the fibrous cervix, the cervix shortens and dilates, which can lead to preterm birth.

The current treatment for cervical insufficiency is a cerclage suture. A cerclage suture is placed early in pregnancy under regional anesthesia. A non-absorbable suture needle makes 4 – 6 passes around the cervix in a purse string fashion. The suture is pulled tight to compress the cervix, and a knot is tied. Near term, the knot is cut, and the cerclage is removed. The rationale of cerclage is to provide compressive support to cervical tissue and thus prevent preterm dilation. Natality records show that cerclage is performed in 0.4% of pregnancies or 15,000 treatments annually in the U.S. alone.

Although the clinical features of cerclage treatment are well known, the biomechanics of cerclage support is poorly understood. In this study, we perform computational modeling of cerclage compression to gain insight into the mechanism of cerclage efficacy. We also study cervical support in two additional devices for cervical treatment: the cervical pessary and the newly designed Cx Device. A pessary is a silicone device that fits around the cervix and aims to decrease cervical stress by modifying the anatomic geometry of the cervix. The Cx Device is a medical device in development as an alternative for cervical cerclage.

The distribution of tissue stretch and stress in the cervix are computed for each device, 1. cerclage, 2. pessary, and 3. Cx Device, and mechanical function are evaluated and compared. Three-dimensional CAD models of representative patient anatomy are created in Solidworks from ultrasound measurements. The patient and device geometries are meshed in Hypermesh using tetrahedral elements, and element sizes are determined from a convergence study. Meshes are imported to FEBio to perform finite element analysis. Maternal reproductive tissue material properties are assigned based on existing mechanical data, and physiologically motivated boundary conditions are applied. Model results will reveal the impact these three forms of treatment have on cervical support, and simulation results will optimize performance, comfort, and fit for Cx Device prototypes.



INNOVATING FOR PROLAPSE REPAIRS USING A COMPUTATIONAL MODELING AND EXPERIMENTAL APPROACH

Katrina Knight(1,2)

1. Department of Bioengineering, University of Pittsburgh, United States of America; 2. Magee-Womens Research Institute, United States of America

1. Abstract

Pelvic organ prolapse (POP) is one of the most common pelvic floor disorders that mainly impacts aging, parous women (women who have given birth). Nearly half of all women aged 50 and over experience symptoms of POP[1, 2]. By the age of 80, approximately 12.6% of women will undergo a surgical repair for POP with estimated annual costs exceeding \$1 billion[3]. With the aging population, the demand for POP treatment and hence surgical cost is expected to rise 50% by 2050[4].

Surgeries that utilize the patient's own tissues to repair POP are associated with high failure rates (up to 70%)[5, 6]. To re-enforce repairs, synthetic meshes are implanted. Current POP meshes are simply hernia meshes re-purposed for POP repairs and initially approved via the FDA 510k mechanism (requiring little to no premarket testing). Unfortunately, this resulted in meshes, that were never specifically designed for the vagina, being implanted in women on a trial-and-error basis. Consequently, mesh usage has been hampered by unacceptably high complication rates which have resulted in numerous lawsuits, the discontinuation of products, and to the eventual halt of the distribution of some products by the FDA. There is currently no surgical treatment for POP that is not without complications. Given the expected rise in the treatment of POP with the aging population, there is an urgent need for an alternative device(s) that affords long-term repair with minimal complications.

Understanding the mechanisms of mesh complications is critical to developing novel solutions for POP repair. This talk will describe how we use computational modelling, mechanical testing, and *in vivo* experimental

approaches to elucidate mechanisms of mesh complications. Learning from the issues with current POP meshes, we can develop a device that is based on scientific evidence and one that is specifically designed for the vagina. Thus, this talk will also highlight how we are using a computational modelling and experimental approach to develop a novel device for POP repair. Ultimately, we anticipate that this research will lead to a product that will benefit millions of women world-wide.

2. References

1. Samuelsson EC et al., *AJOG*. 1999;180(2 1):299-305.
2. Wu JM et al., *Obstet Gynecol*. 2014;123(6):1201-1206.
3. Subak LL et al., *Obstet Gynecol*. 2001;98(4):646-651.
4. Wu JM et al., *Obstet Gynecol*. 2009;114(6):1278-1283.
5. Barber MD et al., *JAMA*. 2014;311(10):1023-1034.
6. Jelovsek JE et al., *JAMA*. 2018;319(15):1554-1565.

Acknowledgements:

The authors would like to thank Dr. Steven Abramowitch, Dr. Pamela Moalli, and members of the Translational Research Laboratories in Urogynecology (TRLU). Also, we thank the National Institutes of Health (K12 HD043441, HD083383, TL1 TR001858), National Science Foundation Graduate Research Fellowship Program (DGE-1247842), Department of Defense (W81XWH-16-1-0133), Magee-Womens Research Institute and Foundation, and the Center for Medical Innovation (University of Pittsburgh) for financially supporting this work.

Corresponding Author: Dr. Katrina Knight
kmk144@pitt.edu

ESTABLISHMENT OF THE *IN VIVO* BIOMECHANICAL PROPERTIES OF THE BLADDER OF CONTINENT AND INCONTINENT WOMEN

Elisabete Silva (1), Sofia Brandão (1,2), Pedro Martins(1,3), Renato Natal (4)

1. LAETA, INEGI, Porto, Portugal; 2. Department of Radiology, Centro Hospitalar de São João-EPE, Faculty of Medicine, University of Porto, Porto, Portugal; 3. ARAID, i3A, University of Zaragoza, Zaragoza, Spain; 4. LAETA, INEGI, Faculty of Engineering, University of Porto, Porto, Portugal.

1. Introduction

Urinary incontinence (UI) has a prevalence of a up to 28%, with stress urinary incontinence (SUI) being the most common form [1,2], characterized by involuntary urinary leakage during physical strain, coughing or an increase in intra-abdominal pressure (IAP). SUI occurs when the intravesical pressure exceeds urethral resistance at which the urethra has the capacity to remain closed [2], and/or pelvic ligaments, are not stabilize the urethra. Assessment of bladder neck (BN) mobility in patients with SUI is essentially clinical, however, the imaging techniques such as ultrasound (US) and magnetic resonance imaging (MRI) are used as a method for evaluating this characteristic. The outcomes of radiographic images have been crucial and used as input for numerical methods.

The aim of the present study was to establish the IAP values and the *in vivo* biomechanical properties of the bladder tissue for two distinct groups (continent women and women with SUI). The numerical simulations of Valsalva maneuver were performed, applying the Ogden hyperelastic constitutive model to the bladder and also the inverse finite element analysis (FEA).

2. Materials and Methods

For this work, in order to evaluate the presence and symptoms of UI, a cohort of 11 women (n=6, Continent (control group) and n=5 with SUI) was recruited and submitted to scanning (MRI). In order to obtain the IAP and *in vivo* biomechanical properties of the bladder in the two distinct groups (continent group (CG) and incontinent group (IG)), it was adapted a 3D computational model (Fig. 1) of the female pelvic cavity [3], that corresponds a nulliparous 24 years old healthy female.

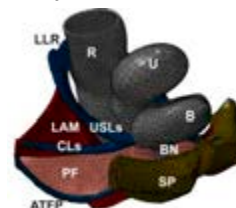


Figure 1. Computational model of the female pelvic cavity.

3. Results

Table 1 presents the material parameters for Ogden constitutive model, applied to the bladder tissue, obtained by inverse FEA for two groups. These parameters were obtained after establishing the IAP values for the CG (3.5 MPa) and adjusting the mechanical properties of support structures and IAP for the IG (5.0 MPa).

Table 1. Material parameters of the bladder in women with and without SUI, and variation between the groups.

variable		CG(n=6)	IG(n=5)	Variation(%)
Ogden	α_1 [MPa]	0.180	0.202	10.89%
	μ_1 [MPa]	4.839	7.720	37.32%

Note: CG: continent group; IG: incontinent group.

4. Discussion and Conclusions

The biomechanical properties for the bladder of the Ogden constitutive model from the CG and IG have a difference of approximately 47% in stiffness, being greater for IG.

5. References

- Jansson MH, et al., *Acta Obst et Gynec Scandinavica* 2021; **100**(12):2193–2201.
- Falah-Hassani K, et al. *Int Uro Journal* 2021; **32**(3):501–552.
- Brandão S, et al.. *J. Biomech Eng* 2017; **139**(8):1–9.

Acknowledgements:

The authors gratefully acknowledge funding from Stimulus of Scientific Employment 2021.00077.CEECIND, financed through FCT. This work was supported by FCT, through INEGI, under LAETA, project UIDB/50022/2020 and UIDP/50022/2020.

EXPERIMENTAL AND COMPUTATIONAL CHARACTERISATION OF OVINE PELVIC TISSUES

Katie Harte (1), Gary Menary (1), Alex B Lennon (1)

1. School of Mechanical and Aerospace Engineering, Queen's University Belfast, Northern Ireland

1. Introduction

Pelvic floor muscles undergo a degree of stretch during vaginal delivery unparalleled elsewhere in the body, causing significant injury in the vagina (VA) and levator ani muscle (LA).¹⁻³ Up to 20-30% of women over 20yrs old and up to 50% over 50 may suffer from pelvic floor disorders.⁴ Challenges with experimental investigation of reproductive biomechanics have led to a shift towards computational modelling, which is heavily dependent on accurate material properties. Current literature lacks accurate anisotropic and time-dependent mechanical properties for pelvic tissues. Furthermore, labour stretches these muscles under time-varying loads and viscoelastic effects are rarely accounted for. This research aims to improve pelvic tissue characterisation using a novel test platform for multiaxial static and viscoelastic testing of pelvic tissues.

2. Materials and Methods

A radial stretcher adapted for soft tissue was designed and built, based on a concept by Schausberger et al.⁵ Three load cells on three of the eight arms, 45° apart, measure force in three directions (X, R, Y; Fig. 1A). An environment chamber held samples in phosphate-buffered solution at 37°C. Ovine VA and LA muscles (6 sheep) were dissected. Uniaxial samples were die-cut in fibre (FD) and cross-fibre directions (CF) for LA and in longitudinal (LD) and circumferential directions (CD) for VA muscles. Radial samples were cut ($\phi = 20$ mm, Figs. 1C). Quasi-static tests were carried out at 6 mm/min following 10 preconditioning cycles. A series of ramp and hold tests were also carried out in both uniaxial and radial modes. Inverse FEA using a combination of FEBio (www.febio.org) and MATLAB® (Mathworks Inc.) was used to fit a constitutive equation consisting of a quasi-linearly viscoelastic neo-Hookean matrix reinforced with a nonlinear continuous fibre distribution to the data.

3. Results and Discussion

Uniaxial tests in both tissues exhibited a non-linear hyperelastic response (Fig 1D).

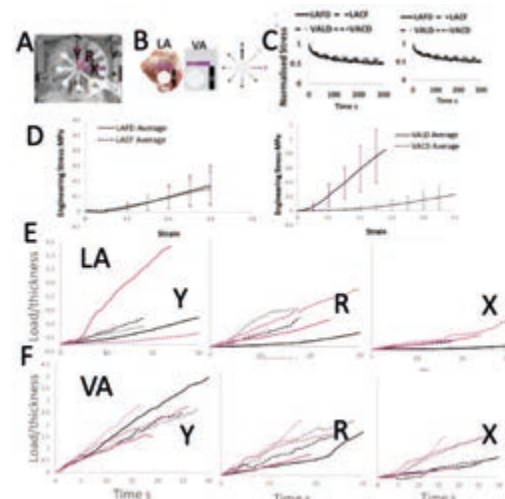


Figure 1: (A) Load cell locations. (B) LA and VA muscle samples for radial and uniaxial. (C) Normalised stress vs time for LA and VA in both uniaxial directions (D) Cauchy stress vs strain for LA and VA uniaxial (E, F) Load/thickness Vs Time multiaxial LA and VA.

Multiaxial tests were stiffest in the fibre (Y) direction (Fig E&F). Ramp and hold uniaxial tests showed little directional dependence in either tissue for relaxation (Fig 1C). Some slowing of relaxation was observed as strain increased in VA but not in LA. Variability was observed across all testing as observed in the literature.^{6,7} Inverse FEA fit a visco-hyperelastic fibre-reinforced model in FEBio to the static tensile and relaxation data, capturing the cross-fibre and fibre-direction response in most specimens. However, it failed to capture the intermediate R-direction in some samples. In conclusion, radial testing demonstrated that single family fibre-reinforced models can capture the FD and CF response, but more complex models of fibre reinforcement may be needed for accurate characterisation in intermediate directions within the tissues.

5. References

- [1] Tracey et al., 2018, *J Mech Behav Biomed Mater*, 79, 213-218
- [2] Boyles et al, *AJOG*, 188(1), 108-115 (2003)
- [3] Subak et al, *Obstet. Gynecol*, 98(4), 646-651.
- [4] Wilson et al., *Obstet. Gynecol*. 2001; 98:398-406
- [5] Schauburger et al., *IEEE-Access* (2015)-3, pp. 556-561.
- [6] Jing et al., 2010, [7] Peña et al., 2011, *J Mech Behav Biomed*.



THE EFFECTS OF RESPIRATORY AND OTHER PHYSIOLOGICAL FACTORS ON CNS FLUID MECHANICS AND TRANSPORT

Lynne E. Bilston

NeuRA & UNSW, Australia

1. Introduction

Circulation of fluid around, into, and out of the CNS is essential for fluid homeostasis and clearance of metabolites and waste products. While cardiovascular contributions to this fluid circulation are well known, albeit not completely understood, more recently, respiration, coughing [1], and other physiological contributors such as sleep and movement have been identified as important factors [2]. However, the biomechanical factors underlying this fluid circulation remain poorly understood.

2. Materials and Methods

Phase-contrast MRI studies of healthy human volunteers during a range of physiological activities, including deep breathing, coughing, sniffing, and yawning have been used to quantify CSF flow in the normal population. These techniques have also been used to define how neurological conditions, such as Chiari I malformation and syringomyelia, alter CSF flow.

Data from these imaging studies have been used both as input to, and validation for, computational models of fluid circulation in the CNS.

3. Results, Discussion and Conclusions

Respiratory manoeuvres significantly alter both blood flow and CSF flows around the brain and spinal cord, predominantly via intrathoracic and abdominal pressure mediated venous blood shifts in the thorax. These effects are more complex than commonly reported [3].

Individual-specific computational models can provide insight into the effects of macroscopic CSF flow dynamics on small-scale fluid

transport into the CNS via perivascular spaces, and across the parenchyma of the CNS.

5. References

1. Lloyd RA et al, *J Physiol*, 598(24): 5789-5805, 2020.
2. Martinac AD & Bilston LE, *Biomech Model Mechanobiol*, 19: 781-800, 2020.
3. Dreha-Kulaczewski, Steffi, et al. *Journal of Neuroscience* 37(9): 2395-2402, 2017.

Acknowledgements:

The author would like to thank the National Health and Medical Research Council of Australia (Grant nos: APP1172988, APP1063628) and the Column of Hope Foundation for providing financial support to this project.



PERSONALIZATION FRAMEWORK – APPLICATIONS ON HUMAN BRAIN, BODY MODELS AND BEYOND

Xiaogai Li

Department of Biomedical Engineering and Health Systems

KTH - Royal Institute of Technology, Sweden

1. Introduction

Finite element (FE) models have become increasingly important numerical tools for understanding how brains get injured during accidents [1, 2], supporting clinical diagnosis [3], developing new treatments [4], and providing insights into mechanical roles into neurosurgical problems [5,6]. Subject-specific models that capture individual anatomical differences are needed for these purposes and beyond. However, developing subject-specific models from scratch can be time-consuming and challenging; an alternative is mesh morphing, which involves displacing nodes of a baseline FE model into a subject model with a displacement field reflecting anatomical differences between both. Mesh morphing is often efficient, but a major challenge is how to achieve good personalization accuracy and element quality as there is often a trade-off between the two, and higher personalization accuracy tends to worsen element quality.

We have previously presented a method to personalize detailed brain models, which proved effective in generating subject-specific models for healthy adult brains [1]. This method has later been extended into a personalization framework [7], which can generate subject-specific brain models for the lifespan from newborn to elderly, and hydrocephalus brain. This *Abstract* aims to further enhance the framework for applications in personalizing skull models, human body models (HBMs), and beyond.

2. Method: Personalization Framework

The personalization framework consists of image registration, mesh morphing, and mesh grouping. Image registration is critical as the resultant displacement field determines personalization accuracy and mesh quality. Three types of image registration pipelines were presented earlier with increasing complexity for

handling more challenging cases that have larger anatomical differences than the baseline [7], including Type I (basic pipeline with 2-step registration), Type II (adding multiple feature steps), and Type III (adding multimodality registration steps). A new type (defined as Type IV here) of registration pipeline is developed here to extend the framework's capacity for other applications when CAD or surface models are available.

3. Applications

The capacity of the newly enriched framework is demonstrated for generating subject-specific brain models, skull models, HBMs of adults and children, and beyond.

4. Discussion and Conclusions

The personalization framework allows efficient generation of brain, skull, and body models, which facilitates personalized simulations. This in turn allows for a better understanding of individuals' injury mechanisms, improving subject-specific diagnosis and treatment.

5. References

1. Li X, Zhou Z, Kleiven S. *Biomech Model Mechanobiol* 20(2): 403-431 (2021).
2. Giordano C, Li X, Kleiven S. *PloS One* 12(11):e0187916 (2017).
3. Li X, Sandler H, Kleiven S. *Forensic Sci Int* 294:173-82 (2019).
4. Wang T, Kleiven S, Li X. *IEEE Trans Biomed Eng* 68(9):2645-53 (2020).
5. Li X, von Holst H, Kleiven S. *J Clin Neurosci* 20(4):509-13 (2013).
6. von Holst H, Li X, Kleiven S. *Acta Neurochir* 154(9):1583-93 (2012).
7. Li X. *Front Bioeng Biotechnol* 9: 706566 (2021).

Acknowledgements

Fundings from Vinnova (nr. 2019-03386), Swedish Research Council (nr. 2020-04724 and 2020-04496) are acknowledged for providing financial support to this project.



THE IMPORTANCE OF USING REGION-DEPENDENT MATERIAL PARAMETERS FOR FULL-SCALE HUMAN BRAIN SIMULATIONS

Emma Griffiths(1)*, Jan Hinrichsen(1), Nina Rieter(1), Silvia Budday(1)

1. Department of Mechanical Engineering, Friedrich-Alexander-Universität Erlangen-Nürnberg, 91058 Erlangen, Germany.

Emma Griffiths, emma.griffiths@fau.de, corresponding author

1. Introduction

Simulations of the brain can provide insights into brain injury, disease, treatment protocols and protective head gear designs [1]. The brain, however, is a very complex organ and thus is complex to model. One aspect is the heterogeneity of various regions of the brain [2]. The extent to which this heterogeneity affects the mechanical response of an FE simulated full brain remains largely unexplored. In this work, we investigate the importance of this heterogeneity.

2. Materials and Methods

A three dimensional brain model was created from MRI images of a brain. It consists of 142900 2x2x2-mm voxel elements and 161253 nodes. A smoothing algorithm was also used on the surface of the brain shown in Fig. 1.

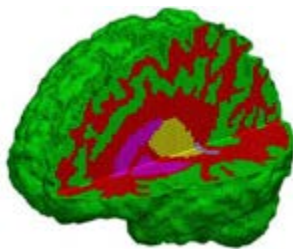


Figure 1: The three dimensional brain model used to investigate the importance of regionally dependent material parameters.

The brain model is segmented into 9 regions and modelled with an isotropic one-term Ogden model has been shown to represent the time-independent, hyperelastic response of the brain. Comparisons between brain models of decreasing heterogeneity were made. Additionally, comparisons using a Poisson's ratio of 0.45 and 0.49 and comparisons between material parameters identified from conditioned samples vs unconditioned samples were made.

3. Results

Clear differences in the strain values were seen between the homogeneous and heterogeneous models as shown in Fig. 2.

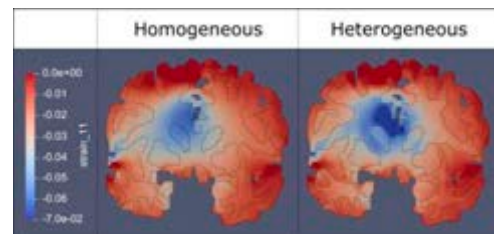


Figure 2: Strain response between a fully heterogeneous and fully homogeneous brain model

4. Discussion and Conclusions

Our results show that regional heterogeneity should be considered in the simulation of large scale brain models. Large differences in the predicted strain values were noted in several regions. The effects of different Poisson's ratios should also be carefully considered as our model showed large differences between the predicted strain values. Finally, it is important for the state of the sample conditioning to be clearly reported as large differences in strain values in the full scale brain model were noted.

5. References

1. Budday S. et al. Arch. Comput. Methods Eng.;27(4):1187-1230 (2019)
2. Reiter, N et al. J. Elast.;145(1-2): 99-116 (2021).

Acknowledgements:

We gratefully acknowledge the financial support by the Deutsche Forschungsgemeinschaft (DFG, German Research Foundation) through the grant BU 3728/1-1.



MECHANICAL CHARACTERIZATION OF HUMAN AND PORCINE BRAIN TISSUE AND HUMAN BRAIN ORGANIDS

Nina Reiter (1), Sarah Nistler (1), Friedrich Paulsen (2), Silvia Budday (1)

1. Institute of Applied Mechanics, Friedrich-Alexander-Universität Erlangen-Nürnberg, Germany;
2. Institute for Functional and Clinical Anatomy, Friedrich-Alexander-Universität Erlangen-Nürnberg, Germany

1. Introduction

Increasing evidence suggests that mechanical forces and signals play an important role for brain development, injury, and disease. Computational models based on continuum mechanics can help to better understand mechanics-related physiological and pathological processes. Since human brain tissue is not always available, experiments to characterize brain tissue are often performed on porcine brain tissue. Here, we compare the mechanical behavior of human and porcine brain tissue to investigate if porcine brain tissue can serve as a substitute for human tissue. Furthermore, we tested human brain organoids, which offer the unique possibility to test living tissue in vitro.

2. Materials and Methods

We obtained nine human brains from body donors who had given their written consent to donate their body to research. Porcine brains were provided by a local butcher. Furthermore, we obtained human brain organoids from the Department of Stem Cell Biology of the University Hospital Erlangen.

We subjected all samples to multimodal mechanical testing including compression, tension, and torsional shear and recorded the applied deformation and the stress response.

3. Results

We observed that human and porcine brain tissue as well as human brain organoids all show similar viscoelastic behavior. However, the three tissue types differed in stiffness. Human brain tissue showed the stiffest response, followed by porcine brain tissue. The human brain organoids showed the softest response.

4. Discussion and Conclusions

The differences in stiffness measured for human and brain tissue could potentially be due to differences in age – porcine brains were taken from 6-month-old pigs, or due to different post mortem testing times – for human brains, more time was required for documentation and preparation prior to testing. Organoids might be softer than brain tissue because of their different internal structure: in contrast to native tissue, organoids have a less diverse cellular network and they do not have an extracellular matrix and vascular network.

In conclusion, porcine brain tissue can be used to understand the general behavior of brain tissue, but data from young pigs might not translate to adult humans. Organoids cannot model the full mechanical response of brain tissue due to their simplified structure. However, they are an interesting platform for research on living cells.

Acknowledgements:

The support from the German Research Foundation (DFG) through the grant BU 3728/1-1 to SB is gratefully acknowledged. We cordially thank Beate Winner and Michaela Farrell for providing the human brain organoids. Furthermore, the authors wish to sincerely thank those who donated their bodies to science so that anatomical research could be performed. Results from such research can potentially improve patient care and increase mankind's overall knowledge. Therefore, these donors and their families deserve our highest gratitude.



MORPHOMETRIC AND BIOMECHANICAL INDICATORS OF CHIARI MALFORMATION I

Javid Abderezaei (1), Aymeric Pionteck (1), Ya-Chen Chuang (1), Alejandro Carrasquilla (2), Gizem Bilgili (1), Tse-An Lu(3), Miriam Scadeng(4), Patrick Fillingham(5), Peter Morgenstern (2), Michael R. Levitt(1, 5), Richard G. Ellenbogen (5), Yang Yang (6,7), Samantha J. Holdsworth (4), Raj Shrivastava (2), Mehmet Kurt (1, 7)

1. Department of Mechanical Engineering, University of Washington, Seattle, WA, USA; 2. Department of Neurosurgery, Icahn School of Medicine at Mount Sinai, New York, NY, USA; 3. Department of Biostatistics, Boston University, Boston, MA, USA; 4. Department of Anatomy and Medical Imaging, Faculty of Medical and Health Sciences & Centre for Brain Research University of Auckland, Auckland, New Zealand; 5. Department of Neurological Surgery, University of Washington, Seattle, WA, USA; 6. Department of Radiology and Biomedical Imaging, University of California, San Francisco, CA, USA; 7. BioMedical Engineering and Imaging Institute, Icahn School of Medicine at Mount Sinai, New York, NY, USA

1. Introduction

Chiari Malformation type 1 (CM-I) is a neurological disorder characterized by morphological defects such as excessive cerebellar tonsillar ectopia and numerous associated manifestations [1,2]. Recently, the intrinsic brain motion during the cardiac cycle has been suggested as a potential diagnostic criterion for CM-I [3]. Recently, a new image processing method called 3D amplified MRI (3D aMRI) was introduced which allows visualizing the brain motion in specific frequency ranges [4, 5]. Here, we compared the brain motion between the healthy and CM-I subjects, and analyzed the correlations between morphometric measurements, brain motion, symptomatology, and surgical outcome.

2. Materials and Methods

With IRB approval, we acquired 3D cine MRI of 14 healthy and 14 CM-I subjects and used 3D aMRI to visualize and measure the brain's intrinsic motion during the cardiac cycle. We also collected symptomatology and surgical treatment data for these patients. We analyzed correlations between morphometric measurements, brain motion, symptomatology and surgical treatment and outcome.

3. Results

Our data suggested that the brain motion was significantly higher in CM-I patients compared to healthy ones ($p < 0.01$), with anterior-posterior (AP) and superior-inferior (SI) displacements in cerebellar tonsils and medulla having the highest differences between healthy and CM-I (45% and 73% increased motion in the CM-I

group; Fig 1). The ratio of neural tissue at the foramen magnum directly correlated with the SI tonsillar motion ($r=0.58$). The tonsillar herniation directly correlated with the tonsils AP motion ($r=0.61$), and medullas AP and ML motion ($r=0.66$, and $r=0.57$). The ML motion of the tonsils was the only indicator of surgical outcome (AUC=0.95), in which subjects with higher motion had an improved outcome.

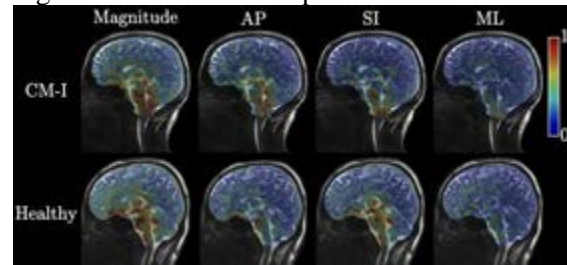


Fig. 1: The maximum displacement of the brain in healthy and CM-I subjects during the cardiac cycle.

4. Discussion and Conclusions

In this work, we have shown preliminary indications that the biomechanical information acquired from 3D aMRI can be used to characterize CM-I and guide surgical decision-making for the CM-I patients.

5. References

- [1] Strahle, J., et al., J. Neurosurg. Pediatr., 2011.
- [2] Taylor, F. R., et al., Curr. Pain Headache Rep., vol. 6, no. 4, pp. 331–337, Aug. 2002.
- [3] Nwotchouang, et al., Ann Biomed Eng, 1-15., 2021.
- [4] Abderezaei, J., et al., Brain Multiphysics, 2021, 100022.
- [5] Terem, I., et al., MRM 2021, 1674-1686.

Acknowledgements:

This research was supported by NIH Grant No. 1R21NS111415-01.

CMBBE 2023

18th International Symposium on Computer Methods
in Biomechanics and Biomedical Engineering

3 - 5 May 2023, Paris, France



Arts et Métiers Institute of Technology

Institut de Biomécanique Humaine

Georges Charpak

155 boulevard de l'Hôpital 75013

Paris France

www.cmbbe-symposium.com

MULTISCALE MODELING OF LIVER METABOLIC PROCESSES: ACUTE AND CHRONIC DISEASES

Jules Dichamp(1), Ahmed Ghallab (2), Géraldine Cellière (1), Noémie Boissier (1), Jan Hengstler (2), Dirk Drasdo (1, 2)

1. INRIA Saclay, France ; 2. IfADO, Germany

1. Introduction

In this work, we focus on two fundamental metabolic processes of the liver: acetaminophen (i.e. paracetamol) and ammonia detoxification, which cover two aspects of liver disease, respectively acute and chronic liver diseases. Acetaminophen is a widely used drug known to generate hepatotoxicity at high dose both *in vitro* and *in vivo*. In the first part of this presentation, we will present a gradually complex model-based approach that permits to extrapolate *in vitro* to *in vivo* acetaminophen hepatotoxicity. The final model obtained is a spatial-temporal resolved model considering the precise micro-architecture of a representative liver lobule (the smallest repetitive functional unit of the liver). On the second part of this presentation, we will focus on ammonia detoxification in the context of a chronic liver disease: fibrosis. Fibrosis can happen after a chronic overdose of a xenobiotic (such as acetaminophen) and is characterized by the deposition of collagen fibres which replace the hepatocytes. We will see how a similar spatial-temporal model focusing on the liver lobule scale can reproduce the modification of the architecture and capture metabolic data.

2. Materials and Methods

The metabolic processes are first derived in a compartment model that represents the set of reactions (either ammonia or acetaminophen detoxification). Those intracellular reactions are then integrated in each cell of a liver lobule which reproduces the key mechanisms of liver detoxification: transport of species in the liver vasculature, uptake by the cells and elimination

by intracellular processes. Blood flow is modelled as Poiseuille flow, accounting for diameter dependent viscosity law. Transport of species is modelled by an advection-reaction equation with source term accounting for the hepatocytes uptakes. This source term is then set as an inflow from the intracellular reactions point of view which are described by a set of ODEs. The ODEs parameters are calibrated in the initial compartment approach.

3. Results

First, in the context of acute liver damage, we show that it is possible to improve the current extrapolation strategy from *in vitro* to *in vivo* hepatotoxicity. In particular, in order to calibrate the data and build a successful extrapolation, one needs to calibrate simultaneously intracellular *in vitro* hepatotoxicity together with *in vivo* pharmacokinetic data. Second, we show that the spatial-temporal model is able to explain the experimentally measured change of ammonia detoxification by modifying the liver architecture accordingly and by a minimal change in the metabolic parameters that we assume arise from the fibrosis process.

4. Discussion and Conclusions

We presented a multiscale model of liver metabolic processes, from the cell to the lobule scale, in two different disease contexts which can successfully explain the available data. Such a model can in principle be extended to other type of metabolites.



PHYSIOLOGICALLY-BASED MODELLING OF LIVER FUNCTIONS

Bastian Kister(1), Rebekka Fendt(1), Vanessa Baier(1), Lars Kuepfer(1)

1. Institute for Systems medicine

with Focus on Organ Interaction, University Hospital RWTH Aachen, Germany

1. Introduction

The liver is the most important organ for the clearance of drugs in the human body. It is also involved in many key physiological processes such as for example enterohepatic circulation (EHC) of bile acids (BA). A comprehensive understanding of liver physiology is hence crucial for many applications in pharmacology and medicine.

2. Materials and Methods

Physiologically-based pharmacokinetic models (PBPK) describe the physiology of the body at a large level of detail (Fig. 1). Organs are explicitly represented in PBPK modelling and they are assigned physiological properties such as organ volumes, surface areas, tissue composition or perfusion rates.

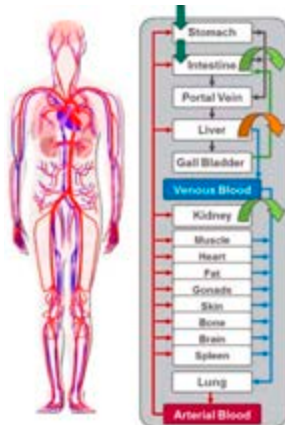


Figure 1: Physiologically-based pharmacokinetic (PBPK) modelling

PBPK models describe the drug pharmacokinetics in plasma and different tissues throughout the body. The models can also be linked to pharmacodynamic model to describe therapeutic as well as toxic side effects of drugs.

3. Results

Parameters in PBPK models are usually informed from population average values, but model parameters can easily be replaced by

patient-specific measurements in order to build personalised PBPK models of individual patients. The benefit of integrating patient-specific measurements on the quality of PK simulations was recently examined with PK data from a specifically designed clinical study [1]. A key outcome of this analysis was that consideration of subject-specific data in personalized PBPK models can indeed increase the accuracy of PK predictions.

In another study, a physiologically-based model of BA metabolism has been developed that describes the EHC of BAs along gut-liver axis [2]. The model has been used to benchmark the clinical cholestasis risk of different hepatotoxic drugs with a PBPK-based workflow. Also, clinical samples from different patient cohorts have been analysed with the model to investigate the effect of disease-related alterations on BA distribution as well as BA composition.

4. Discussion and Conclusions

Our analysis of PK data from individual patients shows the possibilities of PBPK modelling for model-informed precision dosing. Analogously, the investigation of clinical BA samples from different patient cohorts outlines the prospects of physiologically-based models to support the functional understanding of liver diseases. This will contribute to the design of new individualised therapeutic strategies in the future.

5. References

1. Fendt R et al., CPT Pharmacometrics Syst Pharmacol 10, 782-93 (2021).
2. Baier, V et al., Clin Pharmacol Ther 110, 1293-301 (2021).

Acknowledgements:

Authors should acknowledge funding from the German Research Foundation (DFG) – Project-ID 407403224013 – SFB 1382.



INTEGRATED SPATIAL-TEMPORAL AGENT-BASE MODEL FOR SIMULATION OF FIBROTIC SCAR FORMATION

Jieling Zhao (1,2,4), Seddik Hammad (3,4), Mathieu de Langlard (1), Pia Erdoesi (3), Paul Van Liedekerke (1), Jan Hengstler (2), Steven Dooley (3,5), Dirk Drasdo (1,2,5)

1. Inria (Saclay Ile-de-France), France; 2. IfADo, Germany; 3. Medicine Faculty Heidelberg University, Germany; 4. Shared first authorship; 5. Shared corresponding authorship

1. Introduction

Liver fibrosis is characterized by the accumulation of extracellular matrix (ECM) because of exposure of repeated damage. Some computational models such as 2D agent-based models [1] or partial differential equations [2] of liver fibrosis enabled studying the corresponding cellular and molecular mechanisms. Within a 3D single-cell-based model resolving tissue microarchitecture, we have incorporated the collagen fiber mechanics to address fibrosis formation. The pattern-characterizing parameters in this study were obtained through image analysis of histological images from mice experiments. We explored alternative model mechanisms and parameters for a detailed *in silico* study of possible mechanisms that explain the formation of fibrotic walls.

2. Materials and Methods

Mice are exposed to repeated doses of a hepatotoxic drug. Patterns of fibrosis and metabolizing enzymes are analyzed in immunostained histological images. Parameters for the model calibration are estimated such as the distribution of hepatic stellate cells (HSC). The proposed model considers the hepatocytes and other liver cell types as individual geometric objects. The fibrotic collagen fibers and the capillary network, veins of the liver lobule are modeled as semi-flexible chains.

3. Results

The *in silico* model is constructed with the spatial distribution of each of the cell type according to corresponding experimental data. The simulation of a repeated intoxication generating an interplay of hepatic lesion formation and regeneration is run for 3 biological weeks. After each dose, the drug sensitive hepatocytes are killed. Macrophages and HSC are attracted into the lesion to eliminate the dead cells and generate ECM

fibres. HSCs generate ECM fibres while macrophages digest dead hepatocytes and collagen. The healthy hepatocytes surrounding the lesion proliferate to fill the lesion while deforming the collagen network.

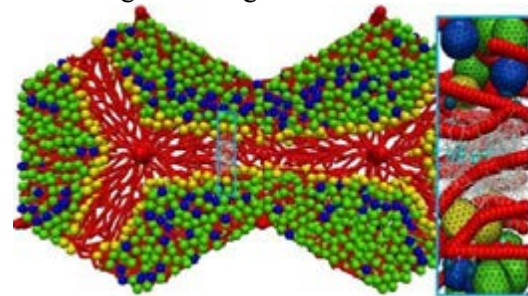


Figure 1: The modeled fibrotic tissue of two liver lobules. Red: sinusoids, Green/Blue/Yellow: quiescent/proliferating/CYP2E1-expressing hepatocytes; White: collagen fibres; Cyan: HSCs; Dark blue: macrophages.

The results show that starting after the second dose the collagen fibres are generated and gradually accumulate. After iterative destruction and partial regeneration cycles over about 3 weeks, the pattern of fibrotic wall is reproduced by this *in-silico* model (Fig. 1).

4. Discussion and Conclusions

Our novel collagen model can explain the pattern formation of liver fibrosis and can run for perturbation simulation to guide pathologists with further test of hypothesis.

5. References

- [1] Dutta-Moscato J, et al. 2014. A multiscale agent-based in silico model of liver fibrosis progression. *Frontiers in Bioeng. & Biotechnol.* 2:18.
- [2] Lara J, et al. 2014. Computational models of liver fibrosis progression for hepatitis C virus chronic infection. *BMC Bioinformatics.* 15: S5.

Acknowledgements:

Funding from LiSyM (Germany PTJ-FKZ: 031L0043) and the iLite project (ANR France, 16-RHUS-0005) is gratefully acknowledged.



A MULTISCALE AND MULTIPHASE DIGITAL TWIN OF FUNCTION-PERFUSION PROCESSES IN THE HUMAN LIVER

Tim Ricken (1), Steffen Gerhäuser (1) Lena Lambers (1) Luis Mandl (1) André Mielke (1)

1. *Institute of Structural Mechanics and Dynamics / University of Stuttgart / Germany*

1. Introduction

As the key organ for metabolic processes in the human body, the human liver is responsible for essential processes like fat storage or the detoxification. Some liver diseases can trigger growth processes in the liver, disrupting important hepatic function-perfusion processes[1].

2. Materials and Methods

To better understand the interplay between hepatic perfusion, metabolism and tissue in the hierarchically organized liver structure, we have developed a multicomponent, poro-elastic multiphasic and multiscale function-perfusion model, cf. [2,3], using a multicomponent mixture theory based on the Theory of Porous Media (TPM, see [4]). The multiscale approach considers the different functional units of the liver, the so-called liver lobules, with an anisotropic blood flow via the sinusoids (slender capillaries between the periportal field and the central vein), and the hepatocytes, where the biochemical metabolic reactions take place. On the lobular scale, we consider a tetraphasic body, composed of a porous solid structure representing healthy tissue, a liquid phase describing the blood, and two solid phases with the ability of growth and depletion representing the fat tissue and the tumor tissue. The phases consist of a carrier phase, called solvent, and solutes, representing microscopic components, e.g. nutrients, dissolved in the solvent. To describe the influences of the resulting tissue growth, the model is enhanced by a kinematic growth approach using a multiplicative split of the deformation gradient into an elastic and a growth part, dependent on the fat accumulation and tumor development. To describe the metabolic processes as well as the production, utilization and storage of the metabolites on the cellular scale, a bi-scale

PDE-ODE approach with embedded coupled ordinary differential equations (ODE) is used.

3. Results

In order to represent realistic conditions of the liver, experimentally or clinically obtained data such as changes in perfusion, material parameters or tissue morphology and geometry are integrated as initial boundary conditions or used for parametrization and validation [5]. Data integration approaches like machine learning are developed for the identification, processing and integration of data.

4. Discussion and Conclusions

A workflow is designed that directly prepares the model for clinical application by (semi-) automatically processing the data, considering uncertainties, and reducing computation time.

5. References

1. Christ, B., ..., Ricken, T. et al. [2017], *Frontiers in Physiology* 8, 906
2. Ricken, T., et al. [2015], *Biomech. Model. Mechanobiol.* 14, 515-536
3. Ricken, T., and Lambers, L. [2019], *GAMM-Mitteilungen* 42(4)
4. Ehlers, W., *Foundations of multiphasic and porous materials* (2002)
5. Seyedpour, S. M., ..., and Ricken, T. [2021], *Frontiers in Physiology* 12, 1563Brodland GW, Veldhuis JH. *PLoS One.* 2012;7(9):e44281 (2012).

Acknowledgements:

This work was funded by the Deutsche Forschungsgemeinschaft (DFG, German Research Foundation) via the following projects: 312860381 (Priority Programme SPP 1886, Subproject 12); 390740016 (Germany's Excellence Strategy EXC 2075/1, Project PN 2-2A); 436883643 (Research Unit Programme FOR5151, Project P7); 465194077 (Priority Programme SPP 2311, Project Sim-LivA); 463296570 (Priority Programme SPP 1158, Antarctica)



HOMOGENIZATION OF THE PERFUSION AND CONTRAST FLUID TRANSPORT IN THE LIVER LOBULES

Eduard Rohan (1), Jana Camprová Turjanicová (1), Vladimír Lukeš (1)

*NTIS- New Technologies for Information Society, Department of Mechanics,
University of West Bohemia, Univerzitní 8, 30100, Pilsen, Czech Republic*

1. Introduction

The contrast fluid (CF) enhanced CT perfusion test belongs to the most frequently used patient investigation. A time bolus of the CF is injected into the vascular system and the CT scans monitor the tissue density using images of the liver slices. We present a model of the blood perfusion and CF transport in the homogenized liver tissue represented by a periodic cell established as a segment of the liver lobulus.

2. Materials and Methods

We employ a recently developed homogenized model of the contrast fluid (CF) transport in the double porosity medium. We consider the primary porosity associated with the sinusoidal network whereas the hepatic tissue involving the bile canaliculi present the dual porosity. In the dual porosity, the diffusion is dominant, accounting for the CF penetration to the space of Disse through the capillary wall fenestration. The multiscale advection velocity fields are given separately by the perfusion model, which is derived using the homogenization of the Stokes flow in pores of the mesoscopic skeleton occupied by the deforming double porosity medium representing the liver parenchyma.

3. Results

The model has been implemented in the in-house developed finite element code SfePy. As the proof of concept, we considered a 3D block of the liver tissue whose the microstructure is described by the liver representative periodic cell (LRPC) constituted by two portal lobulae, such that it contains the liver acinus as a substructure. In Fig. 1, the time space distribution of the CF concentration is displayed for two compartments of the primary

porosities, as associated with the precapillary vessels of the portal (PV) and hepatic (HV) veins.

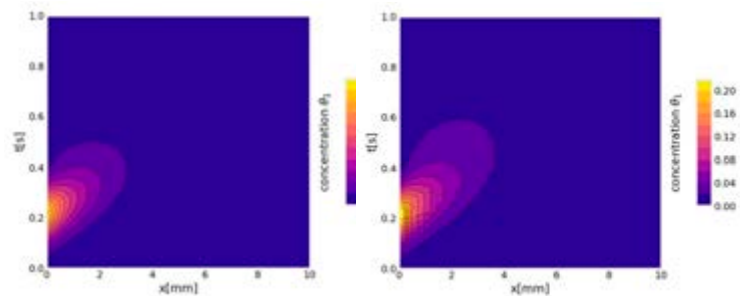


Figure 1: The peak of the concentration bolus arriving in the PV compartment is transported through the dual (sinusoidal) porosity to the HV where it appears more smeared and delayed.

4. Discussion and Conclusions

As a remarkable advantage over the classical phenomenological modelling approaches, the multiscale modelling based on the periodic homogenization method provides mutual influences between the macroscopic phenomena, such as inhomogeneous perfusion, and the local processes relevant to the lobular (mesoscopic) level.

5. References

1. E. Rohan, R. Cimrman, Int J Multiscale Comput. Engrg. 8(1), 2010.
2. E. Rohan, J. Turjanicová, V. Lukeš, Comp & Struct, 251, 106404, 2021.
3. E. Rohan, J. Turjanicová, and V. Liška, PLOS ONE 16(12): e0260068, 2021.
4. E. Rohan, V. Lukeš, and A. Jonášová, J Math Biol., 77:421-454, 2018.

Acknowledgements:

The research has been supported by the grant project GA~22-00863K of the Czech Science Foundation.



MODELLING OF HEMODYNAMICS AND TRANSARTERIAL PARTICLE TRANSPORT IN THE LIVER AT DIFFERENT SCALES

Charlotte Debbaut (1,2), Tim Bomberna (1,2)

1. IBiTech-Biommeda, Ghent University, Belgium; 2. Cancer Research Institute Ghent, Belgium

1. Introduction

As the liver is a highly vascularized organ, its blood circulation plays an important role in many liver-related processes, including organ (dys)function and pathologies (e.g. cirrhosis, hepatocellular carcinoma), as well as treatments (e.g. transplantation and partial hepatectomy procedures). Combined with relevant mass transport phenomena, liver perfusion impacts a multitude of additional applications, e.g. the microsphere transport during transarterial radio- and chemo-embolization procedures, and the cell transport during recellularization for organ bioengineering etc. However, the complexity of liver perfusion is still not fully unravelled. Deeper insights should be gained on the liver's vascular morphology, hemodynamics and mass transport in the vascular compartment. Therefore, we present a summary of our research on (i) imaging and modeling the liver circulation from the macrocirculation up to the microcirculation level, and (ii) a numerical approach to model the hepatic arterial macrocirculation combined with the mass transport of microparticles.

2. Materials and Results

Vascular corrosion casting followed by micro-CT scanning (up to 2.6 μm resolution) and image processing resulted into detailed 3D reconstructions of human and rat liver vascular trees for both normal and cirrhotic conditions. Geometrical characteristics of the vascular trees (branching topology, radii, etc.) were analysed from the macro- to microvascular level [1-2].

Based on the morphological data, perfusion models were built for multiple length scales [1-2]. A whole organ electrical analog model (0D) of human and rat liver perfusion was developed to study machine perfusion, partial hepatectomy procedures and cirrhosis. At the microscale, normal and cirrhotic hepatic perfusion was

modelled using 3D Computational Fluid Dynamics (CFD) to simulate fluid flow through 3D sinusoidal networks and a porous medium liver lobule, revealing a.o. anisotropic permeability properties.

Furthermore, 3D CFD was applied to model particle mass transport in hepatic arterial trees of human livers considering both a continuous fluid phase (blood) and a discrete phase (particles). Doing so, the locoregional delivery of microspheres during radio-/chemo-embolization therapy was simulated [3], and the feasibility of modelling cell transport in case of recellularization strategies for whole liver bioengineering was tested [4]. Results showed a high sensitivity of microsphere and cell distributions to several injection parameters (e.g. injection location) [3-4].

3. Conclusions

An imaging and modelling approach was developed to simulate intrahepatic perfusion and mass transport at different scales. Unique 3D morphological data was obtained, as well as novel models and insights into liver hemodynamics and the mass transport of particles carried by the bloodstream.

5. References

1. Debbaut, C., et al. (2014). Transplantation Proceedings, 46(9), 3143-3146.
2. Peeters, G., et al. (2018). Journal of Anatomy, 232(3), 485-496.
3. Bomberna, T., et al. (2021). Expert Opinion on Drug Delivery, 18(3), 409-422.
4. Bomberna, T., et al. (2021). The International Journal of Artificial Organs, 44(9), 619-619.

Acknowledgements:

The authors would like to thank the Research Foundation – Flanders (FWO) and the Special Research Fund (BOF, Ghent University) for providing financial support to this project.



HYDROMECHANICAL MODELING OF PLANT TISSUE MORPHOGENESIS USING A 3D DEFORMABLE CELL MODEL

Hans Van Cauteren (1), Jef Vangheel (1), Bart Smeets (1), Pieter Verboven (1), Bart Nicolai (1,2)

1. KU Leuven, Belgium; 2. VCBT, Belgium

1. Introduction

Plant growth and morphogenesis are controlled by biochemical and physical processes that guide the coordinated expansion of cells within a tissue. So far, much research has been focussed on elucidating the molecular mechanisms behind plant morphogenesis, but an good understanding of the role of physical constraints in this intricate process is still lacking.

Physical models of cellular growth in plants exist, but often use simplified 2D or 3D vertex geometries. Although very valuable, these models neglect the importance of intercellular adhesion and realistic 3D cell connectivity in morphogenesis. Additionally, plant growth models often assume fast water fluxes and avoid complexity by not including water transport and keeping turgor pressure constant during growth. However, turgor heterogeneity has been observed in plant tissues and water fluxes could have an important contribution in explaining certain growth patterns [1].

2. Materials and Methods

The discrete element method (DEM) was used to model plant cells as deformable visco-elastic shells under turgor pressure (Fig. 1). The shell, representing the cell wall, is characterised by a (bending) stiffness, wall viscosity and wall thickness. A proportional-integral volume controller is used to adjust the cell volume by changing the turgor pressure inside the cell. Furthermore, the model includes intercellular adhesion and irreversible cell separation to represent the mechanics of the middle lamella.

Cell wall growth was added to the model based on the wall growth equations by Lockhart and Ortega [2]. Lastly, symplastic and apoplastic water transport were implemented using basic water transport equations and coupled to the cell

mechanics through turgor pressure by using the volume controller system.

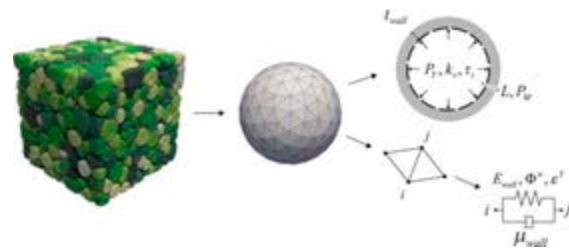


Figure 1: Overview of the DEM model

Finally, simulations were performed using a cuboidal tissue setup, compressed in all directions. The compressive forces were varied to estimate the impact of tissue scale stresses on the resulting growth patterns.

3. Results

The effects of different hydromechanical parameters on growth rate and tissue morphology were analysed.

4. Discussion and Conclusions

In this work, the implementation of a realistic 3D hydromechanical plant growth model using DEM was demonstrated using a number of test cases. In the future, additional complexity should be added to the model (e.g. programmed cell death, effect of plant hormones, spatio-temporal variation of cell properties, etc.), and experimental data on cellular plant growth will be used to validate the model.

5. References

1. Wada H et al., Horticulture Research, 8(1), 1–15 (2021).
2. Ortega J K E, Plant Physiology, 79(1), 318–320 (1985).

Acknowledgements:

The authors would like to thank the Research Foundation – Flanders (SB fellowship H. Van Cauteren, grant no: 1SE3521N) for providing financial support to this project.



DIFFERENCES IN PROPHYLACTIC PERFORMANCE ACROSS WOUND DRESSING TYPES USED TO PROTECT FROM DEVICE-RELATED PRESSURE ULCERS CAUSED BY A CONTINUOUS POSITIVE AIRWAY PRESSURE MASK

Aleksei Orlov (1), Amit Gefen (1)

1. Tel Aviv University, Israel

E-mail: gefen@tauex.tau.ac.il

1. Introduction

Prolonged use of continuous positive airway pressure (CPAP) masks, as often required for noninvasive ventilation during the COVID pandemic time, imposes a risk to facial soft tissue integrity and viability, as these tissues are subjected to sustained deformations caused by tightening of the stiff mask surfaces to the head. The risk of developing CPAP-related pressure ulcers/injuries (CPAP-related-PU) can be reduced through suitable cushioning materials placed at the skin-mask interface, to spread the localised contact forces and disperse the surface and internal tissue stresses.

2. Materials and Methods

Using an integrated experimental-computational approach, we compared the biomechanical protective performance of a popular foam dressing material to that of a market-lead hydrocolloid dressing when applied to protect the facial skin under a CPAP mask. We measured the compressive stiffness properties of both dressing materials, and then fed those to an anatomically-realistic finite element model of the head, with an applied (simulated) CPAP mask. Through this process, we calculated the protective efficacy index (PEI) of the above materials in preventing CPAP-related-PU, which indicates the relative contribution of the dressing type to alleviating the facial soft tissue loads with respect to the no-dressing case..

3. Results

We found that the greatest facial tissue stresses occur at the bridge of the nose and the cheeks, followed by the chin, which is in excellent agreement with reported clinical-epidemiological data concerning facial anatomical sites at-risk for CPAP-related-PU.

The difference in PEIs between the two material types was dramatic at the cheeks, with PEI=64% for the foam dressing with respect to a poor PEI=9% for the hydrocolloid. At the bridge of the nose that difference was lower, but still substantial, PEI=86% for the foam versus PEI=60% for the hydrocolloid. The mean PEI for the entire face was 70% for the foam dressing, and just 23% for the hydrocolloid, indicating that the foam dressing is considerably advantageous over the hydrocolloid for prophylaxis of CPAP-related-PU.

4. Discussion and Conclusions

The tested foam dressing demonstrated high protective efficacy at all the studied facial sites, and was considerably superior to a hydrocolloid dressing for prevention of CPAP-related PU.

Acknowledgements:

Support was received from the European Union's Horizon 2020 research and innovation programme under the Marie Skłodowska-Curie grant agreement No. 811965; project STINTS (Skin Tissue Integrity under Shear), and from Mölnlycke Health Care (Gothenburg, Sweden).

CHARACTERIZATION AND COMPUTATIONAL MODELLING OF SKIN TO BONE INTERACTION THROUGH PEELING TEST

Yves Vallet (1), Cédric Laurent (1), Adrien Baldit (1), Charline Bertholdt (2,3), Rachid Rahouadj (1), Olivier Morel (2,3)

1. CNRS UMR 7239 LEM3 - Université de Lorraine, Nancy, France ; 2. Université de Lorraine, CHRU-NANCY, Pôle de la femme, F-54000 Nancy, France ; 3. IADI INSERM U1254, Rue du Morvan, 54500, Vandoeuvre-lès-Nancy, France

Corresponding author: Yves Vallet, yves.vallet@univ-lorraine.fr

1. Introduction

Fasciae are collagenic tissues permitting a large but finite sliding between organs, but also between skins and its underlying elements [1], [2]. While peeling tests are commonly used in the industry to characterize adhesion between two materials, it has seldomly been used to assess the interactions between two living tissues until recently [3]. Moreover, there is a lack of efficient computational methods in order to transfer peeling test results within finite element modelling at the macrolevel of tissues, with few model parameters. The objective of this study is therefore to introduce a new method to model the tissue interaction between the skin and bone, based on peeling tests on porcine scalp (see Fig.1).



Figure 1: Peeling test performed on porcine scalp. Scale bar: 1 cm

2. Materials and Methods

The model simulating the peeling test has been implemented in Abaqus software, including two deformable solids and a series of connectors elements randomly created via an “ad hoc” Matlab code. The solids are representing the skin and bone and are respectively composed of C3D8 and C3D8R elements. CONN3D2 elements (connectors) have been automatically distributed between the two regarding faces of the solids. The dedicated code permits to link two neighbour nodes within a given radius and

the number of created elements can be controlled. To model the fibres behaviour during the test, each connector has been implemented an elastic linear rigidity, k , and a stretch failure, l_c .

3. Results

These two later parameters have been identified from a set of experimental measured data via the use of a geometric model. An example of the peeling simulation is presented in Figure 2.

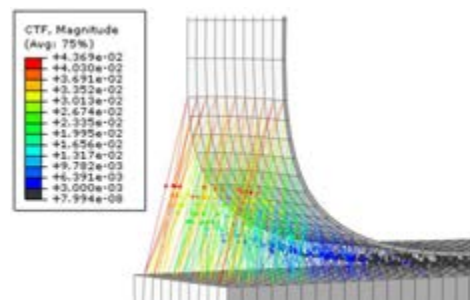


Figure 2: Simulation results of the peeling test using the identified parameters. CTF: connector force (N)

4. Discussion and Conclusions

The developed method successively permitted to reproduce the macroscopic response of the peeling test, modelling the interaction between the two tissues from the identification of only two material parameters and a given series of automatically distributed connectors. This two-parameters model constitutes a new way of simulating the interface between skin and bone, and would notably be useful to model the interaction between the scalp and skull in forthcoming research.

5. References

- Guimberteau JC et al., J. Hand Surg. Eur. Vol. 35, no. 8, pp. 614-622, Oct. 2010
- Camomilla V et al., J. Biomech., vol 62, pp. 1-4, Sep. 2017
- Larose et al., Tissue Eng. Part C Methods, vol 23, no. 3, pp. 180-189, Mar 2020

COMPUTATIONAL MODELLING OF MICRONEEDLE INSERTION AND THERAPEUTIC DRUG DELIVERY

Wenting Shu, Sean Kilroy, Eoin O'Cearbhaill, Aisling Ní Annaidh

UCD Centre for Biomedical Engineering, School of Mechanical and Materials Engineering, University College Dublin, Engineering Building Belfield Dublin 4, Dublin, Ireland

1. Introduction

Microneedles, (MN) can pierce through the tough stratum corneum (SC) layer and reach the dermis directly, resulting in enhanced therapeutic efficacy. However, due to an incomplete understanding of the micro-biomechanics of skin absorption and subsequent therapeutics. MN performance often disappoints in clinical translation. This study aims to couple a state-of-the-art skin tissue model which reflects *in vivo* skin mechanical conditions with a constitutive equation of drug diffusion in tissue.

2. Materials and Methods

Skin tissue is an anisotropic heterogeneous porous media. Hence, the approach taken in the drug diffusion model utilises the aqueous pore pathway hypothesis[1]. This approach describes the diffusion of drug molecules transport through aqueous pores within the intact skin and introduces a hindrance factor (H), a tortuosity parameter (τ) and a porosity parameter (ϕ) into the constitute equation of skin absorption to define the diffusion coefficient (D) in Eq. 1 [1]:

$$D_{eff} = \frac{\phi}{\tau} D^\infty H(\lambda) \quad (1)$$

Coupling skin deformation and subsequent induced strains from MN insertion [2] with a strain-dependent diffusion model, this multi-physics strain-dependent model is currently being adapted to assess drug diffusion from coated MNs [2].

3. Results

The current model considers compression of skin elements due to MN insertion which results in increased tortuosity and decreased porosity volume and radius. This results in an overall reduction in the effective diffusion coefficient for each element. A comparison between the

strain-dependent diffusion model with a strain-independent diffusion model and simple (Fick's law) diffusion model illustrates the overall concentration of drug diffusion with respect to time, as seen in Fig.1.

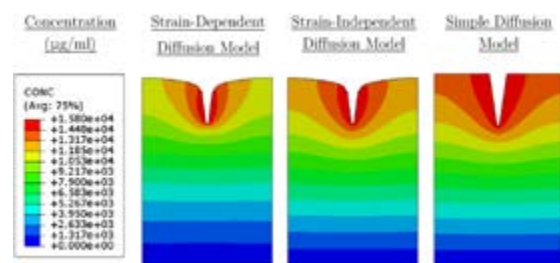


Figure 1: Concentration profiles for drug diffusion modelling.

4. Discussion and Conclusions

The current study developed a state-of-the-art FE model which can elucidate the micro-mechanics of microneedle therapeutics to a degree which has not been previously possible. This study suggests that simple idealised microneedle drug diffusion models significantly overestimate the performance of such drug delivery methods.

5. References

1. Kushner 4th J. et al., J Pharm Sci.;96(12):3263-3282 (2007).
2. Shu, W. et al., Acta Biomater, 135: p. 403-413 (2021).

Acknowledgements:

This work has been funded by a China Scholarship Council (CSC) Grant No. 202008300021 and has emanated from research supported in part by a research grant from Science Foundation Ireland (SFI) under Grant Number 16/RC/3872 and is co-funded under the European Regional Development Fund.



VISCOELASTIC PROPERTIES OF GREY MATTER IN PORCINE SPINAL CORD

Jasdeep Bhinder^{1,2}, Yvan Petit^{1,2}, Atefeh Masoumipour^{1,2}, Elisabeth Laroche^{1,2}, Eric Wagnac^{1,2},

1. Mechanical department, Ecole de technologie supérieure, 1100 rue Notre-Dame Ouest, Montreal, QC H3C 1K3, Canada

2. Research Center, Research Center, CIUSSS Nord de l'île de Montréal, 5400 Gouin Blvd, Montreal, QC H4J 1C5, Canada

1. Introduction

Numerous people suffer from traumatic spinal cord injuries (TSCI) worldwide [1], therefore, understanding post-trauma injury mechanisms becomes vital. In day-to-day life, the spinal cord is subjected to axial cyclic compression. Accordingly, viscoelastic properties of the grey matter of the spinal cord are important, but evaluating these properties experimentally is difficult and lacks mention in the existing literature. The objective of this work is to determine the viscoelastic properties of grey matter by using the well-established technique of inverse finite element modeling (FEM) which is widely adopted for brain tissue [2, 3].

2. Materials and Methods

Spinal cord specimens of 2.25 mm in length were extracted from the thoracic region (T4-T8) of two landrace pigs weighing 58.2 and 65.3 kg. The samples were kept hydrated by regularly spraying phosphate buffer solution. Stress-relaxation testing was conducted in unconfined axial compression mode by applying a strain of 40 % at a strain rate of 0.01 s^{-1} and by maintaining this strain for 1000 seconds. The behavior of the white matter in unconfined compression was taken from the literature [4] and the spinal cord was modeled in Abaqus/CAE2019 using a first-order Odgen material model alongside a 3-parameter Prony series. The viscoelastic properties and compression properties of grey matter were evaluated using the inverse FEM technique by iteratively varying the properties of the grey matter until the properties of the spinal cord model match best with the spinal cord experimental values.

3. Results

The spinal cord displays non-linear hyperelastic behavior with average peak stress of 0.012 MPa

at a strain of 40 %. The average elastic modulus of the spinal cord was 20.5 kPa. During the stress-relaxation test, an average residual stress of 0.001 MPa is observed after 1000 seconds. The inverse FEM approach confirms the existence of heterogeneity within the spinal cord as the grey matter is found to be about 3.2 times stiffer than the white matter. Interestingly, the sum of viscous components derived from curve fitting using the 3-term Prony series is 2.2 times higher for white matter, pointing out that white matter is more viscous compared to grey matter.

4. Discussion and Conclusions

The structural and biological differences between grey and white matter also reflect a difference in their mechanical properties. Histologically, it has been observed that grey matter has a larger density of cell bodies and also owns higher neural cells, while white matter is majorly composed of long-range myelinated axons [5]. The fraction of cells is reported to be directly proportional to stiffness [6] and the same is observed in this study. Henceforth, this work has the potential to pave a way for accurate computational modeling of the TSCI and can assist in determining the biofidelic mechanical properties of the spinal cord.

5. References

1. Lee BB et al., Nature; 52: 110-116: (2014).
2. Pan et al., Frontiers in bioengineering and biotechnology; 1: 1-10: (2013).
3. Feng et al., Journal of Mechanical Behavior of Biomedical Materials; 65: 490-501: (2017).
4. Sparrey and Keaveny. Journal of Biomechanics; 44: 1078-1082: (2011).
5. Yu, JJ. MSc thesis, Biomedical Engineering, University of British Columbia, (2019).
6. Koser DE et al., Biophysical journal; 108: 2137-47: (2015).

IMPLEMENTATION OF THE PATELLAR TENDON REFLEX IN A MUSCLE-DRIVEN ROBOTIC LEG BASED ON BIOINSPIRED MOTOR CONTROL

Tobias Nadler (1), Norman Stutzig (3), Syn Schmitt (1,2)

1. Institute for Modelling and Simulation of Biomechanical Systems, University of Stuttgart, Germany;
2. Stuttgart Center for Simulation Science (SimTech), University of Stuttgart, Germany;
3. Department of Motion and Exercise Science, University of Stuttgart, Germany

1. Introduction

The reflex arc, the neural substrate of a reflex, is fundamental to the physiology of posture and locomotion and to the clinical examination of the nervous system. Understanding the contribution of reflexes to biological motion control has high potential to improve control algorithms (robustness, (learn) performance) in the field of humanoid robots or assistive wearable devices.

2. Materials and Methods

To investigate the contribution of the patellar tendon (monosynaptic) reflex loop to the motor control of humanoid robots, we developed a robot that mimics the human morphology as closely as possible (muscle dynamics (1), muscle activation (2), muscle sensors, muscle attachment points, muscle deflection (3), axes of the joint movements). The neural reflex controller implemented in the biorobotic leg is based on a neuro-musculoskeletal simulation model (4). To validate the robotic model, comparative data from experiments with humans were recorded. A pendulum with eight different start angles (α) was used to trigger the reflex in a standardized manner (Figure 1). We recorded the kinematic data with five high-speed cameras (3.5 pixel/mm; 1000 fps).



a) Bio-robotic leg b) Human leg

Figure 1: Same experimental setup of the bio-robotic leg a) actuated by pneumatic artificial muscles and a human leg b) of a healthy subject.

3. Results

We analyzed the kinematic reflex response of twelve healthy subjects (six male, six female) and compared both individual and mean data with the kinematic reflex response of the leg robot. For the evaluation of the human experiments, the maximum knee angle deflection from 5 trials at each start angle of the pendulum was used (Figure 2).

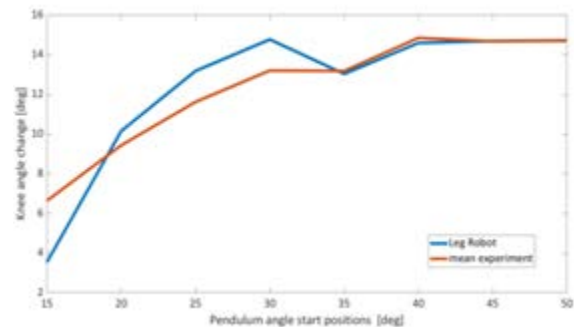


Figure 2: Comparison of the maximum knee angle change (of the eight different start angles of the pendulum) between the robot leg and the mean of twelve subjects.

4. Discussion and Conclusions

We have shown that with our robot model we can reproduce the dynamics of the reflex response in general (reflex times, force generation, kinematics) and tune the control parameters to the individual, subject-specific reflex response.

5. References

1. S. Wolfen et. al., 2018 25th International Conference on Mechatronics and Machine Vision in Practice (M2VIP), p. 1-6 (2018)
2. H. Hatze. Biological cybernetics. 25, p. 103–119 (1977).
3. M. Hammer et. al., Mathematical biosciences. 311, p. 68–81 (2019)
4. K. Stollenmaier et. al., Frontiers in bioengineering and biotechnology. 8, p. 308 (2020)

TOWARDS A REAL-TIME SIMULATOR OF FLOW DIVERTERS DEPLOYMENT BASED ON MODEL ORDER REDUCTION

B. Bisighini^(1,2,3), M. Aguirre⁽¹⁾, B. Pierrat⁽¹⁾, D. Perrin⁽²⁾ and S. Avril⁽¹⁾

1. *École des Mines de Saint-Étienne, France*; 2. *Predisurge, France*; 3. *Università Tor Vergata, Italy*

Beatrice Bisighini: beatrice.bisighini@emse.fr

1. Introduction

Flow diverters (FDs) are very dense braided stents used in the endovascular treatment of cerebral aneurysms. Computational tools could be useful in assisting surgeons in the selection of the best device for a patient, especially in complex cases. However, due to the large amount of degrees of freedom and the necessity to solve the contact with the wall, the computational time required by traditional techniques alone, such as finite element (FE) modelling, is excessively high. Here we propose a feasibility study of a fast and accurate reduced-order (RO) modelling scheme, based on finite element simulations and machine learning, to compute the deployed configuration of FDs within idealised vascular models in real-time.

2. Materials and Methods

High-fidelity simulations: The FD is modelled as a tubular net of interlaced thin wires. The stent structure is discretised using beam elements and deployment simulations are performed using an efficient in-house, open-source FE solver, EndoBeams.jl [1].

Idealised parametric model: Each vessel model is parametrised with 5 geometrical parameters (curvature $2x$, vessel radius, aneurysm radius and centre position) and 1 surgical parameter (deployment site along the vessel centreline).

High-fidelity database: 150 cases are defined for the geometrical and surgical parameters. Corresponding FD deployed configurations are computed, 20% of which are used for testing.

Reduced order model: As in [2], a non-intrusive reduced basis (RB) method is used: the RBs are extracted from the database with the proper orthogonal decomposition and Gaussian process regression is used to predict the

projection coefficients for new parameters values. The RO model is tested by computing the nodal and average absolute error (AE) between FE and approximated solutions among the testing cases.

3. Results

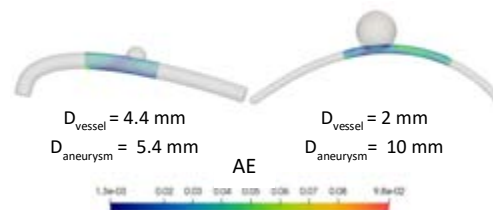


Fig. 1: Predicted solutions for two testing cases with corresponding nodal AE scale.

The average AE decays rapidly as more RBs are considered and, around 15, reaches a stable plateau equal to 0.07 mm with standard deviation 0.08 mm, which results in an acceptable approximation (Fig. 1).

4. Discussion and Conclusions

Using the proposed scheme, the computational cost is reduced from ca 30 minutes to few ms with a controlled loss of accuracy. Current efforts are oriented toward understanding how many parameters are needed to fully describe patient-specific models.

5. References

1. B. Bisighini et al., Advances In Eng. Software, vol. 171, 2022.
2. M. Guo and J. S. Hesthaven, Comput. Methods Appl. Mech. Eng., vol. 341, pp. 807–826, 2018.

Acknowledgements:

This project has received funding from the European Union's Horizon 2020 grant 859836.



GRAPH NEURAL NETWORKS TO PREDICT JUNCTION PRESSURE LOSSES IN REDUCED-ORDER CARDIOVASCULAR MODELLING

Natalia L. Rubio (1), Luca Pegolotti (2), Martin R. Pfaller (2), Jonathan Pham (1),
Eric F. Darve (1), Alison L. Marsden (1, 2)

1. *Stanford Mechanical Engineering, USA*; 2. *Stanford Pediatrics, USA*

Correspondence - Natalia L. Rubio – nrubio@stanford.edu

1. Introduction

Reduced-order models (ROMs) offer an efficient means to approximate bulk quantities in patient-specific cardiovascular hemodynamic models. Compared to expensive 3D computational fluid dynamics (CFD) simulations, they reduce computation by solving a smaller system of equations that governs a simpler but analogous physical system. In particular, the 0D ROM describes the vasculature as an electric circuit in which flow is represented by current and pressure is represented by voltage [1]. The 0D ROM can run in seconds on inexpensive hardware (e.g., laptops). 0D models are widely used in practice but suffer from the inability to accurately characterize fluid dynamics in junctions. This work addresses this issue by using CFD simulations to train a machine learning model to predict pressure drops over vascular junctions.

2. Materials and Methods

We chose to develop a graph neural network (GNN) model to effectively handle junctions with an arbitrary number of inlets and outlets. During training, the GNN parameters are tuned to minimize the mean squared error with respect to the true pressure drop defined by the CFD simulations. We consider two approaches – one in which we directly predict pressure drop over junctions from bulk flow and geometric features and another in which we use only the geometry to predict the characteristic values of electric circuit elements (resistor and inductor) that would represent a junction in the 0D ROM framework. The primary training data for this work is the Vascular Model Repository, a publicly available collection of about 150 hemodynamic 3D CFD simulations of diverse vascular anatomies [2]. Given its diversity, the

relatively small size of this dataset poses challenges regarding model generalization. These challenges are common when applying machine learning techniques to real-world problems in which data are scarce and expensive to generate. We demonstrate and analyse paths towards overcoming these issues using an augmented synthetic dataset.

3. Results

We compare our model against state-of-the-art models commonly used for junction modelling in cardiovascular ROMs and show that we can achieve lower errors on a validation set. We compare the accuracy and generalization capabilities of directly predicting pressure drops versus predicting characteristic values of circuit elements. We also present generalization trends for different dataset sizes and diversities.

4. Discussion and Conclusions

We discuss different approaches to developing a GNN to predict pressure drops over junctions. We explore the GNN model's generalization properties in our setting of limited and diverse training data. Ultimately, we will incorporate the GNN into existing 0D ROM frameworks to increase their accuracy.

5. References

1. M. Mirramezani et al. *Annals of Biomedical Engineering*, 48 (12):2870–2886, 2020.
2. N. M. Wilson, et al. *Journal of Medical Devices*, 7(4):0409231–409231, 2013.

Acknowledgements:

The authors thank the Stanford Graduate Fellowship Program, NSF GRFP, and NIH grants R01LM013120, R01EB029362, and K99HL161313 for financially supporting this work.



LEARNING REDUCED-ORDER MODELS FOR BLOOD FLOW SIMULATIONS USING GRAPH NEURAL NETWORKS

Luca Pegolotti (1), Martin Pfaller (1), Natalia Rubio (2), Eric Darve (2), Alison Marsden (1,2)

1. *Stanford Pediatrics, USA*; 2. *Stanford Mechanical Engineering, USA*

Correspondence – Luca Pegolotti – lpego@stanford.edu

1. Introduction

Reduced-order models (ROMs) are widely used in cardiovascular modeling due to their efficiency [1]. In this work, we aim to develop data-driven ROMs with Graph Neural Networks (GNNs) using simulation data from the Vascular Model Repository (VMR), publicly available at www.vascularmodel.com.

2. Materials and Methods

Similar to classic one-dimensional physics-driven ROMs, our GNN approximates average pressure and flow rate at points (graph nodes) positioned on the vessel centerline. The network is based on MeshGraphNet [2], a recently proposed method to approximate the solution of partial differential equations on unstructured meshes.

In the rollout phase of the method, the GNN uses the state of the system at timestep t^k to compute the increment in pressure and flow rate at each centerline node and reach timestep t^{k+1} . The state of the system includes time-dependent variables (i.e., nodal pressure and flow rate) and time-independent geometrical features. The GNN computation is based on an encode-process-decode algorithm. Node and edge features are first encoded using fully connected neural networks. In the process stage, multiple message passing steps propagate information across neighboring nodes. Finally, the latent node features are decoded using fully connected neural networks.

We train the GNN to minimize the mean squared error between its approximation of pressure and flow rate at the next timestep and the 3D ground truth simulation data extracted from the VMR.

3. Results

Our experiments demonstrate the excellent performance of the GNN on 160 simulations obtained on 5 aorta models with varying boundary conditions. Using 10-fold cross validation, the average errors over all timesteps and mesh nodes are below 1% for both pressure and flow rate and the inference time to perform 400 timesteps is approximately 3 seconds. When considering more simulations from the VMR for training and testing, we achieve average errors around 2% but observe more variability across the dataset.

4. Discussion and Conclusions

We show that GNNs are a valid alternative to physics-driven ROMs given adequate training data. In particular, we focus on the conditions that allow achieving good generalization errors across large numbers of patient-specific geometries and simulation parameters (controlling, for instance, the boundary conditions) from the VMR.

5. References

1. Pfaller et al. *Int J Numer Meth Biomed Engng.* 2022; 38(10):e3639.
2. Pfaff et al. *arXiv:2010.03409* (2020).

Acknowledgements:

This work was supported by NIH Grants R01LM013120, R01EB029362, and K99HL161313. Additional funding was provided by the Stanford Graduate Fellowship. The authors gratefully acknowledge the San Diego Super Computing Center (SDSC) and Intel for providing the computational resources to run the three-dimensional simulations and to train the GNNs presented in this work.

AN APPROACH FOR NEURAL NETWORK FINITE ELEMENT BASED CARDIAC SIMULATIONS

Shruti Motiwale (1), Wenbo Zhang (1), Michael Sacks (1)

1. The University of Texas at Austin, TX, USA

Corresponding author: Michael Sacks, msacks@oden.utexas.edu, 201 E 24th St. Stop C0100 Austin, TX 78712

1. Introduction

Comprehensive image-based computational modelling pipelines are being developed for patient-specific cardiac simulations in health and disease. However, traditional finite element based simulation methods remain a limitation due to their prohibitively slow speeds. In this work, we present a neural network finite element (NNFE) [2,3] approach for cardiac mechanics simulations capable of performing in clinically relevant timeframes.

2. Materials and Methods

We developed a physics-based training scheme using differentiable finite elements to compute the residual force vector of the governing PDE, minimized to find the optimal neural network (NN) parameters. We used NNs for their representation power, and finite elements for defining the problem domain, specifying the boundary conditions, and performing numerical integrations. We incorporated spatially varying fibre structures into a prolate spheroidal model of the left ventricle. A Fung-type material model with active contraction was used [1]. The model was trained against two P-V loops (Fig. 1) and validated against FEM simulations using an identical FEniCS-based model.

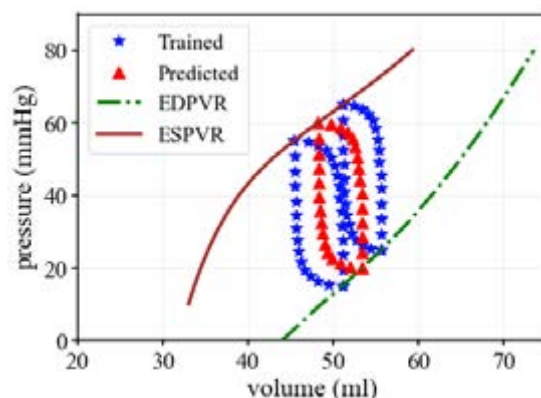


Figure 1: The NNFE model was trained on two PV loops and predicted the third loop.

3. Results

The NNFE model predicted the displacement and the corresponding volume for the predicted PV loop (Fig 1). The mean nodal error between the NNFE solution and the FE solution was 2.32×10^{-2} mm, with a standard deviation of 4.53×10^{-2} mm (Fig. 2a). The NNFE method took 2-3 seconds for each state, whereas the FEM solution took 10-20 min.

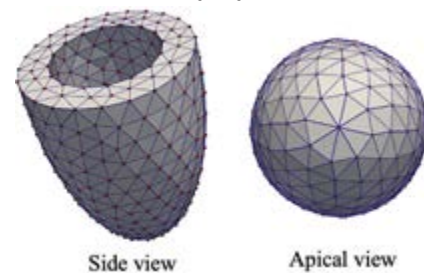


Figure 2: End-diastolic state predicted by the NNFE method (wireframe) overlaid with FEM solution (dots). The NNFE method can accurately capture the twisting, as visible in the apical view.

4. Discussion and Conclusions

We presented the NNFE approach for organ-level functional heart simulations. The NNFE method can be simultaneously trained over the entire range of physiological boundary conditions. The trained NNFE can predict pressure-volume responses for any physiological boundary condition without retraining. We will implement this model to predict cardiac mechanics after a myocardial infarction, and present results at the meeting.

5. References

1. Liu H, et al. Scientific reports 11.1 (2021): 1-15.
2. Zhang W, et al., CMAME 394 (2022): 114871.
3. Sacks M, et al., J Biomech Eng 144.12 (2022)

Acknowledgements:

NIH R01 HL073021, Platform for Advanced Scientific Computing (Swiss Federation).

A COHORT OF PATIENT-SPECIFIC AND VIRTUAL FINITE ELEMENT MODELS OF INTERVERTEBRAL DISCS

Estefano Muñoz-Moya, Morteza Rasouligandomani, Carlos Ruiz, Gemma Piella, Jérôme Noailly
Departament de Tecnologies de la Informació i les Comunicacions, Universitat Pompeu Fabra, España

1. Introduction

Finite element (FE) analyses have been used to study human tissues and organ biomechanics. However, automating patient-specific (PS) Intervertebral Disc (IVD) models can take time and effort to explore the poromechanical behavior of tissues under large deformations [1]. FE studies related to IVD degeneration (DD) have been performed, but no cohorts have yet been generated to explore the particularities of morphology and whether the latter may be a factor in DD [2]. The challenge is to map the different tissues, such as the cartilage endplate (CEP), annulus fibrosus (AF), nucleus pulposus (NP), and transition zone (TZ), in the models. This work aims to generate a finite element mesh repository of PS models through a morphing process and extend it through a virtual cohort employing a statistical shape model (SSM). Simulations are performed to explore the effect of morphology.

2. Materials and Methods

169 3D shapes of lumbar IVDs, from healthy to grade 4 degeneration states, generated during the European My Spine project (FP7-269909), were obtained from MRIs [3]. The segmentations included the AF and the NP. The Bayesian Coherent Point Drift (BCPD) algorithm rigidly and non-rigidly aligned the meshes [4]. A previously validated structural mesh of an IVD was adapted to PS IVD segmentations [1]. The morphing process is carried out in several stages to end with a mesh quality analysis and an assay of the similarity between the morphed model and the segmentation through Hausdorff distance. CEPs, not visible in the images, were created automatically, with a thickness between 0.7 and 1 mm. Subsequently, synthetic IVDs were generated by SSM using the PS cohort. Mechanical simulations of physiological loads were performed, considering a swelling step, 8 hours of sleep, and 16 hours of daytime, applying 0.11 and 0.54 MPa.

3. Results

The PS and a virtual cohort of IVD models were created, all with the same mesh structure and

connectivity. The first twelve modes cover 90% variability, of which the first 3 represent coronal (46 to 52 mm), sagittal (34 to 40 mm), and thickness (7 to 17.5 mm) width. The other modes cover AF bulging and degenerate shapes. There were no differences when comparing the mesh quality of the template model with the PS models, so BCPD maintains the proportions of the relative distances between the nodes. A 94% similarity was obtained between the AF and NP segmentations with their respective meshes. The mechanical variables, such as pore fluid velocity, show substantial variations in TZ between the different models. Clinical imaging has shown DD onsets in the same zone [5].

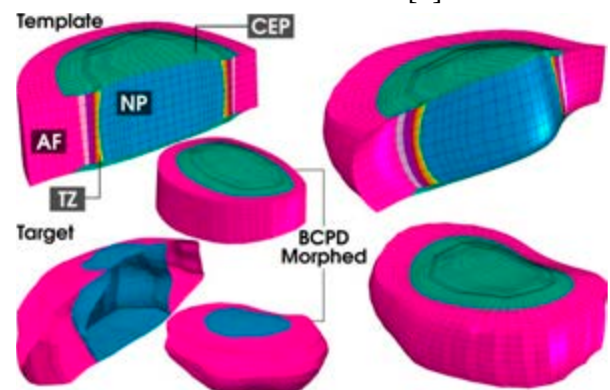


Figure 1: Mesh template, PS and morphed model

4. Impact

The cohort is a unique set of models to explore the effect of multiple geometric variations on the multiphysics and mechanobiology of IVD, including the impact of CEP [2]. The algorithm can create PS FE models from any segmented surface provided by third parties and generate thousands of representative synthetic models of healthy and DD states of IVD.

5. References

1. Ruiz, Wills et al, *Front in Physiology*. 2018.
2. Malandrino et al, *Front in Bioeng Biotech*. 2015.
3. Castro-Mateos et al, *Phys. in Med & Bio*. 2014.
4. O. Hirose et al, *IEEE*. 2021.
5. Lachlan J. Smith et al, *Dis Model Mech*. 2021.

Acknowledgements:

European Commission: Disc4All-MSCA-2020- ITN-ETN GA: 955735; O-Health-ERC-CoG-2021-101044828



FINITE ELEMENT MODELLING OF PRESS-FIT IMPLANT INSERTION

Xiaoyi Min¹ (1), David Heath¹ (2), Stephen Mellon¹ (3), David Murray¹ (4), Laurence Marks¹ (5)

1. Nuffield Department of Orthopaedics, Rheumatology and Musculoskeletal Sciences,
University of Oxford, Oxford, United Kingdom

1. Introduction

Bone damage at the bone-implant interface during press-fit implantation is inevitable. In addition to surgical factors such as interference and insertion load, primary fixation is a function of friction, bone elasticity, plasticity and failure. Press-fit has previously been simulated in finite element (FE) models that required several material parameter inputs [1]. The current study attempted to model press-fit and characterise bone damage with minimal parameters computationally. The objective was to develop a FE model that can compare various fixation element designs.

2. Materials and Methods

The insertion and extraction of a press-fit titanium peg into and out of pre-drilled holes in a plastic bone block (Sawbones Solid Rigid Polyurethane Foam - PCF20) which acted as an analogue of trabecular bone were simulated in Abaqus/Explicit through an axisymmetric model. Interferences from 0.45 mm to 1.06mm that were tested in the experiment were modelled. The peg was modelled as a rigid part and the plastic bone was characterised as an elastic-plastic material with the material stress-strain curve from a uniaxial compression test. A plastic strain-based element deletion mechanism was implemented using the built-in ductile damage feature. Elements that experienced a plastic strain higher than the fracture strain threshold were deleted to avoid heavy distortion and to account for damage at the contact interface. This value was set as the plastic strain value above which a sharp increase in the gradient of the true stress-true plastic strain curve was observed. The frictional coefficient found from a friction test was applied between the foam and the peg. The forces required to push in and pull out the peg were verified against the experiment.

3. Results

The force-displacement curves from FE agreed well with those from experiments (Fig. 1). Also, maximum push-in and pull-out forces from the FE model were both within $\pm 16\%$ of the experimental results for surgically relevant interferences of 0.68 mm, 0.70 mm and 0.92mm.

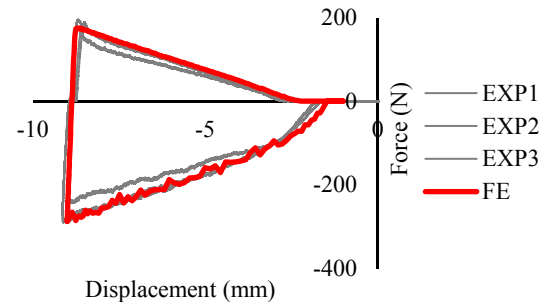


Figure 1: Force-displacement curves from the FE model and experiment for 0.70 mm interference.

4. Discussion and Conclusions

This study proposes a relatively simple FE method of simulating press-fit implantations with plastic strain-controlled element deletion requiring only two inputs: the material stress-strain curves from uniaxial compression tests and the frictional coefficients. This model could potentially provide useful insight into press-fit implant fixation and assist component design optimisations. The future work will focus on further validation of the model with plastic bones of other densities and compressive modulus, animal bone and cadaveric bone. Insertion of rough implants with porous coatings will also be simulated.

5. References

1. Ovesy, M., M. Aeschlimann, and P.K. Zysset, *J Biomech*, 2020. **107**: p. 109844.

DEFINING A PROCESS FOR STRESS REDUCTION IN THE KEEL TRAY INTERFACE IN UNICOMPARTMENTAL KNEE REPLACEMENT TIBIAL COMPONENTS

Laurence Marks (1), David W. Murray (1), Stephen J. Mellon (1)

1. NDORMS, University of Oxford, UK

1. Introduction

Minimal bone resection is advantageous with Unicompartmental Knee Replacement (UKR). The tibial component of the Oxford UKR has never broken. However it is 3mm thick and could potentially be made thinner in smaller sizes. When the tibial component is loaded in a typical ASTM manner¹ the limiting feature in terms of peak stress and therefore durability is the intersection between the keel and tray (Figure 1). Reductions in tray thickness increase the stress at this location, but the available space envelope makes reducing this impossible using simple geometric forms, so a non-parametric optimisation approach has to be adopted.

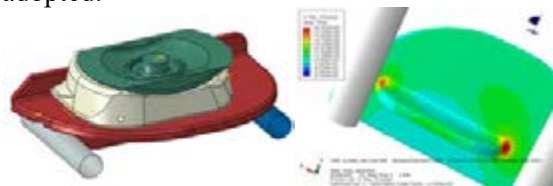


Figure 1: The ASTM test simulation setup, note high stresses at the ends of the keel.

2. Materials and Methods

The optimisation approach uses many solution cycles, the multi part models used for the initial assessments were simplified to run more quickly, whilst providing results within 7% of the more complex model. This speed optimised model is then used in a shape optimisation, and this shape then implemented in the CAD geometry.

Non parametric shape optimisation tools such as TOSCA allow automated stress reduction to be carried out. In basic terms every node in the design optimisation region is allowed to move away from the surface in response to high stress and into the surface in response to low stresses. As multiple runs are carried out stress peaks reduce with a more uniform distribution, both of which improve component durability.

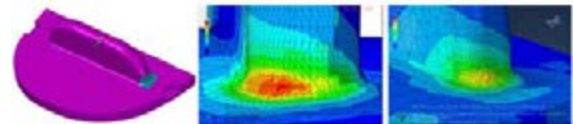


Figure 2: Design optimisation region shown in a contrasting colour. Initial stress distribution and optimised stresses shown.

The forms obtained from the optimisation don't follow simple geometric definitions, so the final CAD model has to be interpreted from these using complex radius definitions. These models were then re-run in the more accurate FEA model to estimate the max. principal stress (P1).

3. Results

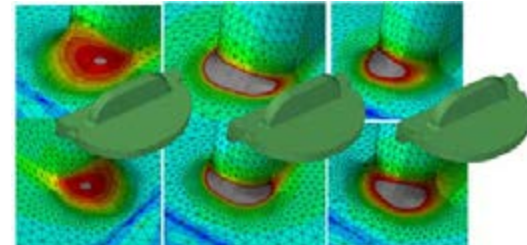


Figure 3: Optimisation informed fillet profiles compared with simply defined alternatives.

With the thinner keel and the maximum allowable simple fillet radius, the peak P1 stress was over 800MPa, the optimised fillet geometry reduced this to 550MPa as shown in Figure 3.

4. Discussion and Conclusions

The predicted increase in stresses at the intersection between the keel and tray induced by thinning the tray were mitigated by optimising the profile. This design fulfils the bone resection constraint and will be validated by mechanical testing

5. References

1. ASTM F3140 - 17, *Standard Test Method for Cyclic Fatigue Testing of Metal Tibial Tray Components of Unicompartmental Knee Joint Replacements* (2017)



IN SILICO CHARACTERIZATION OF MICRO-CT BASED BIOACTIVE GLASS-CERAMIC SCAFFOLDS

Luca D'Andrea (1), Anna De Cet (1), Dario Gastaldi (1), Francesco Baino (2), Enrica Verné (2), Gissur Orlygsson (3), Pasquale Vena (1)

1. Politecnico di Milano, Department of Chemistry, Materials and Chemical Engineering, Italy; 2. Politecnico di Torino, Italy; 3. Innovation Center Iceland (ICI), Iceland

1. Introduction

As the application of bone tissue engineering scaffolds becomes widespread, experimental studies on the effects of different materials and production methods are becoming increasingly complex. Computational models [1] can substantially reduce both the costs and the duration of the development process of these devices.

The morphological and mechanical properties of glass-ceramic scaffolds manufactured through foam replication have been investigated through μ CT-based computational models.

2. Materials and Methods

The scaffolds characterized were obtained using an experimental composition of SiO_2 -based glass-ceramic called 47.5B-32 [2]. Six different temperatures, ranging from 600°C to 850°C, were used during the sintering process.

The 3D reconstruction of the scaffolds was carried out through μ CT images (pixel size 5 μm); two scaffolds for each sintering temperature were considered. The porosity, strut thickness and pore size were determined to characterize the morphology of each cylindrical scaffold, one of which is shown in figure 1.

The mechanical characterization was carried out through finite element based simulations with the ParOSol solver. Through an iterative algorithm allowing for damage-based material evolution [1], longitudinal compression was applied to obtain elastic and strength properties. To appropriately represent the tension-compression strength mismatch of the material, the Drucker-Prager criterion was used.

3. Results

The scaffold porosity varies between 50% and 80%. The average pore dimension for sintering temperatures lower than 700°C is 200-800 μm , while higher temperatures present both large

pores (200-800 μm) and smaller pores (<100 μm). Strut thickness decreases with sintering temperature from 400 μm to 60 μm .

The elastic and strength values of the scaffolds, normalized in respect to the composing material values, also vary between different sintering temperature, ranging from 0.5 to 0.15 and from 0.05 and 0.2 respectively.

4. Discussion and Conclusions

Two sets of scaffolds have been defined, based on sintering temperatures due to morphological and mechanical differences: scaffolds sintered below 690°C, the material's crystallization temperature [2], evidence large pores and thick struts; scaffold sintered at higher temperatures present both large and small pores, reducing the average strut thickness and pore size.

The algorithm used allows for the visualization of the fracture patterns inside the structure. Comparisons with experimental data [2,3] obtained from the same scaffolds that were computationally reconstructed were carried out to confirm the validity of the methodology.

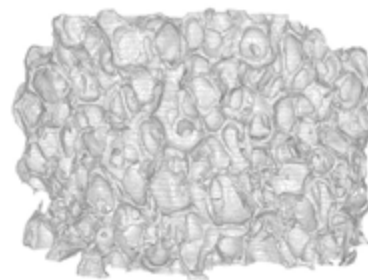


Figure 1: 3D computational reconstruction of a scaffold sintered at 600°C.

5. References

1. E. Farina et al., Acta Mech. Sinica 37(2) 292-306 (2012).
2. E. Fiume et al., Acta Biomater. 119 405-418 (2021).
3. E. Fiume et al., Appl. Sci. 10(22) 8279 (2020).

A PIPELINE FOR IMAGE BASED MODELING OF FASCIA TISSUE IN THE LOWER LEG *IN VIVO*

M.Randika Perera ⁽¹⁾, Samantha Holdsworth ^(2,3), Geoffrey Handsfield ⁽¹⁾

1. Auckland Bioengineering Institute, New Zealand; 2. Mātai Medical Research Institute, Tāirawhiti-Gisborne, New Zealand.; 3. Anatomy and Medical Imaging, The University of Auckland

1. Introduction

A number of studies show the importance of fascia and aponeurosis in understanding force transmission in the musculoskeletal system. A deeper understanding of these tissues can be gleaned from high fidelity computational modelling, but *in vivo* imaging is challenging due to rapid T2* decay times, thwarting image-based modelling workflows. Recent advanced MRI techniques have enabled the potential for connective tissue imaging. This research aims to tune and develop MRI and image processing routines for reliable connective tissue imaging for image-based modelling paradigms to understand the biomechanics of human fascia.

2. Materials and Methods

We imaged thirty participants on two 3T MRI scanners using dual-echo ultrashort echo time (UTE) non-Cartesian MRI with unique vendor versions [1,2]. Spatial resolution ranged between 0.3x0.3 mm² and 0.5x0.5 mm², slice thickness was between 3mm and 5mm. Tissue localization post-processing was used to increase contrast. Following image acquisition, segmentation was performed for deep fascia and lower limb muscles using ITK snap software. Segmentation of fascia involved identifying and marking the boundaries of the tissues in serial axial images. We used segmented datasets to reconstruct the 3D fascia anatomy, which were used to compute tissue volume, length, and thickness. Fascia thickness was computed spatially throughout the lower limb, offering a thickness distribution through the limb. To begin to develop a finite element model of a muscle-fascia system, we created an image-based geometry of one muscle – the tibialis anterior – with and without a sheath of fascia enclosing the muscle (Figure 01).

3. Results and Discussion

Regions of interest displaying fascia are visible in images (Fig 01, arrows). Bright fascia results from the subtraction of a conventional short echo time image from an ultrashort echo time (UTE) image, thus maximizing contrast. Regionally distributed fascia thickness running along the peripheral surface of muscle structures calculated from our customized algorithm presented widths between 1.5mm and 2.0mm, which is consistent with literature [3]. Fascia results demonstrate that, by using dual-echo UTE MRI, fascia tissue is identifiable, measurable, and our *in vivo* results align with literature. Finite element analysis is used to explore our hypothesis that fascia improves force transmission compared to muscle-tendon simulations which omit fascia.

4. Conclusion

Using advanced MRI, this study aimed to image and measure human fascial anatomy *in vivo* and to use imaging to develop a computational finite element model to probe the role of fascia in human movement. We found fascia thickness measurements *in vivo* that are consistent with the literature from dissection studies and we used our imaging results to build a finite element geometry of the tibialis anterior and its surrounding fascia. Future work includes the implementation of muscle contraction simulations to begin to probe the mechanical contributions of fascia to contraction dynamics.

5. References

1. Qian et al. (2008), Magn Reson Med.60:135-145
2. Ma et al. (2017), MR in Biomed.30: 3709.
3. Bhansing et al. (2015), Muscle Nerve,52:534-539

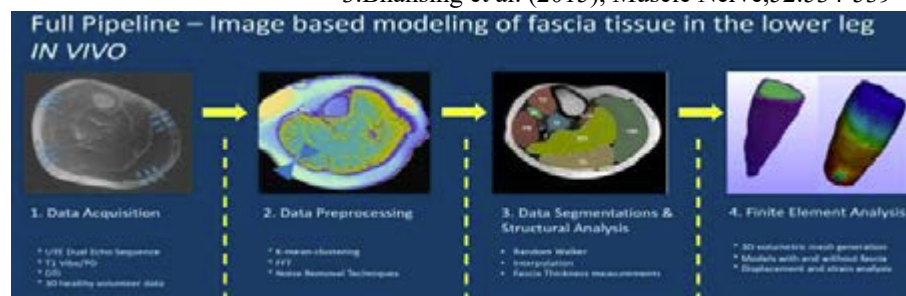


Figure 01



MODELLING MICRONEEDLE INDENTATION AND PENETRATION INTO A SKIN SUBSTITUTE USING A COHESIVE ZONE METHOD

Rachael Joyce(1), Matt Potts (1), Hayley Wyatt (1), Rhys Pullin (1), Sion A Coulman (1), James C Birchall (1) Sam Evans (1)

1. Cardiff University, Wales, UK;

1. Introduction

Microneedle based delivery systems can offer safe and painless delivery of therapeutics and vaccines. However, the success of microneedle systems relies on full and consistent needle penetration. The biomechanics of human skin is complex and therefore modelling skin penetration by a needle at the micron scale is challenging, with few studies published. A silicone skin substitute has therefore been used to develop Finite Element Models that can evaluate indentation and penetration at the micron scale. The models use a cohesive zone method, rather than the commonly published element deletion methods, and will be validated with experimental data collected from Digital Image Correlation (DIC) and μ -CT experiments.

2. Materials and Methods

A quarter model of the silicone, with the dimensions 1x1x3mm, was created with a 4-node tetrahedron mesh. It was then imported into FEBio [1]. A neo-Hookean material model was chosen for the silicone, with a Young's modulus of 0.74MPa. The cohesive zone model was generated by constraining nodes on the fracture surface via tetrahedra with an elastic damage model and free moving tangential to the fracture surface.

The needle, length 1.1mm, was directly imported into FEBio, and meshed with a 4-node tetrahedron mesh. An isotropic elastic material model was used, with a Young's modulus of 2GPa. To stop the overlapping of silicone and needle surfaces, sliding contacts were employed. An explicit solver was then used to run the model.

3. Results

Initial deformation, Figure 1(a), prior to element fracture occurs to approximately

0.1mm. The needle successfully inserted to 0.3mm using the cohesive zone method, as shown in Figure 1(b). A slight bulge is seen at the silicone surface, which is expected as the material is pushed around the needle surface.

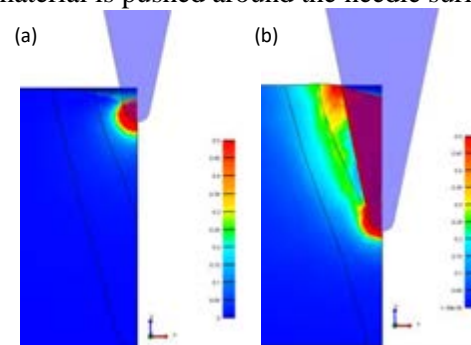


Figure 1: insertion of the microneedle into silicone showing the principal Lagrange strain prior to element fracturing (a) and the insertion at 0.3mm (b).

4. Discussion and Conclusions

Although in its early stages, this model has successfully simulated needle indentation and puncture using a cohesive zone model. This model, unlike the widely used element deletion models, is physically realistic and could therefore provide valuable insights into the mechanics of microneedle penetration and a tool that can be used to optimise needle designs. There are still many unknowns associated with mechanical disruption of the skin during the insertion of a microneedle, however experimental data from μ -CT may validate FEA and provide greater insight.

5. References

1. Maas SA, Ellis BJ, Ateshian GA, Weiss JA. FEBio: Finite Elements for Biomechanics. *J Biomech Eng* 2012;134(1):011005

Acknowledgements:

The authors would like to thank EPSRC (Engineering and Physical Sciences Research Council) for providing financial support to this project.



A DATA-DRIVEN REDUCED ORDER MODEL TO SIMULATE LEFT ATRIUM FLOWS

Caterina Balzotti (1,*), Pierfrancesco Siena (1), Michele Girfoglio (1), Giovanni Stabile (1), Jorge Dueñas-Pamplona (2), José Sierra-Pallares (3), Ignacio Amat-Santos (3,4), Gianluigi Rozza (1)

1. SISSA Mathlab, Italy; 2. Technical University of Madrid, Spain; 3. University of Valladolid, Spain; 4. Clinical University Hospital of Valladolid, Spain;

* Corresponding author: cbalzott@sissa.it, SISSA Mathlab, Trieste, Italy

1. Introduction

Atrial fibrillation (AF) is the most common type of cardiac arrhythmia. AF is usually triggered by irregular electrical impulses from the pulmonary vein root, which cause a random and ineffective contraction of the left atrium (LA). The high incidence rate of stroke for AF patients is associated with thrombus formation occurring within the left atrial appendage (LAA). The latter is a protruding cavity of the LA, whose natural contractility is drastically reduced after AF episodes. For this reason, there is an increasing interest in the study of numerical methods to simulate blood flow dynamics in the LA. This research is based on computational fluid dynamics, which is known to be computationally demanding. Since the computational efficiency of numerical simulators is essential for practical uses, we propose a data-driven reduced order model (ROM) to study LA flows.

2. Materials and Methods

Consider a set \mathcal{P} of parameters, representing a physical state, such as boundary conditions. The dynamics of blood flow in the LA is modelled through parametrized time-dependent Navier-Stokes equations (NS). To determine high residence time and dead zones, the NS equations are coupled with equations for blood age moments as in [1]. Hereafter, we refer to the coupled problem as the *full order model* (FOM). The construction of the ROM is divided into the offline and online phase [2]. The first one consists in the computation of the solutions to the FOM through finite volumes for a set of training parameters $\mathcal{M} \subset \mathcal{P}$; these solutions are collected into the snapshots matrix S , from which we recover the reduced basis space by applying the proper orthogonal decomposition (POD) al-

gorithm; then, the modal coefficients are computed through regression techniques. Finally, given a new parameter $\xi \in \mathcal{P}$, the online phase is reduced to a linear combination between the POD basis and the modal coefficients corresponding to ξ .

3. Results

The results focus on the validation of the ROM through error analysis and computation time comparison. The variables we are mainly interested in are the age blood m_1 , the blood age coefficient of variation, and the wall shear stress. Furthermore, a qualitative comparison between FOM and ROM solutions is shown.

4. Discussion and Conclusions

The medical community has shown a growing interest in numerical methods for LA flows. Our goal is to provide a fast and accurate tool to use in real time. Therefore, we propose a ROM for LA flows, which is powered by a set of high-fidelity solutions, corresponding to a training set of physical conditions, and then reconstructs approximate solutions associated with other physical conditions of interest.

5. References

1. J. Dueñas-Pamplona et al. Morphing the left atrium geometry: a deeper insight into blood stasis within the left atrial appendage. *Appl. Math. Model.*, 2022.
2. J. S. Hesthaven et al. *Certified reduced basis methods for parametrized partial differential equations*. Springer, 2016.

Acknowledgements:

The authors from SISSA want to acknowledge the European Research Council (GA 681447). J.S.-P wants to acknowledge “Movilidad de Investigadores e Investigadoras UVa - Banco Santander 2022” for funding his stay at SISSA.

ASSESSMENT OF IMMERSED BOUNDARY METHODS FOR THE DESIGN OF MEDICAL CIRCULATORY SUPPORT DEVICES

Mathieu Specklin (1), Navideh Abbasnezhad (1), Louis Marcel (1), Smaine Kouidri (1), Danial Pichoy (2), Farid Bakir (1)

1. Arts et Métiers Institute of Technology, CNAM, LIFSE, HESAM University, F-75013 Paris
2. Department of Cardiovascular and Thoracic Surgery, Institute of Cardiology, Pitié Salpêtrière Hospital, Assistance Publique Hôpitaux de Paris (AP-HP), Sorbonne University, F-75013 Paris

1. Introduction

Today's increasing figures of heart failures are concerning in western societies. One of the solutions lies in the use of Medical Circulatory Devices (MCS), whose recent evolutions are detailed in [1]. For their design, a specific attention is paid to negative effects such as hemolysis. This paper investigates the capability of Immersed Boundary Methods (IBMs) to accurately predict both hydro- and hemo- dynamic behaviour of MCS. The device considered here is a centrifugal blood pump.

2. Numerical Methods

IBMs are a set of Computational Fluid Dynamics (CFD) methods in which the presence of an internal obstacle within the flow is not represented through a standard body-fitting grid, but rather through direct modifications of the governing fluid equations. As a result, IBMs allow significant time and effort reduction for the meshing and computation stages, which is of interest for design optimization.

In this paper, the IBM developed in [2] for rotating machinery within OpenFOAM library is used to model the impeller of the pump. This mini-pump operates with a semi-open 5-blades impeller of diameter 35 mm and width 9 mm (2 mm for the blades). In addition, the resulting flow field is used to estimate the hemolysis risk, which represents the damage endured by the red blood cells because of the pump operation. This risk is mainly governed by the shear stress exhibited by the blood flow.

3. Results

As shown in Fig. 1, the IBM predicts the pump head with approx. 10% overestimation. The

trend is in good agreement with experimental data and results from body-fitted simulations.

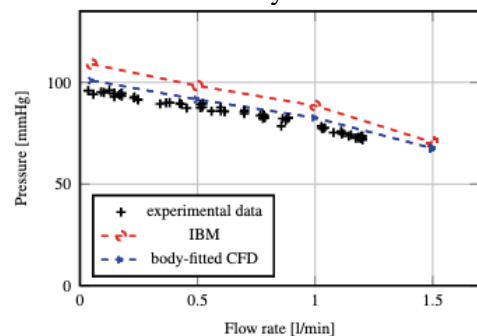


Figure 1: Blood pump characteristic obtained experimentally and numerically.

The numerical method is able to give good insight on the generation of hemolysis within the pump as highlighted in Fig. 2. The high generation zones include the volute walls, the blade trailing edge and the volute tongue.

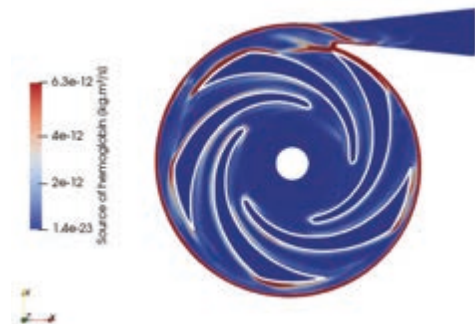


Figure 2: Field of hemoglobin generation on the pump median plane.

4. References

1. Marcel L. et al., Exp. Rev. Med. Dev. 2021 (18), <https://doi.org/10.1080/17434440.2021.1947245>
2. Specklin M. et al., Eur. J. Mech. B Fluids 2018 (70), <https://doi.org/10.1016/j.euromechflu.2018.03.003>

Acknowledgements:

The authors acknowledge the use of the Cassiopee Arts et Métiers Institute of Technology HPC Center.



PREOPERATIVE HEMODYNAMIC SIMULATION OF A PATIENT SPECIFIC EVAR PROCEDURE

Francesco Bardi (1,2,3), Joris Vermunt (1), Jean-Noël Albertini (1), Simona Celi (3), Stéphane Avril (2)

1. *PrediSurge, Saint-Étienne, France*; 2. *MINES Saint-Étienne, France* 3. *BioCardioLab, Fondazione Toscana "G. Monasterio", Italy*

1. Introduction

Complications following abdominal endovascular aortic repair (EVAR) range between 16% and 30% [1]. In this work, we present an *in-silico* approach to preoperatively assess risk of limb occlusion by analysing the hemodynamic behaviour inside an implanted stent-graft.

2. Materials and Methods

A patient-specific simulation of stent-graft deployment was performed using the workflow described in [2]. Vessels were segmented from preoperative CT-scan and meshed with shell elements. The implanted stent-graft was modelled using beam and shell elements, and the deployment simulation was performed using Abaqus explicit solver. From the final configuration, the graft volume was meshed, and a CFD simulation was set up using OpenFOAM V2112. The transient solver rhoPimpleFoam was used, with a time step of 0.1 ms. A pulsatile flow rate waveform, with a peak systolic value of 9 l/min and a period of 0.8 s, was imposed at the inlet and the pressure at the outlets was imposed using the 3-element Windkessel model. Three cardiac cycles were simulated to achieve cycle to cycle convergence.

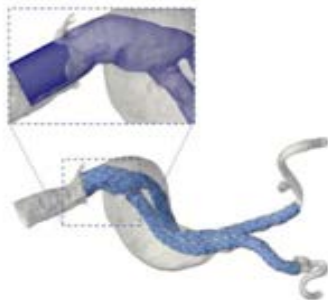


Figure 1: volume mesh from final stent-graft configuration.

3. Results

The deployed configuration of the stent-graft is shown in Fig.1. The velocity magnitude field at the systolic peak is shown in Fig. 2. A recirculation zone is visible downstream of the kinked section of the stent-graft.

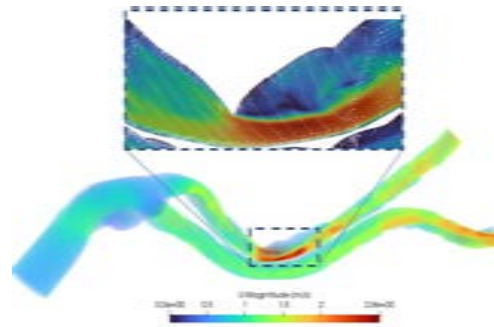


Figure 2: Velocity magnitude field.

4. Discussion and Conclusions

The simulation highlighted a recirculation zone which can be associated with a risk of thrombosis [3]. The proposed workflow could hence represent a valuable tool for the EVAR preoperative planning. In the future, we seek to apply a thrombus formation model and evaluate the sensitivity of the results with respect to the boundary conditions.

5. References

1. Daye D, Walker TG. *Cardiovasc Diagn Ther.* 2018;8(Suppl 1):S138-S156.
2. Perrin D et al., *J Biomech*; 48(10): 1868-1875 (2015).
3. Tasso P et al., *ASME. J Biomech Eng.* November 2018; 140(11): 111003.

Acknowledgements:

MeDiTaTe Project has received funding from the European Union's Horizon 2020 research and innovation programme under Grant Agreement 859836.



PREOPERATIVE HEMODYNAMIC SIMULATION OF A PATIENT SPECIFIC EVAR PROCEDURE

Francesco Bardi (1,2,3), Joris Vermunt (1), Jean-Noël Albertini (1), Simona Celi (3), Stéphane Avril (2)

1. *PrediSurge, Saint-Étienne, France*; 2. *MINES Saint-Étienne, France* 3. *BioCardioLab, Fondazione Toscana "G. Monasterio", Italy*

1. Introduction

Complications following abdominal endovascular aortic repair (EVAR) range between 16% and 30% [1]. In this work, we present an *in-silico* approach to preoperatively assess risk of limb occlusion by analysing the hemodynamic behaviour inside an implanted stent-graft.

2. Materials and Methods

A patient-specific simulation of stent-graft deployment was performed using the workflow described in [2]. Vessels were segmented from preoperative CT-scan and meshed with shell elements. The implanted stent-graft was modelled using beam and shell elements, and the deployment simulation was performed using Abaqus explicit solver. From the final configuration, the graft volume was meshed, and a CFD simulation was set up using OpenFOAM V2112. The transient solver rhoPimpleFoam was used, with a time step of 0.1 ms. A pulsatile flow rate waveform, with a peak systolic value of 9 l/min and a period of 0.8 s, was imposed at the inlet and the pressure at the outlets was imposed using the 3-element Windkessel model. Three cardiac cycles were simulated to achieve cycle to cycle convergence.

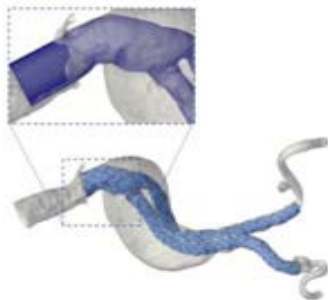


Figure 1: volume mesh from final stent-graft configuration.

3. Results

The deployed configuration of the stent-graft is shown in Fig.1. The velocity magnitude field at the systolic peak is shown in Fig. 2. A recirculation zone is visible downstream of the kinked section of the stent-graft.

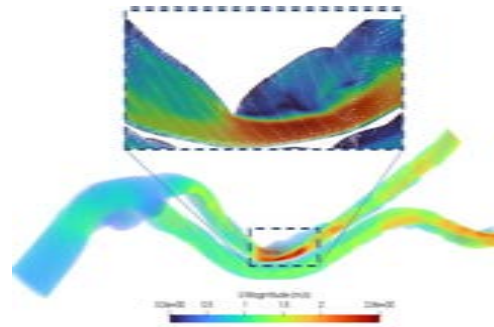


Figure 2: Velocity magnitude field.

4. Discussion and Conclusions

The simulation highlighted a recirculation zone which can be associated with a risk of thrombosis [3]. The proposed workflow could hence represent a valuable tool for the EVAR preoperative planning. In the future, we seek to apply a thrombus formation model and evaluate the sensitivity of the results with respect to the boundary conditions.

5. References

1. Daye D, Walker TG. *Cardiovasc Diagn Ther.* 2018;8(Suppl 1):S138-S156.
2. Perrin D et al., *J Biomech*; 48(10): 1868-1875 (2015).
3. Tasso P et al., *ASME. J Biomech Eng.* November 2018; 140(11): 111003.

Acknowledgements:

MeDiTaTe Project has received funding from the European Union's Horizon 2020 research and innovation programme under Grant Agreement 859836.

A NOVEL MODEL FOR PASSIVE MYOCARDIUM THAT INCORPORATES COMPLETE DIFFUSION TENSOR INFORMATION

Christian Goodbrake (1), Kenneth Meyer (1), Jack Hale (2), Michael Sacks (1)

1. University of Texas, Austin, Oden Institute, Willerson Center for Cardiovascular Modeling and Simulation, United States of America; 2. Université du Luxembourg, Luxembourg

$$\Psi = e^{Q_0 + Q_2^{ABCD} E_{AB} E_{CD} + Q_4^{ABCDEFGH} E_{AB} E_{CD} E_{EF} E_{GH}} \quad (2)$$

1. Introduction

Diffusion Tensor Magnetic Resonance Imaging (DTMRI) is a convenient way to noninvasively locally measure the structure of fibrous biological tissues like axonal tissue and myocardium. We introduce a material model that directly incorporates \mathbf{D} , resolves degeneracy conditions and singularities, and is easily modified to suit other fibrous biological materials.

2. Materials and Methods

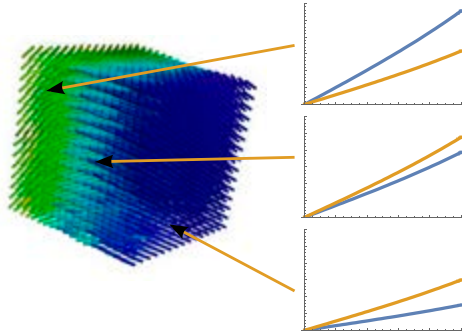


Figure 1: Heterogeneous stress-strain behavior (right) is obtained directly from variation in DTMRI data (left).

Ex-vivo DTMRI data was mapped on 1 cm^3 cubes of ovine myocardium. The diffusion tensor \mathbf{D} is a positive definite symmetric tensor possessing a spectral representation.

$$\mathbf{D} = \sum_{i=1}^3 \lambda_i \mathbf{n}_i \otimes \mathbf{n}_i \quad (1)$$

There are several natural symmetries of such data. We demanded that our model respect these symmetries, in that it gives the same physical predictions for materials that only differ by these symmetry transformations. Our model is a pseudo-elastic material model, so we define a strain energy density Ψ depending on the Lagrange strain tensor \mathbf{E} . In terms of the spectral basis $\{\mathbf{n}_i\}$, and utilizing Einstein summation, this energy takes the form

3. Results

Applying our model to extant data from [2], we obtain an inhomogeneous, anisotropic, material model with fixed global parameters, the inhomogeneity and anisotropy being induced by the diffusion tensor field itself (Figure 1). We perform inverse modeling in FEniCS to find values for structural sensitivities that best captures the behavior of our samples.

4. Discussion and Conclusions

This approach also allows us to describe both healthy and diseased tissue with a single material model when the disease is primarily manifested structurally, since the local DTMRI data captures this structural defect through \mathbf{D} . While the overall form of our model is very similar to previous models, the work we have done ensures that the structure of the DTMRI data is preserved by the final model exactly. Additionally, because we have dense mappings of the diffusion tensor, the resulting inhomogeneous model possesses fine detail at the sub-millimeter scale without requiring manual tuning. In summary, we have developed a flexible material model for myocardium and any other 3D soft tissue that directly incorporates \mathbf{D} in a robust manner.

5. References

1. Zhang W. et al. JMBBM. 2019 Jan; 89:168-198.
2. Li, DS et al., J Mech Behav Biomed Mater, 2020, 103, 103508

Acknowledgements:

The authors would like to thank the National Institutes of Health (Grant no: F32HL162423 to C. Goodbrake and R01 HL073021 and R01 103723 to M. Sacks) for providing financial support to this project.



HEMOLYSIS PREDICTION IN BIOMICROFLUIDIC DEVICES USING RESOLVED CFD-DEM NUMERICAL SIMULATION

Carmine Porcaro (1)(2), Mahdi Saeedipour (1)(2)

1. Department of Particulate Flow Modelling, Johannes Kepler University, A-4040 Linz, Austria;
2. Linz Institute of Technology (LIT), Johannes Kepler University, A-4040 Linz, Austria;

1. Introduction

Hemolysis, namely hemoglobin leakage from red blood cells (RBCs), is an active research topic in blood flow modelling due to its negative effects on accuracy and safety of lab-on-a-chip devices. Microfluidics chips for RBCs sorting and plasma separation could encounter this problem due to their small dimensions that can cause strong RBCs deformation. A resolved Immersed Boundary Method coupling Computational Fluid Dynamics (CFD) and Discrete Element Methods (DEM) is presented for the numerical simulation of hemolysis in bio-microfluidic applications.

2. Materials and Methods

In this study, blood is modelled as a suspension of biological cells, mainly RBCs, in the liquid plasma (Newtonian, incompressible carrier fluid). Therefore, the Navier-Stokes equations are numerically solved through a finite volume approach with an additional penalty term to account for the presence of RBCs. RBCs positions and velocities are updated by solving Newton and Euler equations for conservation of linear and angular momentum. To model the RBCs deformation, a reduced-order model is employed, where each RBC is represented by a clump of overlapping rigid spheres connected by a fictional numerical bond, whose properties are tuned to reproduce the ones of RBCs viscoelastic membrane [1]. A hemolysis index (HI) connected to RBCs deformation is defined using existing strain-based correlations from literature [2].

3. Results

Different micro-channel geometries at different blood hematocrits are considered, showing the influence of these factors on RBCs damage. A statistical analysis is performed to extract

significant biophysical quantities from numerical simulations such as HI distribution at the exit (see Figure 1). Results show reasonable agreement with previous works [3].

4. Conclusions

The present simulation method, although based on a reduced-order model, predicts the hemolysis occurrence with reasonable accuracy compared to literature data. Therefore, it could be used as a reliable and efficient modelling tool for the design and optimization of microfluidic devices.

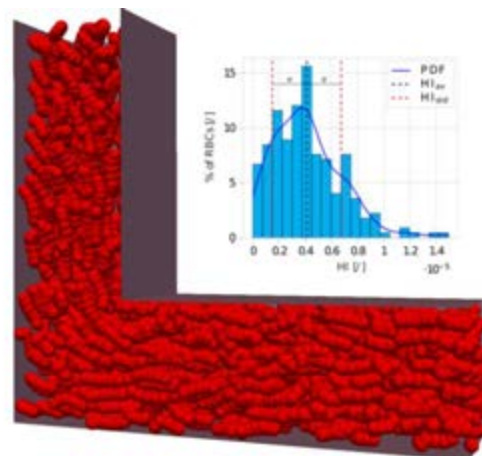


Figure 1: 40% haematocrit channel with statistical analysis of RBCs' HI at the exit.

5. References

1. Nair et al., Computational Particle Mechanics 9, 759-774 (2022)
2. Ezzeldin et al., Annals of Biomedical Engineering 43, 1398-1409 (2015)
3. Gusenbauer et al., Artificial organs 42, 746-755 (2018)

Acknowledgements:

The authors acknowledge the funding support of Linz Institute of Technology (LIT), project number LIT-2020-9-YOU-212.



ANALYSIS OF SKIN TENSION USING MACHINE LEARNING EMULATION TECHNIQUES

Matt Nagle (1, 2), Michel Destrade (5, 2), Michael Fop (3), Aisling Ní Annaidh (2, 4)

1. SFI CRT in Foundations of Data Science, Ireland; 2. School of Mechanical and Materials Engineering, UCD, Ireland; 3. School of Mathematics and Statistics, UCD, Ireland; 4. Charles Institute of Dermatology, UCD, Ireland; 5. School of Mathematical and Statistical Sciences, NUIG, Ireland

1. Introduction

Finite Element Analysis (FEA) is the gold standard method for modelling the complex mechanical behaviour of the skin. Unfortunately, in most circumstances it is too computationally expensive for practical clinical applications. However, using modern machine learning (ML) techniques it is possible to create an emulation model which is a statistical ML model trained on the data generated from the full model of interest (in this case the FEA). These emulators are cheap, fast approximations of the full model. These emulation techniques have been used to great effect in [1,2]. Our goal is to apply similar methods to elastic wave propagation through skin with different material parameters. Furthermore, we would like to build ML architecture to allow for a fast approximation of the inverse FEA problem (i.e. use the velocity of the elastic wave to infer the material parameters of the skin).

2. Materials and Methods

Abaqus was used to develop both two and three-dimensional Finite Element models to model the propagation of an elastic wave through the skin. A training dataset was constructed by randomly generating reasonable values for the skin parameters, performing the full FEA and extracting and storing the resulting waveform and velocity of the wave, see Figure 1.

Using this dataset, ML emulators were trained including Random Forest, XGBoost, Linear Regression, Artificial Neural Networks (ANN), Gaussian Process and a weighted combination of these emulators. Similarly, the ML models to perform an approximation of the FEA can also be trained on the same dataset.

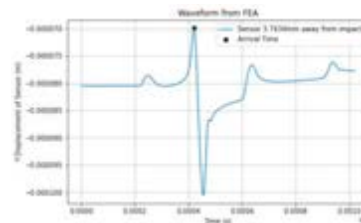


Figure 1: Sample waveform generated by FEA.

3. Results

Using simulated data a provisional ANN which is able to predict the Young's Modulus of skin and also the level of skin tension was developed

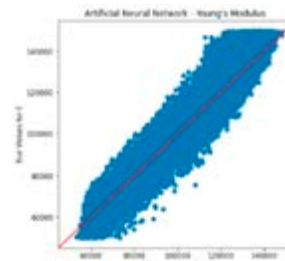


Figure 2: ANN showing ability to predict the Young's Modulus using simulated velocities.

4. Discussion and Conclusions

This study has illustrated proof of concept of the development of a machine learning emulator to infer the fast approximation of an inverse acoustoelastic problem using simulated data. Further development will incorporate a dataset generated through parameterised FEA simulations. This will facilitate the rapid estimation of skin material properties through elastic wave measurements.

5. References

1. Davies V, Noè U, Lazarus A, Gao H, Macdonald B, Berry C, Luo X, Husmeier D. J R Stat Soc Ser C Appl Stat. 2019 Nov;68(5):1555-1576.
2. Stowers C et al., Journal of the Mechanical Behavior of Biomedical Materials; Volume 118, 2021.

CEREBROSPINAL FLUID FORMULATION AFFECTS THE SPINAL CORD DYNAMICS IN TRAUMATIC EVENTS

Lucien Diotalevi (1, 2, 3), Jean-Marc Mac-Thiong (2, 3, 4), Yvan Petit (1, 2, 3)

1. *École de technologie supérieure, Canada*; 2. *CIUSSS Nord de l'île de Montréal, Canada*;
3. *International Laboratory on Spine Imaging and Biomechanics (iLab-Spine), Canada*; 4. *Université de Montréal, Canada*

1. Introduction

The cerebrospinal fluid (CSF) acts as a significant damper to retropulsed bony fragments in the spinal canal, during traumatic events leading to spinal cord injuries (SCI) [1]. Various modelling methods have been attempted but only one study compared their effects, focusing on the kinematics of a retropulsed pellet [2]. The proposed study investigates their effect on the *in situ* dynamics of the spinal cord parenchyma.

2. Materials and Methods

An idealised finite elements model (FEM) of the spinal cord, meninges and CSF was built (Fig. 1), with elements and material laws as described in Diotalevi et al. (2020) [1] and a 0.2 mm characteristic length for CSF elements.

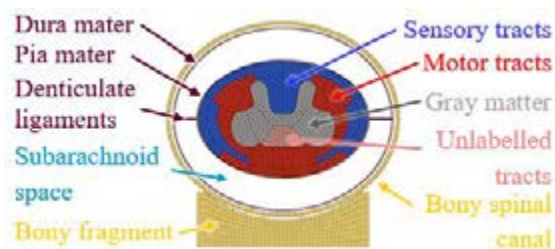


Figure 1: Transverse view of the FEM.

Four main formulations were used for the CSF: langrangian (Solid), pressurised volumes (PV), arbitrary langrangian-eulerian (ALE) and smoothed particles hydrodynamics (SPH). Additionally, the linearity of fluid pressure was investigated using a Newtonian (N) and a Mie-Grünesien (G) equation of state. The fragment was retropulsed at an initial velocity of 5 m.s^{-1} [1]. Three variables were recorded through time: central canal position (CCP), subarachnoid space occlusion (SSO) and strain of the anteroposterior diameter of the spinal cord (CDS). Two-ways intraclass correlation

coefficients (ICC)—random (A,1) and mixed (C,1)— were used to compare results over time.

3. Results

Table 1 summarises ICC results. Variation of pressure linearity presented high ICC in each fluid formulation, and for each variable. ICC between PV and an absence of fluids are higher than between PV and each other fluid formulation. ICC between Solid, ALE and SPH formulations are low to moderate.

	CCP	SSO	CDS
G (Solid, ALE, SPH) vs. N (Solid, ALE, SPH)	>0.99 / >0.99	>0.99 / >0.99	>0.99 / >0.99
Solid vs. ALE vs. SPH	0.60 / 0.72	0.39 / 0.52	0.77 / 0.77
PV vs. No Fluids	0.93 / 0.98	0.30 / 0.54	0.91 / 0.92
PV vs. (Solid, ALE, SPH)	<0.42 / <0.60	<0.03 / <0.03	<0.68 / <0.70

Table 1: ICC(A,1) / ICC(C,1) values between diagrams for each variable.

4. Discussion and Conclusions

The spinal cord dynamics are sensitive to the CSF formulation, but not to pressure linearity. PV formulation is to be avoided, as it deviates from each other fluid formulation and correlates better with an absence of fluids. Experimental data are required to select a formulation.

5. References

1. Diotalevi, L., Bailly, N., Wagnac, É., Mac-Thiong, J.-M., Goulet, J., & Petit, Y. (2020). Clin Biomech, 72, 186-194.
2. Rycman, A., McLachlin, S., & Cronin, D. S. (2022). Int J Num Meth Biomed Eng, e3570.

Acknowledgements:

Funded by the Canada Research Chair in Biomechanics of Head and Spine Injuries (950-231815), at ÉTS.



A UNIFIED FORMULATION FOR FLUID-STRUCTURE-CONTACT INTERACTION

Fannie M. Gerosa (1), Alison L. Marsden (1)

1. Stanford University, Stanford, USA

1. Introduction

Many congenital heart defects may involve valvular anomalies. We aim to use computational methods to model the mechanical behaviour of these anatomies, and ultimately give clinicians insight into malformation development and support surgical planning. Heart valve simulations are extremely complex from both a computational and modelling perspective. We present a numerical framework for fluid-structure interaction (FSI) simulation of heart valves based on a combination of a unified continuum formulation [1] and a penalty-based contact model.

2. Materials and Methods

Fitted and unfitted mesh frameworks have been extensively investigated for application to FSI. Fitted frameworks are ideal for problems with moderate displacement and are commonly coupled with moving mesh techniques. While unfitted formulations are ideal for large deformation simulations, they often suffer from spurious velocity and pressure oscillations and may require ad-hoc intersection and integration procedures.

In this work, we combine a fitted approach with an Arbitrary Lagrangian Eulerian (ALE) description and a unified formulation for FSI.

An unbiased penalty-based formulation for contact is included in the model to avoid solid penetration. Typical contact approaches include realistic and relaxed contact models. In the realistic model, the solid is allowed to reach a zero-gap distance, enabling topological changes to the fluid domain. An alternative approach is to consider a relaxed contact formulation by allowing a small separation between the structure and the contacting solid [2]. We

implement both approaches and compare the results.

The resulting nonlinear fully coupled formulation is solved via the Newton-Raphson method. Moreover, a remeshing technique is included to support large displacement simulations.

3. Results

Numerical examples from academic test cases and idealized valve geometries are used to validate and explore the described methods. A direct comparison between relaxed and realistic contact approaches is considered. In addition, a discussion between a non-consistent and a consistent contact model is included in the analysis.

4. Discussion and Conclusions

In this work, we present and analyse a framework for valvular hemodynamic simulations that includes a finite element-based method featuring a unified description for FSI dynamics, remeshing, and a penalty approach for contact.

5. References

1. Liu J. et al., CMAME 2018, p. 549-597
2. Burman E. et al., ESAIM 2020, p. 531-564

Acknowledgements:

We acknowledge funding from the National Institutes of Health grants 5R01HL159970-02 and 5R01HL129727-06.



VISUALIZING MINERAL STRAIN IN HUMAN BONE BASED ON WIDE-ANGLE X-RAY SCATTERING (WAXS) WITH IN SITU INDENTATION

Imke AK Fiedler (1), Eva M Wölfel (1), Anton Davydok (2), Felix N Schmidt (1), Annika vom Scheidt (1,3), Benjamin Ondruschka (4), Katharina Jähn-Rickert (1), Björn Busse (1)

1. Department of Osteology and Biomechanics, University Medical Center Hamburg-Eppendorf, Germany; 2. Helmholtz-Zentrum Hereon, Institute of Material Physics, Germany; 3. Department of Macroscopic and Clinical Anatomy, Gottfried Schatz Research Center, Medical University of Graz, Austria 4. Department of Legal Medicine, University Medical Center Hamburg-Eppendorf, Germany

Corresponding author address: Lottestr. 55A, 22529 Hamburg, Germany; b.busse@uke.de

1. Introduction

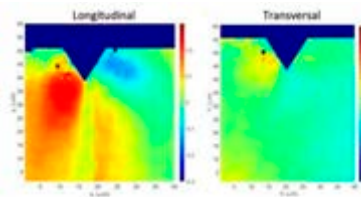
The mechanical properties of bone are provided through distinct structural features found at different length scales [1]. Its deformation at the nanoscale is governed by the interplay between collagen fibrils and mineral particles, which experience fibril strain and mineral strain during loading [2]. The orientation of these components contributes to the ability of bone tissue to withstand different types of loading, e.g. compression or tension [3]. Here, we determine the mineral strain during stepwise indentation in cortical human bone in parallel (longitudinal) and perpendicular (transversal) loading directions to the bone long axis.

2. Materials and Methods

Cortical bone samples from the femoral mid-diaphysis of healthy female individuals were obtained during autopsy at the Department of Legal Medicine (IRB approval present). Five samples (24, 47, 67, 79 years old) were prepared to dimension of 1 x 10mm x 50 μ m. Experiments were performed at P03 nanofocus endstation, PETRA III, DESY, Hamburg, Germany. Samples were positioned perpendicular to the X-ray beam and below a wedge tip, allowing to generate 2D maps (40x40 μ m) directly underneath the loading site. Stepwise indentation was performed along the osteons (longitudinal) and perpendicular to the osteons (transversal). Per sample 5 maps were generated: before loading and at 4 indentation depths. The WAXS signal of each pixel of the map was radially integrated in the region of the 002 peak of hydroxyapatite. After fitting of integrated curves, the peak position was defined, and the q-values were used to calculate the strain field.

3. Results

Mineral strains in longitudinal loading direction were highest in the young case and lower at higher ages, while the mineral strain in transversal loading direction was lower compared to the longitudinal direction in the young case and remained low in the aged cases.



2D maps plotting mineral strain (16 μ m indentation depth, 79 years old) showing higher mineral strains in the longitudinal loading direction.

4. Discussion and Conclusions

We tested a technical setup of synchrotron scanning WAXS with *in situ* indentation [4] for analysing human bone tissue. This is of particular interest because changes in deformation mechanisms of bone at the nanoscale can contribute to the overall fracture risk in disease cases [5]. Our data provides insight into differences in mineral strain depending on the loading scenario directly at the loading sites, and their changes with different ages.

5. References

1. Zimmermann et al., JMBBM 2021;113:104138
2. Schmidt et al., Adv Sci, 2019 6.12:1900287
3. Casanova et al., J R Soc Interface, 2017; 4: 160971
4. Zauner et al., Acta Mater 2022; 239: 118260
5. Wölfel et al., JBMR 2022 (Epub ahead of print)



CONSIDERING NONLOCALITY IN CONTINUUM BONE REMODELLING – A MICROMORPHIC APPROACH

Anna Titlbach (1), Areti Papastavrou (1), Andrew McBride (2), Paul Steinmann (2,3)

1. Nuremberg Tech, Germany; 2. University of Glasgow, United Kingdom 3. Friedrich-Alexander-Universität Erlangen-Nürnberg, Germany;

1. Introduction

In the classical theory of bone remodelling, bone is modelled on the macroscopic scale as continuous matter within a non-linear elastic approach, thus the microstructure of bone is not taken into account. However, this becomes particularly relevant when the material is considered at small scales [1]. Phenomenologically addressing this aspect, we present an approach where bone remodelling is embedded in a micromorphic environment.

2. Materials and Methods

The principle of stationary potential energy requires the internal potential energy density to determine the kinetic quantities associated with the problem

$$\psi_0 = \psi_0^{mac}(\mathbf{F}, \rho_0) + \psi_0^{mic}(\bar{\mathbf{G}}) + \psi_0^{scale}(\mathbf{F}, \bar{\mathbf{F}}). \quad (1)$$

Here, bone is characterized in the macroscopic energy density ψ_0^{mac} by the Neo-Hookean energy density and considers in particular the current density of the body ρ_0 with respect to a reference value ρ_0^* [2,3]. In the novel coupled approach, this is now combined with a micromorphic ψ_0^{mic} and a scale transitioning contribution ψ_0^{scale} . In the former, a length scale parameter describes the size of the micro-continuum and in the latter, a penalty-like parameter is introduced to couple the macro and micro deformation [4].

3. Results

In Figure (1), a femur head is loaded by a force in the vertical direction with the shaft firmly clamped, showing the classical approach on the left compared to the micromorphic approach on the right. By varying the above parameters, the following effects become apparent. A small length scale parameter indicates a fine microstructure of the material and therefore

approaches to the classical case. A large penalty forces the macro and micro deformations to become more and more alike, resulting in a reduction of the dispersion of the density.

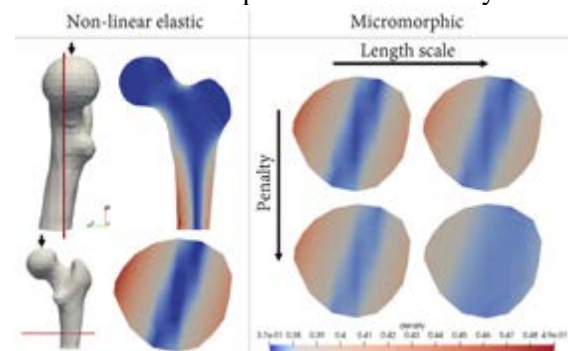


Figure 1: Comparison of the non-linear elastic and the micromorphic approach based on the density distribution in a femoral head.

4. Discussion and Conclusions

By coupling micro and macro deformation in a micromorphic approach, the interaction between the continuum points can be influenced. Thus, areas of the material that are not directly loaded also react to the loading of their neighbors. This manifests itself in a more homogeneous density distribution and thus influences the stiffness of the body.

5. References

1. Hirschberger CB, A Treatise on Micromorphic Continua [PhD thesis]; (2008)
2. Kuhl E et al., Comp. Mechanics; 32:71-88 (2003)
3. Schmidt I et al., CMBBE; 25:1040-1050 (2022)
4. McBride AT et al., CMAME; 371:113320 (2020)

Acknowledgements:

This research was funded by the Deutsche Forschungsgemeinschaft (DFG, German Research Foundation) – 377472739/GRK 2423/1-2019 and the Bavarian Academic Forum (BayWiss) – Consortium ‘Health Care’. The authors are very grateful for this support.

REMODELING OF ISOTROPIC MATERIALS VIA THE HOMOGENIZED CONSTRAINED MIXTURE THEORY AND FINITE PLASTICITY

Felipe Sempéregui, Stéphane Avril

*Mines Saint-Étienne, Univ. Jean Monnet, INSERM, U 1059 Sainbiose, F - 42023,
Saint-Étienne, France*

1. Introduction

The Homogenized Constrained Mixture Theory (H-CMT) is an attractive alternative to simulate remodeling of biological tissues [1], as it is computationally less expensive than its classical counterpart (CMT). The main expression, from which the H-CMT arises, is a stress rate tensor $\dot{\boldsymbol{\sigma}}$ and [1] only verifies his approach by comparing the remodeling of both frameworks (H-CMT and CMT) with unidimensional fibers. In such an example, the referred rank 2 expression can be reduced to a scalar. However, if one wishes to simulate G&R occurring in neo-tissue forming within vascular grafts [2], isotropic materials (e.g., elastin) might remodel as well and the original tensor equation should be solved instead. To the authors' knowledge, no explicit solution to this problem was shown yet and we propose an alternative, which is based on the theory of plasticity and kinematic hardening.

2. Materials and Methods

For our applications, we assume that the strain energy of the isotropic material is a sum of a deviatoric and of a volumetric component, that remodeling is incompressible and that the homeostatic state only affects the stresses isochorically. Then, the backward Euler method is used to transform the rate-like tensor to its incremental counterpart and the deviatoric invariant J_2 is chosen to represent the resulting expression as a scalar. Thus,

$$\begin{aligned} \hat{\boldsymbol{\sigma}}' &= \boldsymbol{\sigma}' - \boldsymbol{\sigma}'_r = \mathbf{0}, \\ J_2 &= 0.5 \hat{\boldsymbol{\sigma}}' : \hat{\boldsymbol{\sigma}}' = 0, \end{aligned} \quad (1)$$

being $\hat{\boldsymbol{\sigma}}$ the relative stress, $\hat{\boldsymbol{\sigma}}'$ is the isochoric stress state, and $\boldsymbol{\sigma}'_r$ is a backstress-like tensor. The scalar J_2 in Eq. 1 can be re-interpreted in terms of the plasticity theory as a yield criterion, which, in turn, allows the user to adapt the H-CMT for isotropic materials in ready-to-use algorithms related to plasticity.

3. Results

Fig. 1 shows the results obtained by setting J_2 as a yield criterion in our FEM algorithm. It presents the stress of an isotropic material evolving from its stress-free configuration towards its homeostatic state $\boldsymbol{\sigma}_{pre}$.

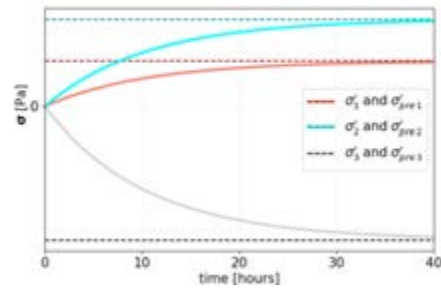


Figure 1: Stress evolution in an isotropic material.

4. Discussion and Conclusions

A yield criterion arose naturally by manipulating the stress rate $\dot{\boldsymbol{\sigma}}$ proposed by [1] and Fig. 1 shows the obtained results after incorporating the expressions of Eq. 1 in a algorithm related to the field of plasticity. The research community of biomechanics can benefit from the intersection of both frameworks and these results show that remodeling of isotropic materials might be interpreted as a standard plastic term.

5. References

1. Cyron, C. J. et al., A homogenized constrained mixture (and mechanical analog) model for growth and remodeling of soft tissue. *Biomechanics and modeling in mechanobiology* 15.6 (2016): 1389-1403.
2. Loerakker, S. et al., Computational modeling for cardiovascular tissue engineering: the importance of including cell behavior in growth and remodeling algorithms. *Current Opinion in Biomedical Engineering* 15 (2020): 1-9.

Acknowledgements:

This project is funded by the European Union's Horizon 2020 research and innovation programme (Grant Agreement 101017523).



COUPLED CHEMO-MECHANO-BIOLOGICAL SIMULATIONS OF EVOLVING OSTEOARTHRITIS: THEORY AND 3-D SIMULATIONS

Muhammed M. Rahman (1), Paul N. Watton (2), Corey P. Neu (3), David M. Pierce (1)

1. University of Connecticut, USA; 2. University of Sheffield, UK; 3. University of Colorado, USA

1. Introduction

Osteoarthritis (OA) is a multifactorial disease of synovial joints with degeneration and loss of articular cartilage as a hallmark feature. While mechanical stimuli are essential to maintain healthy cartilage, overloading (e.g. trauma) and reduced loading (e.g. immobilization) induce molecular and microstructural changes that lead to fibrillation, mechanical softening, and erosion. In response to mechanical stimuli, chondrocytes (the cells within cartilage) express chemicals (e.g. cytokines, growth factors, collagenase, and aggrecanase) which promote degradation or production of constituents, e.g. collagen and proteoglycan. Existing mathematical models of signaling pathways lack mechanical effects while biomechanical models lack the chemical effects [1].

2. Materials and Methods

Leveraging our constitutive model for cartilage [2], we establish evolution equations for key chemical species and solid constituents [3], whereby the progression of OA results in volume loss normal to the articular surface [4]. After implementation in Matlab, we simulate five physically relevant conditions in the knee over 24 months: normal walking, overloading and immobilization in health, and in injury, as well as a therapeutic intervention post injury.

3. Results

Our model predicts homeostasis (i.e. no changes in the constituents) for healthy individuals walking normally. Both overloading and immobilization, i.e. non-physiological loading, increase pro-inflammatory cytokines that upregulate collagenases and aggrecanases resulting in loss of mass of structural constituents, cf. Fig. 1. We also demonstrate that therapeutic interventions produce improvements in the mass of constituents thus recovering thickness of the cartilage layer.

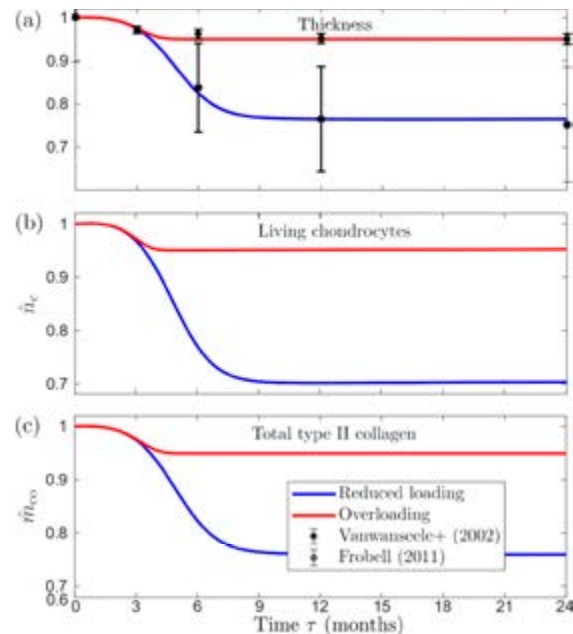


Figure 1: Cartilage evolving in reduced loading (blue) and overloading (red) over 24 months: (a) thickness of cartilage versus experiments [5,6], (b) living chondrocytes, and (c) type II collagen.

4. Discussion and Conclusions

Our proposed framework is a first step towards a new class of computational tools that consider, for the first time, the turnover and production of constituents and cytokines evolving in cartilage.

5. References

1. Baker M et al. *J Math Biol.* 75:985-1024 (2017).
2. Pierce DM et al. *Biomech Model Mechanobiol.* 15:229-244 (2016).
3. Aparicio P et al. *J Biomech.* 49:2321-2330 (2016).
4. Grytsan A et al. *Materials (Basl).* 10:1-19 (2017).
5. Vanwanseele B et al. *Arthritis Rheum.* 46:2073-2078 (2002).
6. Frobell R. *J Bone Joint Surg Am.* 93:1096-1103 (2011).

Acknowledgements:

The authors would like to thank the National Science Foundation (Grant no: 1662429) for providing financial support to this project.



EXTENSION OF BONE HEALING MODEL FROM 2D TO 3D USING FINITE ELEMENT ANALYSIS AND FUZZY LOGIC

Pieter Ansoms (1), Jos Vander Sloten (1), Liesbet Geris (1, 2)

1. Biomechanics section, KU Leuven, Belgium; 2. Biomechanics Research Unit, GIGA in Silico Medicine, University of Liège, Belgium

1. Introduction

Computational bone healing models allow us to explore new and assess existing fixation configurations and treatment strategies in fracture fixation. Simon et al. [1] developed a dynamic, mechanoregulatory model to simulate the complex interactions of mechanical stability, revascularization and tissue differentiation in secondary fracture healing. They used a 2D, axisymmetric finite element (FE) model and fuzzy logic rules to describe five biological processes: angiogenesis, intramembranous ossification, chondrogenesis, cartilage calcification and endochondral ossification, all dependent on local strain state and local blood perfusion. Validation was performed by replication of a sheep experiment by Claes and Heigele [2]. The extension of the existing 2D model to 3D was made in this study.

2. Materials and Methods

The model consisted of an ovine metatarsus with a transverse osteotomy of 3 mm, along with a callus region, as described by [2]. The external fixator was incorporated by a connector element in the FE model. For each of the elements of the callus, three main state variables were stored and updated over time: blood perfusion, cartilage concentration and bone concentration, as explained by [1]. The iterative calculation of these is controlled by a Python script, which performed FEA's and made use of a fuzzy logic algorithm written in Matlab. The fuzzy rules, initial and boundary conditions were taken from [1]. Visualization of the blood perfusion and the tissues in the callus happened at day 14, 28 and 42 after fracture. A value of 1 for perfusion indicates optimal perfusion for bone growth.

3. Results and discussion

Fig. 1 shows the blood perfusion and tissue concentrations and Fig. 2 shows the

interfragmentary motion (IFM). It can be seen that the cartilage (Fig. 1b) and bone (Fig. 1c) concentrations evolve similarly, but the blood perfusion (Fig. 1a) happened faster in 3D than the original model in 2D predicted. Overall, the results in 2D were a lot smoother than those in 3D. The difference in decrease in IFM, along with the blood perfusion values, indicates that the extension of this algorithm to 3D requires a recalibration.

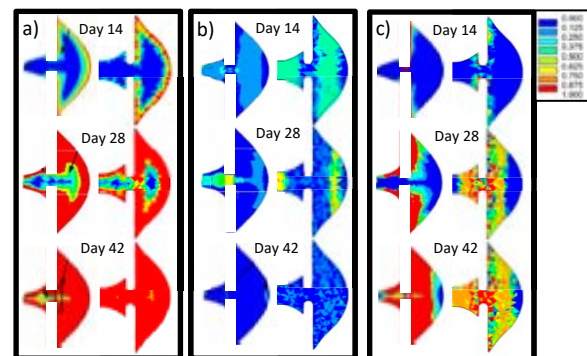


Figure 1: Results comparison: blood perfusion (a), cartilage (b) and bone concentration (c). In each, results from Simon et al. [1] are on the left and this study's results on the right.

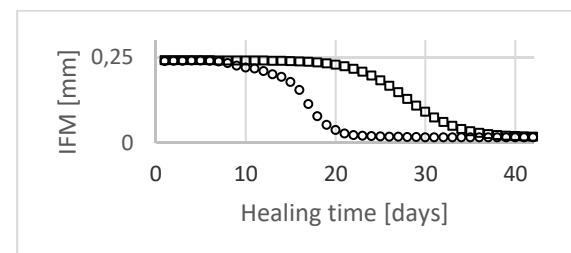


Figure 2: Comparison of IFM: Simon et al. (squares) and this study (circles)

5. References

1. Simon et al., Comput Methods Biomech Biomed Engin, 14(1):79-93 (2011)
2. Claes L, Heigele CA, J Biomech, J Biomech. 32(3):255-266 (1999)

Acknowledgements:

This research is funded by FWO Flanders and by the C2 project 'STIFF' at KU Leuven.



GLIOBLASTOMA RESISTANCE TO TEMOZOLOMIDE: MATHEMATICAL MODELS TO DESIGN OPTIMAL TREATMENTS

Marina Pérez-Aliacar (1)*, Teodora Randelovic (1,2), Jacobo Ayensa-Jiménez (1,2), Manuel Doblaré (1,2,3)

1. Aragon Institute of Engineering Research (I3A), Universidad de Zaragoza, Spain;

2. Aragon Institute of Health Research (IIS Aragon), Spain;

3. Centro de Investigación Biomédica en Red en Bioingeniería, Biomateriales y Nanomedicina (CIBER-BBN), Spain.

*Corresponding autor: Marina Pérez-Aliacar (email: marina.perez@unizar.es)

1. Introduction

Glioblastoma (GBM) is the most common among primary malignant tumours of the central nervous system. In addition, it is also the most lethal, with a median survival rate of 15 months after diagnosis [1], which renders it one of the most challenging malignancies to treat in oncology [2]. The standard of care treatment consists on surgical resection followed by radiotherapy and concomitant and adjuvant chemotherapy with temozolomide (TMZ). While many patients initially respond favourably to treatment, recurrence is almost inevitable and tumours become resistant to therapy [3]. Understanding the biological mechanisms that trigger resistance seems therefore decisive for designing new schemes that contribute to extending the patients' life.

TMZ causes epigenetic changes in GBM cells, that mainly lead to a cytostatic effect (it prevents cells from proliferating). It is believed that cellular heterogeneity plays an important role in resistance acquisition, that is, cells may be considered as an aggregate of different phenotypes reacting differently to stimuli. This different behaviour may in turn depend on their environment and the past stimuli that they have received [4].

2. Materials and Methods

In this work, we use a mathematical model of GBM evolution that, via internal variables that account for phenotypic changes in GBM cells, is able to reproduce the behavioural changes that cells undergo when they are subjected to treatment with TMZ and that eventually lead to

resistance. We define the evolution of the number of cells, TMZ concentration and an internal variable modelling epigenetic changes. Thus, the internal variable allows cells to remind their past states and behave accordingly.

3. Results and Conclusions

Mathematical models such as one the presented here prove to be useful tools for understanding complex processes such as cell adaptation, crucial for the development of new therapies.

The presented model has been calibrated and validated with experimental data of spheroids treated with the clinical treatment schedule. Subsequently, the adjusted model is used as an *in silico* patient in which different treatment schemes can be tested to see which produces the best outcome in terms of tumour regression.

5. References

1. Thakkar et al. (2014) Cancer Epidemiol. Biomarkers Prev. 23, 1985-1996.
2. Alexander and Cloughesy (2017) J. Clin. Oncol., 35(21), 2402-2409.
3. Osuka and Van Meir (2017) J. Clin. Investig. 127(2), 415-426.
4. Stanković et al (2021) Drug Resist. Updat. 55,100753

Acknowledgements:

The authors gratefully acknowledge the financial support from the Spanish Ministry of Science and Innovation and the Research State Agency (project PID2021-126051OB-C41), and the Government of Aragon through the grants for doctoral students.



HYBRID APPROACH TO MODEL EPITHELIAL MONOLAYERS DURING INTRACELLULAR BACTERIAL INFECTION

Raúl Aparicio-Yuste (1,2), Effie E. Bastounis (2), María José Gómez-Benito* (1)

1. Multiscale in Mechanical and Biological Engineering (M2BE), University of Zaragoza, Spain

2. Interfaculty Institute of Microbiology and Infection Medicine, Cluster of Excellence "Controlling Microbes to Fight Infections" (CMFI, EXC 2124), University of Tübingen, Germany

1. Introduction

Listeriosis is a food-borne infection caused by the facultative intracellular bacterial pathogen *Listeria monocytogenes* (*L.m.*). The primary site of infection is the intestine, lined up by a single monolayer of epithelial cells. *In vitro* experiments have elucidated critical information on the mechanisms underlying *L.m.* intercellular spread through the epithelium [1]. Recently, we found that late during infection, a mechanical competition between infected and uninfected cells takes place, that leads to the collective onslaught via extrusion of infected cells, triggered by the uninfected neighbours [2]. How host cells modulate their mechanics during infection and what are the mechanisms that *L.m.* uses to more efficiently disseminate through cell monolayers are still not fully understood. Computational models that simulate infection can yield critical information on how cell mechanics is modulated during infection, for bad or for good of the host.

2. Materials and Methods

A two-dimensional (2D) computational model is proposed here to study the modulation of host cell forces during intracellular bacterial infection. We present a hybrid Finite Element Method (FEM)/Agent-Based Model (ABM) approach to model a cell monolayer in different scenarios [3]. Cells are modelled as discrete particles in the ABM but also as a continuum medium in the FEM. Regarding the cellular force transduction, discrete forces are computed with the ABM. Moreover, we consider the different mechanical properties of infected and uninfected cells based on our experimental observations [2].

3. Results

The model approximates the dynamic behaviour of either an uninfected or infected cell monolayer. Cell displacements are

differentially modulated depending on the infection state of the monolayer as are intra- and inter-cellular monolayer stresses which during infection impact particularly uninfected neighbouring cells which are subjected to larger stresses. We also compute the number of neighbouring cells for any given cell in the monolayer and examine how that changes in uninfected and infected cell monolayers (Fig. 1).

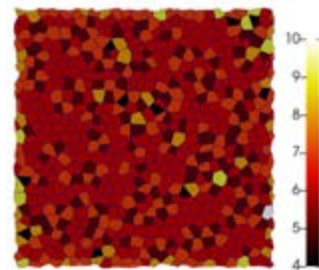


Figure 1: Number of neighbour cells of any given cell pertaining in non-infected cell monolayer

4. Discussion and Conclusions

The mechanics of host epithelial cells play a determinant role in the spread of bacterial infection. Cellular force transduction is key in the mechanical competition that arises during infection. Our model predicts the mechanical behaviour of cells in monolayer during early infection, taking into account the interaction forces and mechanical properties of cells.

5. References

1. Ortega FE, Koslover EF et al., eLife (2019)
2. Bastounis EE et al., Developmental Cell (2021)
3. González-Valverde I et al. Comp. Part. Mech. (2019).

Acknowledgements:

The authors would like to thank the Spanish Ministry of Universities (FPU20/05274) and the MCIN/AEI/10.13039/501100011033, ERDF A way of making Europe (PID2021-124271OB-I00) for providing financial support to this project.

MECHANO-BIOLOGICAL OPTIMIZATION OF SCAFFOLDS TOWARDS ENHANCED BONE REGENERATION

Sara Checa

Julius Wolff Institute, Berlin Institute of Health, Charite-Universitaetsmedizin Berlin

1. Introduction

Large bone defects are a clinical challenge for which current treatment strategies have several drawbacks. A promising treatment alternative is the use of synthetic scaffolds to support the defect endogenous regeneration. Current scaffold design strategies focus on achieving specific mechanical or biological properties, e.g. to match the ones of the tissue being replaced [1], without considering the regeneration process dynamics and its interaction with the scaffold [2]. Here, we propose a computer framework optimising scaffold design to maximise the bone regeneration outcome.

2. Materials and Methods

The computer framework combines a previously developed and validated mechanobiological bone regeneration computer model [2], a surrogate model for bone healing outcome and an optimization algorithm to optimize scaffold design based on the level of regenerated bone volume. As a proof of concept, the computer framework was used to optimize the design of a scaffold with simple cubic pores that is intended to be implanted into a sheep tibia large bone defect [3].

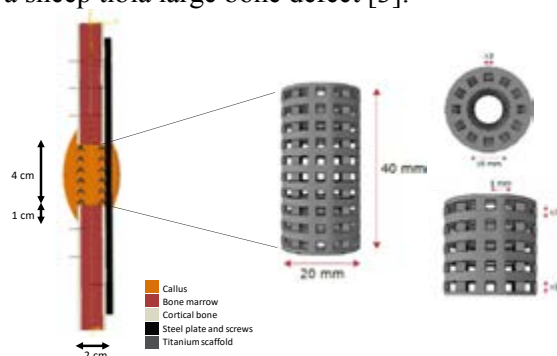


Figure 1: Computer model set-up: longitudinal cut through the defect configuration showing the intact bone extremities, the implanted scaffold and the fixation plate. Scaffold pore dimensions x_1 , x_2 and x_3 were optimized to maximize the regenerated bone volume.

3. Results

The optimization of a titanium scaffold design suggested a very porous design to be optimal for bone regeneration, yielding 96% regenerated bone in the scaffold pores (Fig. 2A). The optimization of a scaffold made of a soft material, with Young's modulus similar to that of granulation tissue, resulted in a scaffold with low porosity and poor regeneration outcome (Fig. 2C).

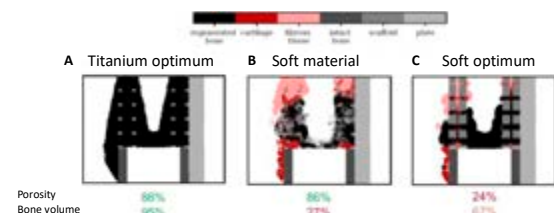


Figure 2: 24-week histology predictions in the mid-sagittal plane for different scaffold designs: (A) optimal titanium scaffold design; (B) scaffold design optimized for titanium but made of soft material; (C) optimal soft material scaffold design.

4. Discussion and Conclusions

We propose here a computational framework for time dependent mechanobiological optimization of 3D-printed scaffolds towards enhanced bone regeneration. Our method is based on the bone regeneration outcome to optimize scaffold design, instead of only the post-surgery mechanical stimulus or scaffold mechanical properties.

5. References

1. Wieding et al, J Mech Behav Biomed. 37:56–68, 2014.
2. Metz et al, Acta Biomater, 101:117-127, 2020.
3. Poblth et al, Sci. Transl. Med. 10, eam8828, 2018

Acknowledgements:

I would like to thank Camille Perier-Metz who carried out this work as a PhD student under my supervision.



MSC MORPHOFUNCTIONAL PROGRAMMING FOR IMPROVED ORTHOPAEDIC IMPLANTATION OUTCOMES

Francisca Melo-Fonseca (1,2,3), Inês Mendes Pinto (3,4), Michael Gasik (5), Filipe S. Silva (1,2), Georgina Miranda (6)

1. Center for MicroElectroMechanical Systems (CMEMS-UMinho), University of Minho, Guimarães, Portugal; 2. LBBELS –Associate Laboratory, Braga, Guimarães, Portugal; 3. International Iberian Nanotechnology Laboratory (INL), Braga, Portugal; 4. Institute for Research and Innovation in Health (i3S), Porto, Portugal; 5. School of Chemical Engineering, Aalto University Foundation, Espoo, Finland; 6. CICECO, Aveiro Institute of Materials, Department of Materials and Ceramic Engineering, University of Aveiro, Aveiro, Portugal

Corresponding author's email: franciscarmelofonseca@gmail.com

1. Introduction

Orthopaedic interventions have risen over the last two decades and are expected to increase due to aging population [1]. Despite advances in orthopaedic implant research, prosthetic failure is often observed, leading to implant replacement. Impaired implant fixation is mainly due to an improper mechanical stimulation at the interface between natural bone and the implant, often composed of Ti6Al4V [2].

At the cellular level, bone remodelling is correlated to the osteoblastic differentiation dynamics of bone-marrow derived mesenchymal stem cells (MSC) in response to changes in their environment [3]. Although the importance of the cytoskeleton as a major mechanotransducer in MSC is widely accepted, it remains elusive how mechanochemical signals regulate MSC differentiation in their interaction with bone and implants.

2. Materials and Methods

Bone marrow-derived human MSC were cultured on Ti6Al4V substrates and a quantitative analysis of the osteogenic potential in different surfaces was performed using exclusively xeno and serum-free culture mediums.

3. Results

The role of the actin network in orchestrating cell dynamics was explored by immunocytochemistry in different Ti6Al4V surfaces and correlated with the osteogenic

commitment of MSC by assessing, for example, calcium deposit levels and expression of osteogenic markers.

4. Discussion and Conclusions

Interactions between human MSC and implant's surface play a critical role in bone regeneration and thus on the biological fixation. The correlation between cellular morphodynamics and the osteogenic capacity of MSC will further pave the way to improve the surface of implants with the most suited ecosystem for bone cells and enhance the biological fixation of orthopaedic implants.

5. References

1. OECD/EU. OECD Publishing, 2021
2. Apostu D et al., Journal of International Medical Research; 46(6):2104-2119 (2018).
3. J. Zonderland L et al., Biomaterials; 268: 120572 (2021)

Acknowledgements:

This work was supported by FCT (Fundação para a Ciência e a Tecnologia) through the grant SFRH/BD/141056/2018 and the projects PTDC/EME-EME/1442/2020, POCI-01-0145-FEDER-030498, UIDB/04436/2019 and UIDP/04436/2020. In addition, this work was developed within the scope of the project CICECO-Aveiro Institute of Materials, UIDB/50011/2020, UIDP/50011/2020 & LA/P/0006/2020, financed by national funds through the FCT/MEC (PIDDAC).



REGULATING CHONDROCYTE BIOSYNTHESIS THROUGH HYPOXIA AND THERMOMECHANICAL STIMULATION

Theofanis Stampoultzis¹, Yanheng Guo¹, Naser Nasrollahzadeh¹, Peyman Karami¹, Dominique P. Pioletti¹

¹Laboratory of Biomechanical Orthopedics, Institute of Bioengineering, EPFL, Switzerland

1. Introduction

It has been demonstrated that chondrocytes respond to a variety of mechanobiological stimuli from their surroundings [1]. According to phenomenological investigations, certain of these cues, including oxygen tension or thermal stress or mechanical loads, may have a significant impact on chondrocyte activity. To date, however, little is understood about how these cues work together to provide a special milieu for chondrocyte activity. Here, we investigate these interactions in order to gain a comprehensive understanding of how well-defined combinations of bio-physical parameters affect transcriptional of chondrocytes. The research's findings demonstrate a strong link between these mechanobiological factors as illustrated by ~14-fold increase in aggrecan (ACAN) expression.

2. Materials and Methods

We encapsulated cells in gelatin-based hydrogels for up to 3 weeks to investigate the uniqueness of the transcriptional effects of diverse biophysical inputs on chondrocyte activity. Gene expression analysis was performed through qPCR method.

Quantitative polymerase chain reaction (qPCR) was executed using the Fast SYBR® Green PCR Master Mix (Applied Biosystems) in a final volume of 20 µl and containing 1 µl of synthesized cDNA.

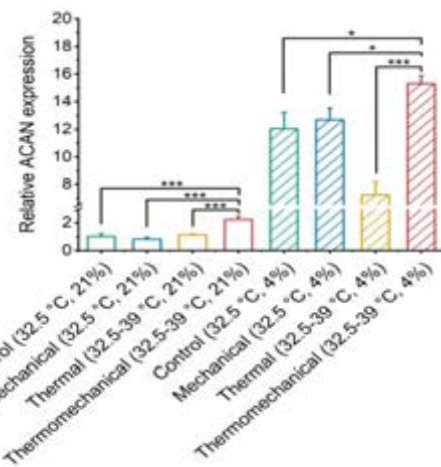


Figure 1: Relative aggrecan expression with regards to different stimuli

3. Results

These findings show how physiologically relevant stimuli interact with one another to increase cell chondro-inductivity.

4. Discussion and Conclusions

The way chondrocytes interpreted and responded to separate dynamic biophysical signals was significantly impacted by oxygen tension during culture.

5. References

1. Nasrollahzadeh, N et al. *elife*. 2022;11(9): e72068.

Acknowledgements:

This research project is supported by a SNF grant # CR2313_159301.

A BONE-ON-CHIP AS A 3D PLATFORM TO ASSESS THE EFFECT OF STEM AGE ON TISSUE FORMATION

Elisa Budyn (1)

1. Ecole Normale Supérieure Paris-Saclay, France

1. Introduction

We present a physiologically relevant 3D environment to form human bone and disk organoids from decellularized bones and either stem cells of different ages or primary committed cells on which regenerative treatments could be tested.

2. Materials and Methods

Our bone-on-chip includes decellularized bones that are recellularized with either human primary adult Mesenchymal Stem Cells (MSCs), primary and cell-line fetal human osteoblast progenitors (FHOB) or human primary annulus fibrosis (hAFC) and nucleus pulposus cells (hNPC). MSCs and FHOBs differentiated into stem cell derived osteocytes (SCDOs) within 30 days and formed bone. AFCs and NPCs formed a collagenous matrix. The systems were long-term cultures up to 26.5 months. Compressive mechanical stimulations applied to the constructs mimicked human walk.

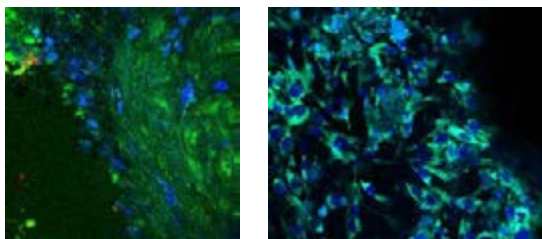


Figure 1: a) MSC in a bone-on-chip b) AF and NP cells in a bone-on-chip.

3. Results

Early and mature osteocytes were identified by the secretion of E11 and SOST under fluorescent confocal microscopy. Bone cells formed mineralized collagen layers of alternating orientations that created an

extracellular matrix able to assemble multiple bones revealing topological cues sensed by the cells within minutes of seeding. The stiffnesses measured using 3-point bending showed primary adult MSCs formed a mineralized tissue of lower flexural stiffness than the fetal cells. FTIR measurements confirmed that Fetal cells produced highly mineralized bone that contained lipids, while adult cells assembled multiple bones to recreate the Haversian structure. AF and NP cells produced collagen Type I and II and almost no minerals.

4. Discussion and Conclusions

The new results confirmed the influence of the age of stem cell on their ability to produce higher quality bone when from younger individuals. The bone-on-chip was also a more suitable environment for the disk cells. All systems were used as an animal-free platform to test medicines for pathologies such as HIV, cancer, and aging.

5. References

1. Budyn, E. et al. *MRS Advances*, 3(26):1443-1455 (2018).
2. Singh, B. et al. *Alternative to Laboratory Animals, Meeting Report*, (2021).
doi.org/10.1177/02611929211025006

Acknowledgements:

The authors thank NSF CMMI BMMB 1214816 EAGER, CNRS INSIS PEPS Mécanique du future, the Farman Institute, Synchrotron 20191708 and 20201633 awards, the *Anatomical Gift Association of Illinois*.

AN *IN SILICO* MODEL TO INVESTIGATE STROMAL CELL-DRIVEN SPROUTING ANGIOGENESIS WITHIN AN ANISOTROPIC SCAFFOLD

Chiara Dazzi (1), Erik Brauer (1), Ansgar Petersen(1), Sara Checa (1)

1. Julius Wolff Institute, Charité – Universitätsmedizin Berlin, Germany

Correspondence: sara.checa@bih-charite.de

1. Introduction

Poor re-vascularization of scaffolds is one of the main hurdles for the clinical use of tissue engineering approaches. Scaffolds with highly aligned channel-like pores showed promising results in large bone defect regeneration *in vivo* [1], however the mechanisms behind scaffold-guided angiogenesis and cells patterning are not fully understood.

During sprouting, endothelial cells (ECs) are known to be sensitive and respond to local mechanical and geometrical cues. ECs interact mechanically with outer-vascular stromal cells (SCs) through cell internally generated traction forces (TFs).

Here, we aim to investigate the role of cell-cell and cell-scaffold mechanical interactions for early sprout formation and SCs patterning within an anisotropic scaffold, using a computer modelling approach.

2. Materials and Methods

An *in silico* multi-scale model of the mechano-regulation of sprouting angiogenesis and SCs organization within a macroporous channel-like collagen scaffold, Fig. 1 A, was developed. The model couples a Finite Element Model (FEM) at the tissue scale, to compute deformations induced by cell TFs within the scaffold, to an Agent-Based Model (ABM) at the cellular scale, describing ECs and SCs activity in response to mechanical signals. Based on current literature, the influence of mechanical stimuli on cell migration, orientation (*durotaxis*, [2]), and vessel sprouting (local strains) was implemented using rule-based approaches.

In silico results of sprout and SCs patterning were compared to dedicated *in vitro* experiments.

3. Results

In silico predictions showed a preferential alignment of vessels and SCs along the channel long-axis, Fig. 1 B-C, in agreement with experimental observations.

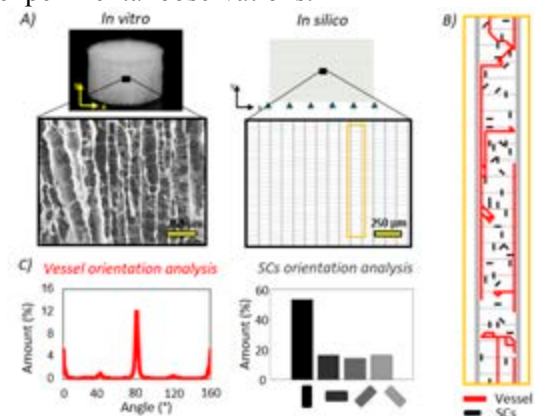


Figure 1: A) *In vitro* [3] vs. *in silico* scaffold architecture; B) *In silico* predictions of vessel and SCs patterning within a scaffold channel; C) Vessels and SCs orientation analyses.

4. Discussion and Conclusions

The model predicted the preferential alignment of vessels and SCs observed experimentally, suggesting that *durotaxis* can explain initial scaffold vascularization and cell alignment within anisotropic scaffolds.

To better understand the influence of SCs forces on sprout patterning, we are currently performing *in silico* experiments of TFs inhibition/activation and outcomes will be compared to the corresponding *in vitro* analyses.

5. References

1. Petersen et al., Nat Commun, 2018
2. Wong et al., Proc Natl Acad Sci U S A, 2014
3. Brauer et al., Adv Sci, 2019

Acknowledgements:

This work was supported by grant CRC 1444 from the DFG.

UNRAVELING THE PHYSICS OF EPITHELIAL JAMMING USING AN ACTIVE FOAM MODEL

Jef Vangheel (1), Steven Ongenaë (1), Bart Smeets (1)

1. MeBioS, KU Leuven, Leuven, Belgium

1. Introduction

During embryonic development, a fluid-to-solid (or vice-versa) transition occurs, known as tissue (un)jamming. Computational models have shown that this transition is controlled by the balance between adhesion and cortical tension, cell motility [1], and tissue porosity [2]. However, the role of cell-cell adhesion on tissue state is still unclear as experiments show that increasing cell-cell adhesion can both fluidise [3] or solidify [4] a confluent tissue. In this work, we use an active 3D foam model to show how this discrepancy can be explained by accounting for cell-cell friction that is ultimately related to adhesion. Particularly, we study cell dynamics in a monolayer of cells in function of cell-cell interfacial tension, cell motility and cell-cell friction.

2. Materials and Methods

Cells are represented as active viscous shells with surface tension γ , adhesive tension ω , and cortex viscosity μ . Cell-cell adhesion is related to cell-cell friction by the cadherin turnover time τ_{ω} . Cells migrate, driven by actin polymerisation at the cell front and retraction at the trailing end, modelled as local pressures P_a on the cell cortex (Fig. 1a).

3. Results

We quantify tissue fluidity by the relative number of neighbour exchanges (T1-transitions, Fig. 1c) in function of individual cell properties (Fig. 1d). We show that cell motility increases number of T1-transitions, and therefore tissue fluidity, and that the effect of cell-cell interfacial tension depends on tissue porosity, consistent with [2]. Furthermore, we find that cell-cell friction increases the characteristic time-scale of T1-transitions, effectively solidifying tissue, in confluent but not in porous epithelium (Fig. 1e).

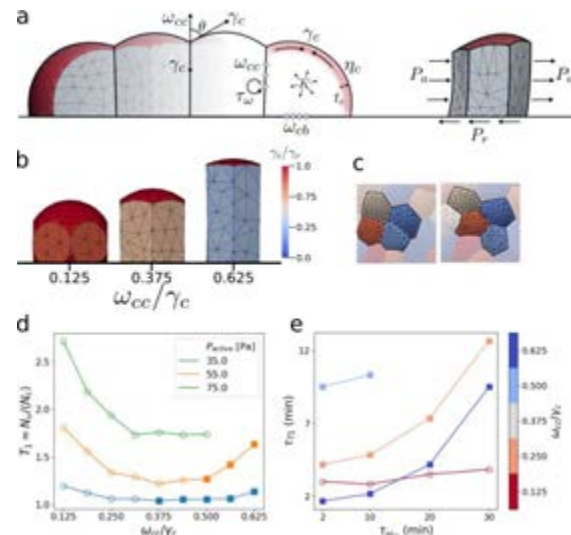


Figure 1: a) Computational model. b) Interfacial tension controls cell shape. c) T1-transition. d) Cell rearrangements in function of interfacial tension and cell motility. Squares indicate confluent tissue, open circles indicate porous tissue. e) Characteristic time of T1-transitions in function of cadherin turnover time and interfacial tension.

4. Discussion and Conclusions

Vertex models show that adhesion can fluidise tissue by decreasing interfacial tension enabling cells to become more deformable [1,2]. However, experiments show solidification is accompanied by adhesion density increase [4]. From our results, we postulate that adhesion not only affects interfacial tension, but also increases friction, eventually solidifying tissue.

5. References

1. Bi D., et al., Phys. Rev. X. 2016; 6(2): 021011
2. Kim S., et al., Nat. Phys. 2021; 17:859-866
3. Park J., et al., Nat. Mater. 2015; 14:1040-1048
4. Garcia S., et al., PNAS. 2015; 112(50):15314-15319

Acknowledgement: The authors would like to thank the Research Foundation Flanders (FWO) (Grant no: 11D9923N) for providing financial support to this project.



IMPROVING DRUG DELIVERY IN THE BRAIN USING MICROBUBBLES COMBINED WITH FOCUSED ULTRASOUND

Qiyao Peng (1), Vivi Rottschäfer (1,2)

1. *Mathematical Institute, Leiden University, The Netherlands;* 2. *Korteweg-de Vries Institute for Mathematics, University of Amsterdam, The Netherlands*

1. Introduction

The brain-blood barrier (BBB) is the major barrier protecting the brain, which consists of endothelial cells that are connected by tight junctions between the neighboring cells. This BBB limits the transport of drugs from the blood into the brain.

To increase the permeability of the BBB and hence drug delivery into the brain, applying a combination of microbubbles (MBs) and focused ultrasound (FUS) shows a great potential [2]. In this process, the MBs start to oscillate due to the FUS and “massage” the membrane of endothelial cells resulting in small, temporary openings in the endothelial cell membrane and in between the cells [2,3]. Most modelling work on MBs revealed relations between the radius of the MBs and the pressure from the FUS, by treating the MBs as a spherical object where the movement of the MB is neglected [1].

2. Materials and Methods

To describe the oscillations of the MB resulting from the driving acoustic pressure of FUS, the Rayleigh-Plesset equation is used [1]:

$$\rho \left(R \frac{d^2 R}{dt^2} + \frac{3}{2} \frac{dR}{dt} \right) = p_i - p_e. \quad (1)$$

Here, ρ is the liquid density, R is the radius of the MB, p_i and p_e represent the pressures inside and outside the MB, respectively.

In our approach, we also take into account the movement of the MBs, combined with the FUS. For that, we no longer assume that the MB is a sphere, or a circle in two-dimensional case. We numerically approximate it with a polygon in two dimensions, by splitting the membrane of MB into many line segments connected by the nodal points. Subsequently, the displacement of every nodal point on the membrane is precisely tracked. The

displacement of the nodal point is determined by multiple processes, such as the blood flow, the acoustic pressure from FUS and the microstreaming caused by the oscillation of the MBs. In this process, shear stress on the endothelial cells is produced [3] which has a significant impact on increasing the permeability of the BBB. When a MB is very close to or collides with the endothelial cells, we assume that a pushing force is exerted by the endothelial cells on the MB to prevent the MB from crossing the membrane.

3. Results

We visualize the process of applying the FUS to the MB that are taken along by the blood flow in a capillary. We especially track the evolution of the geometry of the MB. Furthermore, the impact of the oscillation of the MBs on the endothelial cells is quantified. As far as we know, we are the first to study the influence of FUS on MBs in this setting.

4. Discussion and Conclusions

In this presentation, we present a model that describes the evolution of the geometry of migrating MBs and we compare our results with the model that takes MBs as spherical objects. Our model and results provide a next step towards understanding the influence of MBs combined with FUS on the permeability of the BBB.

5. References

1. De Jong N et al., *Med Biol Eng Comput*; 47: 861-873 (2009).
2. Kooiman K et al., *Advanced Drug Delivery Reviews* 72: 28-48 (2014).
3. Roovers S et al., *Langmuir* 35: 10173-10191 (2019).

PHYSICS INFORMED TISSUE ARCHITECTURE RECONSTRUCTION

Jiří Pešek¹, Mathieu de Langlard¹, Seddik Hamad^{2,3}, Dirk Drasdo¹

1. SIMBIOTX, Inria (Saclay - Île de France), France; 2. Molecular Hepatology Section, Department of Medicine II, Medical Faculty Mannheim Heidelberg University, Mannheim, Germany; 3. Department of Forensic Medicine and Veterinary Toxicology, Faculty of Veterinary Medicine, South Valley University, 83523-Qena, Egypt.

1. Introduction

Microscopic architecture of tissue influences the outcome of many cell processes from signalling, proliferation and, ultimately, the cell fate. In order to study these processes, it is imperative to obtain a realistic and detailed microarchitecture of the tissue. Despite recent advances in imaging and image analysis techniques, they are still insufficient to provide all necessary data for a successful detailed tissue microarchitecture reconstruction directly from the experimental data. This issue is even more pronounced in complex tissues like liver, with many different structures that have to be taken into account. We offer an alternative method where the traditional image analysis is augmented with a model driven tissue reconstruction.

2. Materials and Methods

Deformable cell model (DCM) is a state of the art mechanical model of the cell [1], capable of capturing realistic shapes and mechanical properties. The mechanical nature of the model naturally imposes a mechanical equilibrium in the reconstructed tissue. This additional constraint replaces some of the missing information retrieved from image analysis and thus leads to reconstruction of more realistic cell shapes and thus tissue architecture.

This novel method starts from traditional image analysis to obtain cell nuclei positions and volumes, which are the basis for seeding individual cells, and the outline of relevant structures forming the tissue boundaries (e.g. veins, sinusoids, optionally bile ducts and canaliculi), which are then represented by a triangulated mesh. Inside such environment cells are slowly grown to physiologically realistic sizes subject to the intercellular and cell-boundary adhesive and repulsive forces. This leads to cells a local mechanical equilibrium (see Figure 1 right).

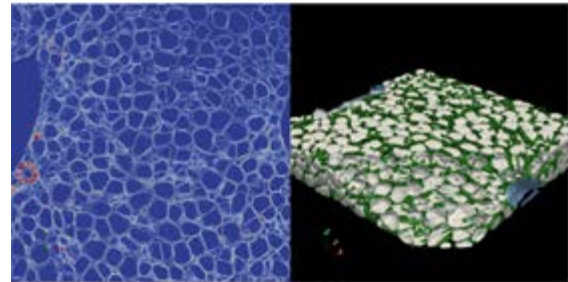


Figure 1: Left: Comparison between reconstructed cell shape and ground truth on a single slice. Right: 3D overview of the reconstructed tissue including cells (white), sinusoids and bile canaliculi (both green) and veins (blue).

3. Results and Conclusions

We reconstructed the tissue microstructure for two biological repeats of mouse liver, where we found a good agreement with the ground truth image (see Figure 1 left) obtained by direct staining of cell surface. The results demonstrate that this method produces qualitatively better results than the morphological watershed transform [2], when starting from the same incomplete information, and comparably to morphological watershed with cell surface provided. Furthermore, the results are robust with respect to chosen mechanical parameters: this new method is thus a prime candidate for tissue microarchitecture reconstruction from incomplete information.

4. References

- [1] Van Liedekerke P, Gannoun L, Loriot A, Johann T, Lemaigre FP, Drasdo D (2022) Quantitative modeling identifies critical cell mechanics driving bile duct lumen formation. *PLoS Comput Biol* 18(2): e1009653.
- [2] Soille, P. (1999). *Morphological image analysis: principles and applications* (Vol. 2, No. 3). Berlin: Springer.

Acknowledgements of funding support:

Agence National de la Recherche (iLite project ref 16-RHUS-0005) and the European Research Council (ERC) under the European Union's Horizon 2020 research and innovation program (Grant No. 864313).



SPHEROID FUSION: ARRESTED COALESCENCE AND JAMMING

Steven Ongenae (1), Jef Vangheel (1), Tom Belpaire (1), Hanna Svitina (2),
Ioannis Papantoniou (2), Bart Smeets (1)

1. MeBioS, KU Leuven, 3001 Leuven, Belgium;

2. Skeletal Biology and Engineering Research Centre, KU Leuven, 3000 Leuven, Belgium

1. Introduction

The fusion assay is commonly used to examine bulk rheological properties of tissue spheroids. While previously tissue spheroids were considered as liquid droplets, the observation that fusion could be locked in an incomplete state, called arrested coalescence, necessitated a visco-elastic description of the evolution of the fusion angle [1-3]. On the other hand, data from cell tracking offers us insight in the fluidisation state of the tissue. Combining both enable us to calibrate an active foam model, so we can link the fusion dynamics with single cell mechanical properties.

2. Materials and Methods

Each cell is simulated as an active viscous shell with a surface tension γ , and cell-cell interfacial tension ω (Fig 1). An active pressure P_A is exerted on the membrane in the polarization direction of the cell. Volume of each cell is conserved using a PI-controller with bulk modulus K . Increasing ω/γ makes the cells more deformable, while increasing P_a promotes cell motility.

3. Results

We identified that an increase in ω/γ results in faster fusion, however, when the level of activity is insufficient, local stresses cannot relax, causing fusion to arrest. At high levels of both ω/γ and P_a fusion is complete and mixing occurs. At low levels of ω/γ , but at high P_a the driving force for fusion is too low to direct the process, causing it to arrest.

4. Discussion and conclusions

Fusion outcome can be mapped on a phase diagram (Fig 2) where we separate zones of fluidised versus jammed tissue and complete versus arrested fusion in function of activity P_a and interfacial tension ω/γ .

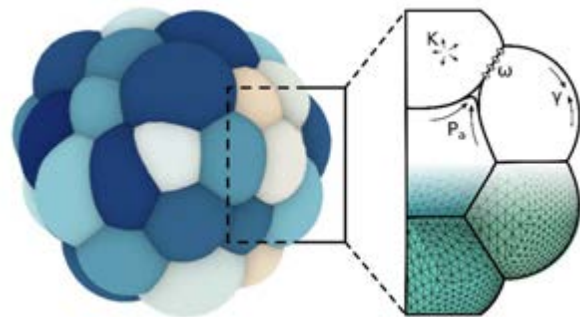


Figure 1: Illustration of a tissue spheroid using an active foam model.

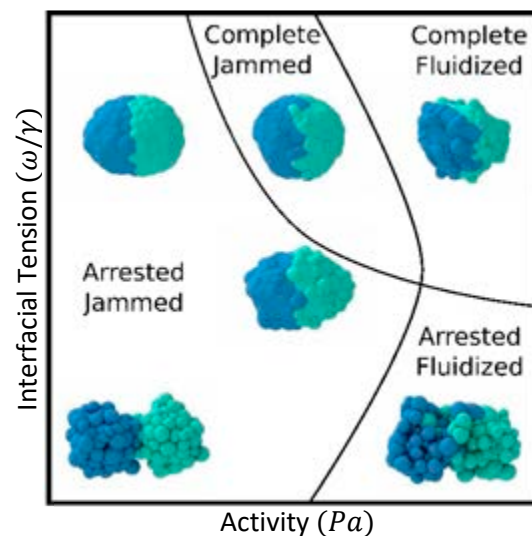


Figure 2: Interplay between cell interfacial tension (ω/γ) and an active pressure P_a illustrates the complexity in outcome of the fusion process.

5. References

1. Oriola D et al., *Soft Matter*; 18(19):3771–3780 (2022).
2. Ongenae S et al., *Frontiers in Physics*; 9:41-48 (2021).
3. Beaune G et al., *Langmuir*; 38(17):5296-5306 (2022).

Acknowledgements:

The authors acknowledges support from KU Leuven internal funding C14/18/055.



NEURAL CREST CELL CONTRACTION CAN DIRECT COLLECTIVE MIGRATION

Ian Manificier (1) (2), William Lalanne (1) (2), Jean-Louis Milan (1) (2)

1. Aix Marseille Univ, CNRS, ISM, Marseille, France; 2. Aix Marseille Univ, APHM, CNRS, ISM, Sainte-Marguerite Hospital, Institute for Locomotion, Department of Orthopaedics and Traumatology, Marseille, France;

1. Introduction

In vertebrates, Neural Crest (NC) cells represent a transient embryonic cell type that undergoes extensive collective migration to various destinations where cells later differentiate into several organs [1]. Interestingly, this collective migration does not rely on predetermined leader cells [2], moreover as cells progress through the tissues they may only use local cues to guide themselves and follow predetermined rules to successfully migrate. Previous NC cell migration models used cell alignment to achieve collective migration [2]. Here we use an agent-based model to demonstrate that persistent migration can be achieved over long distances despite cells lacking an active internal migration alignment mechanism.

2. Materials and Methods

Cells were modelled as 2D particles with a compressive rigidity. Each cell would generate a co-attractant that could diffuse locally. Cells were able to generate filopodia to distally measure local co-attractant concentrations and move to the area where the highest concentration had been measured. As cells came in contact with each other, they would inhibit their ability to generate filopodia in the zone of contact. Cells in contact would become cohesive, however when cells were fully surrounded by other cells their cohesion property differed. To simulate calcium contraction waves, we then induced back to front contraction waves between cells.

3. Results

Distal filopodia co-attractant measurement allowed cells to detect signal of other cells without being overwhelmed by their own. Cells were therefore able to cluster with their nearby neighbors. Cohesion was necessary otherwise

cells would separate after initial contact prevented sustained contact clustering.

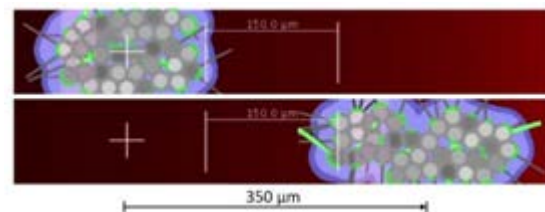


Figure 1: Top view of 2D cell ($n=36$) cluster migrating across a $150 \mu\text{m}$ long interval. Total distance travelled by cell group $350 \mu\text{m}$. Cells are represented by grey disks; their active edge is colored in green from which they emit filopodia (grey and green lines) and secrete co-attractant (purple).

Back to front contraction waves allowed extensive migration in the intended direction. The absence of contraction wave led to insignificant migration (Fig. 1), or unreliable at best. Cohesion properties did impact migration performance and intra-cluster cohesion could be lower than at the periphery.

4. Discussion and Conclusions

Despite cells lacking an active intracellular alignment mechanism the model shows that calcium wave contractions can induce collective migration.

5. References

1. Bronner M, *Histochem Cell Biol.* 2012 Aug; 138(2): 179–186.
2. Szabó A, et al., *J Cell Biol* (2016) 213 (5): 543–555.

Acknowledgements:

No funding was attributed to this work. We thank Roberto Mayor for taking time to answer some of our questions.

CMBBE 2023

18th International Symposium on Computer Methods
in Biomechanics and Biomedical Engineering
3 - 5 May 2023, Paris, France



Arts et Métiers Institute of Technology
Institut de Biomécanique Humaine
Georges Charpak
155 boulevard de l'Hôpital 75013
Paris France

www.cmbbe-symposium.com

DIGITAL NUCLEAR MECHANOBIOLOGY AND CANCER DIAGNOSTICS

G.V.Shivashankar

ETH Zurich & Paul Scherrer Institute, Switzerland
Website: <https://www.psi.ch/en/mgg>

Keynote

Abnormalities in nuclear and chromatin organization are hallmarks of many diseases including cancer and neurodegeneration. However, quantitative methods to analyse nuclear and chromatin abnormalities for early disease diagnostics are still missing. In this talk, I will first describe a digital mechanopathology platform using nuclear and chromatin biomarkers by combining high resolution optical imaging, quantitative single-cell biology, machine learning and functional genomics. I will then demonstrate the sensitivity of this platform to trace tumor progression using human breast tissue microarrays. Finally, I will describe our recently initiated clinical trial using human blood cell chromatin biomarkers for early cancer diagnostics and therapeutic interventions. Collectively, our chromatin biomarkers may have major implications not only in early disease diagnosis, but also for assessing the efficacy of treatments in personalized and precision medicine.

and was the IFOM-NUS Chair Professor (2014-2019) before joining ETH. His scientific awards include the Birla Science Prize in 2006, the Swarnajayanthi Fellowship in 2007, and he was elected to the Indian Academy of Sciences in 2010 and to the EMBO membership in 2019.



Biography

G.V.Shivashankar is currently a Full Professor of Mechano-Genomics at the Department of Health Sciences and Technology, ETH Zurich. He also heads the Laboratory of Nanoscale Biology at the Paul Scherrer Institute, Switzerland. He carried out his PhD at the Rockefeller University (1994-1999) and Postdoctoral research at NEC Research Institute, Princeton USA (1999-2000). He was a tenured faculty at the National Center for Biological Sciences, NCBS-TIFR- Bangalore, India (2000-2009) before relocating to the National University of Singapore (NUS) in 2010. He was the Deputy Director of the Mechanobiology Institute at NUS (2011-2019)

CELL DEFORMABILITY HETEROGENEITY RECOGNITION FROM IN-FLOW MOTION PARAMETERS

Maria Isabella Maremonti (1)*, David Dannhauser (1), Valeria Panzetta (1), Paolo Antonio Netti (1) and Filippo Causa (1)

1. Interdisciplinary Research Centre on Biomaterials (CRIB) and Department of Chemical, Materials and Production Engineering of the University of Naples Federico II, Italy

*Corresponding author: Ph.D. Maria Isabella Maremonti, mariaisabella.maremonti@unina.it.

1. Introduction

Single cell deformability represents a straightforward indicator of changes in cellular states. Especially in cancer diseases, a high cellular heterogeneity has been associated to deformability and then different rheological and mechanical properties, representing a distinctive marker for the detection of different degrees of cancer invasiveness [1]. Nowadays, a variety of microfluidic systems enabled alignment, deformation and/or separation of particles and/or cells for single-cell biophysical and biomechanical analysis [2]. Recently, a straightforward viscoelastic-based microfluidic approach was used to analyse in-flow compressed cells by coupling the classical descriptors of morphological and shape alterations with in-flow orientation angles [3]. Here, we introduce a reduced set of motion parameters as the local cell velocity, the lateral equilibrium position and the orientation angle capable to recognize different levels of cell deformability in a wide range of measurable rheological and mechanical properties.

2. Materials and Methods

In-flow cell analysis has been performed in a label-free manner with in-flow brightfield videos. Thus, we measured dynamic in-flow cell parameters, such as aspect ratio (AR), cell deformation (CD), centroid coordinates (Y) and orientation angles (φ) in the range of $[-90^\circ; 90^\circ]$. For the unsupervised machine learning part, we used a principal component analysis approach (PCA, Figure 1).

3. Results

We introduce a new set of in-flow motion parameters capable to identify the heterogeneity among cell deformability. Firstly, we measured cells deformability by identification of in-flow

motions as Rolling, Tumbling, Swinging, and Tank-Treading, distinctively associated to cell rheological/mechanical properties and then inner compartments (actin and microtubules) organization. Secondly, from a pool of parameters, a PCA revealed dominant features like the local cell velocity, the equilibrium position and the orientation angle variation. These motion parameters clearly defined cell clusters in terms of motion regimes corresponding to specific deformability and rheological/mechanical properties.

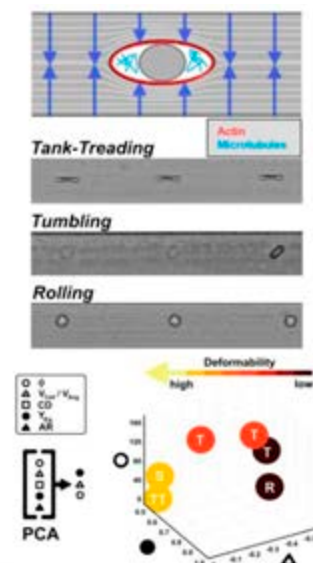


Figure 1: Thanks to a sketch representation we present the compression region of our device where cells perceive a viscoelastic compression. Then, all the interesting features were collected and a PCA was used for the precise classification of cell clusters upon deformability with respect the defined in-flow motion regimes.

4. References

- Lüönd F. et al., Br. J.Cancer.,125, 164–175 2021.
- Zheng Y. et al., LabChip, 13, 2464–2483, 2013.
- Maremonti M. et al., LabChip,24,4611-4622, 2020.



BIOMECHANICAL ANALYSIS OF BRAIN CANCER CELL INVASION BY KINEMATIC FIELD MEASUREMENTS

Aurélie Gangneux (1), Aymerick Gaboriau (2), Laetitia Caille (1), Valéry Valle (1), Marc Mesnil (2), Tanguy Vendeuvre (1,3), Norah Defamie (2), Arnaud Germaneau (1)

1. Institut Pprime, UPR 3346 CNRS, University of Poitiers, ISAE-ENSMA, France; 2. CoMeT Laboratory, University of Poitiers, France; 3. Department of Orthopaedic Surgery and Traumatology, University Hospital of Poitiers, France

1. Introduction

The spread of invasive cancer cells from the primary tumor is the leading cause of death by cancer. The first step of the invasive process involves a specific cell membrane protrusion formation called invadopodia [1]. The particularity of this micrometric structure is their ability to penetrate and to degrade the extracellular matrix (ECM) in order to facilitate cell invasion inside the tissue surrounding the tumor [2]. In this work, we propose a new method to study the displacement and deformation fields responsible for the formation of invadopodia by using brain tumor (glioblastoma) cells, which are known to be highly invasive. This method combines confocal microscopy and volume images correlation techniques.

2. Materials and Methods

The study has been done by using a human glioblastoma cell line (Ln229 cells). The plasma membrane of the cells was marked with a red lipophilic fluorochrome before seeding them on a green-fluorescent ECM (Oregon Green 488 conjugated Gelatin). Volume images of the cells and the ECM were realized during the development of invadopodia with a confocal microscope (Olympus FV3000). A volume image was recorded every 6 minutes during 20 hours. Images were analysed to extract geometry by segmentation techniques. We used digital volume correlation (DVC) method [4] to measure displacement fields of the ECM degraded by invadopodia and the cell in each voxel, and strain fields were computed. A hexahedral mesh of voxel size was applied to the geometry in order to visualize the results through Ansys software.

3. Results

Each element of the mesh is associated with a field value (Fig. 1).

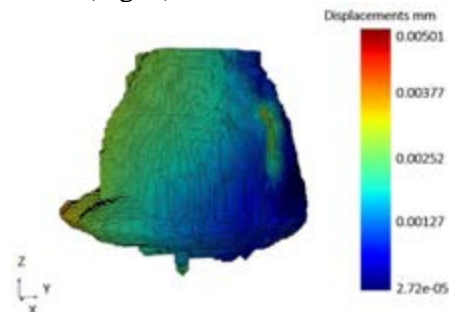


Figure 1: Displacement field (time =12 min).

The internal displacements of the cell were homogeneous around 10^{-3} mm.

4. Discussion and Conclusions

Displacements values are consistent with those obtained in articles using TFM (Traction Force Microscopy) measuring displacement fields only at the cell/ECM interface [4]. The use of confocal microscopy and DVC allowed visualization and quantification of displacement and strain fields inside cell and ECM. These measurements can then be coupled with finite element methods to determine the interaction forces that the cells exert on the ECM or to create a digital twin of the cell.

5. References

1. Murphy D, Courtneige S. NRM. Cell biol. 2011.
2. Wolf, K. et al. Nat. Cell Biol. 2007.
3. Bokam P. et al. JMBBM. 2019.
4. Maskarinec S. et al. PNAS. 2009.

Acknowledgements:

The authors would like to thank the platform ImageUp for providing confocal microscope. Interactive LabEx (ANR-11-LABX-0017-01), Ansys, and Ligue contre le Cancer (Comité de la Vienne) supported this work.



MODELLING OF FORCES EXERTED BY CELLS ON THEIR DIRECT ENVIRONMENT

Fred Vermolen (1,2), Qiyao Peng (3,1), Daphne Weihs (4)

Enter the affiliation information here ("Affiliation" style)

1. Department of Mathematics and Statistics, University of Hasselt, Belgium; 2. Data Science Institute (DSI), University of Hasselt, Belgium; 3. Mathematical Institute, Leiden University, The Netherlands; 4. Faculty of Biomedical Engineering, Technion, Israel

1. Introduction

Cellular forces occur under various circumstances. One can think of muscle cells that exert forces to move a joint, or one may think of forces that are exerted by (myo)fibroblasts during contraction of severely damaged skin. Another example involves cancer cells that exert forces to open channels and cavities to migrate to other parts of the body where they can start new tumour colonies. These biological settings stress the importance of cellular forces. We apply the bio-mathematical principles to simulate pathologies such as skin contraction as a result of deep tissue injury and the metastasis of cancer by cancer cells that migrate between different parts of the body.

2. Materials and Methods

The method that we employ in this research is an agent-based model that treats cells as individual entities, in combination with partial differential equations for the description of the stresses and strains in the computational region (tissue). The boundary of the cell is divided into mesh points that are connected by line elements in 2D and by (triangular) elements in 3D. On the centres of the elements a point force is located, which is modelled by a vectorial Dirac delta distribution. This force is inserted into the balance of momentum that keeps track of displacements and deformations in the entire tissue. Since these deformations can be large locally and since the cells are able to change the local microstructure of the tissue, permanent displacements are included. These permanent displacements are included through a morpho-elastic formalism. Cells are allowed to deform and to migrate as a result of various cues. Since cell migration is affected by the heterogeneous

microstructure of tissues, migration contains a random component.

In our studies, we have done rigorous mathematical analysis in the sense of well-posedness, and we developed finite element solutions to approximate the solution to the resulting problem. Furthermore, the random parts of the model and the uncertainty of input parameters as a result of variations from patient to patient necessitate a sound statistical approach to assess the output data.

3. Results

The model has been applied to deformable cell migration through deformable channels [1], as well as to the contraction of burn injuries, where cells pull on their immediate environment, thereby reducing the wound area. Typical computed results are intervals of confidence, and probability density distributions of the severity of output parameters such as the degree of metastasis of cancer or the extent of skin contraction.

4. Discussion and Conclusions

The models that we present are micro-scale based in the sense that they are applicable to a domain with a limited size since agent-based become computationally expensive when applied to large regions. Larger regions are described by upscaled equations in which cells are described through additional partial differential equations that represent cell densities. An important endeavour that needs to be done is the upscaling that links the microscale to the macroscale. In the presentation, we will briefly assess the first steps that we have taken in this direction.

5. References

1. Peng Q, Vermolen FJ, Weihs D. Biomech Mod MechanoBiol;20:1459-1475 (2022).

MULTISCALE MECHANOBIOLOGICAL ANALYSIS OF THE NEWLY REGENERATED BONE

Pablo Blázquez-Carmona (1), Juan Morgaz (2), Esther Reina-Romo (1)

1. Escuela Técnica Superior de Ingeniería, Universidad de Sevilla, Spain; 2. Hospital Clínico Veterinario, Universidad de Córdoba

1. Introduction

Bone regeneration processes are complex multiscale intrinsic mechanisms in bone tissue whose primary outcome is restoring function and form to a bone insufficiency. The effects of mechanics on the newly formed tissue, occur at the tissue, cellular and even molecular scale. However, at all these scales, the identification of the mechanical parameters and their mechanisms of action are still unknown and continue to be investigated. This concept of mechanical regulation of biological processes is the basis of mechanobiology and is used in this study to understand the multiscale response of the callus and surrounding soft tissues (SST) to mechanical factors during distraction osteogenesis (DO).

2. Materials and Methods

An *in vivo* bone lengthening (BL) treatment was performed in the right-back metatarsus of six female Merino sheep. It consisted of a latency period of one week, a rate of distraction of 1 mm/day and a total distracted length of 15 mm. At the tissue scale, a rheological model based on recorded distraction forces is proposed to assess *in vivo* the impact of the elongation on the SST, including their viscoelastic changes [1].

At the fibril scale, a mathematical model based on *ex vivo* confocal imaging data is developed to understand the fiber rearrangement and structural changes in the early DO callus [2].

3. Results

Tissue scale

The mechanical changes undergone by SST were not in an innate healing and a natural stiffening phase. While SST stiffness barely changes during the first days of distraction, its apparent viscosity strongly increases. This fact suggested a partial loss of its viscoelastic behavior at this stage which could be associated with a structural alteration for tissue

accommodation to elongation. At later stages, the lack of a further structural adaptation to elongation led to strain-hardening.

Fibril scale

Figure 1 exemplifies the structural evolution and orientation distributions of collagen fibers in three of the callus samples analyzed: days 0, 10 and 15 of distraction. As expected, as this phase progresses, collagen fibers reorganize and increase considerably in density.

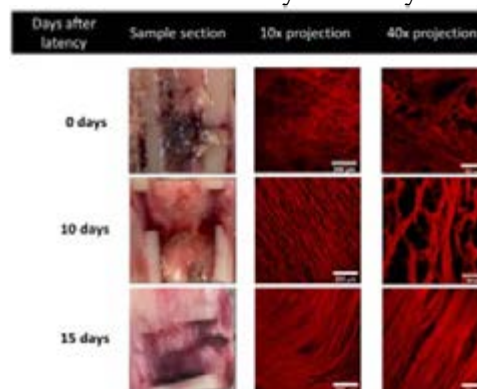


Figure 1: Sum projection of the fluorescence images at different time-points after latency.

4. Discussion and Conclusions

Different monitoring techniques at the tissue and fibril scales have been applied to simultaneously characterize the main biological and mechanical events that occur in DO. This work points out the unquestionable role played by mechanical and structural parameters in the biological regulation of bone regeneration during BL.

5. References

- Blázquez-Carmona P et al., Ann Biomed Eng; 49(4):642-652 (2021).
- Blázquez-Carmona P et al., Ann Biomed Eng; doi: 10.1007/s10439-022-02992-3 (2022).

Acknowledgements:

The authors would like to thank the Government of Spain (Grant no: PID2020-113790RB-I00) for providing financial support to this project.



BIOMECHANICAL DESIGN AND CHARACTERIZATION OF SCAFFOLDS FOR TISSUE ENGINEERING

T. H. V. Pires (1), J. E. Santos (1), A. P. G. Castro (1, 2), P.R Fernandes (1)

1. IDMEC, Instituto Superior Técnico, Universidade de Lisboa, Portugal

2. ESTSetúbal, Instituto Politécnico de Setúbal, Portugal

1. Introduction

The design of scaffolds for tissue engineering (TE) goes from the macroscale, at organ level, to the microscale, to address cell development and tissue growth issues. For instance, scaffolds for bone growth and repair are frequently load bearing devices that should present suitable stiffness and strength while assuring the right environment for cell diffusion and proliferation. This can be achieved with controlled scaffold microstructures to obtain optimal parameters such as porosity, permeability, or wall shear stress (WSS). The present work addresses recent developments on the biomechanical analysis and design of scaffolds using numerical and experimental techniques [1, 2]. Results bring new insights on the most suitable geometries for scaffold production and on methodologies for the development of tailored TE devices.

2. Materials and Methods

This work deals with the analysis of triply periodic minimal surfaces (TPMS) structures to be used as scaffolds in cartilage and bone TE. Geometries manufactured using a 3D MultiJet printer are tested experimentally for permeability using a syringe pump system to measure the pressure drop. The experimental results are compared with computational ones obtained by a CFD analysis [1]. The CFD is also used to estimate the WSS which together with an appropriate optimization strategy allows to obtain the parameters to optimize the scaffold geometry for a target WSS that promotes cellular proliferation and growth [2].



Figure 1: 3D printed scaffold: Schwarz D, Gyroid and Schwarz P geometries with 60% porosity.

3. Results

The correlation between numerical and experimental results obtained for pressure drop is illustrated in figure 2.

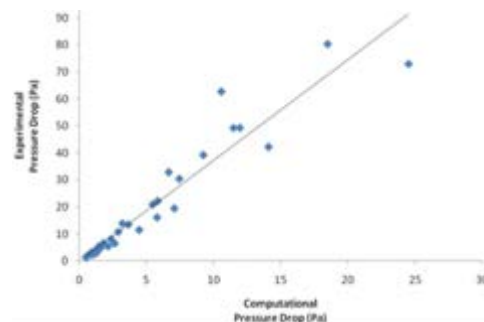


Figure 2: Numerical vs experimental results

4. Discussion and Conclusions

A good correlation between experimental and numerical results was obtained. Higher porosities did not necessarily mean a higher permeability. This implies that the scaffold geometry and its internal curvature need to be considered alongside porosity. Also, the outcomes of these studies indicate Gyroid scaffolds as the most adequate in comparison with the other tested geometries, if one is looking for a fluid-driven favourable environment for cell seeding and proliferation. In terms of the optimization algorithm, it was able to consistently reach the desired average WSS of 5 mPa. Further strategies involving multi-objective optimization will be considered.

5. References

1. Pires T et al., J. Biomech.; 117:110263 (2021).
2. Pires T et al., Materials; 15:7375 (2022).

Acknowledgements:

To Portuguese Science and Technology Foundation, through IDMEC, under LAETA project UIDB/50022/2020.



MULTISCALE MODELLING OF CHONDROCYTE MECHANICAL STIMULATION, A NUMERICAL AND EXPERIMENTAL APPROACH

QUEXADA DIEGO^{A,B*}, JELLALI RACHID^A, LE GOFF ANNE^A, HO BA THO MARIE-CHRISTINE^A, TRABELSI OLFA^A, GARZÓN DIEGO^B

^aUniversité de technologie de Compiègne, CNRS, Biomechanics and Bioengineering, Centre de Recherche Royallieu, CS 60 319 - 60 203 Compiègne Cedex, France ^bNumerical Methods and Modeling Research Group (GNM), Universidad Nacional de Colombia

1. Introduction

Cartilage remains an active research area, especially in cases of injuries or pathologies. In the case of growth plate cartilage, some of the most prevalent diseases are achondroplasia, gaucher's disease, among others (Pauli 2019). In the case of articular cartilage, of all joint diseases, osteoarthritis (OA) has the highest prevalence (Gluck 2015). In this sense, it is important to study the behavior of the main biological agent in cartilage, the chondrocyte. It has been reported that only 3D culture systems are suitable for chondrocyte culture since this prevents dedifferentiation (Lee et al. 2019). Nonetheless under certain conditions, it is possible to maintain chondrocyte phenotype in a 2D monolayer culture. (Yusof and Ramasamy 2017) evaluated the effect of phytoestrogen in chondrocytes on a 2D culture, and they were able to prevent dedifferentiation.

In this work, we explore the effects of different regimes of static and dynamic tension on a 2D chondrocyte monolayer culture. The main objective is to quantify the expression of different components in the extracellular matrix that may play an important role in the mechanobiology of cartilaginous areas. For this purpose, we develop a mathematical model that relates the mechanical strain to the chondrocyte production of GAGS and collagen. This mathematical model is validated with a novel microfluidic device that will subject the monolayer culture to different regimes of tension.

2. Materials and Methods

The mathematical model being developed relates the strain energy per unit volume and the load frequency f , in a certain time interval to the expression of GAGS and collagen v_{col} .

$$v_{col} = \varphi(U_{strain}, f) \quad (1)$$

As shown in figure 1, the device is comprised of the main culture chamber where chondrocytes will be seeded on a flexible polydimethylsiloxane (PDMS) membrane, and culture media is going to be renewed. This membrane will present a tensile strain produced by the negative pressure in two chambers. The amount of tensile strain is calculated in ANSYS and also measured visually with markers on the membrane thanks to the transparency of PDMS.

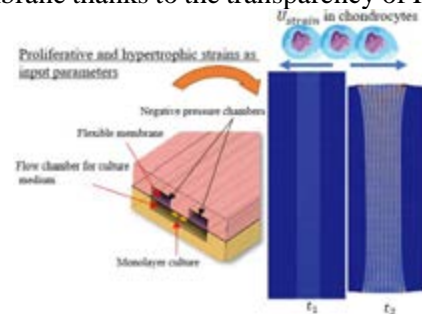


Figure 1: U_{strain} due to tension and microfluidic platform

3. Results

Preliminary results show the microfluidic device can expose the cells to different stimulation regimes with a new methodology. The experimental study is supported by a mathematical model showing how the strain energy may be one of the main mechanical cues in the synthesis of GAGS and collagen.

4. Discussion and Conclusions

This work shows a new approach to analyse the behaviour of cells in a 2D culture subjected to different kinds of mechanical stimuli, this may give insight into different physiological scenarios and identify new treatment targets.

5. References

- Gluck, et al. 2015. *Physiology & behavior* 176(1)
- Lee, et al. 2019. "A Microfluidic Platform for Stimulating Chondrocytes"
- Pauli 2019. *A Comprehensive Clinical Review*.
- Yusof, et al. 2017. "Phytoestrogen (Daidzein) Promotes Chondrogenic Phenotype of Human Chondrocytes in 2D and 3D Culture Systems."



FINITE ELEMENTS OF MULTISCALE MIXTURES (FE2M): APPLICATIONS TO SOFT TISSUES

Ashkan Almasi (1), Phoebe Szarek (1), Tim Ricken (2), David M. Pierce (1)

1. University of Connecticut, USA; 2. University of Stuttgart, DEU

1. Introduction

Estimating intra-tissue stresses in human joints and tissues demands modelling because the required *in-vivo* experiments are impossible or unsafe. The remarkable macro-mechanics of soft tissues derive from the complex micromechanics of their interacting constituents. We aimed to facilitate mechanistic understanding and improved analyses of the multi-scale mechanics of soft tissues and fibrous, engineered materials. To these ends we established validated software tools to predict local micro-mechanics in porous, (engineered) fibrous materials, e.g., fluid-saturated soft tissues, from macroscopic large deformations.

2. Materials and Methods

We combined generalized mixture theory [1] with the multiscale FE²-method [2] (i.e. finite elements (FE) of multiscale mixtures, FE2M) to solve 3-D, two-scale, non-linear, coupled, and time-dependent boundary value problems (BVPs) for fluid-saturated porous materials. To solve the multiscale BVPs we first provide the microscopic representative volume elements (RVEs) with macroscopic quantities as boundary conditions satisfying the Hill-Mandel homogeneity conditions [3]. The microscopic RVEs then provide the first Piola-Kirchhoff stress tensors back to the macroscale model at each integration point. We considered both isotropic, homogeneous RVEs, and those with stiff inclusions or networks of fibres. In the latter case we generate distributions of fibres within RVEs to create networks that are statistically equivalent to those measured in soft tissues, creating SERVES. To validate our implementation, we compared our numerical results from simulations in 3-D plane strain to those obtained by Bartel et al. in 2-D [3,4], and then compared results from standard FE (single-scale) to corresponding multiscale simulations leveraging SERVES within our FE2M scheme.

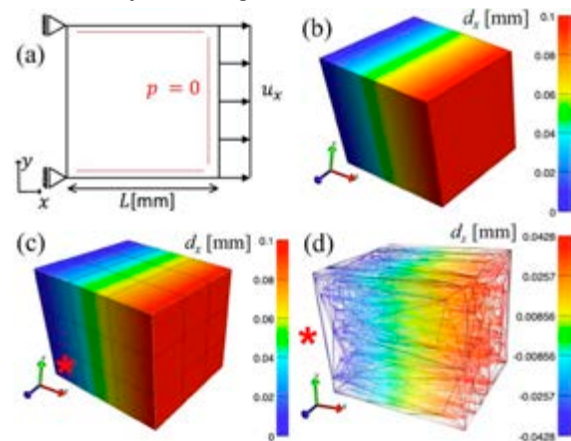


Figure 1: Representative validation comparing standard FE to FE2M using fibrous SERVES: (a) BVP; (b) standard macro model; (c) FE2M macro model; (d) microscale SERVE (elem 3, Gauss-pt 1).

3. Results

We successfully executed FE2M simulations of biphasic (poroelastic) materials, with stiff inclusions or networks of fibres, and validated these results against corresponding single-scale, biphasic FE simulations using mixture theory.

4. Discussion and Conclusions

Emerging multiscale FE²-methods (FE analyses augmented to derive the material behaviours from a distribution of finer scale FE analyses) are ideally suited to bridge the joint, tissue, and intra-tissue scales, but such methods have not yet been applied to multi-phase, fibrous materials. We will leverage our FE2M scheme, e.g., to establish how physical activity propagates micro-damage in cartilage *in vivo*.

5. References

1. Bowen RM, Academic Press, Cambridge (1976).
2. Feyel F, CMAME. 192:3233-3244 (2003).
3. Bartel F et al., PAMM. 15:447-448 (2015).
4. Bartel F et al., PAMM. 17:577-578 (2017).

Acknowledgements:

NSF CAREER 1653358; Gerard Ateshian (Columbia); Steve Maas (University of Utah).



COMPUTATIONAL CHARACTERISATION OF MECHANICAL ENVIRONMENT WITHIN TISSUE ENGINEERING SCAFFOLDS

Feihu Zhao

Zienkiewicz Centre for Computational Engineering and Department of Biomedical Engineering,
Faculty of Science & Engineering, Swansea University, United Kingdom

1. Introduction

In mechanobiological study for tissue engineering (TE) *in vitro*, mechanical stimulation (such as wall shear stress - WSS) is applied via bioreactors to the cells in cell culturing to study cell physiology and pathology. Porous scaffolds are used for housing the cells in three-dimensional cell culturing. It is known that the scaffold porous geometries can influence the scaffold permeability and internal WSS in a bioreactor (e.g., perfusion bioreactor) ¹. To calculate the WSS generated on cells within scaffolds and/or to determine the bioreactor loading, usually computational fluid dynamics (CFD) simulation is needed. However, the limitations are: (i) high time cost of the CFD simulation (in particular for the highly irregular geometries); (ii) accessibility to the CFD model for some experimentalists due to the knowledge gap. To address the limitations, this study aims to develop a simple empirical model for calculating the WSS just based on scaffold permeability.

2. Materials and Methods

To generate the data of WSS and permeability, the scaffolds with two types of pore shapes, cubic shape and gyroid shapes, which represented (i) symmetric pore unit and (ii) non-symmetric pore unit, respectively were generated using MSLattice ². The investigated pore size d and porosity ϕ are in the ranges of 300 – 1000 μm and 60% - 90% respectively. The CFD approach was used for calculating the scaffolds' permeability and resultant WSS. In the CFD model, considering the application context of perfusion bioreactor, we applied the inlet fluid velocity (V_{in}) of 100 $\mu\text{m/s}$, and outlet relative pressure of 0 Pa. The CFD model was solved using finite volume method by ANSYS – CFX. Finally, to obtain the correlation between the permeability (κ) and average WSS (τ_a), regression analysis was

carried out on κ and τ_a of different scaffold geometries.

3. Results

The permeability κ and WSS τ_a are dependent on the scaffold geometries. To correlate κ and τ_a , based on nonlinear regression, a power-law function with the different coefficient values was derived as below:

$$\gamma = A \cdot \kappa^{-0.4793} \quad (1)$$

where, $\gamma = \tau_a / V_{in}$, coefficient $A = 0.002116$ for non-symmetric pore unit (e.g., gyroid pore) with the R-square = 0.9598; $A = 0.001576$ for symmetric pore unit (e.g. cubic pore) with the R-square = 0.7824.

4. Discussion and Conclusions

In this study, a simple empirical model, which can correlate the scaffold permeability with the internal WSS was developed. To verify the accuracy of this empirical model, we tested it with different scaffold geometries. It was found that the average error of prediction by empirical model was 11.3% for scaffolds with non-symmetric pore units; 14.5% for scaffolds assembled by symmetric pore units. More test data will be used for further improving the model accuracy. With the simple empirical equations, researchers / engineers can easily use it for rapidly determining the loading conditions and/or calculating the cellular WSS for mechanobiological study in TE *in vitro* without performing extra computational simulations.

5. References

1. Zhao F et al., Front Bioeng Biotechnol 9: 736489 (2021).
2. Al-Ketan O et al., Mat Design Process Comm 3:1–10 (2021).

Acknowledgements: This study was supported by the Royal Society grant, D3SMechBio (RSG/R2/212280).

INFLUENCE OF CANCER-INDUCED ECM DEGRADATION ON TRACTION FORCE MICROSCOPY: AN IN SILICO STUDY

Alejandro Apolinar-Fernández (1,*), Jorge Barrasa-Fano (2), Hans Van Oosterwyck (2,3), José Antonio Sanz-Herrera (1)

1. *Escuela Técnica Superior de Ingeniería, Universidad de Sevilla, Spain (*,apolinar@us.es); 2. Biomechanics section, Department of Mechanical Engineering, KU Leuven, Belgium; 3. Prometheus division of Skeletal Tissue Engineering, KU Leuven, Belgium*

1. Introduction

Alterations in the mechanical behavior of the extracellular matrix (ECM) as a consequence of the activity of embedded cells have been implicated in many cellular processes [1]. In particular, cancer cell invasion into surrounding tissue is enabled by the remodeling of the collagen microstructure that supports the ECM, achieved by means of the secretion of proteolytic enzymes called metalloproteases [1].

2. Materials and Methods

In this study, we perform *in silico* 3D Traction Force Microscopy (TFM) simulations considering heterogeneity in the mechanical properties of the ECM with the aim of exploring how degradation affects the results obtained in TFM. The space-dependent heterogeneity is retrieved by correlating the parameters that govern a nonlinear hyperelastic model [3,4] to ECM degradation maps obtained numerically. For this purpose, we implemented a mathematical model [2] comprising five nonlinear and coupled PDEs of the reaction-diffusion type that emulates collagen degradation due to its interaction with diffusible metalloprotease MMP-2 and membrane-bound metalloprotease MT1-MMP. The system is solved in a 3D domain simulated in COMSOL Multiphysics, considering a real cell geometry and the surrounding ECM. In addition, the constitutive model is fitted to synthetic shear rheology curves corresponding to different levels of ECM degradation produced by a fibered matrix generator developed by the authors. The results have been adjusted with shear rheology tests that correspond to real collagen hydrogels.

3. Results

Fig. 1 shows an ECM density map for a specific time (3 days) corresponding to a 3D solution (left), associated displacement field without degradation (center), and associated displacement field with degradation (right). An increase of more than 10 times in displacement magnitude is observed between both cases.

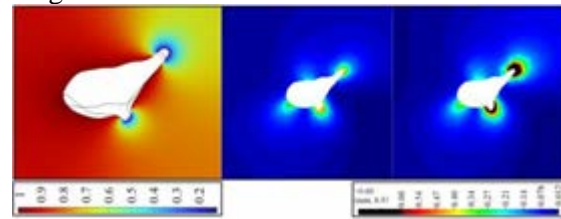


Figure 1: (Left) ECM density map. (Center) displacement magnitude [μm] without degradation. (Right) displacement magnitude [μm] with degradation.

4. Discussion and Conclusions

Displacements and traction magnitude vary significantly in highly degraded regions. The corresponding reduction in matrix stiffness entails an increase in matrix displacements. This leads to an overestimation of cell tractions in classical TFM where a homogeneous and time-invariant matrix is assumed. This work highlights the importance of considering evolving matrices in TFM.

5. References

1. Malandrino et al. *Extreme Mechanics Letters* 21. 2018.
2. Deakin et al. *Frontiers in Oncology* 70(3). 2013.
3. Steinwachs et al. *Nature Methods* 13(2). 2015.
4. Apolinar-Fernández et al. *bioRxiv* 516745. 2022.

Acknowledgements:

A.A.-F. and J.A.S.-H. gratefully acknowledge funding from projects PGC2018-097257-B-C31, US-1261691 and P20-01195. J.B.-F. was supported by KU Leuven internal funding C14/17/111.

A MULTIMODAL HIGH RESOLUTION STRUCTURE-PROPERTY INVESTIGATION OF MINERALIZED FIBROCARTILAGE

Davide Ruffoni

Mechanics of Biological and Bioinspired Materials Laboratory, University of Liège, Belgium

1. Introduction

The biomechanical and biological integration of tendon and ligament into bone is crucial for joint health. The strong differences between the soft tissue and the hard bone make attachment regions vulnerable to high stresses, which may cause failure. The tendon-bone interface features several strategies to enhance strength and damage resistance [1], including the presence of a thin layer of mineralized fibrocartilage (FC) having the critical task of anchoring tendon to bone. Although FC is the target of several pathologies and injuries, this tissue is much less understood than bone and tendon. Unsolved fundamental questions on FC include the structure-property relationship and as the possible communication between bone and tendon cells with FC cells.

2. Materials and Methods

Using the Achilles tendon insertion into calcaneus bone in rats, we are investigating several aspects of FC and subchondral bone (Figure 1). The chosen location features two types of FC which have to solve different tasks: enthesis FC anchors tendon to bone while periosteal FC facilitates tendon sliding. We measured microstructure with micro-computed tomography, mineral content with quantitative backscattered electron imaging and tissue properties with nanoindentation. Second harmonic generation imaging was performed to visualize collagen orientation and cellular functional porosity was investigated on stained samples with confocal microscopy.

3. Results

We highlighted a strong anisotropy of fibrochondrocyte lacunae and channel network at enthesis FC with pores oriented towards the tendon insertion [2]. Moving to material properties, we emphasized a considerable tuning in local mechanical behaviour within mineralized FC provided by matrix

organization beyond mineral content. Enthesis FC featured highly aligned fibres, enhancing anchoring stiffness and strength. Considering the cross-talk between FC and bone, we have unravelled that several fibrocartilage cells, although lacking an underlying communication network (like the osteocytes), still got stained. Further quantification revealed the presence of channels running through the bone-FC interface and connecting the bone cells with fibrocartilage cells, especially at the insertion.

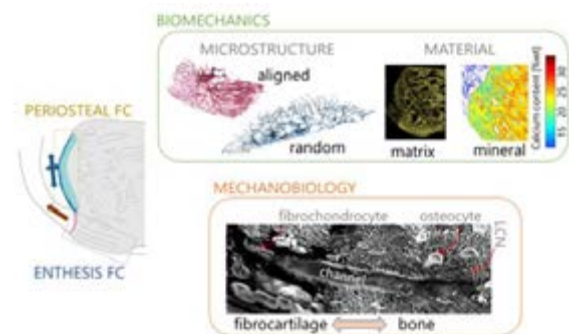


Figure 1: Biomechanical and mechanobiological aspects of fibrocartilage (FC) and bone.

4. Discussion and Conclusions

The specificities of FC biomechanical behaviour in two adjacent regions demonstrate the adaptability of this tissue. The communication paths between FC and bone may suggest new avenues to access mineralized FC with the long-term goal of fighting fibrocartilage pathologies.

5. References

1. Tits and Ruffoni, *Bone Rep*, 14: 1-17, 2021.
2. Tits et al., *Sci Rep*, 11: 16534, 2021.

Acknowledgements:

This ongoing research would not be possible without my PhD candidate Alexandra Tits and our collaborators: E. Plougonven, J.F. Kaux and P. Drion (ULiege), H. van Lenthe (KU Leuven), M. Hartmann and S. Blouin (LBIO, Vienna), R. Weinkamer and M. Rummeler (MPI, Potsdam).



EVALUATION OF ABDOMINAL HERNIA REPAIR USING FINITE ELEMENT MODELLING INCLUDING TISSUE DAMAGE

Baptiste Pillet (1), Gergely Molnár (2), Aline Bel-Brunon (3), Jérôme Molimard (1), Baptiste Pierrat (1)

1. Mines Saint-Étienne, Univ Jean Monnet, INSERM, U 1059 Sainbiose, 42023 Saint-Étienne, France;

2. Univ Lyon, CNRS, INSA Lyon, LaMCoS, UMR5259, 69621 Villeurbanne, France;

3. Univ Lyon, INSA Lyon, CNRS, LaMCoS, UMR5259, 69621 Villeurbanne, France

1. Introduction

Abdominal wall incisional hernia (AWIH) is one of the most frequent complications in visceral surgery. This condition, related to poor healing of the incision, has been correlated with environmental and genetic risk factors [1] (e.g. diabetes, obesity), but also with the surgical closure technique. Besides, the use of a prophylactic mesh has become standard of care. Despite tremendous progress in the treatment, complications remain and reported recurrence rates are still high, up to 30% [2].

In this study, different repair techniques are evaluated, using an original finite element model of the repaired AW that can account for possible damage initiation and development of soft tissues due to active or passive loading.

2. Materials and Methods

The repaired AW model consists in a region of interest including the Linea Alba (LA), segmented from the Visible Human Project, surrounded by rectus muscles (RM). The constitutive model of the different components (LA, RM, mesh, neo-tissues) is hyperelastic and anisotropic. Damage is included through a phase-field approach. Elastic and rupture properties have been identified from tensile experiments up to rupture and peeling tests on repaired porcine AWs. The model has been implemented in 2D in the Fenics framework.

The geometry has been parametrised to describe different populations. Here, two virtual patients are considered: an “average” anatomy, and an “obese” one. Four cases are compared: healthy, incision repaired with suture or mesh, and unrepaired incision.

The loading scenario consists of a preliminary closure of the AW incision by increasing suture tension for cases with sutures, followed by the application of longitudinal and transversal

tension to the boundaries of the model. These tensions have been extracted from a full-scale 3D AW model for three loading conditions: supine, standing and coughing.

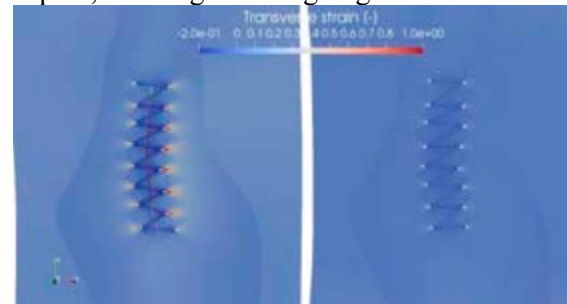


Figure 1: Transverse Green strain for the repaired AW for an obese patient in the standing scenario (left: sutured only; right: sutured with mesh).

3. Results

The model shows widely different damage profiles depending on the loading scenario, repair technique and patient type. We can for instance quantify how much using a mesh reduces transverse strain in the LA and overall tissue damage.

4. Discussion and Conclusions

This model helps evaluating surgical techniques in terms of potential damage initiation in the AW tissues. The originality lies in the full preliminary characterization of tissue behaviour, notably at rupture, and the absence of predefined failure pathway. This fully parametrized model may become a patient-specific assistance tool for visceral surgeons in order to reduce the occurrence of AWIH.

5. References

1. Höer et. al, Chirurg. 73(5):474-80 (2002).
2. Andersen et. al, BMC Surgery. 9:6 (2009).

Acknowledgements:

The authors would like to thank the AuRA région for their financial support.



VALIDATION OF MAXIMUM SHEAR STRAIN AS FE MODEL-BASED PARAMETER FOR POST-TRAUMATIC CARTILAGE DEGENERATION UPON MECHANICAL LOADING

Seyed Ali Elahi (1), Rocío Castro Viñuelas (1), Petri Tanska (2), Rami K. Korhonen (2), Rik Lories (1), Nele Famaey (1), Ilse Jonkers (1)

1. KU Leuven, Belgium; 2. University of Eastern Finland, Finland

1. Introduction

Cartilage degeneration is the hallmark of osteoarthritis (OA) [1]. In post-traumatic OA, even a normal mechanical loading can induce altered tissue strains and cartilage degeneration [2]. Previous studies have linked excessive maximum shear strain (MSS) with proteoglycan matrix associated cartilage degeneration [2]. In this study, we aim to validate finite element (FE) analysis predicted MSS with localized cartilage degeneration upon loading in a post-traumatic *in vitro* OA model.

2. Materials and Methods

Sixteen healthy human hip cartilage explants (8 mm diameter) were harvested from 80 yo female (fractured hip). Half thickness focal defects were created on 8 samples using a scalpel. Both the intact and defect samples were loaded for 7 days using a dynamic loading bioreactor (10% unconfined compression at 1 Hz, 1 hr on - 1 hr off - 1 hr on). On days 1, 3, 5 and 7 of loading, one sample per group was fixed, sectioned and stained with Safranin-O. Glycosaminoglycan (GAG) content was measured using digital densitometry [3].

3D FE models of both defect and intact samples were created in Abaqus, based on the geometry and histological information of the samples before loading. A fibril-reinforced poro-elastic material [3, 4] was used, with model parameters characterized using experimental loading data and inverse FE analysis. One cycle of unconfined compression (10%, 1 Hz) was applied to the model and the localization of MSS and experimental GAG loss was compared.

3. Results

The location of the experimental GAG loss around the crack after day 7 of loading matched the simulated location of MSS in a defect

sample (Figure 1), which was greater than the value of MSS at the same location of intact sample model.

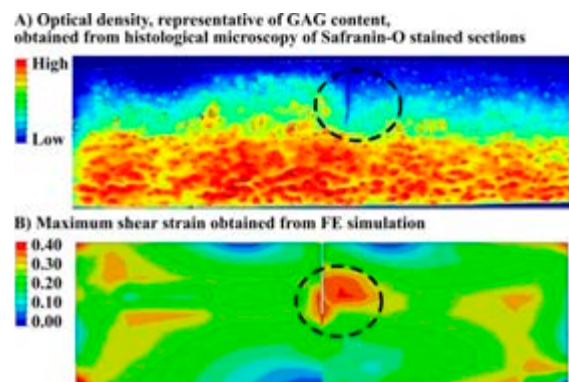


Fig 1: Comparison of A) localized GAG loss around the crack of a defect sample after 7 days of loading (blue zone in the circled area) and B) high MSS in FE simulation of a defect sample (red zone in the circled area).

4. Discussion and Conclusions

The results suggest that the greatest simulated MSS occurs in experimentally measured GAG loss locations. Therefore, FE simulation-based MSS is a valid parameter for adaptive FE models to predict the defect-related changes in localized cartilage degeneration upon mechanical loading.

5. References

1. Alizai et al, Musculoskeletal Radiol, 23, 2019.
2. Elahi SA et al, Front Bioeng Biotech, 9, 2021.
3. Ebrahimi M et al., bioRxiv, 2022.
4. Elahi SA et al, J Mech Behav Biomed Mater; 124, 2021.

Acknowledgements:

This work was supported by Marie Skłodowska Curie Individual Fellowship (CREATION project: MSCA-IF-2019-893771) and KU Leuven Happy Joints project (C14/18/077).



FLUID SHEAR STRESS ON OSTEOCYTE UNDER ULTRASOUND STIMULATION: FINITE-ELEMENT MODEL

Cécile Baron (1), Elise Doveri (2), Philippe Lasaygues (2), Carine Guivier-Curien (1)

1. Aix-Marseille Univ, CNRS, Centrale Marseille, IRPHE UMR 7342, Marseille, France;

2. Aix-Marseille Univ, CNRS, Centrale Marseille, LMA UMR 7031, Marseille France.

1. Introduction

Ultrasound (US) stimulation of bone remodeling remains an open question as the underlying mechanisms involved are still poorly understood. Among the possible hypotheses, the propagation of ultrasonic waves in bone tissue could generate acoustic streaming (AS) resulting in fluid shear stress exerted on the wall of osteocytes known as the mechanosensitive conductors of bone remodeling. Osteocytes are dendritic cells, ubiquitous in the bone extra-cellular matrix (ECM) forming a complex micrometric 3D network called the lacuno-canalicular network (LCN). A first finite-element (FE) model is proposed to investigate the effect of US stimulation on a network of 3 osteocytes aligned in the thickness of an osteon, surrounded by a fluid layer and embedded in a rigid ECM. The influence of a wavy ECM/fluid interface [1] on the wall shear stress (WSS) level is considered.

2. Materials and Methods

In order to implement relevant boundary conditions, we focus on an osteon unit delimited by the cement line (C line) as the outer boundary and the Haversian canal (H canal) as the inner one. Between these two boundaries, we consider a network of 3 osteocytes whose cell body is housed in an ellipsoidal lacuna and connected by one process inside a canaliculus full of fluid considered as salt water at 37°C. A 2D axisymmetric FE model is implemented on Comsol Multiphysics (v. 6.0) to estimate the WSS at the osteocyte surface induced by the AS in the fluid [2]. The boundary conditions are summarized in Table 1. A first order oscillating velocity \mathbf{U}_1 is imposed normal to the ECM/fluid interface to model a harmonic acoustic wave at frequency f of 1 MHz with an amplitude of displacement d_0 equal to 0.4 nm. Two geometries of canaliculus are compared:

straight and wavy.

	Laminar flow	Acoustics
Cement line	Wall (no slip)	Wall (no slip)
H canal	Open boundary	Z continuity
ECM/Fluid	Wall (no slip)	$\mathbf{U}_1(\omega) = i\omega d_0 \mathbf{e}_r$
Fluid/cell	Wall (no slip)	Z continuity

Table 1: Boundary conditions. Z: normal acoustic impedance; $\omega=2\pi f$.

3. Results

The geometry of the canaliculus has a strong influence on the WSS values and spatial pattern (Fig. 1).

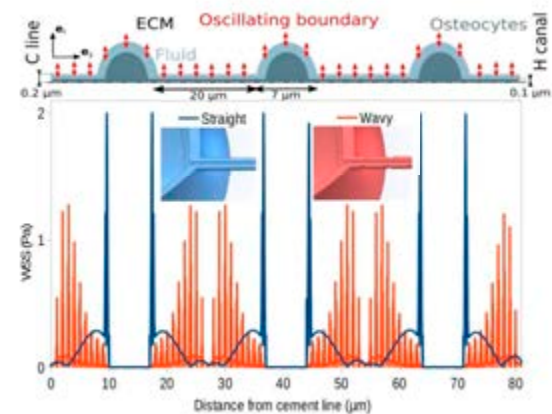


Figure 1: WSS along the wall of the 3 osteocytes.

4. Discussion and Conclusions

This preliminary study shows that, whatever the canaliculus geometry, harmonic ultrasound stimulation can induce WSS level greater than 0.8 Pa, known as the physiological threshold to trigger bone remodeling [3]. Moreover, the model can be improved by integrating the osteocyte elasticity and by adding processes.

5. References

- McNamara L et al. Anat. Rec.; 292(3):355-363 (2009).
- Muller P et Bruus H, Phys. Rev. E; 90(4):043016 (2014).
- Weinbaum S et al., J. Biomech; 27(3):339-360 (1994).



BIOMECHANICS OF VISCERAL PAIN: UNDERSTANDING AND MODELING PERITONEAL ADHESIONS.

Madge Martin*, Thibault Lemaire

CNRS, Univ Paris Est Creteil, Univ Gustave Eiffel, UMR 8208, MSME, F-94010 Créteil, France

*madge.martin@u-pec.fr

1. Introduction

Peritoneal adhesions are pathological fibrotic connections forming between organ surfaces. They typically follow a surgical procedure of the thorax, abdomen or pelvis, or result from inflammatory diseases and can cause small bowel obstruction, chronic pain or infertility. Nowadays, despite a lack of awareness in patients and surgeons, adhesions are now identified as a major economic and health burden. However, the strongest obstacle remains the poor understanding of underlying mechanisms of tissue physiological repair and adhesion formation [1]. Moreover, the role of biomechanics is critical to provide better understanding, prevention and treatments for peritoneal adhesions, especially regarding pain management. Indeed, nociception and mechanics are highly connected [2]. We present a novel and first model of peritoneal adhesions which depicts the main biochemical mechanisms associated with adhesion formation and their mechanical consequences.

2. Materials and Methods

We propose here a 2D model of adhesion formation representing the volume \mathcal{B} between the peritoneal serosa $\partial\mathcal{B}_p$ and the tissue boundary $\partial\mathcal{B}_t$, where the following mechanisms occur: (i) the formation of the fibrin exudate upon tissue insult, (ii) FB-mediated fibrosis and (iii) typical cyclic loading simulating breathing. We implemented a system of partial differential equations depicting the time- and space- dependent evolution of fibrin (F_n), tPA (t_{PA}) and FB (b) concentrations, accounting for fibrin-mediated chemotaxis of FB (sensitivity χ) in volume \mathcal{B} :

$$\frac{\partial}{\partial t} \begin{matrix} b \\ F_n \\ t_{PA} \end{matrix} = \nabla \cdot \begin{bmatrix} \mu_{Fb} \nabla b - \chi b \nabla F_n & b \\ D^{F_n} \nabla F_n & -\mathbf{d} \cdot F_n \\ D^{t_{PA}} \nabla t_{PA} & t_{PA} \end{bmatrix}, \quad (1)$$

where $\mathbf{d} = [a_b, d_{F_n}, d_{t_{PA}}]$ accounts for FB apoptosis \mathcal{A}_b , fibrin (d_{F_n}) and tPA degradation ($d_{t_{PA}}$). The time-derivative of the collagen content c depends linearly on FB activity and collagen degradation. Boundary conditions and material properties are Outside the injury, the coagulation factor tPA is set to a constant flux $\phi_{t_{PA}}^0$ to account for the action of MCs and decreased to 1% $\phi_{t_{PA}}^0$ for a pathological repair.

3. Results

Figure 1 depicts FB seeding into the fibrin exudate, producing collagen. The lines mark the bounds of collagen-rich volumes in adhesive and healthy repairs, respectively (threshold $c \geq 100 \mu\text{g}/\text{mg}$, for dense adhesions). In the case of a healthy repair, the inhibition of fibrin by tPA-mediated fibrinolysis prevents formation of the dense connective tissue (white), thus preserving the mechanical behaviour of the system.

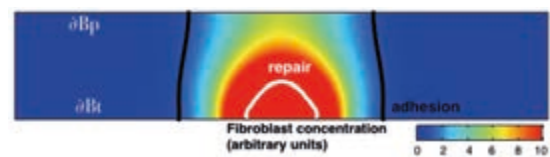


Figure 1: Fibroblast concentration 10 days after tissue trauma, resulting in an adhesive bond (black) or repair (white) depending on fibrinolytic activity.

4. Discussion and Conclusions

This is the first attempt to quantify the mechanisms of adhesion formation. We successfully depicted the main events following tissue trauma. Future work will investigate the next remodelling steps, in particular involving innervation and *in vivo* mechanical stimulation.

5. References

- Hassanabad et al., Biomed; 9(8):867 (2021).
- Feng et al., J Neur Trans; 127(4):415–429 (2008).



SPATIAL AND TEMPORAL WALL SHEAR STRESS DYNAMICS IN EMBRYONIC CHICK HEART AND VASCULATURE ANATOMIES

Kirsten Giesbrecht (1), Simone Rossi (1), Michael Bressan (2), Boyce Griffith (1)

1. Department of Mathematics, University of North Carolina at Chapel Hill, Chapel Hill, NC, USA; 2. Department of Cell Biology and Physiology, University of North Carolina at Chapel Hill, Chapel Hill, NC, USA;

Corresponding author: Kirsten Giesbrecht, kirsteng@live.unc.edu

1. Introduction

Intracardiac fluid factors contribute to heart development, but their mechanosensory role remains poorly understood in cardiogenesis. Altered blood flow can cause defects to arise in the developing heart [1]. Establishing typical temporal and spatial wall shear stress (WSS) patterns throughout the embryonic heart and supporting vasculature is critical to distinguishing pathogenic hemodynamics. Yet, due to the constant pumping and small size of the embryonic heart, WSS cannot easily be measured *in vivo* [2]. We've developed a novel protocol to model blood flow through chick anatomies using the finite element method to reveal precise intracardiac WSS patterns across four heart development stages.

2. Materials and Methods

Chick embryos staged HH16-HH21 were imaged using light-sheet fluorescence microscopy, segmented and meshed. Using the finite element method, we model blood flow through the anatomies described by Eq. 1 and Eq. 2, where p and u are the fluid pressure and

$$\rho \frac{Du}{Dt} + \nabla p - \mu \nabla^2 u - f = 0 \quad (1)$$

velocity fields, respectively. We impose pulsatile pressure driven flow in the inflow and

$$\nabla \cdot u = 0 \quad (2)$$

no slip conditions on vessel walls.

3. Results

The resultant WSS is shown in Fig. 1 during peak flow, deceleration, and minimum flow.

4. Discussion and Conclusions

This is the first computational study examining

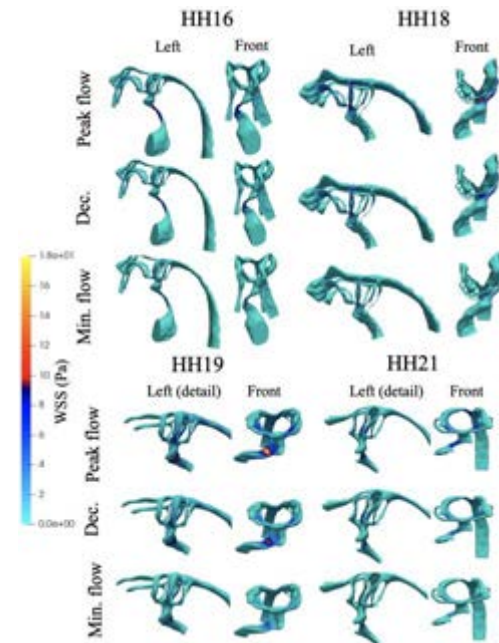


Figure 1: WSS during peak flow, deceleration, and minimum flow from HH16-HH21.

WSS spanning stages HH16-HH21 to include the heart, aortic arches, and dorsal aorta. Peak WSS in HH16 and HH19 occurs in regions that remodel in the subsequent stages HH18 and HH21, respectively, consistent with previous studies [3]. Finally, WSS is elevated in both the aortic arches and heart, which is typically lost on most models with smaller fluid domains.

5. References

1. Menon V et al., J Cardiovasc Dev Dis; 2(2):108-124 (2015).
2. Courchaine K et al., J Cardiovasc Dev Dis; 6(1):11 (2019).
3. Kowalski W et al., PLoS One; 8(3): e60271 (2013).

Acknowledgements:

This research is funded by the American Heart Association Predoctoral Fellowship (# 899419).

MATRIX DEPENDENT EMERGENCE OF BIOFILM STRUCTURE

Tom E. R. Belpaire (1), Jolien Meesters (2), Bram Lories (2) Hans P. Steenackers (2) Bart Smeets (1)

1. Division of Mechatronics, Biostatistics, and Sensors, KU Leuven, Belgium; 2. Centre for Microbial and Plant Genetics, KU Leuven, Belgium

1. Introduction

Biofilms are multicellular communities of bacteria, often engulfed in a self-produced matrix of extracellular polymeric substances (EPS) [1]. Biofilm EPS is notorious for providing mechanical support and serving as a physical barrier against external threats, complicating both the chemical and mechanical eradication of biofilm bacteria [2]. Although the protective effects of biofilms are rather well-studied, how these effects emerge from the production of single bacteria remains challenging [3]. In this work, we study the emergence of structure and the ensuing protective effects of *Salmonella enterica* Typhimurium biofilms with genetically engineered varying levels of EPS production.

2. Materials and Methods

We adopt an interdisciplinary research strategy combining agent-based models of biofilm formation in combination with structural analysis through microscopy. We model biofilm formation through bacterial growth after colonization of the substrate (Fig. 1). EPS is represented as cell-cell viscosity γ and adhesion w . As such, they modulate active extensile stress $\sigma_a = \frac{\gamma L}{t_{div}}$ and adhesive stress $\sigma_w = \frac{w}{L}$, respectively. With L the length of the bacteria, t_{div} the time between bacterial divisions. The final biofilm structure is characterized by cell-cell alignment and local cell density.

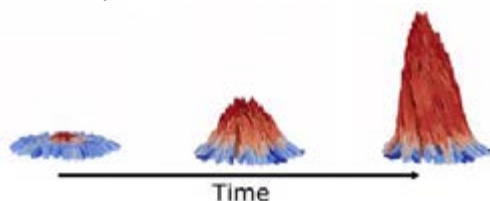


Figure 1: Temporal progression of the agent-based model. Bacteria are colored with respect to their alignment in the direction perpendicular to the surface.

3. Results

We find that both the active extensile and adhesive stress can modulate both the cell-cell alignment and local cell density (Fig. 2). Comparison with empirical biofilm structures indicates that upregulation of matrix production mainly corresponds to an increase in active extensile stress.

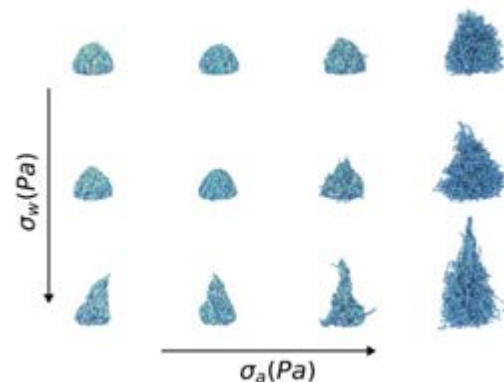


Figure 2: Structural changes in function of active extensile stress σ_a and adhesive stress σ_w .

4. Discussion and Conclusions

In contrast to the current paradigm that increased matrix production increases the protective effects of biofilm formation, our result indicates that increased matrix production can decrease the local cell density of the biofilms and consequently the protective effect.

5. References

1. Costerton, J. W. et al., Microbial biofilms. *Annu. Rev. Microbiol.* 49, 711–745 (1995).
2. Stewart, P. S. Antimicrobial Tolerance in Biofilms. *Microbiol. Spectr.* 3, 269–285 (2015).
3. Hartmann, R. et al. Emergence of three-dimensional order and structure in growing biofilms. *Nat. Phys.* 15, 251–256 (2019).

Acknowledgements:

The authors would like to thank the KU Leuven (Grant no: C14/22/077) for providing financial support to this project.



A MULTISCALE MODEL OF VASCULAR GROWTH AND REMODELING INCLUDING NOTCH SIGNALING

Jordy van Asten (1), Marcos Latorre (2), Cansu Karakaya (1), Frank Baaijens (1), Cecilia Sahlgren (1,3), Tommaso Ristori (1), Jay Humphrey (4), Sandra Loerakker (1)

1. Department of Biomedical Engineering, Eindhoven University of Technology, the Netherlands; 2. Center for Research and Innovation in Bioengineering, Universitat Politècnica de València, Spain; 3. Faculty of Science and Engineering, Biosciences, Åbo Akademi, Turku, Finland; 4. Department of Biomedical Engineering, Yale University, New Haven CT, USA

1. Introduction

Blood vessel growth and remodeling (G&R) is affected by mechanical stimuli. Most computational models include this behavior phenomenologically and do not consider underlying cellular mechanisms [1]. Therefore, they do not allow for studying mutations or interventions that involve these mechanisms. Notch is a key cell-cell signaling pathway in vascular health and disease. It is known to be mediated by strain [2], making it a potential key player contributing to mechano-regulated G&R. Here, we integrated Notch in a G&R framework to reveal its role in vascular G&R and to study Notch interventions to inspire treatment options and advance regenerative medicine.

2. Materials and Methods

A Notch model [2] was coupled to a constrained mixture (CMM) model [1]. The Notch model involved a system of ODEs that describe interactions between receptors and ligands on vascular smooth muscle cells (VSMCs). The CMM modeled the vascular wall as a mixture of elastin, collagen, and VSMCs whose turnover was captured with constitutive equations. Stresses and strains were calculated with Laplace's law and Neo-Hookean and Fung-type material models. Notch activity informed collagen production and VSMC proliferation based on *in vitro* data. A phenomenological contribution was included to account for the turnover due to mechanisms other than Notch.

3. Results

The simulations showed that our model could capture the increase in thickness, collagen content, and VSMC content observed in a hypertensive artery [3] (Fig. 1). Our model further predicted that external Jagged ligands

primarily affected G&R in hypertension in the short term. An increase in VSMC content and a decrease in collagen content was found for soluble ligands, and an opposite response for immobilized ligands (Fig. 1).

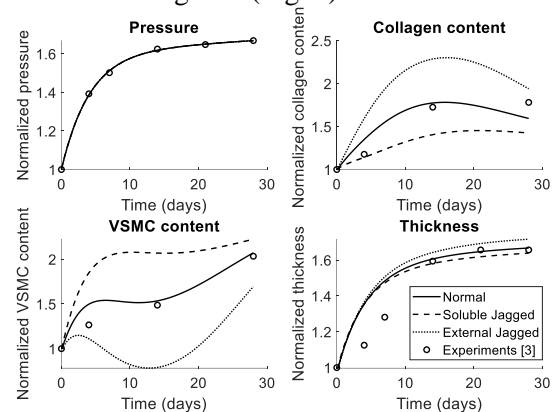


Figure 1. Predicted time course of vascular adaptation to imposed hypertension

4. Discussion and Conclusions

Our multiscale model provides a tool for studying the role of Notch in arterial G&R. Simulations suggest that Notch can contribute to hypertensive growth, mainly by promoting VSMC proliferation, but that other factors are needed to fully capture remodeling. Targeting Notch may provide a way to control vascular G&R and thereby improve vascular regeneration or inspire new treatment strategies.

5. References

- Humphrey, JD et al. *Math Models Methods Appl Sci*, 12(3):407-430 (2002).
- Loerakker, S et al. *PNAS*, 115(16):E3682-E3691 (2018).
- Bersi, M et al. *J R Soc Interface* 14:20170327 (2017).

Acknowledgements:

Funding was received from the European Research Council (Grants 802967 and 771168).

INVESTIGATION OF THE MECHANOBIOLOGICAL REGULATION OF BONE REGENERATION WITHIN SCAFFOLDS IN LARGE BONE DEFECTS COMORBID WITH TYPE 2 DIABETES

Mahdi Jaber (1), Daniela. B. Dias (1), Patrina. S.P.Poh (1), Georg N.Duda (1), Sara Checa (1)

1. Center for Musculoskeletal Biomechanics and Regeneration (Julius Wolff Institute), Charité –
Universitätsmedizin Berlin, Berlin, Germany

1. Introduction

The treatment of large bone defects remains a clinical challenge which gets even more challenging when comorbid with Type 2 Diabetes (T2D). T2D is a metabolic disease known is associated with reduced bone regeneration. Scaffolds have a high potential in the treatment of large bone defects [1]; however, the mechanobiological mechanisms behind bone regeneration within scaffolds in T2D remains largely unknown. This study aims to investigate the mechanobiological regulation of bone regeneration within scaffolds in a large bone defect comorbid with T2D.

2. Materials and Methods

An *in silico* approach that combined finite element (FE) analysis, to determine the mechanical environment, and agent-based models (ABM), describing the biological processes, was used to investigate the bone regeneration within the scaffold in healthy and T2D rats [2]. Gyroid scaffolds were inserted into a large bone defect in a rat femoral osteotomy model (Fig. 1), replicating an experimental setup. Scaffold pores were initially filled with granulation tissue, while PCL material properties were assigned to the scaffold. In the FE models, the T2D was under higher external mechanical loading (healthy: 325 g; T2D: 560 g of body weight). In the ABM, cellular activity in healthy was described using previously described models [3] while in T2D several cellular activities were altered according to findings reported in the existing literature.



Figure 1: CAD model of the rat femur large bone defect filled with a gyroid scaffold and stabilized with a plate.

3. Results

Mechanical strains were higher in the T2D model (Fig. 2). The healing outcome was substantially different between the healthy and T2D. In the healthy case, the bone formed at the walls of the scaffold, similar to *in vivo* observations while the T2D model showed reduced bone formation comparing well with the *in vivo* data (Fig. 2)

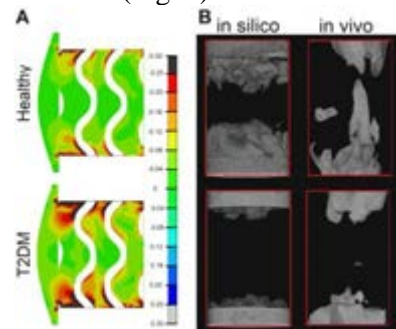


Figure 2: Healthy vs T2D: A) Minimum Principal strains within scaffold pores. B) MicroCT images of regenerated bone

4. Discussion and Conclusions

In Silico results could explain the reduced bone regeneration in T2D within scaffolds as observed *in vivo*. This is in accordance with experimental studies showing reduced healing outcomes in T2D. Future studies will focus on further validating the developed model and the optimization of the scaffold design.

5. References

1. Werner, M et al., *Advanced science*, 2017
2. Perier-Metz et al, *Front. Bioeng. Biotechnol* 2020
3. Checa S et al., *J Biomech*, 2011.

Acknowledgements:

This study was funded by the BMBF, SymBod project 01ZX1910A



MECHANOBIOLOGICAL INFLUENCE OF FIXATION DEVICES ON THE DYNAMIC MANDIBULAR BONE HEALING PROCESS

Vincenzo Orassi (1), Carsten Rendenbach (2), Sara Checa (1)

1. Berlin Institute of Health at Charité – Universitätsmedizin Berlin, Julius Wolff Institute, Germany; 2. Department of Oral and Maxillofacial Surgery, Charité – Universitätsmedizin, Berlin, Germany

1. Introduction

Titanium load-sharing fixation devices are the gold standard in the treatment of mandibular fractures. Recently, new biodegradable materials, e.g. magnesium alloy WE43, have been investigated to overcome titanium limitations [1]. However, due to lower mechanical properties, whether these alternative materials can support mandibular fracture healing remains unknown.

This study aims to investigate the mechanobiological effects of magnesium WE43 fixation devices on the mandibular fracture healing process.

2. Materials and Methods

A 3D finite element model (FEM) of a mandibular body fracture fixated with two parallel miniplates was developed. Material properties of titanium, magnesium WE43, and PLA were assigned to the implants, while granulation tissue properties were assigned to the callus. Physiological muscle forces were applied to simulate unilateral biting (Fig. 1).

Iteratively, the FEM was coupled with a 3D agent-based model (ABM), in which cellular processes, such as migration, proliferation, apoptosis, and differentiation within the callus were simulated according to previously established mechanoregulation rules [2].



Figure 1: Bone healing model: (left) FEM with boundary conditions; (right) ABM with cellular phenotypes and activities.

3. Results

Post-surgery, strains within the healing region induced by titanium, magnesium, and PLA fixation were between 0.03-0.5%, 0.05-0.9%, and 0.4-4.7%, respectively. At day 42, similar bone regeneration was predicted using titanium and magnesium devices, while fibrous tissue formation was predicted using PLA devices (Fig. 2).

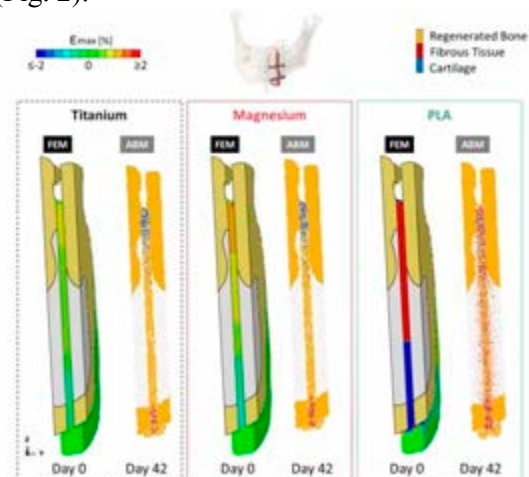


Figure 2: Bone healing model predictions for the different materials (sagittal view of the callus).

4. Discussion and Conclusions

The results of this *in silico* study suggest that magnesium WE43 fixation induced a similar amount of new bone formation compared to clinically-used titanium, thus, it seems able to support the healing process. Future studies will aim to optimize plate design toward an enhanced healing outcome.

5. References

1. Rendenbach et al., Mater. Sci. Eng., 2021.
2. Claes LE, Heigele CA., J. Biomech., 1999.

Acknowledgements:

EU Horizon 2020, InterLynk (grant agreement H2020-NMBP-TR-IND-2020, project ID 953169).



EXPERIMENTAL CALIBRATION OF AN *IN SILICO* MECHANO-BIOLOGICAL MODEL OF BONE HEALING INFLAMMATORY RESPONSE WITH THE SUPPORT OF GENETIC ALGORITHM

Edoardo Borgiani (1,2), Gabriele Nasello (2), Liesbet Geris (1,2)

1. Biomechanics Research Unit, GIGA In Silico Medicine, University of Liège, Belgium;
2. Prometheus, division of Skeletal Tissue Engineering, KU Leuven, Belgium.

1. Introduction

Bone fracture healing is a convoluted process that develops at multiple levels (tissue, cellular, molecular); therefore, using *in silico* multiscale modeling is highly appreciated to investigate its mechano-biological regulation. However, while numerous computer models have been developed to study the repair and remodeling phases of the process, only a few include also the initial inflammatory stage [1]. COMMBINI (COmputational Mechano-biological Model of Bone Injury Immunoresponse) aims to fill this gap as it will simulate mechanical and biological processes that occur within the bone fracture since the initial recruitment of inflammatory cells. We expect to obtain intriguing insights on novel treatments and therapeutics that might enhance the healing of the fracture from the first moments post-injury.

2. Materials and Methods

COMMBINI uses an agent-based model [2] to reproduce biological events that happen at the molecular (pro- and anti-inflammatory cytokines) and cellular level (macrophages) in a 7 mm osteotomy performed in mice, iteratively simulated within a span of three days post-operation. The multiscale interactions are regulated by *in vitro* parametric values found in the literature (e.g. [3]), which we propose to calibrate with *in vivo* immunofluorescent images [4]. The model is calibrated in two steps: sensitivity analysis, followed by evolutionary parametric optimization. Sensitivity analysis is performed on the *in silico* model parameters to evaluate the ones that primarily impact the quantitative outputs of the simulations. The evolutionary optimization employs a genetic algorithm (developed in-house with Python) to assess the combination of values that led the model outputs to a scenario more similar to the experimental one.

3. Results

The model showed a strong sensitivity over the number of total macrophages to variations in the value of proliferation ratio, recruitment factor and debris engulfment. In particular, when optimization is performed over the proliferative parameter, the genetic algorithm converges to a lower ratio ($\hat{k}_p = 5.34 \cdot 10^{-4} \text{ min}^{-1}$) than the one found in literature ($8.33 \cdot 10^{-4} \text{ min}^{-1}$ [3]) (Fig. 1).

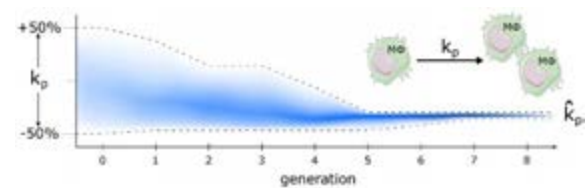


Figure 1: The genetic algorithm calibrates the model by converging to the optimal value for macrophage ($M\Phi$) proliferation ratio (\hat{k}_p).

4. Discussion and Conclusions

COMMBINI is a novel multiscale *in silico* tool to explore the early stages of bone fracture healing. The agent-based model capacity to represent each single immune cell as a single entity allows the calibration with the support of experimental immunofluorescent images. Currently, the model is calibrated with quantitative *in vivo* data; however, it is planned to calibrate according to cell spatial distribution within the callus. Moreover, the coupling of COMMBINI with a mechanical model (finite element analysis, in development) will expand the investigation to mechano-regulated aspects during the inflammatory stage of bone healing.

5. References

1. Lafuente-Gracia & Borgiani et al., Front Bioeng Biotechnol. 2021; 9:703725.
2. Ghaffarizadeh et al., PLoS Comput Biol. 2018; 14(2):e1005991.
3. Chitu et al., Curr Protoc Immunol. 2011; 14.
4. Schlundt et al., Bone. 2018; 106:78-89.

A HYBRID MODEL OF ORGANOIDS MORPHOGENESIS

**Daniel Camacho Gómez (1), Ioritz Sorzabal Bellido (2), Carlos Ortiz de Solórzano Aurusa (2),
José Manuel García Aznar (1), María José Gómez Benito (1)**

1. Department of Mechanical Engineering, Multiscale in Mechanical and Biological Engineering (M2BE), Aragon Institute of Engineering Research (I3A), University of Zaragoza, Spain.; 2. Solid Tumors and Biomarkers Program, IDISNA, and CIBERONC, Center for Applied Medical Research, University of Navarra

1. Introduction

The question of how cells orchestrate their behaviors is crucial to understand morphogenetic processes and how they are formed. In this work, we present a method to simulate the morphogenesis of organoids with an agent-based model that integrates a data-driven algorithm based on artificial intelligence.

2. Materials and Methods

The physics-based model consists of a center-based lattice-free agent-based model that couples cell mechanical interactions and biological functions [1]. On the one hand, we consider that cells interact among themselves using pairwise potential functions in an adhesive repulsive manner. We also consider that cells interact with the extracellular matrix by means of a friction coefficient that represents the dynamic viscosity of the matrix. On the other hand, three decisive biological functions are considered. Thus, we incorporate a mathematical model to regulate cell proliferation. In addition, cells can enter into a quiescent state, in which they remain inactive during a period of time. Finally, cells can secrete fluid, which is modelled by another type of agents, namely particles. These particles represent the fluid and are responsible for the generation and enlargement of the lumen.

To coordinate the cell biological functions, we include a data-driven algorithm based on artificial intelligence that extracts information from the *in vitro* experiments and determine the data metrics used as target values for the simulations.

3. Results

To evaluate the potential of the methodology, we simulated the formation starting from a single cell of the cystic pancreatic tumor

organoid (Fig. 1). Thus, we reproduced the formation of the cystic organoids, coordinating the cell functions spatially and temporarily.

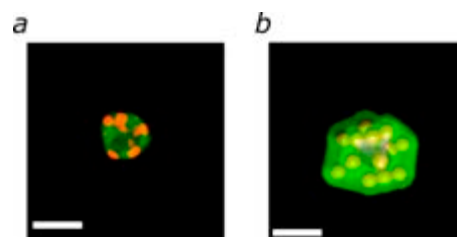


Figure 1: Simulation of cystic organoids. **a.** Snapshot of *in vitro* organoid. **b.** Snapshot of the simulated organoid. All scale bars are 30 μm .

4. Discussion and Conclusions

We presented an agent-based model that uses an artificial intelligence algorithm to unravel the coordination of cellular biological functions. This framework allowed us to simulate the formation of a cystic tumor organoid, understanding how cell functions coordinate.

5. References

1. Camacho-Gómez, D., García-Aznar, J. M., & Gómez-Benito, M. J. (2022). A 3D multi-agent-based model for lumen morphogenesis: the role of the biophysical properties of the extracellular matrix. *Engineering with Computers*, 1-15.

Acknowledgements:

This research was funded by MCIN/AEI/10.13039/501100011033 and ERDF A way of making Europe (Grant No. RTI2018-094494-B-C21, I.S.B., C.O.S.A., J.M.G.A., M.J.G.B.), the European Research Council (ICoMICS Adv grant agreement: 101018587, J.M.G.A., M.J.G.B.), and MCIN/AEI/10.13039/501100011033 and Next Generation EU (ProCanAid Grant No. PLEC2021-007709, D.C.G., J.M.G.A., M.J.G.B.).



POTENTIAL APPLICATIONS FOR MUSCULOSKELETAL MODELLING IN PATIENT CARE

Anna-Maria Liphardt (1)

(1) *Internal Medicine 3 & Deutsches Zentrum für Immuntherapie, Universitätsklinikum Erlangen & Friedrich-Alexander-Universität (FAU) Erlangen-Nürnberg, Erlangen, Germany*

Internal Medicine 3, Ulmenweg 18, 91054 Erlangen, Germany,

E-Mail: anna-maria.liphardt@uk-erlangen.de

S

Main factors shaping the human musculoskeletal system are mechanical loading-resulting from the interaction of our body with the environment and upright locomotion -and gravitational forces acting on the skeleton. Standardized immobilization models allow to investigate the effects of disuse on the skeleton *in vivo* without the presence of injury or disease (1). In immobilization of healthy individuals by bedrest or microgravity, deterioration of the musculoskeletal system is initiated within the first 24hrs of bedrest, and without exercise measures deterioration continues very rapidly (2-4). Musculoskeletal disease can directly degrade musculoskeletal tissue, for example by inflammation acting on the skeleton (5-7), but also results in immobility and unloading. This consequently affects the above-mentioned mechanical factors that shape our skeleton. Likewise, a predominantly seated lifestyle is characterized by lower rates of mechanical loading acting on the skeleton. Likely, in musculoskeletal disease effects of immobilization or disuse and pathological processes acting on the skeleton will accumulate and enhance musculoskeletal deterioration in diseases such as inflammatory arthritis (Figure 1).

On the other hand, simple task such as walking result in acute changes in metabolites of cartilage turnover and markers of inflammation that can be quantified in standardized experiment set-ups (8). This allows to quantify the “missing” stimulus for tissue turnover in immobilization and disuse.

This talk will present musculoskeletal adaptations to changes in the loading environment and disease and discuss the potential of musculoskeletal modelling

approaches to broaden the understanding of the interaction of disease, immobilization and treatment in inflammatory arthritis.



Figure 1: Interaction of factors affecting musculoskeletal health.

5. References

1. Bettis T et al., *Osteop Int.* 29(8):1713-20 (2018).
2. Baecker N et al., *J Appl Physiol.* 95(3):977-82 (2003).
3. Smith SM et al., *Annu Rev Nutr.* 34:377-400 (2014).
4. Frings-Meuthen P et al., *J Musculoskelet Neuronal Interact.* 13(1):45-52 (2013).
5. Kleyer A et al., *Ann Rheum Dis.* 73(5):854-60 (2014).
6. Andreev D et al. *Bone.*;162:116468 (2022).
7. Schett G. *Best Pract Res Clin Rheumatol.* 2017;31(1):53-8.
8. Herger S et al. *F1000Res.*;10:490 (2021).

Acknowledgements:

This project was supported by the German Space Agency (DLR e.V., Projekt 50WB2021) and Deutsche Forschungsgemeinschaft (DFG, German Research Foundation – SFB 1483 – Project-ID 442419336, EmpkinS).



“IN THE WILD” MOVEMENT ANALYSIS OF ARBITRARY MOTIONS

Anne D. Koelewijn (1), Marlies Nitschke (1), Sigrid Leyendecker (2)

1. *Machine Learning and Data Analytics Lab, Department Artificial Intelligence in Biomedical Engineering, Friedrich-Alexander Universität Erlangen-Nürnberg (FAU), Germany;*
2. *Institute of Applied Dynamics, Department of Mechanical Engineering, Friedrich-Alexander-Universität Erlangen-Nürnberg (FAU), Germany*

1. Introduction

Wearable sensors, most prominently inertial sensors, have recently enabled movement analysis “in the wild”, or outside of the lab [1,2]. These analyses allow researchers, coaches, or clinicians insights into the biomechanics of movements in the normal environment.

The main challenges when using inertial sensors are sensor noise and the resulting integration drift, which cause inaccuracies in joint angles. A number of approaches, e.g., Kalman filtering, have been proposed to overcome this drift. One such approach is to use optimal control to create reconstructive simulations of musculoskeletal (MSK) models. This approach allows for a full biomechanical analysis of the resulting simulation [2]. Here, the raw signals (acceleration and angular velocity) are used to avoid the integration drift, while the MSK model acts as a physical filter.

So far, this method was successfully applied to reconstruct running with a 2D musculoskeletal model [2]. Currently, we are investigating if this method is applicable to arbitrary movements, i.e., recordings where the performed movement is unknown. In this talk, we will provide an overview of the optimal control approach and discuss its advantages and challenges.

2. Materials and Methods

We create reconstructive simulations for 2D or 3D MSK models by solving optimal control problems. In these problems, we minimize a weighted objective of tracking error and effort. Tracking error is defined as the difference between measured and simulated accelerations and angular velocities [2]. Effort is estimated using the cubed muscular excitations.

To investigate the method for arbitrary motions, we measured running, curved running, and v-cut motions using inertial sensors and optical motion capture [3]. First, we reconstruct movements using noise-free virtual inertial signals, derived from the optical motion capture

recordings [3]. Then, we will create reconstructions from the measured inertial signals.

3. Results

Fig. 1 shows an exemplary simulation of a v-cut motion. The heading change in this simulation was 35°, while a 90° cut was performed in the experiment.

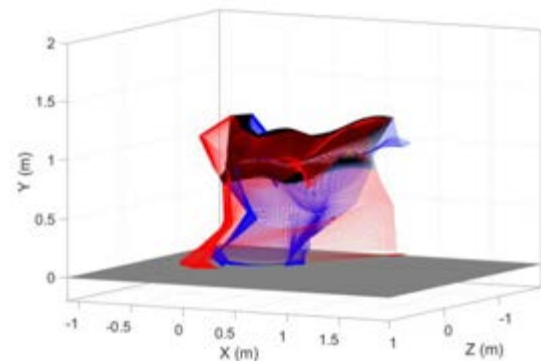


Figure 1 - Stick figures showing a reconstructive simulation of a 90° v-cut.

4. Discussion and Conclusions

Reconstructing arbitrary motions is challenging since we do not have information available to describe the task, e.g., using a periodicity constraint [2]. Therefore, the optimal control problem is not well-defined and optimization is difficult. Currently, we are investigating efficient problem descriptions that do not require a task definition. The task definition could also be derived from the measurements through other data analysis approaches.

5. References

1. Karatsidis A et al.. *Med Eng Phys*, 65: 68-77 (2019).
2. Dorschky et al.. *J Biomech*, 95: 109278 (2019).
3. Nitschke et al., *PeerJ*, in review (2022).

Acknowledgements:

This research was supported by the German Research Foundation (SFB 1483, Project-ID 442419336).



ON THE INCLUSION OF MOTION CAPTURE DATA IN OPTIMAL CONTROL SIMULATIONS OF THE HUMAN HAND

Simon Heinrich(1), Birte Coppers(1,2,3), Anna-Maria Liphardt(1,2,3), Sigrid Leyendecker(1)

(1) *Friedrich-Alexander Universität Erlangen-Nürnberg; Germany* (2) *University Hospital Erlangen; Germany* (3) *Deutsches Zentrum für Immuntherapie, Erlangen; Germany*

Simulations are a powerful tool for many research questions regarding the use of the hand in everyday life. Questions regarding ergonomic design and with clinical relevance, such as the effect of limited range of motion of the thumb are of interest as in [1], can be answered. Including motion capture data in these simulations would enable the analysis of specific human movement. Such data can further be helpful to generate feasible solutions and initial guesses for optimal control problem (OCP) simulations.

Including optical marker data in OCP simulations has originally been investigated in [2]. In that work, the effect of including optical motion capture data within the objective function versus their inclusion in the constraints for the optimization in the OCP simulation has been explored. Further, the effect of data reduction has been investigated, i.e., due to a reduced number of markers, or due to lower sampling rates. This study proposed that it is advantageous to include optical marker data in the constraints and that a data reduction results in inconsistent results, e.g., removing markers with important or unique information – such as markers on the fingertips for arm movements – had a strong influence on the results, while removing markers amid the kinematic chain of the arm did not influence the simulations considerably.

This work considers a torque driven rigid body model of the human hand. It is modelled with 33 degrees of freedom and each of its segments is scaled according to a personalized anthropometry. The joints are assumed to be ideal (infinitely rigid) and to have body fixed axes of rotation. The OCPs are solved by the direct transcription method discrete mechanics and optimal control for constrained systems (DMOCC), see [3]. Using this framework, we also obtain an integrator that can be used for

forward and inverse simulations. All of these simulations preserve the underlying geometric structure of the system as the discretized equations of motion are derived by a discrete variational principal.

In contrast to the model of the human arm during steering and throwing motions considered in [2], we now investigate the effect of optical marker data in the simulation of the model of the human hand with its high complexity in a small volume.

Additionally, there are many open questions regarding the choice of objective functions for the OCP of hand motion as well as regarding selection of relevant data. Other important questions concern which are the optimal parameters for the inclusion of data in relation to data accuracy.

We will be investigating these questions for the human hand. Most insights will be transferable to other musculoskeletal models.

References

- [1] Takahashi R, Miyata N, Maeda Y, Nakanishi Y.: Grasp synthesis considering graspability for a digital hand with limited thumb range of motion, *Adv. Rob.* 2021
- [2] Hoffmann R, Taetz B, Miezal M, Bleser G, Leyendecker S.: On optical data-guided optimal control simulations of human motion, *Multibody Syst Dyn* 2020
- [3] Leyendecker S, Ober-Blöbaum S, Marsden J. E, Ortiz M.: Discrete mechanics and optimal control for constrained systems, *Optim. Control Appl. Methods* 2009

Acknowledgements:

This work was supported by the German Research Foundation (DFG) under Grant SFB 1483 – Project-ID 442419336

Modeling and simulation of surface bone growth based on thermodynamic principles

Jean-François Ganghoffer¹, Ibrahim Goda²

¹LEM3 – Université de Lorraine – CNRS. 7, rue Félix Savart. 57073 Metz Cedex, France

²Université Bourgogne Franche-Comté, FEMTO-ST Institute, Département Mécanique Appliquée, 24 rue de l'Épitaphe, 25000 Besançon, France

E-mail addresses: jean-francois.ganghoffer@univ-lorraine.fr (J.-F. Ganghoffer), ibrahim.goda02@gmail.com; Ibrahim.goda@femto-st.fr (I. Goda)

Abstract

Unlike inactive systems, living biological systems have the advantage of being able to adapt to their environment through growth. Growth is a phenomenon unique to biological tissues, which is mainly driven by accretion processes, whereby new living tissues are added only on the surface of the growing body, due to the action of generating cells. The aim of this contribution is to develop a model for material accretion in the context of the thermodynamics of continuous media. A relation between the accretion velocity and a conjugated driving force based on Eshelby stress tensor is derived from the optimum condition of the zero thermodynamic potential. Numerical simulations are subsequently carried out in the biomechanical context of bone external remodeling to elucidate the apposition of bone mineral onto the surface of proximal femur sample subjected to physiological loads.

Keywords: *Surface accretion; Proximal femur; Eshelby stress; Bone external remodeling; Numerical simulations.*

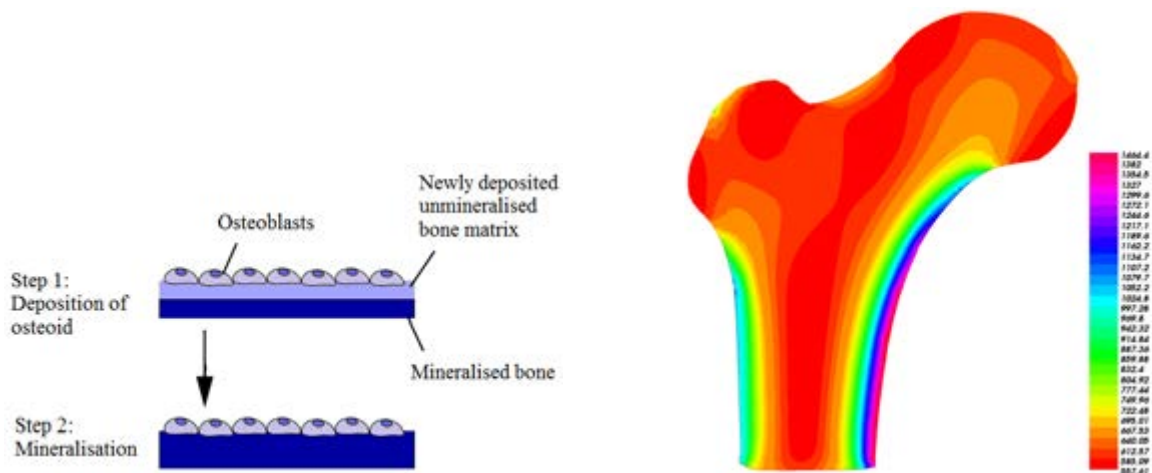


Figure 1: Schematic representation of the bone accretion process (left) and bone density distribution after 50-accretion timestep (right).



OSTEOARTHRITIS PATIENTS CLASSIFICATION BASED ON SUPPORT VECTOR MACHINES.

Maria Segarra-Queralt (1), Mar Galofre (1), Laura Tio (2), Jordi Monfort (2), Gemma Piella (1), Jérôme Noailly (1)

1. BCN MedTech, Spain; 2. IMIM, Barcelona, Spain

1. Introduction

Diagnosis of knee osteoarthritis (OA) is based on symptomatology, i.e. joint stiffness and pain. The latter is assessed through questionnaires such as the WOMAC which has a high level of subjectivity, because the ache is independent of image-based signs and is modulated by the patient's psychological status, in addition to biological factors [1]. Finding non-linear relations among data shall allow data-based prediction models in OA able to reduce the subjectivity in clinical decision-making. To this end, this study explores possible relationships among clinical and molecular data in a cohort of women diagnosed with OA, through a Support Vector Machine (SVM).

2. Materials and Methods

In SVM, each input patient data is divided into two known output categories in a feature, x_n , space regarding a hyperplane. [2] A Youden's test has been done in each classifier to find the best appropriate threshold value to classify binarily OA-related descriptors i.e., catastrophism (CA), depression (DE), effusion (EF), functionality (FU), joint pain (JP), rigidity (RI), sensitization (SE) and synovitis (SY). Women (n=51) with Kellgren-Lawrence grade 2-3 OA are further classified using eight combinations of the aforementioned features. Parallely, synovial liquid (SL) proteomic measurements from patients with effusion (n=25) are further used as input, i.e., IL-6, IL-8, IL-4, TNF- α , IL-18, INF- γ , IL-17, IL-1RA, and VEGF. The accuracy of the most influential feature (based on its relative weight (w_n) when classifying as lineal kernels are used) is then evaluated against AUC-ROC curves.

3. Results

Fig. 1 shows the importance of each feature for each classifier. Fig. 2 shows the ROC curves and AUC values for the most influential inputs (Fig. 1, black squares) based on w_n values.

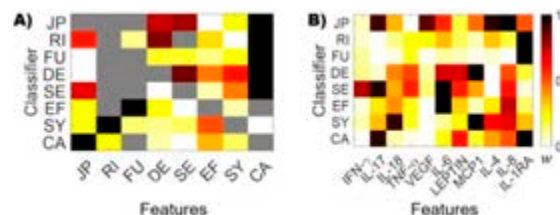


Figure 1: SVM with A) clinical data and B) SL data. Grey, omitted features.

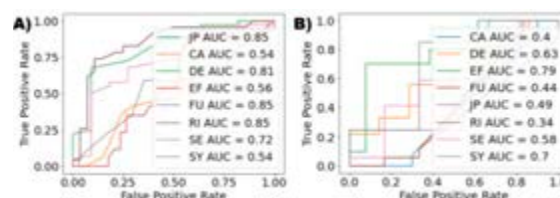


Figure 2: AUC-ROC curves for the most relevant input features of A) clinical data and B) SL.

4. Discussion and Conclusions

CA is the most influential parameter in classifying OA descriptors, Fig. 1A) and better discriminates WOMAC-derived descriptors (JP, FU and RI) in Fig. 2. Inflammation (SY and EF) is better classified by SL data (Fig.1,2 B), i.e., IL-6 and MCP1, emphasizing the role of innate immunity in OA. [3] IL-1RA looks influential, Fig. 1B), and has been studied as a possible regenerative treatment. [4] The use of SL information shall help identify new objective descriptors for OA diagnosis & treatment. These might allow to better understand the relative weight of the patient subjective measures (CA) and possible co-morbidities (DE) that strongly interfere with the diagnosis & decision-making.

5. References

- Schaible, HG. *Curr Rheumatol Rep.* 14, (2012).
- Vapnik, V. *Mach Learn* 20, (1995).
- Millerand, M. *OA and Car.* 28, (2020).
- Baltzer, A. *OA and Car.* 17, (2009).

Acknowledgements: Catalan & Spanish Governments (2020FI_b00680;STRATO-PID2021126469ob-C21-2), European Commission (MSCA-TN-ETN-2020-Disc4Ail-955735, ERC-2021-CoG-O-Health-101044828).



FEMORAL GROWTH PLATE STRESSES IN CHILDREN QUANTIFIED WITH A SEMI-AUTOMATED MULTI-SCALE MODELING WORKFLOW

Willi Koller (1), Basílio Gonçalves (1), Arnold Baca (1), Hans Kainz (1)

1. Centre for Sport Science and University Sports, University of Vienna, Austria

1. Introduction

A multi-scale workflow based on musculoskeletal simulations (MSK) and mechanobiological finite element (FE) analysis can be used to estimate growth plate loading and femoral growth trends [1,2]. Personalizing the model in this workflow is time-consuming and therefore previous studies included small sample sizes ($n < 4$) or generic FE models [3,4]. The aim of this study was to develop a semi-automated toolbox to perform this workflow and to quantify intra-subject variability in growth plate stresses in typically developing (TD) children and children with cerebral palsy (CP).

2. Materials and Methods

Magnetic resonance images (MRI) and three-dimensional gait analysis data of 13 TD children and 8 children with CP was analysed for this study. Muscle and joint contact forces were estimated with MSK simulations. A semi-automated workflow to create subject-specific FE models including femoral geometry, growth plate shape and location based on MRI segmentation was developed. Using muscle and joint contact forces from the MSK simulation as loading conditions, FE analysis were performed for all participants.

The growth rate due to mechanical loading was estimated for each element of the growth plate as the osteogenic index (OI) [5] quantified based on the obtained principal stresses from the FE analysis [1,2]. A colour scheme was used to visualize and compare OI values between participants. OI heatmaps were divided into five regions (Fig. 1a). Intra-subject variability was assessed with OpenCV's template matching and by comparing the region with highest mean values between the left and right side of each participant. Within groups, the regions with the highest mean value was identified.

3. Results

When comparing the left with the right growth plate of each participant, the highest OI value occurred at different regions in 30.8% ($n=4$) of

TD children and in 62.5% ($n=5$) of children with CP. Image comparison of the heatmaps showed significantly higher ($p < 0.01$) intra-subject variability in children with CP compared to TD children.

In 61.5% ($n=16$) of the TD femurs the highest OI value was observed in the posterior region of the growth plate followed by the medial region (27%; $n=7$). In children with CP the lateral (50%; $n=8$) followed by the posterior (31%; $n=5$) region were the areas with the most occurred maximum OI values (Fig. 1b).

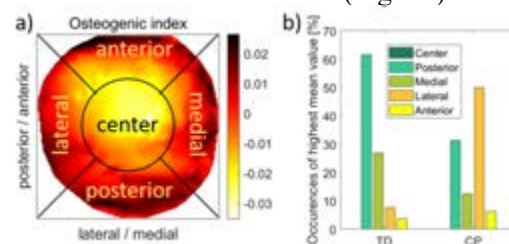


Figure 1: a) shows an example OI heatmap divided into five regions; b) shows the region with highest OI in TD and CP children.

4. Discussion and Conclusions

Intra-subject variability in growth plate stresses was higher in CP than in TD children, which could be caused by the higher variability in CP compared to TD gait. The observed different OI pattern in many children with CP compared to our TD children might be the reason for the development of femoral abnormalities, e.g. increased anteversion angle. Our simulation results can be used as reference values for further investigations. Furthermore, we will share our workflow with the community to enable peers to conduct mechanobiological growth studies with larger sample sizes and enhance our understanding of femoral growth.

5. References

1. Carriero et al, *Comp Meth Bio Bio Eng*, 14:253–262, 2011.
2. Kainz et al, *PLOS ONE*, 15:e0235966, 2020.
3. Yadav et al, *Med Eng & Phys*, S1350453321000217, 2021
4. Shefelbine et al, *Annals of Biomed Eng*, 32:297–305, 2004
5. Stevens et al, *J. Orthop Res*, 17: 646–653, 1999



THEORETICAL CONSIDERATIONS FOR PATIENT-SPECIFIC MODELLING BASED ON OBSERVABLE STATE VARIABLES

Gerard A. Ateshian (1), Courtney A. Petersen (1), Jeffrey A. Weiss (2)

1. Columbia University, United States; 2. University of Utah, United States

1. Introduction

One of the primary goals of the biomechanics of soft and hard tissues is the identification of mechanical factors that may lead to tissue failure in subject-specific populations. The ability to predict tissue failure prior to its occurrence can alter treatment strategies for specific individuals afflicted by well-understood pathologies. For example, it is common to use bone density measurements acquired from non-invasive imaging to assess the risk of bone fracture due to osteoporosis. Upon finding an elevated risk, subjects may be prescribed suitable medications to reduce the occurrence of bone fracture. The success of this standard of care became possible only because extensive *in vitro* biomechanical testing of trabecular bone samples demonstrated a very strong correlation between apparent bone density and failure strength (1).

Here, we address fundamental theoretical considerations that should guide biomedical engineers in the formulation of patient-specific computational modelling strategies, based on imaging modalities.

2. Material Properties of Tissues

Fundamentally, properties of any material represent fitted coefficients in constitutive models that describe functions of state, such as the stress tensor σ , the heat flux vector q , the free energy density Ψ_r , etc. By definition, functions of state represent non-observable measures that appear in the governing equations of mechanics, such as the equations of conservation of mass, momentum, and energy, or the axiom of entropy inequality.

A constitutive model relates a function of state to state variables, such as the strain tensor, temperature, temperature gradient, and concentrations of constituents. Though the classical fields of mechanics rarely enforce this requirement strictly, in our recent theoretical studies we have emphasized that state variables

must always represent observable variables (2, 3). In practice, since we live in three-dimensional space and one-dimensional time, the only observable variables are length, area, volume and time, and measures that can be derived from them, such as force and strain.

3. Non-Invasive Patient-Specific Imaging

Non-invasive imaging modalities can only report observable state variables related to space and time. Most commonly, imaging modalities provide measures of tissue geometry. Other measures, such as bone density measurements, or sodium magnetic resonance imaging, represent measures of tissue composition. Diffusion tensor imaging provides a measure of tissue anisotropy. Ultrasound imaging may be used for measuring pulse wave velocity in various tissues.

4. Discussion and Conclusions

A fundamental theoretical constraint on patient-specific computational modelling is the inability to measure material properties non-invasively in individual subjects. The best strategy for patient-specific computational modelling is to perform extensive *in vitro* testing of tissue samples to relate their failure properties to observable measures that can be characterized from non-invasive imaging. We surmise that the concepts outlined here are intuitively understood by most investigators. A formal confirmation of the underlying theoretical reasons for these limitations may help guide the approach of investigators toward the resolution of this challenge.

5. References

1. Carter DR, Hayes WC. Science. 1976;194(4270):1174-6.
2. Ateshian GA, Kroupa KR, Petersen CA, Zimmerman BK, Maas SA, Weiss JA. J Biomech Eng. 2023;145(4).
3. Ateshian GA, Zimmerman BK. J Biomech Eng. 2022;144(4).

Acknowledgements:

National Institutes of Health (R01GM083925).

VERTEBRAL BODY TETHERING FOR IDIOPATHIC SCOLIOSIS: A PARAMETRIC FEM STUDY OF IMPLANT AND PATIENT FACTORS

Cooper Dickinson (1), Megan Roser (1), J Paige Little (1)

1. *Biomechanics & Spine Research Group, Centre for Children's Health Research, School of Mechanical, Medical and Process Engineering, Queensland Uni of Technology, Australia*

1. Introduction

Vertebral body tethering (VBT) is utilised to surgically manage adolescent idiopathic scoliosis (AIS) spinal deformity. A flexible tether applies tension to vertebral bodies on the convex side of the major structural curve, via vertebral screws inserted into the anterior vertebral body. The tether applies an asymmetrical tension-compression stress across the tethered spinal vertebrae in the immature spine, imparting a differential propensity for bone growth modulation. The current study sought to parametrically explore the effect of implant- and patient- factors on immediate post-op outcome.

2. Materials and Methods

A patient-specific FEM representing the osseoligamentous thoracolumbar spine and ribcage for a 10-year-old AIS patient was analysed. The patient's deformity was right-side major thoracic (T5-T12), and the FEM had previously been validated [1]. The PET tether was 2nd-order, linear elastic continuum elements ($E=800\text{MPa}$, $\nu=0.3$), connecting laterally oriented screw continuum elements ($E=108\text{GPa}$, $\nu=0.3$) across nonlinear intervertebral discs (IVD) (Annulus ground matrix: Mooney-Rivlin $C_{10}=0.7$, $C_{01}=0.2$; Collagen fibres: tension-only, $E = 500\text{MPa}$, $\nu=0.3$; Nucleus: Incompressible fluid). The L5 inferior endplate was fixed, and T1 laterally constrained. Implant/Tether factors: Segmental tether tension and tether diameter (ie. Stiffness) were modified (Table 1). Patient factors: To reflect age-related changes in fibre bundle morphology and IVD anatomy [2], collagen fibre stiffness and angle was modified to reflect varying IVD stiffness with age (Table 1). Predicted change in corrected Cobb angle and vertebral endplate stress was calculated.

Table 1: FEM parameters varied

Tether	Values
--------	--------

Tension*	200N, 350N** (mean clinically measured), 700N, 1050N
Diameter	4mm, 5mm **, 6mm
Patient	Values
Fibre stiffness	250MPa, 500MPa**, 600MPa
Fibre angle	15°, **30°, 45°, 60° (NB. 30±15°, mean for adult IVD)

* Max. force - Apical level; Based on intra-op measured tether forces; all other level-wise forces scaled according to intra-op measures, ** Baseline

2. Results

Increased tether tension resulted in increased Cobb angle correction, while increased tether diameter and fibre angle/stiffness resulted in decreased predicted correction for the baseline force condition. Increased collagen fibre stiffness showed minimal variation in vertebral endplate stress (no appreciable difference in propensity for growth modulation), and immediate post-op Cobb angle correction decreased (<1°). With increasing fibre angle, Cobb angle correction decreased (17%) and maximum tensile/compressive stress on the concave/convex endplates (respectively) increased (10%).

4. Discussion and Conclusions

Taken together, predicted results for vertebral endplate stress and deformity correction imply increasing tether tension may result in an improved post-op Cobb correction, but this may be dependent upon the individual patient's IVD properties, which are themselves age-related and varying with progressive IVD growth. The results of these analyses shed light on clinically observed VBT outcomes [3] whereby growth modulation is observed post-op, but not in all patients.

5. References

- Little JP, Adam, CJ, Spine, 34(2), (2009).
- Pickering et al., FrBioEngBiotech; 15(9), (2021)
- Roser M et al, ICORS2022 confrence, Edinburgh.

Endovascular aneurysm repair (EVAR) has become a standard treatment of abdominal aortic aneurysm (AAA), given that EVAR is associated with superior intraoperative outcomes and similar long-term survival compared with open repair. EVAR consists in implanting an endograft, or stent-graft (stent covered with an impermeable fabric) into the aneurysm sac through endovascular navigation, only requiring a small incision in the femoral artery. Once the stent-graft is successfully positioned and deployed, the impermeable fabric works as a pressure isolation barrier, preventing the transmission of systemic pressure to the weakened aneurysm wall. For this reason, shrinkage of the aneurysm sac is commonly accepted as clinical evidence for a successful EVAR. In this work, we propose to study the effects using numerical simulation. We set up a 3D finite-element model of post-EVAR vascular adaptation within an open-source finite-element code, which was initially developed for growth and remodelling (G&R). We modelled the endograft with a set of uniaxial prestrained springs that apply radial forces on the inner surface of the artery. Constitutive equations, momentum balance equations, and equations related to the mechanobiology of the artery were formulated based on the homogenized constrained mixture theory. We performed a sensitivity analysis by varying different selected parameters, namely oversizing and compliance of the stent-graft, gain parameters related to collagen G&R, and the residual pressure in the aneurysm sac. This permitted us to evaluate how each factor influences post-EVAR vascular adaptation. It was found that oversizing, compliance, or gain parameters have a limited influence compared to that of the residual pressure in the aneurysm sac, which was found to play a critical role in the stability of aneurysm after stent-graft implantation. An excessive residual pressure larger than 50 mmHg can induce a continuous expansion of the aneurysm while a moderate residual pressure below this critical threshold yields continuous shrinkage of the aneurysm. Moreover, it was found that elderly patients, with relatively lower amounts of remnant elastin in the arterial wall, are more sensitive to the effect of residual pressure. Therefore, these results show that elderly patients may present higher potential risk of aortic sac expansion due to intra-aneurysm sac pressure after EVAR than for younger patients.



IN-VIVO BILAYER MATERIAL YOUNG MODULI IDENTIFICATION UNDER SMALL DEFORMATION USING ONLY SUCTION

Nathanael Connesson (1), Yohan Payan (1), Noemie Briot (1), Pierre-Alain Barraud (1)

1. Univ. Grenoble Alpes, CNRS, UMR 5525, VetAgro Sup, Grenoble INP, TIMC, 38000 Grenoble, France

Email: nathanael.connesson@univ-grenoble-alpes.fr

1. Introduction

In vivo, patient specific and non-invasive mechanical characterisation of biological soft tissue is challenging, even under moderate quasi-static loading and small deformations. Among other technical solutions, suction-based devices enable the acquisition of experimental data under relatively well controlled boundary and loading situations. However, (i) the usual aspiration head design constraints drastically limit the number of used aspiration aperture diameter [1], (ii) the underlying tissues are often assumed to be homogeneous during inverse identification, and (iii) inverse identifications usually imply time-consuming postprocessing that hinders any clinical application. An original suction system and method is implemented as a step toward dealing with these limitations.

2. Materials and Methods

An original suction system is proposed based on volume measurements [2], which enable extreme customisation of the suction aperture shape and diameter. Cyclic partial vacuum (repeatability) was applied under small deformation using 9 suction cups of aperture diameters ranging from 4 to 30 mm both on silicone reference phantoms (with different upper layer thicknesses) and *in vivo* on the abdominal tissue of a healthy volunteer. Each cup extract tissue mechanical behaviour information integrated over about one diameter depth [3]. The tissue in-depth heterogeneity thus differently affects the pressure-tissue volume curves depending on the suction diameter.

A cost function was built to minimize the squared distance between the 9 experimental pressure-tissue volume curves with their simulated counterparts assuming a bilayer structure (two Neo Hookean layers) defined by three main parameters: the upper and lower

layer Young's Moduli and the upper layer thickness. A real time evaluation of the simulated pressure volume curves was implemented by interpolating a Finite Elements database so that these three parameters, including the upper layer thickness, minimizing the cost function were identified in less than one minute. The parameter identifiability was also evaluated.

The silicone reference mechanical properties were characterized during classical tensile tests. The silicone upper layers thicknesses were measured by annexe destructive measurement. The reference skin thickness of abdomen was measured using Bmode ultrasound imaging (natural contrast between the epidermis and fat).

3. Results

On a bilayer controlled silicone phantoms with superficial upper layer thickness of 3 mm, Young's moduli identified by suction and uniaxial tension presented a relative difference lower than 10%. Preliminary tests on *in vivo* abdomen tissue provided the skin and underlying adipose tissue Young's Moduli at 54 ± 1 kPa and 4.8 ± 0.1 kPa respectively. The skin upper thickness was of 2.21 ± 0.033 mm using Bmode ultrasound and 2.15 ± 0.05 mm using only suction data.

4. Discussion and Conclusions

The whole process results on controlled silicone phantoms were considered fully satisfactory. The identified Young moduli of skin and fat are in good accordance with literature data.

5. References

1. Luboz V *et al.*, Annals of biomedical engineering, 2014, 42(11):2369--2378
2. Elahi SA *et al.*, Journal of Mechanics in Medicine and Biology, 2018, 18(04):1850037
3. Zhao R *et al.*, Acta biomaterialia, 2011,7(3):1220--1227



STIFFNESS MATTERS: AN IMPROVED IN VIVO FAILURE RISK ASSESSMENT OF ASCENDING THORACIC AORTIC ANEURYSMS

Klaas Vander Linden (1), Emma Vanderveken (2), Amber Hendrickx (2), Lauranne Maes (1), Heleen Fehervary (1), Lucas Van Hoof (3), Filip Rega (3), Bart Meuris (3), Nele Famaey (1)

1. Biomechanics Section, Mechanical engineering, KU Leuven, Belgium

2. Department of Cardiovascular Sciences, KU Leuven, Belgium

3. Department of Cardiac Surgery, University Hospitals Leuven, Belgium

1. Introduction

Dissection and rupture are feared complications of an ascending thoracic aortic aneurysm (ATAA) related to mechanical failure of the wall. The aortic diameter is currently used to predict the risk of complications and to decide when to surgically resect the aneurysm. However, it has been shown that this criterion lacks accuracy [1]. To define better predictors, we performed a retrospective personalized failure risk analysis, including clinical, geometrical, histological and mechanical data of 30 patients.

2. Materials and Methods

For each patient, uniaxial tensile tests in both directions i were performed to determine the wall strength P_{ii}^s (i =circumferential, axial). Material parameters were fitted against *in vitro* planar biaxial data and *in vivo* pressure-diameter relationships at diastole and systole [2]. Using the resulting material properties and *in vivo* data, the maximal *in vivo* stress at systole P_{ii}^* was calculated, assuming a thick-walled axisymmetric geometry. The retrospective failure risk (Λ) was then defined as $\Lambda_{ii} = \frac{P_{ii}^*}{P_{ii}^s}$.

Three possible clinically accessible predictors were compared: the maximal diameter at systole (D_{sys}), the area-based distensibility coefficient ($DC_A = \frac{D_{sys}^2 - D_{dia}^2}{D_{dia}^2(p_{sys} - p_{dia})}$), and volume-based distensibility coefficient ($DC_V = \frac{V_{sys} - V_{dia}}{V_{dia}(p_{sys} - p_{dia})}$), with V_{sys} and V_{dia} the aneurysm volume at systole and diastole computed from the patient's 4D CT scan, and p_{sys} and p_{dia} the corresponding systolic and diastolic pressure, respectively. Logistic regression was performed and correlations were determined using the Spearman rank test.

3. Results

Figure 1 shows the failure risk Λ_{ii} in function of the studied clinically accessible predictors.

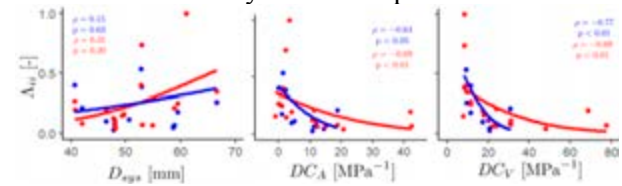


Figure 1: The failure risk Λ_{ii} in function of three different predictors (D_{sys} , DC_A , DC_V). Red and blue colours indicate the circumferential and axial direction, respectively. Solid lines represent the regression model. The correlation coefficients (ρ) with corresponding p-values are also shown. The solid lines show the predictions made by the logistic regression.

4. Discussion and Conclusions

By conducting a retrospective personalized failure risk assessment of ATAA patients, we were able to identify and compare clinically accessible aneurysm failure risk predictors. Figure 1 shows that mechanical predictors, *i.e.* the distensibility coefficients, outperform predictors based on geometrical features alone, *i.e.* the aortic diameter, in predicting wall failure. The volume-based DC has the best predictive power as it also takes the axial stretch into account. This study also shows clear evidence to include multiphasic scans in clinical practice when assessing the risk of aneurysm failure.

5. References

1. Pape *et al.* Circulation 2007; 116 (10) 1120-1127
2. Maes *et al.* J. Mech. Behav. Biomed. Mater. 2019; 94:124-135

Acknowledgements:

The authors would like to thank Research Foundation – Flanders (FWO) (Grants no: SB1SA9119N, SB1S56317) and KU Leuven (C2-ADAPT) for providing financial support to this project.

BIOMECHANICAL MODELING OF ABDOMINAL AORTIC ANEURYSM TOWARDS OBJECTIVE CLINICAL DECISION MAKING

T.Christian Gasser^{1,2}

1. KTH Royal Institute of Technology, Sweden; 2. University of Southern Denmark, Denmark

1. Introduction

Abdominal Aortic Aneurysm (AAA) disease [1], the local enlargement of the infrarenal aorta, is a serious condition that causes many deaths, especially in men exceeding 65 years of age [2]. Over the past quarter of a century, computational biomechanical models have been developed towards the assessment of AAA rupture risk [3], technology that is now on the verge of being integrated within the clinical decision-making process, see figure 1.

2. Materials and Methods

We performed a literature survey to summarize and critically discuss the individual biomechanical approaches to predict AAA rupture risk. The review examined the specific modeling assumptions and reports the outcome of clinical validation studies. Several refinements concern model individualization that goes beyond a patient-specific vessel geometry, as well as the use of probabilistic frameworks. First data from probabilistic biomechanical models indicate an improvement over the purely deterministic modeling of AAA rupture risk [4,5]. Whilst an isotropic elastic model that reflects the non-linearity of the AAA wall provides sufficiently accurate wall stress predictions, it is the strength of the aneurysmatic wall that requires much more attention.

3. Results, Discussion and Conclusions

AAA rupture is a localized event in the aneurysm wall, and the maximum diameter, the parameter used in the clinics to assess AAA rupture risk, is limited in its ability to effectively indicate risk. In contrast, a biomechanical model allows for the estimation of the wall's local mechanical loading, i.e. its risk of local rupture. However, little is known concerning the actual failure mechanisms of the diseased vessel wall. Fundamental aspects of fracture have not been explored and the most fundamental parameters in fracture mechanics, such as the fracture energy of the AAA wall are still unknown. In addition, many biomechanical models are not validated and therefore have not garnered significant clinician attention. A simulation model represents the real objective or process to the desired degree of complexity -- it should be guided by clinical needs rather than by integrating all available

(biomechanical) information to the given problem [6]. Recent developments utilizing Machine Learning [7] seems to be beneficial to better predict growth [8] and rupture [9] of AAAs; research results that need to be confirmed in larger clinical studies.

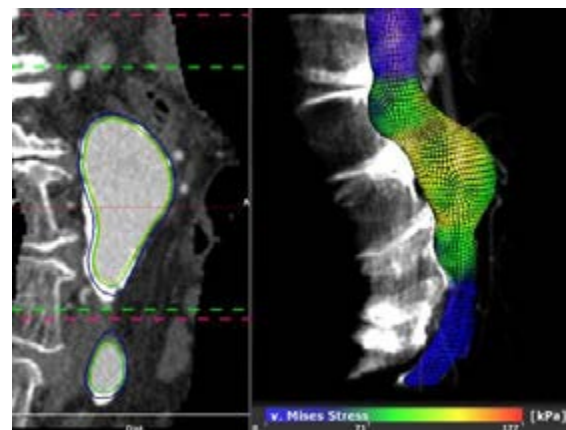


Figure 1: Patient-specific risk assessment of a small Abdominal Aortic Aneurysm (AAA) using A4clinicsRE software (Vascops GmbH, Austria). Left: Segmentation from Computed Tomography-Angiography images. Right: Predicted von Mises Stress in the AAA wall.

5. References

1. N Sakalihan, et al, Nature Reviews Disease Primers 4, 2018.
2. J Golledge, Nat. Reviews Cardiology 16, 2019.
3. TC Gasser TC et al, Int J Num Meth Biomedical Engrg 10.1002/cnm.3587, 2022.
4. S Polzer et al, J Vascular Surgery 2020; 71.
5. L Bruder, et al, PLoS ONE 2020; 15.
6. TC Gasser TC. Springer Nature 2021.
7. TK Chung et al, Applications in Engineering Science, 10, 2022.
8. M Lindquist Liljeqvist, et al. Sci. Rep. 11,10.
9. M Alloisio, et al. Eur. J. Vasc. Endovasc. Surg 63, e34-e35.

Acknowledgements:

Financial support through the project grant No 2020-04447 from the Swedish Research Council.

POROMECHANICAL MODELLING OF KNEE JOINT: SUBJECT-SPECIFIC VS GENERIC MODELS BASED ON 39 PATIENTS

Ruoqi Deng (1), Olivia L Bruce (1), Kalin D Gibbons (2), Clare K Fitzpatrick (2), LePing Li (1)

1. University of Calgary, Canada; 2. Boise State University, USA

1. Introduction

Subject-specific knee finite element modelling is time-consuming and technically challenging due to complex joint topology and multiple mechanical contacts involving several hard and soft tissues. It was even more challenging when we implemented the time variable to simulate fluid pressure and flow in the cartilaginous tissues. Various simplifications and modelling errors with a few subjects have led to diverse or even conflicting results in the literature. Diverse approaches coupled with population variability may have resulted in subjective or subject-specific conclusions [1]. Our research aims to understand the consequence of population diversity, including sex and ethnic differences in knee anatomy and tissue properties, through modelling of a large population to find generic and subject-specific biomechanical behaviours. The objective of the present study was to develop a generic knee modelling approach with statistical shape modelling (SSM) [2].

2. Methods

Two generic knee models have been so far created, respectively, for the left and right knees of 39 healthy subjects (45-69 years, white male) using a previously developed SSM workflow [3]. As an essential step for all subject-specific models, tissue geometries of each knee were reconstructed with MRIs (The Osteoarthritis Initiative) and meshed using an automated hexahedral meshing approach. The SSM approach used the Coherent Point Drift algorithm to establish node correspondence between individuals' point clouds for the bones, cartilages, and menisci. Following alignment of the point clouds, principal component analysis was applied to the registered knee joint data to extract the principal modes of variation. Cartilages and menisci were modelled as fibril-reinforced fluid-saturated materials using a previously developed constitutive model. The

creep response of the knee in full extension was then simulated with the generic models and selected subject-specific models, which included a 600-N force ramped in 1s and remained constant for 6000s.

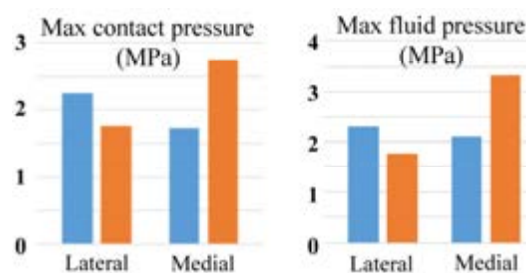


Figure 1: Contact and fluid pressures at 1s in the lateral and medial tibial cartilages for the average (blue) and subject-specific (orange) right knees. (Statistics will be available at the conference.)

3. Results

Cohort averaged and subject-specific results are shown in Fig. 1 where the result from the generic model represents the general or average response of the cohort while the result from a specific knee shows individual response.

4. Discussion and Conclusions

We have tested the feasibility of SSM in the poromechanical modelling of human knee joint using both left and right knees of 39 subjects. Joint mechanics for a cohort may be better understood with statistical results from average, individual models and the principal modes.

5. References

1. Erdemir A et al., J Biomech Eng 141: 071002 (2019).
2. Rao C et al., Med Eng Phy 35: 1450-6 (2013).
3. Bruce OL et al., Comput Methods Biomech Biomed Eng 25: 875-86 (2022).

Acknowledgements

Cette recherche a été financée par le Conseil de recherches en sciences naturelles et en génie du Canada.



APONEUROSIS HETEROGENEOUS MATERIAL PROPERTIES: EVIDENCE AND IMPLICATIONS FOR MUSCLE STRAIN

Benjamin Wheatley (1), Olivia Dyer (2), Mark Seeley (2)

1. Bucknell University, USA; 2. Geisinger Medical Center, USA

1. Introduction

Aponeurosis plays a vital role in muscle-tendon unit function [1], yet little is known of the structure-function properties of aponeurosis [2]. Specifically, it is unclear how aponeurosis material properties and microstructure vary from tendon insertion to muscle midbelly. We hypothesized that aponeurosis would exhibit a higher modulus and less wavy collagen towards the tendon insertion site, where forces in aponeurosis are likely to be greater.

2. Materials and Methods

Aponeurosis samples were fixed either unstretched or at 5% tensile stretch and imaged with scanning electron microscopy (n=10). Collagen waviness was measured. Tensile testing was performed at 0.05% strain/sec until failure (n=15) with strain tracking digital image correlation. Collagen waviness and stress-strain data was separated into two equal size regions: the insertion region (closer to tendon) and the transition region (closer to midbelly) (Figure 1). A finite element model of the average aponeurosis sample geometry was developed for fitting constitutive parameters to experimental stress-strain data. Three different constitutive formulations were implemented for model fitting: 1) homogeneous modulus, 2) linearly increasing or decreasing modulus with aponeurosis length, or 3) a log-normal modulus distribution. A finite element model of a representative muscle slice was developed for the simulation of 20% tensile strain and 50 N/cm² active contraction [3] for each of the three assumptions of aponeurosis heterogeneity.

3. Results

Unstretched aponeurosis microstructure exhibited a mean collagen bundle waviness value of 1.17 (p=0.055 between regions) and stretched aponeurosis exhibited decreases in waviness to 1.05 (p<0.001 stretched-

unstretched, p=0.45 between regions). The transition region exhibited a stiffer stress-stretch response (Figure 1A). Heterogeneous finite element modelling showed a strong fit to experimental data (Figure 1A) and variable linear modulus (Figure 1B). Variations in aponeurosis homogeneity greatly affected muscle first principal strain (Figure 1C).

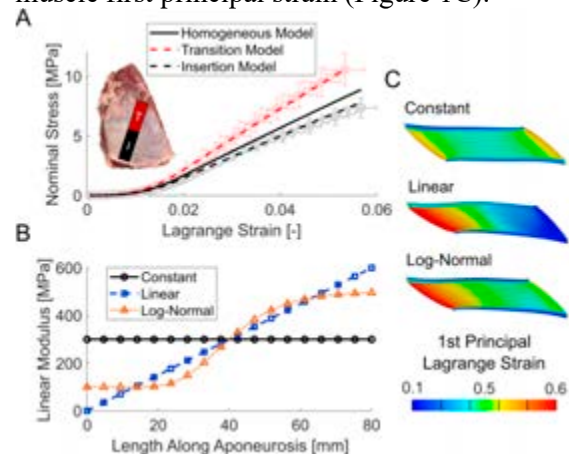


Figure 1: A) Experimental stress-strain data (mean and SEM bars) and model fits. B) Variability of linear region modulus as a function of length along aponeurosis. C) Effect of aponeurosis homogeneity on muscle strain after stretch-contraction.

4. Discussion and Conclusions

We observed a higher aponeurosis modulus in the transition region versus the insertion region, which contradicted our hypothesis. Structural differences in collagen waviness between these two regions was trending towards statistical significance. Finite element analysis further suggested that heterogeneous modelling of aponeurosis modulus could greatly affect muscle strain and thus muscle function *in vivo*, which warrants further investigation [3,4].

5. References

1. Herzog, W. BMC Biomed Eng., 28(1), 2019.
2. Grega, K. J Mech Behav Biomed., 110, 2020.
3. Wheatley, B. J Biomech Eng, 140(8), 2018.
4. Knaus, K., J Biomech., 30, 2022.



MECHANICAL CHARACTERIZATION OF NORMAL AND DECELLULARIZED BREAST TISSUES

Ana Margarida Teixeira (1), António Diogo André (1), Rossana Correia (2), Maria da Luz Barroso (3), Horácio Costa (3), Pedro Martins (4,5)

1. FEUP/INEGI, Portugal; 2. HEMS, i3s, Portugal; 3. CHVNGE, Serviço Cirurgia Plástica, Portugal; 4. INEGI/LAETA, Portugal; 5. i3A, Universidad de Zaragoza, Spain

1. Introduction

Female breast cancer was the most prevalent cancer worldwide (2020), and, for women, it had the highest mortality [1]. Many women perform a mastectomy or lumpectomy to fight the disease, which is normally followed by breast reconstruction, using silicone implants [2]. To find better alternatives for this procedure and improve the understanding of breast tissues, it is important to investigate their mechanical properties, including the mechanical behaviour of the extracellular matrix (ECM). It is known that the mechanical properties change along the life of a woman [3]. Therefore, the aim of this study is to mechanically characterize normal and decellularized breast tissues.

2. Materials and Methods

11 samples were collected from 3 patients who underwent a mammary reduction surgery. Samples were cut with diameter=20mm and height=10mm and tested using a 5mm flat-ended cylindrical indenter, a 10N load cell and a saline bath at 37°C. Only one sample was decellularized, following the protocol of [4]. A two-step mechanical protocol was defined: (I) preconditioning, using 20 cycles with 10% strain at 30%/min; (II) stress-relaxation test, using a load up to 30% strain at 30%/min, hold for 360s at the final position and unload up to 0% at the same rate. Histology was performed on normal samples, to assess the tissue's types.

3. Results

The mathematical approach was based on the work of Delaine-Smith et al. [5], and the proposed models were applied in the two linear regions of the loading curve. Depending on the model, the results (mean \pm standard error of mean) for normal breast tissues varied between 3.27 ± 0.41 kPa and 8.94 ± 1.13 kPa, for the first linear region, and between 21.09 ± 4.03 kPa and

57.66 ± 11.02 kPa, for the second linear region. For the decellularized sample, the Young's modulus was between 3.27-8.94 kPa and 85.27-233.16 kPa, for the first and second linear regions, respectively. Afterwards, the percentage of relaxation was calculated, and the values were $\approx 77 \pm 2\%$ for normal breast tissues and $\approx 94\%$ for the decellularized sample.

4. Discussion and Conclusions

The results obtained for the stiffness of normal breast tissues are in accordance with the values found in literature [3]. Comparing with the decellularized sample, the stiffness of the second linear region and the percentage of relaxation were higher for the decellularized sample. Considering relaxation, the equilibrium state of normal breast tissues requires more time. However, for the decellularized sample, a quasi-equilibrium state was already achieved with 360s. This study aims to improve the understanding of the mechanical behaviour of breast tissues, including the ECM, an important step for future tissue engineering solutions.

5. References

1. Sung et al., CA: Cancer J. Clin., 71(3):209–249 (2021).
2. Rocco et al., Procedia CIRP, 49:183–187 (2016).
3. Ramião et al., Biomech Model in Mechanobiol, 15(5):1307–1323 (2016).
4. Sesli et al., Turk. J. Biol., 42(6):537–547 (2018).
5. Delaine-Smith et al., J Mech Behav Biomed Mater, 60, 401–415 (2016).

Acknowledgements:

The authors gratefully acknowledge funding from FCT, Portugal, under grant 2020.08718.BD, from research unit LAETA and from project MImBI - PTDC/EME-APL/29875/2017 financed through FEDER and FCT.



MYXOMATOUS DEGENERATION OF THE MITRAL VALVE; COLLAGEN STRUCTURE AND MECHANICAL BEHAVIOR

**Mohammad Javad Sadeghinia (1), Robert Matongo Persson (2,3), Stig Urheim (2,3),
Gerhard A. Holzapfel (1,4), Bjørn Skallerud (1), Victorien Prot (1)**

1. Department of Structural Engineering, Norwegian University of Science and Technology (NTNU), Norway; 2. Haukeland University Hospital, Department of Heart Disease, Norway; 3. Institute of Clinical Science, University of Bergen, Norway; 4. Institute of Biomechanics, Graz University of Technology, Austria

1. Introduction

The mitral valve provides unidirectional blood flow from the left atrium to the left ventricle. Myxomatous degeneration is one of the main causes of mitral regurgitation [1]. It is associated with disrupted collagen fibers, which are the main mechanical load carriers in the mitral valve leaflets [2]. Therefore, an accurate mechanical characterization of the myxomatous leaflets requires a detailed investigation of the collagen structure in addition to mechanical tests. To the best of our knowledge, there is only one study on the mechanical characterization of myxomatous tissue by Barber et al. [3], which lacks the necessary detailed investigation of the collagen fibers required for material modeling.

2. Materials and Methods

This study was approved by the Regional Ethical Committee of West Norway, and all procedures followed national and EU ethical regulations. Myxomatous tissue samples are acquired peroperatively from patients requiring surgery. Healthy human mitral valves were obtained from post-mortem donors. Upon explantation, the sample is snap-frozen, stored in a biobank, and transported to the testing facility in liquid nitrogen. Before testing, it is thawed in 1×Phosphate-buffered saline (PBS) at room temperature.

Mechanical behavior is investigated with planar mechanical biaxial tests in 1×PBS at 37°C. Immediately after the mechanical tests, the tissue is chemically fixed and cleared. The cleared tissue is imaged throughout its thickness using second harmonic imaging microscopy. The collagen fiber structure is quantified using image analysis. Finally, tissue behavior is

characterized by an informed constitutive model.

3. Results

Planar biaxial tests revealed anisotropic mechanical behavior of the myxomatous tissue. This contrasts with the previous reports using uniaxial testing of myxomatous MV leaflets [3]. Nonetheless, the anisotropic mechanical response is verified by the anisotropic quantified collagen fiber distribution.

Nevertheless, results show that myxomatous samples show a variable mean fiber orientation across the thickness. Samples also demonstrated a lower concentration parameter for collagen distribution, i.e., a higher dispersion value.

4. Discussion and Conclusions

We demonstrated that myxomatous degeneration is associated with disrupted collagen fibers that affect the mechanical behavior of the leaflets. Collagen structure is quantified throughout the thickness and tissue behavior is examined using planar biaxial tests. This information is used in informed constitutive modeling that has the potential to improve predictability in novel surgical techniques and enables a better assessment of post-operative outcomes.

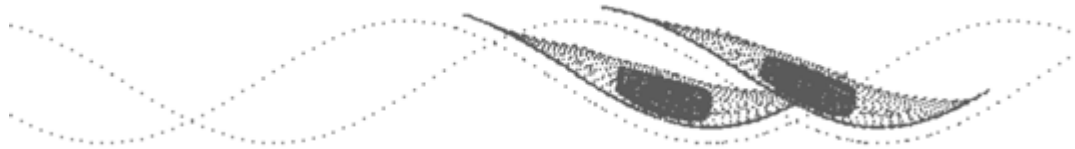
5. References

- [1] Carpentier A., Adams D., Filsoufi F. Carpentier's Reconstructive Valve Surgery. Medicine (Elsevier, 2010).
- [2] Levine R.A. et al. Nat. Rev. Cardiol. 12, 689–710 (2015).
- [3] Barber J.E. et al. J. Thorac. Cardiovasc. Surg. 122, 955–962 (2001).

***In silico* avatars of cells to predict cell migration on travelling waves**

Jean-Louis Milan¹, Maxime Vassaux², Laurent Pieuchot³, Karine Anselme³, Ian Manificier¹

1. Aix Marseille University, CNRS, ISM, Marseille, France
2. IPR Institute of Physics, UMR UR1 CNRS 6251, Rennes 1 University, France
3. Institut de Science des Matériaux de Mulhouse, University of Haute Alsace, 68057 Mulhouse, France



Introduction

We showed previously that cell migration is guided towards concave areas by a curvature gradient [1]. We called this phenomenon *curvotaxis* that is not induced by gravity. We showed that curvotaxis is a mechanobiological process involving the cytoskeleton and nucleus. The nucleus, is pushed by apical cortex pressure and is consequently displaced toward concave areas where the stress is lower [2, 3]. Influenced by the repositioning of the nucleus, the cell migrates to concave areas until a more relaxed mechanical state is reached. Nonetheless static curved surfaces guide cell migration only locally. We hypothesize that changing curvature dynamically by generating travelling waves at the surface of the substrate should stimulate and drive cell migration over large distances. Verifying our hypothesis directly by *in vitro* methods would require a long-time to develop the working prototype of a dynamic wavy substrate able to stimulate and drive cell migration. We proposed to verify it first using *in silico* with cell avatars.

Methods

We have developed *in silico* cell avatars that reproduce the mechanisms by which the cells sense the curvature of the substrate dynamically during cell migration [2, 3]. Cell model is a network of mechanical interactions that reproduce the contractile and dynamic structure of the cytoskeleton bound to the extracellular environment via focal adhesions. The cell model, in open access [4] is developed using LMGC90, a computational framework dedicated to non-smooth contact dynamics and multi interaction systems. Waves of 10 μm of amplitude and 160 μm of wave-length were simulated at the surface of a virtual substrate at a speed of 4 μm /iteration. Migration of the cellular model was then initiated and driven by curvotaxis.

Results

The cell model follows the progression of the wave and migrates indefinitely as long as the wave exists. Influenced by the travelling wave, the nucleus moves towards the concavity and the cell migrates in that direction. When retaining the same wavelength and velocity parameters, the speed of the cellular avatar decreased by a third when we lowered the amplitude of the wave 5 μm . But, with a wave amplitude of 20 μm , cell model migrated 1.5 times faster.

Discussion & Conclusion

Using the model, concerning the impact of travelling waves on cell migration, we answer a question that would otherwise be hard to directly address by experimental means. We propose the first *in-silico* proof-of-concept to guide cell migration by generating travelling waves. This will help in the designing of dynamic substrates to stimulate cell migration *in vitro*. Our *in-silico* avatar of migrating cells can later be implemented for cell engineering and lab-on-chip technology, as a live augmented reality tool to drive smart substrate actuation and control cells *in vitro*.

- [1] Pieuchot *et al.*, *Nature Commun.*, 2018, <https://doi.org/10.1038/s41467-018-06494-6>.
- [2] Vassaux *et al.*, *Biophys. J.*, 2019, <https://doi.org/10.1016/j.bpj.2019.07.022>.
- [3] Vassaux *et al.*, *Adv. Struct. Materials*, 2020, https://doi.org/10.1007/978-3-030-50464-9_12
- [4] Vassaux *et al.*, *Zenodo available in Github* <https://doi.org/10.5281/zenodo.1187087>



COMPUTED-TOMOGRAPHIC IMAGING FOR THE *IN VIVO* REGENERATION OF CRITICAL-SIZED CERAMIC SCAFFOLDS

Pablo Blázquez-Carmona (1,2), Francisco Javier Martínez-Vázquez (1), Juan Mora-Macías (3), Jaime Domínguez-Abascal (1), Esther Reina-Romo (1)

1. Universidad de Sevilla, Spain; 2. Universidad de Cádiz, Spain; 3. Universidad de Huelva, Huelva.

1. Introduction

Tissue engineering (TE) is an emerging biomedical field focused on designing porous structures, called scaffolds, to address the current limited graft availability for critical-sized treatments [2]. Specifically, bioceramic became a good standard owing to their proven biocompatibility and osteoinductivity [2]. Given the small pool of *in vivo* experiments in large animals, this work aims to apply imaging techniques in ovine defects treated with TE to elucidate the effectiveness attributed to ceramic frameworks in comparison to other regeneration processes with shared orthopaedic applications, such as bone transport or tissue grafting.

2. Materials and Methods

TE surgeries were performed *in vivo* on the right-back metatarsus of eight skeletally-mature merino sheep. It consisted of the replacement of a 15-mm bone segment by a hydroxyapatite scaffold (59% of porosity, 360 μ m of pore size) externally stabilized. Computed tomographic (CT) scans of the operated limb were taken at different time-points of the consolidation phase to quantify the evolution of the callus geometry and mineral density (BMD). CT images of the contralateral limb were recorded as control data. Phantoms were also included as a screening tool to correlate mineral density with the segmented Hounsfield unit. The stacks were thresholded and analysed using the medical software InVesalius[®] and ImageJ[®]. Data were finally fitted to logistic function to evaluate the general tendency (R-square > 0.7 and p-value > 0.01).

3. Results

Fig. 1 validates the success of the applied clinical treatment through the progressive recovery of the cortical properties. The callus geometry started close to healthy values due to the patient-specific scaffold's design.

Volumetric peaks prior to remodelling were reached approximately after 6 months, being over twice that in the original bone. At this stage, the defect already recovered 85% of the contralateral mineral density.

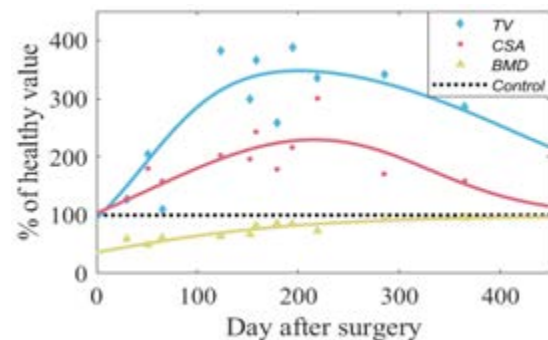


Figure 1: Evolution of the total volume (TV), cross-sectional area (CSA), and mineral density (BMD) of the TE callus as a % of the contralateral values.

4. Discussion and Conclusions

Compared with previous studies in the same bone model, the callus volume and cross-section seem to be significantly higher than distraction strategies [1]. Furthermore, our scaffold exhibited a 18% faster mineral densification than mixed phosphate-polymer structures [3]. In closing, pure ceramic scaffold offers efficient mineralization at the cost of a delay in complete remodelling.

5. References

- Blázquez-Carmona P et al., Ann Biomed Eng; 49(4):1209-1221 (2021).
- Karageorgiou V, Kaplan D, Biomaterials; 26(27):5474-5491 (2005).
- Pobloth A-M et al., J Tissue Eng Regen Med; 12(4):897-911 (2018).

Acknowledgements:

The authors would like to thank the Government of Spain (Grant no: PID2020-113790RB-I00) for providing financial support to this project.



BIOMECHANICS OF BACTERIA : THEORY AND EXPERIMENT

Rui Han (1), Xiqiao Feng (2), Waldemar Vollmer (3), Paul Stoodley (4), Jinju Chen (1)*

1. School of Engineering, Newcastle University, UK; 2. Department of Engineering Mechanics, Tsinghua University, China; 3. Biosciences Institute, Newcastle University, UK; 4. Department of Microbial Infection and Immunity and the Department of Orthopaedics, The Ohio State University, United States

1. Introduction

Cell growth, division, and motility, strongly depend on their mechanical properties and interactions with the environments [1]. Cell wall provides a protection of bacteria and maintains their mechanical integrity by resisting deformation arising from the adhesion forces of bacteria attached to a substratum surface and other external stimuli. Cell integrity is maintained by the osmotic difference between the cytoplasm extracellular environment, known as turgor. Both bacterial cell wall stiffness and turgor are important for bacterial survival and adaptation, but they are difficult to be determined simultaneously.

2. Materials and Methods

We have adopted atomic force microscopy (AFM) nanoindentation using both pyramid and spherical probes, finite element simulations and theoretical models to simultaneously determine the cell wall stiffness and turgor of the given bacteria at different chemical environment. Clinical isolates *S. epidermidis* FH8 were immobilised on mica prior to AFM nanoindentation. These bacteria were in three different osmolarity environments: DI water, phosphate-buffered saline (PBS), and 100 mM CaCl₂ solution.

3. Results

Fig.1 shows the cell wall stiffness and turgor determined by combined experimental and modelling approach. For bacterial mechanics, we also expect some viscoelastic characteristics due to the combination of the polymeric nature of the bacterial cell wall and cytoplasm. As expected, we did observe a hysteresis in the force-distance curves due to the viscoelastic characteristics of bacteria [2]. We found energy loss and elastic energy during AFM indentation

were highest for bacteria in DI water, followed by PBS, and then by 100 mM CaCl₂.

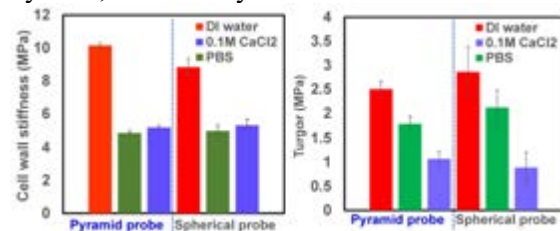


Figure 1. Comparisons of (a) cell wall stiffness and (b) turgor for *S. epidermidis* in DI water, PBS, and 100 mM CaCl₂, respectively. N = 36.

4. Discussion and Conclusions

Based on the combined experimental and modelling approaches, we have revealed that the cell wall stiffness for individual cells correlated well with the turgor. The use of pyramid and spherical probes yields consistent results. We have demonstrated that higher osmolarity reduce the apparent bacterial modulus by decreasing both cell wall stiffness and turgor. By analysing energy loss and elastic energy during indentation tests, we have discovered that the change in turgor is associated with a change in the viscosity of the cell. Our methodology can be adapted to other bacteria with different shapes. The approach presented here can also be adapted to study how bacterial mechanics contribute to survival in the presence of antibiotics or within a host.

5. References

1. Furchtgott L, Wingreen N S, Huang, KC. Mol Microbiol, 2011, 81, 340-353.
2. Han R, et al., Nanoscale, 2022, 14, 12060 - 12068

Acknowledgements:

The authors acknowledge funding from the Engineering and Physical Sciences Research Council (EP/R025606/1, EP/V049615/1, EP/T002778/1) and PhD scholarship from Chinese Scholarship Council and Newcastle University.